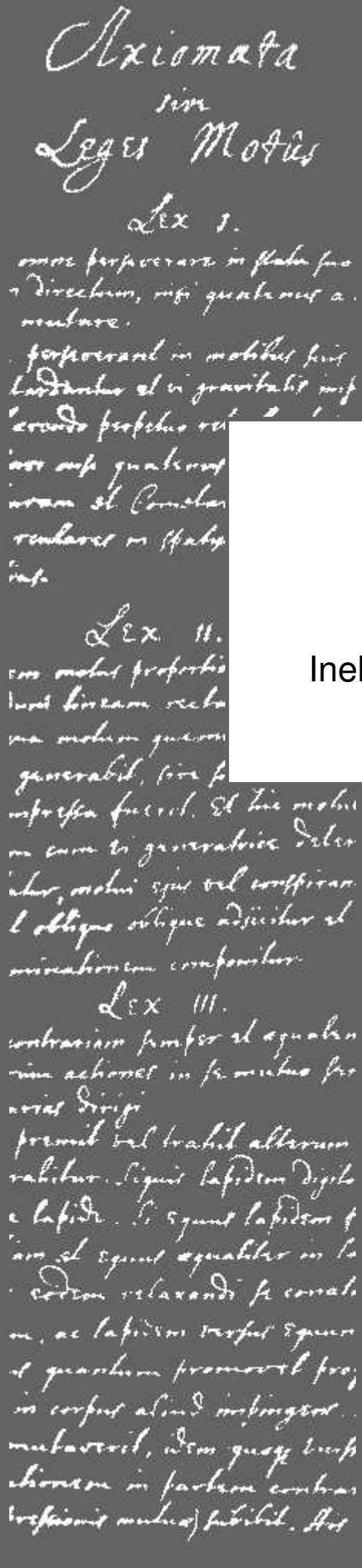

Technische Universität
Kaiserslautern

A. Menzel

Frontiers in Inelastic Continuum Mechanics

UKL / LTM T 07–03 September 2007
Lehrstuhl für Technische Mechanik

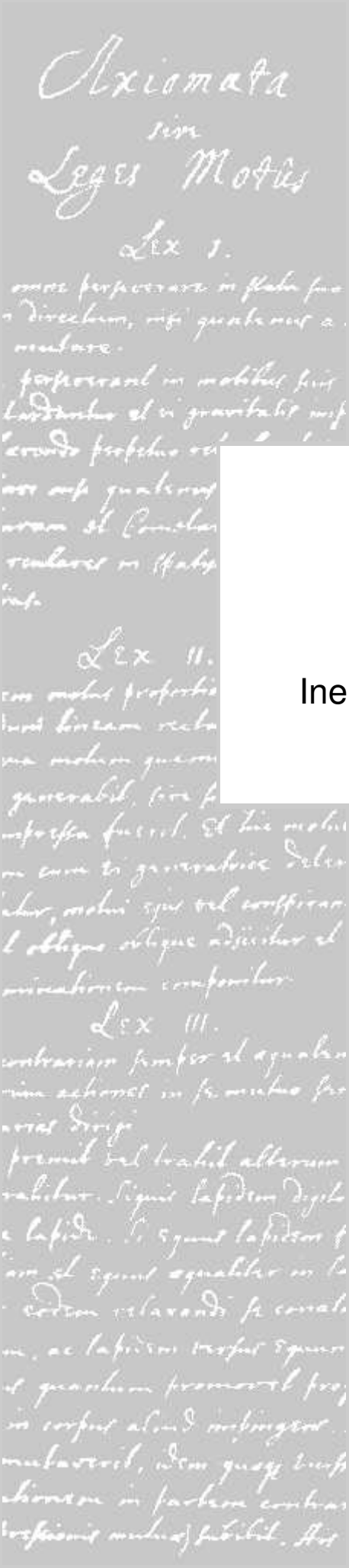

Technische Universität
Kaiserslautern

A. Menzel

Frontiers in Inelastic Continuum Mechanics

UKL / LTM T 07–03 September 2007
Lehrstuhl für Technische Mechanik

Frontiers in Inelastic Continuum Mechanics

Andreas Menzel

key words continuum mechanics, configurational mechanics, finite deformation, plasticity, continuum dislocations, kinematic hardening, biological tissues, anisotropy, remodelling, growth, anisotropy, finite elements

Bibliografische Information Der Deutschen Bibliothek
Die Deutsche Bibliothek verzeichnet diese Publikation in der Deutschen Nationalbibliografie; detaillierte bibliographische Daten sind im Internet über **http://dnb.ddb.de** abrufbar.

Bibliographic information published by Die Deutschen Bibliothek
Die Deutsche Bibliothek lists this publication in the Deutschen Nationalbibliografie; detailed bibliographic data is available in the Internet at **http://dnb.ddb.de**.

Herausgeber: Fachbereich Maschinenbau und Verfahrenstechnik
Lehrstuhl für Technische Mechanik
Postfach 3049
Technische Universität Kaiserslautern
D–67653 Kaiserslautern

Verlag: Technische Universität Kaiserslautern

Druck: Technische Universität Kaiserslautern
ZBT – Abteilung Foto–Repro–Druck

D–386

http://kluedo.ub.uni-kl.de

Als Manuskript gedruckt, Printed in Germany

ISSN 1610–4641
ISBN 978–3–939432–55–5

Frontiers in Inelastic Continuum Mechanics

vom Fachbereich Maschinenbau und Verfahrenstechnik
der Technischen Universität Kaiserslautern
zur Erlangung der venia legendi für das Fach
Mechanik
angenommene Habilitationsschrift

von
Dr.–Ing. Andreas Menzel
aus Hannover

Referenten:	Prof. P. Steinmann
	Prof. G.A. Maugin
	Prof. R.W. Ogden
Tag der Einreichung:	22. November 2005
Vollzug des Habilitationsverfahrens:	31. Mai 2006

Preface

This work has been carried out during the period from 2002 to 2005 at the Chair of Applied Mechanics at the University of Kaiserslautern.

First of all, I want to thank Professor Paul Steinmann for his continuous support over the past ten years and serving as a referee. Inspiring discussions, the friendly working environment at the Chair of Applied Mechanics, the freedom to follow different fields of research, and the opportunity to be involved in several scientific projects had a great impact on my work. Moreover, I thank Professor Gérard Maugin and Professor Ray Ogden for acting as referees of this thesis. Their openness and interest in my work as well as stimulating discussions at various occasions were a great motivation over the past years and invaluably contributed to this thesis.

I gratefully appreciate my colleagues at the Chair of Applied Mechanics at the University of Kaiserslautern who provided such a pleasant working atmosphere. In particular I thank Dr. Franz Josef Barth and Natalia Kondratieva for their support, help, and encouragement. I also greatly benefited from collaborating with the Department of Applied Mechanics at Chalmers University of Technology. Working together with Professor Magnus Ekh, Göran Johansson, Ph.D., and Professor Kenneth Runesson was not only very fruitful but especially of great pleasure. Most of all, I thank my family for their continuous support, tolerance, patience, and understanding.

Kaiserslautern, September 2007 Andreas Menzel

Contents

1 Introduction

The appropriate modelling of inelastic solid continua is among the most challenging tasks in applied and theoretical mechanics. This active field of research is located at the intersection of engineering disciplines, physics, materials sciences, and mathematics and has attracted studies not only within the last decades but over centuries. Nevertheless, reliable constitutive models to which (almost) all scientists in these communities agree, seem to reduce to linear elastic concepts so that severe assumptions must be accepted which lead to a rather limited applicability. Even though this strong statement might be too pessimistic, it reflects the necessity to develop fundamental theories and modelling strategies for inelastic deformation processes that capture physically relevant and experimentally observed phenomena. Giving solely some representative examples, the description of irreversible deformations, plastic distortions, dislocations, damage mechanisms, substructure evolution, growth processes and so forth are of particular interest. Two aspects turn out to be of cardinal importance for the appropriate modelling of such effects, namely

(i) the consideration of inhomogeneities (together with their evolution) that affect constitutive properties of the material of interest;

(ii) the incorporation of internal and residual stresses (for instance caused by inhomogeneities).

Modelling approaches that account for inhomogeneities of materials usually result in a rather mathematical formalism based on concepts borrowed from differential geometry. The evolution of such inhomogeneities is commonly considered to be driven by so–called configurational forces. Furthermore, the incorporation of pre–stressed states or, in other words, configurations raises various questions which appear to be fully understood only for the linear elastic case.

The purpose of this introduction is twofold: on the one hand, general modelling concepts for (i) the incorporation of inhomogeneities, (ii) internal stresses, and related topics are briefly reviewed from a personal perspective. On the other hand, we summarise the contents of the subsequent chapters within which formulations for typical inelastic phenomena as plasticity, damage, growth, remodelling, and so forth are addressed. Besides the development of constitutive frameworks, fundamental aspects as for instance effects stemming from incompatibilities and configurational balance relations are preliminarily discussed in detail. The derived sets of constitutive equations combined with related balance equations are usually too complex to obtain analytical solutions. As such, emphasis will also be placed on numerical strategies with particular emphasis on the finite element method.

1.1 Inhomogeneities

For the following elaborations, we assume the constitutive behaviour of the considered body B, which is embedded into a three–dimensional space, to be characterised by the Helmholtz free energy ψ. In view of an elastic material, the scalar–valued tensor function ψ consequently depends (i) on the deformation gradient $\boldsymbol{F}$, (ii) on the material placements $\boldsymbol{X}$ of particles,

and (iii) possibly on a so–called material isomorphism $\boldsymbol{K}$, which transforms elements of the tangent space of the particular material configuration to the tangent space of the some chosen reference configuration. Accordingly, the Helmholtz free energy density allows representation as

$$\psi_{\mathrm{k}} \doteq \psi_{\mathrm{k}}(\bar{\boldsymbol{F}}) = \psi_{\mathrm{k}}(\boldsymbol{F}\cdot\boldsymbol{K}(\boldsymbol{X})) \equiv J_{\mathrm{k}}\,\psi_0(\boldsymbol{F};\boldsymbol{X}) \quad \text{with} \quad J_{\mathrm{k}} = \det(\boldsymbol{K}) > 0\,, \tag{1.1}$$

so that the underlying material symmetry (at $\boldsymbol{X}$) with respect to $\boldsymbol{K}$ is determined by

$$\psi_{\mathrm{k}}(\bar{\boldsymbol{F}}) = \psi_{\mathrm{k}}(\bar{\boldsymbol{F}}\cdot\boldsymbol{Q}) \quad \forall\ \bar{\boldsymbol{F}} \in \mathbb{L}_+\,, \tag{1.2}$$

wherein $\boldsymbol{Q} \in \mathbb{U}_+$ has been assumed. Moreover, Christoffel symbols of the second kind and with respect to the material connection, as here represented by means of $\boldsymbol{K}$, are characterised via

$$\Gamma^L_{\ NM}(\boldsymbol{X}) = k^\alpha_{\ N,M}(\boldsymbol{X})\,K^L_{\ \alpha}(\boldsymbol{X}) = -\,k^\alpha_{\ N}(\boldsymbol{X})\,K^L_{\ \alpha,M}(\boldsymbol{X}) \tag{1.3}$$

with the notation $\{\bullet\}_{,M}$ abbreviating partial differentiation and $\boldsymbol{k} = \boldsymbol{K}^{-1}$. The skew–symmetric part of $\Gamma^L_{\ NM}(\boldsymbol{X})$, namely $T^L_{\ MN}(\boldsymbol{X}) = \frac{1}{2}\,[\,\Gamma^L_{\ MN}(\boldsymbol{X}) - \Gamma^L_{\ NM}(\boldsymbol{X})\,]$, is denoted as torsion and represents the density of the distributions of inhomogeneities. Practically speaking, $T^L_{\ MN}(\boldsymbol{X})$ is directly related to so–called dislocation densities. For detailed elaborations we refer the reader to Schouten (1989), Lodge (1974), Kröner (1981), Davini (1988) or Maugin (1993) and references cited therein.

The overall modelling concept itself is often also denoted as the introduction of a local rearrangement and dates back to the pioneering works by Noll (1958, 1967, 1972); see also Wang and Truesdell (1973), Truesdell and Noll (2004), Truesdell (1977), Wang and Bloom (1974) or Epstein and Maugin (1990), the recent monograph by Bertram (2003) and the contributions in Del Piero and Owen (2004) as well as references cited therein. Moreover, the action of the material isomorphism $\boldsymbol{K}$ is directly related to the multiplicative decomposition of the deformation gradient into a reversible contribution $\boldsymbol{F}_{\mathrm{e}} \equiv \bar{\boldsymbol{F}}$ and an irreversible part $\boldsymbol{F}_{\mathrm{p}} \equiv \boldsymbol{k}$; compare Lee (1969), Mandel (1974), Kröner (1960) or Lubarda (1999) among others.

Apparently, the properties of $\boldsymbol{K}$ significantly affect the constitutive response of the material. Conceptually speaking, this second–order tensor allows to account for inhomogeneities so that residual stresses after unloading are naturally incorporated. In general, $\boldsymbol{K}$ is not integrable so that incompatibilities come into the picture and $\nabla^{\mathrm{t}}_{\boldsymbol{X}} \times \boldsymbol{k} \neq \boldsymbol{0}$. In other words, the configuration related to the tangent space to which $\boldsymbol{k}$ points is not connected. Consequently, this material isomorphism cannot be derived from a single vector field but rather transforms infinitesimal line elements, say $\mathrm{d}\boldsymbol{X} = \boldsymbol{K}\cdot\mathrm{d}\boldsymbol{x}_{\mathrm{k}}$ and $\mathrm{d}\boldsymbol{x}_{\mathrm{k}} = \boldsymbol{k}\cdot\mathrm{d}\boldsymbol{X}$, respectively. A field representation of $\boldsymbol{K}$ requires the introduction of tensor potentials which is addressed in section 1.1.1. Subsequently, transformations of related differential operators are discussed, see section 1.1.2.

1.1.1 Helmholtz decomposition of tensor fields

Recall the Helmholtz decomposition of some vector field $\boldsymbol{v}(\boldsymbol{X})$ into an irrotational and a solenoidal part

$$\boldsymbol{v}(\boldsymbol{X}) = \nabla_{\boldsymbol{X}} a(\boldsymbol{X}) + \nabla^{\mathrm{t}}_{\boldsymbol{X}} \times \boldsymbol{b}(\boldsymbol{X}) + \boldsymbol{v}_c\,, \tag{1.4}$$

wherein $a(\boldsymbol{X})$ and $\boldsymbol{b}(\boldsymbol{X})$ denote a scalar and a vector potential of sufficient smoothness – with $\nabla^{\mathrm{t}}_{\boldsymbol{X}} \times \nabla_{\boldsymbol{X}} a(\boldsymbol{X}) = \boldsymbol{0}$ and $\nabla_{\boldsymbol{X}} \cdot (\nabla^{\mathrm{t}}_{\boldsymbol{X}} \times \boldsymbol{b}(\boldsymbol{X})) = 0$ being obvious – and $\boldsymbol{v}_c = \mathrm{const}$; see section 1.5 for notational details. For a related decomposition of a second–oder tensor field, $\boldsymbol{T}(\boldsymbol{X}) = \boldsymbol{j}_j(\boldsymbol{X}) \otimes \boldsymbol{i}_j(\boldsymbol{X})$ say, we follow the lines of derivation highlighted in Dassios and Lindell (2001) and note

$$\boldsymbol{T}(\boldsymbol{X}) = \boldsymbol{j}_j(\boldsymbol{X}) \otimes [\,\boldsymbol{i}_j(\boldsymbol{X}) \cdot \boldsymbol{e}_i\,]\,\boldsymbol{e}_i = \boldsymbol{j}_j(\boldsymbol{X}) \otimes \boldsymbol{i}_j(\boldsymbol{X}) \cdot \boldsymbol{e}_i \otimes \boldsymbol{e}_i = \boldsymbol{v}_i(\boldsymbol{X}) \otimes \boldsymbol{e}_i\,. \tag{1.5}$$

Making use of eq.(1.4) renders the alternative format

$$\begin{aligned} \boldsymbol{T}(\boldsymbol{X}) &= [\ \nabla_{\boldsymbol{X}} a_i(\boldsymbol{X}) \quad + \nabla^{\mathrm{t}}_{\boldsymbol{X}} \times \ \boldsymbol{b}_i(\boldsymbol{X})\ ] \cdot \boldsymbol{e}_i \ + \boldsymbol{T}_c \\ &= \nabla_{\boldsymbol{X}} (\ a_i(\boldsymbol{X})\, \boldsymbol{e}_i\ ) + \nabla^{\mathrm{t}}_{\boldsymbol{X}} \times (\ \boldsymbol{b}_i(\boldsymbol{X}) \otimes \boldsymbol{e}_i\ ) + \boldsymbol{T}_c \\ &= \nabla_{\boldsymbol{X}} \boldsymbol{a}(\boldsymbol{X}) \quad + \nabla^{\mathrm{t}}_{\boldsymbol{X}} \times \ \boldsymbol{B}(\boldsymbol{X}) \quad + \boldsymbol{T}_c\,, \end{aligned} \tag{1.6}$$

whereby $\{\boldsymbol{e}_i\}$ denotes a material space–attached orthonormal frame, $\boldsymbol{T}_c = \mathrm{const}$, and a divergence–free ansatz for $\boldsymbol{b}_i(\boldsymbol{X})$, or $\boldsymbol{B}(\boldsymbol{X})$ respectively, is obviously sufficient; compare also Kröner (1958). The vector potential $\boldsymbol{a}(\boldsymbol{X})$ as well as the tensor potential $\boldsymbol{B}(\boldsymbol{X})$ also exhibit the representations highlighted in eqs.(1.4,1.6) so that renaming arguments and assembling terms results in

$$\boldsymbol{T}(\boldsymbol{X}) = \nabla^2_{\boldsymbol{X}\otimes\boldsymbol{X}} a(\boldsymbol{X}) + \nabla_{\boldsymbol{X}} (\ \nabla^{\mathrm{t}}_{\boldsymbol{X}} \times \boldsymbol{b}(\boldsymbol{X})\ ) + \nabla^{\mathrm{t}}_{\boldsymbol{X}} \times (\ \nabla^{\mathrm{t}}_{\boldsymbol{X}} \times \boldsymbol{C}(\boldsymbol{X})\ ) + \boldsymbol{T}_c\,. \tag{1.7}$$

The tensor potential $\boldsymbol{C}(\boldsymbol{X})$ can also be rewritten by means of eq.(1.7), for instance in terms of some potentials $q(\boldsymbol{X})$, $\boldsymbol{r}(\boldsymbol{X})$ and $\boldsymbol{S}(\boldsymbol{X})$. Due to the fact that the curl operation is applied to $\boldsymbol{C}(\boldsymbol{X})$, additional constrains might be introduced, to be specific $\nabla_{\boldsymbol{X}} q = \boldsymbol{0}$, $\nabla^{\mathrm{t}}_{\boldsymbol{X}} \times \boldsymbol{r} = \boldsymbol{0}$, $\nabla_{\boldsymbol{X}} \cdot \boldsymbol{S} = [\,\nabla_{\boldsymbol{X}} \boldsymbol{S}\,] : \boldsymbol{I} = \boldsymbol{0}$ and $[\,\nabla^2_{\boldsymbol{X}\otimes\boldsymbol{X}} \boldsymbol{S}\,] : \boldsymbol{I} = \boldsymbol{0}$. In this regard, divergence–free tensor potentials $\boldsymbol{C}(\boldsymbol{X})$ allow representation via eq.(1.5) combined with a (vectorial) null divergence, namely

$$\boldsymbol{C}(\boldsymbol{X}) = \boldsymbol{c}_i(\nabla_{\boldsymbol{X}} \boldsymbol{\chi}(\boldsymbol{X}), \boldsymbol{\chi}(\boldsymbol{X}), \boldsymbol{X}) \otimes \boldsymbol{e}_i \quad \text{with} \quad \nabla_{\boldsymbol{X}} \cdot \boldsymbol{c}_i = \boldsymbol{0}\,, \tag{1.8}$$

whereby $\boldsymbol{\chi}(\boldsymbol{X})$ is assumed to be a twice continuously differentiable mapping; compare Olver (1993) and Šilhavý (1997). By further reducing $\boldsymbol{c}_i$ to homogeneous null divergences so that $\boldsymbol{c}_i = \boldsymbol{c}_i(\nabla_{\boldsymbol{X}} \boldsymbol{\chi}(\boldsymbol{X}))$, we obtain

$$\boldsymbol{c}_i(\nabla_{\boldsymbol{X}} \boldsymbol{\chi}(\boldsymbol{X})) = \boldsymbol{l}_i + \boldsymbol{E} : [\,\nabla^{\mathrm{t}}_{\boldsymbol{X}} \boldsymbol{\chi} \cdot \boldsymbol{M}_i\,] + \mathrm{cof}^{\mathrm{t}}(\nabla_{\boldsymbol{X}} \boldsymbol{\chi}) \cdot \boldsymbol{n}_i \tag{1.9}$$

for the material configuration endowed with placements $\boldsymbol{X} \in \mathbb{R}^3$ being connected and $\boldsymbol{l}_i, \boldsymbol{M}_i, \boldsymbol{n}_i = \mathrm{const}$. To verify that eq.(1.9) is divergence–free, one simply takes into account the definition of the permutation tensor $\boldsymbol{E}$ as well as the Piola identity; compare appendices A and C.

In view of deformation processes of solid continua, eqs.(1.6,1.7) can be applied to, for instance, $\boldsymbol{F}$ or $\boldsymbol{k}$, respectively. To give two examples, we observe on the one hand that the total deformation gradient allows convenient representation by means of eq.(1.6), namely $\boldsymbol{F} = \nabla_{\boldsymbol{X}} \boldsymbol{\varphi} \equiv \nabla_{\boldsymbol{X}} \boldsymbol{u} + \boldsymbol{I}$. The contributions of the tensor potential $\boldsymbol{B}$ apparently vanish so that $\nabla^{\mathrm{t}}_{\boldsymbol{X}} \times \boldsymbol{F} = \boldsymbol{0}$ and $\boldsymbol{F}$ relates elements of tangent spaces attached to connected configurations. On the other hand, we apply eq.(1.7) to the material isomorphism $\boldsymbol{k}$. The contribution $\nabla^{\mathrm{t}}_{\boldsymbol{X}} \times \nabla^{\mathrm{t}}_{\boldsymbol{X}} \times \boldsymbol{C}$ then takes the interpretation as representing the so–called incompatibility of $\boldsymbol{C}$; see for instance Lodge (1951) or references cited in Menzel and Steinmann (1998). For $\nabla^{\mathrm{t}}_{\boldsymbol{X}} \times \boldsymbol{k} \neq \boldsymbol{0}$, this local rearrangement points towards a non–connected configuration.

1.1.2 Transformations of divergence and curl operations

Apart from the elaboration of fundamental properties of the material isomorphism $\boldsymbol{K}$, it is also of interest to identify related differential operations. The introduction of corresponding gradient operations is straightforward, since $\boldsymbol{K}$ itself transforms infinitesimal line elements, as mentioned in section 1.1, so that $\nabla_{\boldsymbol{x}_{\mathrm{k}}}\{\bullet\} = \nabla_{\boldsymbol{X}}\{\bullet\} \cdot \boldsymbol{K}$ and $\nabla_{\boldsymbol{X}}\{\bullet\} = \nabla_{\boldsymbol{x}_{\mathrm{k}}}\{\bullet\} \cdot \boldsymbol{k}$, respectively. In view of the divergence or curl operation, however, such transformations turn out to be rather advanced for the general case where contributions of $\boldsymbol{k}$ stemming from $\boldsymbol{B}$ or $\boldsymbol{C}$ in eqs.(1.6,1.7) do not vanish. One reason among others consists of the fact that the standard

Piola identity is no longer valid as soon as incompatibilities are incorporated; see de Saxcé (2001) for detailed derivations or appendix C where the incorporation of so–called dislocation density tensors is additionally addressed.

In this regard, let $\boldsymbol{\Upsilon}$ be a second–order tensor which is either entirely settled in the so–called reference configuration or represents a two–point tensor by analogy with $\boldsymbol{k}$. Moreover, we introduce $\boldsymbol{v}$ via the Piola transformation $\boldsymbol{\Upsilon} = \boldsymbol{v} \cdot \operatorname{cof}(\boldsymbol{k})$. With these assumptions at hand, the divergence operation $\nabla_{\boldsymbol{x}_\mathrm{k}} \cdot \{\bullet\}$ as well as the curl operation $\nabla^\mathrm{t}_{\boldsymbol{x}_\mathrm{k}} \times \{\bullet\}$ are determined by

$$\begin{aligned} \nabla_{\boldsymbol{X}} \cdot \boldsymbol{\Upsilon} \quad &= \boldsymbol{v} \cdot [\, \nabla_{\boldsymbol{X}} \cdot \operatorname{cof}(\boldsymbol{k}) \,] \, + \, J_\mathrm{k} \, \nabla_{\boldsymbol{x}_\mathrm{k}} \cdot \boldsymbol{v} \,, \\ \nabla^\mathrm{t}_{\boldsymbol{X}} \times (\, \boldsymbol{v} \cdot \boldsymbol{k} \,) \, &= \boldsymbol{v} \cdot [\, \nabla^\mathrm{t}_{\boldsymbol{X}} \times \boldsymbol{k} \,] \quad + [\, \nabla^\mathrm{t}_{\boldsymbol{x}_\mathrm{k}} \times \boldsymbol{v} \,] \cdot \operatorname{cof}(\boldsymbol{k}) \,, \end{aligned} \tag{1.10}$$

whereby use of transformation relations for permutation tensors as highlighted in appendix A has been made. If $\boldsymbol{k}$ can be derived from a vector potential, recall for instance eq.(1.6), the Piola identity holds and the curl of $\boldsymbol{k}$ vanishes so that $\nabla_{\boldsymbol{X}} \cdot \operatorname{cof}(\boldsymbol{k}) = \boldsymbol{0}$ and $\nabla^\mathrm{t}_{\boldsymbol{X}} \times \boldsymbol{k} = \boldsymbol{0}$. To give an example for the corresponding reduced format of eq.(1.10), assume $\boldsymbol{k} = \nabla_{\boldsymbol{X}} \boldsymbol{\varphi} = \boldsymbol{F}$ together with $\boldsymbol{\Upsilon} = \boldsymbol{\Pi}^\mathrm{t} = \boldsymbol{\sigma}^\mathrm{t} \cdot \operatorname{cof}(\boldsymbol{F})$ denoting the Piola stress tensor. Accordingly, we recover the well–known relation $\nabla_{\boldsymbol{X}} \cdot \boldsymbol{\Pi}^\mathrm{t} = J \, \nabla_{\boldsymbol{x}} \cdot \boldsymbol{\sigma}^\mathrm{t}$ for $\boldsymbol{x} = \boldsymbol{\varphi}(\boldsymbol{X})$.

1.2 Internal stresses

A continuum might exhibit internal and residual stresses for absent body forces and surface traction so that related pre–stressed configurations are energetic. Moreover, such pre–stressed bodies also allow interpretation as pre–deformed continua since any removal of these type of stresses would violate the conditions of continuity. Nevertheless, residual stresses must be in equilibrium, namely $\nabla_{\boldsymbol{X}} \cdot \boldsymbol{\Pi}^\mathrm{t}_\mathrm{res} = \boldsymbol{0}$ in the considered material configuration $\mathcal{B}_0$ together with $\boldsymbol{\Pi}^\mathrm{t}_\mathrm{res} \cdot \boldsymbol{N} = \boldsymbol{0}$ on $\partial\mathcal{B}_0$ for $\boldsymbol{N}$ denoting the outward surface normal. With these relations at hand, we furthermore conclude that

$$\begin{aligned} \int_{\mathcal{B}_0} \boldsymbol{\Pi}^\mathrm{t}_\mathrm{res} \, \mathrm{d}V_0 \, &= \int_{\mathcal{B}_0} \quad \boldsymbol{\Pi}^\mathrm{t}_\mathrm{res} \cdot \nabla_{\boldsymbol{X}} \boldsymbol{X} \, \mathrm{d}V_0 \\ &= \int_{\partial\mathcal{B}_0} [\, \boldsymbol{\Pi}^\mathrm{t}_\mathrm{res} \cdot \boldsymbol{N} \,] \otimes \boldsymbol{X} \, \mathrm{d}A_0 - \int_{\mathcal{B}_0} [\, \nabla_{\boldsymbol{X}} \cdot \boldsymbol{\Pi}^\mathrm{t}_\mathrm{res} \,] \otimes \boldsymbol{X} \, \mathrm{d}V_0 = \boldsymbol{0} \,, \end{aligned} \tag{1.11}$$

see the contribution by Ogden in Holzapfel and Ogden (2003, pp. 65–108) and Chadwick (1999) or Ogden (1997) in view of the applied integral theorem. Apparently, the distribution of $\boldsymbol{\Pi}^\mathrm{t}_\mathrm{res}$ must be inhomogeneous to satisfy eq.(1.11) and also influences the material symmetry related to the constitutive response of the body B.

The incorporation of residual stresses and the formulation of constitutive relations for pre–stressed bodies has attracted studies for several decades. A classical and enlightening survey of this topic is given by Biot (1965). The reader is also referred to the contributions on initial stresses by Green et al. (1952), Truesdell (1966), Ieşan (1989), Ciarletta and Ieşan (1993) and Haupt et al. (1992) as well as to the elaborations on internal constraints in Antman (1995) and Podio–Guidugli (2000). The pioneering work on residual stresses by Hoger is documented in a series of papers (mainly in the J. Elasticity), for instance (1993a, 1993b, 1993c, 1996, 1997), see also the contribution by Skalak et al. (1996). In view of finite deformation theories, a key modelling concept thereby consists of the incorporation of residual stresses as an additional argument into the Helmholtz free energy density; see the contributions in Boehler (1987) or Antman (1995) for an overview on the underlying representation theorems. Apparently, the overall material response then turns out to be anisotropic since residual stresses are in general

not aligned with the subsequent loading path. However, various approaches for the incorporation of residual resses have been developed from different perspectives. In this regard, numerous models for the evolution of the material isomorphism $\boldsymbol{K}$, as introduced in eq.(1.1), are suggested in the literature. The evolution of $\boldsymbol{K}$ might for instance be driven by its energetically conjugate (stress–) quantity or by the corresponding torsion T^{L}_{MN}. However, evolution equations are often also derived from scalar–valued potentials, so–called yield functions in the context of irreversible plastic deformations. In the following, some well–established as well as recently developed modelling concepts are summarised which, by some means or other, account for internal stresses:

(i) Similar to the previously mentioned incorporation of residual stresses into the Helmholtz free energy density ψ_0, an inelastic potential Φ might also additionally account for so–called back–stresses. These supplementary stress contributions, $\boldsymbol{\Pi}^{\mathrm{t}}_{\mathrm{b}}(\boldsymbol{X})$ say, which typically are deformation–induced, act similar to internal stresses and thereby influence the evolution of the material isomorphism via

$$\mathrm{D}_t\boldsymbol{k}(\boldsymbol{X}) \propto \partial_{\boldsymbol{\Pi}^{\mathrm{t}}_{\mathrm{k}}}\Phi(\boldsymbol{\Pi}^{\mathrm{t}}_{\mathrm{k}}, \boldsymbol{\Pi}^{\mathrm{t}}_{\mathrm{b}}(\boldsymbol{X})) \quad \text{for} \quad \boldsymbol{\Pi}^{\mathrm{t}}_{\mathrm{k}} \doteq \partial_{\boldsymbol{k}}\psi_0\big|_{\boldsymbol{F}}\,, \tag{1.12}$$

wherein $\mathrm{D}_t\{\bullet\}$ denotes the material time derivative. For a general review, the reader is referred to the monographs by Lubliner (1990), Lemaitre and Chaboche (1998), Maugin (1992) or Menzel et al. (2005b) and references cited therein.

(ii) The type of evolution equation highlighted in eq.(1.12) does not explicitly distinguish between the compatible and incompatible contributions of $\boldsymbol{k}$; recall for instance the decomposition in eq.(1.7). Since incompatibilities, or in other words non–connected reference configurations, are directly related to internal stresses, separate evolution equations for $\nabla^{\mathrm{t}}_{\boldsymbol{X}} \times \boldsymbol{k}$ are of particular interest. In this regard, Acharya developed a continuum dislocation mechanics theory in a series of papers (2001, 2003, 2004). The therein proposed evolution equation for the underlying incompatibility measure is of the type

$$\begin{aligned} \mathrm{L}^{\mathrm{k}}_t\, \nabla^{\mathrm{t}}_{\boldsymbol{X}} \times \boldsymbol{k} \;&=\; \mathrm{D}_t\, \nabla^{\mathrm{t}}_{\boldsymbol{X}} \times \boldsymbol{k} - \mathrm{D}_t\boldsymbol{k} \cdot \boldsymbol{K} \cdot \nabla^{\mathrm{t}}_{\boldsymbol{X}} \times \boldsymbol{k} \\ &\propto\; \nabla^{\mathrm{t}}_{\boldsymbol{X}} \times \big([\, \nabla^{\mathrm{t}}_{\boldsymbol{X}} \times \boldsymbol{k}\,] \times \boldsymbol{b}_{\mathrm{k}} \big) - s\, \nabla^{\mathrm{t}}_{\boldsymbol{X}} \times \boldsymbol{\Pi}^{\mathrm{t}}_{\mathrm{k}}\,, \end{aligned} \tag{1.13}$$

whereby $s > 0$ weights a source–type term and $\boldsymbol{b}_{\mathrm{k}}$ takes the interpretation as a material volume force (vector) stemming from inhomogeneities of the material.

(iii) Besides separately addressing the evolution of incompatibilities as in eq.(1.13), one could also account for particular micro–structures of the material. A classical example is thereby provided by crystalline continua where, on the level of single crystals, orientations of individual slip systems are incorporated. The projection of a representative stress tensor, as for instance $\boldsymbol{\Pi}^{\mathrm{t}}_{\mathrm{k}}$, onto such a slip system I is commonly assumed to drive a plastic slip parameter γ_I. In addition to this so–called Schmid stress $\tau_{\mathrm{k}\,I}$, projected back–stresses $\tau_{\mathrm{b}\,I}$ can furthermore be introduced. The particular format of these back–stresses are commonly related to the stress fields which are induced by edge and screw dislocations in linear elastic infinitely expanded media. However, it is not only the existence of dislocations itself which causes internal stresses but also how these dislocations are distributed in space. To take such effects into account, gradients of representative dislocation density measures are additionally incorporated into the constitutive equations for the Schmid–type back–stresses $\tau_{\mathrm{b}\,I}$. For detailed background informations we refer the reader to the monographs by Phillips (2001) and Nemat–Nasser (2004) or the contributions by Evers et al. (2004a, 2004b) and references cited therein. Alternatively, one could also introduce gradients of, for instance, $\boldsymbol{k}$ into the Helmholtz free energy density and determine back–stress–type tensors from hyperelastic formats; see Menzel and Steinmann (2000) or Liebe et al. (2003) among others.

(iv) Apart from that, one could also introduce further balance relations; besides the standard balance of linear momentum representation related to so–called macro–forces, an additional relation balancing so–called micro–forces might be accounted for. Apparently, both sets of equations are accompanied by boundary conditions, see Capriz (1989) for a general review. To give an example in the context of crystal–plasticity, $\nabla_{\boldsymbol{X}} \cdot \boldsymbol{v}_I + \tau_I = w_I$ together with $t_I = \boldsymbol{v}_I \cdot \boldsymbol{N} = t_I^p$ (on the surface) represents such a balance law; compare Gurtin (2000b, 2002). The (resolved) shear stress or rather Schmid stress thereby couples the micro– and the macro–system. Conceptually speaking, τ_I takes the interpretation as a source term and represents forces acting on the underlying system of dislocations. Moreover, the vectorial flux $\boldsymbol{v}_I$ thereby allows interpretation as a stress stemming from interactions across surfaces. Apparently, thermodynamic considerations restrict constitutive relations for instance of $\boldsymbol{v}_I$.

This short list is by far not complete and could substantially be extended.

1.3 Configurational forces

Inhomogeneities and defects are objects often directly observable in experiments. The interaction of such quantities combined with effects due to, for instance, stresses is usually related to the concept of forces. Consequently, such forces represent dual objects with respect to energetically conjugated objects. To give an example, the force acting on a crack tip is energetically conjugated to the movement of the crack tip through the material. Similarly, the movement of defects like dislocation–type structures through the ambient material results in related energy variations. As such, these so–called configurational forces are not observed by analogy to Newtonian forces in physical space but act as energetically conjugated quantities with respect to configurational or rather material displacements. Alternative denominations for these configurational forces are proposed in the literature, for example the identification as material forces, pseudo–forces or energetic driving forces are equivalently used. Moreover, various lines of derivations to access these configurational forces have been developed. In the following, we first briefly summarise a field–theoretical approach in section 1.3.1 while two different applications are elaborated later on: on the one hand, the classical fracture-mechanics-related problems of a peeling tape and the so–called trousers test are discussed in section 1.3.2 and 1.3.3, wherein configurational forces are naturally accounted for. The examples can be expressed by means of scalar–valued equations which are interpreted by means of simple analytical and numerical investigations. On the other hand, configurational forces embedded into a finite element framework for single–slip crystal–plasticity are elaborated in section 1.3.4. That section also includes an alternative derivation of a material balance of linear momentum representation.

1.3.1 Field–theoretical formulation

Let the body of interest be appropriately modelled by an elastic simple continuum so that the corresponding Lagrangian L does not depend on higher derivatives in space and time. Accordingly, the kinetic energy depends on $\mathrm{D}_t\boldsymbol{\varphi}$, or rather on $\|\mathrm{D}_t\boldsymbol{\varphi}\|$, the stored energy is assumed to be a function of $\nabla_{\boldsymbol{X}}\boldsymbol{\varphi}$ and $\boldsymbol{X}$, while the loading potential is defined in terms of $\boldsymbol{\varphi}$ and $\boldsymbol{X}$, respectively. The equations of motion are directly related to the stationarity of L, namely

$$I(\boldsymbol{\varphi}, V_0) = \int_{\mathcal{B}_0} L(\boldsymbol{\varphi}, \nabla_{\boldsymbol{X}}\boldsymbol{\varphi}, \mathrm{D}_t\boldsymbol{\varphi}, \boldsymbol{X}) \; \mathrm{d}V_0 \quad \longrightarrow \quad \text{stat.} \tag{1.14}$$

for $\boldsymbol{x} = \boldsymbol{\varphi}(\boldsymbol{X}, t) \in C^2$. Alternatively, one might find a set of independent geometric objects, or in fact components, represented by $\boldsymbol{q}(\boldsymbol{\xi})$ with $\boldsymbol{\xi} = [\, \boldsymbol{X}, t\,]$ which replaces $\boldsymbol{\varphi}(\boldsymbol{\xi})$ in eq.(1.14) so that $L(\boldsymbol{q}, \nabla_{\boldsymbol{\xi}}\boldsymbol{q}, \boldsymbol{\xi})$. Next, variations of $\boldsymbol{q}$ are introduced via $\delta\boldsymbol{q} := \partial_\varepsilon \boldsymbol{q}_\varepsilon(\boldsymbol{q}(\boldsymbol{\xi}), \boldsymbol{\xi}_\varepsilon, \varepsilon)|_{\varepsilon=0}$, whereby $\boldsymbol{\xi}_\varepsilon = \boldsymbol{\xi}$ and $\boldsymbol{q}_\varepsilon = \boldsymbol{q}$ for $\varepsilon = 0$. Accordingly, we obtain

$$\delta I(\boldsymbol{q}, V_0) = \int_{\mathcal{B}_0 \times \mathcal{T}} \partial_{\boldsymbol{q}} L \cdot \delta\boldsymbol{q} + \partial_{\nabla_{\boldsymbol{\xi}}\boldsymbol{q}} L : \delta\, \nabla_{\boldsymbol{\xi}}\boldsymbol{q} + \partial_{\boldsymbol{X}} L \cdot \delta\boldsymbol{X} \;\; \mathrm{d}V_0\, \mathrm{d}t \tag{1.15}$$

and, furthermore, make use of $\nabla_{\boldsymbol{\xi}} \cdot [\, \delta\boldsymbol{q} \cdot \partial_{\nabla_{\boldsymbol{\xi}}\boldsymbol{q}} L\,] = [\, \nabla_{\boldsymbol{\xi}} \cdot \partial_{\nabla_{\boldsymbol{\xi}}\boldsymbol{q}} L\,] \cdot \delta\boldsymbol{q} + \partial_{\nabla_{\boldsymbol{\xi}}\boldsymbol{q}} L : \delta\, \nabla_{\boldsymbol{\xi}}\boldsymbol{q}$ which enables us to rewrite eq.(1.15) under the assumption $\delta\boldsymbol{X} \doteq \boldsymbol{0}$ as

$$\delta I(\boldsymbol{q}, V_0) = \int_{\mathcal{B}_0 \times \mathcal{T}} \big[\, \partial_{\boldsymbol{q}} L - \nabla_{\boldsymbol{\xi}} \cdot \partial_{\nabla_{\boldsymbol{\xi}}\boldsymbol{q}} L \,\big] \cdot \delta\boldsymbol{q} \;\; \mathrm{d}V_0\, \mathrm{d}t \doteq 0 \;\; + \;\; \mathrm{bc} \quad \forall\, \delta\boldsymbol{q}\,. \tag{1.16}$$

The local format of eq.(1.16), namely $\partial_{\boldsymbol{q}} L - \nabla_{\boldsymbol{\xi}} \cdot \partial_{\nabla_{\boldsymbol{\xi}}\boldsymbol{q}} L = 0 \;\forall\, \boldsymbol{X}$, recovers the Euler–Lagrange equation; compare for instance Ericksen (1977), Hanyga (1985) or Marsden and Hughes (1994) and see Maugin (1993) for derivations in view of non–simple materials like gradient continua. In other words, the pointwise representation of eq.(1.16) is a null Lagrangian – in general, equations of this type can be added to the Euler–Lagrange equation without affecting the Euler–Lagrange equation itself (apart from boundary conditions); see Šilhavý (1997) for further details. Moreover, the computation of $\delta L(\boldsymbol{q}, \nabla_{\boldsymbol{\xi}}\boldsymbol{q}, \boldsymbol{\xi})$ not only by means of $\delta\boldsymbol{q}$ but also with respect to variations of $\boldsymbol{\xi}$ is directly related to Noether's theorem. The expression for the corresponding current $\boldsymbol{\zeta}$, which is to be conserved or rather balanced, results in

$$\boldsymbol{\zeta} = L\, \partial_\varepsilon \boldsymbol{\xi}_\varepsilon\big|_{\varepsilon=0} + \big[\, \partial_\varepsilon \boldsymbol{q}_\varepsilon - \nabla_{\boldsymbol{\xi}}\boldsymbol{q} \cdot \partial_\varepsilon \boldsymbol{\xi}_\varepsilon \,\big]\big|_{\varepsilon=0} \cdot\, \partial_{\nabla_{\boldsymbol{\xi}}\boldsymbol{q}} L\,, \tag{1.17}$$

see Maugin (1993) and Olver (1993) for detailed background informations. Assuming that $\boldsymbol{\xi}_\varepsilon$ is characterised by a space–time translation of $\boldsymbol{\xi}$ (so that no adequate variation of $\boldsymbol{q}$ exists), eq.(1.17) reduces to

$$\begin{aligned} &\boldsymbol{\Lambda}^{\mathrm{t}} = L\, \boldsymbol{I}^{\mathrm{t}} - [\, \nabla_{\boldsymbol{\xi}}\boldsymbol{q}\,]^{\mathrm{t}} \cdot \partial_{\nabla_{\boldsymbol{\xi}}\boldsymbol{q}} L \qquad\qquad \text{such that} \\ &\nabla_{\boldsymbol{\xi}} \cdot \boldsymbol{\Lambda}^{\mathrm{t}} = \boldsymbol{0}\,, \;\; \nabla_{\boldsymbol{\xi}} \cdot \boldsymbol{\zeta} = 0 \quad \text{if} \quad L \doteq L(\boldsymbol{q}, \nabla_{\boldsymbol{\xi}}\boldsymbol{q}) \;\;, \end{aligned} \tag{1.18}$$

compare Maugin (1993). Apart from this rather general format, possibly more familiar representations are recovered by separating differentiation with respect to $\boldsymbol{\xi}$ into the gradient operation in space $\nabla_{\boldsymbol{X}}\{\bullet\}$ (at fixed t) and the material time derivative $\mathrm{D}_t\{\bullet\}$ (at fixed $\boldsymbol{X}$). Then, the energy–momentum (un–) balance equations related to eq.(1.18) allows an alternative representation as

$$\mathrm{D}_t \boldsymbol{P} = \nabla_{\boldsymbol{X}} \cdot \boldsymbol{\Sigma}^{\mathrm{t}} + \boldsymbol{B}_0 \quad \text{together with} \quad \mathrm{D}_t H = \nabla_{\boldsymbol{X}} \cdot \boldsymbol{Q} + S_0\,, \tag{1.19}$$

wherein

$$\begin{aligned} \boldsymbol{P} &= -\, \partial_{\mathrm{D}_t\boldsymbol{q}} L \cdot \nabla_{\boldsymbol{X}}\boldsymbol{q}\,, & H &= \;\; \partial_{\mathrm{D}_t\boldsymbol{q}} L \cdot \mathrm{D}_t\boldsymbol{q} - L\,, \\ \boldsymbol{\Sigma}^{\mathrm{t}} &= -\, L\, \boldsymbol{I}^{\mathrm{t}} - [\, \nabla_{\boldsymbol{X}}\boldsymbol{q}\,]^{\mathrm{t}} \cdot \partial_{\nabla_{\boldsymbol{X}}\boldsymbol{q}} L\,, & \boldsymbol{Q} &= -\, \mathrm{D}_t\boldsymbol{q} \cdot \partial_{\nabla_{\boldsymbol{X}}\boldsymbol{q}} L\,, \\ \boldsymbol{B}_0 &= \;\; \partial_{\boldsymbol{X}} L\,, & S_0 &= -\, \partial_t L \end{aligned} \tag{1.20}$$

with $S_0 = 0$ due to energy conservation (L does not explicitly depend on time). Possible inhomogeneities of the body of interest are taken into account since $\boldsymbol{X}$ is one of the arguments which (explicitly) determines the Lagrangian L. Accordingly, the contribution $\boldsymbol{B}_0$ does in general not vanish and takes the interpretation as a configurational (volume) force. Both, $\boldsymbol{\Sigma}^{\mathrm{t}}$ as well as $\boldsymbol{B}_0$ are illustrated by means of applications in the following.

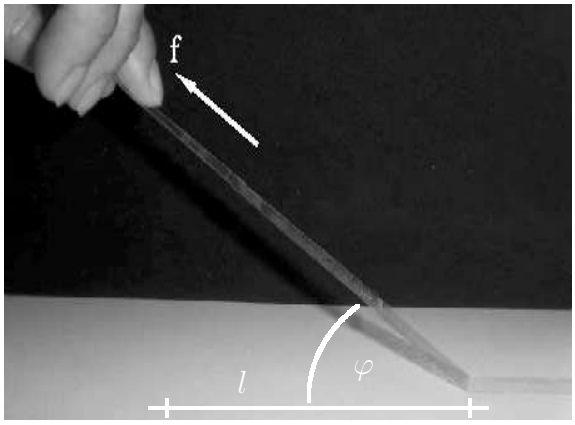

Figure 1.1: Peeling tapes: 'experimental setup'.

1.3.2 Peeling tapes

Peeling tapes provide a familiar application of configurational forces experienced in every–day life. We assume such a tape to be homogeneous and purely elastic; the analysis of peeling phenomena for inelastic tapes, however, is more advanced, see for instance Cotterell et al. (2003). Furthermore, the tape is accepted to be loaded under tension so that for example bending effects are neglected; the reader is referred to Kinloch et al. (1994), O'Reilly (2007), and references cited in theses work for an analysis that additionally accounts for bending. The peel test itself allows interpretation as an adhesion problem, see Kaelble (1971) for a general survey. Consequently, a key feature for the subsequent elaborations consists in the introduction of a surface energy, whereby we adopt the lines of derivations highlighted in Ericksen (1998a).

Let the reference configuration of a tape with width w and thickness $t \ll w$, as the one displayed in figure 1.1, be represented by the interval $X \in [\,0, L\,]$. A conservative load $\mathbf{f} = \mathrm{f}\,\boldsymbol{e} = \mathrm{f}\,[\,\cos(\varphi)\,\boldsymbol{e}_1 + \sin(\varphi)\,\boldsymbol{e}_2\,]$ is applied to the free ending of the tape so that the scalar product of $\mathbf{f}$ with the related displacement vector $\boldsymbol{u} = d\,\boldsymbol{e} - l\,\boldsymbol{e}_1$ renders the external load potential

$$\varpi^{\mathrm{ext}} = -\,\mathbf{f}\cdot\boldsymbol{u} = -\,\mathrm{f}\,[\,d - l\,\cos(\varphi)\,] \qquad \text{with} \qquad d = \int_{\bar{X}}^{L} \lambda\,\mathrm{d}x\,, \tag{1.21}$$

wherein $\lambda > 0$ denotes the stretch and $\bar{X} = L - l$. Besides establishing a (convex) Helmholtz free energy density $\psi_0(\lambda)$ with $\psi_0(1) = 0$ and $\partial_\lambda \psi_0|_{\lambda=1} = 0$ for $w, t \doteq \mathrm{const}$, we additionally introduce a surface energy by means of the simple ansatz

$$\varpi^{\mathrm{sur}} \doteq G\,l\,w\,, \tag{1.22}$$

whereby $G > 0$ acts as a material parameter that remains to be determined from experiments. By assembling terms we obtain the thermodynamic potential

$$\varpi = w\,t\int_{\bar{X}}^{L} \psi_0(\lambda)\,\mathrm{d}x - \mathrm{f}\,[\,d - l\,\cos(\varphi)\,] + G\,l\,w\,. \tag{1.23}$$

With these relations at hand, variations of two quantities are of particular interest, namely $\bar{X}$ (or l) and λ. While variations of $\bar{X}$, in other words the parameter that characterises the crack tip position, are related to configurational forces, we next elaborate on variations with respect to λ, i.e. $\delta\varpi|_{\varphi,\bar{X}} = 0\ \forall\,\delta\lambda$, and obtain the equilibrium condition (in physical space)

$$\exists!\ \lambda \in \mathbb{R}_+ \qquad w\,t\,\partial_\lambda\psi_0(\lambda) = w\,t\,\sigma = \mathrm{f} \tag{1.24}$$

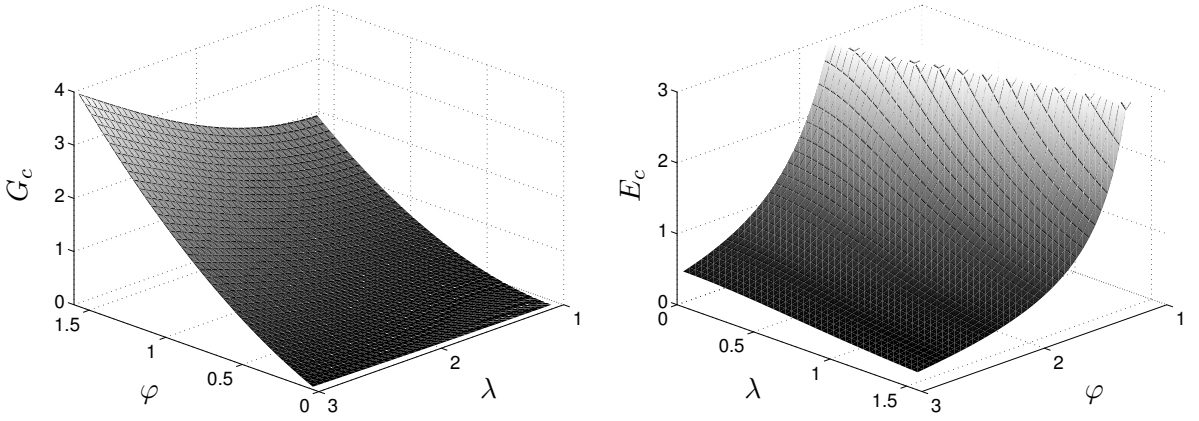

Figure 1.2: Peeling tapes for $\varepsilon = \lambda - 1$: critical surface energy parameter G_c for $E = 1$, $t = 1$ and critical elasticity parameter E_c for $G = 1$, $t = 1$ – both vs. the stretch λ and angle of attack φ at $\eta = 0$.

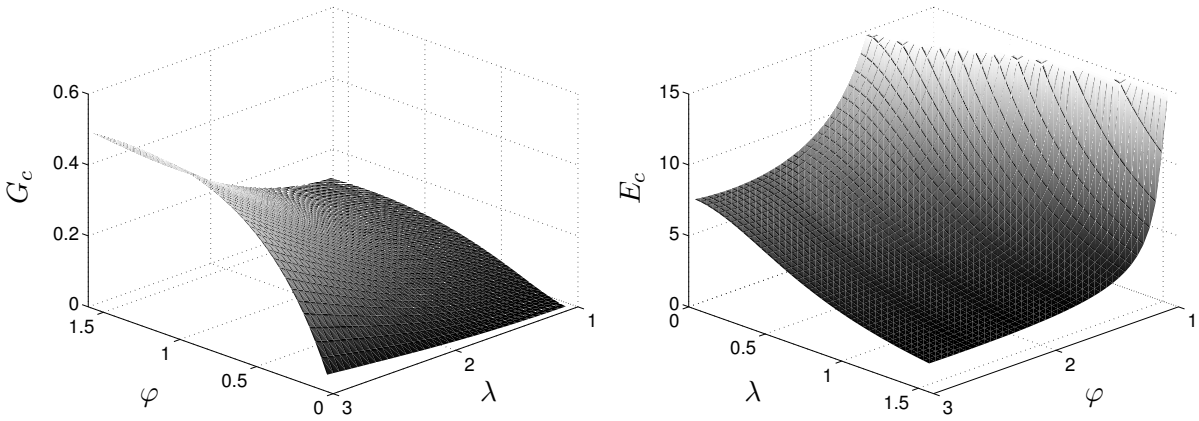

Figure 1.3: Peeling tapes for $\varepsilon = \ln(\lambda)$: critical surface energy parameter G_c for $E = 1$, $t = 1$ and critical elasticity parameter E_c for $G = 1$, $t = 1$ – both vs. the stretch λ and angle of attack φ at $\eta = 0$.

since the tape is assumed to deform homogeneously ($d = \lambda\, l$). Evaluation of eq.(1.23) at equilibrium states results in

$$\varpi(\lambda, \varphi; l)\big|_{\partial_\lambda \varpi = 0} = l\, w \left[t \left[\psi_0(\lambda) - \left[\lambda - \cos(\varphi) \right] \sigma \right] + G \right] = l\, w\, \eta(\lambda, \varphi)\,. \tag{1.25}$$

Concerning variations or rather extrema of eq.(1.25) with respect to l (or $\bar{X}$), minima of ϖ are observed at $l = L$ ($\bar{X} = 0$) for $\eta < 0$ and, respectively, at $l = 0$ ($\bar{X} = L$) for $\eta > 0$, while ϖ turns out to be independent of l ($\bar{X}$) if $\eta = 0$. Obviously, $l = 0$ means that the entire tape is still fixed and $l = L$ stands for the tape being completely peeled off. Moreover, $l = 0$ results in $\varpi = 0$ so that $\eta > 0$ serves as a criterion to detect stable configurations. Consequently, $\eta = 0$ characterises states at which peeling of the tape is initiated and eq.(1.25) can be used to analyse whether the tape begins to peel off or not. To visualise this relation, we assume a St.–Venant–Kirchhoff–type constitutive equation, namely $\psi_0 = \frac{1}{2}\, E\, \varepsilon^2$ with $\varepsilon(\lambda)$ denoting a representative strain measure. Based on eq.(1.25) and $\eta = 0$ we conclude that, say, critical values of the material parameters – such that $G \geq G_c$ respectively $E \leq E_c$ in order to prevent peeling – follow as

$$\begin{aligned} G_c &= t \left[\left[\lambda - \cos(\varphi) \right] E\, \varepsilon\, \partial_\lambda \varepsilon - \tfrac{1}{2}\, E\, \varepsilon^2 \right], \\ E_c &= \frac{G}{t \left[\left[\lambda - \cos(\varphi) \right] \varepsilon\, \partial_\lambda \varepsilon - \frac{1}{2}\, \varepsilon^2 \right]}\,. \end{aligned} \tag{1.26}$$

Qualitative graphical representations of $G_c(\lambda, \varphi)|_{E,t}$ as well as of $E_c(\lambda, \varphi)|_{G,t}$ are highlighted in figure 1.2 and 1.3 for two different strain measures – to be specific, $\varepsilon = \lambda - 1$ and $\varepsilon = \ln(\lambda)$.

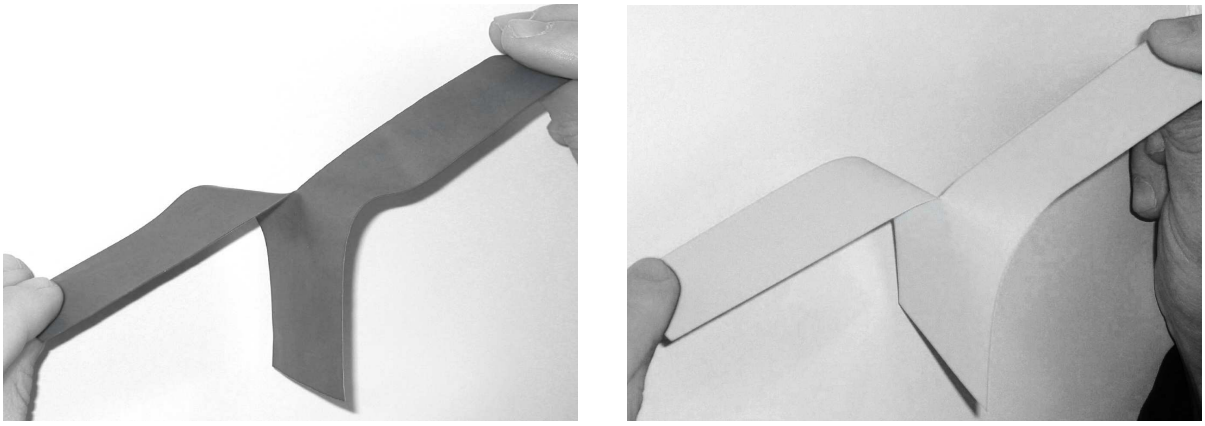

Figure 1.4: Trousers test: 'experimental setup' for rubber (left) and paper (right).

Despite the fact that a totally peeled–off tape still sustains stresses for the model at hand, one could interpret properties of η by investigating $\partial_\lambda \eta|_\varphi$. Apparently, one has $\eta|_{\lambda=1} = G > 0$ and $\partial_\lambda \eta|_\varphi = -t\,[\,\lambda - \cos(\varphi)\,]\,\partial^2_{\lambda\lambda}\psi_0 < 0$, recall that ψ_0 has been assumed to be convex, so that the initially positive value continuously decreases with deformation until the critical state is reached. Apart from the so–called soft peeling problem reviewed above, one could also study hard peeling where stability properties – here reflected by $\partial_\lambda \eta|_\varphi$ – turn out, as expected, to be in contrast to the case of soft peeling; compare Ericksen (1998a) or see the discussion of imposed forces and imposed displacements in the context of crack propagation in Freund (1990). Moreover, the dynamical peeling of tapes has been elaborated by, for example, Burridge and Keller (1978), in the contribution by Podio–Guidugli in Steinmann and Maugin (2005, pp. 253–260), and by Pede et al. (2006).

1.3.3 Trousers test

In addition to the surface–energy–based approach highlighted in section 1.3.2, we next directly make use of the Griffith criterion – both approaches, however, being inherently related. The reader is referred to, for instance, Sanford (2003) and Freund (1990) for reviews on the classical Griffith theory. While the peeling problem is mainly dominated by mode I conditions – in general mode II is activated as well – the subsequently discussed so–called trousers test is a typical example for mode III loading; see figure 1.4 for a sketch of the experimental setup. The following elaborations are based on the contributions by Rivlin and Thomas (1953) and Sawyers and Rivlin (1974).

As displayed in figure 1.4, the thickness of the homogeneous specimen is much smaller that its width, i.e. $t \ll w = w_I + w_{II}$ whereby $w_{I,II}$ denote the width of 'leg' I and II. Next, we introduce different domains of interest, namely the region A where external loads are applied, followed by a part B (for each 'leg') assumed to undergo homogeneous deformations, the rupture zone C, and the region of the unloaded ending D. By analogy with the notation introduced for peeling tapes, the length of the 'crack' is denoted as l. Apparently, A and C can be assumed to remain stationary as long as D exists so that the evolution of B is directly related to crack propagation. The homogeneous deformation in B is accepted to be isochoric with the longitudinal stretch λ and identical transverse stretches. Accordingly, the first and second invariants of the right Cauchy–Green tensor read $I_1 = \lambda^2 + 2\,\lambda^{-1}$ and $I_2 = \lambda^{-2} + 2\,\lambda$. By means of a hyperelastic ansatz for the stress contribution one receives

$$\sigma(\lambda) = \partial_\lambda \psi_0 = 2\,[\,\lambda - \lambda^{-2}\,]\,[\,\partial_{I_1}\psi_0 + \lambda^{-1}\,\partial_{I_2}\psi_0\,] \tag{1.27}$$

so that the applied longitudinal force allows representation as $\mathrm{f} = t\,w_I\,\sigma(\lambda_I) = t\,w_{II}\,\sigma(\lambda_{II})$.

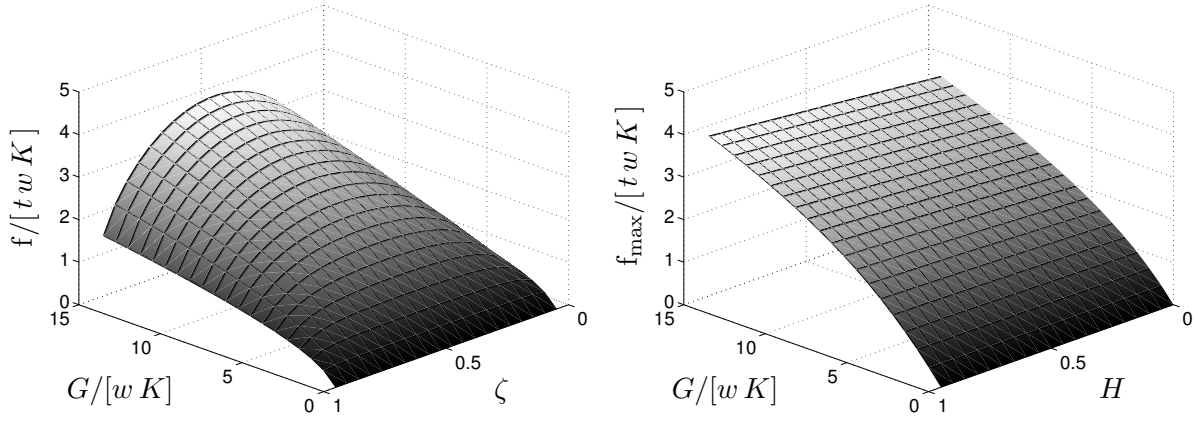

Figure 1.5: Trousers test: longitudinal force as a function of G and ζ for $H = 1$ and maximum longitudinal force as a function of G and H for $\zeta = \frac{1}{2}$.

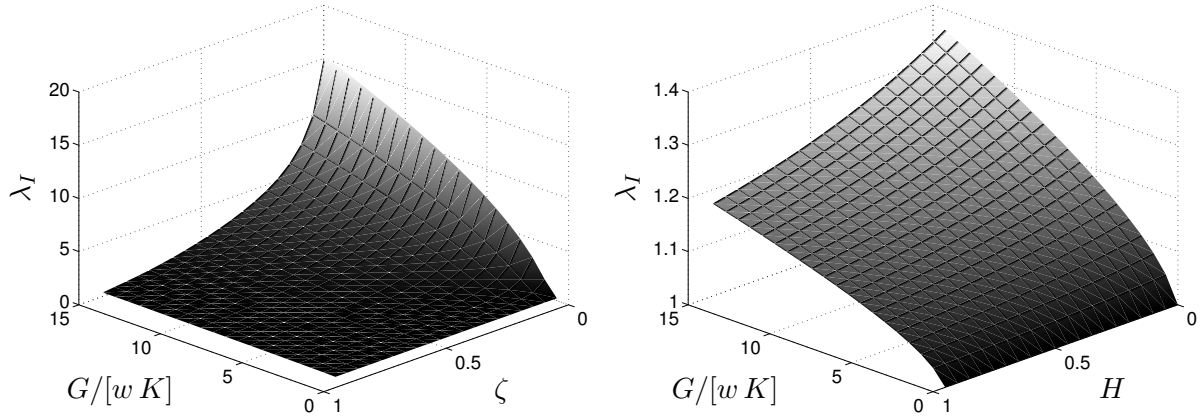

Figure 1.6: Trousers test: longitudinal stretch λ_I as a function of G and ζ for $H = 1$ and longitudinal stretch λ_I as a function of G and H for $\zeta = \frac{1}{2}$.

To particularise the constitutive behaviour, we make use of a Mooney–Rivlin material, namely $\psi_0 = K\,[\,[\,I_1 - 3\,] + H\,[\,I_2 - 3\,]\,]$ such that $\partial_{I_1}\psi_0 = K$ and $\partial_{I_2}\psi_0 = KH$. In view of applying the Griffith criterion – a crack grows in case the rate of released strain energy exceeds the energy required to form new surfaces – we obtain for the problem at hand

$$\frac{\mathrm{f}\,[\lambda_I + \lambda_{II}\,]}{t}\,\mathrm{d}l - [\,w_I\,W_0(\lambda_I) + w_{II}\,W_0(\lambda_{II})\,]\,\mathrm{d}l = G \tag{1.28}$$

and incorporation of the constitutive model chosen renders

$$\begin{aligned}\frac{\mathrm{f}\,[\lambda_I + \lambda_{II}\,]}{w\,t\,K} \;-\;& \zeta\,\big[\,\lambda_I^2 + 2\,\lambda_I^{-1} - 3 + H\,[\,\lambda_I^{-2} + 2\,\lambda_I - 3\,]\,\big] \\ -\;& [\,1-\zeta\,]\,\big[\,\lambda_{II}^2 + 2\,\lambda_{II}^{-1} - 3 + H\,[\,\lambda_{II}^{-2} + 2\,\lambda_{II} - 3\,]\,\big] \;=\; \frac{G}{w\,K}\end{aligned} \tag{1.29}$$

with $\zeta = w_I/w \in [0,1]$. Based on this relation, quantities of interest $\{\lambda_I, \lambda_{II}, \mathrm{f}/[\,w\,t\,K\,]\}$ can iteratively be computed for $\{\zeta, G/[\,w\,K\,], H\}$ given. Representative results are displayed in figure 1.5 and 1.6, whereby for convenience we choose K and w equal to one (obviously, the results turn out to be independent of t). It is interesting to note, that the maximum force can be supported for $\zeta = \frac{1}{2}$ or rather $w_I = w_{II}$; compare figure 1.5. In contrast, small strain linear elasticity yields $\mathrm{f}_{\max}$ independent of ζ. To be specific, $\psi_0 = \frac{1}{2}\,E\,[\,\lambda - 1\,]^2$ results in $2\,\mathrm{f}\,/\,t = G$. As expected, figure 1.6 underlines that $\lambda_I \to 1$ for $\zeta \to 1$.

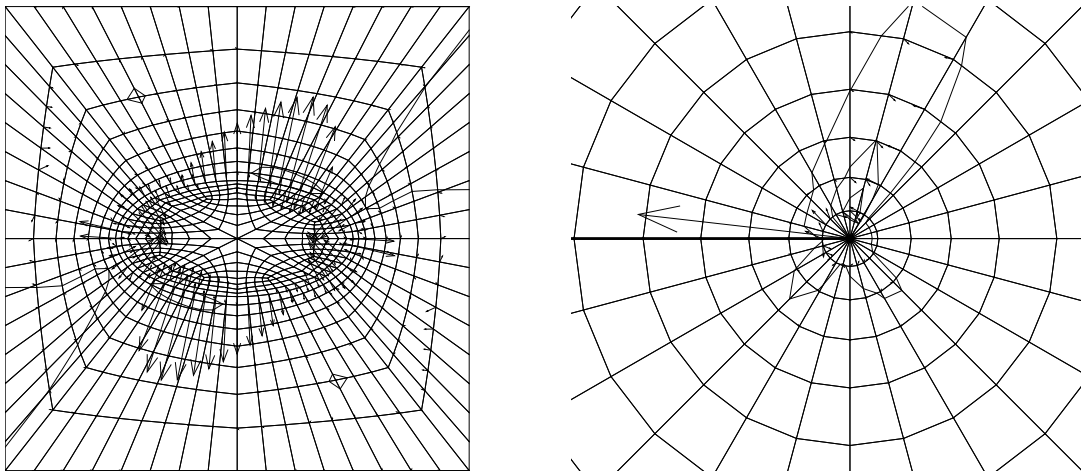

Figure 1.7: Crystal plasticity: material surface forces for an elliptic inclusion and at a crack tip.

1.3.4 Crystal plasticity

As previously mentioned in section 1.3, we next briefly review applications of configurational forces for inelastic continua in a finite element context. The reader is referred to Menzel et al. (2004, 2005a) for a detailed outline of the subsequently reviewed approach. As a prototype model, single–slip crystal–plasticity is investigated so that $\mathrm{D}_t\boldsymbol{k} \equiv \mathrm{D}_t\boldsymbol{F}_{\mathrm{p}} \doteq \mathrm{D}_t\gamma\, \boldsymbol{s} \otimes \boldsymbol{m}$. Without loss of generality, we restrict ourselves to associated evolution equations for $\boldsymbol{F}_{\mathrm{p}}$ and a proportional hardening parameter κ, whereby the underlying yield function is determined by a Schmid–type stress and a hardening stress. For notational simplicity, use of the abbreviations $\boldsymbol{\alpha} = [\, \boldsymbol{F}_{\mathrm{p}}, \kappa \,]$ and $\boldsymbol{A} = [\, \partial_{\boldsymbol{F}_{\mathrm{p}}}\psi_0, \partial_\kappa \psi_0 \,]$ is made.

To set the stage for applying the 'material force method', we derive the (quasi–static) material balance of linear momentum representation by investigation the transformation of its spatial format to the material configuration, in other words $-\boldsymbol{F}^{\mathrm{t}} \cdot [\, \nabla_{\boldsymbol{x}} \cdot \boldsymbol{\Pi}^{\mathrm{t}} + \boldsymbol{b}_0 \,] = \nabla_{\boldsymbol{X}} \cdot \boldsymbol{\Sigma}^{\mathrm{t}} + \boldsymbol{B}_0 = \boldsymbol{0}$. The approach itself is elaborated later on in detail, see chapter 2, and as a result we obtain

$$\boldsymbol{\Sigma}^{\mathrm{t}} = \psi_0\, \boldsymbol{I} - \boldsymbol{F}^{\mathrm{t}} \cdot \boldsymbol{\Pi}^{\mathrm{t}} \quad \text{and} \quad \boldsymbol{B}_0 = -\,\boldsymbol{A} \circ \nabla_{\boldsymbol{X}}\, \boldsymbol{\alpha} - \partial_{\boldsymbol{X}}\, \psi_0 - \boldsymbol{F}^{\mathrm{t}} \cdot \boldsymbol{b}_0\,, \tag{1.30}$$

compare section 1.3.1. With these relations at hand, we next consider the material equilibrium condition which is satisfied if the underlying surface and volume forces sum up to zero, namely

$$\mathbf{f}_{\mathrm{sur}} + \mathbf{f}_{\mathrm{vol}} = \boldsymbol{0} \quad \text{with} \quad \mathbf{f}_{\mathrm{sur}} = \int_{\partial\mathcal{B}_0} \boldsymbol{\Sigma}^{\mathrm{t}} \cdot \boldsymbol{N}\, \mathrm{d}A \quad \text{and} \quad \mathbf{f}_{\mathrm{vol}} = \int_{\mathcal{B}_0} \boldsymbol{B}_0\, \mathrm{d}V_0\,, \tag{1.31}$$

whereby $\boldsymbol{N}$ denotes the correlated surface normal. The weak form expression $\boldsymbol{\Theta} \cdot [\, \mathbf{f}_{\mathrm{sur}} + \mathbf{f}_{\mathrm{vol}} \,] = 0 \;\forall\, \boldsymbol{\Theta} \in \mathcal{B}_0$ is recovered from

$$\begin{aligned} 0 &= \int_{\mathcal{B}_0} \boldsymbol{W} \cdot [\, \nabla_{\boldsymbol{X}} \cdot \boldsymbol{\Sigma}^{\mathrm{t}} + \boldsymbol{B}_0 \,]\, \mathrm{d}V_0 \qquad \forall\, \boldsymbol{W} \in H^1_0(\mathcal{B}_0) && (1.32)\\ &= \int_{\mathcal{B}_0} \nabla_{\boldsymbol{X}} \cdot (\, \boldsymbol{W} \cdot \boldsymbol{\Sigma}^{\mathrm{t}} \,) - \nabla_{\boldsymbol{X}} \boldsymbol{W} : \boldsymbol{\Sigma}^{\mathrm{t}} + \boldsymbol{W} \cdot \boldsymbol{B}_0\, \mathrm{d}V_0 && (1.33)\\ &= \underbrace{\int_{\partial\mathcal{B}_0} \boldsymbol{W} \cdot \boldsymbol{\Sigma}^{\mathrm{t}} \cdot \boldsymbol{N}\, \mathrm{d}A_0}_{W_{\mathrm{sur}}} - \underbrace{\int_{\mathcal{B}_0} \nabla_{\boldsymbol{X}} \boldsymbol{W} : \boldsymbol{\Sigma}^{\mathrm{t}}\, \mathrm{d}V_0}_{W_{\mathrm{int}}} + \underbrace{\int_{\mathcal{B}_0} \boldsymbol{W} \cdot \boldsymbol{B}_0\, \mathrm{d}V_0}_{W_{\mathrm{vol}}} && (1.34) \end{aligned}$$

if the constant test functions $\boldsymbol{\Theta}$ coincide with the material virtual displacements $\boldsymbol{W}$, compare Steinmann (2000). On this basis, standard finite element approximation techniques – see also

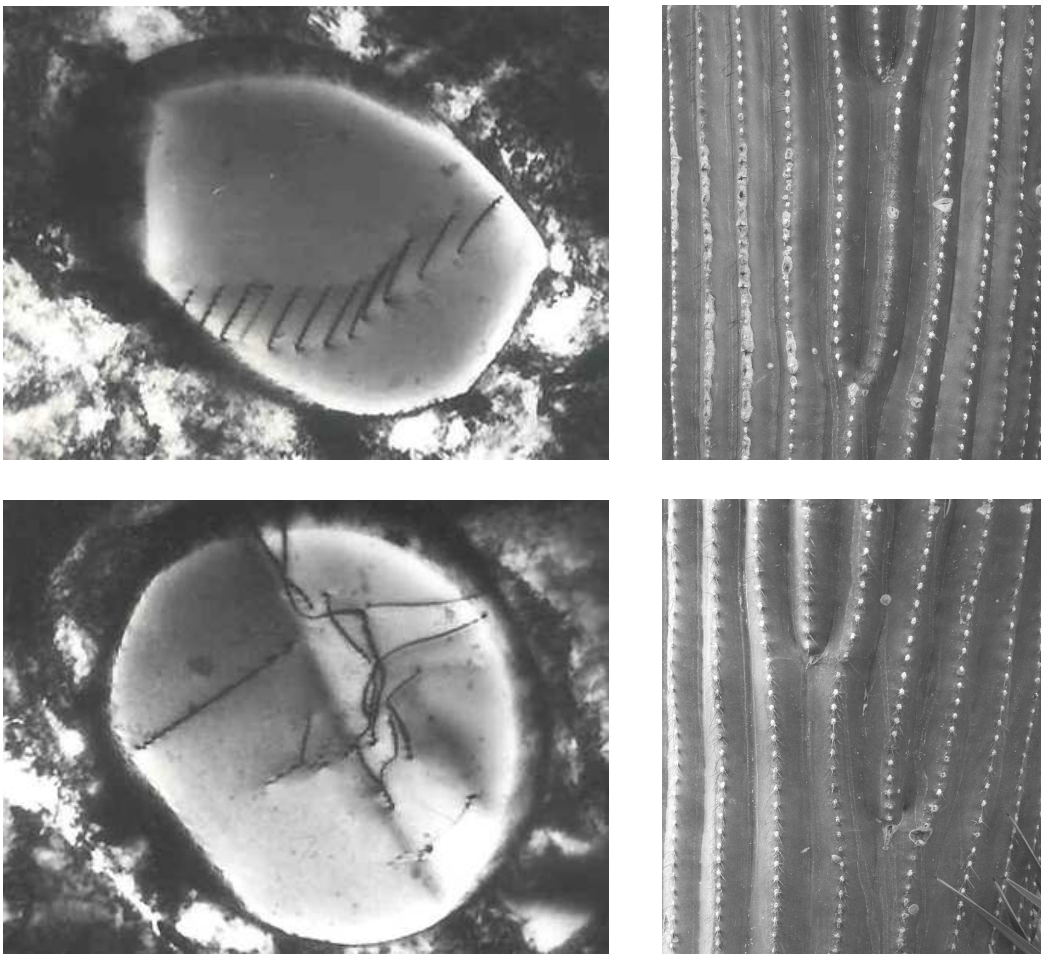

Figure 1.8: Chapter 2: dislocation structures in crystalline metals (http://en.wikipedia.org/wiki/Dislocation) and 'biological materials'.

remark 2.5.1 in this regard – render

$$W^{h\,e}_{\rm int} = \sum_{k=1}^{n_{\rm en}} \boldsymbol{W}_k \cdot \int_{\mathcal{B}^e_0} \boldsymbol{\Sigma}^{\rm t} \cdot \nabla_{\boldsymbol{X}} N^k_\varphi \, {\rm d}V_0 \,, \qquad W^{h\,e}_{\rm vol} = \sum_{k=1}^{n_{\rm en}} \boldsymbol{W}_k \cdot \int_{\mathcal{B}^e_0} N^k_\varphi \, \boldsymbol{B}_0 \, {\rm d}V_0 \tag{1.35}$$

and motivate the introduction of the global discrete nodal point (material) force

$$\mathbf{F}^h_{{\rm sur}\,K} = \mathop{\mathbf{A}}_{e=1}^{n_{\rm el}} \int_{\mathcal{B}^e_0} \boldsymbol{\Sigma}^{\rm t} \cdot \nabla_{\boldsymbol{X}} N^k_\varphi - N^k_\varphi \, \boldsymbol{B}_0 \, {\rm d}V_0 = \mathbf{F}^h_{{\rm int}\,K} - \mathbf{F}^h_{{\rm vol}\,K} \,. \tag{1.36}$$

Since the (material) force acting on a singular part of the surface of a body, as it is for instance the case for a cracked specimen, is often of particular interest, we next consider the subdomain $\mathcal{V}_0 \subseteq \mathcal{B}_0$ with singular and regular boundary $\partial\mathcal{V}^{\rm s}_0 \cup \partial\mathcal{V}^{\rm r}_0 = \partial\mathcal{V}_0$, $\partial\mathcal{V}^{\rm s}_0 \cap \partial\mathcal{V}^{\rm r}_0 = \emptyset$ and a correlated surface normal $\boldsymbol{N}$. By analogy with eq.(1.31) one consequently obtains

$$-\,\mathbf{f}^{\rm s}_{\rm sur} = \mathbf{f}^{\rm r}_{\rm sur} + \mathbf{f}_{\rm vol} = \int_{\partial\mathcal{V}^{\rm r}_0} \boldsymbol{\Sigma}^{\rm t} \cdot \boldsymbol{N} \, {\rm d}A_0 + \int_{\mathcal{V}_0} \boldsymbol{B}_0 \, {\rm d}V_0 \,. \tag{1.37}$$

Keeping the case of a crack tip singularity in mind, we observe that eq.(1.37) reduces to the (vectorial) J–integral for $\partial\mathcal{V}^{\rm r}_0 \to 0$, to be specific $\mathbf{j} = -\,\mathbf{f}^{\rm s}_{\rm sur} = \lim_{\partial\mathcal{V}^{\rm r}_0 \to 0} \int_{\partial\mathcal{V}^{\rm r}_0} \boldsymbol{\Sigma}^{\rm t} \cdot \boldsymbol{N} \, {\rm d}A$. In view of finite element applications, however, the discrete (vectorial) J–integral is computed from eq.(1.36), namely

$$\mathbf{J}^h \approx \sum_K \mathbf{F}^h_{{\rm vol}\,K} - \mathbf{F}^h_{{\rm int}\,K} \qquad K \in \mathbb{V}_0 \setminus \partial\mathbb{V}^{\rm r}_0 \,. \tag{1.38}$$

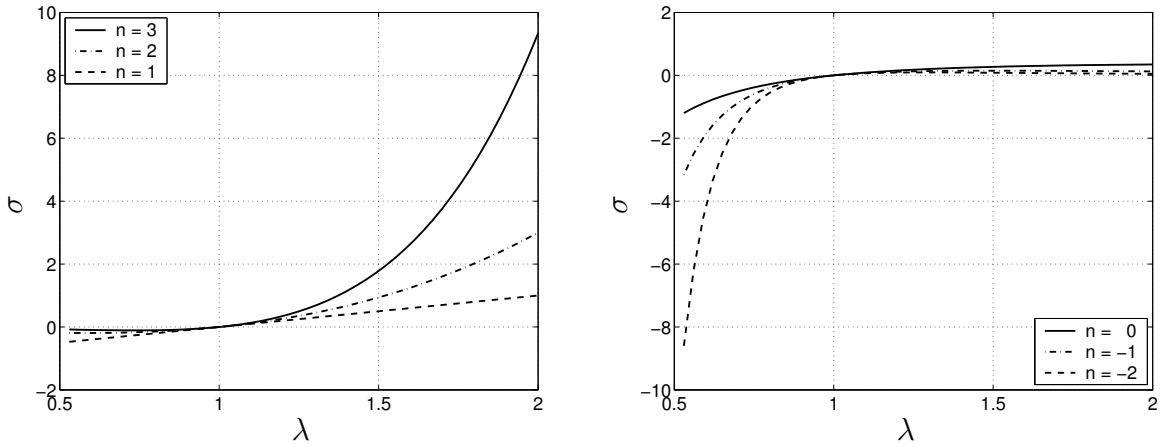

Figure 1.9: Chapter 3: stress (σ) versus stretch (λ) relations for one–dimensional elasticity based on generalised strain measures ($\varepsilon_{(n)}$).

Practically speaking, the numerical evaluation is carried out over the discrete domain $\mathbb{V}_0$, determined by finite element nodes K, except the regular part of the considered boundary. Note that spurious nodal forces due to an insufficient discretisation of the specimen are thereby implicitly incorporated.

Figure 1.7 shows two representative finite element simulations related to the computation of material surface forces with respect to an elliptic inclusion and a crack tip. The slip systems of the inclusion are chosen different in orientation compared to the ambient material. This heterogeneity together with the underlying plastic anisotropy is reflected by the fact that the distribution of the calculated surface forces possess no 'axial' symmetry. Similarly, the force acting on the crack tip is not aligned with the (horizontal) crack itself. Apart from that, moving finite element nodes, or rather the boundary of the inclusion and the crack tip, respectively, opposite to the direction of the material surface forces results in a decrease of the potential energy.

1.4 Goals of this work and modus operandi

Fundamental theoretical concepts and essential modelling approaches for inelastic continua are reviewed and developed in chapters 2 and 3. With these elaborations in hand, different application are then elaborated in chapters 4, 5, and 6. Particular emphasis is thereby placed on anisotropy, plasticity, kinematic hardening, continuum damage as well as growth phenomena and remodelling of biological tissues.

Chapter 2 The main goal of this chapter consists in the elaboration of the material or rather configurational mechanics in the context of multiplicative elastoplasticity. This nowadays well–established approach, which is inherently related to the concept of a material isomorphism or in other words to a local rearrangement, is adopted as a paradigm for the general modelling of finite inelasticity. The overall motion in space is throughout assumed to be compatible and sufficiently smooth. According to the underlying configurations, namely the material and the spatial configuration as well as what we call the intermediate configuration, different representations of balance of linear momentum are set up for the static case. The underlying flux terms are thereby identified as stress tensors of Piola– and Cauchy–type and are assumed to derive from a Helmholtz free energy density function, thus taking hyperelastic formats. Moreover, the incorporated source terms, namely the configurational volume forces,

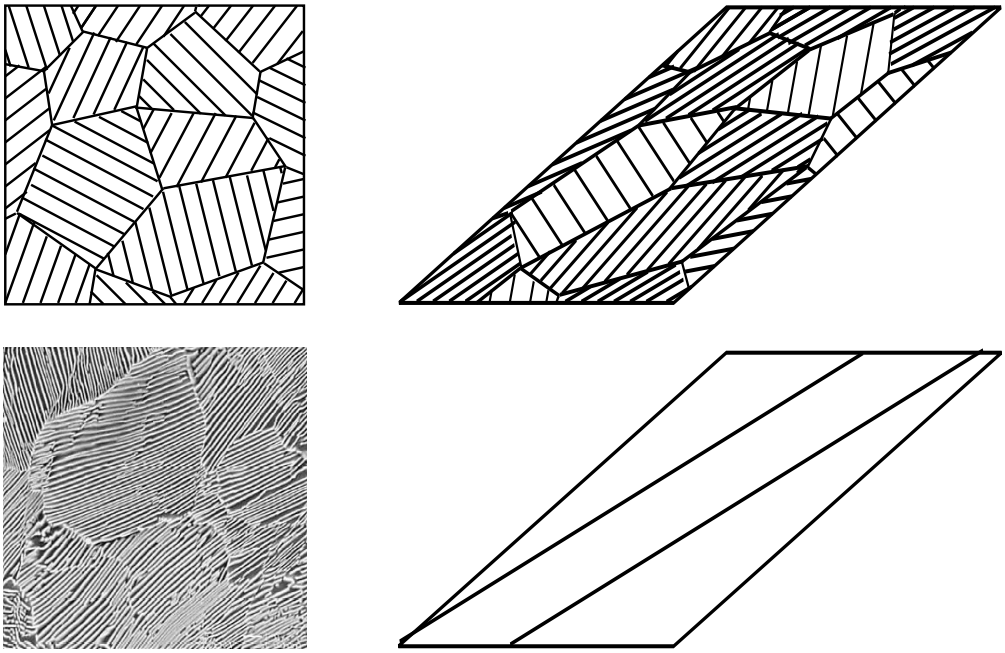

Figure 1.10: Chapter 5: photography (Zelin (2002)) and illustration of initial perlitic microstructure with randomly oriented grains, sketch of a deformed microstructure with aligned grains, and induced texture–like orientation on a macroscopic scale of observation (compare Johansson et al. (2005b)).

are identified by comparison arguments. These quantities include gradients of distortions as well as dislocation density tensors; see figure 1.8 for an illustration of typical dislocation structures. In particular those dislocation density tensors related to the elastic or plastic distortion do not vanish due to the general incompatibility of the intermediate configuration. As a result, configurational volume forces which are settled in the intermediate configuration embody non–vanishing dislocation density tensors while their material counterparts directly incorporate non–vanishing gradients of distortions. This fundamental property enables us to recover the celebrated Peach–Koehler forces for finite inelasticity, acting on a single dislocation, from the intermediate configuration volume forces.

Chapter 3 Application of generalised strain measures to finite inelasticity based on the multiplicative decomposition of the total deformation gradient is discussed in chapter 3. The underlying symmetry properties of the material are modelled via the incorporation of structural tensors while the evolution of any inelastic spin is neglected. Appropriate pushforward and pullback transformations of particular generalised strain measures to different configurations enable the setup of anisotropic hyperelastic formats with respect to all configurations of interest. This rather general formalism turns out be convenient in view of for instance efficient numerical algorithms and computational applications investigated in subsequent chapters. A simple or rather trivial example for the constitutive modelling by means of generalised strain measure is highlighted in figure 1.9. To be specific, one–dimensional and purely elastic response in terms of the strain measures $\varepsilon_{(n)}(\lambda) = [\,\lambda^n - 1\,]/n$ for $n \neq 0$ and $\varepsilon_{(0)}(\lambda) = \ln(\lambda)$ is investigated, whereby $\lambda > 0$ denotes the stretch. Related stresses are derived from a St.–Venant–Kirchhoff–type Helmholtz free energy density, $\psi_0 = \frac{1}{2}\,E\,\varepsilon^2_{(n)}$, so that hyperelastic formats result in $\sigma(\lambda; n) = \partial_\lambda \psi_0 = E\,\varepsilon_{(n)}(\lambda)\,\lambda^{n-1}$. The computations shown in figure 1.9 are based on $E = 1$ together with $n \in \{-2, -1, 0, 1, 2, 3\}$ and, moreover, suggest the (additive) combination of different generalised strain measures; compare remark 3.2.2.

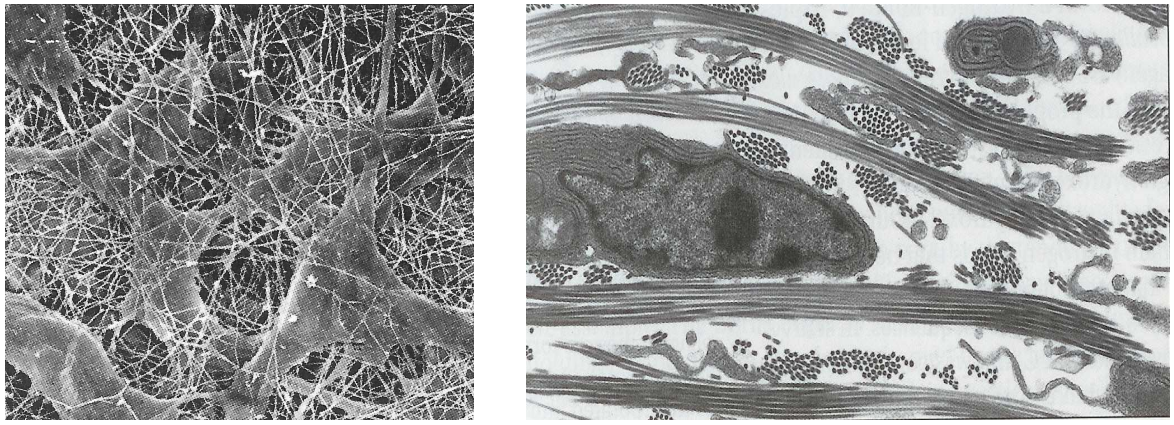

Figure 1.11: Chapter 6: connective tissue; network of collagen fibrils and orthogonal fibre bundles around fibroblasts (Alberts et al. (1994)).

Chapter 4 The objective of chapter 4 is the formulation and algorithmic treatment of a phenomenological framework to capture anisotropic geometrically nonlinear inelasticity. We consider in particular the coupling of viscoplasticity with anisotropic continuum damage whereby both, proportional and kinematic hardening are taken into account. As a main advantage of the proposed formulation, standard continuum damage models with respect to a fictitious isotropic configuration can be adopted and conveniently extended to anisotropic continuum damage. The key assumption is based on the introduction of a damage tangent map that acts as an affine pre–deformation. Conceptually speaking, we deal with an Euclidian space with respect to a non–constant metric. The evolution of this tensor is directly related to the degradation of the material and allows the modelling of specific classes of elastic anisotropy. In analogy to the damage mapping, we introduce an internal variable that determines a back–stress tensor via a hyperelastic format and thereby enables the incorporation of plastic anisotropy. Numerical issues arising when integrating the obtained system of non–linear equation related to the so–called local problem due to implicit integration algorithms, are also discussed in detail. It is shown that algorithms like staggered iteration and quasi–Newton techniques are superior to a pure Newton approach when the CPU–time is compared. However, the drawback of the staggered and the quasi–Newton technique is that rather small time steps must be taken to ensure convergence, which can be of importance when applying complex constitutive models in a finite element program. Finally, several numerical examples underline the applicability of the proposed finite strain framework.

Chapter 5 A macroscopic model for deformation–induced anisotropy due to substructure evolution at large strains is proposed within a thermodynamically consistent framework. The model is motivated via experimental observations on the mechanism of formation of nanostructure and dissolution of, for instance, cementite in a pearlitic steel during high pressure. Although such pearlitic grains have a preferred direction determined by cementite lamellas (embedded in a softer ferrite matrix), initial random orientation of the grains is interpreted as initial macroscopic isotropy. However, the oriented grains tend to align after large shear deformation. Each (pearlitic) grain is viewed as approximately transversely isotropic, whereby the (cementite) lamellas determine the orientation of (the normal to) the isotropy plane, see figure 1.10 for a graphical illustration. As key features of the formulation developed in chapter 5, reorientation of a representative direction vector is driven by an appropriate stress measure. Apart form that, a so–called substructure metric is additionally determined by two scalars. The evolution of one of theses quantities is directly related to the evolution of the other scalar, which enables to conveniently set up a thermodynamically consistent formulation.

Chapter 6 A theoretical and computational framework for anisotropic growth phenomena of biological tissues under finite deformations is developed in chapter 6. Besides the incorporation of a referential mass source, anisotropic growth is addressed by means of a multiplicative decomposition of the overall deformation gradient into an elastic and a growth distortion. As a key idea of the proposed phenomenological approach, fibre families or rather structural tensors are introduced, which allow the description of transversely isotropic and orthotropic material behaviour; see figure 1.11 for illustrations of collageneous tissues in this regard. Based on these additional arguments, anisotropic growth is modelled via appropriate evolution equations for the fibre diameters or rather the strength of the fibres. Two different saturation–type formulations are thereby developed, namely an energy–driven approach as well as a stress–driven formulation. As a driving force for the stress–driven framework, projected quantities of a configurational growth stress tensor are advocated. Moreover, remodelling is addressed by means of a reorientation framework for the fibre directions, which is guided by analysing critical energy points. In other words, a time–dependent formulation is developed which aligns the fibre directions according to the principal stretch directions. One of the main benefits of the proposed models consists in the opportunity to separately address the evolution of the strength and the direction of fibre families. It is then straightforward to set up appropriate integration algorithms such that the developed framework fits nicely into finite element algorithms. Finally, several representative numerical examples underline the applicability of the proposed formulation by examining growth and resorption in volume and density together with fibre reorientation.

1.5 Notation

Before we begin, a word on notation: The referential position vector in Euclidian space is identified with $\boldsymbol{X}$. Furthermore, let $\boldsymbol{a}$, $\boldsymbol{b}$ denote two vectors and $\boldsymbol{A}$, $\boldsymbol{B}$, $\boldsymbol{C}$ three second–order tensors. The third–order permutation tensor is abbreviated by $\boldsymbol{E}$ possessing the properties $\boldsymbol{E} : \boldsymbol{E} = 2\,\boldsymbol{I}$, $\boldsymbol{E} \cdot \boldsymbol{E} = 2\,\mathsf{I}^{\mathrm{skw}}$ and $\boldsymbol{E} \cdot \boldsymbol{E} : \boldsymbol{A} = 2\,\boldsymbol{A}^{\mathrm{skw}}$; see also appendix A where further transformations and non–Cartesian representations are additionally reviewed. The tensor $\boldsymbol{I}$ symbolises the second–order identity and the skew–symmetric fourth–order identity has been introduced as $\mathsf{I}^{\mathrm{skw}} = \frac{1}{2}\,[\,\boldsymbol{I} \,\overline{\otimes}\, \boldsymbol{I} - \boldsymbol{I} \,\underline{\otimes}\, \boldsymbol{I}\,]$ with the non–standard dyadic products being defined via $[\,\boldsymbol{A} \,\overline{\otimes}\, \boldsymbol{B}\,] \cdot \boldsymbol{C} = \boldsymbol{A} \cdot \boldsymbol{C} \cdot \boldsymbol{B}^{\mathrm{t}}$ and $[\,\boldsymbol{A} \,\underline{\otimes}\, \boldsymbol{B}\,] \cdot \boldsymbol{C} = \boldsymbol{A} \cdot \boldsymbol{C}^{\mathrm{t}} \cdot \boldsymbol{B}^{\mathrm{t}}$, respectively. Therein, $\{\bullet\}^{\mathrm{t}}$ characterises the transposed of the second–order tensor $\{\bullet\}$ while the dual of $\{\bullet\}$ is denoted as $\{\bullet\}^{\mathrm{d}}$; however, we often also use $\{\bullet\}^{\mathrm{t}}$ instead of $\{\bullet\}^{\mathrm{d}}$. Consequently, the skew–symmetric part of $\boldsymbol{A}$ is determined by $\boldsymbol{A}^{\mathrm{skw}} = \mathsf{I}^{\mathrm{skw}} : \boldsymbol{A} = \frac{1}{2}\,[\,\boldsymbol{A} - \boldsymbol{A}^{\mathrm{t}}\,]$.

In the following, differential operators are frequently used, namely the gradient $\nabla_{\boldsymbol{X}} \boldsymbol{A}$, the divergence $\nabla_{\boldsymbol{X}} \cdot \boldsymbol{A} := \nabla_{\boldsymbol{X}} \boldsymbol{A} : \boldsymbol{I}$ and the curl operation $\nabla^{\mathrm{t}}_{\boldsymbol{X}} \times \boldsymbol{A} := -\nabla^{\mathrm{skw}}_{\boldsymbol{X}} \boldsymbol{A} : \boldsymbol{E} = -\nabla_{\boldsymbol{X}} \boldsymbol{A} : \boldsymbol{E}$. As an interesting side aspect, one observes the relation $[\,\nabla^{\mathrm{t}}_{\boldsymbol{X}} \times \boldsymbol{A}\,] \cdot \boldsymbol{E} = -\,2\,\nabla_{\boldsymbol{X}} \boldsymbol{A} : \mathsf{I}^{\mathrm{skw}}$. Furthermore, let $\partial_{\{\circ\}}\{\bullet\}$ denote the partial or rather explicit derivative of $\{\bullet\}$ with respect to some (tensorial) quantity $\{\circ\}$.

The vector product of two vectors and (the outer product) of a second–order tensor and a vector as well as of two second–order tensors are determined by $\boldsymbol{a} \times \boldsymbol{b} = [\,\boldsymbol{a} \otimes \boldsymbol{b}\,] : \boldsymbol{E}$, $\boldsymbol{A} \times \boldsymbol{a} = [\,\boldsymbol{A} \otimes \boldsymbol{a}\,] : \boldsymbol{E}$ and $\boldsymbol{A} \times \boldsymbol{B} = [\,\boldsymbol{A} \cdot \boldsymbol{B}^{\mathrm{t}}\,] : \boldsymbol{E}$, respectively. Moreover, the cofactor is introduced as $\mathrm{cof}(\boldsymbol{A}) = \partial_{\boldsymbol{A}} \det(\boldsymbol{A}) = \det(\boldsymbol{A})\,\boldsymbol{A}^{-\mathrm{t}}$ with $\boldsymbol{A}^{-\mathrm{t}} \cdot \boldsymbol{A}^{\mathrm{t}} = \boldsymbol{I}$.

Finally, we commonly apply identical symbols for functions and their values. The notation for one and the same symbol might also slightly vary from chapter to chapter by for instance modifying the denomination of $\{\bullet\}$ to $\{\widehat{\bullet}\}$ and so forth.

2 Configurational forces and continuum dislocations for multiplicative elastoplasticity

The commonly applied framework of Newtonian mechanics addresses the movement of particles in physical space. Contrary, within Eshelbian or configurational mechanics emphasis is placed on variations of placements of particles in material space. The first approach will consequently be denoted as the spatial motion problem in this work while the latter approach is referred to as the material motion problem. The concept of configurational mechanics is particularly suited for the modelling of defects, dislocations, inhomogeneities, heterogeneities, phase boundaries and so forth in, for example, solid mechanics since these phenomena are driven by configurational forces as present in configurational balance of linear momentum representations. A brief review of fundamental concepts is given by, for instance, Podio–Guidugli (2001, 2002). The consideration of forces acting on defects dates back to the pioneering works by Eshelby; see Markenscoff and Gupta (2006) and in particular Eshelby (1951, 1956). Nowadays several monographs elaborate the concept of configurational mechanics and mechanics in material space; see Maugin (1993), Šilhavý (1997), Gurtin (2000a), Kienzler and Hermann (2000), and Asaro and Lubarda (2006, chapt. 21) or the survey articles by Gurtin (1995), Maugin (1995), Steinmann (2002b), Yavari et al. (2006) and the contributions in Steinmann and Maugin (2005). Related numerical formulations based on a purely elastic response date back to the contributions by Govindjee and Mihalic (1996, 1998), Braun (1997) and Steinmann (2000). Computational strategies for plastic response have recently been discussed in Menzel et al. (2004, 2005a) and Nguyen et al. (2005). Moreover, the constitutive modelling of finite inelasticity in the present context is addressed by, for example, Svendsen (2001), Cleja-Ţigoiu and Maugin (2000), Menzel and Steinmann (2003c) and Gross et al. (2003) among others. Eshelby–type stress tensors thereby commonly serve as the driving quantity for the plastic distortion rate or for an appropriate symmetric part thereof. For specific applications these stress tensors are often replaced with Mandel–type stresses, compare Mandel (1974).

In this chapter, particular emphasis is placed on the configurational balance of linear momentum expressions and related configurational volume forces stemming from inelastic deformation processes. Elaborations in this context often incorporate a local rearrangement, or rather material isomorphism, based on an additional linear tangent map or directly apply a multiplicative decomposition of the total deformation gradient; see for instance the pioneering works by Noll (1958, 1967, 1972) or Truesdell and Noll (2004), Wang and Truesdell (1973) and Lee (1969) among others. For a review on the underlying basic concepts we refer the reader to the recent monographs by Haupt (2000), Lubarda (2002) and Bertram (2005) as well as to references cited therein. This local rearrangement transformation, or the inelastic part of the total deformation gradient, allows interpretation as plastic distortion. Related configurational volume forces have so far been referred to the reference or rather material configuration. They usually incorporate, besides contributions stemming from explicit dependencies on material placements, gradients of the plastic distortion. Detailed derivations are highlighted in a series of papers by Epstein and Maugin (1990, 1996), Maugin and Epstein (1998), Epstein (2002) and Maugin (2003), see also Epstein and Bucataru (2003). Skew–symmetric portions of the plastic distortion gradient allow interpretation as dislocation density tensor related to appropriate Burgers density vectors. The underlying configurational volume forces accordingly possess contributions stemming from geometrically necessary dislocations. This property turns

out to be of cardinal importance and establishes a connection on the one hand with classical continuum dislocation theories – see for instance Kondo (1952), Bilby et al. (1955), Kosevich (1979), de Wit (1981), Vanalis and Panoskaltsis (2005) or the monographs by Phillips (2001), Hull and Bacon (2001), Bulatov and Cai (2006) as well as the applications in Liu et al. (2006) – and on the other hand with nonlocal continuum theories: see for example the contributions in Rogula (1982) and Eringen (2002) as well as references cited therein. Early works based on the incorporation of dislocation density tensors date back to the contributions by Seeger (1955), Kröner (1958, 1960) and Kröner and Seeger (1959). Several continuum dislocation theories have been advocated since then, whereby special emphasis has in particular been placed on the modelling of geometrically necessary dislocations. Naming solely a brief personal collection of related references, we refer the reader to the contributions by Steinmann (1996), Le and Stumpf (1998), Menzel and Steinmann (2000), Acharya and Bassani (2000), Cermelli and Gurtin (2001, 2002), Gurtin (2002, 2004) and Gurtin and Needleman (2005).

As previously emphasised, we elaborate configurational balance of linear momentum representations with respect to what we call the material, intermediate and spatial configuration and derive correlated volume forces in this chapter. It turns out that the deduced formats with respect to the intermediate configuration recapture the celebrated Peach–Koehler force, compare Peach and Koehler (1950). Fundamental characteristics of this force, which drives the movement of single dislocations, are reviewed in various publications, monographs and textbooks; see Kosevich (1979), Maugin (1993), Nembach (1997), Phillips (2001), Hull and Bacon (2001), Indenbom and Orlov (1968), Ericksen (1995, 1998b), Rogula (1977) and references cited in these works. In this chapter we mainly follow the lines of derivation presented in Steinmann (2002a) and Menzel and Steinmann (2005, 2007) and develop a rigorous framework for configurational balance of linear momentum representations embedded into the finite deformation kinematics of multiplicative elastoplasticity. As a special application, particular volume forces possess the format of a Peach–Koehler–type force which has also been applied to the modelling of plasticity by other authors, see for instance the recent publication by Han et al. (2005) among others. For the sake of clarity, the structure of this chapter is somewhat formal. Conceptually speaking, we set the stage – for essential kinematical concepts, balance of linear momentum, hyperelastic formats and volume forces – by introducing the spatial, material and intermediate motion problem. Sought relations are then obtained by comparison arguments so that derivations of some expression are repeated. Apparently, this highly structured approach turns out to be rather helpful for a systematic and rigorous formulation of configurational balance relations. These derivations are, apart from other essential aspects, based on the following key approaches:

(i) Piola transformations are consequently applied to various two–point tensors, for instance dislocation density tensors and stress tensors – see for instance eqs.(2.4,2.43) – so that appropriate representations of these quantities with respect to solely one single configuration are obtained. The fundamental Piola transformation is highlighted, for example, in the pioneering monograph by Murnaghan (1951).

(ii) The commonly applied Piola identity is no longer valid for incompatible configurations. Consequently, divergence operations with respect to the intermediate configuration must be modified according to the underlying incompatibilities so that related balance of linear momentum representations take a non–standard format, see for instance eqs.(2.44,2.48,2.50,2.52). A detailed derivation is given in appendix C.

(iii) Based on a Helmholtz free energy density function, stress tensors of hyperelastic format are introduced. It is of cardinal importance to precisely distinguish between those quantities which are fixed and those with respect to which we compute derivatives, compare section 2.3 and as well as the related discussion in Ogden (2001b). It turns out

that both Cauchy stress tensors introduced for the spatial motion problem, as well as both Cauchy–type stresses of the intermediate motion problem coincide pairwise. The Cauchy–type stress tensors which are related to the material motion problem, however, possess different representations.

(iv) The introduced hyperelastic stresses are compared within a rather formal scheme in section 2.3.4: we give attention to three different combinations of two different Piola–type stress tensors which pairwise point to one and the same configuration. Related Cauchy stress tensors can directly be compared with each other since they are also settled in one and the same configuration. Taking finally Piola–type stress tensors into account which point in the opposite direction as those Piola–type stresses considered above, renders combinations with correlated Cauchy stress tensors. The three different types of examined Cauchy stresses are, apparently, settled in three different configurations, i.e. in what we call the spatial, intermediate and material configuration.

(v) With these stress tensors in hand, appropriate representations of volume forces in different configurations are derived by the key assumption that the corresponding balances of linear momentum are related by pullback or pushforward transformations.

The chapter is organised as follows: Essential kinematics are reviewed in section 2.1. This covers fundamental concepts according to the multiplicative decomposition of the deformation gradient as well as the introduction and comparison of related dislocation density tensors. The applied dislocation density tensors, which are introduced as two–point tensors as well as quantities being settled in only one single configuration, capture the description of geometrically necessary dislocations which is usually not explicitely mentioned. Here and in the subsequent sections, particular emphasis is placed on the spatial, intermediate and material motion problem and key results are additionally summarised in comprehensive tables for convenience of the reader. Different representations of balance of linear momentum are addressed in section 2.2, whereby the intermediate and material motion problem are introduced by analogy with the spatial motion problem. It turns out to be of cardinal importance to take a modified Piola identity into account since the intermediate configuration is in general incompatible. Hyperelastic stress formats for the fluxes in the balance of linear momentum are stated in section 2.3, whereby elaborations for the intermediate and material motion problem again follow by arguments of duality. Both, the appropriate definition of an underlying Helmholtz free energy density as well as a precise distinction between those quantities which are fixed and those with respect to which derivatives are computed are essential steps for the definition of theses hyperelastic formats. Based on these elaborations, different balance of linear momentum representations are compared in section 2.4. This part constitutes the main body of this chapter since configurational volume forces, i.e. the source terms in the configurational balance of linear momentum, are explicitly identified. They naturally incorporate gradients of the elastic and plastic distortion, the total deformation gradient or correlated dislocation density tensors. Moreover, the hyperelastic formats introduced in section 2.3 are recovered. A classical application is reviewed in section 2.5, namely the celebrated Peach–Koehler force acting on a single dislocation. The chapter is concluded with a discussion in section 2.6 where also the properties and applications of essential balance of linear momentum representations are addressed. Important but technical derivations, as for instance the extension of the classical Piola identity to incompatible configurations, are highlighted in appendices A–C.

2.1 Essential kinematics

Let $\mathcal{B}_0 \subset \mathbb{E}^3$ denote some reference or rather material configuration of the body B of interest. The corresponding tangent and co–tangent (or dual) spaces at a particular $\boldsymbol{X} \in \mathcal{B}_0$ are abbreviated by $T\mathcal{B}_0$ and $T^*\mathcal{B}_0$, respectively. Following standard conventions, let $\mathcal{B}_t \subset \mathbb{E}^3$ characterise the current or rather spatial configuration of B at time $t \in \mathcal{T} \subset \mathbb{R}$ whereas $T\mathcal{B}_t$ and $T^*\mathcal{B}_t$ denominate the correlated tangent spaces at a particular $\boldsymbol{x} \in \mathcal{B}_t$. In line with well–established finite elastoplasticity theories, we assume the existence of a generally incompatible (stress–free) intermediate configuration equipped with the tangent spaces $T\mathcal{B}_{\mathrm{p}}$ and $T^*\mathcal{B}_{\mathrm{p}}$, respectively. Having in mind that the three configurations are finite–dimensional, we can map elements of different tangent spaces in one and the same configuration via appropriate metric tensors.

2.1.1 Spatial motion problem

The commonly considered spatial motion problem takes the interpretation as describing the movement of physical particles through the ambient space while fixing their material position. The corresponding nonlinear spatial motion as based on this Lagrangian point of view reads

$$\boldsymbol{\varphi} : \mathcal{B}_0 \times \mathcal{T} \to \mathcal{B}_t\,, \quad \boldsymbol{X} \mapsto \boldsymbol{x} = \boldsymbol{\varphi}(\boldsymbol{X}, t) \tag{2.1}$$

and the related deformation gradient is multiplicatively decomposed into the inverse elastic (reversible) distortion and the plastic (irreversible) distortion, namely

$$\begin{aligned} \nabla_{\boldsymbol{X}} \boldsymbol{\varphi} = \boldsymbol{F} \doteq \boldsymbol{F}_{\mathrm{e}} \cdot \boldsymbol{F}_{\mathrm{p}} : T\mathcal{B}_0 \to T\mathcal{B}_t\,, \quad J &= \det(\boldsymbol{F}) > 0\,, \\ \boldsymbol{F}_{\mathrm{p}} : T\mathcal{B}_0 \to T\mathcal{B}_{\mathrm{p}}\,, \quad J_{\mathrm{p}} &= \det(\boldsymbol{F}_{\mathrm{p}}) > 0\,, \\ \boldsymbol{F}_{\mathrm{e}} : T\mathcal{B}_{\mathrm{p}} \to T\mathcal{B}_t\,, \quad J_{\mathrm{e}} &= \det(\boldsymbol{F}_{\mathrm{e}}) > 0\,, \end{aligned} \tag{2.2}$$

with $\nabla_{\boldsymbol{X}}\{\bullet\}$ characterising the gradient operator with respect to $\boldsymbol{X}$ at fixed time t. The spatial configuration is thereby assumed to be compatible, i.e

$$\begin{aligned} [\![\boldsymbol{\varphi}]\!] = \oint_{\mathcal{C}_t} \mathrm{d}\boldsymbol{x} \qquad\qquad &= \oint_{\mathcal{C}_0} \boldsymbol{F} \cdot \mathrm{d}\boldsymbol{X} \\ = \int_{\mathcal{A}_0} \nabla^{\mathrm{t}}_{\boldsymbol{X}} \times \boldsymbol{F} \cdot \boldsymbol{N}\, \mathrm{d}A_0 =: \int_{\mathcal{A}_0} \boldsymbol{A}^{\mathrm{t}} \cdot \boldsymbol{N}\, \mathrm{d}A_0 &=: \int_{\mathcal{A}_0} \boldsymbol{b}_0^{\mathrm{bur}}\, \mathrm{d}A_0 \doteq \boldsymbol{0} \end{aligned} \tag{2.3}$$

such that the corresponding local format yields a vanishing dislocation density tensor $\boldsymbol{A}^{\mathrm{t}}$ and a vanishing Burgers density vector $\boldsymbol{b}_0^{\mathrm{bur}}$, respectively.[1] Please note, that the two–point tensor $\boldsymbol{A}^{\mathrm{t}}$ can be related to the spatial configuration via the appropriate Piola transformation

$$\boldsymbol{d}^{\mathrm{t}} := \boldsymbol{A}^{\mathrm{t}} \cdot \mathrm{cof}(\boldsymbol{F}^{-1}) \quad \text{with} \quad \boldsymbol{A}^{\mathrm{t}} = \nabla^{\mathrm{t}}_{\boldsymbol{X}} \times \boldsymbol{F} = -\nabla_{\boldsymbol{X}} \boldsymbol{F} : \boldsymbol{E}_0 \doteq \boldsymbol{0}\,, \tag{2.4}$$

where $\boldsymbol{E}_0$ denotes the third–order permutation tensor, compare appendix A. Further transformations of $\boldsymbol{A}^{\mathrm{t}}$ to the material and intermediate configuration or alternative two–point representations are straightforward but omitted for the sake of brevity. Taking next the material time derivative of some quantity of interest at fixed $\boldsymbol{X}$ is abbreviated by the notation $\mathrm{D}_t\{\bullet\}$. To give an example, the spatial velocity consequently takes the representation

$$\boldsymbol{v} = \mathrm{D}_t \boldsymbol{\varphi} \quad \text{such that} \quad \nabla_{\boldsymbol{X}} \boldsymbol{v} = \mathrm{D}_t \boldsymbol{F}\,. \tag{2.5}$$

Figure 2.1 summarises essential kinematic tensors of the spatial motion problem for convenience of the reader.

[1] The dislocation density tensors in this work are identified with geometrically necessary dislocations even though we usually do not explicitly place emphasis on this property.

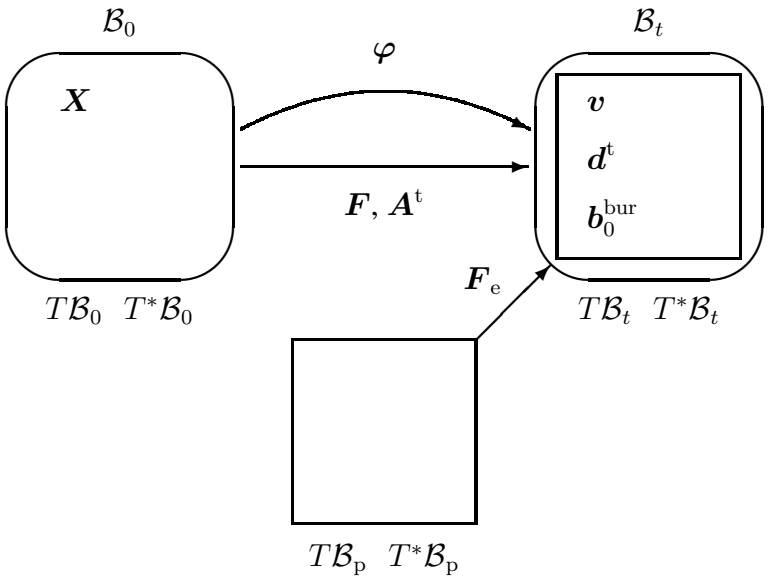

Figure 2.1: Spatial motion problem: essential kinematics.

2.1.2 Material motion problem

Similar to the spatial motion problem, we next focus on the material motion problem which takes the interpretation as describing the movement of physical particles through the ambient material while fixing their spatial position. The corresponding nonlinear material motion as based on this Eulerian–type point of view reads

$$\boldsymbol{\Phi} : \mathcal{B}_t \times \mathcal{T} \to \mathcal{B}_0 \,, \quad \boldsymbol{x} \mapsto \boldsymbol{X} = \boldsymbol{\Phi}(\boldsymbol{x}, t) \tag{2.6}$$

and the related deformation gradient is multiplicatively decomposed into the elastic (reversible) distortion and the inverse plastic (irreversible) distortion, namely

$$\begin{aligned} \nabla_{\boldsymbol{x}} \boldsymbol{\Phi} = \boldsymbol{f} \doteq \boldsymbol{f}_{\mathrm{p}} \cdot \boldsymbol{f}_{\mathrm{e}} : T\mathcal{B}_t \to T\mathcal{B}_0 \,, \quad j &= \det(\boldsymbol{f}) > 0 \,, \\ \boldsymbol{f}_{\mathrm{e}} : T\mathcal{B}_t \to T\mathcal{B}_{\mathrm{p}} \,, \quad j_{\mathrm{e}} &= \det(\boldsymbol{f}_{\mathrm{e}}) > 0 \,, \\ \boldsymbol{f}_{\mathrm{p}} : T\mathcal{B}_{\mathrm{p}} \to T\mathcal{B}_0 \,, \quad j_{\mathrm{p}} &= \det(\boldsymbol{f}_{\mathrm{p}}) > 0 \,, \end{aligned} \tag{2.7}$$

with $\nabla_{\boldsymbol{x}}\{\bullet\}$ characterising the gradient operator with respect to $\boldsymbol{x}$ at fixed time t. The material configuration is thereby also assumed to be compatible, i.e

$$\begin{aligned} [\![\boldsymbol{\Phi}]\!] = \oint_{\mathcal{C}_0} \mathrm{d}\boldsymbol{X} \qquad\qquad &= \oint_{\mathcal{C}_t} \boldsymbol{f} \cdot \mathrm{d}\boldsymbol{x} \\ = \int_{\mathcal{A}_t} \nabla^{\mathrm{t}}_{\boldsymbol{x}} \times \boldsymbol{f} \cdot \boldsymbol{n} \, \mathrm{d}A_t =: \int_{\mathcal{A}_t} \boldsymbol{a}^{\mathrm{t}} \cdot \boldsymbol{n} \, \mathrm{d}A_t &=: \int_{\mathcal{A}_t} \boldsymbol{B}_t^{\mathrm{bur}} \, \mathrm{d}A_t \doteq \boldsymbol{0} \end{aligned} \tag{2.8}$$

such that the corresponding local format yields a vanishing dislocation density tensor $\boldsymbol{a}^{\mathrm{t}}$ and a vanishing Burgers density vector $\boldsymbol{B}_t^{\mathrm{bur}}$, respectively. Please note, that the two–point tensor $\boldsymbol{a}^{\mathrm{t}}$ can be related to the material configuration via the appropriate Piola transformation

$$\boldsymbol{D}^{\mathrm{t}} := \boldsymbol{a}^{\mathrm{t}} \cdot \mathrm{cof}(\boldsymbol{f}^{-1}) \quad \text{with} \quad \boldsymbol{a}^{\mathrm{t}} = \nabla^{\mathrm{t}}_{\boldsymbol{x}} \times \boldsymbol{f} = -\nabla_{\boldsymbol{x}} \boldsymbol{f} : \boldsymbol{E}_t \doteq \boldsymbol{0} \,, \tag{2.9}$$

whereby the applied permutation tensor $\boldsymbol{E}_t$ is defined in appendix A. Further transformations of $\boldsymbol{a}^{\mathrm{t}}$ to the spatial and intermediate configuration or alternative two–point representations are straightforward but omitted for the sake of brevity. Taking next the spatial time derivative of

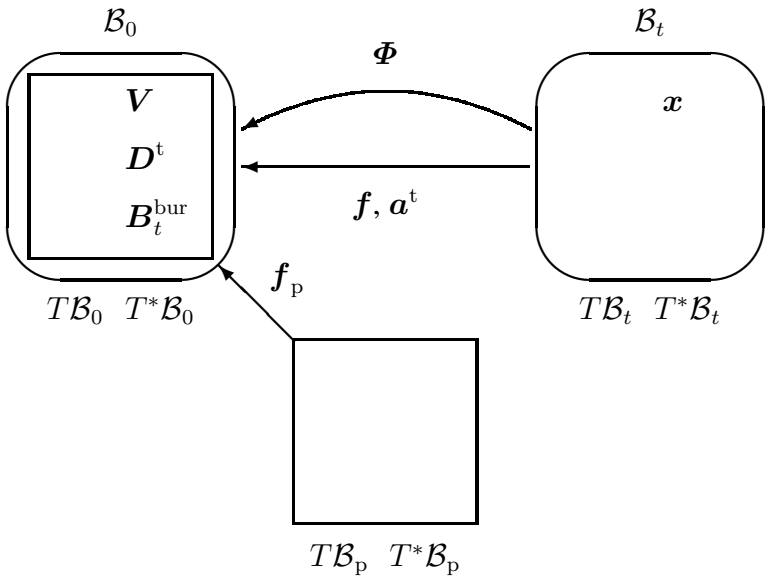

Figure 2.2: Material motion problem: essential kinematics.

some quantity of interest at fixed $\boldsymbol{x}$ is abbreviated by the notation $\mathrm{d}_t\{\bullet\}$. To give an example, the material velocity consequently takes the representation

$$\boldsymbol{V} = \mathrm{d}_t\boldsymbol{\Phi} \quad \text{such that} \quad \nabla_{\boldsymbol{x}}\boldsymbol{V} = \mathrm{d}_t\boldsymbol{f}\,. \tag{2.10}$$

Figure 2.2 summarises essential kinematic tensors of the material motion problem for convenience of the reader.

2.1.3 Intermediate motion problem

Due to the incompatible nature of the considered intermediate configuration, we cannot assume the existence of a differentiable mapping that relates placements of particles in the intermediate configuration to corresponding placements in the material or spatial configuration. Infinitesimal line elements, however, are mapped via

$$\mathrm{d}\widetilde{\boldsymbol{x}} := \boldsymbol{F}_{\mathrm{p}} \cdot \mathrm{d}\boldsymbol{X} = \boldsymbol{f}_{\mathrm{e}} \cdot \mathrm{d}\boldsymbol{x} =: \mathrm{d}\bar{\boldsymbol{X}} \quad \text{so that} \quad \mathrm{d}\widetilde{\boldsymbol{x}} \equiv \mathrm{d}\bar{\boldsymbol{X}}\,. \tag{2.11}$$

With these relations in hand, differential operations with respect to the intermediate configuration can formally be defined, namely a 'gradient' operator

$$\widetilde{\nabla}\{\bullet\} := \nabla_{\boldsymbol{X}}\{\bullet\} \cdot \boldsymbol{F}_{\mathrm{p}}^{-1} = \nabla_{\boldsymbol{x}}\{\bullet\} \cdot \boldsymbol{f}_{\mathrm{e}}^{-1} =: \bar{\nabla}\{\bullet\} \tag{2.12}$$

so that the corresponding 'divergence' and 'curl' operators result in

$$\widetilde{\nabla} \cdot \{\bullet\}^{\mathrm{t}} := \widetilde{\nabla}\{\bullet\}^{\mathrm{t}} : \boldsymbol{I}_{\mathrm{p}}^{\mathrm{t}} = \bar{\nabla}\{\bullet\}^{\mathrm{t}} : \boldsymbol{I}_{\mathrm{p}}^{\mathrm{t}} =: \bar{\nabla} \cdot \{\bullet\}^{\mathrm{t}} \tag{2.13}$$

as well as

$$\widetilde{\nabla}^{\mathrm{t}} \times \{\bullet\} := -\widetilde{\nabla}\{\bullet\} : \boldsymbol{E}_{\mathrm{p}} = -\bar{\nabla}\{\bullet\} : \boldsymbol{E}_{\mathrm{p}} =: \bar{\nabla}^{\mathrm{t}} \times \{\bullet\}\,, \tag{2.14}$$

whereby the second–order identity $\boldsymbol{I}_{\mathrm{p}}$ is explicitely defined in section 2.3.3 and the permutation tensor $\boldsymbol{E}_{\mathrm{p}}$ is elaborated in appendix A. Based on these properties, non–vanishing dislocation density tensors are introduced next.

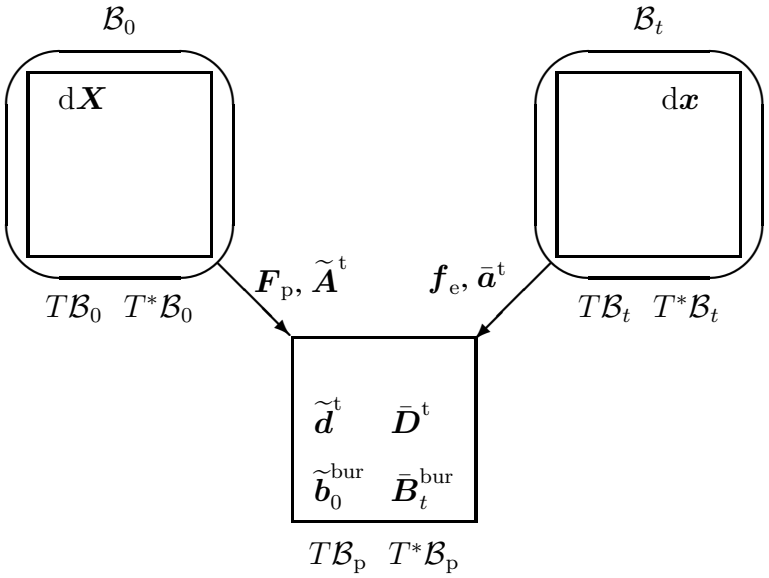

Figure 2.3: Intermediate motion problem: essential kinematics.

On the one hand, we take into account the plastic distortion and obtain

$$\begin{aligned}\int_{\mathcal{C}_\mathrm{p}} \mathrm{d}\widetilde{\boldsymbol{x}} &= \oint_{\mathcal{C}_0} \boldsymbol{F}_\mathrm{p} \cdot \mathrm{d}\boldsymbol{X} \\ &= \int_{\mathcal{A}_0} \nabla^\mathrm{t}_{\boldsymbol{X}} \times \boldsymbol{F}_\mathrm{p} \cdot \boldsymbol{N}\, \mathrm{d}A_0 =: \int_{\mathcal{A}_0} \widetilde{\boldsymbol{A}}^\mathrm{t} \cdot \boldsymbol{N}\, \mathrm{d}A_0 =: \int_{\mathcal{A}_0} \widetilde{\boldsymbol{b}}_0^\mathrm{bur}\, \mathrm{d}A_0 \neq \boldsymbol{0}\,,\end{aligned} \tag{2.15}$$

where neither the dislocation density tensor $\widetilde{\boldsymbol{A}}^\mathrm{t}$ nor the Burgers density vector $\widetilde{\boldsymbol{b}}_0^\mathrm{bur}$ equal zero. Application of a Piola transformation with respect to the plastic dislocation density tensor in eq.(2.15) results in

$$\widetilde{\boldsymbol{d}}^\mathrm{t} := \widetilde{\boldsymbol{A}}^\mathrm{t} \cdot \mathrm{cof}(\boldsymbol{F}_\mathrm{p}^{-1}) \quad \text{with} \quad \widetilde{\boldsymbol{A}}^\mathrm{t} = \nabla^\mathrm{t}_{\boldsymbol{X}} \times \boldsymbol{F}_\mathrm{p} = -\nabla_{\boldsymbol{X}} \boldsymbol{F}_\mathrm{p} : \boldsymbol{E}_0 \neq \boldsymbol{0}\,. \tag{2.16}$$

Further transformations of $\widetilde{\boldsymbol{A}}^\mathrm{t}$ to the spatial and material configuration or alternative two–point representations are straightforward but omitted for the sake of brevity. On the other hand, we take into account the elastic distortion and obtain

$$\begin{aligned}\int_{\mathcal{C}_\mathrm{p}} \mathrm{d}\bar{\boldsymbol{X}} &= \oint_{\mathcal{C}_t} \boldsymbol{f}_\mathrm{e} \cdot \mathrm{d}\boldsymbol{x} \\ &= \int_{\mathcal{A}_t} \nabla^\mathrm{t}_{\boldsymbol{x}} \times \boldsymbol{f}_\mathrm{e} \cdot \boldsymbol{n}\, \mathrm{d}A_t =: \int_{\mathcal{A}_t} \bar{\boldsymbol{a}}^\mathrm{t} \cdot \boldsymbol{n}\, \mathrm{d}A_t =: \int_{\mathcal{A}_t} \bar{\boldsymbol{B}}_t^\mathrm{bur}\, \mathrm{d}A_t \neq \boldsymbol{0}\,,\end{aligned} \tag{2.17}$$

where neither the dislocation density tensor $\bar{\boldsymbol{a}}^\mathrm{t}$ nor the Burgers density vector $\bar{\boldsymbol{B}}_t^\mathrm{bur}$ equal zero. Application of a Piola transformation with respect to the elastic dislocation density tensor in eq.(2.17) results in

$$\bar{\boldsymbol{D}}^\mathrm{t} := \bar{\boldsymbol{a}}^\mathrm{t} \cdot \mathrm{cof}(\boldsymbol{f}_\mathrm{e}^{-1}) \quad \text{with} \quad \bar{\boldsymbol{a}}^\mathrm{t} = \nabla^\mathrm{t}_{\boldsymbol{x}} \times \boldsymbol{f}_\mathrm{e} = -\nabla_{\boldsymbol{x}} \boldsymbol{f}_\mathrm{e} : \boldsymbol{E}_t \neq \boldsymbol{0}\,. \tag{2.18}$$

Further transformations of $\bar{\boldsymbol{a}}^\mathrm{t}$ to the material and spatial configuration or alternative two–point representations are straightforward but omitted for the sake of brevity.

In conclusion, we formally defined transformations of gradient operations with respect to different configurations. Concerning the divergence and curl operation, however, it turns out

Table 2.1: Transformations related to the dislocation density tensors $\boldsymbol{A}^{\mathrm{t}} = \nabla^{\mathrm{t}}_{\boldsymbol{X}} \times \boldsymbol{F}$ and $\boldsymbol{a}^{\mathrm{t}} = \nabla^{\mathrm{t}}_{\boldsymbol{x}} \times \boldsymbol{f}$.

	$\boldsymbol{A}^{\mathrm{t}}$	$\boldsymbol{d}^{\mathrm{t}}$	$\boldsymbol{a}^{\mathrm{t}}$	$\boldsymbol{D}^{\mathrm{t}}$
$\boldsymbol{A}^{\mathrm{t}}$	$\bullet$	$\boldsymbol{d}^{\mathrm{t}} \cdot \mathrm{cof}(\boldsymbol{F})$	$-\boldsymbol{F} \cdot \boldsymbol{a}^{\mathrm{t}} \cdot \mathrm{cof}(\boldsymbol{F})$	$-\boldsymbol{F} \cdot \boldsymbol{D}^{\mathrm{t}}$
$\boldsymbol{d}^{\mathrm{t}}$	$\boldsymbol{A}^{\mathrm{t}} \cdot \mathrm{cof}(\boldsymbol{f})$	$\bullet$	$-\boldsymbol{F} \cdot \boldsymbol{a}^{\mathrm{t}}$	$-\boldsymbol{F} \cdot \boldsymbol{D}^{\mathrm{t}} \cdot \mathrm{cof}(\boldsymbol{f})$
$\boldsymbol{a}^{\mathrm{t}}$	$-\boldsymbol{f} \cdot \boldsymbol{A}^{\mathrm{t}} \cdot \mathrm{cof}(\boldsymbol{f})$	$-\boldsymbol{f} \cdot \boldsymbol{d}^{\mathrm{t}}$	$\bullet$	$\boldsymbol{D}^{\mathrm{t}} \cdot \mathrm{cof}(\boldsymbol{f})$
$\boldsymbol{D}^{\mathrm{t}}$	$-\boldsymbol{f} \cdot \boldsymbol{A}^{\mathrm{t}}$	$-\boldsymbol{f} \cdot \boldsymbol{d}^{\mathrm{t}} \cdot \mathrm{cof}(\boldsymbol{F})$	$\boldsymbol{a}^{\mathrm{t}} \cdot \mathrm{cof}(\boldsymbol{F})$	$\bullet$

that for instance the fundamental Piola identity is no longer valid as soon as one of the configurations of interest possesses incompatibilities. A detailed review addressing necessary modifications is given in appendix C; see also the discussion in section 1.1.2. Figure 2.3 summarises essential kinematic tensors of the intermediate motion problem for convenience of the reader.

2.1.4 Comparison of the spatial, material, and intermediate motion problem

The main objective of the subsequent section consists in deriving relations between the previously introduced deformation gradients, distortions and dislocation density tensors. In this regard, the relation between the spatial and the material motion problem, as reflected by eqs.(2.1,2.6), is of cardinal importance in the progressing of the work. Practically speaking, combinations of both motions are assumed to render identity mappings, namely

$$\boldsymbol{\iota}_{\mathcal{B}_0} \doteq \boldsymbol{\Phi} \circ \boldsymbol{\varphi} \quad \text{and} \quad \boldsymbol{\iota}_{\mathcal{B}_t} \doteq \boldsymbol{\varphi} \circ \boldsymbol{\Phi} \tag{2.19}$$

such that the underlying linear tangent maps are related via

$$\begin{aligned} \boldsymbol{F}^{-1} &\equiv \boldsymbol{f}\,, & \boldsymbol{F}_{\mathrm{e}}^{-1} &\equiv \boldsymbol{f}_{\mathrm{e}}\,, & \boldsymbol{F}_{\mathrm{p}}^{-1} &\equiv \boldsymbol{f}_{\mathrm{p}} \qquad \text{with} \\ J^{-1} &\equiv j\,, & J_{\mathrm{e}}^{-1} &\equiv j_{\mathrm{e}}\,, & J_{\mathrm{p}}^{-1} &\equiv j_{\mathrm{p}}\,. \end{aligned} \tag{2.20}$$

Furthermore, the relation between the material and spatial time derivative is well–established as

$$\mathrm{D}_t\{\bullet\} = \mathrm{d}_t\{\bullet\} + \nabla_{\boldsymbol{x}}\{\bullet\} \cdot \boldsymbol{v} \quad \text{and} \quad \mathrm{d}_t\{\bullet\} = \mathrm{D}_t\{\bullet\} + \nabla_{\boldsymbol{X}}\{\bullet\} \cdot \boldsymbol{V}\,, \tag{2.21}$$

respectively, and in addition it is straightforward to derive the transformation

$$\boldsymbol{v} = -\boldsymbol{F} \cdot \boldsymbol{V} \quad \text{and} \quad \boldsymbol{V} = -\boldsymbol{f} \cdot \boldsymbol{v} \tag{2.22}$$

between the spatial and material velocity.

For convenience of the reader, table 2.1 and 2.2 anticipate results by summarising transformations between dislocation density tensors. Nevertheless, detailed derivations are discussed in the following.

2.1.4.1 Total spatial motion versus total material motion

The relation between the dislocation density tensors $\boldsymbol{A}^{\mathrm{t}}$ and $\boldsymbol{a}^{\mathrm{t}}$ follows directly from $\nabla_{\boldsymbol{x}}(\boldsymbol{F} \cdot \boldsymbol{f}) = \boldsymbol{0}$ or $\nabla_{\boldsymbol{X}}(\boldsymbol{f} \cdot \boldsymbol{F}) = \boldsymbol{0}$ which renders

$$-\nabla_{\boldsymbol{X}}\boldsymbol{F} = \boldsymbol{F} \cdot \nabla_{\boldsymbol{x}}\boldsymbol{f} : [\,\boldsymbol{F} \,\overline{\otimes}\, \boldsymbol{F}\,]\,, \tag{2.23}$$

Table 2.2: Transformations related to the dislocation density tensors $\widetilde{\boldsymbol{A}}^{\mathrm{t}} = \nabla^{\mathrm{t}}_{\boldsymbol{X}} \times \boldsymbol{F}_{\mathrm{p}}$ and $\bar{\boldsymbol{a}}^{\mathrm{t}} = \nabla^{\mathrm{t}}_{\boldsymbol{x}} \times \boldsymbol{f}_{\mathrm{e}}$.

	$\widetilde{\boldsymbol{A}}^{\mathrm{t}}$	$\widetilde{\boldsymbol{d}}^{\mathrm{t}} \equiv \bar{\boldsymbol{D}}^{\mathrm{t}}$	$\bar{\boldsymbol{a}}^{\mathrm{t}}$	$\bar{\boldsymbol{A}}^{\mathrm{t}}$	$\widetilde{\boldsymbol{a}}^{\mathrm{t}}$
$\widetilde{\boldsymbol{A}}^{\mathrm{t}}$	$\bullet$	$\widetilde{\boldsymbol{d}}^{\mathrm{t}} \cdot \mathrm{cof}(\boldsymbol{F}_{\mathrm{p}})$	$\bar{\boldsymbol{a}}^{\mathrm{t}} \cdot \mathrm{cof}(\boldsymbol{F})$	$-\boldsymbol{f}_{\mathrm{e}} \cdot \bar{\boldsymbol{A}}^{\mathrm{t}} \cdot \mathrm{cof}(\boldsymbol{F}_{\mathrm{p}})$	$-\boldsymbol{F}_{\mathrm{p}} \cdot \widetilde{\boldsymbol{a}}^{\mathrm{t}} \cdot \mathrm{cof}(\boldsymbol{F}_{\mathrm{p}})$
$\widetilde{\boldsymbol{d}}^{\mathrm{t}} \equiv \bar{\boldsymbol{D}}^{\mathrm{t}}$	$\widetilde{\boldsymbol{A}}^{\mathrm{t}} \cdot \mathrm{cof}(\boldsymbol{f}_{\mathrm{p}})$	$\bullet$	$\bar{\boldsymbol{a}}^{\mathrm{t}} \cdot \mathrm{cof}(\boldsymbol{F}_{\mathrm{e}})$	$-\boldsymbol{f}_{\mathrm{e}} \cdot \bar{\boldsymbol{A}}^{\mathrm{t}}$	$-\boldsymbol{F}_{\mathrm{p}} \cdot \widetilde{\boldsymbol{a}}^{\mathrm{t}}$
$\bar{\boldsymbol{a}}^{\mathrm{t}}$	$\widetilde{\boldsymbol{A}}^{\mathrm{t}} \cdot \mathrm{cof}(\boldsymbol{f})$	$\widetilde{\boldsymbol{d}}^{\mathrm{t}} \cdot \mathrm{cof}(\boldsymbol{f}_{\mathrm{e}})$	$\bullet$	$-\boldsymbol{f}_{\mathrm{e}} \cdot \bar{\boldsymbol{A}}^{\mathrm{t}} \cdot \mathrm{cof}(\boldsymbol{f}_{\mathrm{e}})$	$-\boldsymbol{F}_{\mathrm{p}} \cdot \widetilde{\boldsymbol{a}}^{\mathrm{t}} \cdot \mathrm{cof}(\boldsymbol{f}_{\mathrm{e}})$
$\bar{\boldsymbol{A}}^{\mathrm{t}}$	$-\boldsymbol{F}_{\mathrm{e}} \cdot \widetilde{\boldsymbol{A}}^{\mathrm{t}} \cdot \mathrm{cof}(\boldsymbol{f}_{\mathrm{p}})$	$-\boldsymbol{F}_{\mathrm{e}} \cdot \widetilde{\boldsymbol{d}}^{\mathrm{t}}$	$-\boldsymbol{F}_{\mathrm{e}} \cdot \bar{\boldsymbol{a}}^{\mathrm{t}} \cdot \mathrm{cof}(\boldsymbol{F}_{\mathrm{e}})$	$\bullet$	$\boldsymbol{F} \cdot \widetilde{\boldsymbol{a}}^{\mathrm{t}}$
$\widetilde{\boldsymbol{a}}^{\mathrm{t}}$	$-\boldsymbol{f}_{\mathrm{p}} \cdot \widetilde{\boldsymbol{A}}^{\mathrm{t}} \cdot \mathrm{cof}(\boldsymbol{f}_{\mathrm{p}})$	$-\boldsymbol{f}_{\mathrm{p}} \cdot \widetilde{\boldsymbol{d}}^{\mathrm{t}}$	$-\boldsymbol{f}_{\mathrm{p}} \cdot \bar{\boldsymbol{a}}^{\mathrm{t}} \cdot \mathrm{cof}(\boldsymbol{F}_{\mathrm{e}})$	$\boldsymbol{f} \cdot \bar{\boldsymbol{A}}^{\mathrm{t}}$	$\bullet$

compare eqs.(2.4,2.9). As a result, we observe that

$$-\nabla_{\boldsymbol{X}} \boldsymbol{F} : \boldsymbol{E}_0 = \boldsymbol{F} \cdot \nabla_{\boldsymbol{x}} \boldsymbol{f} : [\, \boldsymbol{F} \,\overline{\otimes}\, \boldsymbol{F} \,] : \boldsymbol{E}_0 = J\, \boldsymbol{F} \cdot \nabla_{\boldsymbol{x}} \boldsymbol{f} : \boldsymbol{E}_t \cdot \boldsymbol{f}^{\mathrm{t}} \tag{2.24}$$

with the sought transformation taking the formats

$$-\boldsymbol{A}^{\mathrm{t}} = \boldsymbol{F} \cdot \boldsymbol{a}^{\mathrm{t}} \cdot \mathrm{cof}(\boldsymbol{F}) = \boldsymbol{F} \cdot \boldsymbol{D}^{\mathrm{t}} \quad \text{and} \quad -\boldsymbol{a}^{\mathrm{t}} = \boldsymbol{f} \cdot \boldsymbol{A}^{\mathrm{t}} \cdot \mathrm{cof}(\boldsymbol{f}) = \boldsymbol{f} \cdot \boldsymbol{d}^{\mathrm{t}} \tag{2.25}$$

together with $-\boldsymbol{D}^{\mathrm{t}} = \boldsymbol{f} \cdot \boldsymbol{d}^{\mathrm{t}} \cdot \mathrm{cof}(\boldsymbol{F})$ as well as $-\boldsymbol{d}^{\mathrm{t}} = \boldsymbol{F} \cdot \boldsymbol{D}^{\mathrm{t}} \cdot \mathrm{cof}(\boldsymbol{f})$ now being obvious.

2.1.4.2 Plastic intermediate motion versus elastic intermediate motion

Following the same lines of derivation for the relations between non–vanishing dislocation density tensors based on the plastic and elastic distortion, the expressions

$$\nabla_{\boldsymbol{X}} \boldsymbol{F} = \widetilde{\nabla} \boldsymbol{F}_{\mathrm{e}} : [\, \boldsymbol{F}_{\mathrm{p}} \,\overline{\otimes}\, \boldsymbol{F}_{\mathrm{p}} \,] + \boldsymbol{F}_{\mathrm{e}} \cdot \nabla_{\boldsymbol{X}} \boldsymbol{F}_{\mathrm{p}} \tag{2.26}$$

and likewise

$$\nabla_{\boldsymbol{x}} \boldsymbol{f} = \bar{\nabla} \boldsymbol{f}_{\mathrm{p}} : [\, \boldsymbol{f}_{\mathrm{e}} \,\overline{\otimes}\, \boldsymbol{f}_{\mathrm{e}} \,] + \boldsymbol{f}_{\mathrm{p}} \cdot \nabla_{\boldsymbol{x}} \boldsymbol{f}_{\mathrm{e}} \tag{2.27}$$

turn out to be of cardinal importance. Eqs.(2.26,2.27) motivate in particular the relation between elastic and plastic dislocation density tensors

$$\boldsymbol{f}_{\mathrm{e}} \cdot \boldsymbol{A}^{\mathrm{t}} = -\boldsymbol{f}_{\mathrm{e}} \cdot \nabla_{\boldsymbol{X}} \boldsymbol{F} : \boldsymbol{E}_0 = \widetilde{\boldsymbol{A}}^{\mathrm{t}} + \boldsymbol{f}_{\mathrm{e}} \cdot \bar{\boldsymbol{A}}^{\mathrm{t}} \cdot \mathrm{cof}(\boldsymbol{F}_{\mathrm{p}}) = \boldsymbol{0} \tag{2.28}$$

with

$$\widetilde{\boldsymbol{A}}^{\mathrm{t}} = -\nabla_{\boldsymbol{X}} \boldsymbol{F}_{\mathrm{p}} : \boldsymbol{E}_0 = J_{\mathrm{p}}\, \boldsymbol{f}_{\mathrm{e}} \cdot \widetilde{\nabla} \boldsymbol{F}_{\mathrm{e}} : \boldsymbol{E}_{\mathrm{p}} \cdot \boldsymbol{f}_{\mathrm{p}}^{\mathrm{t}} = -\boldsymbol{f}_{\mathrm{e}} \cdot \bar{\boldsymbol{A}}^{\mathrm{t}} \cdot \mathrm{cof}(\boldsymbol{F}_{\mathrm{p}})\,, \tag{2.29}$$

whereby $\bar{\boldsymbol{A}}^{\mathrm{t}} = \widetilde{\nabla}^{\mathrm{t}} \times \boldsymbol{F}_{\mathrm{e}} : T^*\mathcal{B}_{\mathrm{p}} \to T\mathcal{B}_t$ points opposite to $\bar{\boldsymbol{a}}^{\mathrm{t}}$, as well as

$$\boldsymbol{F}_{\mathrm{p}} \cdot \boldsymbol{a}^{\mathrm{t}} = -\boldsymbol{F}_{\mathrm{p}} \cdot \nabla_{\boldsymbol{x}} \boldsymbol{f} : \boldsymbol{E}_t = \bar{\boldsymbol{a}}^{\mathrm{t}} + \boldsymbol{F}_{\mathrm{p}} \cdot \widetilde{\boldsymbol{a}}^{\mathrm{t}} \cdot \mathrm{cof}(\boldsymbol{f}_{\mathrm{e}}) = \boldsymbol{0} \tag{2.30}$$

with

$$\bar{\boldsymbol{a}}^{\mathrm{t}} = -\nabla_{\boldsymbol{x}} \boldsymbol{f}_{\mathrm{e}} : \boldsymbol{E}_t = j_{\mathrm{e}}\, \boldsymbol{F}_{\mathrm{p}} \cdot \bar{\nabla} \boldsymbol{f}_{\mathrm{p}} : \boldsymbol{E}_{\mathrm{p}} \cdot \boldsymbol{F}_{\mathrm{e}}^{\mathrm{t}} = -\boldsymbol{F}_{\mathrm{p}} \cdot \widetilde{\boldsymbol{a}}^{\mathrm{t}} \cdot \mathrm{cof}(\boldsymbol{f}_{\mathrm{e}})\,, \tag{2.31}$$

whereby $\widetilde{\boldsymbol{a}}^{\mathrm{t}} = \bar{\nabla}^{\mathrm{t}} \times \boldsymbol{f}_{\mathrm{p}} : T^*\mathcal{B}_{\mathrm{p}} \to T\mathcal{B}_0$ points opposite to $\widetilde{\boldsymbol{A}}^{\mathrm{t}}$. By analogy with eq.(2.23), it is straightforward to compute

$$-\nabla_{\boldsymbol{X}} \boldsymbol{F}_{\mathrm{p}} = \boldsymbol{F}_{\mathrm{p}} \cdot \bar{\nabla} \boldsymbol{f}_{\mathrm{p}} : [\, \boldsymbol{F}_{\mathrm{p}} \,\overline{\otimes}\, \boldsymbol{F}_{\mathrm{p}} \,] \quad \text{and} \quad -\nabla_{\boldsymbol{x}} \boldsymbol{f}_{\mathrm{e}} = \boldsymbol{f}_{\mathrm{e}} \cdot \widetilde{\nabla} \boldsymbol{F}_{\mathrm{e}} : [\, \boldsymbol{f}_{\mathrm{e}} \,\overline{\otimes}\, \boldsymbol{f}_{\mathrm{e}} \,] \tag{2.32}$$

which constitute the essential kinematic relations for the derivation of the sought expressions

$$\widetilde{\boldsymbol{A}}^{\mathrm{t}} = \boldsymbol{F}_{\mathrm{p}} \cdot \bar{\nabla} \boldsymbol{f}_{\mathrm{p}} : [\, \boldsymbol{F}_{\mathrm{p}} \,\overline{\otimes}\, \boldsymbol{F}_{\mathrm{p}} \,] : \boldsymbol{E}_0 = -\boldsymbol{F}_{\mathrm{p}} \cdot \widetilde{\boldsymbol{a}}^{\mathrm{t}} \cdot \mathrm{cof}(\boldsymbol{F}_{\mathrm{p}}) = \bar{\boldsymbol{a}}^{\mathrm{t}} \cdot \mathrm{cof}(\boldsymbol{F}) \tag{2.33}$$

and

$$\bar{\boldsymbol{a}}^{\mathrm{t}} = \boldsymbol{f}_{\mathrm{e}} \cdot \widetilde{\nabla} \boldsymbol{F}_{\mathrm{e}} : [\, \boldsymbol{f}_{\mathrm{e}} \,\overline{\otimes}\, \boldsymbol{f}_{\mathrm{e}} \,] : \boldsymbol{E}_t = -\boldsymbol{f}_{\mathrm{e}} \cdot \bar{\boldsymbol{A}}^{\mathrm{t}} \cdot \mathrm{cof}(\boldsymbol{f}_{\mathrm{e}}) = \widetilde{\boldsymbol{A}}^{\mathrm{t}} \cdot \mathrm{cof}(\boldsymbol{f})\,. \tag{2.34}$$

With these relations in hand, it is possible to compare those distortion–based dislocation density tensors that are entirely settled in the intermediate configuration, i.e.

$$\widetilde{\boldsymbol{d}}^{\mathrm{t}} = \widetilde{\boldsymbol{A}}^{\mathrm{t}} \cdot \mathrm{cof}(\boldsymbol{f}_{\mathrm{p}}) = -\boldsymbol{f}_{\mathrm{e}} \cdot \bar{\boldsymbol{A}}^{\mathrm{t}} = \bar{\boldsymbol{a}}^{\mathrm{t}} \cdot \mathrm{cof}(\boldsymbol{F}_{\mathrm{e}}) = \bar{\boldsymbol{D}}^{\mathrm{t}} \tag{2.35}$$

and

$$\bar{\boldsymbol{D}}^{\mathrm{t}} = \bar{\boldsymbol{a}}^{\mathrm{t}} \cdot \mathrm{cof}(\boldsymbol{F}_{\mathrm{e}}) = -\boldsymbol{F}_{\mathrm{p}} \cdot \widetilde{\boldsymbol{a}}^{\mathrm{t}} = \widetilde{\boldsymbol{A}}^{\mathrm{t}} \cdot \mathrm{cof}(\boldsymbol{f}_{\mathrm{p}}) = \widetilde{\boldsymbol{d}}^{\mathrm{t}}\,, \tag{2.36}$$

compare eqs.(2.16,2.18). Based on this, we additionally summarise the combinations

$$\bar{\boldsymbol{A}}^{\mathrm{t}} = -\boldsymbol{F}_{\mathrm{e}} \cdot \bar{\boldsymbol{a}}^{\mathrm{t}} \cdot \mathrm{cof}(\boldsymbol{F}_{\mathrm{e}}) = \boldsymbol{F} \cdot \widetilde{\boldsymbol{a}}^{\mathrm{t}} = -\boldsymbol{F}_{\mathrm{e}} \cdot \widetilde{\boldsymbol{A}}^{\mathrm{t}} \cdot \mathrm{cof}(\boldsymbol{f}_{\mathrm{p}}) = -\boldsymbol{F}_{\mathrm{e}} \cdot \bar{\boldsymbol{D}}^{\mathrm{t}} \tag{2.37}$$

and

$$\widetilde{\boldsymbol{a}}^{\mathrm{t}} = -\boldsymbol{f}_{\mathrm{p}} \cdot \widetilde{\boldsymbol{A}}^{\mathrm{t}} \cdot \mathrm{cof}(\boldsymbol{F}_{\mathrm{p}}) = \boldsymbol{f} \cdot \bar{\boldsymbol{A}}^{\mathrm{t}} = -\boldsymbol{f}_{\mathrm{p}} \cdot \bar{\boldsymbol{a}}^{\mathrm{t}} \cdot \mathrm{cof}(\boldsymbol{F}_{\mathrm{e}}) = -\boldsymbol{f}_{\mathrm{p}} \cdot \widetilde{\boldsymbol{d}}^{\mathrm{t}}\,. \tag{2.38}$$

Remark 2.1.1 *At first glance, the introduction of dislocation density tensors based on the inverse elastic distortion $\boldsymbol{F}_{\mathrm{e}}$ for the spatial motion problem and the inverse plastic distortion $\boldsymbol{f}_{\mathrm{p}}$ for the material motion problem seems to be straightforward. The incompatibility of the intermediate configuration, however, does not permit the computation of (vanishing) 'closed' curve integrals in analogy to eqs.(2.3,2.8) as $\oint_{\mathcal{C}_0} \mathrm{d}\boldsymbol{X}$ or $\oint_{\mathcal{C}_t} \mathrm{d}\boldsymbol{x}$, compare also eqs.(2.15,2.17) as well as eq.(1.10). Applying Stokes' theorem with respect to incompatible configurations requires modifications of its standard format according to the lines of derivation highlighted for Gauß' theorem in appendix C, see section 1.1 for further details. Nevertheless, (non–vanishing) dislocation density tensors in terms of $\boldsymbol{F}_{\mathrm{e}}$ and $\boldsymbol{f}_{\mathrm{p}}$ are derived in, for example, eqs.(2.29,2.31).*

Remark 2.1.2 *The connection between the dislocation density tensors as highlighted in eqs.(2.33,2.34) allows alternative derivation via the definition of the corresponding Burgers density vectors as introduced in eqs.(2.15,2.17). To be specific, from $\int_{\mathcal{C}_{\mathrm{p}}} \mathrm{d}\widetilde{\boldsymbol{x}} \equiv \int_{\mathcal{C}_{\mathrm{p}}} \mathrm{d}\bar{\boldsymbol{X}} \neq \boldsymbol{0}$ we observe the equivalent relations*

$$\int_{\mathcal{A}_0} \widetilde{\boldsymbol{A}}^{\mathrm{t}} \cdot \boldsymbol{N}\, \mathrm{d}A_0 = \int_{\mathcal{A}_t} \widetilde{\boldsymbol{A}}^{\mathrm{t}} \cdot \mathrm{cof}(\boldsymbol{f}) \cdot \boldsymbol{n}\, \mathrm{d}A_t \doteq \int_{\mathcal{A}_t} \bar{\boldsymbol{a}}^{\mathrm{t}} \cdot \boldsymbol{n}\, \mathrm{d}A_t \tag{2.39}$$

and

$$\int_{\mathcal{A}_t} \bar{\boldsymbol{a}}^{\mathrm{t}} \cdot \boldsymbol{n}\, \mathrm{d}A_t = \int_{\mathcal{A}_0} \bar{\boldsymbol{a}}^{\mathrm{t}} \cdot \mathrm{cof}(\boldsymbol{F}) \cdot \boldsymbol{N}\, \mathrm{d}A_0 \doteq \int_{\mathcal{A}_0} \widetilde{\boldsymbol{A}}^{\mathrm{t}} \cdot \boldsymbol{N}\, \mathrm{d}A_0\,. \tag{2.40}$$

The frequently applied notation

$$\widetilde{\boldsymbol{A}}^{\mathrm{t}} \cdot \mathrm{cof}(\boldsymbol{f}_{\mathrm{p}}) = \bar{\boldsymbol{a}}^{\mathrm{t}} \cdot \mathrm{cof}(\boldsymbol{F}_{\mathrm{e}}) \tag{2.41}$$

is immediately obtained from the pointwise formats of eqs.(2.39,2.40), namely $\widetilde{\boldsymbol{A}}^{\mathrm{t}} \cdot \mathrm{cof}(\boldsymbol{f}) = \bar{\boldsymbol{a}}^{\mathrm{t}}$ and $\bar{\boldsymbol{a}}^{\mathrm{t}} \cdot \mathrm{cof}(\boldsymbol{F}) = \widetilde{\boldsymbol{A}}^{\mathrm{t}}$, which recaptures eqs.(2.33,2.34). Please note that the relations highlighted in eqs.(2.39,2.40) also reflect the compatibility of the reference and current configuration where the surface integration has been carried out.

2.2 Balance of linear momentum

Balance of linear momentum is traditionally based on Newton's second axiom and set up in the spatial configuration ($T^*\mathcal{B}_t$). The corresponding flux terms (stresses) as based on the spatial motion problem are alternatively two–point tensors or totally settled in the spatial configuration. Thereby, these two possible options are related via appropriate Piola transformations. Nevertheless, we can establish balance equations referring either to the material configuration ($T^*\mathcal{B}_0$) or to the intermediate configuration ($T^*\mathcal{B}_{\mathrm{p}}$). These so–called configurational balance equations are consequently based on the material and intermediate motion problem and the corresponding options for the flux terms (stresses) are again related via appropriate Piola transformations. For the sake of clarity, we restrict ourselves to the quasi static case and assume conservation of mass.

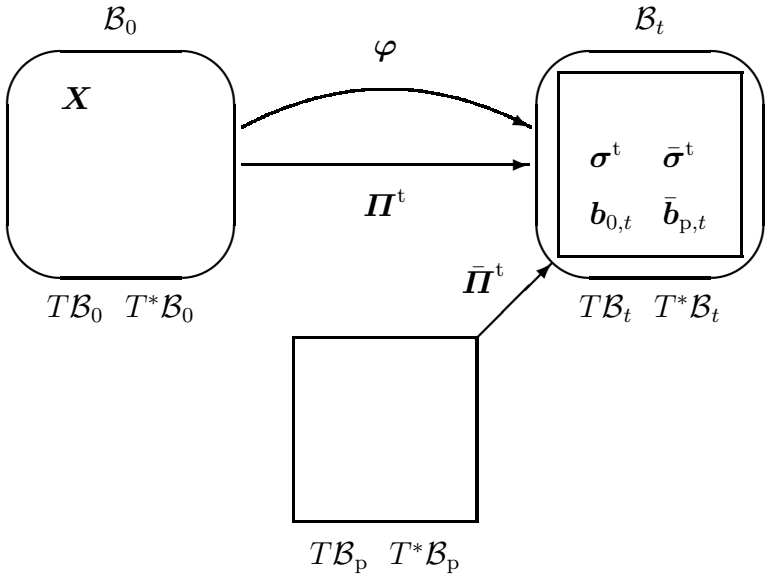

Figure 2.4: Spatial motion problem: linear momentum flux and source terms.

2.2.1 Spatial motion problem

Balance of linear momentum for the spatial motion problem is commonly formulated in terms of two different flux terms, namely either the spatial motion Piola stress $\boldsymbol{\Pi}^{\mathrm{t}}$ or the spatial motion Cauchy stress $\boldsymbol{\sigma}^{\mathrm{t}}$, respectively.[2] The Piola stress thereby constitutes a two–point tensor with respect to the material and spatial configuration. The corresponding balance of linear momentum equations read

$$\nabla_{\boldsymbol{X}} \cdot \boldsymbol{\Pi}^{\mathrm{t}} + \boldsymbol{b}_0 = \boldsymbol{0} \quad \text{and} \quad \nabla_{\boldsymbol{x}} \cdot \boldsymbol{\sigma}^{\mathrm{t}} + \boldsymbol{b}_t = \boldsymbol{0} \quad \in T^*\mathcal{B}_t \tag{2.42}$$

with

$$\boldsymbol{\sigma}^{\mathrm{t}} := \boldsymbol{\Pi}^{\mathrm{t}} \cdot \mathrm{cof}(\boldsymbol{f}) \quad \text{and} \quad \boldsymbol{b}_t := j\, \boldsymbol{b}_0 \,, \tag{2.43}$$

whereby $\boldsymbol{b}_{0,t} := \boldsymbol{b}_{0,t}^{\mathrm{int}} + \boldsymbol{b}_{0,t}^{\mathrm{ext}}$ account for external body forces, as for instance gravitation, and possibly internal body forces, which will be specified later on.

Alternatively, we can formally introduce the spatial motion elastic Piola stress $\bar{\boldsymbol{\Pi}}^{\mathrm{t}}$ and a corresponding spatial motion elastic Cauchy stress $\bar{\boldsymbol{\sigma}}^{\mathrm{t}}$. The Piola stress thereby constitutes a two–point tensor with respect to the intermediate and spatial configuration. The postulated equivalent balance of linear momentum equations read

$$\bar{\nabla} \cdot \bar{\boldsymbol{\Pi}}^{\mathrm{t}} - \bar{\boldsymbol{\Pi}}^{\mathrm{t}} \cdot [\, \boldsymbol{f}_{\mathrm{e}} \times \bar{\boldsymbol{A}} \,] + \bar{\boldsymbol{b}}_{\mathrm{p}} = \boldsymbol{0} \quad \text{and} \quad \nabla_{\boldsymbol{x}} \cdot \bar{\boldsymbol{\sigma}}^{\mathrm{t}} + \bar{\boldsymbol{b}}_t = \boldsymbol{0} \quad \in T^*\mathcal{B}_t \,, \tag{2.44}$$

compare appendix C, with

$$\bar{\boldsymbol{\sigma}}^{\mathrm{t}} := \bar{\boldsymbol{\Pi}}^{\mathrm{t}} \cdot \mathrm{cof}(\boldsymbol{f}_{\mathrm{e}}) \quad \text{and} \quad \bar{\boldsymbol{b}}_t := j_{\mathrm{e}}\, \bar{\boldsymbol{b}}_{\mathrm{p}} \,, \tag{2.45}$$

whereby $\bar{\boldsymbol{b}}_{\mathrm{p},t} := \bar{\boldsymbol{b}}_{\mathrm{p},t}^{\mathrm{int}} + \bar{\boldsymbol{b}}_{\mathrm{p},t}^{\mathrm{ext}}$ account for external body forces, as for instance gravitation, and internal body forces, which will be specified later on. The modified Piola identity with respect to the intermediate divergence operator $\bar{\nabla} \cdot \{\bullet\}$ is reviewed in appendix C.

Figure 2.4 displays the stress tensors and volume force vectors introduced above.

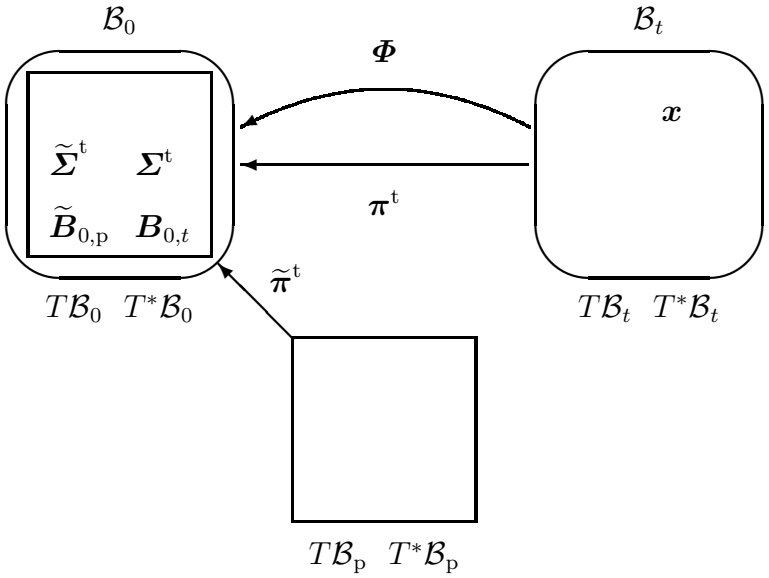

Figure 2.5: Material motion problem: linear momentum flux and source terms.

2.2.2 Material motion problem

Balance of linear momentum for the material motion problem is, by analogy with section 2.2.1, formulated in terms of two different flux terms, namely either the material motion Piola stress $\boldsymbol{\pi}^{\mathrm{t}}$ or the material motion Cauchy stress $\boldsymbol{\Sigma}^{\mathrm{t}}$, respectively.[3] The Piola stress thereby constitutes a two–point tensor with respect to the spatial and material configuration. The corresponding equivalent balance of linear momentum equations read

$$\nabla_{\boldsymbol{x}} \cdot \boldsymbol{\pi}^{\mathrm{t}} + \boldsymbol{B}_t = \boldsymbol{0} \quad \text{and} \quad \nabla_{\boldsymbol{X}} \cdot \boldsymbol{\Sigma}^{\mathrm{t}} + \boldsymbol{B}_0 = \boldsymbol{0} \quad \in T^*\mathcal{B}_0 \tag{2.46}$$

with

$$\boldsymbol{\Sigma}^{\mathrm{t}} := \boldsymbol{\pi}^{\mathrm{t}} \cdot \mathrm{cof}(\boldsymbol{F}) \quad \text{and} \quad \boldsymbol{B}_0 := J\, \boldsymbol{B}_t \,, \tag{2.47}$$

whereby $\boldsymbol{B}_{t,0} := \boldsymbol{B}_{t,0}^{\mathrm{int}} + \boldsymbol{B}_{t,0}^{\mathrm{ext}}$ account for external body forces, as for instance gravitation, and internal body forces, which will be specified later on.

Alternatively, we can formally introduce the material motion plastic Piola stress $\widetilde{\boldsymbol{\pi}}^{\mathrm{t}}$ and a corresponding material motion plastic Cauchy stress $\widetilde{\boldsymbol{\Sigma}}^{\mathrm{t}}$. The Piola stress thereby constitutes a two–point tensor with respect to the intermediate and material configuration. The postulated equivalent balance of linear momentum equations read

$$\widetilde{\nabla} \cdot \widetilde{\boldsymbol{\pi}}^{\mathrm{t}} - \widetilde{\boldsymbol{\pi}}^{\mathrm{t}} \cdot [\, \boldsymbol{F}_{\mathrm{p}} \times \widetilde{\boldsymbol{a}}\,] + \widetilde{\boldsymbol{B}}_{\mathrm{p}} = \boldsymbol{0} \quad \text{and} \quad \nabla_{\boldsymbol{X}} \cdot \widetilde{\boldsymbol{\Sigma}}^{\mathrm{t}} + \widetilde{\boldsymbol{B}}_0 = \boldsymbol{0} \quad \in T^*\mathcal{B}_0 \,, \tag{2.48}$$

compare appendix C, with

$$\widetilde{\boldsymbol{\Sigma}}^{\mathrm{t}} := \widetilde{\boldsymbol{\pi}}^{\mathrm{t}} \cdot \mathrm{cof}(\boldsymbol{F}_{\mathrm{p}}) \quad \text{and} \quad \widetilde{\boldsymbol{B}}_0 := J_{\mathrm{p}}\, \widetilde{\boldsymbol{B}}_{\mathrm{p}} \,, \tag{2.49}$$

whereby $\widetilde{\boldsymbol{B}}_{\mathrm{p},0} := \widetilde{\boldsymbol{B}}_{\mathrm{p},0}^{\mathrm{int}} + \widetilde{\boldsymbol{B}}_{\mathrm{p},0}^{\mathrm{ext}}$ account for external body forces, as for instance gravitation, and internal body forces, which will be specified later on. The modified Piola identity with respect to the intermediate divergence operator $\widetilde{\nabla} \cdot \{\bullet\}$ is reviewed in appendix C.

Figure 2.5 displays the stress tensors and volume force vectors introduced above.

[2] The transposed is chosen by convention so that traction follows from $\boldsymbol{\sigma}^{\mathrm{t}} \cdot \boldsymbol{n}$, thus the first index of the stress tensor refers to the surface normal.

[3] What we call the material motion Cauchy stress $\boldsymbol{\Sigma}^{\mathrm{t}}$ is frequently referred to as the Eshelby stress tensor and exhibits the classical energy momentum format, compare Eshelby (1951, 1956).

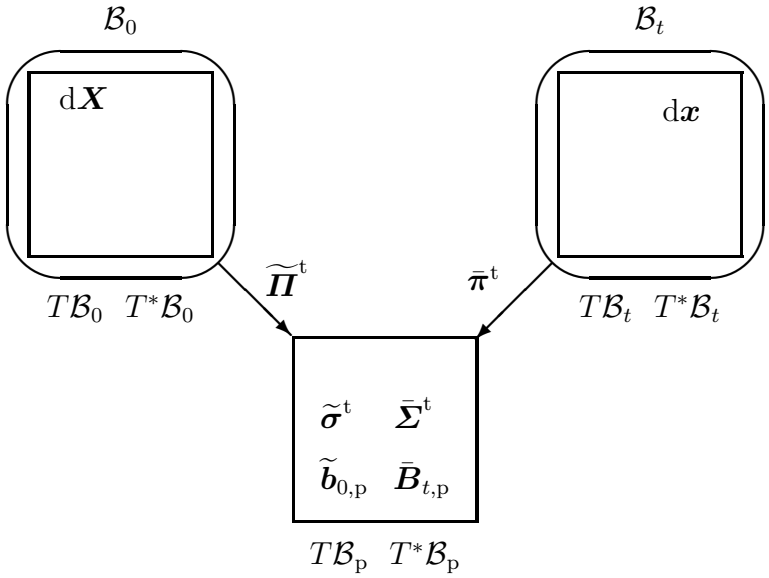

Figure 2.6: Intermediate motion problem: linear momentum flux and source terms.

2.2.3 Intermediate motion problem

Balance of linear momentum for the intermediate motion problem is, by analogy with sections 2.2.1 and 2.2.2, formulated in terms of two different Piola–type flux terms, namely either the intermediate motion plastic Piola stress $\widetilde{\boldsymbol{\Pi}}^{\mathrm{t}}$ or the intermediate motion elastic Piola stress $\bar{\boldsymbol{\pi}}^{\mathrm{t}}$, respectively. The setup of the corresponding intermediate motion plastic Cauchy stress $\widetilde{\boldsymbol{\sigma}}^{\mathrm{t}}$ as well as of the intermediate motion elastic Cauchy stress $\bar{\boldsymbol{\Sigma}}^{\mathrm{t}}$ is straightforward. The Piola stresses thereby constitute two–point tensors with respect to the material and intermediate configuration for the plastic intermediate motion problem and with respect to the spatial and intermediate configuration for the elastic intermediate motion problem. The postulated equivalent balance of linear momentum equations formally read

$$\nabla_{\boldsymbol{X}} \cdot \widetilde{\boldsymbol{\Pi}}^{\mathrm{t}} + \widetilde{\boldsymbol{b}}_0 = \boldsymbol{0} \quad \text{and} \quad \widetilde{\nabla} \cdot \widetilde{\boldsymbol{\sigma}}^{\mathrm{t}} - \widetilde{\boldsymbol{\sigma}}^{\mathrm{t}} \cdot [\, \boldsymbol{F}_{\mathrm{p}} \times \widetilde{\boldsymbol{a}} \,] + \widetilde{\boldsymbol{b}}_{\mathrm{p}} = \boldsymbol{0} \quad \in T^*\mathcal{B}_{\mathrm{p}} \,, \tag{2.50}$$

compare appendix C, with

$$\widetilde{\boldsymbol{\sigma}}^{\mathrm{t}} := \widetilde{\boldsymbol{\Pi}}^{\mathrm{t}} \cdot \mathrm{cof}(\boldsymbol{f}_{\mathrm{p}}) \quad \text{and} \quad \widetilde{\boldsymbol{b}}_{\mathrm{p}} := j_{\mathrm{p}}\, \widetilde{\boldsymbol{b}}_0 \tag{2.51}$$

and

$$\nabla_{\boldsymbol{x}} \cdot \bar{\boldsymbol{\pi}}^{\mathrm{t}} + \bar{\boldsymbol{B}}_t = \boldsymbol{0} \quad \text{and} \quad \bar{\nabla} \cdot \bar{\boldsymbol{\Sigma}}^{\mathrm{t}} - \bar{\boldsymbol{\Sigma}}^{\mathrm{t}} \cdot [\, \boldsymbol{f}_{\mathrm{e}} \times \bar{\boldsymbol{A}} \,] + \bar{\boldsymbol{B}}_{\mathrm{p}} = \boldsymbol{0} \quad \in T^*\mathcal{B}_{\mathrm{p}} \,, \tag{2.52}$$

compare appendix C, with

$$\bar{\boldsymbol{\Sigma}}^{\mathrm{t}} := \bar{\boldsymbol{\pi}}^{\mathrm{t}} \cdot \mathrm{cof}(\boldsymbol{F}_{\mathrm{e}}) \quad \text{and} \quad \bar{\boldsymbol{B}}_{\mathrm{p}} := J_{\mathrm{e}}\, \bar{\boldsymbol{B}}_t \,, \tag{2.53}$$

whereby $\widetilde{\boldsymbol{b}}_{0,\mathrm{p}} := \widetilde{\boldsymbol{b}}^{\mathrm{int}}_{0,\mathrm{p}} + \widetilde{\boldsymbol{b}}^{\mathrm{ext}}_{0,\mathrm{p}}$ and $\bar{\boldsymbol{B}}_{t,\mathrm{p}} := \bar{\boldsymbol{B}}^{\mathrm{int}}_{t,\mathrm{p}} + \bar{\boldsymbol{B}}^{\mathrm{ext}}_{t,\mathrm{p}}$, respectively, account for external body forces, as for instance gravitation, and internal body forces, which will be specified later on. The modified Piola identity with respect to the intermediate divergence operators $\widetilde{\nabla} \cdot \{\bullet\}$ and $\bar{\nabla} \cdot \{\bullet\}$ is reviewed in appendix C.

Figure 2.6 displays the stress tensors and volume force vectors introduced above.

2.3 Hyperelastic stress formats based on a Helmholtz free energy function

In order to compare the various representations of balance of linear momentum proposed in section 2.2, we firstly introduce hyperelastic formats for the corresponding stresses in the following section 2.3 and secondly address derivations of correlated volume forces in section 2.4. Based on the standard argumentation of rational thermomechanics, the adopted hyperelastic formats are based on the idea, that constitutive equations are defined in terms of a Helmholtz free energy density. Without loss of generality we restrict ourselves to the isothermal case and do not elaborate particular evolution or balance equations for, e.g., the plastic distortion for the sake of conceptual clarity. As the key assumption the postulated Helmholtz free energy density potential depends only on the elastic distortion and possibly on the material placement of particles. In addition, invariance requirements further constrain how the Helmholtz free energy density depends on its arguments. We will not place special emphasis on invariance conditions under superposed orientation preserving spatial isometries. Translational invariance, however, is of cardinal importance for the problem at hand. As a result, the Helmholtz free energy density must not depend on the spatial placement of particles, $\boldsymbol{x} = \boldsymbol{\varphi}(\boldsymbol{X}, t)$, but solely on material placements, $\boldsymbol{X} = \boldsymbol{\Phi}(\boldsymbol{x}, t)$. Moreover, we consequently obtain vanishing internal volume or rather self forces for the spatial motion problem, $\boldsymbol{b}_{0,t}^{\text{int}} = \boldsymbol{0}$.

Following these preliminary statements, let (with a slight misuse of notation) the Helmholtz free energy density be defined as

$$\psi_0(\boldsymbol{F}, \boldsymbol{F}_{\text{p}}; \boldsymbol{X}) = \psi_0(\boldsymbol{F} \cdot \boldsymbol{f}_{\text{p}}; \boldsymbol{X}) = \psi_0(\boldsymbol{F}_{\text{e}}; \boldsymbol{X}) \,. \tag{2.54}$$

In order to relate this Helmholtz free energy density per material unit volume to intermediate and spatial unit volumes, we additionally mention the transformations

$$\psi_0 = J_{\text{p}}\, \psi_{\text{p}} = J\, \psi_t \quad \text{s.t.} \quad \psi_{\text{p}} = j_{\text{p}}\, \psi_0 = J_{\text{e}}\, \psi_t \quad \text{or} \quad \psi_t = j_{\text{e}}\, \psi_{\text{p}} = j\, \psi_0 \,. \tag{2.55}$$

2.3.1 Spatial motion problem

The commonly accepted constitutive equation for the spatial motion Piola stress reads

$$\boldsymbol{\Pi}^{\text{t}} = \partial_{\boldsymbol{F}} \psi_0|_{\boldsymbol{F}_{\text{p}}} \,. \tag{2.56}$$

From eqs.(2.43,2.55) we additionally observe that the spatial motion Cauchy stress allows representation in energy momentum format

$$\boldsymbol{\sigma}^{\text{t}} = \partial_{\boldsymbol{F}} \psi_0|_{\boldsymbol{F}_{\text{p}}} \cdot \text{cof}(\boldsymbol{f}) = \psi_t\, \boldsymbol{I}_t^{\text{t}} - \boldsymbol{f}^{\text{t}} \cdot \partial_{\boldsymbol{f}} \psi_t|_{\boldsymbol{f}_{\text{p}}} \,, \tag{2.57}$$

whereby $\boldsymbol{I}_t = \boldsymbol{F} \cdot \boldsymbol{f} = \boldsymbol{f}^{\text{t}} \cdot \boldsymbol{F}^{\text{t}} = \boldsymbol{F}_{\text{e}} \cdot \boldsymbol{f}_{\text{e}} = \boldsymbol{f}_{\text{e}}^{\text{t}} \cdot \boldsymbol{F}_{\text{e}}^{\text{t}} : T\mathcal{B}_t \to T\mathcal{B}_t$ denotes the second–order identity in the spatial configuration and use of the relation $\partial_{\boldsymbol{F}} \psi_t|_{\boldsymbol{F}_{\text{p}}} = -\, \boldsymbol{f}^{\text{t}} \cdot \partial_{\boldsymbol{f}} \psi_t|_{\boldsymbol{f}_{\text{p}}} \cdot \boldsymbol{f}^{\text{t}}$ has been made.

For the second family of stresses, we define the spatial motion elastic Piola stress to take the format

$$\bar{\boldsymbol{\Pi}}^{\text{t}} := \partial_{\boldsymbol{F}_{\text{e}}} \psi_{\text{p}} \,. \tag{2.58}$$

From eqs.(2.45,2.55) we additionally observe that the spatial motion elastic Cauchy stress then allows representation in energy momentum format

$$\bar{\boldsymbol{\sigma}}^{\text{t}} = \partial_{\boldsymbol{F}_{\text{e}}} \psi_{\text{p}} \cdot \text{cof}(\boldsymbol{f}_{\text{e}}) = \psi_t\, \boldsymbol{I}_t^{\text{t}} - \boldsymbol{f}_{\text{e}}^{\text{t}} \cdot \partial_{\boldsymbol{f}_{\text{e}}} \psi_t \,, \tag{2.59}$$

whereby use of the relation $\partial_{\boldsymbol{F}_{\text{e}}} \psi_t = -\, \boldsymbol{f}_{\text{e}}^{\text{t}} \cdot \partial_{\boldsymbol{f}_{\text{e}}} \psi_t \cdot \boldsymbol{f}_{\text{e}}^{\text{t}}$ has been made.

Table 2.3: Transformations related to the Piola–type stresses $\boldsymbol{\Pi}^{\mathrm{t}} = \partial_{\boldsymbol{F}}\psi_0|_{\boldsymbol{F}_{\mathrm{p}}}$, $\bar{\boldsymbol{\Pi}}^{\mathrm{t}} = \partial_{\boldsymbol{F}_{\mathrm{e}}}\psi_{\mathrm{p}}$ and $\widetilde{\boldsymbol{\Pi}}^{\mathrm{t}} = \partial_{\boldsymbol{F}_{\mathrm{p}}}\psi_0|_{\boldsymbol{F}}$.

	$\boldsymbol{\Pi}^{\mathrm{t}}$	$\bar{\boldsymbol{\Pi}}^{\mathrm{t}}$	$\widetilde{\boldsymbol{\Pi}}^{\mathrm{t}}$
$\boldsymbol{\Pi}^{\mathrm{t}}$	$\bullet$	$\bar{\boldsymbol{\Pi}}^{\mathrm{t}} \cdot \mathrm{cof}(\boldsymbol{F}_{\mathrm{p}})$	$\psi_0\, \boldsymbol{f}^{\mathrm{t}} - \boldsymbol{f}_{\mathrm{e}}^{\mathrm{t}} \cdot \widetilde{\boldsymbol{\Pi}}^{\mathrm{t}}$
$\bar{\boldsymbol{\Pi}}^{\mathrm{t}}$	$\boldsymbol{\Pi}^{\mathrm{t}} \cdot \mathrm{cof}(\boldsymbol{f}_{\mathrm{p}})$	$\bullet$	$\psi_{\mathrm{p}}\, \boldsymbol{f}_{\mathrm{e}}^{\mathrm{t}} - \boldsymbol{f}_{\mathrm{e}}^{\mathrm{t}} \cdot \widetilde{\boldsymbol{\Pi}}^{\mathrm{t}} \cdot \mathrm{cof}(\boldsymbol{f}_{\mathrm{p}})$
$\widetilde{\boldsymbol{\Pi}}^{\mathrm{t}}$	$\psi_0\, \boldsymbol{f}_{\mathrm{p}}^{\mathrm{t}} - \boldsymbol{F}_{\mathrm{e}}^{\mathrm{t}} \cdot \boldsymbol{\Pi}^{\mathrm{t}}$	$\psi_0\, \boldsymbol{f}_{\mathrm{p}}^{\mathrm{t}} - \boldsymbol{F}_{\mathrm{e}}^{\mathrm{t}} \cdot \bar{\boldsymbol{\Pi}}^{\mathrm{t}} \cdot \mathrm{cof}(\boldsymbol{F}_{\mathrm{p}})$	$\bullet$
$\boldsymbol{\pi}^{\mathrm{t}}$	$\psi_t\, \boldsymbol{F}^{\mathrm{t}} - \boldsymbol{F}^{\mathrm{t}} \cdot \boldsymbol{\Pi}^{\mathrm{t}} \cdot \mathrm{cof}(\boldsymbol{f})$	$\psi_t\, \boldsymbol{F}^{\mathrm{t}} - \boldsymbol{F}^{\mathrm{t}} \cdot \bar{\boldsymbol{\Pi}}^{\mathrm{t}} \cdot \mathrm{cof}(\boldsymbol{f}_{\mathrm{e}})$	$\boldsymbol{F}_{\mathrm{p}}^{\mathrm{t}} \cdot \widetilde{\boldsymbol{\Pi}}^{\mathrm{t}} \cdot \mathrm{cof}(\boldsymbol{f})$
$\widetilde{\boldsymbol{\pi}}^{\mathrm{t}}$	$\boldsymbol{F}^{\mathrm{t}} \cdot \boldsymbol{\Pi}^{\mathrm{t}} \cdot \mathrm{cof}(\boldsymbol{f}_{\mathrm{p}})$	$\boldsymbol{F}^{\mathrm{t}} \cdot \bar{\boldsymbol{\Pi}}^{\mathrm{t}}$	$\psi_{\mathrm{p}}\, \boldsymbol{F}_{\mathrm{p}}^{\mathrm{t}} - \boldsymbol{F}_{\mathrm{p}}^{\mathrm{t}} \cdot \widetilde{\boldsymbol{\Pi}}^{\mathrm{t}} \cdot \mathrm{cof}(\boldsymbol{f}_{\mathrm{p}})$
$\bar{\boldsymbol{\pi}}^{\mathrm{t}}$	$\psi_t\, \boldsymbol{F}_{\mathrm{e}}^{\mathrm{t}} - \boldsymbol{F}_{\mathrm{e}}^{\mathrm{t}} \cdot \boldsymbol{\Pi}^{\mathrm{t}} \cdot \mathrm{cof}(\boldsymbol{f})$	$\psi_t\, \boldsymbol{F}_{\mathrm{e}}^{\mathrm{t}} - \boldsymbol{F}_{\mathrm{e}}^{\mathrm{t}} \cdot \bar{\boldsymbol{\Pi}}^{\mathrm{t}} \cdot \mathrm{cof}(\boldsymbol{f}_{\mathrm{e}})$	$\widetilde{\boldsymbol{\Pi}}^{\mathrm{t}} \cdot \mathrm{cof}(\boldsymbol{f})$
$\boldsymbol{\sigma}^{\mathrm{t}}$	$\boldsymbol{\Pi}^{\mathrm{t}} \cdot \mathrm{cof}(\boldsymbol{f})$	$\bar{\boldsymbol{\Pi}}^{\mathrm{t}} \cdot \mathrm{cof}(\boldsymbol{f}_{\mathrm{e}})$	$\psi_t\, \boldsymbol{I}_t^{\mathrm{t}} - \boldsymbol{f}_{\mathrm{e}}^{\mathrm{t}} \cdot \widetilde{\boldsymbol{\Pi}}^{\mathrm{t}} \cdot \mathrm{cof}(\boldsymbol{f})$
$\widetilde{\boldsymbol{\sigma}}^{\mathrm{t}}$	$\psi_{\mathrm{p}}\, \boldsymbol{I}_{\mathrm{p}}^{\mathrm{t}} - \boldsymbol{F}_{\mathrm{e}}^{\mathrm{t}} \cdot \boldsymbol{\Pi}^{\mathrm{t}} \cdot \mathrm{cof}(\boldsymbol{f}_{\mathrm{p}})$	$\psi_{\mathrm{p}}\, \boldsymbol{I}_{\mathrm{p}}^{\mathrm{t}} - \boldsymbol{F}_{\mathrm{e}}^{\mathrm{t}} \cdot \bar{\boldsymbol{\Pi}}^{\mathrm{t}}$	$\widetilde{\boldsymbol{\Pi}}^{\mathrm{t}} \cdot \mathrm{cof}(\boldsymbol{f}_{\mathrm{p}})$
$\boldsymbol{\Sigma}^{\mathrm{t}}$	$\psi_0\, \boldsymbol{I}_0^{\mathrm{t}} - \boldsymbol{F}^{\mathrm{t}} \cdot \boldsymbol{\Pi}^{\mathrm{t}}$	$\psi_0\, \boldsymbol{I}_0^{\mathrm{t}} - \boldsymbol{F}^{\mathrm{t}} \cdot \bar{\boldsymbol{\Pi}}^{\mathrm{t}} \cdot \mathrm{cof}(\boldsymbol{F}_{\mathrm{p}})$	$\boldsymbol{F}_{\mathrm{p}}^{\mathrm{t}} \cdot \widetilde{\boldsymbol{\Pi}}^{\mathrm{t}}$
$\widetilde{\boldsymbol{\Sigma}}^{\mathrm{t}}$	$\boldsymbol{F}^{\mathrm{t}} \cdot \boldsymbol{\Pi}^{\mathrm{t}}$	$\boldsymbol{F}^{\mathrm{t}} \cdot \bar{\boldsymbol{\Pi}}^{\mathrm{t}} \cdot \mathrm{cof}(\boldsymbol{F}_{\mathrm{p}})$	$\psi_0\, \boldsymbol{I}_0^{\mathrm{t}} - \boldsymbol{F}_{\mathrm{p}}^{\mathrm{t}} \cdot \widetilde{\boldsymbol{\Pi}}^{\mathrm{t}}$

2.3.2 Material motion problem

The, by now, well–accepted constitutive equation for the material motion Piola stress reads

$$\boldsymbol{\pi}^{\mathrm{t}} = \partial_{\boldsymbol{f}}\psi_t|_{\boldsymbol{f}_{\mathrm{p}}} \,. \tag{2.60}$$

From eqs.(2.47,2.55) we additionally observe that the material motion Cauchy stress allows representation in energy momentum format

$$\boldsymbol{\Sigma}^{\mathrm{t}} = \partial_{\boldsymbol{f}}\psi_t|_{\boldsymbol{f}_{\mathrm{p}}} \cdot \mathrm{cof}(\boldsymbol{F}) = \psi_0\, \boldsymbol{I}_0^{\mathrm{t}} - \boldsymbol{F}^{\mathrm{t}} \cdot \partial_{\boldsymbol{F}}\psi_0|_{\boldsymbol{F}_{\mathrm{p}}} \,, \tag{2.61}$$

whereby $\boldsymbol{I}_0 = \boldsymbol{f} \cdot \boldsymbol{F} = \boldsymbol{F}^{\mathrm{t}} \cdot \boldsymbol{f}^{\mathrm{t}} = \boldsymbol{f}_{\mathrm{p}} \cdot \boldsymbol{F}_{\mathrm{p}} = \boldsymbol{F}_{\mathrm{p}}^{\mathrm{t}} \cdot \boldsymbol{f}_{\mathrm{p}}^{\mathrm{t}} : T\mathcal{B}_0 \to T\mathcal{B}_0$ denotes the second–order identity in the material configuration and use of the relation $\partial_{\boldsymbol{f}}\psi_0|_{\boldsymbol{f}_{\mathrm{p}}} = -\,\boldsymbol{F}^{\mathrm{t}} \cdot \partial_{\boldsymbol{F}}\psi_0|_{\boldsymbol{F}_{\mathrm{p}}} \cdot \boldsymbol{F}^{\mathrm{t}}$ has been made.

For the second family of stresses, we define the material motion plastic Piola stress to take the format

$$\widetilde{\boldsymbol{\pi}}^{\mathrm{t}} := \partial_{\boldsymbol{f}_{\mathrm{p}}}\psi_{\mathrm{p}}|_{\boldsymbol{f}} \,. \tag{2.62}$$

From eqs.(2.49,2.55) we additionally observe that the material motion plastic Cauchy stress then allows representation in energy momentum format

$$\widetilde{\boldsymbol{\Sigma}}^{\mathrm{t}} = \partial_{\boldsymbol{f}_{\mathrm{p}}}\psi_{\mathrm{p}}|_{\boldsymbol{f}} \cdot \mathrm{cof}(\boldsymbol{F}_{\mathrm{p}}) = \psi_0\, \boldsymbol{I}_0^{\mathrm{t}} - \boldsymbol{F}_{\mathrm{p}}^{\mathrm{t}} \cdot \partial_{\boldsymbol{F}_{\mathrm{p}}}\psi_0|_{\boldsymbol{F}} \,, \tag{2.63}$$

whereby use of the relation $\partial_{\boldsymbol{f}_{\mathrm{p}}}\psi_0|_{\boldsymbol{f}} = -\,\boldsymbol{F}_{\mathrm{p}}^{\mathrm{t}} \cdot \partial_{\boldsymbol{F}_{\mathrm{p}}}\psi_0|_{\boldsymbol{F}} \cdot \boldsymbol{F}_{\mathrm{p}}^{\mathrm{t}}$ has been made.

Table 2.4: Transformations related to the Piola–type stresses $\boldsymbol{\pi}^{\mathrm{t}} = \partial_{\boldsymbol{f}} \psi_t|_{\boldsymbol{f}_{\mathrm{p}}}$, $\widetilde{\boldsymbol{\pi}}^{\mathrm{t}} = \partial_{\boldsymbol{f}_{\mathrm{p}}} \psi_{\mathrm{p}}|_{\boldsymbol{f}}$ and $\bar{\boldsymbol{\pi}}^{\mathrm{t}} = \partial_{\boldsymbol{f}_{\mathrm{e}}} \psi_t$.

	$\boldsymbol{\pi}^{\mathrm{t}}$	$\widetilde{\boldsymbol{\pi}}^{\mathrm{t}}$	$\bar{\boldsymbol{\pi}}^{\mathrm{t}}$
$\boldsymbol{\Pi}^{\mathrm{t}}$	$\psi_0\, \boldsymbol{f}^{\mathrm{t}} - \boldsymbol{f}^{\mathrm{t}} \cdot \boldsymbol{\pi}^{\mathrm{t}} \cdot \mathrm{cof}(\boldsymbol{F})$	$\boldsymbol{f}^{\mathrm{t}} \cdot \widetilde{\boldsymbol{\pi}}^{\mathrm{t}} \cdot \mathrm{cof}(\boldsymbol{F}_{\mathrm{p}})$	$\psi_0\, \boldsymbol{f}^{\mathrm{t}} - \boldsymbol{f}_{\mathrm{e}}^{\mathrm{t}} \cdot \bar{\boldsymbol{\pi}}^{\mathrm{t}} \cdot \mathrm{cof}(\boldsymbol{F})$
$\bar{\boldsymbol{\Pi}}^{\mathrm{t}}$	$\psi_{\mathrm{p}}\, \boldsymbol{f}_{\mathrm{e}}^{\mathrm{t}} - \boldsymbol{f}^{\mathrm{t}} \cdot \boldsymbol{\pi}^{\mathrm{t}} \cdot \mathrm{cof}(\boldsymbol{F}_{\mathrm{e}})$	$\boldsymbol{f}^{\mathrm{t}} \cdot \widetilde{\boldsymbol{\pi}}^{\mathrm{t}}$	$\psi_{\mathrm{p}}\, \boldsymbol{f}_{\mathrm{e}}^{\mathrm{t}} - \boldsymbol{f}_{\mathrm{e}}^{\mathrm{t}} \cdot \bar{\boldsymbol{\pi}}^{\mathrm{t}} \cdot \mathrm{cof}(\boldsymbol{F}_{\mathrm{e}})$
$\widetilde{\boldsymbol{\Pi}}^{\mathrm{t}}$	$\boldsymbol{f}_{\mathrm{p}}^{\mathrm{t}} \cdot \boldsymbol{\pi}^{\mathrm{t}} \cdot \mathrm{cof}(\boldsymbol{F})$	$\psi_0\, \boldsymbol{f}_{\mathrm{p}}^{\mathrm{t}} - \boldsymbol{f}_{\mathrm{p}}^{\mathrm{t}} \cdot \widetilde{\boldsymbol{\pi}}^{\mathrm{t}} \cdot \mathrm{cof}(\boldsymbol{F}_{\mathrm{p}})$	$\bar{\boldsymbol{\pi}}^{\mathrm{t}} \cdot \mathrm{cof}(\boldsymbol{F})$
$\boldsymbol{\pi}^{\mathrm{t}}$	$\bullet$	$\psi_t\, \boldsymbol{F}^{\mathrm{t}} - \widetilde{\boldsymbol{\pi}}^{\mathrm{t}} \cdot \mathrm{cof}(\boldsymbol{f}_{\mathrm{e}})$	$\boldsymbol{F}_{\mathrm{p}}^{\mathrm{t}} \cdot \bar{\boldsymbol{\pi}}^{\mathrm{t}}$
$\widetilde{\boldsymbol{\pi}}^{\mathrm{t}}$	$\psi_{\mathrm{p}}\, \boldsymbol{F}_{\mathrm{p}}^{\mathrm{t}} - \boldsymbol{\pi}^{\mathrm{t}} \cdot \mathrm{cof}(\boldsymbol{F}_{\mathrm{e}})$	$\bullet$	$\psi_{\mathrm{p}}\, \boldsymbol{F}_{\mathrm{p}}^{\mathrm{t}} - \boldsymbol{F}_{\mathrm{p}}^{\mathrm{t}} \cdot \bar{\boldsymbol{\pi}}^{\mathrm{t}} \cdot \mathrm{cof}(\boldsymbol{F}_{\mathrm{e}})$
$\bar{\boldsymbol{\pi}}^{\mathrm{t}}$	$\boldsymbol{f}_{\mathrm{p}}^{\mathrm{t}} \cdot \boldsymbol{\pi}^{\mathrm{t}}$	$\psi_t\, \boldsymbol{F}_{\mathrm{e}}^{\mathrm{t}} - \boldsymbol{f}_{\mathrm{p}}^{\mathrm{t}} \cdot \widetilde{\boldsymbol{\pi}}^{\mathrm{t}} \cdot \mathrm{cof}(\boldsymbol{f}_{\mathrm{e}})$	$\bullet$
$\boldsymbol{\sigma}^{\mathrm{t}}$	$\psi_t\, \boldsymbol{I}_t^{\mathrm{t}} - \boldsymbol{f}^{\mathrm{t}} \cdot \boldsymbol{\pi}^{\mathrm{t}}$	$\boldsymbol{f}^{\mathrm{t}} \cdot \widetilde{\boldsymbol{\pi}}^{\mathrm{t}} \cdot \mathrm{cof}(\boldsymbol{f}_{\mathrm{e}})$	$\psi_t\, \boldsymbol{I}_t^{\mathrm{t}} - \boldsymbol{f}_{\mathrm{e}}^{\mathrm{t}} \cdot \bar{\boldsymbol{\pi}}^{\mathrm{t}}$
$\widetilde{\boldsymbol{\sigma}}^{\mathrm{t}}$	$\boldsymbol{f}_{\mathrm{p}}^{\mathrm{t}} \cdot \boldsymbol{\pi}^{\mathrm{t}} \cdot \mathrm{cof}(\boldsymbol{F}_{\mathrm{e}})$	$\psi_{\mathrm{p}}\, \boldsymbol{I}_{\mathrm{p}}^{\mathrm{t}} - \boldsymbol{f}_{\mathrm{p}}^{\mathrm{t}} \cdot \widetilde{\boldsymbol{\pi}}^{\mathrm{t}}$	$\bar{\boldsymbol{\pi}}^{\mathrm{t}} \cdot \mathrm{cof}(\boldsymbol{F}_{\mathrm{e}})$
$\boldsymbol{\Sigma}^{\mathrm{t}}$	$\boldsymbol{\pi}^{\mathrm{t}} \cdot \mathrm{cof}(\boldsymbol{F})$	$\psi_0\, \boldsymbol{I}_0^{\mathrm{t}} - \widetilde{\boldsymbol{\pi}}^{\mathrm{t}} \cdot \mathrm{cof}(\boldsymbol{F}_{\mathrm{p}})$	$\boldsymbol{F}_{\mathrm{p}}^{\mathrm{t}} \cdot \bar{\boldsymbol{\pi}}^{\mathrm{t}} \cdot \mathrm{cof}(\boldsymbol{F})$
$\widetilde{\boldsymbol{\Sigma}}^{\mathrm{t}}$	$\psi_0\, \boldsymbol{I}_0^{\mathrm{t}} - \boldsymbol{\pi}^{\mathrm{t}} \cdot \mathrm{cof}(\boldsymbol{F})$	$\widetilde{\boldsymbol{\pi}}^{\mathrm{t}} \cdot \mathrm{cof}(\boldsymbol{F}_{\mathrm{p}})$	$\psi_0\, \boldsymbol{I}_0^{\mathrm{t}} - \boldsymbol{F}_{\mathrm{p}}^{\mathrm{t}} \cdot \bar{\boldsymbol{\pi}}^{\mathrm{t}} \cdot \mathrm{cof}(\boldsymbol{F})$

2.3.3 Intermediate motion problem

The constitutive equation for the intermediate motion plastic Piola stress is defined as

$$\widetilde{\boldsymbol{\Pi}}^{\mathrm{t}} := \partial_{\boldsymbol{F}_{\mathrm{p}}} \psi_0|_{\boldsymbol{F}} \,. \tag{2.64}$$

From eqs.(2.51,2.55) we additionally observe that the intermediate motion plastic Cauchy stress then allows representation in energy momentum format

$$\widetilde{\boldsymbol{\sigma}}^{\mathrm{t}} = \partial_{\boldsymbol{F}_{\mathrm{p}}} \psi_0|_{\boldsymbol{F}} \cdot \mathrm{cof}(\boldsymbol{f}_{\mathrm{p}}) = \psi_{\mathrm{p}}\, \boldsymbol{I}_{\mathrm{p}}^{t} - \boldsymbol{f}_{\mathrm{p}}^{\mathrm{t}} \cdot \partial_{\boldsymbol{f}_{\mathrm{p}}} \psi_{\mathrm{p}}|_{\boldsymbol{f}} \,, \tag{2.65}$$

whereby $\boldsymbol{I}_{\mathrm{p}} = \boldsymbol{F}_{\mathrm{p}} \cdot \boldsymbol{f}_{\mathrm{p}} = \boldsymbol{f}_{\mathrm{p}}^{\mathrm{t}} \cdot \boldsymbol{F}_{\mathrm{p}}^{\mathrm{t}} = \boldsymbol{f}_{\mathrm{e}} \cdot \boldsymbol{F}_{\mathrm{e}} = \boldsymbol{F}_{\mathrm{e}}^{\mathrm{t}} \cdot \boldsymbol{f}_{\mathrm{e}}^{\mathrm{t}} : T\mathcal{B}_{\mathrm{p}} \rightarrow T\mathcal{B}_{\mathrm{p}}$ denotes the second–order identity in the intermediate configuration and use of the relation $\partial_{\boldsymbol{F}_{\mathrm{p}}} \psi_{\mathrm{p}}|_{\boldsymbol{F}} = -\, \boldsymbol{f}_{\mathrm{p}}^{\mathrm{t}} \cdot \partial_{\boldsymbol{f}_{\mathrm{p}}} \psi_{\mathrm{p}}|_{\boldsymbol{f}} \cdot \boldsymbol{f}_{\mathrm{p}}^{\mathrm{t}}$ has been made.

For the second family of stresses, we define the intermediate motion elastic Piola stress to take the format

$$\bar{\boldsymbol{\pi}}^{\mathrm{t}} := \partial_{\boldsymbol{f}_{\mathrm{e}}} \psi_t \,. \tag{2.66}$$

From eqs.(2.53,2.55) we additionally observe that the material motion elastic Cauchy stress then allows representation in energy momentum format

$$\bar{\boldsymbol{\Sigma}}^{\mathrm{t}} = \partial_{\boldsymbol{f}_{\mathrm{e}}} \psi_t \cdot \mathrm{cof}(\boldsymbol{F}_{\mathrm{e}}) = \psi_{\mathrm{p}}\, \boldsymbol{I}_{\mathrm{p}}^{\mathrm{t}} - \boldsymbol{F}_{\mathrm{e}}^{\mathrm{t}} \cdot \partial_{\boldsymbol{F}_{\mathrm{e}}} \psi_{\mathrm{p}} \,, \tag{2.67}$$

whereby use of the relation $\partial_{\boldsymbol{f}_{\mathrm{e}}} \psi_{\mathrm{p}} = -\, \boldsymbol{F}_{\mathrm{e}}^{\mathrm{t}} \cdot \partial_{\boldsymbol{F}_{\mathrm{e}}} \psi_{\mathrm{p}} \cdot \boldsymbol{F}_{\mathrm{e}}^{\mathrm{t}}$ has been made.

2.3.4 Comparison of the spatial, material, and intermediate motion problem

The main objective of the subsequent section consists in the derivation of relations between the previously introduced stresses. As point of departure, Piola and Cauchy stress tensors contributing to a balance of linear momentum representation in one and the same configuration,

Table 2.5: Transformations related to the Cauchy–type stresses $\boldsymbol{\sigma}^{\mathrm{t}} = \boldsymbol{\Pi}^{\mathrm{t}} \cdot \mathrm{cof}(\boldsymbol{f}) = \bar{\boldsymbol{\Pi}}^{\mathrm{t}} \cdot \mathrm{cof}(\boldsymbol{f}_{\mathrm{e}}) = \bar{\boldsymbol{\sigma}}^{\mathrm{t}}$, $\widetilde{\boldsymbol{\sigma}}^{\mathrm{t}} = \widetilde{\boldsymbol{\Pi}}^{\mathrm{t}} \cdot \mathrm{cof}(\boldsymbol{f}_{\mathrm{p}}) = \bar{\boldsymbol{\pi}}^{\mathrm{t}} \cdot \mathrm{cof}(\boldsymbol{F}_{\mathrm{e}}) = \bar{\boldsymbol{\Sigma}}^{\mathrm{t}}$, $\boldsymbol{\Sigma}^{\mathrm{t}} = \boldsymbol{\pi}^{\mathrm{t}} \cdot \mathrm{cof}(\boldsymbol{F})$ and $\widetilde{\boldsymbol{\Sigma}}^{\mathrm{t}} = \widetilde{\boldsymbol{\pi}}^{\mathrm{t}} \cdot \mathrm{cof}(\boldsymbol{F}_{\mathrm{p}})$.

	$\boldsymbol{\sigma}^{\mathrm{t}} \equiv \bar{\boldsymbol{\sigma}}^{\mathrm{t}}$	$\widetilde{\boldsymbol{\sigma}}^{\mathrm{t}} \equiv \bar{\boldsymbol{\Sigma}}^{\mathrm{t}}$	$\boldsymbol{\Sigma}^{\mathrm{t}}$	$\widetilde{\boldsymbol{\Sigma}}^{\mathrm{t}}$
$\boldsymbol{\Pi}^{\mathrm{t}}$	$\boldsymbol{\sigma}^{\mathrm{t}} \cdot \mathrm{cof}(\boldsymbol{F})$	$\psi_0\, \boldsymbol{f}^{\mathrm{t}} - \boldsymbol{f}^{\mathrm{t}}_{\mathrm{e}} \cdot \widetilde{\boldsymbol{\sigma}}^{\mathrm{t}} \cdot \mathrm{cof}(\boldsymbol{F}_{\mathrm{p}})$	$\psi_0\, \boldsymbol{f}^{\mathrm{t}} - \boldsymbol{f}^{\mathrm{t}} \cdot \boldsymbol{\Sigma}^{\mathrm{t}}$	$\boldsymbol{f}^{\mathrm{t}} \cdot \widetilde{\boldsymbol{\Sigma}}^{\mathrm{t}}$
$\bar{\boldsymbol{\Pi}}^{\mathrm{t}}$	$\boldsymbol{\sigma}^{\mathrm{t}} \cdot \mathrm{cof}(\boldsymbol{F}_{\mathrm{e}})$	$\psi_{\mathrm{p}}\, \boldsymbol{f}^{\mathrm{t}}_{\mathrm{e}} - \boldsymbol{f}^{\mathrm{t}}_{\mathrm{e}} \cdot \widetilde{\boldsymbol{\sigma}}^{\mathrm{t}}$	$\psi_{\mathrm{p}}\, \boldsymbol{f}^{\mathrm{t}}_{\mathrm{e}} - \boldsymbol{f}^{\mathrm{t}} \cdot \boldsymbol{\Sigma}^{\mathrm{t}} \cdot \mathrm{cof}(\boldsymbol{f}_{\mathrm{p}})$	$\boldsymbol{f}^{\mathrm{t}} \cdot \widetilde{\boldsymbol{\Sigma}}^{\mathrm{t}} \cdot \mathrm{cof}(\boldsymbol{f}_{\mathrm{p}})$
$\widetilde{\boldsymbol{\Pi}}^{\mathrm{t}}$	$\psi_0\, \boldsymbol{f}^{\mathrm{t}}_{\mathrm{p}} - \boldsymbol{F}^{\mathrm{t}}_{\mathrm{e}} \cdot \boldsymbol{\sigma}^{\mathrm{t}} \cdot \mathrm{cof}(\boldsymbol{F})$	$\widetilde{\boldsymbol{\sigma}}^{\mathrm{t}} \cdot \mathrm{cof}(\boldsymbol{F}_{\mathrm{p}})$	$\boldsymbol{f}^{\mathrm{t}}_{\mathrm{p}} \cdot \boldsymbol{\Sigma}^{\mathrm{t}}$	$\psi_0\, \boldsymbol{f}^{\mathrm{t}}_{\mathrm{p}} - \boldsymbol{f}^{\mathrm{t}}_{\mathrm{p}} \cdot \widetilde{\boldsymbol{\Sigma}}^{\mathrm{t}}$
$\boldsymbol{\pi}^{\mathrm{t}}$	$\psi_t\, \boldsymbol{F}^{\mathrm{t}} - \boldsymbol{F}^{\mathrm{t}} \cdot \boldsymbol{\sigma}^{\mathrm{t}}$	$\boldsymbol{F}^{\mathrm{t}}_{\mathrm{p}} \cdot \widetilde{\boldsymbol{\sigma}}^{\mathrm{t}} \cdot \mathrm{cof}(\boldsymbol{f}_{\mathrm{e}})$	$\boldsymbol{\Sigma}^{\mathrm{t}} \cdot \mathrm{cof}(\boldsymbol{f})$	$\psi_t\, \boldsymbol{F}^{\mathrm{t}} - \widetilde{\boldsymbol{\Sigma}}^{\mathrm{t}} \cdot \mathrm{cof}(\boldsymbol{f})$
$\widetilde{\boldsymbol{\pi}}^{\mathrm{t}}$	$\boldsymbol{F}^{\mathrm{t}} \cdot \boldsymbol{\sigma}^{\mathrm{t}} \cdot \mathrm{cof}(\boldsymbol{F}_{\mathrm{e}})$	$\psi_{\mathrm{p}}\, \boldsymbol{F}^{\mathrm{t}}_{\mathrm{p}} - \boldsymbol{F}^{\mathrm{t}}_{\mathrm{p}} \cdot \widetilde{\boldsymbol{\sigma}}^{\mathrm{t}}$	$\widetilde{\boldsymbol{\sigma}}^{\mathrm{t}} \cdot \mathrm{cof}(\boldsymbol{f}_{\mathrm{p}})$	$\widetilde{\boldsymbol{\Sigma}}^{\mathrm{t}} \cdot \mathrm{cof}(\boldsymbol{f}_{\mathrm{p}})$
$\bar{\boldsymbol{\pi}}^{\mathrm{t}}$	$\psi_t\, \boldsymbol{F}^{\mathrm{t}}_{\mathrm{e}} - \boldsymbol{F}^{\mathrm{t}}_{\mathrm{e}} \cdot \boldsymbol{\sigma}^{\mathrm{t}}$	$\widetilde{\boldsymbol{\sigma}}^{\mathrm{t}} \cdot \mathrm{cof}(\boldsymbol{F}_{\mathrm{e}})$	$\boldsymbol{f}^{\mathrm{t}}_{\mathrm{p}} \cdot \boldsymbol{\Sigma}^{\mathrm{t}} \cdot \mathrm{cof}(\boldsymbol{f})$	$\psi_t\, \boldsymbol{F}^{\mathrm{t}}_{\mathrm{e}} - \boldsymbol{f}^{\mathrm{t}}_{\mathrm{p}} \cdot \widetilde{\boldsymbol{\Sigma}}^{\mathrm{t}} \cdot \mathrm{cof}(\boldsymbol{f})$
$\boldsymbol{\sigma}^{\mathrm{t}}$	$\bullet$	$\psi_t\, \boldsymbol{I}^{\mathrm{t}}_t - \boldsymbol{f}^{\mathrm{t}}_{\mathrm{e}} \cdot \widetilde{\boldsymbol{\sigma}}^{\mathrm{t}} \cdot \mathrm{cof}(\boldsymbol{f}_{\mathrm{e}})$	$\psi_t\, \boldsymbol{I}^{\mathrm{t}}_t - \boldsymbol{f}^{\mathrm{t}} \cdot \boldsymbol{\Sigma}^{\mathrm{t}} \cdot \mathrm{cof}(\boldsymbol{f})$	$\boldsymbol{f}^{\mathrm{t}} \cdot \widetilde{\boldsymbol{\Sigma}}^{\mathrm{t}} \cdot \mathrm{cof}(\boldsymbol{f})$
$\widetilde{\boldsymbol{\sigma}}^{\mathrm{t}}$	$\psi_{\mathrm{p}}\, \boldsymbol{I}^{\mathrm{t}}_{\mathrm{p}} - \boldsymbol{F}^{\mathrm{t}}_{\mathrm{e}} \cdot \boldsymbol{\sigma}^{\mathrm{t}} \cdot \mathrm{cof}(\boldsymbol{F}_{\mathrm{e}})$	$\bullet$	$\boldsymbol{f}^{\mathrm{t}}_{\mathrm{p}} \cdot \boldsymbol{\Sigma}^{\mathrm{t}} \cdot \mathrm{cof}(\boldsymbol{f}_{\mathrm{p}})$	$\psi_{\mathrm{p}}\, \boldsymbol{I}^{\mathrm{t}}_{\mathrm{p}} - \boldsymbol{f}^{\mathrm{t}}_{\mathrm{p}} \cdot \widetilde{\boldsymbol{\Sigma}}^{\mathrm{t}} \cdot \mathrm{cof}(\boldsymbol{f}_{\mathrm{p}})$
$\boldsymbol{\Sigma}^{\mathrm{t}}$	$\psi_0\, \boldsymbol{I}^{\mathrm{t}}_0 - \boldsymbol{I}^{\mathrm{t}}_{\mathrm{p}} \cdot \boldsymbol{\sigma}^{\mathrm{t}} \cdot \mathrm{cof}(\boldsymbol{F})$	$\boldsymbol{F}^{\mathrm{t}}_{\mathrm{p}} \cdot \widetilde{\boldsymbol{\sigma}}^{\mathrm{t}} \cdot \mathrm{cof}(\boldsymbol{F}_{\mathrm{p}})$	$\bullet$	$\psi_0\, \boldsymbol{I}^{\mathrm{t}}_0 - \widetilde{\boldsymbol{\Sigma}}^{\mathrm{t}}$
$\widetilde{\boldsymbol{\Sigma}}^{\mathrm{t}}$	$\boldsymbol{F}^{\mathrm{t}} \cdot \boldsymbol{\sigma}^{\mathrm{t}} \cdot \mathrm{cof}(\boldsymbol{F})$	$\psi_0\, \boldsymbol{I}^{\mathrm{t}}_0 - \boldsymbol{F}^{\mathrm{t}}_{\mathrm{p}} \cdot \widetilde{\boldsymbol{\sigma}}^{\mathrm{t}} \cdot \mathrm{cof}(\boldsymbol{F}_{\mathrm{p}})$	$\psi_0\, \boldsymbol{I}^{\mathrm{t}}_0 - \boldsymbol{\Sigma}^{\mathrm{t}}$	$\bullet$

i.e. either the spatial, intermediate or material configuration, are compared. The corresponding energy momentum formats as well as correlated Piola stress tensors, are also addressed. Adhering to this procedure, some derivations are, apparently, repeated. For completeness, however, we prefer to apply this highly structured approach.

For convenience of the reader, tables 2.3–2.5 anticipate results by summarising transformations between representative stress tensors. Nevertheless, detailed derivations are discussed in the following.

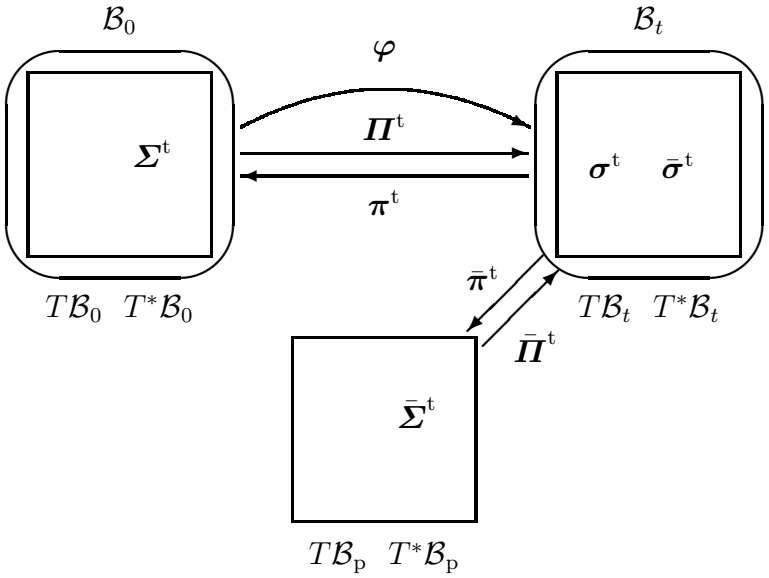

Figure 2.7: Total and elastic spatial motion stresses versus total and elastic material motion stresses.

2.3.4.1 Total and elastic spatial motion versus total and elastic material motion

First, we compare the spatial motion Piola stress tensors $\boldsymbol{\Pi}^{\mathrm{t}}$ and $\bar{\boldsymbol{\Pi}}^{\mathrm{t}}$ with the spatial motion Cauchy stresses $\boldsymbol{\sigma}^{\mathrm{t}}$ and $\bar{\boldsymbol{\sigma}}^{\mathrm{t}}$ as introduced in sections 2.3.1–2.3.3. The material motion counterparts $\boldsymbol{\pi}^{\mathrm{t}}$, $\bar{\boldsymbol{\pi}}^{\mathrm{t}}$ and $\boldsymbol{\Sigma}^{\mathrm{t}}$, $\bar{\boldsymbol{\Sigma}}^{\mathrm{t}}$ are also addressed, compare figure 2.7.

When placing emphasis on Piola–type stresses associated with the spatial motion problem but related to different Helmholtz free energy densities, we expect their relation to be determined via Piola transformations and consequently observe from eqs.(2.56,2.58,2.45)

$$\boldsymbol{\Pi}^{\mathrm{t}} = J_{\mathrm{p}}\, \partial_{\boldsymbol{F}} \psi_{\mathrm{p}}|_{\boldsymbol{F}_{\mathrm{p}}} = \bar{\boldsymbol{\Pi}}^{\mathrm{t}} \cdot \mathrm{cof}(\boldsymbol{F}_{\mathrm{p}}) = \bar{\boldsymbol{\sigma}}^{\mathrm{t}} \cdot \mathrm{cof}(\boldsymbol{F})\,, \tag{2.68}$$

whereby use of $\partial_{\boldsymbol{F}} W_{\{\bullet\}}|_{\boldsymbol{F}_{\mathrm{p}}} = \partial_{\boldsymbol{F}_{\mathrm{e}}} W_{\{\bullet\}} \cdot \boldsymbol{f}_{\mathrm{p}}^{\mathrm{t}}$ has been made. Based on the definitions in section 2.2.1, it thus turns out that the spatial motion Cauchy stress and the spatial motion elastic Cauchy stress coincide, i.e.

$$\boldsymbol{\sigma}^{\mathrm{t}} = \boldsymbol{\Pi}^{\mathrm{t}} \cdot \mathrm{cof}(\boldsymbol{f}) = \bar{\boldsymbol{\Pi}}^{\mathrm{t}} \cdot \mathrm{cof}(\boldsymbol{f}_{\mathrm{e}}) = \bar{\boldsymbol{\sigma}}^{\mathrm{t}}\,. \tag{2.69}$$

The relations of the spatial motion Cauchy stresses to the material and intermediate motion Piola stresses, however, take the common configurational format. For the material motion problem, eqs.(2.57,2.60,2.61) render

$$\boldsymbol{\sigma}^{\mathrm{t}} = \psi_t\, \boldsymbol{I}_t^{\mathrm{t}} - \boldsymbol{f}^{\mathrm{t}} \cdot \boldsymbol{\pi}^{\mathrm{t}} = \psi_t\, \boldsymbol{I}_t^{\mathrm{t}} - \boldsymbol{f}^{\mathrm{t}} \cdot \boldsymbol{\Sigma}^{\mathrm{t}} \cdot \mathrm{cof}(\boldsymbol{f})\,. \tag{2.70}$$

It is then straightforward to derive the relations

$$\boldsymbol{\Pi}^{\mathrm{t}} = \psi_0\, \boldsymbol{f}^{\mathrm{t}} - \boldsymbol{f}^{\mathrm{t}} \cdot \boldsymbol{\pi}^{\mathrm{t}} \cdot \mathrm{cof}(\boldsymbol{F}) = \psi_0\, \boldsymbol{f}^{\mathrm{t}} - \boldsymbol{f}^{\mathrm{t}} \cdot \boldsymbol{\Sigma}^{\mathrm{t}} \tag{2.71}$$

and

$$\bar{\boldsymbol{\Pi}}^{\mathrm{t}} = \psi_{\mathrm{p}}\, \boldsymbol{f}_{\mathrm{e}}^{\mathrm{t}} - \boldsymbol{f}^{\mathrm{t}} \cdot \boldsymbol{\pi}^{\mathrm{t}} \cdot \mathrm{cof}(\boldsymbol{F}_{\mathrm{e}}) = \psi_{\mathrm{p}}\, \boldsymbol{f}_{\mathrm{e}}^{\mathrm{t}} - \boldsymbol{f}^{\mathrm{t}} \cdot \boldsymbol{\Sigma}^{\mathrm{t}} \cdot \mathrm{cof}(\boldsymbol{f}_{\mathrm{p}}) \tag{2.72}$$

from eq.(2.69). For the intermediate motion problem, eqs.(2.59,2.66,2.67) and eq.(2.69) lead to

$$\bar{\boldsymbol{\sigma}}^{\mathrm{t}} = \psi_t\, \boldsymbol{I}_t^{\mathrm{t}} - \boldsymbol{f}_{\mathrm{e}}^{\mathrm{t}} \cdot \bar{\boldsymbol{\pi}}^{\mathrm{t}} = \psi_t\, \boldsymbol{I}_t^{\mathrm{t}} - \boldsymbol{f}_{\mathrm{e}}^{\mathrm{t}} \cdot \bar{\boldsymbol{\Sigma}}^{\mathrm{t}} \cdot \mathrm{cof}(\boldsymbol{f}_{\mathrm{e}})\,. \tag{2.73}$$

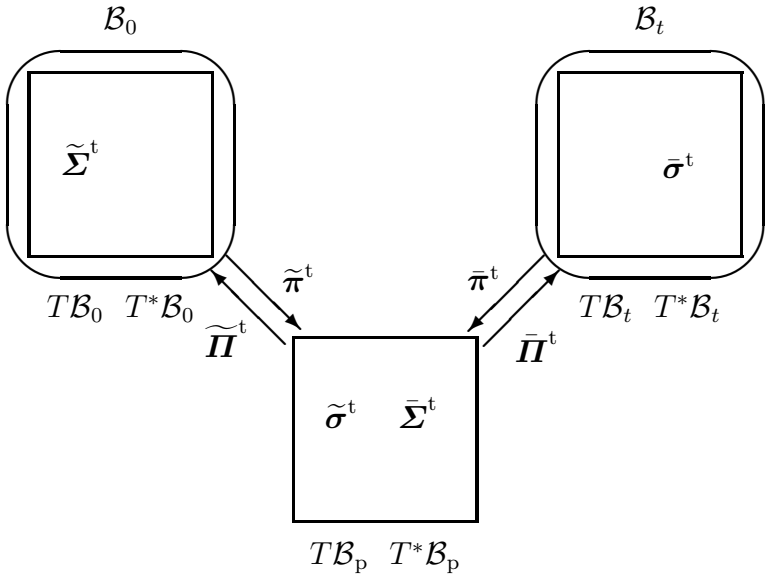

Figure 2.8: Plastic and elastic intermediate motion stresses versus plastic material and elastic spatial motion stresses.

It is then straightforward to derive the relations

$$\boldsymbol{\Pi}^{\mathrm{t}} = \psi_0\, \boldsymbol{f}^{\mathrm{t}} - \boldsymbol{f}_{\mathrm{e}}^{\mathrm{t}} \cdot \bar{\boldsymbol{\pi}}^{\mathrm{t}} \cdot \mathrm{cof}(\boldsymbol{F}) = \psi_0\, \boldsymbol{f}^{\mathrm{t}} - \boldsymbol{f}_{\mathrm{e}}^{\mathrm{t}} \cdot \bar{\boldsymbol{\Sigma}}^{\mathrm{t}} \cdot \mathrm{cof}(\boldsymbol{F}_{\mathrm{p}}) \tag{2.74}$$

and

$$\bar{\boldsymbol{\Pi}}^{\mathrm{t}} = \psi_{\mathrm{p}}\, \boldsymbol{f}_{\mathrm{e}}^{\mathrm{t}} - \boldsymbol{f}_{\mathrm{e}}^{\mathrm{t}} \cdot \bar{\boldsymbol{\pi}}^{\mathrm{t}} \cdot \mathrm{cof}(\boldsymbol{F}_{\mathrm{e}}) = \psi_{\mathrm{p}}\, \boldsymbol{f}_{\mathrm{e}}^{\mathrm{t}} - \boldsymbol{f}_{\mathrm{e}}^{\mathrm{t}} \cdot \bar{\boldsymbol{\Sigma}}^{\mathrm{t}}\,. \tag{2.75}$$

from eq.(2.69). Moreover, the comparison of eqs.(2.68,2.69) with eqs.(2.70–2.72) and eqs.(2.73–2.75) results in

$$\boldsymbol{\pi}^{\mathrm{t}} = \boldsymbol{F}_{\mathrm{p}}^{\mathrm{t}} \cdot \bar{\boldsymbol{\pi}}^{\mathrm{t}} \quad \text{and} \quad \boldsymbol{\Sigma}^{\mathrm{t}} = \boldsymbol{F}_{\mathrm{p}}^{\mathrm{t}} \cdot \bar{\boldsymbol{\Sigma}}^{\mathrm{t}} \cdot \mathrm{cof}(\boldsymbol{F}_{\mathrm{p}}) = \boldsymbol{\pi}^{\mathrm{t}} \cdot \mathrm{cof}(\boldsymbol{F})\,. \tag{2.76}$$

Note that $\boldsymbol{\pi}^{\mathrm{t}}$ and $\bar{\boldsymbol{\pi}}^{\mathrm{t}}$ are defined with respect to the same Helmholtz free energy density and consequently transform via a tangent map and not via a Piola transformation, the alternative derivation consequently reads

$$\boldsymbol{\pi}^{\mathrm{t}} = \partial_{\boldsymbol{f}} \psi_t|_{\boldsymbol{f}_{\mathrm{p}}} = \boldsymbol{F}_{\mathrm{p}}^{\mathrm{t}} \cdot \partial_{\boldsymbol{f}_{\mathrm{e}}} \psi_t = \boldsymbol{F}_{\mathrm{p}}^{\mathrm{t}} \cdot \bar{\boldsymbol{\pi}}^{\mathrm{t}}\,. \tag{2.77}$$

and verifies eq.(2.76). Furthermore, the considerations above are in line with derivations in finite elasticity since the intermediate configuration allows interpretation as a stress–free reference configuration.

2.3.4.2 Plastic and elastic intermediate motion versus plastic material and elastic spatial motion

Second, we compare the intermediate motion plastic and elastic Piola stresses $\widetilde{\boldsymbol{\Pi}}^{\mathrm{t}}$ and $\bar{\boldsymbol{\pi}}^{\mathrm{t}}$ with the intermediate motion plastic and elastic Cauchy stresses $\widetilde{\boldsymbol{\sigma}}^{\mathrm{t}}$ and $\bar{\boldsymbol{\Sigma}}^{\mathrm{t}}$ as introduced in sections 2.3.1–2.3.3. The spatial and material motion counterparts $\bar{\boldsymbol{\Pi}}^{\mathrm{t}}$, $\widetilde{\boldsymbol{\pi}}^{\mathrm{t}}$ and $\bar{\boldsymbol{\sigma}}^{\mathrm{t}}$, $\widetilde{\boldsymbol{\Sigma}}^{\mathrm{t}}$ are also addressed, compare figure 2.8.

When placing emphasis on Piola–type stresses associated with the intermediate motion problem but related to different Helmholtz free energy densities, we expect their relation to be determined via Piola transformations and consequently observe from eqs.(2.64,2.66,2.53)

$$\widetilde{\boldsymbol{\Pi}}^{\mathrm{t}} = J\, \partial_{\boldsymbol{F}_{\mathrm{p}}} \psi_t|_{\boldsymbol{F}} = \bar{\boldsymbol{\pi}}^{\mathrm{t}} \cdot \mathrm{cof}(\boldsymbol{F}) = \bar{\boldsymbol{\Sigma}}^{\mathrm{t}} \cdot \mathrm{cof}(\boldsymbol{F}_{\mathrm{p}})\,, \tag{2.78}$$

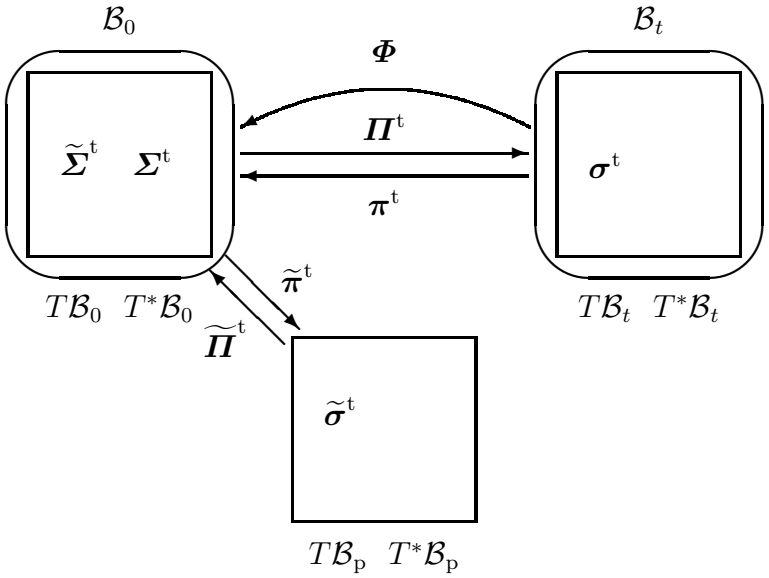

Figure 2.9: Plastic and total material motion stresses versus plastic and total spatial motion stresses.

whereby use of $\partial_{\boldsymbol{F}_{\mathrm{p}}} W_{\{\bullet\}}|_{\boldsymbol{F}} = \partial_{\boldsymbol{f}_{\mathrm{e}}} W_{\{\bullet\}} \cdot \boldsymbol{f}^{\mathrm{t}}$ has been made. Based on the definitions in section 2.2.3, it thus turns out that the intermediate motion plastic Cauchy stress and the intermediate motion elastic Cauchy stress coincide, i.e.

$$\widetilde{\boldsymbol{\sigma}}^{\mathrm{t}} = \widetilde{\boldsymbol{\Pi}}^{\mathrm{t}} \cdot \mathrm{cof}(\boldsymbol{f}_{\mathrm{p}}) = \bar{\boldsymbol{\pi}}^{\mathrm{t}} \cdot \mathrm{cof}(\boldsymbol{F}_{\mathrm{e}}) = \bar{\boldsymbol{\Sigma}}^{\mathrm{t}} \,. \tag{2.79}$$

The relations of the intermediate motion stress tensor to the elastic spatial and the plastic material motion stresses, however, take the common configurational format. For the material motion problem, eqs.(2.65,2.62,2.63) render

$$\widetilde{\boldsymbol{\sigma}}^{\mathrm{t}} = \psi_{\mathrm{p}}\, \boldsymbol{I}^{\mathrm{t}}_{\mathrm{p}} - \boldsymbol{f}^{\mathrm{t}}_{\mathrm{p}} \cdot \widetilde{\boldsymbol{\pi}}^{\mathrm{t}} = \psi_{\mathrm{p}}\, \boldsymbol{I}^{\mathrm{t}}_{\mathrm{p}} - \boldsymbol{f}^{\mathrm{t}}_{\mathrm{p}} \cdot \widetilde{\boldsymbol{\Sigma}}^{\mathrm{t}} \cdot \mathrm{cof}(\boldsymbol{f}_{\mathrm{p}}) \,. \tag{2.80}$$

It is then straightforward to derive the relations

$$\widetilde{\boldsymbol{\Pi}}^{\mathrm{t}} = \psi_0\, \boldsymbol{f}^{\mathrm{t}}_{\mathrm{p}} - \boldsymbol{f}^{\mathrm{t}}_{\mathrm{p}} \cdot \widetilde{\boldsymbol{\pi}}^{\mathrm{t}} \cdot \mathrm{cof}(\boldsymbol{F}_{\mathrm{p}}) = \psi_0\, \boldsymbol{f}^{\mathrm{t}}_{\mathrm{p}} - \boldsymbol{f}^{\mathrm{t}}_{\mathrm{p}} \cdot \widetilde{\boldsymbol{\Sigma}}^{\mathrm{t}} \tag{2.81}$$

and

$$\bar{\boldsymbol{\pi}}^{\mathrm{t}} = \psi_t\, \boldsymbol{F}^{\mathrm{t}}_{\mathrm{e}} - \boldsymbol{f}^{\mathrm{t}}_{\mathrm{p}} \cdot \widetilde{\boldsymbol{\pi}}^{\mathrm{t}} \cdot \mathrm{cof}(\boldsymbol{f}_{\mathrm{e}}) = \psi_t\, \boldsymbol{F}^{\mathrm{t}}_{\mathrm{e}} - \boldsymbol{f}^{\mathrm{t}}_{\mathrm{p}} \cdot \widetilde{\boldsymbol{\Sigma}}^{\mathrm{t}} \cdot \mathrm{cof}(\boldsymbol{f}) \tag{2.82}$$

from eq.(2.79). For the spatial motion problem, eqs.(2.67,2.58,2.59) and eq.(2.78) lead to

$$\bar{\boldsymbol{\Sigma}}^{\mathrm{t}} = \psi_{\mathrm{p}}\, \boldsymbol{I}^{\mathrm{t}}_{\mathrm{p}} - \boldsymbol{F}^{\mathrm{t}}_{\mathrm{e}} \cdot \bar{\boldsymbol{\Pi}}^{\mathrm{t}} = \psi_{\mathrm{p}}\, \boldsymbol{I}^{\mathrm{t}}_{\mathrm{p}} - \boldsymbol{F}^{\mathrm{t}}_{\mathrm{e}} \cdot \bar{\boldsymbol{\sigma}}^{\mathrm{t}} \cdot \mathrm{cof}(\boldsymbol{F}_{\mathrm{e}}) \,. \tag{2.83}$$

It is then straightforward to derive the relations

$$\widetilde{\boldsymbol{\Pi}}^{\mathrm{t}} = \psi_0\, \boldsymbol{f}^{\mathrm{t}}_{\mathrm{p}} - \boldsymbol{F}^{\mathrm{t}}_{\mathrm{e}} \cdot \bar{\boldsymbol{\Pi}}^{\mathrm{t}} \cdot \mathrm{cof}(\boldsymbol{F}_{\mathrm{p}}) = \psi_0\, \boldsymbol{f}^{\mathrm{t}}_{\mathrm{p}} - \boldsymbol{F}^{\mathrm{t}}_{\mathrm{e}} \cdot \bar{\boldsymbol{\sigma}}^{\mathrm{t}} \cdot \mathrm{cof}(\boldsymbol{F}) \tag{2.84}$$

and

$$\bar{\boldsymbol{\pi}}^{\mathrm{t}} = \psi_t\, \boldsymbol{F}^{\mathrm{t}}_{\mathrm{e}} - \boldsymbol{F}^{\mathrm{t}}_{\mathrm{e}} \cdot \bar{\boldsymbol{\Pi}}^{\mathrm{t}} \cdot \mathrm{cof}(\boldsymbol{f}_{\mathrm{e}}) = \psi_t\, \boldsymbol{F}^{\mathrm{t}}_{\mathrm{e}} - \boldsymbol{F}^{\mathrm{t}}_{\mathrm{e}} \cdot \bar{\boldsymbol{\sigma}}^{\mathrm{t}} \tag{2.85}$$

from eq.(2.79). Moreover, the comparison of eqs.(2.78,2.79) with eqs.(2.80–2.82) and eqs.(2.83–2.85) results in

$$\widetilde{\boldsymbol{\pi}}^{\mathrm{t}} = \boldsymbol{F}^{\mathrm{t}} \cdot \bar{\boldsymbol{\Pi}}^{\mathrm{t}} \quad \text{and} \quad \widetilde{\boldsymbol{\Sigma}}^{\mathrm{t}} = \boldsymbol{F}^{\mathrm{t}} \cdot \bar{\boldsymbol{\sigma}}^{\mathrm{t}} \cdot \mathrm{cof}(\boldsymbol{F}) = \widetilde{\boldsymbol{\pi}}^{\mathrm{t}} \cdot \mathrm{cof}(\boldsymbol{F}_{\mathrm{p}}) \,. \tag{2.86}$$

Note that $\widetilde{\boldsymbol{\pi}}^{\mathrm{t}}$ and $\bar{\boldsymbol{\Pi}}^{\mathrm{t}}$ are defined with respect to the same Helmholtz free energy density and consequently transform via a tangent map and not via a Piola transformation, the alternative derivation consequently reads

$$\widetilde{\boldsymbol{\pi}}^{\mathrm{t}} = \partial_{\boldsymbol{f}_{\mathrm{p}}} \psi_{\mathrm{p}}|_{\boldsymbol{f}} = \boldsymbol{F}^{\mathrm{t}} \cdot \partial_{\boldsymbol{F}_{\mathrm{e}}} \psi_{\mathrm{p}} = \boldsymbol{F}^{\mathrm{t}} \cdot \bar{\boldsymbol{\Pi}}^{\mathrm{t}} \,. \tag{2.87}$$

and verifies eq.(2.86).

2.3.4.3 Plastic and total material motion versus plastic and total spatial motion

Third, we compare the material motion plastic and total Piola stress tensors $\widetilde{\boldsymbol{\pi}}^{\mathrm{t}}$ and $\boldsymbol{\pi}^{\mathrm{t}}$ with the material motion plastic and total Cauchy stresses $\widetilde{\boldsymbol{\Sigma}}^{\mathrm{t}}$ and $\boldsymbol{\Sigma}^{\mathrm{t}}$ as introduced in sections 2.3.1–2.3.3. The intermediate and spatial motion counterparts $\widetilde{\boldsymbol{\Pi}}^{\mathrm{t}}$, $\boldsymbol{\Pi}^{\mathrm{t}}$ and $\widetilde{\boldsymbol{\sigma}}^{\mathrm{t}}$, $\boldsymbol{\sigma}^{\mathrm{t}}$ are also addressed, compare figure 2.9.

When placing emphasis on Piola–type stresses associated with the material motion problem but related to different Helmholtz free energy densities, we expect their relation to be determined via Piola transformations. For the problem at hand, however, it is not the elastic distortion which serves as a dual quantity for one of the considered Piola–type stresses; consequently we observe from eqs.(2.62,2.60,2.47)

$$\begin{aligned} \widetilde{\boldsymbol{\pi}}^{\mathrm{t}} &= \partial_{\boldsymbol{f}_{\mathrm{p}}} (\, j_{\mathrm{p}}\, \psi_0 \,)|_{\boldsymbol{f}} \\ &= \psi_{\mathrm{p}}\, \boldsymbol{F}_{\mathrm{p}}^{\mathrm{t}} + J_{\mathrm{e}}\, \partial_{\boldsymbol{f}_{\mathrm{p}}} \psi_t|_{\boldsymbol{f}} \quad = \psi_{\mathrm{p}}\, \boldsymbol{F}_{\mathrm{p}}^{\mathrm{t}} - \partial_{\boldsymbol{f}} \psi_t|_{\boldsymbol{f}_{\mathrm{p}}} \cdot \mathrm{cof}(\boldsymbol{F}_{\mathrm{e}}) \\ &= \psi_{\mathrm{p}}\, \boldsymbol{F}_{\mathrm{p}}^{\mathrm{t}} - \boldsymbol{\pi}^{\mathrm{t}} \cdot \mathrm{cof}(\boldsymbol{F}_{\mathrm{e}}) \;=\; \psi_{\mathrm{p}}\, \boldsymbol{F}_{\mathrm{p}}^{\mathrm{t}} - \boldsymbol{\Sigma}^{\mathrm{t}} \cdot \mathrm{cof}(\boldsymbol{f}_{\mathrm{p}}) \,, \end{aligned} \tag{2.88}$$

whereby use of $\partial_{\boldsymbol{f}_{\mathrm{p}}} \psi_t|_{\boldsymbol{f}} = \boldsymbol{F}^{\mathrm{t}} \cdot \partial_{\boldsymbol{F}_{\mathrm{e}}} \psi_t$ and $\partial_{\boldsymbol{f}} \psi_t|_{\boldsymbol{f}_{\mathrm{p}}} = -\, \boldsymbol{F}^{\mathrm{t}} \cdot \partial_{\boldsymbol{F}_{\mathrm{e}}} \psi_t \cdot \boldsymbol{F}_{\mathrm{e}}^{\mathrm{t}}$ has been made so that

$$\partial_{\boldsymbol{f}_{\mathrm{p}}} \psi_t|_{\boldsymbol{f}} = -\, \partial_{\boldsymbol{f}} \psi_t|_{\boldsymbol{f}_{\mathrm{p}}} \cdot \boldsymbol{f}_{\mathrm{e}}^{\mathrm{t}} \,. \tag{2.89}$$

Based on the definitions in section 2.2.2 and eq.(2.88), it thus turns out that the material motion plastic and total Cauchy stress do not coincide, i.e.

$$\widetilde{\boldsymbol{\Sigma}}^{\mathrm{t}} = \widetilde{\boldsymbol{\pi}}^{\mathrm{t}} \cdot \mathrm{cof}(\boldsymbol{F}_{\mathrm{p}}) = \psi_0\, \boldsymbol{I}_0^{\mathrm{t}} - \boldsymbol{\pi}^{\mathrm{t}} \cdot \mathrm{cof}(\boldsymbol{F}) = \psi_0\, \boldsymbol{I}_0^{\mathrm{t}} - \boldsymbol{\Sigma}^{\mathrm{t}} \,. \tag{2.90}$$

The relations of the material motion stresses to the corresponding spatial motion stresses, however, take the common configurational format besides a Piola–type transformation. For the intermediate motion problem, eqs.(2.63,2.64,2.65) render

$$\widetilde{\boldsymbol{\Sigma}}^{\mathrm{t}} = \psi_0\, \boldsymbol{I}_0^{\mathrm{t}} - \boldsymbol{F}_{\mathrm{p}}^{\mathrm{t}} \cdot \widetilde{\boldsymbol{\Pi}}^{\mathrm{t}} = \psi_0\, \boldsymbol{I}_0^{\mathrm{t}} - \boldsymbol{F}_{\mathrm{p}}^{\mathrm{t}} \cdot \widetilde{\boldsymbol{\sigma}}^{\mathrm{t}} \cdot \mathrm{cof}(\boldsymbol{F}_{\mathrm{p}}) \,. \tag{2.91}$$

It is then straightforward to derive the relations

$$\widetilde{\boldsymbol{\pi}}^{\mathrm{t}} = \psi_{\mathrm{p}}\, \boldsymbol{F}_{\mathrm{p}}^{\mathrm{t}} - \boldsymbol{F}_{\mathrm{p}}^{\mathrm{t}} \cdot \widetilde{\boldsymbol{\Pi}}^{\mathrm{t}} \cdot \mathrm{cof}(\boldsymbol{f}_{\mathrm{p}}) = \psi_{\mathrm{p}}\, \boldsymbol{F}_{\mathrm{p}}^{\mathrm{t}} - \boldsymbol{F}_{\mathrm{p}}^{\mathrm{t}} \cdot \widetilde{\boldsymbol{\sigma}}^{\mathrm{t}} \tag{2.92}$$

and

$$\boldsymbol{\pi}^{\mathrm{t}} = \boldsymbol{F}_{\mathrm{p}}^{\mathrm{t}} \cdot \widetilde{\boldsymbol{\Pi}}^{\mathrm{t}} \cdot \mathrm{cof}(\boldsymbol{f}) = \boldsymbol{F}_{\mathrm{p}}^{\mathrm{t}} \cdot \widetilde{\boldsymbol{\sigma}}^{\mathrm{t}} \cdot \mathrm{cof}(\boldsymbol{f}_{\mathrm{e}}) \tag{2.93}$$

from eq.(2.90). For the spatial motion problem, eqs.(2.61,2.56,2.57) and eq.(2.88) lead to

$$\boldsymbol{\Sigma}^{\mathrm{t}} = \psi_0\, \boldsymbol{I}_0^{\mathrm{t}} - \boldsymbol{F}^{\mathrm{t}} \cdot \boldsymbol{\Pi}^{\mathrm{t}} = \psi_0\, \boldsymbol{I}_0^{\mathrm{t}} - \boldsymbol{F}^{\mathrm{t}} \cdot \boldsymbol{\sigma}^{\mathrm{t}} \cdot \mathrm{cof}(\boldsymbol{F}) \,. \tag{2.94}$$

It is then straightforward to derive the relations

$$\widetilde{\boldsymbol{\pi}}^{\mathrm{t}} = \boldsymbol{F}^{\mathrm{t}} \cdot \boldsymbol{\Pi}^{\mathrm{t}} \cdot \mathrm{cof}(\boldsymbol{f}_{\mathrm{p}}) = \boldsymbol{F}^{\mathrm{t}} \cdot \boldsymbol{\sigma}^{\mathrm{t}} \cdot \mathrm{cof}(\boldsymbol{F}_{\mathrm{e}}) \tag{2.95}$$

and

$$\boldsymbol{\pi}^{\mathrm{t}} = \psi_t\, \boldsymbol{F}^{\mathrm{t}} - \boldsymbol{F}^{\mathrm{t}} \cdot \boldsymbol{\Pi}^{\mathrm{t}} \cdot \mathrm{cof}(\boldsymbol{f}) = \psi_t\, \boldsymbol{F}^{\mathrm{t}} - \boldsymbol{F}^{\mathrm{t}} \cdot \boldsymbol{\sigma}^{\mathrm{t}} \tag{2.96}$$

from eq.(2.90). Moreover, the comparison of eqs.(2.88,2.90) with eqs.(2.91–2.93) and eqs.(2.94–2.96) results in

$$\widetilde{\boldsymbol{\Pi}}^{\mathrm{t}} = \psi_0\, \boldsymbol{f}_{\mathrm{p}}^{\mathrm{t}} - \boldsymbol{F}_{\mathrm{e}}^{\mathrm{t}} \cdot \boldsymbol{\Pi}^{\mathrm{t}} \quad \text{and} \quad \widetilde{\boldsymbol{\sigma}}^{\mathrm{t}} = \psi_{\mathrm{p}}\, \boldsymbol{I}_{\mathrm{p}}^{\mathrm{t}} - \boldsymbol{F}_{\mathrm{e}}^{\mathrm{t}} \cdot \boldsymbol{\sigma}^{\mathrm{t}} \cdot \mathrm{cof}(\boldsymbol{F}_{\mathrm{e}}) = \bar{\boldsymbol{\pi}}^{\mathrm{t}} \cdot \mathrm{cof}(\boldsymbol{F}_{\mathrm{e}})\,. \tag{2.97}$$

Note that $\widetilde{\boldsymbol{\Pi}}^{\mathrm{t}}$ and $\boldsymbol{\Pi}^{\mathrm{t}}$ are defined with respect to one and the same Helmholtz free energy density but transform by analogy to eq.(2.88); the alternative derivation consequently reads

$$\begin{aligned} \widetilde{\boldsymbol{\Pi}}^{\mathrm{t}} &= \partial_{\boldsymbol{F}_{\mathrm{p}}}(\, J_{\mathrm{p}}\, \psi_{\mathrm{p}}\,)|_{\boldsymbol{F}} \\ &= \psi_0\, \boldsymbol{f}_{\mathrm{p}}^{\mathrm{t}} + J_{\mathrm{p}}\, \partial_{\boldsymbol{F}_{\mathrm{p}}} \psi_{\mathrm{p}}|_{\boldsymbol{F}} = \psi_0\, \boldsymbol{f}_{\mathrm{p}}^{\mathrm{t}} - \boldsymbol{F}_{\mathrm{e}}^{\mathrm{t}} \cdot \partial_{\boldsymbol{F}} \psi_0|_{\boldsymbol{F}_{\mathrm{p}}} \\ &= \psi_0\, \boldsymbol{f}_{\mathrm{p}}^{\mathrm{t}} - \boldsymbol{F}_{\mathrm{e}}^{\mathrm{t}} \cdot \boldsymbol{\Pi}^{\mathrm{t}} \quad = \psi_0\, \boldsymbol{f}_{\mathrm{p}}^{\mathrm{t}} - \boldsymbol{F}_{\mathrm{e}}^{\mathrm{t}} \cdot \boldsymbol{\sigma}^{\mathrm{t}} \cdot \mathrm{cof}(\boldsymbol{F}) \end{aligned} \tag{2.98}$$

and verifies eq.(2.97), whereby use of $\partial_{\boldsymbol{F}_{\mathrm{p}}} \psi_{\mathrm{p}}|_{\boldsymbol{F}} = -\,\boldsymbol{F}_{\mathrm{e}}^{\mathrm{t}} \cdot \partial_{\boldsymbol{F}_{\mathrm{e}}} \psi_{\mathrm{p}} \cdot \boldsymbol{f}_{\mathrm{p}}^{\mathrm{t}}$ and $\partial_{\boldsymbol{F}} \psi_{\mathrm{p}}|_{\boldsymbol{F}_{\mathrm{p}}} = \partial_{\boldsymbol{F}_{\mathrm{e}}} \psi_{\mathrm{p}} \cdot \boldsymbol{f}_{\mathrm{p}}^{\mathrm{t}}$ has been made so that

$$\partial_{\boldsymbol{F}_{\mathrm{p}}} \psi_{\mathrm{p}}|_{\boldsymbol{F}} = -\,\boldsymbol{F}_{\mathrm{e}}^{\mathrm{t}} \cdot \partial_{\boldsymbol{F}} \psi_{\mathrm{p}}|_{\boldsymbol{F}_{\mathrm{p}}}\,. \tag{2.99}$$

According to the fact that $\boldsymbol{\Sigma}^{\mathrm{t}} \neq \widetilde{\boldsymbol{\Sigma}}^{\mathrm{t}}$, which is in contrast to the previous elaborations in sections 2.3.4.1 and 2.3.4.2 where $\boldsymbol{\sigma}^{\mathrm{t}} \equiv \bar{\boldsymbol{\sigma}}^{\mathrm{t}}$ and $\widetilde{\boldsymbol{\sigma}}^{\mathrm{t}} \equiv \bar{\boldsymbol{\Sigma}}^{\mathrm{t}}$, we finally mention the interesting relations

$$\begin{aligned} \widetilde{\boldsymbol{\Sigma}}^{\mathrm{t}} &= \boldsymbol{F}^{\mathrm{t}} \cdot \boldsymbol{\Pi}^{\mathrm{t}}\,, & \boldsymbol{\Sigma}^{\mathrm{t}} &= \boldsymbol{F}_{\mathrm{p}}^{\mathrm{t}} \cdot \widetilde{\boldsymbol{\Pi}}^{\mathrm{t}}\,, \\ \widetilde{\boldsymbol{\Sigma}}^{\mathrm{t}} &= \boldsymbol{F}^{\mathrm{t}} \cdot \bar{\boldsymbol{\Pi}}^{\mathrm{t}} \cdot \mathrm{cof}(\boldsymbol{F}_{\mathrm{p}})\,, & \boldsymbol{\Sigma}^{\mathrm{t}} &= \boldsymbol{F}_{\mathrm{p}}^{\mathrm{t}} \cdot \bar{\boldsymbol{\pi}}^{\mathrm{t}} \cdot \mathrm{cof}(\boldsymbol{F}) \end{aligned} \tag{2.100}$$

which directly follow from eq.(2.90).

Remark 2.3.1 *Apparently, the derived set of stress tensors is by far not complete in the sense that further stress tensors are frequently applied in continuum mechanics and theory of materials – for instance Kirchhoff– and Mandel–type stress tensors. With the relations summarised in tables 2.3–2.5 at hand, however, the derivation of these additional stresses becomes obvious. In this regard, we consider the elaborated stress tensors as essential quantities which serve as a platform to examine other stresses as well. For the sake of clarity, we do not place emphasis on the illustration of further stresses since these tensors would not yield any additional (physical) inside for the problem at hand.*

Remark 2.3.2 *A similar modelling concept as the multiplicative decomposition, which is adopted in this work, was pioneered by Noll and is often denoted as a material isomorphism or a local rearrangement; see the introduction of this chapter and section 1.1: let* $\boldsymbol{k} : T\mathcal{B}_0 \rightarrow T\mathcal{B}_{\mathrm{k}}$ *with* $j_{\mathrm{k}} = \det(\boldsymbol{k}) > 0$ *characterise this mapping such that the Helmholtz free energy density is defined by means of* $\psi_0 = j_{\mathrm{k}}\, \psi_{\mathrm{k}}(\boldsymbol{F} \cdot \boldsymbol{k}^{-1}; \boldsymbol{X})$*. When identifying* $\boldsymbol{k}$ *with* $\boldsymbol{F}_{\mathrm{p}}$ *it is straightforward to introduce dislocation density tensors in terms of* $\nabla^{\mathrm{t}}_{\boldsymbol{X}} \times \boldsymbol{k}$*. The incorporation of* $\nabla^{\mathrm{t}}_{\boldsymbol{x}} \times (\boldsymbol{k} \cdot \boldsymbol{f})$*, however, is commonly not addressed.*

Remark 2.3.3 *Even though we have not placed any emphasis on dissipation inequalities so far, the introduced hyperelastic stress formats are apparently based on the well–established Coleman–Noll entropy principle. To give an example, we consider the isothermal representation of the Clausius–Duhem inequality and set up a hyperelastic format for, for example, the total spatial motion Piola stress. In this regard, the dissipation inequality reads*

$$\mathsf{D}_0 = \boldsymbol{\Pi}^{\mathrm{t}} : \mathrm{D}_t \boldsymbol{F} - \mathrm{D}_t \psi_0 - \boldsymbol{b}_0^{\mathrm{int}} \cdot \boldsymbol{v} = J_{\mathrm{p}}\, \mathsf{D}_{\mathrm{p}} = J\, \mathsf{D}_t \geq 0\,, \tag{2.101}$$

compare eq.(2.55), from which we derive the relation

$$\begin{aligned}
\mathsf{D}_{\mathrm{p}} &= j_{\mathrm{p}} \, [\quad \boldsymbol{\Pi}^{\mathrm{t}} \, - \, \partial_{\boldsymbol{F}} \psi_0|_{\boldsymbol{F}_{\mathrm{p}}} \qquad] : \quad \mathrm{D}_t \boldsymbol{F} - j_{\mathrm{p}} \, \partial_{\boldsymbol{F}_{\mathrm{p}}} \psi_0|_{\boldsymbol{F}} : \mathrm{D}_t \boldsymbol{F}_{\mathrm{p}} \\
&= - \, [\, \psi_{\mathrm{p}} \, \boldsymbol{f}_{\mathrm{p}}^{\mathrm{t}} \, + \, \partial_{\boldsymbol{F}_{\mathrm{p}}} \psi_{\mathrm{p}}|_{\boldsymbol{F}} \qquad] : \quad \mathrm{D}_t \boldsymbol{F}_{\mathrm{p}} \\
&= - \, [\, \psi_{\mathrm{p}} \, \boldsymbol{I}_{\mathrm{p}}^{\mathrm{t}} \, + \, \partial_{\boldsymbol{F}_{\mathrm{p}}} \psi_{\mathrm{p}}|_{\boldsymbol{F}} \cdot \boldsymbol{F}_{\mathrm{p}}^{\mathrm{t}} \,] : [\, \mathrm{D}_t \boldsymbol{F}_{\mathrm{p}} \cdot \boldsymbol{f}_{\mathrm{p}} \,] \\
&= - \, [\, \psi_{\mathrm{p}} \, \boldsymbol{I}_{\mathrm{p}}^{\mathrm{t}} \, - \, \boldsymbol{f}_{\mathrm{p}}^{\mathrm{t}} \cdot \partial_{\boldsymbol{f}_{\mathrm{p}}} \psi_{\mathrm{p}}|_{\boldsymbol{F}} \,] : [\, \mathrm{D}_t \boldsymbol{F}_{\mathrm{p}} \cdot \boldsymbol{f}_{\mathrm{p}} \,] \\
&= - \, \widetilde{\boldsymbol{\sigma}}^{\mathrm{t}} : [\, \mathrm{D}_t \boldsymbol{F}_{\mathrm{p}} \cdot \boldsymbol{f}_{\mathrm{p}} \,] \, = \, - \, \bar{\boldsymbol{\Sigma}}^{\mathrm{t}} : [\, \mathrm{D}_t \boldsymbol{F}_{\mathrm{p}} \cdot \boldsymbol{f}_{\mathrm{p}} \,] \, \geq \, 0
\end{aligned} \tag{2.102}$$

by lines of argumentation previously reviewed in this section – see for instance eqs.(2.56,2.65). Note that the material time derivative of the plastic distortion can alternatively be rewritten as $\mathrm{D}_t \boldsymbol{F}_{\mathrm{p}} = \mathrm{d}_t \boldsymbol{F}_{\mathrm{p}} - \nabla_{\boldsymbol{X}} \boldsymbol{F}_{\mathrm{p}} \cdot \boldsymbol{V}$*, compare eqs.(2.5,2.10,2.22), so that the dissipation inequality (2.102) allows representation, for example, as*

$$\begin{aligned}
\mathsf{D}_0 &= - \, J_{\mathrm{p}} \, [\, \widetilde{\boldsymbol{\sigma}}^{\mathrm{t}} \cdot \boldsymbol{f}_{\mathrm{p}}^{\mathrm{t}} \,] : [\, \mathrm{d}_t \boldsymbol{F}_{\mathrm{p}} \quad - \, \nabla_{\boldsymbol{X}} \boldsymbol{F}_{\mathrm{p}} \cdot \boldsymbol{V} \,] \\
&= - \qquad \widetilde{\boldsymbol{\Pi}}^{\mathrm{t}} \qquad : [\, \mathrm{d}_t \boldsymbol{F}_{\mathrm{p}} \quad - \, \nabla_{\boldsymbol{X}} \boldsymbol{F}_{\mathrm{p}} \cdot \boldsymbol{V} \,] \\
&= - \qquad \boldsymbol{\Sigma}^{\mathrm{t}} : [\, \boldsymbol{f}_{\mathrm{p}} \cdot \mathrm{d}_t \boldsymbol{F}_{\mathrm{p}} \,] \, - \, [\, \boldsymbol{B}_0 + \partial_{\boldsymbol{X}} \psi_0 + J \, \boldsymbol{F}^{\mathrm{t}} \cdot \boldsymbol{b}_0^{\mathrm{ext}} \,] \cdot \boldsymbol{V} \, \geq 0
\end{aligned} \tag{2.103}$$

whereby use of eqs.(2.51,2.70) and the later on derived volume force $\boldsymbol{B}_0$ *has been made; compare eqs.(2.46,2.110). For the sake of brevity, however, we do not place emphasis on different representations of eqs.(2.101–2.103) – for instance in the context of different motion problems – but refer the reader to the review by Steinmann (2002b) as well as to Maugin (2006).*

2.4 Volume forces

As previously mentioned at the beginning of section 2.3, we next identify configurational volume forces which have formally been introduced in section 2.2. Apparently, these elaborations are intrinsically related to the hyperelastic formats developed in section 2.3 and constitute the key contribution of this chapter. The cardinal importance of these forces is underpinned by the fact that they involve driving forces acting on defects, inhomogeneities, heterogeneities and so forth. As point of departure, we apply as the fundamental requirement that appropriate pullback and pushforward transformations of different representations of the balance of linear momentum coincide, which enables us to relate the various volume forces. It turns out that gradients of the elastic and plastic distortion and especially dislocation density tensors, as introduced in section 2.1, are explicitly incorporated. To set the stage, we preliminarily review fundamental pullback and pushforward transformations well–known from finite elasticity and thereby discuss the basic derivation procedure in detail, see appendix B. The same modus operandi will then be applied in general to express the various volume forces particularly in the intermediate configuration.

2.4.1 Starting from spatial motion balance of linear momentum representations

The main objective of this section consists in the derivation of representations for the volume forces $\boldsymbol{B}_{0,t}$ and $\bar{\boldsymbol{B}}_{t,\mathrm{p}}$ introduced in eqs.(2.46,2.52).

2.4.1.1 Pullback to the material configuration

First, recall that the balance of linear momentum representations in eqs.(2.42,2.46) are related via

$$\begin{aligned} \mathbf{0} &= -\boldsymbol{F}^{\mathrm{t}} \cdot \left[J\ \nabla_{\boldsymbol{x}} \cdot \boldsymbol{\sigma}^{\mathrm{t}} + \boldsymbol{b}_0^{\mathrm{ext}} \right] \\ &= -\boldsymbol{F}^{\mathrm{t}} \cdot \left[\nabla_{\boldsymbol{X}} \cdot \boldsymbol{\Pi}^{\mathrm{t}} + \boldsymbol{b}_0^{\mathrm{ext}} \right] \\ &=: \nabla_{\boldsymbol{X}} \cdot \boldsymbol{\Sigma}^{\mathrm{t}} + \boldsymbol{B}_0 \,, \end{aligned} \tag{2.104}$$

compare appendix C, with $\boldsymbol{b}_0^{\mathrm{int}} = \mathbf{0}$. Now, we reformulate the transformed divergence of $\boldsymbol{\Pi}^{\mathrm{t}}$ by

$$-\boldsymbol{F}^{\mathrm{t}} \cdot [\, \nabla_{\boldsymbol{X}} \cdot \boldsymbol{\Pi}^{\mathrm{t}} \,] = -\nabla_{\boldsymbol{X}} \cdot (\, \boldsymbol{F}^{\mathrm{t}} \cdot \boldsymbol{\Pi}^{\mathrm{t}} \,) + \nabla_{\boldsymbol{X}} \boldsymbol{F}^{\mathrm{t}} : \boldsymbol{\Pi}^{\mathrm{t}} \tag{2.105}$$

in order to relate both material divergence operations in eq.(2.104). Note that $\nabla_{\boldsymbol{X}} \boldsymbol{F}$ contributes to the dislocation density tensor introduced in eq.(2.4) which, however, vanishes for the compatible spatial configuration. The second term on the right–hand side of eq.(2.105) allows representation as

$$\nabla_{\boldsymbol{X}} \boldsymbol{F}^{\mathrm{t}} : \boldsymbol{\Pi}^{\mathrm{t}} = \boldsymbol{\Pi}^{\mathrm{t}} : \nabla_{\boldsymbol{X}} \boldsymbol{F} - \boldsymbol{\Pi} \times \boldsymbol{A} \,, \tag{2.106}$$

see appendix B for a detailed derivation. As a result, the dislocation density tensor $\boldsymbol{A}^{\mathrm{t}}$ is automatically included. The first term on the right–hand side of eq.(2.106) is next rewritten as

$$\boldsymbol{\Pi}^{\mathrm{t}} : \nabla_{\boldsymbol{X}} \boldsymbol{F} = \nabla_{\boldsymbol{X}} \cdot (\, \psi_0\, \boldsymbol{I}_0^{\mathrm{t}} \,) - \widetilde{\boldsymbol{\Pi}}^{\mathrm{t}} : \nabla_{\boldsymbol{X}} \boldsymbol{F}_{\mathrm{p}} - \partial_{\boldsymbol{X}} \psi_0 \,, \tag{2.107}$$

whereby the hyperelastic formats in eqs.(2.56,2.64) and eq.(2.54) are applied. Assembling terms then renders

$$\begin{aligned} \mathbf{0} = \quad & \nabla_{\boldsymbol{X}} \cdot (\, \psi_0\, \boldsymbol{I}_0^{\mathrm{t}} - \boldsymbol{F}^{\mathrm{t}} \cdot \boldsymbol{\Pi}^{\mathrm{t}} \,) \\ & - \boldsymbol{\Pi} \times \boldsymbol{A} - \widetilde{\boldsymbol{\Pi}}^{\mathrm{t}} : \nabla_{\boldsymbol{X}} \boldsymbol{F}_{\mathrm{p}} - \partial_{\boldsymbol{X}} \psi_0 - \boldsymbol{F}^{\mathrm{t}} \cdot \boldsymbol{b}_0^{\mathrm{ext}} \\ =: \quad & \nabla_{\boldsymbol{X}} \cdot \boldsymbol{\Sigma}^{\mathrm{t}} + \boldsymbol{B}_0 \end{aligned} \tag{2.108}$$

from which we identify the sought expressions for the material motion Cauchy stress

$$\boldsymbol{\Sigma}^{\mathrm{t}} = \psi_0\, \boldsymbol{I}_0^{\mathrm{t}} - \boldsymbol{F}^{\mathrm{t}} \cdot \boldsymbol{\Pi}^{\mathrm{t}} \tag{2.109}$$

and the corresponding volume force

$$\boldsymbol{B}_0^{\mathrm{int}} = -\boldsymbol{\Pi} \times \boldsymbol{A} - \widetilde{\boldsymbol{\Pi}}^{\mathrm{t}} : \nabla_{\boldsymbol{X}} \boldsymbol{F}_{\mathrm{p}} - \partial_{\boldsymbol{X}} \psi_0 \tag{2.110}$$

with $\boldsymbol{B}_0^{\mathrm{ext}} = -\boldsymbol{F}^{\mathrm{t}} \cdot \boldsymbol{b}_0^{\mathrm{ext}}$. Note that the definition of $\boldsymbol{\Sigma}^{\mathrm{t}}$ recaptures eqs.(2.71,2.94). Alternatively, one obtains

$$\boldsymbol{B}_t^{\mathrm{int}} = -\boldsymbol{F}^{\mathrm{t}} \cdot [\, \boldsymbol{\sigma} \times \boldsymbol{d} \,] - j\, \widetilde{\boldsymbol{\Pi}}^{\mathrm{t}} : \nabla_{\boldsymbol{X}} \boldsymbol{F}_{\mathrm{p}} - \partial_{\boldsymbol{X}} \psi_t \tag{2.111}$$

and $\boldsymbol{B}_t^{\mathrm{ext}} = -\boldsymbol{F}^{\mathrm{t}} \cdot \boldsymbol{b}_t^{\mathrm{ext}}$ from eqs.(2.4,2.43,2.47); a detailed derivation is reviewed in appendix B. Furthermore, rearranging terms results in

$$\boldsymbol{b}_0^{\mathrm{ext}} = -\boldsymbol{f}^{\mathrm{t}} \cdot [\, \boldsymbol{\Pi} \times \boldsymbol{A} \,] - \widetilde{\boldsymbol{\Pi}}^{\mathrm{t}} : \nabla_{\boldsymbol{x}} \boldsymbol{F}_{\mathrm{p}} - \boldsymbol{f}^{\mathrm{t}} \cdot \partial_{\boldsymbol{X}} \psi_0 - \boldsymbol{f}^{\mathrm{t}} \cdot \boldsymbol{B}_0 \tag{2.112}$$

and likewise

$$\boldsymbol{b}_t^{\mathrm{ext}} = -\boldsymbol{\sigma} \times \boldsymbol{d} - j\, \widetilde{\boldsymbol{\Pi}}^{\mathrm{t}} : \nabla_{\boldsymbol{x}} \boldsymbol{F}_{\mathrm{p}} - \boldsymbol{f}^{\mathrm{t}} \cdot \partial_{\boldsymbol{X}} \psi_t - \boldsymbol{f}^{\mathrm{t}} \cdot \boldsymbol{B}_t \,. \tag{2.113}$$

2.4.1.2 Pullback to the intermediate configuration

Second, we relate the balance of linear momentum representations in eqs.(2.44,2.52) via

$$\begin{aligned} \mathbf{0} = & - \boldsymbol{F}_{\mathrm{e}}^{\mathrm{t}} \cdot \big[J_{\mathrm{e}} \, \nabla_{\boldsymbol{x}} \cdot \bar{\boldsymbol{\sigma}}^{\mathrm{t}} + \bar{\boldsymbol{b}}_{\mathrm{p}}^{\mathrm{ext}} \big] \\ = & - \boldsymbol{F}_{\mathrm{e}}^{\mathrm{t}} \cdot \big[\bar{\nabla} \cdot \bar{\boldsymbol{\Pi}}^{\mathrm{t}} - \bar{\boldsymbol{\Pi}}^{\mathrm{t}} \cdot [\boldsymbol{f}_{\mathrm{e}} \times \bar{\boldsymbol{A}}] + \bar{\boldsymbol{b}}_{\mathrm{p}}^{\mathrm{ext}} \big] \\ =: & \bar{\nabla} \cdot \bar{\boldsymbol{\Sigma}}^{\mathrm{t}} - \bar{\boldsymbol{\Sigma}}^{\mathrm{t}} \cdot [\boldsymbol{f}_{\mathrm{e}} \times \bar{\boldsymbol{A}}] + \bar{\boldsymbol{B}}_{\mathrm{p}} \, , \end{aligned} \tag{2.114}$$

compare appendix C, with $\bar{\boldsymbol{b}}_{\mathrm{p}}^{\mathrm{int}} = \mathbf{0}$ and $\bar{\boldsymbol{A}}^{\mathrm{t}} \neq \mathbf{0}$. Now, we reformulate the transformed divergence of $\bar{\boldsymbol{\Pi}}^{\mathrm{t}}$ by

$$- \boldsymbol{F}_{\mathrm{e}}^{\mathrm{t}} \cdot [\bar{\nabla} \cdot \bar{\boldsymbol{\Pi}}^{\mathrm{t}}] = - \bar{\nabla} \cdot (\boldsymbol{F}_{\mathrm{e}}^{\mathrm{t}} \cdot \bar{\boldsymbol{\Pi}}^{\mathrm{t}}) + \bar{\nabla} \boldsymbol{F}_{\mathrm{e}}^{\mathrm{t}} : \bar{\boldsymbol{\Pi}}^{\mathrm{t}} \tag{2.115}$$

in order to relate both intermediate divergence operations in eq.(2.114). Note that $\bar{\nabla} \boldsymbol{F}_{\mathrm{e}}$ contributes to the dislocation density tensor introduced in eq.(2.29) which does not vanish for the incompatible intermediate configuration. The second term on the right–hand side of eq.(2.115) allows representation as

$$\bar{\nabla} \boldsymbol{F}_{\mathrm{e}}^{\mathrm{t}} : \bar{\boldsymbol{\Pi}}^{\mathrm{t}} = \bar{\boldsymbol{\Pi}}^{\mathrm{t}} : \bar{\nabla} \boldsymbol{F}_{\mathrm{e}} - \bar{\boldsymbol{\Pi}} \times \bar{\boldsymbol{A}} \, , \tag{2.116}$$

see appendix B for a detailed derivation. As a result, the dislocation density tensor $\bar{\boldsymbol{A}}^{\mathrm{t}}$ is automatically incorporated. The first term on the right–hand side of eq.(2.116) is next rewritten as

$$\bar{\boldsymbol{\Pi}}^{\mathrm{t}} : \bar{\nabla} \boldsymbol{F}_{\mathrm{e}} = \bar{\nabla} \cdot (\psi_{\mathrm{p}} \, \boldsymbol{I}_{\mathrm{p}}^{\mathrm{t}}) - \boldsymbol{f}_{\mathrm{p}}^{\mathrm{t}} \cdot \partial_{\boldsymbol{X}} \psi_{\mathrm{p}} \, , \tag{2.117}$$

whereby the hyperelastic formats in eq.(2.58) and eq.(2.54) are included. Assembling terms then renders

$$\begin{aligned} \mathbf{0} = & \quad \bar{\nabla} \cdot (\psi_{\mathrm{p}} \, \boldsymbol{I}_{\mathrm{p}}^{\mathrm{t}} - \boldsymbol{F}_{\mathrm{e}}^{\mathrm{t}} \cdot \bar{\boldsymbol{\Pi}}^{\mathrm{t}}) + \boldsymbol{F}_{\mathrm{e}}^{\mathrm{t}} \cdot \bar{\boldsymbol{\Pi}}^{\mathrm{t}} \cdot [\boldsymbol{f}_{\mathrm{e}} \times \bar{\boldsymbol{A}}] - \bar{\boldsymbol{\Pi}} \times \bar{\boldsymbol{A}} \\ & - \boldsymbol{f}_{\mathrm{p}}^{\mathrm{t}} \cdot \partial_{\boldsymbol{X}} \psi_{\mathrm{p}} - \boldsymbol{F}_{\mathrm{e}}^{\mathrm{t}} \cdot \bar{\boldsymbol{b}}_{\mathrm{p}}^{\mathrm{ext}} \\ =: & \quad \bar{\nabla} \cdot \bar{\boldsymbol{\Sigma}}^{\mathrm{t}} - \bar{\boldsymbol{\Sigma}}^{\mathrm{t}} \cdot [\boldsymbol{f}_{\mathrm{e}} \times \bar{\boldsymbol{A}}] + \bar{\boldsymbol{B}}_{\mathrm{p}} \end{aligned} \tag{2.118}$$

from which we identify the sought expressions for the material motion elastic Cauchy stress

$$\bar{\boldsymbol{\Sigma}}^{\mathrm{t}} = \psi_{\mathrm{p}} \, \boldsymbol{I}_{\mathrm{p}}^{\mathrm{t}} - \boldsymbol{F}_{\mathrm{e}}^{\mathrm{t}} \cdot \bar{\boldsymbol{\Pi}}^{\mathrm{t}} \tag{2.119}$$

and the corresponding volume force

$$\begin{aligned} \bar{\boldsymbol{B}}_{\mathrm{p}}^{\mathrm{int}} = & [\bar{\boldsymbol{\Sigma}}^{\mathrm{t}} + \boldsymbol{F}_{\mathrm{e}}^{\mathrm{t}} \cdot \bar{\boldsymbol{\Pi}}^{\mathrm{t}}] \cdot [\boldsymbol{f}_{\mathrm{e}} \times \bar{\boldsymbol{A}}] - \bar{\boldsymbol{\Pi}} \times \bar{\boldsymbol{A}} - \boldsymbol{f}_{\mathrm{p}}^{\mathrm{t}} \cdot \partial_{\boldsymbol{X}} \psi_{\mathrm{p}} \\ = & \quad [\psi_{\mathrm{p}} \, \boldsymbol{f}_{\mathrm{e}} - \bar{\boldsymbol{\Pi}}] \times \bar{\boldsymbol{A}} - \boldsymbol{f}_{\mathrm{p}}^{\mathrm{t}} \cdot \partial_{\boldsymbol{X}} \psi_{\mathrm{p}} \end{aligned} \tag{2.120}$$

with $\bar{\boldsymbol{B}}_{\mathrm{p}}^{\mathrm{ext}} = - \boldsymbol{F}_{\mathrm{e}}^{\mathrm{t}} \cdot \bar{\boldsymbol{b}}_{\mathrm{p}}^{\mathrm{ext}}$. Note that the definition of $\bar{\boldsymbol{\Sigma}}^{\mathrm{t}}$ recaptures eqs.(2.83,2.75). Alternatively, one obtains

$$\bar{\boldsymbol{B}}_{t}^{\mathrm{int}} = \boldsymbol{F}_{\mathrm{e}}^{\mathrm{t}} \cdot \big[[\psi_t \, \boldsymbol{I}_t - \bar{\boldsymbol{\sigma}}] \times \bar{\boldsymbol{d}} \big] - \boldsymbol{f}_{\mathrm{p}}^{\mathrm{t}} \cdot \partial_{\boldsymbol{X}} \psi_t \tag{2.121}$$

and $\bar{\boldsymbol{B}}_{t}^{\mathrm{ext}} = - \boldsymbol{F}_{\mathrm{e}}^{\mathrm{t}} \cdot \bar{\boldsymbol{b}}_{t}^{\mathrm{ext}}$ from eqs.(2.45,2.53) with $\bar{\boldsymbol{d}}^{\mathrm{t}} = \bar{\boldsymbol{A}}^{\mathrm{t}} \cdot \mathrm{cof}(\boldsymbol{f}_{\mathrm{e}})$; a detailed derivation is reviewed in appendix B. Furthermore, rearranging terms results in

$$\bar{\boldsymbol{b}}_{\mathrm{p}}^{\mathrm{ext}} = \boldsymbol{f}_{\mathrm{e}}^{\mathrm{t}} \cdot \big[[\psi_{\mathrm{p}} \, \boldsymbol{f}_{\mathrm{e}} - \bar{\boldsymbol{\Pi}}] \times \bar{\boldsymbol{A}} \big] - \boldsymbol{f}^{\mathrm{t}} \cdot \partial_{\boldsymbol{X}} \psi_{\mathrm{p}} - \boldsymbol{f}_{\mathrm{e}}^{\mathrm{t}} \cdot \bar{\boldsymbol{B}}_{\mathrm{p}} \tag{2.122}$$

and likewise

$$\bar{\boldsymbol{b}}_{t}^{\mathrm{ext}} = [\psi_t \, \boldsymbol{I}_t - \bar{\boldsymbol{\sigma}}] \times \bar{\boldsymbol{d}} - \boldsymbol{f}^{\mathrm{t}} \cdot \partial_{\boldsymbol{X}} \psi_t - \boldsymbol{f}_{\mathrm{e}}^{\mathrm{t}} \cdot \bar{\boldsymbol{B}}_{t} \, . \tag{2.123}$$

A fundamental difference between the derived volume forces in eqs.(2.110,2.111) and eqs.(2.120,2.121) is given by the fact that $\bar{\boldsymbol{B}}_{\mathrm{p},t}^{\mathrm{int}}$ incorporate non–vanishing gradients of distortions solely via dislocation density tensors.

2.4.2 Starting from material motion balance of linear momentum representations

The main objective of this section consists in the derivation of representations for the volume forces $\boldsymbol{b}_{t,0}$ and $\widetilde{\boldsymbol{b}}_{\mathrm{p},0}$ introduced in eqs.(2.46,2.48).

2.4.2.1 Pushforward to the spatial configuration

First, recall that the balance of linear momentum representations in eqs.(2.46,2.42) are related via

$$\begin{aligned} \boldsymbol{0} &= -\boldsymbol{f}^{\mathrm{t}} \cdot \left[\, j\, \nabla_{\boldsymbol{X}} \cdot \boldsymbol{\Sigma}^{\mathrm{t}} + \boldsymbol{B}_t \,\right] \\ &= -\boldsymbol{f}^{\mathrm{t}} \cdot \left[\, \nabla_{\boldsymbol{x}} \cdot \boldsymbol{\pi}^{\mathrm{t}} + \boldsymbol{B}_t \,\right] \\ &=: \qquad \nabla_{\boldsymbol{x}} \cdot \boldsymbol{\sigma}^{\mathrm{t}} + \boldsymbol{b}_t^{\mathrm{ext}} \,, \end{aligned} \tag{2.124}$$

compare appendix C, with $\boldsymbol{b}_t^{\mathrm{int}} = \boldsymbol{0}$. Now, we reformulate the transformed divergence of $\boldsymbol{\pi}^{\mathrm{t}}$ by

$$-\boldsymbol{f}^{\mathrm{t}} \cdot [\, \nabla_{\boldsymbol{x}} \cdot \boldsymbol{\pi}^{\mathrm{t}} \,] = -\nabla_{\boldsymbol{x}} \cdot (\, \boldsymbol{f}^{\mathrm{t}} \cdot \boldsymbol{\pi}^{\mathrm{t}} \,) + \nabla_{\boldsymbol{x}} \boldsymbol{f}^{\mathrm{t}} : \boldsymbol{\pi}^{\mathrm{t}} \tag{2.125}$$

in order to relate both spatial divergence operations in eq.(2.124). Note that $\nabla_{\boldsymbol{x}} \boldsymbol{f}$ contributes to the dislocation density tensor introduced in eq.(2.9) which, however, vanishes for the compatible material configuration. The second term on the right–hand side of eq.(2.125) allows representation as

$$\nabla_{\boldsymbol{x}} \boldsymbol{f}^{\mathrm{t}} : \boldsymbol{\pi}^{\mathrm{t}} = \boldsymbol{\pi}^{\mathrm{t}} : \nabla_{\boldsymbol{x}} \boldsymbol{f} - \boldsymbol{\pi} \times \boldsymbol{a} \,, \tag{2.126}$$

see appendix B for a detailed derivation. As a result, the dislocation density tensor $\boldsymbol{a}^{\mathrm{t}}$ is automatically incorporated. The first term on the right–hand side of eq.(2.126) is next rewritten as

$$\boldsymbol{\pi}^{\mathrm{t}} : \nabla_{\boldsymbol{x}} \boldsymbol{f} = \nabla_{\boldsymbol{x}} \cdot (\, \psi_t\, \boldsymbol{I}_t^{\mathrm{t}} \,) - [\, j_{\mathrm{e}}\, \widetilde{\boldsymbol{\pi}}^{\mathrm{t}} - \psi_t\, \boldsymbol{F}_{\mathrm{p}}^{\mathrm{t}} \,] : \nabla_{\boldsymbol{x}} \boldsymbol{f}_{\mathrm{p}} - \boldsymbol{f}^{\mathrm{t}} \cdot \partial_{\boldsymbol{X}} \psi_t \,, \tag{2.127}$$

whereby the hyperelastic formats in eqs.(2.60,2.62) and eq.(2.54) are included. Assembling terms then renders

$$\begin{aligned} \boldsymbol{0} = \quad & \nabla_{\boldsymbol{x}} \cdot (\, \psi_t\, \boldsymbol{I}_t^{\mathrm{t}} - \boldsymbol{f}^{\mathrm{t}} \cdot \boldsymbol{\pi}^{\mathrm{t}} \,) \\ & - \boldsymbol{\pi} \times \boldsymbol{a} + [\, \psi_t\, \boldsymbol{F}_{\mathrm{p}}^{\mathrm{t}} - j_{\mathrm{e}}\, \widetilde{\boldsymbol{\pi}}^{\mathrm{t}} \,] : \nabla_{\boldsymbol{x}} \boldsymbol{f}_{\mathrm{p}} - \boldsymbol{f}^{\mathrm{t}} \cdot \partial_{\boldsymbol{X}} \psi_t - \boldsymbol{f}^{\mathrm{t}} \cdot \boldsymbol{B}_t \\ =: \quad & \nabla_{\boldsymbol{x}} \cdot \boldsymbol{\sigma}^{\mathrm{t}} + \boldsymbol{b}_t^{\mathrm{ext}} \end{aligned} \tag{2.128}$$

from which we identify the sought expressions for the spatial motion Cauchy stress

$$\boldsymbol{\sigma}^{\mathrm{t}} = \psi_t\, \boldsymbol{I}_t^{\mathrm{t}} - \boldsymbol{f}^{\mathrm{t}} \cdot \boldsymbol{\pi}^{\mathrm{t}} \tag{2.129}$$

and the corresponding volume force

$$\boldsymbol{b}_t^{\mathrm{ext}} = -\boldsymbol{\pi} \times \boldsymbol{a} + [\, \psi_t\, \boldsymbol{F}_{\mathrm{p}}^{\mathrm{t}} - j_{\mathrm{e}}\, \widetilde{\boldsymbol{\pi}}^{\mathrm{t}} \,] : \nabla_{\boldsymbol{x}} \boldsymbol{f}_{\mathrm{p}} - \boldsymbol{f}^{\mathrm{t}} \cdot \partial_{\boldsymbol{X}} \psi_t - \boldsymbol{f}^{\mathrm{t}} \cdot \boldsymbol{B}_t \tag{2.130}$$

with $\boldsymbol{b}_t^{\mathrm{ext}} = -\boldsymbol{f}^{\mathrm{t}} \cdot \boldsymbol{B}_t^{\mathrm{ext}}$. Note that the definition of $\boldsymbol{\sigma}^{\mathrm{t}}$ recaptures eqs.(2.70,2.96). Alternatively, one obtains

$$\boldsymbol{b}_0^{\mathrm{ext}} = -\boldsymbol{f}^{\mathrm{t}} \cdot [\, \boldsymbol{\Sigma} \times \boldsymbol{D} \,] + [\, \psi_0\, \boldsymbol{F}_{\mathrm{p}}^{\mathrm{t}} - J_{\mathrm{p}}\, \widetilde{\boldsymbol{\pi}}^{\mathrm{t}} \,] : \nabla_{\boldsymbol{x}} \boldsymbol{f}_{\mathrm{p}} - \boldsymbol{f}^{\mathrm{t}} \cdot \partial_{\boldsymbol{X}} \psi_0 - \boldsymbol{f}^{\mathrm{t}} \cdot \boldsymbol{B}_0 \tag{2.131}$$

and $\boldsymbol{b}_0^{\mathrm{ext}} = -\boldsymbol{f}^{\mathrm{t}} \cdot \boldsymbol{B}_0^{\mathrm{ext}}$ from eqs.(2.9,2.47,2.43); a detailed derivation is reviewed in appendix B. Furthermore, rearranging terms results in

$$\boldsymbol{B}_t^{\mathrm{int}} = -\boldsymbol{F}^{\mathrm{t}} \cdot [\, \boldsymbol{\pi} \times \boldsymbol{a} \,] + [\, \psi_t\, \boldsymbol{F}_{\mathrm{p}}^{\mathrm{t}} - j_{\mathrm{e}}\, \widetilde{\boldsymbol{\pi}}^{\mathrm{t}} \,] : \nabla_{\boldsymbol{X}} \boldsymbol{f}_{\mathrm{p}} - \partial_{\boldsymbol{X}} \psi_t \tag{2.132}$$

and likewise

$$\boldsymbol{B}_0^{\mathrm{int}} = -\boldsymbol{\Sigma} \times \boldsymbol{D} + [\, \psi_0\, \boldsymbol{F}_{\mathrm{p}}^{\mathrm{t}} - J_{\mathrm{p}}\, \widetilde{\boldsymbol{\pi}}^{\mathrm{t}} \,] : \nabla_{\boldsymbol{X}} \boldsymbol{f}_{\mathrm{p}} - \partial_{\boldsymbol{X}} \psi_0 \,. \tag{2.133}$$

2.4.2.2 Pushforward to the intermediate configuration

Second, we relate the balance of linear momentum representations in eqs.(2.48,2.50) via

$$\begin{aligned} \mathbf{0} = & - \boldsymbol{f}_{\mathrm{p}}^{\mathrm{t}} \cdot \big[j_{\mathrm{p}} \, \nabla_{\boldsymbol{X}} \cdot \widetilde{\boldsymbol{\Sigma}}^{\mathrm{t}} + \widetilde{\boldsymbol{B}}_{\mathrm{p}} \big] \\ = & - \boldsymbol{f}_{\mathrm{p}}^{\mathrm{t}} \cdot \big[\widetilde{\nabla} \cdot \widetilde{\boldsymbol{\pi}}^{\mathrm{t}} - \widetilde{\boldsymbol{\pi}}^{\mathrm{t}} \cdot [\boldsymbol{F}_{\mathrm{p}} \times \widetilde{\boldsymbol{a}}] + \widetilde{\boldsymbol{B}}_{\mathrm{p}} \big] \\ =: & \quad \widetilde{\nabla} \cdot \widetilde{\boldsymbol{\sigma}}^{\mathrm{t}} - \widetilde{\boldsymbol{\sigma}}^{\mathrm{t}} \cdot [\boldsymbol{F}_{\mathrm{p}} \times \widetilde{\boldsymbol{a}}] + \widetilde{\boldsymbol{b}}_{\mathrm{p}} \, , \end{aligned} \tag{2.134}$$

compare appendix C, with $\widetilde{\boldsymbol{a}} \neq \mathbf{0}$. Now, we reformulate the transformed divergence of $\widetilde{\boldsymbol{\pi}}^{\mathrm{t}}$ by

$$- \boldsymbol{f}_{\mathrm{p}}^{\mathrm{t}} \cdot [\widetilde{\nabla} \cdot \widetilde{\boldsymbol{\pi}}^{\mathrm{t}}] = - \widetilde{\nabla} \cdot (\boldsymbol{f}_{\mathrm{p}}^{\mathrm{t}} \cdot \widetilde{\boldsymbol{\pi}}^{\mathrm{t}}) + \widetilde{\nabla} \boldsymbol{f}_{\mathrm{p}}^{\mathrm{t}} : \widetilde{\boldsymbol{\pi}}^{\mathrm{t}} \tag{2.135}$$

in order to relate both intermediate divergence operations in eq.(2.134). Note that $\widetilde{\nabla} \boldsymbol{f}_{\mathrm{p}}$ contributes to the dislocation density tensor introduced in eq.(2.31) which does not vanish for the incompatible intermediate configuration. The second term on the right–hand side of eq.(2.135) allows representation as

$$\widetilde{\nabla} \boldsymbol{f}_{\mathrm{p}}^{\mathrm{t}} : \widetilde{\boldsymbol{\pi}}^{\mathrm{t}} = \widetilde{\boldsymbol{\pi}}^{\mathrm{t}} : \widetilde{\nabla} \boldsymbol{f}_{\mathrm{p}} - \widetilde{\boldsymbol{\pi}} \times \widetilde{\boldsymbol{a}} \, , \tag{2.136}$$

see appendix B for a detailed derivation. As a result, the dislocation density tensor $\widetilde{\boldsymbol{a}}^{\mathrm{t}}$ is automatically incorporated. The first term on the right–hand side of eq.(2.136) is next rewritten as

$$\widetilde{\boldsymbol{\pi}}^{\mathrm{t}} : \widetilde{\nabla} \boldsymbol{f}_{\mathrm{p}} = \widetilde{\nabla} \cdot (\psi_{\mathrm{p}} \boldsymbol{I}_{\mathrm{p}}^{\mathrm{t}}) + [\psi_{\mathrm{p}} \boldsymbol{F}^{\mathrm{t}} - J_{\mathrm{e}} \boldsymbol{\pi}^{\mathrm{t}}] : \widetilde{\nabla} \boldsymbol{f} - \boldsymbol{f}_{\mathrm{p}}^{\mathrm{t}} \cdot \partial_{\boldsymbol{X}} \psi_{\mathrm{p}} \, , \tag{2.137}$$

whereby the hyperelastic formats in eqs.(2.60,2.62) and eq.(2.54) are included. Assembling terms then renders

$$\begin{aligned} \mathbf{0} = & \quad \widetilde{\nabla} \cdot (\psi_{\mathrm{p}} \boldsymbol{I}_{\mathrm{p}}^{\mathrm{t}} - \boldsymbol{f}_{\mathrm{p}}^{\mathrm{t}} \cdot \widetilde{\boldsymbol{\pi}}^{\mathrm{t}}) + \boldsymbol{f}_{\mathrm{p}}^{\mathrm{t}} \cdot \widetilde{\boldsymbol{\pi}}^{\mathrm{t}} \cdot [\boldsymbol{F}_{\mathrm{p}} \times \widetilde{\boldsymbol{a}}] - \widetilde{\boldsymbol{\pi}} \times \widetilde{\boldsymbol{a}} \\ & + [\psi_{\mathrm{p}} \boldsymbol{F}^{\mathrm{t}} - J_{\mathrm{e}} \boldsymbol{\pi}^{\mathrm{t}}] : \widetilde{\nabla} \boldsymbol{f} - \boldsymbol{f}_{\mathrm{p}}^{\mathrm{t}} \cdot \partial_{\boldsymbol{X}} \psi_{\mathrm{p}} - \boldsymbol{f}_{\mathrm{p}}^{\mathrm{t}} \cdot \widetilde{\boldsymbol{B}}_{\mathrm{p}} \\ =: & \quad \widetilde{\nabla} \cdot \widetilde{\boldsymbol{\sigma}}^{\mathrm{t}} - \widetilde{\boldsymbol{\sigma}}^{\mathrm{t}} \cdot [\boldsymbol{F}_{\mathrm{p}} \times \widetilde{\boldsymbol{a}}] + \widetilde{\boldsymbol{b}}_{\mathrm{p}} \end{aligned} \tag{2.138}$$

from which we identify the sought expressions for the intermediate motion plastic Cauchy stress

$$\widetilde{\boldsymbol{\sigma}}^{\mathrm{t}} = \psi_{\mathrm{p}} \boldsymbol{I}_{\mathrm{p}}^{\mathrm{t}} - \boldsymbol{f}_{\mathrm{p}}^{\mathrm{t}} \cdot \widetilde{\boldsymbol{\pi}}^{\mathrm{t}} \tag{2.139}$$

and the corresponding volume force

$$\begin{aligned} \widetilde{\boldsymbol{b}}_{\mathrm{p}} = & [\widetilde{\boldsymbol{\sigma}}^{\mathrm{t}} + \boldsymbol{f}_{\mathrm{p}}^{\mathrm{t}} \cdot \widetilde{\boldsymbol{\pi}}^{\mathrm{t}}] \cdot [\boldsymbol{F}_{\mathrm{p}} \times \widetilde{\boldsymbol{a}}] - \widetilde{\boldsymbol{\pi}} \times \widetilde{\boldsymbol{a}} \\ & + [\psi_{\mathrm{p}} \boldsymbol{F}^{\mathrm{t}} - J_{\mathrm{e}} \boldsymbol{\pi}^{\mathrm{t}}] : \widetilde{\nabla} \boldsymbol{f} - \boldsymbol{f}_{\mathrm{p}}^{\mathrm{t}} \cdot \partial_{\boldsymbol{X}} \psi_{\mathrm{p}} - \boldsymbol{f}_{\mathrm{p}}^{\mathrm{t}} \cdot \widetilde{\boldsymbol{B}}_{\mathrm{p}} \\ = & [\psi_{\mathrm{p}} \boldsymbol{F}_{\mathrm{p}} - \widetilde{\boldsymbol{\pi}}] \times \widetilde{\boldsymbol{a}} + [\psi_{\mathrm{p}} \boldsymbol{F}^{\mathrm{t}} - J_{\mathrm{e}} \boldsymbol{\pi}^{\mathrm{t}}] : \widetilde{\nabla} \boldsymbol{f} - \boldsymbol{f}_{\mathrm{p}}^{\mathrm{t}} \cdot \partial_{\boldsymbol{X}} \psi_{\mathrm{p}} - \boldsymbol{f}_{\mathrm{p}}^{\mathrm{t}} \cdot \widetilde{\boldsymbol{B}}_{\mathrm{p}} \, . \end{aligned} \tag{2.140}$$

Note that the definition of $\widetilde{\boldsymbol{\sigma}}^{\mathrm{t}}$ recaptures eqs.(2.80,2.92). Alternatively, one obtains

$$\begin{aligned} \widetilde{\boldsymbol{b}}_0 = & \quad \boldsymbol{f}_{\mathrm{p}}^{\mathrm{t}} \cdot \big[[\psi_0 \boldsymbol{I}_0 - \widetilde{\boldsymbol{\Sigma}}] \times \widetilde{\boldsymbol{D}} \big] \\ & + [\psi_0 \boldsymbol{F}^{\mathrm{t}} - J \boldsymbol{\pi}^{\mathrm{t}}] : \widetilde{\nabla} \boldsymbol{f} - \boldsymbol{f}_{\mathrm{p}}^{\mathrm{t}} \cdot \partial_{\boldsymbol{X}} \psi_0 - \boldsymbol{f}_{\mathrm{p}}^{\mathrm{t}} \cdot \widetilde{\boldsymbol{B}}_0 \end{aligned} \tag{2.141}$$

from eqs.(2.63,2.65) with $\widetilde{\boldsymbol{D}}^{\mathrm{t}} = \widetilde{\boldsymbol{a}}^{\mathrm{t}} \cdot \mathrm{cof}(\boldsymbol{F}_{\mathrm{p}})$; a detailed derivation is reviewed in appendix B. Furthermore, rearranging terms results in

$$\begin{aligned} \widetilde{\boldsymbol{B}}_{\mathrm{p}} = & \quad \boldsymbol{F}_{\mathrm{p}}^{\mathrm{t}} \cdot \big[[\psi_{\mathrm{p}} \boldsymbol{F}_{\mathrm{p}} - \widetilde{\boldsymbol{\pi}}] \times \widetilde{\boldsymbol{a}} \big] \\ & + [\psi_{\mathrm{p}} \boldsymbol{F}^{\mathrm{t}} - J_{\mathrm{e}} \boldsymbol{\pi}^{\mathrm{t}}] : \nabla_{\boldsymbol{X}} \boldsymbol{f} - \partial_{\boldsymbol{X}} \psi_{\mathrm{p}} - \boldsymbol{F}_{\mathrm{p}}^{\mathrm{t}} \cdot \widetilde{\boldsymbol{b}}_{\mathrm{p}} \end{aligned} \tag{2.142}$$

and likewise

$$\begin{aligned} \widetilde{\boldsymbol{B}}_0 = & \quad [\psi_0 \boldsymbol{I}_0 - \widetilde{\boldsymbol{\Sigma}}] \times \widetilde{\boldsymbol{D}} \\ & + [\psi_0 \boldsymbol{F}^{\mathrm{t}} - J \boldsymbol{\pi}^{\mathrm{t}}] : \nabla_{\boldsymbol{X}} \boldsymbol{f} - \partial_{\boldsymbol{X}} \psi_0 - \boldsymbol{F}_{\mathrm{p}}^{\mathrm{t}} \cdot \widetilde{\boldsymbol{b}}_0 \, . \end{aligned} \tag{2.143}$$

2.4.3 Starting from intermediate motion balance of linear momentum representations

The main objective of this section consists in the derivation of representations for the volume forces $\widetilde{\boldsymbol{B}}_{0,\mathrm{p}}$ and $\bar{\boldsymbol{b}}_{t,\mathrm{p}}$ introduced in eqs.(2.48,2.44).

2.4.3.1 Pullback to the material configuration

First, we relate the balance of linear momentum representations in eqs.(2.50,2.48) via

$$\begin{aligned} \boldsymbol{0} = & - \boldsymbol{F}_{\mathrm{p}}^{\mathrm{t}} \cdot \big[J_{\mathrm{p}} \, \widetilde{\nabla} \cdot \widetilde{\boldsymbol{\sigma}}^{\mathrm{t}} \quad - \widetilde{\boldsymbol{\sigma}}^{\mathrm{t}} \cdot [\, \boldsymbol{F}_{\mathrm{p}} \times \widetilde{\boldsymbol{a}} \,] + \widetilde{\boldsymbol{b}}_0 \ \big] \\ = & - \boldsymbol{F}_{\mathrm{p}}^{\mathrm{t}} \cdot \big[\quad \nabla_{\boldsymbol{X}} \cdot \widetilde{\boldsymbol{\Pi}}^{\mathrm{t}} \qquad\qquad + \widetilde{\boldsymbol{b}}_0 \ \big] \\ =: & \qquad \nabla_{\boldsymbol{X}} \cdot \widetilde{\boldsymbol{\Sigma}}^{\mathrm{t}} \qquad\qquad + \widetilde{\boldsymbol{B}}_0 \, , \end{aligned} \tag{2.144}$$

compare appendix C, with $\widetilde{\boldsymbol{a}}^{\mathrm{t}} \neq \boldsymbol{0}$. Now, we reformulate the transformed divergence of $\widetilde{\boldsymbol{\Pi}}^{\mathrm{t}}$ by

$$- \boldsymbol{F}_{\mathrm{p}}^{\mathrm{t}} \cdot [\, \nabla_{\boldsymbol{X}} \cdot \widetilde{\boldsymbol{\Pi}}^{\mathrm{t}} \,] = - \nabla_{\boldsymbol{X}} \cdot (\, \boldsymbol{F}_{\mathrm{p}}^{\mathrm{t}} \cdot \widetilde{\boldsymbol{\Pi}}^{\mathrm{t}} \,) + \nabla_{\boldsymbol{X}} \boldsymbol{F}_{\mathrm{p}}^{\mathrm{t}} : \widetilde{\boldsymbol{\Pi}}^{\mathrm{t}} \tag{2.145}$$

in order to relate both material divergence operations in eq.(2.144). Note that $\nabla_{\boldsymbol{X}} \boldsymbol{F}_{\mathrm{p}}$ contributes to the dislocation density tensor introduced in eq.(2.16) which does not vanish for the incompatible intermediate configuration. The second term on the right–hand side of eq.(2.145) allows representation as

$$\nabla_{\boldsymbol{X}} \boldsymbol{F}_{\mathrm{p}}^{\mathrm{t}} : \widetilde{\boldsymbol{\Pi}}^{\mathrm{t}} = \widetilde{\boldsymbol{\Pi}}^{\mathrm{t}} : \nabla_{\boldsymbol{X}} \boldsymbol{F}_{\mathrm{p}} - \widetilde{\boldsymbol{\Pi}} \times \widetilde{\boldsymbol{A}} \, , \tag{2.146}$$

see appendix B for a detailed derivation. As a result, the dislocation density tensor $\widetilde{\boldsymbol{A}}^{\mathrm{t}}$ is automatically incorporated. The first term on the right–hand side of eq.(2.146) is next rewritten as

$$\widetilde{\boldsymbol{\Pi}}^{\mathrm{t}} : \nabla_{\boldsymbol{X}} \boldsymbol{F}_{\mathrm{p}} = \nabla_{\boldsymbol{X}} \cdot (\, \psi_0 \, \boldsymbol{I}_0^{\mathrm{t}} \,) - \boldsymbol{\Pi}^{\mathrm{t}} : \nabla_{\boldsymbol{X}} \boldsymbol{F} - \partial_{\boldsymbol{X}} \psi_0 \, , \tag{2.147}$$

whereby the hyperelastic formats in eqs.(2.64,2.56) and eq.(2.54) are included. Assembling terms then renders

$$\begin{aligned} \boldsymbol{0} = & \quad \nabla_{\boldsymbol{X}} \cdot (\, \psi_0 \, \boldsymbol{I}_0^{\mathrm{t}} - \boldsymbol{F}_{\mathrm{p}}^{\mathrm{t}} \cdot \widetilde{\boldsymbol{\Pi}}^{\mathrm{t}} \,) - \widetilde{\boldsymbol{\Pi}} \times \widetilde{\boldsymbol{A}} \\ & - \boldsymbol{\Pi}^{\mathrm{t}} : \nabla_{\boldsymbol{X}} \boldsymbol{F} - \partial_{\boldsymbol{X}} \psi_0 - \boldsymbol{F}_{\mathrm{p}}^{\mathrm{t}} \cdot \widetilde{\boldsymbol{b}}_0 \\ =: & \quad \nabla_{\boldsymbol{X}} \cdot \widetilde{\boldsymbol{\Sigma}}^{\mathrm{t}} + \widetilde{\boldsymbol{B}}_0 \end{aligned} \tag{2.148}$$

from which we identify the sought expressions for the material motion plastic Cauchy stress

$$\widetilde{\boldsymbol{\Sigma}}^{\mathrm{t}} = \psi_0 \, \boldsymbol{I}_0^{\mathrm{t}} - \boldsymbol{F}_{\mathrm{p}}^{\mathrm{t}} \cdot \widetilde{\boldsymbol{\Pi}}^{\mathrm{t}} \tag{2.149}$$

and the corresponding volume force

$$\widetilde{\boldsymbol{B}}_0 = - \widetilde{\boldsymbol{\Pi}} \times \widetilde{\boldsymbol{A}} - \boldsymbol{\Pi}^{\mathrm{t}} : \nabla_{\boldsymbol{X}} \boldsymbol{F} - \partial_{\boldsymbol{X}} \psi_0 - \boldsymbol{F}_{\mathrm{p}}^{\mathrm{t}} \cdot \widetilde{\boldsymbol{b}}_0 \, . \tag{2.150}$$

Note that the definition of $\widetilde{\boldsymbol{\Sigma}}^{\mathrm{t}}$ recaptures eqs.(2.81,2.91). Alternatively, one obtains

$$\widetilde{\boldsymbol{B}}_{\mathrm{p}} = - \boldsymbol{F}_{\mathrm{p}}^{\mathrm{t}} \cdot [\, \widetilde{\boldsymbol{\sigma}} \times \widetilde{\boldsymbol{d}} \,] - j_{\mathrm{p}} \, \boldsymbol{\Pi}^{\mathrm{t}} : \nabla_{\boldsymbol{X}} \boldsymbol{F} - \partial_{\boldsymbol{X}} \psi_{\mathrm{p}} - \boldsymbol{F}_{\mathrm{p}}^{\mathrm{t}} \cdot \widetilde{\boldsymbol{b}}_{\mathrm{p}} \tag{2.151}$$

from eqs.(2.16,2.51,2.49); a detailed derivation is reviewed in appendix B. Furthermore, rearranging terms results in

$$\widetilde{\boldsymbol{b}}_0 = - \boldsymbol{f}_{\mathrm{p}}^{\mathrm{t}} \cdot [\, \widetilde{\boldsymbol{\Pi}} \times \widetilde{\boldsymbol{A}} \,] - \boldsymbol{\Pi}^{\mathrm{t}} : \widetilde{\nabla} \boldsymbol{F} - \boldsymbol{f}_{\mathrm{p}}^{\mathrm{t}} \cdot \partial_{\boldsymbol{X}} \psi_0 - \boldsymbol{f}_{\mathrm{p}}^{\mathrm{t}} \cdot \widetilde{\boldsymbol{B}}_0 \tag{2.152}$$

and likewise

$$\widetilde{\boldsymbol{b}}_{\mathrm{p}} = - \widetilde{\boldsymbol{\sigma}} \times \widetilde{\boldsymbol{d}} - j_{\mathrm{p}} \, \boldsymbol{\Pi}^{\mathrm{t}} : \widetilde{\nabla} \boldsymbol{F} - \boldsymbol{f}_{\mathrm{p}}^{\mathrm{t}} \cdot \partial_{\boldsymbol{X}} \psi_{\mathrm{p}} - \boldsymbol{f}_{\mathrm{p}}^{\mathrm{t}} \cdot \widetilde{\boldsymbol{B}}_{\mathrm{p}} \, . \tag{2.153}$$

2.4.3.2 Pushforward to the spatial configuration

Second, we relate the balance of linear momentum representations in eqs.(2.52,2.44) via

$$\begin{aligned} \mathbf{0} &= -\boldsymbol{f}_{\mathrm{e}}^{\mathrm{t}} \cdot \big[\, j_{\mathrm{e}}\, \bar{\nabla} \cdot \bar{\boldsymbol{\Sigma}}^{\mathrm{t}} - \bar{\boldsymbol{\Sigma}}^{\mathrm{t}} \cdot [\, \boldsymbol{f}_{\mathrm{e}} \times \bar{\boldsymbol{A}}\,] + \bar{\boldsymbol{B}}_t \,\big] \\ &= -\boldsymbol{f}_{\mathrm{e}}^{\mathrm{t}} \cdot \big[\, \nabla_{\boldsymbol{x}} \cdot \bar{\boldsymbol{\pi}}^{\mathrm{t}} + \bar{\boldsymbol{B}}_t \,\big] \\ &=: \nabla_{\boldsymbol{x}} \cdot \bar{\boldsymbol{\sigma}}^{\mathrm{t}} + \bar{\boldsymbol{b}}_t^{\mathrm{ext}}\,, \end{aligned} \tag{2.154}$$

compare appendix C, with $\bar{\boldsymbol{b}}_t^{\mathrm{int}} = \mathbf{0}$ and $\bar{\boldsymbol{A}}^{\mathrm{t}} \neq \mathbf{0}$. Now, we reformulate the transformed divergence of $\bar{\boldsymbol{\pi}}^{\mathrm{t}}$ by

$$-\boldsymbol{f}_{\mathrm{e}}^{\mathrm{t}} \cdot [\, \nabla_{\boldsymbol{x}} \cdot \bar{\boldsymbol{\pi}}^{\mathrm{t}}\,] = -\nabla_{\boldsymbol{x}} \cdot (\, \boldsymbol{f}_{\mathrm{e}}^{\mathrm{t}} \cdot \bar{\boldsymbol{\pi}}^{\mathrm{t}}\,) + \nabla_{\boldsymbol{x}}\, \boldsymbol{f}_{\mathrm{e}}^{\mathrm{t}} : \bar{\boldsymbol{\pi}}^{\mathrm{t}} \tag{2.155}$$

in order to relate both spatial divergence operations in eq.(2.154). Note that $\nabla_{\boldsymbol{x}} \boldsymbol{f}_{\mathrm{e}}$ contributes to the dislocation density tensor introduced in eq.(2.18) which does not vanish for the incompatible intermediate configuration. The second term on the right–hand side of eq.(2.155) allows representation as

$$\nabla_{\boldsymbol{x}}\, \boldsymbol{f}_{\mathrm{e}}^{\mathrm{t}} : \bar{\boldsymbol{\pi}}^{\mathrm{t}} = \bar{\boldsymbol{\pi}}^{\mathrm{t}} : \nabla_{\boldsymbol{x}}\, \boldsymbol{f}_{\mathrm{e}} - \bar{\boldsymbol{\pi}} \times \bar{\boldsymbol{a}}\,, \tag{2.156}$$

see appendix B for a detailed derivation. As a result, the dislocation density tensor $\bar{\boldsymbol{A}}^{\mathrm{t}}$ is automatically incorporated. The first term on the right–hand side of eq.(2.156) is next rewritten as

$$\bar{\boldsymbol{\pi}}^{\mathrm{t}} : \nabla_{\boldsymbol{x}} \boldsymbol{f}_{\mathrm{e}} = \nabla_{\boldsymbol{x}} \cdot (\, \psi_t\, \boldsymbol{I}_t^{\mathrm{t}}\,) - \boldsymbol{f}^{\mathrm{t}} \cdot \partial_{\boldsymbol{X}} \psi_t\,, \tag{2.157}$$

whereby the hyperelastic formats in eq.(2.66) and eq.(2.54) are included. Assembling terms then renders

$$\begin{aligned} \mathbf{0} &= \nabla_{\boldsymbol{x}} \cdot (\, \psi_t\, \boldsymbol{I}_t^{\mathrm{t}} - \boldsymbol{f}_{\mathrm{e}}^{\mathrm{t}} \cdot \bar{\boldsymbol{\pi}}^{\mathrm{t}}\,) - \bar{\boldsymbol{\pi}} \times \bar{\boldsymbol{a}} - \boldsymbol{f}^{\mathrm{t}} \cdot \partial_{\boldsymbol{X}} \psi_t - \boldsymbol{f}_{\mathrm{e}}^{\mathrm{t}} \cdot \bar{\boldsymbol{B}}_t \\ &=: \nabla_{\boldsymbol{x}} \cdot \bar{\boldsymbol{\sigma}}^{\mathrm{t}} + \bar{\boldsymbol{b}}_t^{\mathrm{ext}} \end{aligned} \tag{2.158}$$

from which we identify the sought expressions for the spatial motion elastic Cauchy stress

$$\bar{\boldsymbol{\sigma}}^{\mathrm{t}} = \psi_t\, \boldsymbol{I}_t^{\mathrm{t}} - \boldsymbol{f}_{\mathrm{e}}^{\mathrm{t}} \cdot \bar{\boldsymbol{\pi}}^{\mathrm{t}} \tag{2.159}$$

and the corresponding volume force

$$\bar{\boldsymbol{b}}_t^{\mathrm{ext}} = -\bar{\boldsymbol{\pi}} \times \bar{\boldsymbol{a}} - \boldsymbol{f}^{\mathrm{t}} \cdot \partial_{\boldsymbol{X}} \psi_t - \boldsymbol{f}_{\mathrm{e}}^{\mathrm{t}} \cdot \bar{\boldsymbol{B}}_t \tag{2.160}$$

with $\bar{\boldsymbol{b}}_t^{\mathrm{ext}} = -\boldsymbol{f}_{\mathrm{e}}^{\mathrm{t}} \cdot \bar{\boldsymbol{B}}_t^{\mathrm{ext}}$. Note that the definition of $\bar{\boldsymbol{\sigma}}^{\mathrm{t}}$ recaptures eq.(2.73). Alternatively, one obtains

$$\bar{\boldsymbol{b}}_{\mathrm{p}}^{\mathrm{ext}} = -\boldsymbol{f}_{\mathrm{e}}^{\mathrm{t}} \cdot [\, \bar{\boldsymbol{\Sigma}} \times \bar{\boldsymbol{D}}\,] - \boldsymbol{f}^{\mathrm{t}} \cdot \partial_{\boldsymbol{X}} \psi_{\mathrm{p}} - \boldsymbol{f}_{\mathrm{e}}^{\mathrm{t}} \cdot \bar{\boldsymbol{B}}_{\mathrm{p}} \tag{2.161}$$

and $\bar{\boldsymbol{b}}_{\mathrm{p}}^{\mathrm{ext}} = -\boldsymbol{f}_{\mathrm{e}}^{\mathrm{t}} \cdot \bar{\boldsymbol{B}}_{\mathrm{p}}^{\mathrm{ext}}$ from eqs.(2.18,2.53,2.45); a detailed derivation is reviewed in appendix B. Furthermore, rearranging terms results in

$$\bar{\boldsymbol{B}}_t^{\mathrm{int}} = -\boldsymbol{F}_{\mathrm{e}}^{\mathrm{t}} \cdot [\, \bar{\boldsymbol{\pi}} \times \bar{\boldsymbol{a}}\,] - \boldsymbol{f}_{\mathrm{p}}^{\mathrm{t}} \cdot \partial_{\boldsymbol{X}} \psi_t \tag{2.162}$$

and likewise

$$\bar{\boldsymbol{B}}_{\mathrm{p}}^{\mathrm{int}} = -\bar{\boldsymbol{\Sigma}} \times \bar{\boldsymbol{D}} - \boldsymbol{f}_{\mathrm{p}}^{\mathrm{t}} \cdot \partial_{\boldsymbol{X}} \psi_{\mathrm{p}}\,. \tag{2.163}$$

A fundamental difference between the derived volume forces in eqs.(2.150,2.151) and eqs.(2.160,2.161) is given by the fact that $\bar{\boldsymbol{b}}_{t,\mathrm{p}}^{\mathrm{ext}}$ incorporate gradients of distortions solely via dislocation density tensors.

Table 2.6: Transformations related to the spatial motion volume forces $\boldsymbol{b}_t^{\text{ext}} = \bar{\boldsymbol{b}}_t^{\text{ext}}$.

	$\boldsymbol{b}_t^{\text{ext}} = \bar{\boldsymbol{b}}_t^{\text{ext}} \in T^*\mathcal{B}_t$				
$\widetilde{\boldsymbol{b}}_0 \in T^*\mathcal{B}_{\text{p}}$	$-\ \boldsymbol{f}_{\text{p}}^{\text{t}} \cdot [\,\widetilde{\boldsymbol{\Pi}} \times \widetilde{\boldsymbol{A}}\,]$	$-\ \boldsymbol{f}_{\text{p}}^{\text{t}} \cdot \partial_{\boldsymbol{X}} \psi_0$	$-\ J$	$\boldsymbol{F}_{\text{e}}^{\text{t}} \cdot \boldsymbol{b}_t^{\text{ext}}$
$\widetilde{\boldsymbol{b}}_{\text{p}} \in T^*\mathcal{B}_{\text{p}}$	$-\ \widetilde{\boldsymbol{\sigma}} \times \widetilde{\boldsymbol{d}}$	$-\ \boldsymbol{f}_{\text{p}}^{\text{t}} \cdot \partial_{\boldsymbol{X}} \psi_{\text{p}}$	$-\ J_{\text{e}}$	$\boldsymbol{F}_{\text{e}}^{\text{t}} \cdot \boldsymbol{b}_t^{\text{ext}}$
$= \bar{\boldsymbol{B}}_{\text{p}}$	$= -\ \bar{\boldsymbol{\Sigma}} \times \bar{\boldsymbol{D}}$	$-\ \boldsymbol{f}_{\text{p}}^{\text{t}} \cdot \partial_{\boldsymbol{X}} \psi_{\text{p}}$	$-\ J_{\text{e}}$	$\boldsymbol{F}_{\text{e}}^{\text{t}} \cdot \boldsymbol{b}_t^{\text{ext}}$
$\bar{\boldsymbol{B}}_t \in T^*\mathcal{B}_{\text{p}}$	$-\ \boldsymbol{F}_{\text{e}}^{\text{t}} \cdot [\,\bar{\boldsymbol{\pi}} \times \bar{\boldsymbol{a}}\,]$	$-\ \boldsymbol{f}_{\text{p}}^{\text{t}} \cdot \partial_{\boldsymbol{X}} \psi_t$	$-$	$\boldsymbol{F}_{\text{e}}^{\text{t}} \cdot \boldsymbol{b}_t^{\text{ext}}$
$\widetilde{\boldsymbol{B}}_0 \in T^*\mathcal{B}_0$	$-\ \boldsymbol{\Pi}^{\text{t}} : \nabla_{\boldsymbol{X}} \boldsymbol{F}$		$+\ J$	$\boldsymbol{F}^{\text{t}} \cdot \boldsymbol{b}_t^{\text{ext}}$
$\boldsymbol{B}_0 \in T^*\mathcal{B}_0$	$-\ \widetilde{\boldsymbol{\Pi}}^{\text{t}} : \nabla_{\boldsymbol{X}} \boldsymbol{F}_{\text{p}}$	$-\ \partial_{\boldsymbol{X}} \psi_0$	$-\ J$	$\boldsymbol{F}^{\text{t}} \cdot \boldsymbol{b}_t^{\text{ext}}$

2.4.4 Comparison of the spatial, material, and intermediate motion problem

The main objective of the subsequent section consists of the examination of further relations between the various volume forces. We perform the subsequent elaborations in order to (double–) check the previously obtained expressions which have been identified via (i) setting up different balance of linear momentum representations; (ii) introducing hyperelastic stress formats; (iii) relating different balance of linear momentum representations by means of pullback or pushforward transformations; (iv) arguments of comparison. As such, the following sections 2.4.4.1–2.4.4.3 are not mandatory and those readers mainly interested in the obtained results might skip these final verifications and continue with section 2.5. As point of departure, relations between Cauchy–type stress tensors together with the corresponding balance of linear momentum representations serve for the identification of the coherence between different volume forces. Following this procedure, some derivations are, apparently, repeated. For clarity's sake, however, we prefer to apply this highly structured approach.

For convenience of the reader, table 2.6 anticipates results by summarising transformations between representative configurational volume forces, whereby we restrict ourselves to (as compact as possible) illustrations in terms of $j\,\boldsymbol{b}_0^{\text{ext}} = \boldsymbol{b}_t^{\text{ext}} = \bar{\boldsymbol{b}}_t^{\text{ext}} = j_{\text{e}}\,\bar{\boldsymbol{b}}_{\text{p}}^{\text{ext}}$. As a fundamental property, we observe that $\widetilde{\boldsymbol{b}}_{0,\text{p}}, \bar{\boldsymbol{B}}_{\text{p},t} \in T^*\mathcal{B}_{\text{p}}$ incorporate gradients of distortions solely via dislocation density tensors whereas theses quantities directly occur within the representations of $\widetilde{\boldsymbol{B}}_{\text{p},0}, \boldsymbol{B}_{0,t} \in T^*\mathcal{B}_0$. As an interesting side aspect, $\widetilde{\boldsymbol{B}}_{\text{p},0}$ do not include any inhomogeneities stemming from explicit dependencies of the Helmholtz free energy density on material placements.

2.4.4.1 Spatial versus intermediate and material volume forces

First, recall that $\boldsymbol{b}_t = \bar{\boldsymbol{b}}_t$ explicitly follows from $\boldsymbol{\sigma}^{\text{t}} = \bar{\boldsymbol{\sigma}}^{\text{t}}$, compare eqs.(2.42,2.44,2.69), whereby $\boldsymbol{b}_{0,t}^{\text{int}}$ and $\bar{\boldsymbol{b}}_{\text{p},t}^{\text{int}}$ vanish due to translational invariance in physical space. Based on the representations highlighted in eqs.(2.113,2.123,2.130,2.160), we observe

$$
\begin{aligned}
\boldsymbol{b}_t^{\text{ext}} = \bar{\boldsymbol{b}}_t^{\text{ext}} &= -\,\boldsymbol{\sigma} \times \boldsymbol{d} - j\,\widetilde{\boldsymbol{\Pi}}^{\text{t}} : \nabla_{\boldsymbol{x}} \boldsymbol{F}_{\text{p}} && - \boldsymbol{f}^{\text{t}} \cdot \partial_{\boldsymbol{X}} \psi_t - \boldsymbol{f}^{\text{t}} \cdot \boldsymbol{B}_t \\
&= -\,[\,\bar{\boldsymbol{\sigma}} - \psi_t\,\boldsymbol{I}_t\,] \times \bar{\boldsymbol{d}} && - \boldsymbol{f}^{\text{t}} \cdot \partial_{\boldsymbol{X}} \psi_t - \boldsymbol{f}_{\text{e}}^{\text{t}} \cdot \bar{\boldsymbol{B}}_t \\
&= -\,\boldsymbol{\pi} \times \boldsymbol{a} - [\,j_{\text{e}}\,\widetilde{\boldsymbol{\pi}}^{\text{t}} - \psi_t\,\boldsymbol{F}_{\text{p}}^{\text{t}}\,] : \nabla_{\boldsymbol{x}} \boldsymbol{f}_{\text{p}} && - \boldsymbol{f}^{\text{t}} \cdot \partial_{\boldsymbol{X}} \psi_t - \boldsymbol{f}^{\text{t}} \cdot \boldsymbol{B}_t \\
&= -\,\bar{\boldsymbol{\pi}} \times \bar{\boldsymbol{a}} && - \boldsymbol{f}^{\text{t}} \cdot \partial_{\boldsymbol{X}} \psi_t - \boldsymbol{f}_{\text{e}}^{\text{t}} \cdot \bar{\boldsymbol{B}}_t
\end{aligned}
\tag{2.164}
$$

with the computation of $\boldsymbol{b}_0^{\text{ext}}$ and $\bar{\boldsymbol{b}}_{\text{p}}^{\text{ext}}$ being obvious. On the one hand it is straightforward to verify

$$j\,\widetilde{\boldsymbol{\Pi}}^{\text{t}} : \nabla_{\boldsymbol{x}}\boldsymbol{F}_{\text{p}} = [\, j_{\text{e}}\,\widetilde{\boldsymbol{\pi}}^{\text{t}} - \psi_t\,\boldsymbol{F}_{\text{p}}^{\text{t}}\,] : \nabla_{\boldsymbol{x}}\boldsymbol{f}_{\text{p}} = -\,j\,\widetilde{\boldsymbol{\Pi}}^{\text{t}} : [\,\boldsymbol{F}_{\text{p}}\,\overline{\otimes}\,\boldsymbol{F}_{\text{p}}\,] : \nabla_{\boldsymbol{x}}\boldsymbol{f}_{\text{p}} \tag{2.165}$$

from eqs.(2.92,2.4,2.9) and basic kinematic considerations, whereby $\boldsymbol{d}^{\text{t}} = \boldsymbol{0}$ as well as $\boldsymbol{a}^{\text{t}} = \boldsymbol{0}$. On the other hand, eq.(2.164) renders

$$\bar{\boldsymbol{\pi}} \times \bar{\boldsymbol{a}} = [\,\bar{\boldsymbol{\sigma}} - \psi_t\,\boldsymbol{I}_t\,] \times \bar{\boldsymbol{d}} = \big[\,[\,\psi_t\,\boldsymbol{I}_t - \bar{\boldsymbol{\sigma}}\,]\cdot\boldsymbol{F}_{\text{e}}\,\big] \times \bar{\boldsymbol{a}}\,, \tag{2.166}$$

wherein $\bar{\boldsymbol{d}}^{\text{t}} = \bar{\boldsymbol{A}}^{\text{t}} \cdot \text{cof}(\boldsymbol{f}_{\text{e}}) = -\,\boldsymbol{F}_{\text{e}} \cdot \bar{\boldsymbol{a}}^{\text{t}}$ and which recaptures eqs.(2.73,2.85); see appendix B for notational details. These elaborations enable us to formally relate the configurational volume forces $\boldsymbol{B}_t$ and $\bar{\boldsymbol{B}}_t$ via

$$\begin{aligned}
\boldsymbol{B}_t &= -\,j\,\widetilde{\boldsymbol{\Pi}}^{\text{t}} : \nabla_{\boldsymbol{X}}\boldsymbol{F}_{\text{p}} &&+\ \boldsymbol{F}^{\text{t}} \cdot \big[\,[\,\bar{\boldsymbol{\sigma}} - \psi_t\,\boldsymbol{I}_t\,] \times \bar{\boldsymbol{d}}\,\big] &&+\ \boldsymbol{F}_{\text{p}}^{\text{t}} \cdot \bar{\boldsymbol{B}}_t \\
&= -\,j\,\widetilde{\boldsymbol{\Pi}}^{\text{t}} : \nabla_{\boldsymbol{X}}\boldsymbol{F}_{\text{p}} &&+\ \boldsymbol{F}^{\text{t}} \cdot [\,\bar{\boldsymbol{\pi}} \times \bar{\boldsymbol{a}}\,] &&+\ \boldsymbol{F}_{\text{p}}^{\text{t}} \cdot \bar{\boldsymbol{B}}_t \\
&= -\,[\, j_{\text{e}}\,\widetilde{\boldsymbol{\pi}}^{\text{t}} - \psi_t\,\boldsymbol{F}_{\text{p}}^{\text{t}}\,] : \nabla_{\boldsymbol{X}}\boldsymbol{f}_{\text{p}} &&+\ \boldsymbol{F}^{\text{t}} \cdot \big[\,[\,\bar{\boldsymbol{\sigma}} - \psi_t\,\boldsymbol{I}_t\,] \times \bar{\boldsymbol{d}}\,\big] &&+\ \boldsymbol{F}_{\text{p}}^{\text{t}} \cdot \bar{\boldsymbol{B}}_t \\
&= -\,[\, j_{\text{e}}\,\widetilde{\boldsymbol{\pi}}^{\text{t}} - \psi_t\,\boldsymbol{F}_{\text{p}}^{\text{t}}\,] : \nabla_{\boldsymbol{X}}\boldsymbol{f}_{\text{p}} &&+\ \boldsymbol{F}^{\text{t}} \cdot [\,\bar{\boldsymbol{\pi}} \times \bar{\boldsymbol{a}}\,] &&+\ \boldsymbol{F}_{\text{p}}^{\text{t}} \cdot \bar{\boldsymbol{B}}_t\,.
\end{aligned} \tag{2.167}$$

Summarising, we finally conclude

$$\begin{aligned}
\boldsymbol{B}_t &= -\,j\,\widetilde{\boldsymbol{\Pi}}^{\text{t}} : \nabla_{\boldsymbol{X}}\boldsymbol{F}_{\text{p}} + \boldsymbol{F}^{\text{t}} \cdot [\,\bar{\boldsymbol{\pi}} \times \bar{\boldsymbol{a}}\,] + \boldsymbol{F}_{\text{p}}^{\text{t}} \cdot \bar{\boldsymbol{B}}_t \\
&= -\,j\,\nabla_{\boldsymbol{X}}\boldsymbol{F}_{\text{p}}^{\text{t}} : \widetilde{\boldsymbol{\Pi}}^{\text{t}} - j\,\widetilde{\boldsymbol{\Pi}} \times \widetilde{\boldsymbol{A}} + \boldsymbol{F}^{\text{t}} \cdot [\,\bar{\boldsymbol{\pi}} \times \bar{\boldsymbol{a}}\,] + \boldsymbol{F}_{\text{p}}^{\text{t}} \cdot \bar{\boldsymbol{B}}_t \\
&= -\,[\,\nabla_{\boldsymbol{x}}\boldsymbol{F}_{\text{p}}^{\text{t}} \cdot \text{cof}(\boldsymbol{f}^{\text{t}})\,] : \widetilde{\boldsymbol{\Pi}}^{\text{t}} + \boldsymbol{F}_{\text{p}}^{\text{t}} \cdot \bar{\boldsymbol{B}}_t \\
&= -\,\nabla_{\boldsymbol{x}}\boldsymbol{F}_{\text{p}}^{\text{t}} : \bar{\boldsymbol{\pi}}^{\text{t}} + \boldsymbol{F}_{\text{p}}^{\text{t}} \cdot \bar{\boldsymbol{B}}_t\,,
\end{aligned} \tag{2.168}$$

see eqs.(2.29,2.34,2.78) and appendix B.

2.4.4.2 Intermediate versus spatial and material volume forces

Second, recall that $\widetilde{\boldsymbol{b}}_{\text{p}} = \bar{\boldsymbol{B}}_{\text{p}}$ follows directly from $\widetilde{\boldsymbol{\sigma}}^{\text{t}} = \bar{\boldsymbol{\Sigma}}^{\text{t}}$, compare eqs.(2.50,2.52,2.79). Based on the representations highlighted in eqs.(2.120,2.140,2.153,2.163) we observe

$$\begin{aligned}
\widetilde{\boldsymbol{b}}_{\text{p}} = \bar{\boldsymbol{B}}_{\text{p}} &= -\,[\,\bar{\boldsymbol{\Pi}} - \psi_{\text{p}}\,\boldsymbol{f}_{\text{e}}\,] \times \bar{\boldsymbol{A}} &&-\ \boldsymbol{f}_{\text{p}}^{\text{t}} \cdot \partial_{\boldsymbol{X}}\psi_{\text{p}} - \boldsymbol{F}_{\text{e}}^{\text{t}} \cdot \bar{\boldsymbol{b}}_{\text{p}}^{\text{ext}} \\
&= -\,[\,\widetilde{\boldsymbol{\pi}} - \psi_{\text{p}}\,\boldsymbol{F}_{\text{p}}\,] \times \widetilde{\boldsymbol{a}} \\
&\quad -\,[\, J_{\text{e}}\,\boldsymbol{\pi}^{\text{t}} - \psi_{\text{p}}\,\boldsymbol{F}^{\text{t}}\,] : \widetilde{\nabla}\boldsymbol{f} &&-\ \boldsymbol{f}_{\text{p}}^{\text{t}} \cdot \partial_{\boldsymbol{X}}\psi_{\text{p}} - \boldsymbol{f}_{\text{p}}^{\text{t}} \cdot \widetilde{\boldsymbol{B}}_{\text{p}} \\
&= -\,\widetilde{\boldsymbol{\sigma}} \times \widetilde{\boldsymbol{d}} - j_{\text{p}}\,\boldsymbol{\Pi}^{\text{t}} : \widetilde{\nabla}\boldsymbol{F} &&-\ \boldsymbol{f}_{\text{p}}^{\text{t}} \cdot \partial_{\boldsymbol{X}}\psi_{\text{p}} - \boldsymbol{f}_{\text{p}}^{\text{t}} \cdot \widetilde{\boldsymbol{B}}_{\text{p}} \\
&= -\,\bar{\boldsymbol{\Sigma}} \times \bar{\boldsymbol{D}} &&-\ \boldsymbol{f}_{\text{p}}^{\text{t}} \cdot \partial_{\boldsymbol{X}}\psi_{\text{p}} - \boldsymbol{F}_{\text{e}}^{\text{t}} \cdot \bar{\boldsymbol{b}}_{\text{p}}^{\text{ext}}
\end{aligned} \tag{2.169}$$

with the computation of $\widetilde{\boldsymbol{b}}_0$ and $\bar{\boldsymbol{B}}_t$ being obvious. On the one hand it is straightforward to verify

$$[\,\bar{\boldsymbol{\Pi}} - \psi_{\text{p}}\,\boldsymbol{f}_{\text{e}}\,] \times \bar{\boldsymbol{A}} = \bar{\boldsymbol{\Sigma}} \times \bar{\boldsymbol{D}} = -\,[\,\bar{\boldsymbol{\Sigma}} \cdot \boldsymbol{f}_{\text{e}}\,] \times \bar{\boldsymbol{A}} \tag{2.170}$$

from eqs.(2.75,2.83,2.29,2.35). On the other hand, eq.(2.169) renders

$$\begin{aligned}
[\,\widetilde{\boldsymbol{\pi}} - \psi_{\text{p}}\,\boldsymbol{F}_{\text{p}}\,] \times \widetilde{\boldsymbol{a}} &= \quad j_{\text{p}}\,\boldsymbol{\Pi}^{\text{t}} : \widetilde{\nabla}\boldsymbol{F} - [\, J_{\text{e}}\,\boldsymbol{\pi}^{\text{t}} - \psi_{\text{p}}\,\boldsymbol{F}^{\text{t}}\,] : \widetilde{\nabla}\boldsymbol{f} + \widetilde{\boldsymbol{\sigma}} \times \widetilde{\boldsymbol{d}} \\
&= \quad j_{\text{p}}\,\boldsymbol{\Pi}^{\text{t}} : \widetilde{\nabla}\boldsymbol{F} + [\, j_{\text{p}}\,\boldsymbol{F}^{\text{t}} \cdot \boldsymbol{\Pi}^{\text{t}} \cdot \boldsymbol{F}^{\text{t}}\,] : \widetilde{\nabla}\boldsymbol{f} \\
&\quad + [\,\psi_{\text{p}}\,\boldsymbol{I}_{\text{p}} - \widetilde{\boldsymbol{\pi}} \cdot \boldsymbol{f}_{\text{p}}\,] \times \widetilde{\boldsymbol{d}} \\
&= \quad \big[\,[\,\widetilde{\boldsymbol{\pi}} \cdot \boldsymbol{f}_{\text{p}} - \psi_{\text{p}}\,\boldsymbol{I}_{\text{p}}\,] \cdot \boldsymbol{F}_{\text{p}}\,\big] \times \widetilde{\boldsymbol{a}}\,,
\end{aligned} \tag{2.171}$$

whereby use of eqs.(2.70,2.96,2.38) and basic kinematic relations has been made; see appendix B for notational details. Apparently, eq.(2.171) recaptures eqs.(2.80,2.92). These elaborations enable us to formally relate the configurational volume forces $\bar{\boldsymbol{b}}_{\mathrm{p}}^{\mathrm{ext}}$ and $\widetilde{\boldsymbol{B}}_{\mathrm{p}}$ via

$$\begin{aligned}
\bar{\boldsymbol{b}}_{\mathrm{p}}^{\mathrm{ext}} &= -\,\boldsymbol{f}_{\mathrm{e}}^{\mathrm{t}}\cdot\big[\,[\,\bar{\boldsymbol{\Pi}}-\psi_{\mathrm{p}}\,\boldsymbol{f}_{\mathrm{e}}\,]\times\bar{\boldsymbol{A}}\,\big]\;+\;\boldsymbol{f}_{\mathrm{e}}^{\mathrm{t}}\cdot[\,\widetilde{\boldsymbol{\pi}}-\psi_{\mathrm{p}}\,\boldsymbol{F}_{\mathrm{p}}\,]\times\widetilde{\boldsymbol{a}}\\
&\quad+\,[\,J_{\mathrm{e}}\,\boldsymbol{\pi}^{\mathrm{t}}-\psi_{\mathrm{p}}\,\boldsymbol{F}^{\mathrm{t}}\,]:\nabla_{\boldsymbol{x}}\boldsymbol{f}\qquad+\;\boldsymbol{f}^{\mathrm{t}}\cdot\widetilde{\boldsymbol{B}}_{\mathrm{p}}\\
&= -\,\boldsymbol{f}_{\mathrm{e}}^{\mathrm{t}}\cdot\big[\,[\,\bar{\boldsymbol{\Pi}}-\psi_{\mathrm{p}}\,\boldsymbol{f}_{\mathrm{e}}\,]\times\bar{\boldsymbol{A}}\,\big]\;+\;\boldsymbol{f}_{\mathrm{e}}^{\mathrm{t}}\cdot[\,\widetilde{\boldsymbol{\sigma}}\times\widetilde{\boldsymbol{d}}\,]\\
&\quad+\,j_{\mathrm{p}}\,\boldsymbol{\Pi}^{\mathrm{t}}:\nabla_{\boldsymbol{x}}\boldsymbol{F}\qquad\qquad\qquad+\;\boldsymbol{f}^{\mathrm{t}}\cdot\widetilde{\boldsymbol{B}}_{\mathrm{p}}\\
&= -\,\boldsymbol{f}_{\mathrm{e}}^{\mathrm{t}}\cdot[\,\bar{\boldsymbol{\Sigma}}\times\bar{\boldsymbol{D}}\,]\qquad\qquad\qquad+\;\boldsymbol{f}_{\mathrm{e}}^{\mathrm{t}}\cdot[\,\widetilde{\boldsymbol{\pi}}-\psi_{\mathrm{p}}\,\boldsymbol{F}_{\mathrm{p}}\,]\times\widetilde{\boldsymbol{a}}\\
&\quad+\,[\,J_{\mathrm{e}}\,\boldsymbol{\pi}^{\mathrm{t}}-\psi_{\mathrm{p}}\,\boldsymbol{F}^{\mathrm{t}}\,]:\nabla_{\boldsymbol{x}}\boldsymbol{f}\qquad+\;\boldsymbol{f}^{\mathrm{t}}\cdot\widetilde{\boldsymbol{B}}_{\mathrm{p}}\\
&= -\,\boldsymbol{f}_{\mathrm{e}}^{\mathrm{t}}\cdot[\,\bar{\boldsymbol{\Sigma}}\times\bar{\boldsymbol{D}}\,]\qquad\qquad\qquad+\;\boldsymbol{f}_{\mathrm{e}}^{\mathrm{t}}\cdot[\,\widetilde{\boldsymbol{\sigma}}\times\widetilde{\boldsymbol{d}}\,]\\
&\quad+\,j_{\mathrm{p}}\,\boldsymbol{\Pi}^{\mathrm{t}}:\nabla_{\boldsymbol{x}}\boldsymbol{F}\qquad\qquad\qquad+\;\boldsymbol{f}^{\mathrm{t}}\cdot\widetilde{\boldsymbol{B}}_{\mathrm{p}}\,.
\end{aligned}\tag{2.172}$$

Summarising, we finally conclude

$$\bar{\boldsymbol{b}}_{\mathrm{p}}^{\mathrm{ext}}=j_{\mathrm{p}}\,\boldsymbol{\Pi}^{\mathrm{t}}:\nabla_{\boldsymbol{x}}\boldsymbol{F}+\boldsymbol{f}^{\mathrm{t}}\cdot\widetilde{\boldsymbol{B}}_{\mathrm{p}}\,,\tag{2.173}$$

see eqs.(2.35,2.79).

2.4.4.3 Material versus spatial and intermediate volume forces

Third, recall that $\boldsymbol{B}_0\neq\widetilde{\boldsymbol{B}}_0$ follows directly from $\boldsymbol{\Sigma}^{\mathrm{t}}\neq\widetilde{\boldsymbol{\Sigma}}^{\mathrm{t}}$, compare eqs.(2.46,2.48,2.90). Based on the representations highlighted in eqs.(2.110,2.133) and eqs.(2.143,2.150), however, we observe

$$\begin{aligned}
\boldsymbol{B}_0 &= -\,\boldsymbol{\Pi}\times\boldsymbol{A}\;-\;\widetilde{\boldsymbol{\Pi}}^{\mathrm{t}}:\nabla_{\boldsymbol{X}}\boldsymbol{F}_{\mathrm{p}}\qquad\qquad-\;\partial_{\boldsymbol{X}}\psi_0\;-\;\boldsymbol{F}^{\mathrm{t}}\cdot\boldsymbol{b}_0^{\mathrm{ext}}\\
&= -\,\boldsymbol{\Sigma}\times\boldsymbol{D}\;-\;[\,J_{\mathrm{p}}\,\widetilde{\boldsymbol{\pi}}^{\mathrm{t}}-\psi_0\,\boldsymbol{F}_{\mathrm{p}}^{\mathrm{t}}\,]:\nabla_{\boldsymbol{X}}\boldsymbol{f}_{\mathrm{p}}\;-\;\partial_{\boldsymbol{X}}\psi_0\;-\;\boldsymbol{F}^{\mathrm{t}}\cdot\boldsymbol{b}_0^{\mathrm{ext}}\,,
\end{aligned}\tag{2.174}$$

wherein $\boldsymbol{A}^{\mathrm{t}}=\boldsymbol{0}$ as well as $\boldsymbol{D}^{\mathrm{t}}=\boldsymbol{0}$ and which is directly verified via eq.(2.165). By analogy with eq.(2.174), we consequently conclude

$$\begin{aligned}
\widetilde{\boldsymbol{B}}_0 &= -\,[\,\widetilde{\boldsymbol{\Sigma}}-\psi_0\,\boldsymbol{I}_0\,]\times\widetilde{\boldsymbol{D}}\;-\;[\,J\,\boldsymbol{\pi}^{\mathrm{t}}-\psi_0\,\boldsymbol{F}^{\mathrm{t}}\,]:\nabla_{\boldsymbol{X}}\boldsymbol{f}\;-\;\partial_{\boldsymbol{X}}\psi_0\;-\;\boldsymbol{F}_{\mathrm{p}}^{\mathrm{t}}\cdot\widetilde{\boldsymbol{b}}_0\\
&= -\,\widetilde{\boldsymbol{\Pi}}\times\widetilde{\boldsymbol{A}}\qquad\qquad-\;\boldsymbol{\Pi}^{\mathrm{t}}:\nabla_{\boldsymbol{X}}\boldsymbol{F}\qquad\qquad-\;\partial_{\boldsymbol{X}}\psi_0\;-\;\boldsymbol{F}_{\mathrm{p}}^{\mathrm{t}}\cdot\widetilde{\boldsymbol{b}}_0
\end{aligned}\tag{2.175}$$

which is easily proven by the relations

$$[\,\widetilde{\boldsymbol{\Sigma}}-\psi_0\,\boldsymbol{I}_0\,]\times\widetilde{\boldsymbol{D}}=\big[\,[\,\psi_0\,\boldsymbol{I}_0-\widetilde{\boldsymbol{\Sigma}}\,]\cdot\boldsymbol{F}_{\mathrm{p}}\,\big]\times\widetilde{\boldsymbol{A}}=\widetilde{\boldsymbol{\Pi}}\times\widetilde{\boldsymbol{A}}\,,\tag{2.176}$$

whereby $\widetilde{\boldsymbol{D}}^{\mathrm{t}}=-\,\boldsymbol{f}_{\mathrm{p}}\cdot\widetilde{\boldsymbol{A}}^{\mathrm{t}}$, and

$$\begin{aligned}
[\,J\,\boldsymbol{\pi}^{\mathrm{t}}-\psi_0\,\boldsymbol{F}^{\mathrm{t}}\,]:\nabla_{\boldsymbol{X}}\boldsymbol{f} &= [\,\psi_0\,\boldsymbol{F}^{\mathrm{t}}-J\,\boldsymbol{\pi}^{\mathrm{t}}\,]:[\,\boldsymbol{f}\,\overline{\otimes}\,\boldsymbol{f}\,]:\nabla_{\boldsymbol{X}}\boldsymbol{F}\\
&= [\,\psi_0\,\boldsymbol{f}^{\mathrm{t}}-\boldsymbol{f}^{\mathrm{t}}\cdot\boldsymbol{\pi}^{\mathrm{t}}\cdot\mathrm{cof}(\boldsymbol{F})\,]:\nabla_{\boldsymbol{X}}\boldsymbol{F}=\boldsymbol{\Pi}^{\mathrm{t}}:\nabla_{\boldsymbol{X}}\boldsymbol{F}\,,
\end{aligned}\tag{2.177}$$

respectively; recall eqs.(2.81,2.91) as well as eqs.(2.71,2.96). Apparently, the configurational volume forces $\boldsymbol{B}_0$ and $\widetilde{\boldsymbol{B}}_0$ in eqs.(2.46,2.48) are connected via eq.(2.90), namely

$$\begin{aligned}
\nabla_{\boldsymbol{X}}\cdot\boldsymbol{\Sigma}^{\mathrm{t}}+\boldsymbol{B}_0 &= \nabla_{\boldsymbol{X}}\cdot(\,\psi_0\,\boldsymbol{I}_0^{\mathrm{t}}-\widetilde{\boldsymbol{\Sigma}}^{\mathrm{t}}\,)+\boldsymbol{B}_0\\
&= \nabla_{\boldsymbol{X}}\cdot(\,\psi_0\,\boldsymbol{I}_0^{\mathrm{t}}-\boldsymbol{\Sigma}^{\mathrm{t}}\,)+\widetilde{\boldsymbol{B}}_0=\nabla_{\boldsymbol{X}}\cdot\widetilde{\boldsymbol{\Sigma}}^{\mathrm{t}}+\widetilde{\boldsymbol{B}}_0
\end{aligned}\tag{2.178}$$

such that

$$\boldsymbol{B}_0 = \nabla_{\boldsymbol{X}} \cdot (\psi_0 \, \boldsymbol{I}_0^{\mathrm{t}} - 2 \, \boldsymbol{\Sigma}^{\mathrm{t}}) + \widetilde{\boldsymbol{B}}_0 = \nabla_{\boldsymbol{X}} \cdot (2 \, \widetilde{\boldsymbol{\Sigma}}^{\mathrm{t}} - \psi_0 \, \boldsymbol{I}_0^{\mathrm{t}}) + \widetilde{\boldsymbol{B}}_0 \, . \tag{2.179}$$

This relation finally enables us to conclude

$$\begin{aligned}
\boldsymbol{b}_0^{\mathrm{ext}} = \quad & \boldsymbol{f}^{\mathrm{t}} \cdot \big[\, \widetilde{\boldsymbol{\Pi}} \times \widetilde{\boldsymbol{A}} - \nabla_{\boldsymbol{X}} \cdot (2 \, \widetilde{\boldsymbol{\Sigma}}^{\mathrm{t}} - \psi_0 \, \boldsymbol{I}_0^{\mathrm{t}}) \, \big] \\
& - \widetilde{\boldsymbol{\Pi}}^{\mathrm{t}} : \nabla_{\boldsymbol{x}} \boldsymbol{F}_{\mathrm{p}} + \boldsymbol{\Pi}^{\mathrm{t}} : \nabla_{\boldsymbol{x}} \boldsymbol{F} + \boldsymbol{f}_{\mathrm{e}}^{\mathrm{t}} \cdot \widetilde{\boldsymbol{b}}_0 \\
= \quad & \boldsymbol{f}^{\mathrm{t}} \cdot \big[\, \widetilde{\boldsymbol{\Pi}} \times \widetilde{\boldsymbol{A}} - 2 \, \nabla_{\boldsymbol{X}} \cdot \widetilde{\boldsymbol{\Sigma}}^{\mathrm{t}} + \widetilde{\boldsymbol{\Pi}}^{\mathrm{t}} : \nabla_{\boldsymbol{X}} \boldsymbol{F}_{\mathrm{p}} + \boldsymbol{\Pi}^{\mathrm{t}} : \nabla_{\boldsymbol{X}} \boldsymbol{F} + \partial_{\boldsymbol{X}} \psi_0 \, \big] \\
& - \widetilde{\boldsymbol{\Pi}}^{\mathrm{t}} : \nabla_{\boldsymbol{x}} \boldsymbol{F}_{\mathrm{p}} + \boldsymbol{\Pi}^{\mathrm{t}} : \nabla_{\boldsymbol{x}} \boldsymbol{F} + \boldsymbol{f}_{\mathrm{e}}^{\mathrm{t}} \cdot \widetilde{\boldsymbol{b}}_0 \\
= \quad & \boldsymbol{f}^{\mathrm{t}} \cdot \big[\, \widetilde{\boldsymbol{\Pi}} \times \widetilde{\boldsymbol{A}} - 2 \, \nabla_{\boldsymbol{X}} \cdot \widetilde{\boldsymbol{\Sigma}}^{\mathrm{t}} \, \big] + 2 \, \boldsymbol{\Pi}^{\mathrm{t}} : \nabla_{\boldsymbol{x}} \boldsymbol{F} + \partial_{\boldsymbol{X}} \psi_0 + \boldsymbol{f}_{\mathrm{e}}^{\mathrm{t}} \cdot \widetilde{\boldsymbol{b}}_0 \\
= \, - \, & \boldsymbol{f}^{\mathrm{t}} \cdot \big[\, \widetilde{\boldsymbol{\Pi}} \times \widetilde{\boldsymbol{A}} \, \big] - \boldsymbol{f}^{\mathrm{t}} \cdot \partial_{\boldsymbol{X}} \psi_0 - \boldsymbol{f}_{\mathrm{e}}^{\mathrm{t}} \cdot \widetilde{\boldsymbol{b}}_0 \, ,
\end{aligned} \tag{2.180}$$

whereby use of $\boldsymbol{A}^{\mathrm{t}} = \boldsymbol{0}$ and eqs.(2.147,2.48,2.150) has been made. An alternative derivation of eq.(2.180) is based on the relation $\boldsymbol{b}_0^{\mathrm{ext}} = J_{\mathrm{p}} \, \bar{\boldsymbol{b}}_{\mathrm{p}}^{\mathrm{ext}} (\bar{\boldsymbol{B}}_{\mathrm{p}} = \widetilde{\boldsymbol{b}}_{\mathrm{p}})$, recall eqs.(2.43,2.45) and eqs.(2.122,2.161), namely

$$\begin{aligned}
\boldsymbol{b}_0^{\mathrm{ext}} &= - \, J_{\mathrm{p}} \, \boldsymbol{f}_{\mathrm{e}}^{\mathrm{t}} \cdot \big[\, \bar{\boldsymbol{\Sigma}} \times \bar{\boldsymbol{D}} \, \big] - \boldsymbol{f}^{\mathrm{t}} \cdot \partial_{\boldsymbol{X}} \psi_0 - \boldsymbol{f}_{\mathrm{e}}^{\mathrm{t}} \cdot \widetilde{\boldsymbol{b}}_0 \\
&= - \, \boldsymbol{f}^{\mathrm{t}} \cdot \big[\, \widetilde{\boldsymbol{\Pi}} \times \widetilde{\boldsymbol{A}} \, \big] \quad - \boldsymbol{f}^{\mathrm{t}} \cdot \partial_{\boldsymbol{X}} \psi_0 - \boldsymbol{f}_{\mathrm{e}}^{\mathrm{t}} \cdot \widetilde{\boldsymbol{b}}_0 \, ,
\end{aligned} \tag{2.181}$$

whereby eqs.(2.161,2.35,2.78) have been applied; see also appendix B.

Remark 2.4.1 *The elaborations above enable us to review all relations between the derived volume forces – similar to the dislocation density tensors and stresses in tables 2.1–2.5. For physical reasons, however, we are in particular interested in representations of configurational volume forces with respect to* $\boldsymbol{b}_{t,0}^{\mathrm{ext}}$ *and* $\bar{\boldsymbol{b}}_{t,\mathrm{p}}^{\mathrm{ext}}$ *as summarised in table 2.6. The underlying derivations are straightforward, for example*

$$\begin{aligned}
\widetilde{\boldsymbol{b}}_{\mathrm{p}} &= - \, \widetilde{\boldsymbol{\sigma}} \times \widetilde{\boldsymbol{d}} - j_{\mathrm{p}} \, \boldsymbol{\Pi}^{\mathrm{t}} : \widetilde{\nabla} \boldsymbol{F} - \boldsymbol{f}_{\mathrm{p}}^{\mathrm{t}} \cdot \partial_{\boldsymbol{X}} \psi_{\mathrm{p}} - \boldsymbol{f}_{\mathrm{p}}^{\mathrm{t}} \cdot \widetilde{\boldsymbol{B}}_{\mathrm{p}} \\
&= - \, \widetilde{\boldsymbol{\sigma}} \times \widetilde{\boldsymbol{d}} - j_{\mathrm{p}} \, \boldsymbol{\Pi}^{\mathrm{t}} : \widetilde{\nabla} \boldsymbol{F} - \boldsymbol{f}_{\mathrm{p}}^{\mathrm{t}} \cdot \partial_{\boldsymbol{X}} \psi_{\mathrm{p}} + j_{\mathrm{p}} \, \boldsymbol{\Pi}^{\mathrm{t}} : \bar{\nabla} \boldsymbol{F} - \boldsymbol{F}^{\mathrm{t}} \cdot \bar{\boldsymbol{b}}_{\mathrm{p}}^{\mathrm{ext}} \\
&= - \, \widetilde{\boldsymbol{\sigma}} \times \widetilde{\boldsymbol{d}} - \boldsymbol{f}_{\mathrm{p}}^{\mathrm{t}} \cdot \partial_{\boldsymbol{X}} \psi_{\mathrm{p}} - \boldsymbol{F}^{\mathrm{t}} \cdot \bar{\boldsymbol{b}}_{\mathrm{p}}^{\mathrm{ext}} \, ,
\end{aligned} \tag{2.182}$$

recall eqs.(2.153,2.173), with $\widetilde{\boldsymbol{\sigma}} \times \widetilde{\boldsymbol{d}} = \bar{\boldsymbol{\Sigma}} \times \bar{\boldsymbol{D}}$ *being obvious from eqs.(2.35,2.79). Most of these results are given previously in this section.*

2.5 Peach–Koehler force

A classical example of a material or rather configurational force is highlighted in the subsequent section, namely a representation of the celebrated Peach–Koehler force that we propose to express in the intermediate configuration. Since this configurational volume force should be located in the incompatible intermediate configuration, we consequently take volume forces in $T^*\mathcal{B}_{\mathrm{p}}$ into account; see the summary in table 2.6. Let $\widetilde{\mathbf{F}} = \bar{\mathbf{F}} \in T^*\mathcal{B}_{\mathrm{p}}$ denote such a

configurational force, so that the following alternative expressions apply

$$\begin{aligned}
\widetilde{\mathbf{F}} &= \int_{\mathcal{V}_0} \widetilde{\boldsymbol{b}}_0 \;\; \mathrm{d}V_0 \;=\; -\int_{\mathcal{V}_0} \boldsymbol{f}_{\mathrm{p}}^{\mathrm{t}} \cdot [\, \widetilde{\boldsymbol{\Pi}} \times \widetilde{\boldsymbol{A}} \,] \;\mathrm{d}V_0 \\
&= \int_{\mathcal{V}_{\mathrm{p}}} \widetilde{\boldsymbol{b}}_{\mathrm{p}} \;\; \mathrm{d}V_{\mathrm{p}} \;=\; -\int_{\mathcal{V}_{\mathrm{p}}} \quad \widetilde{\boldsymbol{\sigma}} \times \widetilde{\boldsymbol{d}} \quad \mathrm{d}V_{\mathrm{p}} \\
&= \int_{\mathcal{V}_{\mathrm{p}}} \bar{\boldsymbol{B}}_{\mathrm{p}} \; \mathrm{d}V_{\mathrm{p}} \;=\; -\int_{\mathcal{V}_{\mathrm{p}}} \quad \bar{\boldsymbol{\Sigma}} \times \bar{\boldsymbol{D}} \quad \mathrm{d}V_{\mathrm{p}} \\
&= \int_{\mathcal{V}_t} \bar{\boldsymbol{B}}_t \;\; \mathrm{d}V_t \;=\; -\int_{\mathcal{V}_t} \boldsymbol{F}_{\mathrm{e}}^{\mathrm{t}} \cdot [\, \bar{\boldsymbol{\pi}} \times \bar{\boldsymbol{a}} \,] \quad \mathrm{d}V_t \;=\; \bar{\mathbf{F}} \,,
\end{aligned} \tag{2.183}$$

wherein any dependence of the Helmholtz free energy density on material placements, $\partial_{\boldsymbol{X}} \psi_0$, as well as external volume forces, $\boldsymbol{b}_t^{\mathrm{ext}}$, have been neglected for conceptual simplicity. Please note that eq.(2.183) incorporates solely dislocation density tensors in contrast to volume forces in $T^*\mathcal{B}_0$, compare table 2.6, which therefore are less suitable concerning the derivation of a Peach–Koehler force. This quantity, as a paradigm of a configurational volume force, takes the interpretation as driving a single dislocation. Accordingly, we represent such a single dislocation in the domain of interest via $\widetilde{\boldsymbol{A}}^{\mathrm{t}} \doteq \delta_0 \, \widetilde{\boldsymbol{b}}_0^{\mathrm{bur}} \otimes \widetilde{\boldsymbol{T}}_0$ and $\widetilde{\boldsymbol{d}}^{\mathrm{t}} \doteq \delta_{\mathrm{p}} \, \widetilde{\boldsymbol{b}}_{\mathrm{p}}^{\mathrm{bur}} \otimes \widetilde{\boldsymbol{T}}_{\mathrm{p}} \equiv \delta_{\mathrm{p}} \, \bar{\boldsymbol{B}}_{\mathrm{p}}^{\mathrm{bur}} \otimes \bar{\boldsymbol{T}}_{\mathrm{p}} \doteq \bar{\boldsymbol{D}}^{\mathrm{t}}$ as well as $\bar{\boldsymbol{a}}^{\mathrm{t}} \doteq \delta_t \, \bar{\boldsymbol{B}}_t^{\mathrm{bur}} \otimes \bar{\boldsymbol{T}}_t$, wherein $J_{\mathrm{p}} \, \delta_0 = \delta_{\mathrm{p}} = j_{\mathrm{e}} \, \delta_t$ denote Dirac–delta distributions , so that

$$\begin{aligned}
\widetilde{\mathbf{F}}^{\mathrm{PK}} &= -\int_{\mathcal{V}_0} \quad \boldsymbol{f}_{\mathrm{p}}^{\mathrm{t}} \cdot \big[\, \widetilde{\boldsymbol{\Pi}} \times \; [\, \delta_0 \, \widetilde{\boldsymbol{b}}_0^{\mathrm{bur}} \otimes \widetilde{\boldsymbol{T}}_0]^{\mathrm{t}} \,\big] \; \mathrm{d}V_0 \\
&= -\int_{\mathcal{L}_{\mathrm{p}}} \mathrm{cof}(\boldsymbol{F}_{\mathrm{p}}) \cdot \big[\, [\, \widetilde{\boldsymbol{\Pi}} \cdot \widetilde{\boldsymbol{b}}_{\mathrm{p}}^{\mathrm{bur}} \,] \times \widetilde{\boldsymbol{T}}_0 \quad \big] \; \mathrm{d}L_{\mathrm{p}} \\
&= -\int_{\mathcal{V}_{\mathrm{p}}} \quad \widetilde{\boldsymbol{\sigma}} \times \; [\, \delta_{\mathrm{p}} \, \widetilde{\boldsymbol{b}}_{\mathrm{p}}^{\mathrm{bur}} \otimes \widetilde{\boldsymbol{T}}_{\mathrm{p}} \,]^{\mathrm{t}} \quad \mathrm{d}V_{\mathrm{p}} \\
&= -\int_{\mathcal{L}_{\mathrm{p}}} \quad [\, \widetilde{\boldsymbol{\sigma}} \cdot \widetilde{\boldsymbol{b}}_{\mathrm{p}}^{\mathrm{bur}} \,] \times \widetilde{\boldsymbol{T}}_{\mathrm{p}} \quad \mathrm{d}L_{\mathrm{p}} \\
&= -\int_{\mathcal{V}_{\mathrm{p}}} \quad \bar{\boldsymbol{\Sigma}} \times [\, \delta_{\mathrm{p}} \, \bar{\boldsymbol{B}}_{\mathrm{p}}^{\mathrm{bur}} \otimes \bar{\boldsymbol{T}}_{\mathrm{p}} \,]^{\mathrm{t}} \quad \mathrm{d}V_{\mathrm{p}} \\
&= -\int_{\mathcal{L}_{\mathrm{p}}} \quad [\, \bar{\boldsymbol{\Sigma}} \cdot \bar{\boldsymbol{B}}_{\mathrm{p}}^{\mathrm{bur}} \,] \times \bar{\boldsymbol{T}}_{\mathrm{p}} \quad \mathrm{d}L_{\mathrm{p}} \\
&= -\int_{\mathcal{V}_t} \quad \boldsymbol{F}_{\mathrm{e}}^{\mathrm{t}} \cdot \big[\, \bar{\boldsymbol{\pi}} \times [\, \delta_t \, \bar{\boldsymbol{B}}_t^{\mathrm{bur}} \otimes \bar{\boldsymbol{T}}_t \,]^{\mathrm{t}} \,\big] \; \mathrm{d}V_t \\
&= -\int_{\mathcal{L}_{\mathrm{p}}} \mathrm{cof}(\boldsymbol{f}_{\mathrm{e}}) \cdot \big[\, [\, \bar{\boldsymbol{\pi}} \cdot \bar{\boldsymbol{B}}_{\mathrm{p}}^{\mathrm{bur}} \,] \times \bar{\boldsymbol{T}}_t \quad \big] \; \mathrm{d}L_{\mathrm{p}} \;=\; \bar{\mathbf{F}}^{\mathrm{PK}}
\end{aligned} \tag{2.184}$$

with $j_{\mathrm{p}} \, \widetilde{\boldsymbol{b}}_0^{\mathrm{bur}} = \widetilde{\boldsymbol{b}}_{\mathrm{p}}^{\mathrm{bur}} = \bar{\boldsymbol{B}}_{\mathrm{p}}^{\mathrm{bur}} = J_{\mathrm{e}} \, \bar{\boldsymbol{B}}_t^{\mathrm{bur}} \in T\mathcal{B}_{\mathrm{p}}$ being defined by means of eqs.(2.15,2.17), see also remark 2.1.2. The unit vectors $\widetilde{\boldsymbol{T}}_{\mathrm{p}} \equiv \bar{\boldsymbol{T}}_{\mathrm{p}} \in T\mathcal{B}_{\mathrm{p}}$ characterise the tangent according to the dislocation line $\mathcal{L}_{\mathrm{p}}$ while $\widetilde{\boldsymbol{T}}_0 = \boldsymbol{f}_{\mathrm{p}} \cdot \widetilde{\boldsymbol{T}}_{\mathrm{p}} \in T\mathcal{B}_0$ and $\bar{\boldsymbol{T}}_t = \boldsymbol{F}_{\mathrm{e}} \cdot \bar{\boldsymbol{T}}_{\mathrm{p}} \in T\mathcal{B}_t$, respectively. Note the familiar format of the Peach–Koehler force per unit length, $[\, \widetilde{\boldsymbol{\sigma}} \cdot \widetilde{\boldsymbol{b}}_{\mathrm{p}}^{\mathrm{bur}} \,] \times \widetilde{\boldsymbol{T}}_{\mathrm{p}} \equiv [\, \bar{\boldsymbol{\Sigma}} \cdot \bar{\boldsymbol{B}}_{\mathrm{p}}^{\mathrm{bur}} \,] \times \bar{\boldsymbol{T}}_{\mathrm{p}}$, nevertheless in terms of intermediate motion plastic or elastic Cauchy

stresses that allow representation in energy momentum format; compare the discussion in Ericksen (1998b).

2.5.1 Application to crystal plasticity

A demonstrative application of the derived Peach–Koehler force consists of its relation to continuum crystal–plasticity formulations. In order to briefly review this classical modelling approach, we adopt the representation of $\bar{\mathrm{F}}^{\mathrm{PK}}$ determined for instance in terms of $\bar{\boldsymbol{\Sigma}}^{\mathrm{t}}$, elaborations based on different stress tensors being straightforward. From eq.(2.67) we conclude that the second part of $\bar{\boldsymbol{\Sigma}}^{\mathrm{t}}$, together with a change in sign, apparently coincides with the celebrated intermediate configuration Mandel stress tensor.

Now, let a slip system I in the intermediate configuration be defined in terms of the slip direction $\bar{\boldsymbol{S}}_I$ and the slip normal $\bar{\boldsymbol{M}}_I$ with $\bar{\boldsymbol{S}}_I \cdot \bar{\boldsymbol{M}}_I = 0$. The corresponding projected Schmid stress consequently results in

$$\tau_I = -\bar{\boldsymbol{S}}_I \cdot \bar{\boldsymbol{\Sigma}}^{\mathrm{t}} \cdot \bar{\boldsymbol{M}}_I = \bar{\boldsymbol{S}}_I \cdot \boldsymbol{F}_{\mathrm{e}}^{\mathrm{t}} \cdot \partial_{\boldsymbol{F}_{\mathrm{e}}} \psi_{\mathrm{p}} \cdot \bar{\boldsymbol{M}}_I \tag{2.185}$$

and usually serves as the fundamental quantity for the definition of appropriate yield functions for crystal–plasticity formulation in stress space. The identical contribution is obtained by taking an edge dislocation into account, where the Burgers density vector is aligned according to the slip direction – say $\bar{\boldsymbol{S}}_I \equiv \bar{\boldsymbol{B}}^{\mathrm{bur}}_{\mathrm{p}\,I} / \| \bar{\boldsymbol{B}}^{\mathrm{bur}}_{\mathrm{p}\,I} \| \perp \bar{\boldsymbol{T}}_{\mathrm{p}\,I}$, and projecting the Peach–Koehler force on the slip direction

$$-\bar{\boldsymbol{S}}_I \cdot \big[\, [\, \bar{\boldsymbol{\Sigma}} \cdot \bar{\boldsymbol{S}}_I \,] \times \bar{\boldsymbol{T}}_{\mathrm{p}\,I} \, \big] = -\bar{\boldsymbol{S}}_I \cdot \bar{\boldsymbol{\Sigma}}^{\mathrm{t}} \cdot [\, \bar{\boldsymbol{T}}_{\mathrm{p}\,I} \times \bar{\boldsymbol{S}}_I \,] = -\bar{\boldsymbol{S}}_I \cdot \bar{\boldsymbol{\Sigma}}^{\mathrm{t}} \cdot \bar{\boldsymbol{M}}_I = \tau_I \,. \tag{2.186}$$

Arguing the other way round, the projected Peach–Koehler force justifies the common consideration of the classical Schmid stress. Finally, recall that the projected Peach–Koehler force (weighted by the length of the Burgers density vector) is frequently adopted within a constitutive ansatz for the glide velocity $\bar{V}_I$ of a dislocation along $\bar{\boldsymbol{S}}_I$ via the elementary relation

$$-\bar{V}_I = B^{-1}\, \bar{\mathrm{F}}^{\mathrm{PK}}_I \quad \text{with} \quad \bar{\mathrm{F}}^{\mathrm{PK}}_I = -\bar{\boldsymbol{B}}^{\mathrm{bur}}_{\mathrm{p}\,I} \cdot \bar{\boldsymbol{\Sigma}}^{\mathrm{t}} \cdot \bar{\boldsymbol{M}}_I \,, \tag{2.187}$$

whereby the material parameter $B > 0$ is commonly denoted as drag coefficient. From the general relation between spatial and material motion time derivatives and velocities, eqs.(2.5,2.10,2.22), as well as eq.(2.70) we conclude that the classical ansatz in eq.(2.187) results in a positive contribution (quadratic format) to the dissipation inequality.

2.5.2 Application to continuum plasticity

While the previously highlighted studies in section 2.5.1 basically reviewed fundamentals of nowadays classical crystal–plasticity formulations, we next discuss a continuum plasticity framework related to the very active research field of continuum and discrete dislocation mechanics. Consequently, the incorporated volume forces do, in general, not reduce to the Peach–Koehler format even though the single or discrete dislocation case is principally captured. To establish a general and physically sound framework wherein size effects, residual stresses and so forth are appropriately incorporated is, by far, out of the scope of this chapter. Nevertheless, the following analysis might serve as a platform for further elaborations. To be specific, we will assume intermediate configuration volume forces to drive the evolution of, for instance, the plastic distortion velocity. As such, dislocation density tensors are automatically incorporated. Moreover, dislocation density tensors will also directly contribute to the evolution equation set up in the sequel. For the sake of brevity, however, we restrict

ourselves to a constitutive ansatz for the material time derivative of the plastic distortion in the progression of this section and do not place further emphasis on relations between different time derivatives or the evolution of the elastic distortion.

In this regard, we propose the following evolution equation

$$\mathrm{D}_t \boldsymbol{F}_{\mathrm{p}} \cdot \boldsymbol{f}_{\mathrm{p}} = - \boldsymbol{F}_{\mathrm{p}} \cdot \mathrm{D}_t \, \boldsymbol{f}_{\mathrm{p}} \doteq \widetilde{\boldsymbol{d}}^{\mathrm{t}} \times \widetilde{\boldsymbol{v}} \tag{2.188}$$

whereby $\mathrm{D}_t \boldsymbol{F}_{\mathrm{p}} \cdot \boldsymbol{f}_{\mathrm{p}} = \mathrm{d}_t \boldsymbol{F}_{\mathrm{p}} \cdot \boldsymbol{f}_{\mathrm{p}} - [\, \nabla_{\boldsymbol{X}} \boldsymbol{F}_{\mathrm{p}} \cdot \boldsymbol{V} \,] \cdot \boldsymbol{f}_{\mathrm{p}} = \mathrm{d}_t \boldsymbol{F}_{\mathrm{p}} \cdot \boldsymbol{f}_{\mathrm{p}} + [\, \nabla_{\boldsymbol{x}} \boldsymbol{F}_{\mathrm{p}} \cdot \boldsymbol{v} \,] \cdot \boldsymbol{f}_{\mathrm{p}}$ is commonly denoted as the plastic velocity 'gradient' and $\widetilde{\boldsymbol{v}}$ takes the interpretation as dislocation velocity, compare eq.(2.188). As the key constitutive assumption we apply

$$\widetilde{\boldsymbol{v}} := - \widetilde{\boldsymbol{p}}(\widetilde{\boldsymbol{d}}^{\mathrm{t}}, \widetilde{\boldsymbol{\xi}}) \cdot \widetilde{\boldsymbol{b}}_{\mathrm{p}} \tag{2.189}$$

with $\widetilde{\boldsymbol{\xi}}$ collecting additional arguments besides the intermediate dislocation density tensor, which enter $\widetilde{\boldsymbol{p}}$. Conceptually speaking, the dislocation velocity, driving the plastic distortion evolution, is determined via a mapping of the intermediate configuration volume force. This volume force, i.e. $\widetilde{\boldsymbol{b}}_{\mathrm{p}}$, in the present context incorporates a continuum dislocation density tensor but, as previously mentioned, also could be related so discrete or rather single dislocations. Finally, as a first modelling ansatz, the second–order tensor $\widetilde{\boldsymbol{p}}$ in eq.(2.189) is assumed as

$$\widetilde{\boldsymbol{p}} := \Phi \; b \, B^{-1} \, \boldsymbol{G}_{\mathrm{p}}^{-1} \quad \text{with} \quad \Phi \doteq \mathcal{H}\big(\| \widetilde{\boldsymbol{b}}_{\mathrm{p}} \| - \widetilde{b}_{\mathrm{p}\,Y} \big) \quad \text{and} \quad b, B > 0 \,, \tag{2.190}$$

wherein $\boldsymbol{G}_{\mathrm{p}}$ denotes the co–variant metric in the intermediate configuration.The scalar–valued function Φ constrains the evolution of the plastic distortion velocity and acts in analogy to a yield criterion in classical continuum (ideal) plasticity formulations so that $\widetilde{b}_{\mathrm{p}\,Y} > 0$ corresponds to a (constant) threshold value. Alternatively, one might also make use of the Macaulay bracket instead of the Heaviside function in eq.(2.190).

Remark 2.5.1 *The constitutive modelling and related numerical implementations, for example within a finite element context, for single–crystalline materials is nowadays well–established; see for instance Havner (1992), Nemat–Nasser (2004), Miehe and Schröder (2001) or Schmidt–Baldassari (2003). Algorithmic concepts for dislocation–based formulations, as the framework proposed above, have only recently been addressed; the reader is referred to Evers et al. (2004a, 2004b) or Maciejewski and Dłużewski (2004). Internal variables, as $\boldsymbol{F}_{\mathrm{p}}$ for the problem at hand, can either be introduced at the so–called (finite element) node–point–level or, alternatively, at the integration–point–level (by analogy with the first concept, one could also introduce a second–order tensor as additional degree of freedom which is then enforced to coincide with $\boldsymbol{F}_{\mathrm{p}}$ at the integration points by, for example, incorporation of penalty terms or applying Lagrange multiplier methods). While gradients of these quantities can directly be computed within the node–point–based approach, additional projection techniques must be implemented for the integration–point–based formulation, compare the discussion in Menzel et al. (2004, 2005a). To give an example, a least square approximation renders*

$$\boldsymbol{F}_{\mathrm{p}\,k}^{\mathrm{pro}} = \left[\mathop{\mathsf{A}}_{e=1}^{n_{\mathrm{el}}} \int_{\mathcal{B}^e} N^k \, N^l \, \mathrm{d}V_0 \right]^{-1} \mathop{\mathsf{A}}_{e=1}^{n_{\mathrm{el}}} \int_{\mathcal{B}^e} N^l \, \boldsymbol{F}_{\mathrm{p}}^h \, \mathrm{d}V_0 \,, \tag{2.191}$$

wherein the notation $\lceil \{\bullet\} \rfloor$ abbreviates a lumped diagonalisation format and N^k characterise shape functions, so that $\nabla_{\boldsymbol{X}} \boldsymbol{F}_{\mathrm{p}}^h = \sum_{k=1}^{n_{\mathrm{en}}} \boldsymbol{F}_{\mathrm{p}\,k}^{\mathrm{pro}} \otimes \nabla_{\boldsymbol{X}} N^k$ follows straightforwardly. Eqs.(2.188,2.191) together with eq.(2.16) can conveniently be combined with the (most) simple Euler forward integration scheme, namely $\boldsymbol{F}_{\mathrm{p}}^{n+1} \doteq \boldsymbol{F}_{\mathrm{p}}^n + \Delta t \; \mathrm{D}_t \boldsymbol{F}_{\mathrm{p}}^n$ with $\Delta t = t_{n+1} - t_n > 0$.

Remark 2.5.2 *Plastic distortion evolution can only be activated within the proposed continuum plasticity framework if the initial distribution of the plastic distortion itself is inhomogeneous; otherwise* $\nabla_{\boldsymbol{X}} \boldsymbol{F}_{\mathrm{p}} = \boldsymbol{0}$ *results in* $\widetilde{\boldsymbol{d}}^{\mathrm{t}} = \boldsymbol{0}$ *as well as* $\widetilde{\boldsymbol{v}} = \boldsymbol{0}$*, respectively. To compute simple academic examples,* $\boldsymbol{F}_{\mathrm{p}}|_{t_0} \doteq \lambda_{\mathrm{p}\,i}\, \boldsymbol{h}_{\mathrm{p}\,i} \otimes \boldsymbol{h}_0^i$ *can be generated by random (for instance at the integration–point–level within a finite element formulation), compare eq.(1.5). The (non–negative) stretches* $\lambda_{\mathrm{p}\,i}$ *might thereby be restricted to* $J_{\mathrm{p}}|_{t_0} \doteq 1$ *while* $\{\boldsymbol{h}_{\mathrm{p}\,i}\}$ *and* $\{\boldsymbol{h}_0^i\}$ *represent orthonormal frames, for example, determined in terms of randomly generated Eulerian angles; compare eq.(6.84). Concerning physically (more) realistic simulations, experimental data for the initial plastic distortion distribution based on digital processing techniques are applied in Dłużewski et al. (2004).*

Remark 2.5.3 *Similar to classical crystal– or continuum plasticity formulations, the evolution equation in eq.(2.188) for the plastic distortion automatically renders compatible contributions* $(\nabla^{\mathrm{t}}_{\boldsymbol{X}} \times \boldsymbol{F}^{\mathrm{com}}_{\mathrm{p}} = \boldsymbol{0})$ *together with incompatible parts* $(\nabla^{\mathrm{t}}_{\boldsymbol{X}} \times \boldsymbol{F}^{\mathrm{inc}}_{\mathrm{p}} \neq \boldsymbol{0})$ *of the plastic distortion. For physical reasons as well as from the modelling point of view, however, it might be favourable to generally distinguish between the evolution of dislocation density tensors and related distortion contributions embedded in the corresponding null space. To give an example, such an ansatz for* $\mathrm{L}^{\mathrm{p}}_t \widetilde{\boldsymbol{A}}^{\mathrm{t}} = \mathrm{D}_t \widetilde{\boldsymbol{A}}^{\mathrm{t}} - \mathrm{D}_t \boldsymbol{F}_{\mathrm{p}} \cdot \boldsymbol{f}_{\mathrm{p}} \cdot \widetilde{\boldsymbol{A}}^{\mathrm{t}}$ *could, in principle, be introduced as for instance*

$$\mathrm{L}^{\mathrm{p}}_t \widetilde{\boldsymbol{A}}^{\mathrm{t}} \propto \nabla^{\mathrm{t}}_{\boldsymbol{X}} \times [\, \widetilde{\boldsymbol{A}}^{\mathrm{t}} \times \widetilde{\boldsymbol{b}}_0 \,] - s\, \nabla^{\mathrm{t}}_{\boldsymbol{X}} \times \widetilde{\boldsymbol{\Pi}}^{\mathrm{t}} \,, \tag{2.192}$$

whereby the second part, weighted by $s > 0$*, takes the interpretation as a source term. The overall framework itself has been developed in a series of papers by Acharya (2001, 2003, 2004) and for a related review on null divergences the reader is referred to the monographs by Olver (1993) and Šilhavý (1997). An alternative modelling approach is elaborated in Epstein and Elżanowski (2003) and Elżanowski and Preston (2007), see also references cited in these contributions, where the plastic distortion evolution is (self–) driven in terms of the correlated torsion tensor, and section 1.1.*

2.6 Discussion

The main goal of this chapter was the elaboration of configurational balance of linear momentum representations embedded into an inelastic and finite deformation framework. A multiplicative decomposition of the deformation gradient has been adopted and served as a general setting for the modelling of finite inelasticity. Application of the developed approach to, for instance, viscoelastic behaviour or growth phenomena is straightforward even though special emphasis has been placed on elastoplastic response in this work. Compatibility of the spatial and material configuration has been assumed throughout while the underlying intermediate configuration is generally incompatible. Due to these basic geometrical properties, one obtains non–vanishing dislocation density tensors in terms of the elastic or plastic distortion. Several versions of theses quantities have been highlighted, whereby two–point formats as well as representations entirely settled in one configuration have been developed. From the physical or rather material modelling point of view, these tensors are commonly related to geometrically necessary dislocations. Moreover, dislocation density tensors also directly contributed to particular configurational balance of linear momentum representations since the normally applied Piola identity is not valid in its standard format as soon as incompatible configurations are considered.

Motivated by the assumption of a Helmholtz free energy density which depends on the elastic distortion, hyperelastic stress formats have been introduced. Piola and Cauchy stress tensors with respect to different configurations were discussed in detail and also their relations have been highlighted. As an interesting aspect, it turned out that different versions of material motion Cauchy stresses do not coincide while their spatial and intermediate motion counterparts are pairwise identical. The particular representations of the constitutive stress formats were recaptured when deriving the corresponding configurational volume forces by comparing balance of linear momentum representations of different motion problems. External spatial volume forces thereby allowed interpretation as applied loads according, for instance, to gravitation and internal spatial volume forces must vanish due to spatial translational invariance. The derived formats of intermediate and material volume forces, however, additionally incorporate appropriate combinations of stresses and gradients of distortions besides possible terms stemming from dependencies of the Helmholtz free energy density on material placements of particles. It thereby turned out that gradients of distortions directly contribute to material volume forces while these quantities are incorporated via dislocation density tensors into intermediate volume forces. This property is of cardinal importance and reflects the idea that the celebrated Peach–Koehler force is settled in the incompatible intermediate configuration for the kinematical framework at hand. Consequently, the derived representation of the Peach–Koehler force would not have been accessible when restricting the present configurational approach to material balance of linear momentum expressions.

Conceptually speaking, a non–vanishing Burgers density vector is introduced with respect to the incompatible intermediate configuration. The formulation is either based on the incorporation of the plastic or elastic distortion. By analogy with these two definitions, two lines of deriving intermediate volume forces come into the picture which apparently refer to the plastic and elastic intermediate motion balance of linear momentum. The related Cauchy stresses and volume forces consequently coincide and the Peach–Koehler force takes a classical format similar to the small strain setting. In this regard, the definition of this celebrated configurational force within an inelastic finite deformation framework seems to be clarified. Furthermore, not only the small strain case is naturally included within the presented framework but also purely elastic finite deformations. To be specific, by setting either the plastic or elastic distortion equal to the identity – so that either the spatial motion gradient coincides with the inverse elastic distortion or the material motion gradient equals the inverse plastic distortion – renders non–vanishing Burgers density vectors in the material or spatial configuration, respectively. The total motion, however, is then no longer compatible but apart from that, all equations derived in this contribution can be carried over to the case of elastic incompatibilities.

In conclusion, we discussed and derived four fundamentally different representations of balance of linear momentum:

(i) The commonly applied quasi static equilibrium condition in $T^*\mathcal{B}_t$ is illustrated by eqs.(2.42,2.44), namely

$$\begin{aligned} \mathbf{0} &= \nabla_{\boldsymbol{x}} \cdot (\, \boldsymbol{\Pi}^{\mathrm{t}} \cdot \mathrm{cof}(\boldsymbol{f})\,) + \boldsymbol{b}_t = \nabla_{\boldsymbol{x}} \cdot (\, \bar{\boldsymbol{\Pi}}^{\mathrm{t}} \cdot \mathrm{cof}(\boldsymbol{f}_{\mathrm{e}})\,) + \bar{\boldsymbol{b}}_t \\ \text{with} \quad \boldsymbol{\Pi}^{\mathrm{t}} &= \partial_{\boldsymbol{F}} \psi_0|_{\boldsymbol{F}_{\mathrm{p}}}\,, \quad \bar{\boldsymbol{\Pi}}^{\mathrm{t}} = \partial_{\boldsymbol{F}_{\mathrm{e}}} \psi_{\mathrm{p}} \\ \text{and} \quad \boldsymbol{b}_t &= \boldsymbol{b}_t^{\mathrm{ext}} = \bar{\boldsymbol{b}}_t^{\mathrm{ext}} = \bar{\boldsymbol{b}}_t\,. \end{aligned} \tag{2.193}$$

Note that the divergence operation acts on identical Cauchy stresses. Moreover, internal volume force contributions vanish due to spatial translational invariance and the remaining terms take the interpretation as external loads.

(ii) The balance of linear momentum representations in $T^*\mathcal{B}_\mathrm{p}$ are illustrated by eqs.(2.50,2.52), namely

$$\begin{aligned}
\mathbf{0} &= \widetilde{\nabla} \cdot (\, \widetilde{\boldsymbol{\Pi}}^{\mathrm{t}} \cdot \mathrm{cof}(\boldsymbol{f}_\mathrm{p})\,) \; - \; [\, \widetilde{\boldsymbol{\Pi}}^{\mathrm{t}} \cdot \mathrm{cof}(\boldsymbol{f}_\mathrm{p})\,] \cdot [\, \boldsymbol{F}_\mathrm{p} \times \widetilde{\boldsymbol{a}}\,] \; + \; \widetilde{\boldsymbol{b}}_\mathrm{p} \\
&= \bar{\nabla} \cdot (\, \bar{\boldsymbol{\pi}}^{\mathrm{t}} \cdot \mathrm{cof}(\boldsymbol{F}_\mathrm{e})\,) \; - \; [\, \bar{\boldsymbol{\pi}}^{\mathrm{t}} \cdot \mathrm{cof}(\boldsymbol{F}_\mathrm{e})\,] \cdot [\, \boldsymbol{f}_\mathrm{e} \times \bar{\boldsymbol{A}}\,] \; + \; \bar{\boldsymbol{B}}_\mathrm{p} \\
\text{with} \quad \widetilde{\boldsymbol{\Pi}}^{\mathrm{t}} &= \partial_{\boldsymbol{F}_\mathrm{p}} \psi_0|_{\boldsymbol{F}}\,, \quad \bar{\boldsymbol{\pi}}^{\mathrm{t}} = \partial_{\boldsymbol{f}_\mathrm{e}} \psi_t \\
\text{and} \quad \widetilde{\boldsymbol{b}}_\mathrm{p} &= -\, \widetilde{\boldsymbol{\sigma}}^{\mathrm{t}} \times \widetilde{\boldsymbol{d}} \; - \boldsymbol{f}_\mathrm{p}^{\mathrm{t}} \cdot \partial_{\boldsymbol{X}} \psi_\mathrm{p} - J_\mathrm{e}\, \boldsymbol{F}_\mathrm{e}^{\mathrm{t}} \cdot \boldsymbol{b}_t^{\mathrm{ext}} \\
&= -\, \bar{\boldsymbol{\Sigma}}^{\mathrm{t}} \times \bar{\boldsymbol{D}} - \boldsymbol{f}_\mathrm{p}^{\mathrm{t}} \cdot \partial_{\boldsymbol{X}} \psi_\mathrm{p} - J_\mathrm{e}\, \boldsymbol{F}_\mathrm{e}^{\mathrm{t}} \cdot \boldsymbol{b}_t^{\mathrm{ext}} \; = \; \bar{\boldsymbol{B}}_\mathrm{p}\,.
\end{aligned} \tag{2.194}$$

Note that the divergence operations act on identical Cauchy–type stresses whereby additional contributions stemming from the incompatibility of the intermediate configuration are acknowledged. Moreover, $\boldsymbol{F}_\mathrm{p} \times \widetilde{\boldsymbol{a}} = \boldsymbol{f}_\mathrm{e} \times \bar{\boldsymbol{A}}$ must hold throughout since $\widetilde{\boldsymbol{b}}_\mathrm{p} = \bar{\boldsymbol{B}}_\mathrm{p}$ and $\widetilde{\boldsymbol{\Pi}}^{\mathrm{t}} \cdot \mathrm{cof}(\boldsymbol{f}_\mathrm{p}) = \bar{\boldsymbol{\pi}}^{\mathrm{t}} \cdot \mathrm{cof}(\boldsymbol{F}_\mathrm{e})$, compare eq.(2.79). This condition results in $\boldsymbol{F}_\mathrm{p} \cdot \widetilde{\boldsymbol{a}}^{\mathrm{t}} = \boldsymbol{f}_\mathrm{e} \cdot \bar{\boldsymbol{A}}^{\mathrm{t}}$ which is verified by eqs.(2.37,2.38). Apparently, dislocation density tensors are also incorporated into the corresponding volume forces which enabled us to derive Peach–Koehler force formats embedded into a framework for finite inelasticity.

(iii) On the one hand, an established material balance of linear momentum representation in $T^*\mathcal{B}_0$ is illustrated by eq.(2.46), namely

$$\begin{aligned}
\mathbf{0} &= \nabla_{\boldsymbol{X}} \cdot (\, \boldsymbol{F}_\mathrm{p}^{\mathrm{t}} \cdot \widetilde{\boldsymbol{\Pi}}^{\mathrm{t}}\,) + \boldsymbol{B}_0 \\
\text{with} \quad \widetilde{\boldsymbol{\Pi}}^{\mathrm{t}} &= \partial_{\boldsymbol{F}_\mathrm{p}} \psi_0|_{\boldsymbol{F}} \\
\text{and} \quad \boldsymbol{B}_0 &= -\, \widetilde{\boldsymbol{\Pi}}^{\mathrm{t}} : \nabla_{\boldsymbol{X}} \boldsymbol{F}_\mathrm{p} - \partial_{\boldsymbol{X}} \psi_0 - J\, \boldsymbol{F}^{\mathrm{t}} \cdot \boldsymbol{b}_t^{\mathrm{ext}}\,.
\end{aligned} \tag{2.195}$$

Note that the commonly derived material balance of linear momentum version, as based on the framework of local rearrangements, follows by analogy with eq.(2.195); compare remark 2.3.2. The underlying stress tensor, which we call material motion Cauchy stress $\boldsymbol{\Sigma}^{\mathrm{t}} = \boldsymbol{F}_\mathrm{p}^{\mathrm{t}} \cdot \widetilde{\boldsymbol{\Pi}}^{\mathrm{t}}$, is commonly referred to as the Eshelby stress or energy momentum tensor. Moreover, the obtained volume force in eq.(2.195) directly incorporates the gradient of the underlying material isomorphisms or, in the present context, plastic distortion. It is also interesting to recall the relation $\widetilde{\boldsymbol{\Pi}}^{\mathrm{t}} : \nabla_{\boldsymbol{X}} \boldsymbol{F}_\mathrm{p} = \boldsymbol{\Sigma}^{\mathrm{t}} : [\, \boldsymbol{f}_\mathrm{p} \cdot \nabla_{\boldsymbol{X}} \boldsymbol{F}_\mathrm{p}\,]$ with $\boldsymbol{f}_\mathrm{p} \cdot \nabla_{\boldsymbol{X}} \boldsymbol{F}_\mathrm{p}$ taking the interpretation as the corresponding connection.

(iv) On the other hand, an alternative material balance of linear momentum representations in $T^*\mathcal{B}_0$ is illustrated by eq.(2.48), namely

$$\begin{aligned}
\mathbf{0} &= \nabla_{\boldsymbol{X}} \cdot (\, \boldsymbol{F}^{\mathrm{t}} \cdot \boldsymbol{\Pi}^{\mathrm{t}}\,) + \widetilde{\boldsymbol{B}}_0 \\
\text{with} \quad \boldsymbol{\Pi}^{\mathrm{t}} &= \partial_{\boldsymbol{F}} \psi_0|_{\boldsymbol{F}_\mathrm{p}} \\
\text{and} \quad \widetilde{\boldsymbol{B}}_0 &= -\, \boldsymbol{\Pi}^{\mathrm{t}} : \nabla_{\boldsymbol{X}} \boldsymbol{F} - J\, \boldsymbol{F}^{\mathrm{t}} \cdot \boldsymbol{b}_t^{\mathrm{ext}}\,,
\end{aligned} \tag{2.196}$$

which seems to be unrecognised in the literature so far. Note that the underlying stress tensor, which we call material motion plastic Cauchy stress $\widetilde{\boldsymbol{\Sigma}}^{\mathrm{t}} = \boldsymbol{F}^{\mathrm{t}} \cdot \boldsymbol{\Pi}^{\mathrm{t}}$, is commonly referred to as the (material) Mandel stress. Moreover, the obtained volume force in eq.(2.195) directly incorporates the gradient of the deformation gradient while no dependencies on material placements of the particle occur. It is also interesting to recall the relation $\boldsymbol{\Pi}^{\mathrm{t}} : \nabla_{\boldsymbol{X}} \boldsymbol{F} = \widetilde{\boldsymbol{\Sigma}}^{\mathrm{t}} : [\, \boldsymbol{f} \cdot \nabla_{\boldsymbol{X}} \boldsymbol{F}\,]$ with $\boldsymbol{f} \cdot \nabla_{\boldsymbol{X}} \boldsymbol{F}$ taking the interpretation as the corresponding torsion–free connection due to overall compatibility. This balance

of linear momentum representation is in particular suitable for numerical applications since (i) solely standard stresses as the spatial motion Piola stress tensor need to be computed; (ii) neither gradients of the plastic and elastic distortion nor any directly related dislocation density tensors are incorporated. Practically speaking, besides the computation of $\nabla_{\boldsymbol{X}}\boldsymbol{F}$ conventional techniques can be adopted within, for instance, a standard finite element setting.

In conclusion, we derived material and, what we call, intermediate representations of balance of linear momentum in addition to the spatial format which classically defines equilibrium in physical space. Two key steps within this derivation are (i) the extension of the Piola identity to incompatible configurations, appendix C; (ii) the relation between Piola stresses based on the plastic distortion and the total motion stresses, eqs.(2.88,2.98). The obtained intermediate and material volume forces recaptured the celebrated Peach–Koehler force and gave rise to the incorporation of the gradient of the plastic distortion and total deformation gradient. Apparently, these configurational volume forces serve as a platform for the definition of appropriate evolution equations for, for example, slip systems, continuum dislocations, defects, inhomogeneities and so forth.

3 Generalised strain measures for multiplicative elastoplasticity

The application of different stretch representations and strain measures within nonlinear continuum mechanics has been under discussion for several decades; see for instance the fundamental contributions by Murnaghan (1937), Kauderer (1949) or Richter (1952), and Truesdell and Toupin (1960) or Eringen (1962) for an overview. When referring to generalised strain measures, we commonly think of sufficiently smooth monotone tensor functions with respect to an appropriate deformation field. The spectral decomposition theorem thereby allows convenient interpretation in terms of principal stretches. These ideas date back to the pioneering contributions by Seth (1964) and Hill (1968). Particular emphasis on logarithmic strains has been placed, for example, by Hoger (1987), Sansour (2001), and Xiao and Chen (2003) among others. For a general overview we refer the reader to the monographs by Biot (1965), Ogden (1997), and Šilhavý (1997) or Havner (1992) and Lubarda (2002) where inelastic material behaviour is addressed.

The formulation of nonlinear constitutive response as based on the introduction of different deformation and strain measures as well as higher–order terms constitutes a traditional but still very active field of research; see for instance the classical modelling approaches elaborated in the monographs by Murnaghan (1951) and Kauderer (1958). Apparently, for particular applications where the total strains might remain rather small, it is – from the modelling point of view – attractive to introduce St.–Venant–Kirchhoff–type constitutive equations in terms of generalised strain measures. Conceptually speaking, the sought nonlinear response is incorporated via specific strain measures with respect to which the quadratic format of the strain energy function is retained. In this regard, the well–established framework of linear elasticity is adopted and combined with generalised strain measures which then constitutes an essential part of the constitutive modelling itself. It is well–known, however, that the region of ellipticity is rather restricted for these approaches; see, for example, Bruhns et al. (2001) for a detailed discussion based on an isotropic setting in terms of logarithmic strains. Nevertheless, one of the main advantages of a St.–Venant–Kirchhoff–type ansatz consists in the fact that the backbone of anisotropic linear elasticity can directly be combined with nonlinearities related to appropriate generalised strain measures; see for instance the monograph by Green and Adkins (1970) and references cited therein. For detailed surveys the reader is also referred to the contributions by Mehrabadi and Cowin (1995, 1990) and Rychlewski (1995). A delightful representation of Hooke's law, say, in anisotropic linear elasticity is provided by the introduction of Kelvin modes, or, in other words, the application of the spectral decomposition theorem to the elasticity tensor; see for example Kelvin (1856), Elata and Rubin (1994), Sutcliffe (1992), Xiao (1997), Martins (1999), and Pericak–Spector et al. (1999).

Recently, Papadopoulos and Lu (1998, 2001) introduced generalised strain measures to a strain–space formulation of finite isotropic and anisotropic elastoplasticity, see also the contributions by Miehe et al. (2002) or Schröder et al. (2002). Along this direction, we focus on a stress–space framework in the sequel and model the underlying symmetry of the material via structural tensors which – at least formally – enables us to overcome the structure of a St.–Venant–Kirchhoff–type ansatz. The essential point of departure thereby consists in applying the fundamental covariance principle to the Helmholtz free energy density. Following these ideas, as discussed in Menzel (2005b), allows to set up a convenient formulation (especially

for numerical applications) in terms of spatial arguments. Detailed background information of the fundamental covariance principle is provided in, for instance, the monograph by Marsden and Hughes (1994) while its application to anisotropic response has been elaborated by Lu and Papadopoulos (2000) and Menzel and Steinmann (2003c, 2003d), see also Svendsen (2001).

In the following, particular emphasis is placed on the multiplicative decomposition of the deformation gradient into an elastic and inelastic contribution, see for example Haupt (2000), references cited therein, and chapter 2. Concerning notation, we distinguish between co– and contra–variant base vectors. The reader is referred to Eringen (1971a, 1971b) or Lodge (1964, 1974) for further background information in this regard. The Helmholtz free energy density is assumed to incorporate the total deformation gradient as well as the elastic distortion. Accordingly, different types of material behaviour – typically elasticity, plasticity or viscoelasticty – are included within the proposed framework. Based on these deformation quantities, various strain tensors can be introduced – naming solely some of theses measures, classical strain tensors are typically identified with, for instance, Biot–, Green–Lagrange – and Almansi strains, tensors of Green or Karni–Reiner–type, etc. In this study, however, we mainly focus on strain tensors of the Seth–Hill family. These generalised strain measures are introduced with respect to different configurations in the sequel. Moreover, we carefully distinguish between strain tensors of co– and contra–variant type. In this regard, the main goal of this chapter consists in the elaboration of these strain measures embedded into the framework of general covariance of the Helmholtz free energy density. This finally enables us to clearly develop pushforward and pullback transformations between generalised strains and correlated hyperelastic stress tensors in different configurations. As such, this study might on the one hand seem slightly technical or rather formal, but on the other hand it reviews established formulations and gives new insight into the geometric interpretation of the relations between strain and stress quantities in one and the same as well as different configurations. With these elaborations in hand, evolution equations for the inelastic distortion or related strain measures are discussed. By analogy with the transformations between different strain tensors, one observes similar relations for the driving forces entering these evolution equations. As a main result, essential equations for anisotropic inelasticity together with anisotropic elasticity in terms of entirely spatial arguments are derived which is of particular interest for efficient numerical simulations based on, for example, finite element techniques.

The chapter is organised as follows: In section 3.1 we formally review essential kinematic relations based on a multiplicative decomposition of the total deformation gradient. Various stretch tensors are thereby introduced and particular emphasis is placed on the application of the spectral decomposition theorem. Based on these elaborations, the definition of Seth–Hill–type strain measures is discussed in section 3.2. Apart from distinguishing between co– and contra–variant generalised strain measures, we additionally derive transformation relations between different strain measures in one and the same configuration as well as between strain measures in different configurations. Next, the Helmholtz free energy density is introduced in terms of appropriate strain tensors and an additional structural tensors, say; see section 3.3. The Helmholtz free energy density is thereby defined in terms of two contributions – one with respect to the total deformation gradient while the other one refers to the elastic distortion – so that classical modelling approaches, as for instance elasticity, plasticity or viscoelasticity are embodied. Appropriate stress tensors as well as typical evolution equations are elaborated in section 3.4. An alternative approach of Green–Naghdi–type is discussed in section 3.5.

3.1 Deformation measures

By analogy with section 2.1.1, let $\boldsymbol{\varphi}(\boldsymbol{X},t) : \mathcal{B}_0 \times \mathcal{T} \to \mathcal{B}_t \,|\, \boldsymbol{X} \times t \mapsto \boldsymbol{x}$ represent the nonlinear motion of the body B of interest with the corresponding linear tangent map $\boldsymbol{F} = \nabla_{\boldsymbol{X}} \boldsymbol{\varphi}$. In the following, we once more adopt the common ansatz that the elastic part of the deformation gradient is defined as $\boldsymbol{F}_{\mathrm{e}} \doteq \boldsymbol{F} \cdot \boldsymbol{f}_{\mathrm{p}}$, namely

$$\begin{aligned} \boldsymbol{F} = \nabla_{\boldsymbol{X}} \boldsymbol{\varphi} \doteq \boldsymbol{F}_{\mathrm{e}} \cdot \boldsymbol{F}_{\mathrm{p}} : T\mathcal{B}_0 \to T\mathcal{B}_t\,, \quad \boldsymbol{F}_{\mathrm{p}} : T\mathcal{B}_0 \to T\mathcal{B}_{\mathrm{p}}\,, \quad \boldsymbol{F}_{\mathrm{e}} : T\mathcal{B}_{\mathrm{p}} \to T\mathcal{B}_t \\ \text{with} \quad \det(\boldsymbol{F})\,,\ \det(\boldsymbol{F}_{\mathrm{e}})\,,\ \det(\boldsymbol{F}_{\mathrm{p}}) > 0\,. \end{aligned} \tag{3.1}$$

The adopted multiplicative decomposition allows interpretation as a local rearrangement or rather material isomorphism and also gives rise to a generally incompatible, and possibly stress–free, intermediate configuration $\mathcal{B}_{\mathrm{p}}$; compare chapter 2. Furthermore, let the introduced configurations, which are embedded into the three–dimensional Euclidian space, be equipped with the co–variant and contra–variant metric tensors

$$\begin{aligned} \boldsymbol{G} &: T\mathcal{B}_0 \to T^*\mathcal{B}_0\,, & \boldsymbol{G}^{-1} &= \det{}^{-1}(\boldsymbol{G})\ \ \mathrm{cof}(\boldsymbol{G}) &&: T^*\mathcal{B}_0 \to T\mathcal{B}_0\,, \\ \boldsymbol{G}_{\mathrm{p}} &: T\mathcal{B}_{\mathrm{p}} \to T^*\mathcal{B}_{\mathrm{p}}\,, & \boldsymbol{G}_{\mathrm{p}}^{-1} &= \det{}^{-1}(\boldsymbol{G}_{\mathrm{p}})\ \mathrm{cof}(\boldsymbol{G}_{\mathrm{p}}) &&: T^*\mathcal{B}_{\mathrm{p}} \to T\mathcal{B}_{\mathrm{p}}\,, \\ \boldsymbol{g} &: T\mathcal{B}_t \to T^*\mathcal{B}_t\,, & \boldsymbol{g}^{-1} &= \det{}^{-1}(\boldsymbol{g})\ \ \mathrm{cof}(\boldsymbol{g}) &&: T^*\mathcal{B}_t \to T\mathcal{B}_t\,. \end{aligned} \tag{3.2}$$

Next, the polar decomposition theorem is (formally) applied to the linear tangent maps in eq.(3.1) so that appropriate stretch tensors are conveniently defined via

$$\boldsymbol{F} = \boldsymbol{R} \cdot \boldsymbol{U} = \boldsymbol{v} \cdot \boldsymbol{R}\,, \quad \boldsymbol{F}_{\mathrm{p}} = \boldsymbol{R}_{\mathrm{p}} \cdot \boldsymbol{U}_{\mathrm{p}} = \boldsymbol{v}_{\mathrm{p}} \cdot \boldsymbol{R}_{\mathrm{p}} \quad \text{and} \quad \boldsymbol{F}_{\mathrm{e}} = \boldsymbol{R}_{\mathrm{e}} \cdot \boldsymbol{U}_{\mathrm{e}} = \boldsymbol{v}_{\mathrm{e}} \cdot \boldsymbol{R}_{\mathrm{e}}\,. \tag{3.3}$$

The proper orthogonal part of the inelastic, i.e. irreversible, part is (usually) not uniquely determined, $\boldsymbol{F} = \boldsymbol{v}_{\mathrm{e}} \cdot \boldsymbol{R}_{\mathrm{e}} \cdot \boldsymbol{R}_{\mathrm{p}} \cdot \boldsymbol{U}_{\mathrm{p}} = \boldsymbol{v}_{\mathrm{e}} \cdot \boldsymbol{R}_{\mathrm{e}} \cdot \boldsymbol{Q} \cdot \boldsymbol{Q}^{\mathrm{t}} \cdot \boldsymbol{R}_{\mathrm{p}} \cdot \boldsymbol{U}_{\mathrm{p}} = \boldsymbol{v}_{\mathrm{e}} \cdot \boldsymbol{R}'_{\mathrm{e}} \cdot \boldsymbol{R}'_{\mathrm{p}} \cdot \boldsymbol{U}_{\mathrm{p}}$ with $\boldsymbol{Q} \cdot \boldsymbol{Q}^{\mathrm{t}} = \boldsymbol{I}_{\mathrm{p}}$ and the stretch tensors in eq.(3.3) can alternatively be introduced as the square root of appropriate symmetric deformation tensors; see eqs.(3.10–3.15,3.17) below. Moreover, the application of the spectral decomposition theorem renders

$$\begin{aligned} \boldsymbol{F} &= \lambda_k\ \boldsymbol{n}_k \ \otimes \boldsymbol{N}^k\,, & \boldsymbol{R} &= \ \ \boldsymbol{n}_k \otimes \boldsymbol{N}^k\,, \\ \boldsymbol{U} &= \lambda_k\ \boldsymbol{N}_k \otimes \boldsymbol{N}^k\,, & \boldsymbol{v} &= \lambda_k\ \boldsymbol{n}_k \otimes \boldsymbol{n}^k \end{aligned} \tag{3.4}$$

and

$$\begin{aligned} \boldsymbol{F}_{\mathrm{p}} &= \lambda_{\mathrm{p}k}\ \widehat{\boldsymbol{n}}_{\mathrm{p}k} \ \otimes \boldsymbol{N}^k_{\mathrm{p}}\,, & \boldsymbol{R}_{\mathrm{p}} &= \ \ \widehat{\boldsymbol{n}}_{\mathrm{p}k} \otimes \boldsymbol{N}^k_{\mathrm{p}}\,, \\ \boldsymbol{U}_{\mathrm{p}} &= \lambda_{\mathrm{p}k}\ \boldsymbol{N}_{\mathrm{p}k} \otimes \boldsymbol{N}^k_{\mathrm{p}}\,, & \widehat{\boldsymbol{v}}_{\mathrm{p}} &= \lambda_{\mathrm{p}k}\ \widehat{\boldsymbol{n}}_{\mathrm{p}k} \otimes \widehat{\boldsymbol{n}}^k_{\mathrm{p}} \end{aligned} \tag{3.5}$$

as well as

$$\begin{aligned} \boldsymbol{F}_{\mathrm{e}} &= \lambda_{\mathrm{e}k}\ \boldsymbol{n}_{\mathrm{e}k} \ \otimes \widehat{\boldsymbol{N}}^k_{\mathrm{e}}\,, & \boldsymbol{R}_{\mathrm{e}} &= \ \ \boldsymbol{n}_{\mathrm{e}k} \otimes \widehat{\boldsymbol{N}}^k_{\mathrm{e}}\,, \\ \widehat{\boldsymbol{U}}_{\mathrm{e}} &= \lambda_{\mathrm{e}k}\ \widehat{\boldsymbol{N}}_{\mathrm{e}k} \otimes \widehat{\boldsymbol{N}}^k_{\mathrm{e}}\,, & \boldsymbol{v}_{\mathrm{e}} &= \lambda_{\mathrm{e}k}\ \boldsymbol{n}_{\mathrm{e}k} \otimes \boldsymbol{n}^k_{\mathrm{e}}\,, \end{aligned} \tag{3.6}$$

see also Goddard and Ledniczky (1997) for further elaborations. Here and in the progression of this chapter, the summation convention over, for example, $k = 1,2,3$ is implied. The incorporated eigenvectors are unit vectors in the sense that

$$\begin{aligned} \boldsymbol{N}^{(k)} \cdot \boldsymbol{G}^{-1} \cdot \boldsymbol{N}^{(k)} &= \boldsymbol{N}_{(k)} \cdot \boldsymbol{G} \ \ \cdot \boldsymbol{N}_{(k)} \\ &= \boldsymbol{N}^{(k)}_{\mathrm{p}} \cdot \boldsymbol{G}^{-1} \cdot \boldsymbol{N}^{(k)}_{\mathrm{p}} = \boldsymbol{N}_{\mathrm{p}\,(k)} \cdot \boldsymbol{G} \cdot \boldsymbol{N}_{\mathrm{p}\,(k)} = 1 \end{aligned} \tag{3.7}$$

and

$$\begin{aligned} \widehat{\boldsymbol{N}}^{(k)}_{\mathrm{e}} \cdot \boldsymbol{G}^{-1}_{\mathrm{p}} \cdot \widehat{\boldsymbol{N}}^{(k)}_{\mathrm{e}} &= \widehat{\boldsymbol{N}}_{\mathrm{e}\,(k)} \cdot \boldsymbol{G}_{\mathrm{p}} \ \ \cdot \widehat{\boldsymbol{N}}_{\mathrm{e}\,(k)} \\ &= \widehat{\boldsymbol{n}}^{(k)}_{\mathrm{p}} \ \ \cdot \boldsymbol{G}^{-1}_{\mathrm{p}} \cdot \widehat{\boldsymbol{n}}^{(k)}_{\mathrm{p}} \ \ = \widehat{\boldsymbol{n}}_{\mathrm{p}\,(k)} \cdot \boldsymbol{G}_{\mathrm{p}} \cdot \widehat{\boldsymbol{n}}_{\mathrm{p}\,(k)} = 1 \end{aligned} \tag{3.8}$$

as well as

$$\begin{aligned} \boldsymbol{n}_{\mathrm{e}}^{(k)} \cdot \boldsymbol{g}^{-1} \cdot \boldsymbol{n}_{\mathrm{e}}^{(k)} &= \boldsymbol{n}_{\mathrm{e}\,(k)} \cdot \boldsymbol{g} \quad \cdot \boldsymbol{n}_{\mathrm{e}\,(k)} \\ &= \boldsymbol{n}^{(k)} \cdot \boldsymbol{g}^{-1} \cdot \boldsymbol{n}^{(k)} = \boldsymbol{n}_{(k)} \cdot \boldsymbol{g} \cdot \boldsymbol{n}_{(k)} = 1\,, \end{aligned} \tag{3.9}$$

with the notation (k) indicating that the summation over k is (here) excluded.

Based on these relations, it is now straightforward to introduce different deformation tensors, for instance

$$\begin{aligned} \boldsymbol{C} &= \boldsymbol{f} \star \boldsymbol{g} = \lambda_k^2 \;\; \boldsymbol{N}^k \otimes \boldsymbol{N}^k\,, \qquad \boldsymbol{B} = \boldsymbol{f} \star \boldsymbol{g}^{-1} = \lambda_k^{-2}\; \boldsymbol{N}_k \otimes \boldsymbol{N}_k\,, \\ \boldsymbol{c} &= \boldsymbol{F} \star \boldsymbol{G} = \lambda_k^{-2}\; \boldsymbol{n}^k \otimes \boldsymbol{n}^k\,, \qquad \boldsymbol{b} = \boldsymbol{F} \star \boldsymbol{G}^{-1} = \lambda_k^2 \;\; \boldsymbol{n}_k \otimes \boldsymbol{n}_k \end{aligned} \tag{3.10}$$

and

$$\begin{aligned} \boldsymbol{C}_{\mathrm{p}} &= \boldsymbol{f}_{\mathrm{p}} \star \boldsymbol{G}_{\mathrm{p}} = \lambda_{\mathrm{p}\,k}^2\; \boldsymbol{N}_{\mathrm{p}}^k \otimes \boldsymbol{N}_{\mathrm{p}}^k\,, \quad \boldsymbol{B}_{\mathrm{p}} = \boldsymbol{f}_{\mathrm{p}} \star \boldsymbol{G}_{\mathrm{p}}^{-1} = \lambda_{\mathrm{p}\,k}^{-2}\; \boldsymbol{N}_{\mathrm{p}\,k} \otimes \boldsymbol{N}_{\mathrm{p}\,k}\,, \\ \widehat{\boldsymbol{c}}_{\mathrm{p}} &= \boldsymbol{F}_{\mathrm{p}} \star \boldsymbol{G} = \lambda_{\mathrm{p}\,k}^{-2}\; \widehat{\boldsymbol{n}}_{\mathrm{p}}^k \otimes \widehat{\boldsymbol{n}}_{\mathrm{p}}^k\,, \quad \widehat{\boldsymbol{b}}_{\mathrm{p}} = \boldsymbol{F}_{\mathrm{p}} \star \boldsymbol{G}^{-1} = \lambda_{\mathrm{p}\,k}^2\; \widehat{\boldsymbol{n}}_{\mathrm{p}\,k} \otimes \widehat{\boldsymbol{n}}_{\mathrm{p}\,k} \end{aligned} \tag{3.11}$$

as well as

$$\begin{aligned} \widehat{\boldsymbol{C}}_{\mathrm{e}} &= \boldsymbol{f}_{\mathrm{e}} \star \boldsymbol{g} = \lambda_{\mathrm{e}\,k}^2\; \widehat{\boldsymbol{N}}_{\mathrm{e}}^k \otimes \widehat{\boldsymbol{N}}_{\mathrm{e}}^k\,, \quad \widehat{\boldsymbol{B}}_{\mathrm{e}} = \boldsymbol{f}_{\mathrm{e}} \star \boldsymbol{g}^{-1} = \lambda_{\mathrm{e}\,k}^{-2}\; \widehat{\boldsymbol{N}}_{\mathrm{e}\,k} \otimes \widehat{\boldsymbol{N}}_{\mathrm{e}\,k}\,, \\ \boldsymbol{c}_{\mathrm{e}} &= \boldsymbol{F}_{\mathrm{e}} \star \boldsymbol{G}_{\mathrm{p}} = \lambda_{\mathrm{e}\,k}^{-2}\; \boldsymbol{n}_{\mathrm{e}}^k \otimes \boldsymbol{n}_{\mathrm{e}}^k\,, \quad \boldsymbol{b}_{\mathrm{e}} = \boldsymbol{F}_{\mathrm{e}} \star \boldsymbol{G}_{\mathrm{p}}^{-1} = \lambda_{\mathrm{e}\,k}^2\; \boldsymbol{n}_{\mathrm{e}\,k} \otimes \boldsymbol{n}_{\mathrm{e}\,k}\,, \end{aligned} \tag{3.12}$$

wherein the notation $\star$ abbreviates the linear action in terms of the preceding tensor, see also remarks 3.1.1 and 3.1.2. These tensors are essentially characterised by metric coefficients with respect to particular configurations, which provides a nice geometrical interpretation of the above transformations, and can alternatively be expressed in terms of the right and left stretch tensors as reviewed in eqs.(3.4–3.6). In this context, the action of the proper orthogonal tensors $\boldsymbol{R}$, $\boldsymbol{R}_{\mathrm{p}}$ and $\boldsymbol{R}_{\mathrm{e}}$ on the considered metric tensors are a priori included and the remaining relations read

$$\boldsymbol{C} = \boldsymbol{U}^{-1} \star\, \boldsymbol{G}\,, \quad \boldsymbol{B} = \boldsymbol{U}^{-1} \star\, \boldsymbol{G}^{-1}\,, \quad \boldsymbol{c} = \boldsymbol{v} \star\, \boldsymbol{g}\,, \quad \boldsymbol{b} = \boldsymbol{v} \star\, \boldsymbol{g}^{-1} \tag{3.13}$$

and

$$\boldsymbol{C}_{\mathrm{p}} = \boldsymbol{U}_{\mathrm{p}}^{-1} \star\, \boldsymbol{G}\,, \quad \boldsymbol{B}_{\mathrm{p}} = \boldsymbol{U}_{\mathrm{p}}^{-1} \star\, \boldsymbol{G}^{-1}\,, \quad \widehat{\boldsymbol{c}}_{\mathrm{p}} = \widehat{\boldsymbol{v}}_{\mathrm{p}} \star\, \boldsymbol{G}_{\mathrm{p}}\,, \quad \widehat{\boldsymbol{b}}_{\mathrm{p}} = \widehat{\boldsymbol{v}}_{\mathrm{p}} \star\, \boldsymbol{G}_{\mathrm{p}}^{-1} \tag{3.14}$$

as well as

$$\widehat{\boldsymbol{C}}_{\mathrm{e}} = \widehat{\boldsymbol{U}}_{\mathrm{e}}^{-1} \star\, \boldsymbol{G}_{\mathrm{p}}\,, \quad \widehat{\boldsymbol{B}}_{\mathrm{e}} = \widehat{\boldsymbol{U}}_{\mathrm{e}}^{-1} \star\, \boldsymbol{G}_{\mathrm{p}}^{-1}\,, \quad \boldsymbol{c}_{\mathrm{e}} = \boldsymbol{v}_{\mathrm{e}} \star\, \boldsymbol{g}\,, \quad \boldsymbol{b}_{\mathrm{e}} = \boldsymbol{v}_{\mathrm{e}} \star\, \boldsymbol{g}^{-1}\,, \tag{3.15}$$

compare remark 3.1.1 and 3.1.2.

Remark 3.1.1 *In order to represent the transformations in eqs.(3.10–3.15) in more detail, we introduce the dual quantities of the linear tangent maps and stretch tensors, respectively. Placing emphasis on the overall motion of the considered body B, one consequently obtains*

$$\begin{aligned} \boldsymbol{F}^{\mathrm{d}} &= \lambda_k \;\; \boldsymbol{N}^k \otimes \boldsymbol{n}_k\,, \qquad \boldsymbol{f}^{\mathrm{d}} = \lambda_k^{-1}\; \boldsymbol{n}^k \otimes \boldsymbol{N}_k\,, \\ \boldsymbol{R}^{\mathrm{d}} &= \quad\; \boldsymbol{N}^k \otimes \boldsymbol{n}_k\,, \qquad \boldsymbol{R}^{-\mathrm{d}} = \quad\; \boldsymbol{n}^k \otimes \boldsymbol{N}_k\,, \\ \boldsymbol{U}^{\mathrm{d}} &= \lambda_k \;\; \boldsymbol{N}^k \otimes \boldsymbol{N}_k\,, \qquad \boldsymbol{U}^{-\mathrm{d}} = \lambda_k^{-1}\; \boldsymbol{N}^k \otimes \boldsymbol{N}_k\,, \\ \boldsymbol{v}^{\mathrm{d}} &= \lambda_k \;\; \boldsymbol{n}^k \otimes \boldsymbol{n}_k\,, \qquad \boldsymbol{v}^{-\mathrm{d}} = \lambda_k^{-1}\; \boldsymbol{n}^k \otimes \boldsymbol{n}_k\,, \end{aligned} \tag{3.16}$$

so that

$$\begin{aligned}
\boldsymbol{C} &= \boldsymbol{F}^{\mathrm{d}} \cdot \boldsymbol{g} \cdot \boldsymbol{F} &&= \boldsymbol{U}^{\mathrm{d}} \cdot \boldsymbol{G} \cdot \boldsymbol{U}\,, \\
\boldsymbol{B} &= \boldsymbol{f} \cdot \boldsymbol{g}^{-1} \cdot \boldsymbol{f}^{\mathrm{d}} &&= \boldsymbol{U}^{-1} \cdot \boldsymbol{G}^{-1} \cdot \boldsymbol{U}^{-\mathrm{d}}\,, \\
\boldsymbol{c} &= \boldsymbol{f}^{\mathrm{d}} \cdot \boldsymbol{G} \cdot \boldsymbol{f} &&= \boldsymbol{v}^{-\mathrm{d}} \cdot \boldsymbol{g} \cdot \boldsymbol{v}^{-1}\,, \\
\boldsymbol{b} &= \boldsymbol{F} \cdot \boldsymbol{G}^{-1} \cdot \boldsymbol{F}^{\mathrm{d}} &&= \boldsymbol{v} \cdot \boldsymbol{g}^{-1} \cdot \boldsymbol{v}^{\mathrm{d}}\,.
\end{aligned} \tag{3.17}$$

By analogy with eq.(3.16) we obtain the definitions of $\boldsymbol{f}$, $\boldsymbol{R}^{-1}$, $\boldsymbol{U}^{-1}$ and $\boldsymbol{v}^{-1}$ which are obvious and not additionally summarised. With these relations in hand, a corresponding outline in terms of $\boldsymbol{F}_{\mathrm{p}}$ and $\boldsymbol{F}_{\mathrm{e}}$ is straightforward and therefore omitted.

Remark 3.1.2 *Deformation tensors as highlighted in eqs.(3.10–3.12) are usually introduced as either co– or contra–variant tensors. Alternatively, one could also define mixed–variant deformation tensors, see for example Marsden and Hughes (1994). In this context, we first introduce the transposition of mixed–variant tensors and second set up appropriate deformation tensors. By analogy with remark 3.1.1, special emphasis is placed on the overall motion of the considered body $\mathcal{B}$. In this regard, the relation between the transposed and the dual of the deformation gradient – to be specific $\boldsymbol{F}^{\mathrm{t}} = \boldsymbol{G}^{-1} \cdot \boldsymbol{F}^{\mathrm{d}} \cdot \boldsymbol{g}$ – together with the previously introduced spectral decomposition theorem results in*

$$\begin{aligned}
\boldsymbol{F}^{\mathrm{t}} &= \lambda_k\ \boldsymbol{N}_k \otimes \boldsymbol{n}^k\,, & \boldsymbol{f}^{\mathrm{t}} &= \lambda_k^{-1}\ \boldsymbol{n}_k \otimes \boldsymbol{N}^k\,, \\
\boldsymbol{R}^{\mathrm{t}} &= \boldsymbol{N}_k \otimes \boldsymbol{n}^k = \boldsymbol{R}^{-1}\,, & \boldsymbol{R}^{-\mathrm{t}} &= \boldsymbol{n}_k \otimes \boldsymbol{N}^k = \boldsymbol{R}\,, \\
\boldsymbol{U}^{\mathrm{t}} &= \boldsymbol{U}\,, & \boldsymbol{v}^{\mathrm{t}} &= \boldsymbol{v}\,.
\end{aligned} \tag{3.18}$$

Moreover, we additionally note the relations

$$\boldsymbol{G}^{-1} \cdot \boldsymbol{N}^k = \boldsymbol{N}_k\,, \quad \boldsymbol{G} \cdot \boldsymbol{N}_k = \boldsymbol{N}^k\,, \quad \boldsymbol{g}^{-1} \cdot \boldsymbol{n}^k = \boldsymbol{n}_k\,, \quad \boldsymbol{g} \cdot \boldsymbol{n}_k = \boldsymbol{n}^k\,. \tag{3.19}$$

Now, with the transposition operation being defined, the well–established transformations between right and left stretch tensors

$$\boldsymbol{U} = \boldsymbol{R}^{\mathrm{t}} \cdot \boldsymbol{v} \cdot \boldsymbol{R}\,, \quad \boldsymbol{U}_{\mathrm{p}} = \boldsymbol{R}_{\mathrm{p}}^{\mathrm{t}} \cdot \widehat{\boldsymbol{v}}_{\mathrm{p}} \cdot \boldsymbol{R}_{\mathrm{p}}\,, \quad \widehat{\boldsymbol{U}}_{\mathrm{p}} = \boldsymbol{R}_{\mathrm{e}}^{\mathrm{t}} \cdot \boldsymbol{v}_{\mathrm{e}} \cdot \boldsymbol{R}_{\mathrm{e}} \tag{3.20}$$

become evident – the inverse relation, as for instance $\boldsymbol{v} = \boldsymbol{R} \cdot \boldsymbol{U} \cdot \boldsymbol{R}^{\mathrm{t}}$, being obvious. Finally, these elaborations allow on the one hand to reiterate the definition of second order identities as

$$\begin{aligned}
\boldsymbol{f} \cdot \boldsymbol{F} &= \boldsymbol{F}^{\mathrm{t}} \cdot \boldsymbol{f}^{\mathrm{t}} = \boldsymbol{R}^{\mathrm{t}} \cdot \boldsymbol{R} &&= \boldsymbol{N}_k \otimes \boldsymbol{N}^k = \boldsymbol{I}_0\,, \\
\boldsymbol{F} \cdot \boldsymbol{f} &= \boldsymbol{f}^{\mathrm{t}} \cdot \boldsymbol{F}^{\mathrm{t}} = \boldsymbol{R} \cdot \boldsymbol{R}^{\mathrm{t}} &&= \boldsymbol{n}_k \otimes \boldsymbol{n}^k = \boldsymbol{I}_t\,, \\
& \boldsymbol{F}^{\mathrm{d}} \cdot \boldsymbol{f}^{\mathrm{d}} = \boldsymbol{R}^{\mathrm{d}} \cdot \boldsymbol{R}^{-\mathrm{d}} &&= \boldsymbol{N}^k \otimes \boldsymbol{N}_k = \boldsymbol{I}_0^{\mathrm{d}}\,, \\
& \boldsymbol{f}^{\mathrm{d}} \cdot \boldsymbol{F}^{\mathrm{d}} = \boldsymbol{R}^{-\mathrm{d}} \cdot \boldsymbol{R}^{\mathrm{d}} &&= \boldsymbol{n}^k \otimes \boldsymbol{n}_k = \boldsymbol{I}_t^{\mathrm{d}}\,,
\end{aligned} \tag{3.21}$$

and, on the other hand, enable us to introduce the sought mixed–variant deformation tensors via

$$\begin{aligned}
\boldsymbol{C}^{\natural} &= \boldsymbol{F}^{\mathrm{t}} \cdot \boldsymbol{F} = \boldsymbol{U} \cdot \boldsymbol{U} &&= \lambda_k^2\ \boldsymbol{N}_k \otimes \boldsymbol{N}^k = \boldsymbol{G}^{-1} \cdot \boldsymbol{C}\,, \\
\boldsymbol{B}^{\natural} &= \boldsymbol{f} \cdot \boldsymbol{f}^{\mathrm{t}} = \boldsymbol{U}^{-\mathrm{d}} \cdot \boldsymbol{U}^{-\mathrm{d}} &&= \lambda_k^{-2}\ \boldsymbol{N}_k \otimes \boldsymbol{N}^k = \boldsymbol{B} \cdot \boldsymbol{G}\,, \\
\boldsymbol{c}^{\natural} &= \boldsymbol{f}^{\mathrm{t}} \cdot \boldsymbol{f} = \boldsymbol{v}^{-\mathrm{d}} \cdot \boldsymbol{v}^{-\mathrm{d}} &&= \lambda_k^{-2}\ \boldsymbol{n}_k \otimes \boldsymbol{n}^k = \boldsymbol{g}^{-1} \cdot \boldsymbol{c}\,, \\
\boldsymbol{b}^{\natural} &= \boldsymbol{F} \cdot \boldsymbol{F}^{\mathrm{t}} = \boldsymbol{v} \cdot \boldsymbol{v} &&= \lambda_k^2\ \boldsymbol{n}_k \otimes \boldsymbol{n}^k = \boldsymbol{b} \cdot \boldsymbol{g}\,,
\end{aligned} \tag{3.22}$$

so that $\boldsymbol{B} \cdot \boldsymbol{C} = \boldsymbol{B}^{\natural} \cdot \boldsymbol{C}^{\natural} = \boldsymbol{C}^{\natural} \cdot \boldsymbol{B}^{\natural} = \boldsymbol{I}_0$ and $\boldsymbol{b} \cdot \boldsymbol{c} = \boldsymbol{b}^{\natural} \cdot \boldsymbol{c}^{\natural} = \boldsymbol{c}^{\natural} \cdot \boldsymbol{b}^{\natural} = \boldsymbol{I}_t$. With these relations in hand, a corresponding outline in terms of $\boldsymbol{F}_{\mathrm{p}}$ and $\boldsymbol{F}_{\mathrm{e}}$ is straightforward and therefore omitted.

3.2 Generalised strain measures

The geometric interpretation of strain measures (in one configuration) consists in the point of view that

‘strain means change of metric with time’.

In order to compare the metric coefficients, according to a particular particle of the body B, at two different states of deformation, we must analyse these quantities (or powers thereof) in one and the same configuration. In this regard, the transformations highlighted in eqs.(3.10–3.12) are of cardinal importance.

One classical strain tensor family is provided by the so–called Seth–Hill strain measures; compare Seth (1964) and Hill (1968). Adopting this framework, the corresponding class of co–variant strains in $\mathcal{B}_0$ reads

$$\boldsymbol{E}_{(m)}(\boldsymbol{C};\boldsymbol{G}) = \begin{cases} \frac{1}{m}\,[\,\lambda_k^m - 1\,]\;\boldsymbol{N}^k \otimes \boldsymbol{N}^k = \frac{1}{m}\,[\,\boldsymbol{G}\cdot\boldsymbol{U}^m - \boldsymbol{G}\,] \\ \qquad\qquad\qquad\qquad\qquad\quad = \frac{1}{m}\,\big[\,\boldsymbol{G}\cdot[\,\boldsymbol{G}^{-1}\cdot\boldsymbol{C}\,]^{\frac{m}{2}} - \boldsymbol{G}\,\big] \\ \frac{1}{2}\;\ln(\lambda_k^2) \qquad \boldsymbol{N}^k \otimes \boldsymbol{N}^k = \frac{1}{2}\;\ln(\boldsymbol{G}\cdot\boldsymbol{U}^2) \\ \qquad\qquad\qquad\qquad\qquad\quad = \frac{1}{2}\;\ln(\boldsymbol{C}) \qquad\qquad \text{if } m=0 \end{cases} \tag{3.23}$$

with $m \geq 0$. Herein, powers of the pullback of the spatial co–variant metric $\boldsymbol{g}$ are compared with the material co–variant metric $\boldsymbol{G}$. It is clearly seen, that the spectral decomposition theorem (which is the standard representation for strain measures of the Seth–Hill family) renders strain eigenvalues that allow interpretation as being monotone functions in terms of the principal stretches; to be specific, $E_{(m)\,k}(\lambda_k)$ with $E_{(m)\,k}|_{\lambda_k=1} = 0$ and $\partial_{\lambda_k} E_{(m)\,k}|_{\lambda_k=1} = 1$ which is assumed to hold throughout for the subsequent strain measures. Commonly applied representations are, for example, the logarithmic Hencky strains ($m = 0$), the Biot strain measure ($m = 1$), and the right Cauchy–Green strain tensor ($m = 2$). The scalar quantity m in eq.(3.23) is restricted to remain non–negative. Strain measures in $\mathcal{B}_0$ that incorporate the inverse stretch are consequently introduced as contra–variant tensors, namely

$$\boldsymbol{K}_{(m)}(\boldsymbol{B};\boldsymbol{G}^{-1}) = \begin{cases} \frac{1}{m}\,[\,1-\lambda_k^{-m}\,]\;\boldsymbol{N}_k \otimes \boldsymbol{N}_k = \frac{1}{m}\,[\,\boldsymbol{G}^{-1} - \boldsymbol{U}^{-m}\cdot\boldsymbol{G}^{-1}\,] \\ \qquad\qquad\qquad\qquad\qquad\quad = \frac{1}{m}\,\big[\,\boldsymbol{G}^{-1} - \boldsymbol{G}^{-1}\cdot[\,\boldsymbol{G}\cdot\boldsymbol{B}\,]^{\frac{m}{2}}\,\big] \\ -\frac{1}{2}\;\ln(\lambda_k^{-2}) \qquad \boldsymbol{N}_k \otimes \boldsymbol{N}_k = -\frac{1}{2}\;\ln(\boldsymbol{U}^{-2}\cdot\boldsymbol{G}^{-1}) \\ \qquad\qquad\qquad\qquad\qquad\quad = -\frac{1}{2}\;\ln(\boldsymbol{B}) \qquad\qquad \text{if } m=0 \end{cases} \tag{3.24}$$

with $m \geq 0$. Herein powers of the pullback of the spatial contra–variant metric $\boldsymbol{g}^{-1}$ are compared with the material contra–variant metric $\boldsymbol{G}^{-1}$.

A similar setup in $\mathcal{B}_{\mathrm{p}}$ is obtained if the pullback of the spatial metric tensor is not performed via the total deformation gradient $\boldsymbol{F}$ but in terms of solely its reversible part $\boldsymbol{F}_{\mathrm{e}}$. In this context, the following strain measures take the interpretation of an elastic setting with respect

to $\mathcal{B}_{\rm p}$. By analogy with eq.(3.23) we obtain

$$\widehat{\boldsymbol{E}}_{{\rm e}\,(m)}(\widehat{\boldsymbol{C}}_{\rm e};\boldsymbol{G}_{\rm p}) = \begin{cases} \frac{1}{m}\,[\,\lambda_{{\rm e}\,k}^{m}-1\,]\;\widehat{\boldsymbol{N}}_{\rm e}^{k}\otimes\widehat{\boldsymbol{N}}_{\rm e}^{k} = \frac{1}{m}\,[\,\boldsymbol{G}_{\rm p}\cdot\widehat{\boldsymbol{U}}_{\rm e}^{\,m}-\boldsymbol{G}_{\rm p}\,] \\ \qquad\qquad\qquad\qquad\qquad\quad = \frac{1}{m}\,\Big[\,\boldsymbol{G}_{\rm p}\cdot[\,\boldsymbol{G}_{\rm p}^{-1}\cdot\widehat{\boldsymbol{C}}_{\rm e}\,]^{\frac{m}{2}}-\boldsymbol{G}_{\rm p}\,\Big] \\ \frac{1}{2}\;\ln(\lambda_{{\rm e}\,k}^{2}) \quad \widehat{\boldsymbol{N}}_{\rm e}^{k}\otimes\widehat{\boldsymbol{N}}_{\rm e}^{k} = \frac{1}{2}\;\ln(\boldsymbol{G}_{\rm p}\cdot\widehat{\boldsymbol{U}}_{\rm e}^{\,2}) \\ \qquad\qquad\qquad\qquad\qquad\quad = \frac{1}{2}\;\ln(\widehat{\boldsymbol{C}}_{\rm e}) \qquad\qquad \text{if } m=0 \end{cases} \tag{3.25}$$

and eq.(3.24) corresponds to

$$\widehat{\boldsymbol{K}}_{{\rm e}\,(m)}(\widehat{\boldsymbol{B}}_{\rm e};\boldsymbol{G}_{\rm p}^{-1}) = \begin{cases} \frac{1}{m}\,[\,1-\lambda_{{\rm e}\,k}^{-m}\,]\;\widehat{\boldsymbol{N}}_{{\rm e}\,k}\otimes\widehat{\boldsymbol{N}}_{{\rm e}\,k} = \frac{1}{m}\,[\,\boldsymbol{G}_{\rm p}^{-1}-\widehat{\boldsymbol{U}}_{\rm e}^{\,-m}\cdot\boldsymbol{G}_{\rm p}^{-1}\,] \\ \qquad\qquad\qquad\qquad\qquad\quad = \frac{1}{m}\,\Big[\,\boldsymbol{G}_{\rm p}^{-1}-\boldsymbol{G}_{\rm p}^{-1}\cdot[\,\boldsymbol{G}_{\rm p}\cdot\widehat{\boldsymbol{B}}_{\rm e}\,]^{\frac{m}{2}}\,\Big] \\ -\;\frac{1}{2}\;\ln(\lambda_{{\rm e}\,k}^{-2}) \quad \widehat{\boldsymbol{N}}_{{\rm e}\,k}\otimes\widehat{\boldsymbol{N}}_{{\rm e}\,k} = -\;\frac{1}{2}\;\ln(\widehat{\boldsymbol{U}}_{\rm e}^{\,-2}\cdot\boldsymbol{G}_{\rm p}^{-1}) \\ \qquad\qquad\qquad\qquad\qquad\quad = -\;\frac{1}{2}\;\ln(\widehat{\boldsymbol{B}}_{\rm e}) \qquad\qquad \text{if } m=0 \end{cases} \tag{3.26}$$

whereby the restriction $m \geq 0$ is assumed to hold for both types of strain measures, i.e. for the co–variant tensors $\widehat{\boldsymbol{E}}_{{\rm e}\,(m)}$ as well as for the contra–variant tensors $\widehat{\boldsymbol{K}}_{{\rm e}\,(m)}$.

While the previously highlighted strain measures are defined in terms of pullback operations of metric tensors in $\mathcal{B}_t$ to $\mathcal{B}_0$ or to $\mathcal{B}_{\rm p}$, respectively, we can alternatively introduce pushforward transformations of metric tensors in either $\mathcal{B}_0$ or $\mathcal{B}_{\rm p}$ to $\mathcal{B}_t$. Comparing the obtained deformation tensors with metric tensors in $\mathcal{B}_t$, we observe alternative strain measures which, conceptually speaking, are related to the inverse motion problem; see chapter 2 for a general review. By analogy with eqs.(3.23,3.24), we obtain the co–variant spatial strain family

$$\boldsymbol{e}_{(m)}(\boldsymbol{c};\boldsymbol{g}) = \begin{cases} \frac{1}{m}\,[\,1-\lambda_{k}^{-m}\,]\;\boldsymbol{n}^{k}\otimes\boldsymbol{n}^{k} = \frac{1}{m}\,[\,\boldsymbol{g}-\boldsymbol{g}\cdot\boldsymbol{v}^{-m}\,] \\ \qquad\qquad\qquad\qquad\quad = \frac{1}{m}\,\big[\,\boldsymbol{g}-\boldsymbol{g}\cdot[\,\boldsymbol{g}^{-1}\cdot\boldsymbol{c}\,]^{\frac{m}{2}}\,\big] \\ -\;\frac{1}{2}\;\ln(\lambda_{k}^{-2}) \quad \boldsymbol{n}^{k}\otimes\boldsymbol{n}^{k} = -\;\frac{1}{2}\;\ln(\boldsymbol{g}\cdot\boldsymbol{v}^{-2}) \\ \qquad\qquad\qquad\qquad\quad = -\;\frac{1}{2}\;\ln(\boldsymbol{c}) \qquad\quad \text{if } m=0 \end{cases} \tag{3.27}$$

and the contra–variant counterpart reads

$$\boldsymbol{k}_{(m)}(\boldsymbol{b};\boldsymbol{g}^{-1}) = \begin{cases} \frac{1}{m}\,[\,\lambda_{k}^{m}-1\,]\;\boldsymbol{n}_{k}\otimes\boldsymbol{n}_{k} = \frac{1}{m}\,[\,\boldsymbol{v}^{m}\cdot\boldsymbol{g}^{-1}-\boldsymbol{g}^{-1}\,] \\ \qquad\qquad\qquad\qquad\quad = \frac{1}{m}\,\big[\,\boldsymbol{g}^{-1}\cdot[\,\boldsymbol{g}\cdot\boldsymbol{b}\,]^{\frac{m}{2}}-\boldsymbol{g}^{-1}\,\big] \\ \frac{1}{2}\;\ln(\lambda_{k}^{2}) \quad \boldsymbol{n}_{k}\otimes\boldsymbol{n}_{k} = \frac{1}{2}\;\ln(\boldsymbol{v}^{2}\cdot\boldsymbol{g}^{-1}) \\ \qquad\qquad\qquad\qquad\quad = \frac{1}{2}\;\ln(\boldsymbol{b}) \qquad\quad \text{if } m=0 \end{cases} \tag{3.28}$$

for $m \geq 0$.

Finally, we place emphasis on the reversible part of the deformation gradient $\boldsymbol{F}_{\rm e}$ instead of the total tangent map $\boldsymbol{F}$ and obtain the spatial co–variant strain measures

$$\boldsymbol{e}_{{\rm e}\,(m)}(\boldsymbol{c}_{\rm e};\boldsymbol{g}) = \begin{cases} \frac{1}{m}\,[\,1-\lambda_{{\rm e}\,k}^{-m}\,]\;\boldsymbol{n}_{\rm e}^{k}\otimes\boldsymbol{n}_{\rm e}^{k} = \frac{1}{m}\,[\,\boldsymbol{g}-\boldsymbol{g}\cdot\boldsymbol{v}_{\rm e}^{m}\,] \\ \qquad\qquad\qquad\qquad\quad = \frac{1}{m}\,\big[\,\boldsymbol{g}-\boldsymbol{g}\cdot[\,\boldsymbol{g}^{-1}\cdot\boldsymbol{c}_{\rm e}\,]^{\frac{m}{2}}\,\big] \\ -\;\frac{1}{2}\;\ln(\lambda_{{\rm e}\,k}^{-2}) \quad \boldsymbol{n}_{\rm e}^{k}\otimes\boldsymbol{n}_{\rm e}^{k} = -\;\frac{1}{2}\;\ln(\boldsymbol{g}\cdot\boldsymbol{v}_{\rm e}^{-2}) \\ \qquad\qquad\qquad\qquad\quad = -\;\frac{1}{2}\;\ln(\boldsymbol{c}_{\rm e}) \qquad\quad \text{if } m=0 \end{cases} \tag{3.29}$$

similarly to eqs.(3.25,3.26), with the corresponding contra–variant representation consequently taking the format

$$\boldsymbol{k}_{\mathrm{e}\,(m)}(\boldsymbol{b}_{\mathrm{e}};\boldsymbol{g}^{-1}) = \begin{cases} \frac{1}{m}\,[\,\lambda_{\mathrm{e}\,k}^{m}-1\,]\;\boldsymbol{n}_{\mathrm{e}\,k}\otimes\boldsymbol{n}_{\mathrm{e}\,k} = \frac{1}{m}\,[\,\boldsymbol{v}_{\mathrm{e}}^{m}\cdot\boldsymbol{g}^{-1}-\boldsymbol{g}^{-1}\,] \\ \qquad\qquad\qquad\qquad\qquad\quad = \frac{1}{m}\,\big[\,\boldsymbol{g}^{-1}\cdot[\,\boldsymbol{g}\cdot\boldsymbol{b}_{\mathrm{e}}\,]^{\frac{m}{2}}-\boldsymbol{g}^{-1}\,\big] \\ \frac{1}{2}\;\ln(\lambda_{\mathrm{e}\,k}^{2}) \quad \boldsymbol{n}_{\mathrm{e}\,k}\otimes\boldsymbol{n}_{\mathrm{e}\,k} = \frac{1}{2}\;\ln(\boldsymbol{v}_{\mathrm{e}}^{2}\cdot\boldsymbol{g}^{-1}) \\ \qquad\qquad\qquad\qquad\qquad\quad = \frac{1}{2}\;\ln(\boldsymbol{b}_{\mathrm{e}}) \qquad\qquad \text{if } m=0 \end{cases} \tag{3.30}$$

for $m \geq 0$.

Remark 3.2.1 *The previously highlighted list of Seth–Hill–type strain measures is by far not complete – for instance the deformation tensors $\boldsymbol{C}_{\mathrm{p}}$ and $\boldsymbol{B}_{\mathrm{p}}$ have, up to now, not been incorporated. In this regard, a typical example is provided by, for example,*

$$\boldsymbol{E}_{\mathrm{p}\,(2)}(\boldsymbol{C};\boldsymbol{C}_{\mathrm{p}}) \doteq \boldsymbol{F}_{\mathrm{p}}^{-1}\star\widehat{\boldsymbol{E}}_{\mathrm{e}\,(2)}(\widehat{\boldsymbol{C}}_{\mathrm{e}};\boldsymbol{G}_{\mathrm{p}}) = \tfrac{1}{2}\,[\,\boldsymbol{C}-\boldsymbol{C}_{\mathrm{p}}\,] \tag{3.31}$$

with $\boldsymbol{E}_{\mathrm{p}\,(2)}\cdot\boldsymbol{G}^{-1}\cdot\boldsymbol{C} \neq \boldsymbol{C}\cdot\boldsymbol{G}^{-1}\cdot\boldsymbol{E}_{\mathrm{p}\,(2)}$ while $\widehat{\boldsymbol{E}}_{\mathrm{e}\,(m)}\cdot\boldsymbol{G}_{\mathrm{p}}^{-1}\cdot\widehat{\boldsymbol{C}}_{\mathrm{e}} = \widehat{\boldsymbol{C}}_{\mathrm{e}}\cdot\boldsymbol{G}_{\mathrm{p}}^{-1}\cdot\widehat{\boldsymbol{E}}_{\mathrm{e}\,(m)}$ constantly holds. Since absolute tensor representations (besides spectral decompositions) are applied in this work and any additional assumption on isotropy is avoided, we predominantly restrict ourselves to the strains highlighted in eqs.(3.23–3.30). Moreover, appropriate evolution equations of, for instance, the irreversible part of the deformation gradient will be related to appropriate rates of strain measures in this work. In other words, the inelastic spin of $\boldsymbol{F}_{\mathrm{p}}$ will be neglected. Please note that the presented (kinematical) framework is not restricted to one single intermediate configuration but also allows extension to the combination of several intermediate configurations, see Meggyes (2001) for an outline. Even though it seems to be natural to introduce mixed–variant strain measures, compare remark 3.1.2, we refer to the highlighted co– or contra–variant strains in the following.

Remark 3.2.2 *Seth–Hill–type strain measures represent solely one particular family of strain tensors. The general definition of strain measures is commonly introduced in terms of the strain eigenvalues, s_k say, which are monotone functions with respect to appropriate principal stretches, λ_k say, with $s_k(\lambda_k)|_{\lambda_k=1} = 0$ and $\partial_{\lambda_k}s_k(\lambda_k)|_{\lambda_k=1} = 1$. This enables us to define admissible strain families in terms of for instance combinations of Seth–Hill–type strain measures like*

$$\boldsymbol{\Xi}_{(m)} = \tfrac{1}{2}\,[\,\boldsymbol{E}_{(m)}+\boldsymbol{G}\cdot\boldsymbol{K}_{(m)}\cdot\boldsymbol{G}\,] = \begin{cases} \frac{1}{2\,m}\;[\,\boldsymbol{G}\cdot\boldsymbol{U}^{m}-\boldsymbol{U}^{-m}\cdot\boldsymbol{G}\,] \\ \frac{1}{4}\quad [\,\ln(\boldsymbol{G}\cdot\boldsymbol{U}^{2})-\ln(\boldsymbol{G}\cdot\boldsymbol{U}^{-2})\,] \quad \text{if } m=0 \end{cases} \tag{3.32}$$

or

$$\boldsymbol{\Gamma}_{(m,n)} = \tfrac{1}{2}\,[\,\boldsymbol{E}_{(m)}+\boldsymbol{E}_{(n)}\,] = \begin{cases} \frac{1}{2\,m}\,\boldsymbol{G}\cdot\boldsymbol{U}^{m}+\frac{1}{2\,n}\,\boldsymbol{G}\cdot\boldsymbol{U}^{n}-[\,\frac{1}{2\,m}+\frac{1}{2\,n}\,]\,\boldsymbol{G} \\ \frac{1}{2\,m}\,\boldsymbol{G}\cdot\boldsymbol{U}^{m}+\frac{1}{4}\,\ln(\boldsymbol{G}\cdot\boldsymbol{U}^{2})-\frac{1}{2\,m}\,\boldsymbol{G} \quad \text{if } m=0 \end{cases} \tag{3.33}$$

for $m,n \geq 0$ – with the outline for $m > 0$ but $n = 0$ as well as $\boldsymbol{\Gamma}_{(0,0)} = \boldsymbol{E}_{(0)}$ being obvious; see e.g. Dłużewski (2000) or Billington (2003) where several applications based on the introduction of $\boldsymbol{\Xi}_{(2)}$ are elaborated. The setup of similar strains of contra–variant nature, derivations with respect to other configurations and the combination of more than solely two strain tensors are straightforward and therefore omitted.

Furthermore, the spectral decomposition enables us to represent strain measures as isotropic tensor functions based on the eigenvalues of other strain tensors, for instance,

$$\boldsymbol{E}_{(m)} = \boldsymbol{E}_{(m)}(\boldsymbol{E}_{(n)}) = \begin{cases} \frac{1}{m}\,\big[\,[\,n\,E_{(n)\,k}+1\,]^{\frac{m}{n}}-1\,\big] & \boldsymbol{N}^k\otimes\boldsymbol{N}^k \\ \frac{1}{m}\,\big[\,[\exp(2\,E_{(n)\,k})]^{\frac{m}{2}}-1\,\big] & \boldsymbol{N}^k\otimes\boldsymbol{N}^k \text{ if } n=0 \\ \frac{1}{2}\,\ln\big([\,n\,E_{(n)\,k}+1\,]^{\frac{2}{n}}\big) & \boldsymbol{N}^k\otimes\boldsymbol{N}^k \text{ if } m=0 \end{cases} \tag{3.34}$$

wherein $E_{(n>0)\,k} = \frac{1}{n}\,[\,\lambda^n - 1\,]$ *and* $E_{(0)\,k} = \frac{1}{2}\,\ln(\lambda_k^2)$ *abbreviate the set of eigenvalues with respect to* $\boldsymbol{E}_{(n)}$*,* $m \geq 0$ *as well as* $n \geq 0$ *and the case* $m = n = 0$ *being trivial.*

Finally, note that general strain tensors are not restricted to represent tensors in solely one single configuration – even though the geometric interpretation of strain as change of metric with time is then formally lost. In this regard, Böck and Holzapfel (2004) recently introduced the strain tensor $\boldsymbol{\Upsilon} = \frac{1}{2}\,[\,\boldsymbol{F} - \boldsymbol{f}^{\mathrm{t}}\,]$ *possessing the property* $\|\boldsymbol{\Upsilon}^{\mathrm{d}}\cdot\boldsymbol{g}\cdot\boldsymbol{\Upsilon}\| \to \infty$ *for* $\det(\boldsymbol{F}) \to \infty$ *or* $\det(\boldsymbol{F}) \to 0$*, the latter case (possibly) becoming more important in view of, for instance, numerical applications.*

Remark 3.2.3 *A volumetric / isochoric split of generalised strain measures follows straightforwardly by replacing the considered strain tensor with its unimodular part. To give an example, let* $\{\bullet\}$ *abbreviate a representative strain measure so that* $\{\bullet\} \;\mapfrom\; \{\bullet\}^{\mathrm{iso}} = \det{}^{-1/3}(\{\bullet\})\,\{\bullet\}$ *represents the corresponding unimodular part; see Papadopoulos and Lu (1998, 2001) and Miehe and Lambrecht (2001) for detailed outlines.*

3.2.1 Relations between different strain measures in one configuration

The previously highlighted introduction of Seth–Hill–type strain measures suggests that there exist transformations which map co–variant strain tensors onto contra–variant representations within one strain family and within one configuration. Taking the particular format of the linear tangent maps as reviewed in eqs.(3.4–3.6) into account, one observes the fundamental relation

$$\boldsymbol{E}_{(m)}\cdot\boldsymbol{G}^{-1} = \boldsymbol{C}^{\frac{m}{2}}\cdot\boldsymbol{K}_{(m)} \quad\longleftrightarrow\quad \boldsymbol{K}_{(m)}\cdot\boldsymbol{G} = \boldsymbol{B}^{\frac{m}{2}}\cdot\boldsymbol{E}_{(m)} \tag{3.35}$$

for those strain measures set up in eqs.(3.23,3.24) with respect to $\mathcal{B}_0$. As an interesting side aspect, eq.(3.35) generally holds for $m \geq 0$. Similarly, we obtain the corresponding strain tensors in the intermediate configuration $\mathcal{B}_{\mathrm{p}}$

$$\widehat{\boldsymbol{E}}_{\mathrm{e}\,(m)}\cdot\boldsymbol{G}_{\mathrm{p}}^{-1} = \widehat{\boldsymbol{C}}_{\mathrm{e}}^{\frac{m}{2}}\cdot\widehat{\boldsymbol{K}}_{\mathrm{e}\,(m)} \quad\longleftrightarrow\quad \widehat{\boldsymbol{K}}_{\mathrm{e}\,(m)}\cdot\boldsymbol{G}_{\mathrm{p}} = \widehat{\boldsymbol{B}}_{\mathrm{e}}^{\frac{m}{2}}\cdot\widehat{\boldsymbol{E}}_{\mathrm{e}\,(m)}\,, \tag{3.36}$$

recall eqs.(3.25,3.26). When placing emphasis on the spatial configuration $\mathcal{B}_t$, eqs.(3.27–3.30) consequently result in

$$\begin{aligned} \boldsymbol{e}_{(m)}\cdot\boldsymbol{g}^{-1} &= \boldsymbol{c}^{\frac{m}{2}}\cdot\boldsymbol{k}_{(m)} \quad\longleftrightarrow\quad \boldsymbol{k}_{(m)}\cdot\boldsymbol{g} &= \boldsymbol{b}^{\frac{m}{2}}\cdot\boldsymbol{e}_{(m)}\,, \\ \boldsymbol{e}_{\mathrm{e}\,(m)}\cdot\boldsymbol{g}^{-1} &= \boldsymbol{c}_{\mathrm{e}}^{\frac{m}{2}}\cdot\boldsymbol{k}_{\mathrm{e}\,(m)} \quad\longleftrightarrow\quad \boldsymbol{k}_{\mathrm{e}\,(m)}\cdot\boldsymbol{g} &= \boldsymbol{b}_{\mathrm{e}}^{\frac{m}{2}}\cdot\boldsymbol{e}_{\mathrm{e}\,(m)}\,. \end{aligned} \tag{3.37}$$

Remark 3.2.4 *Please note that the transformations above allow alternative representation in terms of appropriate stretches, to give an example*

$$\begin{aligned} \boldsymbol{E}_{(m)}\cdot\boldsymbol{G}^{-1} &= \boldsymbol{C}^{\frac{m}{2}}\cdot\boldsymbol{K}_{(m)} &&= \boldsymbol{U}^{\mathrm{d}\,\frac{m}{2}}\cdot\boldsymbol{G}\cdot\boldsymbol{U}^{\frac{m}{2}}\cdot\boldsymbol{K}_{(m)} \\ &= \boldsymbol{U}^{\mathrm{d}\,\frac{m}{2}}\cdot\boldsymbol{G}\cdot\boldsymbol{K}_{(m)}\cdot\boldsymbol{U}^{\mathrm{d}\,\frac{m}{2}} &&= \boldsymbol{U}^{\mathrm{d}\,\frac{m}{2}}\cdot\boldsymbol{G}\cdot\boldsymbol{K}_{(m)}\cdot\boldsymbol{G}\cdot\boldsymbol{U}^{\frac{m}{2}}\cdot\boldsymbol{G}^{-1}\,, \end{aligned} \tag{3.38}$$

whereby use of eq.(3.17) has been made.

3.2.2 Relations between different strain measures in different configurations

In addition to the transformation relations of strain measures in one configuration, the by far more interesting task consists in the correlations between strain measures in different configurations. Without these connections, typical pushforward and pullback transformations between the introduced configurations of interest (namely application of the fundamental covariance principle with respect to, for instance, the Helmholtz free energy), as commonly applied in computational inelasticity, would not be accessible.

In this context, we first observe

$$\boldsymbol{R} \star \boldsymbol{E}_{(m)} \cdot \boldsymbol{g}^{-1} = \boldsymbol{g} \cdot \boldsymbol{k}_{(m)} \,, \qquad \boldsymbol{R} \star \boldsymbol{K}_{(m)} \cdot \boldsymbol{g} = \boldsymbol{g}^{-1} \cdot \boldsymbol{e}_{(m)} \tag{3.39}$$

as well as

$$\boldsymbol{R}_{\mathrm{e}} \star \widehat{\boldsymbol{E}}_{\mathrm{e}\,(m)} \cdot \boldsymbol{g}^{-1} = \boldsymbol{g} \cdot \boldsymbol{k}_{\mathrm{e}\,(m)} \,, \qquad \boldsymbol{R}_{\mathrm{e}} \star \widehat{\boldsymbol{K}}_{\mathrm{e}\,(m)} \cdot \boldsymbol{g} = \boldsymbol{g}^{-1} \cdot \boldsymbol{e}_{\mathrm{e}\,(m)} \tag{3.40}$$

which becomes obvious from the underlying spectral decomposition theorem and, practically speaking, identifies identical eigenvalues

$$E_{(m)\,k} = k_{(m)\,k} \,, \qquad K_{(m)\,k} = e_{(m)\,k} \,, \qquad \widehat{E}_{\mathrm{e}\,(m)\,k} = k_{\mathrm{e}\,(m)\,k} \,, \qquad \widehat{K}_{\mathrm{e}\,(m)\,k} = e_{\mathrm{e}\,(m)\,k} \,, \tag{3.41}$$

wherein the abbreviation $E_{(m)\,k}$ collects the eigenvalues of $\boldsymbol{E}_{(m)}$, etc.; compare remark 3.2.4. Apparently, eqs.(3.39–3.41) hold for $m \geq 0$. Based on these relations, taking the transformations between the underlying eigenvectors into account and recalling eqs.(3.4–3.6), we second obtain the sought transformations, namely on the one hand by analogy with eq.(3.39)

$$\begin{aligned} \boldsymbol{F} \star \boldsymbol{E}_{(m)} \cdot \boldsymbol{g}^{-1} &= \boldsymbol{c} \cdot \boldsymbol{k}_{(m)} \,, & \boldsymbol{F} \star \boldsymbol{K}_{(m)} \cdot \boldsymbol{g} &= \boldsymbol{b} \cdot \boldsymbol{e}_{(m)} \,, \\ \boldsymbol{f} \star \boldsymbol{k}_{(m)} \cdot \boldsymbol{G} &= \boldsymbol{B} \cdot \boldsymbol{E}_{(m)} \,, & \boldsymbol{f} \star \boldsymbol{e}_{(m)} \cdot \boldsymbol{G}^{-1} &= \boldsymbol{C} \cdot \boldsymbol{K}_{(m)} \,, \end{aligned} \tag{3.42}$$

while, on the other hand, the representation which stems for eq.(3.40) reads

$$\begin{aligned} \boldsymbol{F}_{\mathrm{e}} \star \widehat{\boldsymbol{E}}_{\mathrm{e}\,(m)} \cdot \boldsymbol{g}^{-1} &= \boldsymbol{c}_{\mathrm{e}} \cdot \boldsymbol{k}_{\mathrm{e}\,(m)} \,, & \boldsymbol{F}_{\mathrm{e}} \star \widehat{\boldsymbol{K}}_{\mathrm{e}\,(m)} \cdot \boldsymbol{g} &= \boldsymbol{b}_{\mathrm{e}} \cdot \boldsymbol{e}_{\mathrm{e}\,(m)} \,, \\ \boldsymbol{f}_{\mathrm{e}} \star \boldsymbol{k}_{\mathrm{e}\,(m)} \cdot \boldsymbol{G}_{\mathrm{p}} &= \widehat{\boldsymbol{B}}_{\mathrm{e}} \cdot \widehat{\boldsymbol{E}}_{\mathrm{e}\,(m)} \,, & \boldsymbol{f}_{\mathrm{e}} \star \boldsymbol{e}_{\mathrm{e}\,(m)} \cdot \boldsymbol{G}_{\mathrm{p}}^{-1} &= \widehat{\boldsymbol{C}}_{\mathrm{e}} \cdot \widehat{\boldsymbol{K}}_{\mathrm{e}\,(m)} \,. \end{aligned} \tag{3.43}$$

Remark 3.2.5 *Please note that the transformations above allow alternative representation in terms of appropriate stretches, to give an example*

$$\begin{aligned} \boldsymbol{F} \star \boldsymbol{E}_{(m)} \cdot \boldsymbol{g}^{-1} &= \boldsymbol{v}^{-\mathrm{d}} \cdot \boldsymbol{R} \star \boldsymbol{E}_{(m)} \cdot \boldsymbol{v}^{-1} \cdot \boldsymbol{g}^{-1} &&= \boldsymbol{v}^{-\mathrm{d}} \cdot \boldsymbol{g} \cdot \boldsymbol{k}_{(m)} \cdot \boldsymbol{g} \cdot \boldsymbol{v}^{-1} \cdot \boldsymbol{g}^{-1} \\ &= \boldsymbol{v}^{-\mathrm{d}} \cdot \boldsymbol{g} \cdot \boldsymbol{k}_{(m)} \cdot \boldsymbol{v}^{-\mathrm{d}} &&= \boldsymbol{v}^{-\mathrm{d}} \cdot \boldsymbol{g} \cdot \boldsymbol{v}^{-1} \cdot \boldsymbol{k}_{(m)} \\ &= \boldsymbol{c} \cdot \boldsymbol{k}_{(m)} \,, \end{aligned} \tag{3.44}$$

whereby use of eqs.(3.17,3.39) has been made.

3.3 Helmholtz free energy density

In order to incorporate both types of generalised strains, namely those measures referring to the total deformation as well as those tensors which allow interpretation as an elastic setting with respect to $\mathcal{B}_{\mathrm{p}}$, we accept (with a slight misuse of notation) the following additive split of the Helmholtz free energy density

$$\psi_0(\boldsymbol{F}, \boldsymbol{F}_{\mathrm{p}}, \boldsymbol{A}_0; \boldsymbol{X}) = \psi_0^0(\boldsymbol{E}_{(m)}, \boldsymbol{G}^{-1}, \boldsymbol{A}_0; \boldsymbol{X}) + \psi_0^{\mathrm{e}}(\widehat{\boldsymbol{E}}_{\mathrm{e}\,(m)}, \boldsymbol{G}_{\mathrm{p}}^{-1}, \boldsymbol{A}_{\mathrm{p}}; \boldsymbol{X}) \,. \tag{3.45}$$

The additional quantities $\boldsymbol{A}_0$ and $\boldsymbol{A}_{\rm p} = \boldsymbol{F}_{\rm p} \star \boldsymbol{A}_0$ represent a contra–variant second order tensor which is assumed to be symmetric. Further arguments – which enable for instance the modelling of different hardening effects – are neglected for the sake of simplicity. With eq.(3.45) in hand, the fundamental covariance relation apparently allows us to rewrite the Helmholtz free energy density as

$$\begin{aligned}\psi_0(\boldsymbol{F},\boldsymbol{F}_{\rm p},\boldsymbol{A}_0;\boldsymbol{X}) &= \psi_0^0(\boldsymbol{E}_{(m)},\boldsymbol{G}^{-1},\boldsymbol{A}_0;\boldsymbol{X}) &&+\ \psi_0^{\rm e}(\boldsymbol{E}_{{\rm e}\,(m)},\boldsymbol{B}_{\rm p},\boldsymbol{A}_0;\boldsymbol{X})\\ &= \psi_0^0(\widehat{\boldsymbol{E}}_{(m)},\widehat{\boldsymbol{b}}_{\rm p},\boldsymbol{A}_{\rm p};\boldsymbol{X}) &&+\ \psi_0^{\rm e}(\widehat{\boldsymbol{E}}_{{\rm e}\,(m)},\boldsymbol{G}_{\rm p}^{-1},\boldsymbol{A}_{\rm p};\boldsymbol{X})\\ &= \psi_0^0(\boldsymbol{c}\cdot\boldsymbol{k}_{(m)}\cdot\boldsymbol{g},\boldsymbol{b},\boldsymbol{A}_t;\boldsymbol{X}) &&+\ \psi_0^{\rm e}(\boldsymbol{c}_{\rm e}\cdot\boldsymbol{k}_{{\rm e}\,(m)}\cdot\boldsymbol{g},\boldsymbol{b}_{\rm e},\boldsymbol{A}_t;\boldsymbol{X})\end{aligned} \tag{3.46}$$

with $\boldsymbol{E}_{{\rm e}\,(m)} = \boldsymbol{f}_{\rm p} \star \widehat{\boldsymbol{E}}_{{\rm e}\,(m)}$, $\widehat{\boldsymbol{E}}_{(m)} = \boldsymbol{F}_{\rm p} \star \boldsymbol{E}_{(m)}$ and $\boldsymbol{A}_t = \boldsymbol{F} \star \boldsymbol{A}_0$. The reader is referred to, for instance, Marsden and Hughes (1994), and references cited therein, for background information on the covariance principle. A particular application of this fundamental principle is the invariance of the Helmholtz free energy density under superposed material isometries (onto the arguments of ψ_0 with respect to the representation highlighted in eq.$(3.46)_1$). Conceptually speaking, the Helmholtz free energy is characterised by an isotropic tensor function determined via two sets of invariants. For clarity's sake, but without loss of generality we will assume $\boldsymbol{A}_0$ to remain constant during a deformation process in the progression of this work. Each set of invariants consequently includes solely five invariants, to be specific

$$\begin{aligned} I_j \ &= \boldsymbol{I}_0 : [\,\boldsymbol{E}_{(m)}\cdot\boldsymbol{G}^{-1}\,]^j && = \boldsymbol{I}_{\rm p} : [\,\widehat{\boldsymbol{E}}_{(m)}\cdot\widehat{\boldsymbol{b}}_{\rm p}\,]^j\\ &= \boldsymbol{I}_t : \big[\,[\,\boldsymbol{c}\cdot\boldsymbol{k}_{(m)}\cdot\boldsymbol{g}\,]\cdot\boldsymbol{b}\,\big]^j && = \boldsymbol{I}_t : [\,\boldsymbol{g}\cdot\boldsymbol{k}_{(m)}\,]^j\,,\\ I_{\alpha+3} \ &= \boldsymbol{I}_0 : \big[\,\boldsymbol{E}_{(m)}\cdot[\,\boldsymbol{G}^{-1}\cdot\boldsymbol{E}_{(m)}\,]^{\alpha-1}\cdot\boldsymbol{A}_0\,\big] && = \boldsymbol{I}_{\rm p} : \Big[\,\widehat{\boldsymbol{E}}_{(m)}\cdot[\,\widehat{\boldsymbol{b}}_{\rm p}\cdot\widehat{\boldsymbol{E}}_{(m)}\,]^{\alpha-1}\cdot\boldsymbol{A}_{\rm p}\,\Big]\\ &= \boldsymbol{I}_t : \big[\,[\,\boldsymbol{c}\cdot\boldsymbol{k}_{(m)}\cdot\boldsymbol{g}\,]\cdot[\,\boldsymbol{b}\cdot\boldsymbol{c}\cdot\boldsymbol{k}_{(m)}\cdot\boldsymbol{g}\,]^{\alpha-1}\cdot\boldsymbol{A}_t\,\big]\,, \end{aligned} \tag{3.47}$$

and

$$\begin{aligned} I_{{\rm e}\,j} \ &= \boldsymbol{I}_0 : [\,\boldsymbol{E}_{{\rm e}\,(m)}\cdot\boldsymbol{B}_{\rm p}\,]^j && = \boldsymbol{I}_{\rm p} : [\,\widehat{\boldsymbol{E}}_{{\rm e}\,(m)}\cdot\boldsymbol{G}_{\rm p}^{-1}\,]^j\\ &= \boldsymbol{I}_t : \big[\,[\,\boldsymbol{c}_{\rm e}\cdot\boldsymbol{k}_{{\rm e}\,(m)}\cdot\boldsymbol{g}\,]\cdot\boldsymbol{b}_{\rm e}\,\big]^j && = \boldsymbol{I}_t : [\,\boldsymbol{g}\cdot\boldsymbol{k}_{{\rm e}\,(m)}\,]^j\,,\\ I_{{\rm e}\,\alpha+3} \ &= \boldsymbol{I}_0 : \big[\,\boldsymbol{E}_{{\rm e}\,(m)}\cdot[\,\boldsymbol{B}_{\rm p}\cdot\boldsymbol{E}_{{\rm e}\,(m)}\,]^{\alpha-1}\cdot\boldsymbol{A}_0\,\big] && = \boldsymbol{I}_{\rm p} : \Big[\,\widehat{\boldsymbol{E}}_{{\rm e}\,(m)}\cdot[\,\boldsymbol{G}_{\rm p}^{-1}\cdot\widehat{\boldsymbol{E}}_{{\rm e}\,(m)}\,]^{\alpha-1}\cdot\boldsymbol{A}_{\rm p}\,\Big]\\ &= \boldsymbol{I}_t : \big[\,[\,\boldsymbol{c}_{\rm e}\cdot\boldsymbol{k}_{{\rm e}\,(m)}\cdot\boldsymbol{g}\,]\cdot[\,\boldsymbol{b}_{\rm e}\cdot\boldsymbol{c}_{\rm e}\cdot\boldsymbol{k}_{{\rm e}\,(m)}\cdot\boldsymbol{g}\,]^{\alpha-1}\cdot\boldsymbol{A}_t\,\big] \end{aligned} \tag{3.48}$$

with $j = 1,2,3$ and $\alpha = 1,2$, compare eq.(3.17). The underlying (elastic) symmetry group $\mathbb{G}$ of the considered body B, as based on the subsequent hyperelastic formats of representative stresses, based on for instance ψ_0^0, is defined via

$$\mathbb{G} = \{\boldsymbol{Q} \in \mathbb{O}^3 \mid \boldsymbol{Q} \star \boldsymbol{A}_0 = \boldsymbol{A}_0\}\,, \tag{3.49}$$

see, e.g., Boehler (1979) or the contributions in Boehler (1987). A typical example is provided by transversal isotropic symmetry so that $\boldsymbol{A}_0 \doteq \boldsymbol{v}_0 \otimes \boldsymbol{v}_0$ while orthotropy can be reflected via $\boldsymbol{A}_0 \doteq \boldsymbol{v}_0 \otimes \boldsymbol{v}_0 - \boldsymbol{w}_0 \otimes \boldsymbol{w}_0$, whereby $\boldsymbol{v}_0 \cdot \boldsymbol{G} \cdot \boldsymbol{w}_0 = 0$; see e.g. Zhang and Rychlewsky (1990) and Zheng and Spencer (1993) for the definition of ('general') structural tensors characterising crystalline and non–crystalline symmetries.

Remark 3.3.1 *It is obvious that the Helmholtz free energy density as represented in eq.(3.45) can be generalised by replacing the single argument $\boldsymbol{A}_0$ in ψ_0^0 and $\psi_0^{\rm e}$ with series $\boldsymbol{A}_{0\,1,\ldots,q}$ and*

$\boldsymbol{A}_{0\,q+1,\ldots,r}$ of tensors, respectively. Moreover, both sets also allow consideration as internal variables such that these arguments would evolve during the deformation process. In this regard, the reader is referred to Menzel and Steinmann (2003a, 2003c).

Remark 3.3.2 *Please note that the highlighted format of the Helmholtz free energy in, for instance, eq.(3.45) captures several standard approaches of typical (isothermal) 'constitutive models', namely hyperelasticity ($\psi_0 = \psi_0^0$), plasticity ($\psi_0 = \psi_0^{\mathrm{e}}$) or viscoelasticity ($\psi_0 = \psi_0^0 + \psi_0^{\mathrm{e}}$, the generalisation to several viscosity terms, $\psi_0(\boldsymbol{F}, \boldsymbol{F}_{\mathrm{p}_{1,\ldots,s}}; \boldsymbol{X}) \doteq \psi_0^0(\boldsymbol{F}; \boldsymbol{X}) + \sum_{s=1}^{S} \psi_{0_s}^{\mathrm{e}}(\boldsymbol{F}, \boldsymbol{F}_{\mathrm{p}_s}; \boldsymbol{X})$, being straightforward).*

3.4 Coleman–Noll entropy principle

The pointwise format of the isothermal Clausius–Duhem inequality reads

$$\mathsf{D}_0 = \boldsymbol{\Pi}^{\mathrm{d}} : \mathrm{D}_t\,\boldsymbol{F} - \mathrm{D}_t\,\psi_0 = \boldsymbol{\Pi}^{\mathrm{d}} : \mathrm{D}_t\,\boldsymbol{F} - \left.\frac{\partial \psi_0}{\partial \boldsymbol{F}}\right|_{\boldsymbol{F}_{\mathrm{p}}} : \mathrm{D}_t\,\boldsymbol{F} - \left.\frac{\partial \psi_0}{\partial \boldsymbol{F}_{\mathrm{p}}}\right|_{\boldsymbol{F}} : \mathrm{D}_t\,\boldsymbol{F}_{\mathrm{p}} \geq 0\,, \quad (3.50)$$

whereby the notation $\mathrm{D}_t\{\bullet\}$ characterises the material time derivative. From eq.(3.45) and $\widehat{\boldsymbol{C}}_{\mathrm{e}} = \boldsymbol{f}_{\mathrm{p}}^{\mathrm{d}} \cdot \boldsymbol{C} \cdot \boldsymbol{f}_{\mathrm{p}}$, recall eq.(3.1) and eqs.(3.10-3.12), we obtain

$$\left.\frac{\partial \psi_0}{\partial \boldsymbol{F}}\right|_{\boldsymbol{F}_{\mathrm{p}}} = \frac{\partial \psi_0^0}{\partial \boldsymbol{E}_{(m)}} : \frac{\partial \boldsymbol{E}_{(m)}}{\partial \boldsymbol{C}} : \frac{\partial \boldsymbol{C}}{\partial \boldsymbol{F}} + \frac{\partial \psi_0^{\mathrm{e}}}{\partial \widehat{\boldsymbol{E}}_{\mathrm{e}\,(m)}} : \frac{\partial \widehat{\boldsymbol{E}}_{\mathrm{e}\,(m)}}{\partial \widehat{\boldsymbol{C}}_{\mathrm{e}}} : \left.\frac{\partial \widehat{\boldsymbol{C}}_{\mathrm{e}}}{\partial \boldsymbol{F}}\right|_{\boldsymbol{F}_{\mathrm{p}}} \quad (3.51)$$

as well as

$$\left.\frac{\partial \psi_0}{\partial \boldsymbol{F}_{\mathrm{p}}}\right|_{\boldsymbol{F}} = \frac{\partial \psi_0^{\mathrm{e}}}{\partial \widehat{\boldsymbol{E}}_{\mathrm{e}\,(m)}} : \frac{\partial \widehat{\boldsymbol{E}}_{\mathrm{e}\,(m)}}{\partial \widehat{\boldsymbol{C}}_{\mathrm{e}}} : \left.\frac{\partial \widehat{\boldsymbol{C}}_{\mathrm{e}}}{\partial \boldsymbol{F}_{\mathrm{p}}}\right|_{\boldsymbol{F}}\,, \quad (3.52)$$

compare, for example, Govindjee and Reese (1997). In order to abbreviate notation, we introduce symmetric stress tensors of second Piola–Kirchhoff–type which are essentially based on commonly applied projection operators, to be specific

$$\begin{aligned}
\tfrac{1}{2}\,\boldsymbol{S}^0 &= \boldsymbol{T}^0_{(m)} : \mathsf{P}_{(m)}\,, & \tfrac{1}{2}\,\widehat{\boldsymbol{S}}^{\mathrm{e}} &= \widehat{\boldsymbol{T}}^{\mathrm{e}}_{(m)} : \widehat{\mathsf{P}}_{(m)} \quad \text{with} \\
\boldsymbol{T}^0_{(m)} &= \left.\frac{\partial \psi_0^0}{\partial \boldsymbol{E}_{(m)}}\right|_{\boldsymbol{F}_{\mathrm{p}}}\,, & \widehat{\boldsymbol{T}}^{\mathrm{e}}_{(m)} &= \frac{\partial \psi_0^{\mathrm{e}}}{\partial \widehat{\boldsymbol{E}}_{\mathrm{e}\,(m)}} \qquad \text{and} \\
\mathsf{P}_{(m)} &= \frac{\partial \boldsymbol{E}_{(m)}}{\partial \boldsymbol{C}}\,, & \widehat{\mathsf{P}}^{\mathrm{e}}_{(m)} &= \frac{\partial \widehat{\boldsymbol{E}}_{\mathrm{e}\,(m)}}{\partial \widehat{\boldsymbol{C}}_{\mathrm{e}}}\,,
\end{aligned} \quad (3.53)$$

see also remark 3.4.1. Based on these notations, the computation of the derivatives $\partial_{\boldsymbol{F}} \boldsymbol{C}$, $\partial_{\boldsymbol{F}} \widehat{\boldsymbol{C}}_{\mathrm{e}}\big|_{\boldsymbol{F}_{\mathrm{p}}}$ and $\partial_{\boldsymbol{F}_{\mathrm{p}}} \widehat{\boldsymbol{C}}_{\mathrm{e}}\big|_{\boldsymbol{F}}$ finally renders

$$\begin{aligned}
\mathsf{D}_0 = &\left[\boldsymbol{\Pi}^{\mathrm{d}} - \boldsymbol{g} \cdot \boldsymbol{F} \cdot \boldsymbol{S}^0 - \boldsymbol{g} \cdot \boldsymbol{F} \cdot \boldsymbol{f}_{\mathrm{p}} \cdot \widehat{\boldsymbol{S}}^{\mathrm{e}} \cdot \boldsymbol{f}_{\mathrm{p}}^{\mathrm{d}}\right] : \mathrm{D}_t\,\boldsymbol{F} \\
&+ \left[\widehat{\boldsymbol{C}}_{\mathrm{e}} \cdot \widehat{\boldsymbol{S}}^{\mathrm{e}} \cdot \boldsymbol{f}_{\mathrm{p}}^{\mathrm{d}}\right] : \mathrm{D}_t\,\boldsymbol{F}_{\mathrm{p}} \geq 0\,.
\end{aligned} \quad (3.54)$$

It is now straightforward to adopt the standard argumentation of rational thermodynamics and to introduce a hyperelastic constitutive equation for the Piola stress tensor

$$\boldsymbol{\Pi}^{\mathrm{d}} \doteq \boldsymbol{g} \cdot \boldsymbol{F} \cdot \boldsymbol{S}^0 + \boldsymbol{g} \cdot \boldsymbol{F} \cdot \boldsymbol{f}_{\mathrm{p}} \cdot \widehat{\boldsymbol{S}}^{\mathrm{e}} \cdot \boldsymbol{f}_{\mathrm{p}}^{\mathrm{d}} \quad (\text{dual: } \mathrm{D}_t\,\boldsymbol{F}) \quad (3.55)$$

in addition to the remaining part of the dissipation inequality

$$\mathsf{D}_0 = \Big[\, \widehat{\boldsymbol{C}}_{\mathrm{e}} \cdot \widehat{\boldsymbol{S}}^{\mathrm{e}} \cdot \boldsymbol{f}_{\mathrm{p}}^{\mathrm{d}} \,\Big] : \mathrm{D}_t \boldsymbol{F}_{\mathrm{p}} \geq 0 \,. \tag{3.56}$$

Now, standard pullback operations to the material configuration result in

$$\begin{aligned} \boldsymbol{M}^{\mathrm{d}} &= \boldsymbol{C} \cdot \boldsymbol{S}^0 + \boldsymbol{C} \cdot \boldsymbol{f}_{\mathrm{p}} \cdot \widehat{\boldsymbol{S}}^{\mathrm{e}} \cdot \boldsymbol{f}_{\mathrm{p}}^{\mathrm{d}} \quad \text{(dual: } \boldsymbol{L}) \,, \\ \boldsymbol{S} &= \boldsymbol{S}^0 + \boldsymbol{f}_{\mathrm{p}} \cdot \widehat{\boldsymbol{S}}^{\mathrm{e}} \cdot \boldsymbol{f}_{\mathrm{p}}^{\mathrm{d}} \quad \text{(dual: } \mathrm{D}_t \boldsymbol{C}) \,, \\ \mathsf{D}_0 &= \Big[\, \boldsymbol{C} \cdot \boldsymbol{f}_{\mathrm{p}} \cdot \widehat{\boldsymbol{S}}^{\mathrm{e}} \cdot \boldsymbol{f}_{\mathrm{p}}^{\mathrm{d}} \,\Big] : \boldsymbol{L}_{\mathrm{p}} \geq 0 \,, \end{aligned} \tag{3.57}$$

whereby symmetry relations and the following notations have been applied

$$\boldsymbol{L} = \boldsymbol{f} \cdot \mathrm{D}_t \boldsymbol{F} \quad \longrightarrow \quad \mathrm{D}_t \boldsymbol{C} = 2\, [\, \boldsymbol{C} \cdot \boldsymbol{L} \,]^{\mathrm{sym}} \,, \quad \boldsymbol{L}_{\mathrm{p}} = \boldsymbol{f}_{\mathrm{p}} \cdot \mathrm{D}_t \boldsymbol{F}_{\mathrm{p}} \,. \tag{3.58}$$

Likewise, standard pushforward transformations to the spatial setting consequently yield

$$\begin{aligned} \boldsymbol{m}^{\mathrm{d}} &= \boldsymbol{g} \cdot \boldsymbol{\tau}^0 + \boldsymbol{g} \cdot \boldsymbol{\tau}^{\mathrm{e}} \quad \text{(dual: } \boldsymbol{l}) \,, \\ \boldsymbol{\tau} &= \boldsymbol{\tau}^0 + \boldsymbol{\tau}^{\mathrm{e}} \quad \text{(dual: } \mathrm{L}_t \boldsymbol{g}) \,, \\ \mathsf{D}_0 &= \Big[\, \boldsymbol{g} \cdot \boldsymbol{F}_{\mathrm{e}} \cdot \widehat{\boldsymbol{S}}^{\mathrm{e}} \cdot \boldsymbol{F}_{\mathrm{e}}^{\mathrm{d}} \,\Big] : \boldsymbol{l}_{\mathrm{p}} = \big[\, \boldsymbol{F}_{\mathrm{e}}^{\mathrm{d}} \cdot \boldsymbol{g} \cdot \boldsymbol{\tau}^{\mathrm{e}} \cdot \boldsymbol{f} \,\big] : \mathrm{D}_t \boldsymbol{F}_{\mathrm{p}} \geq 0 \end{aligned} \tag{3.59}$$

with

$$\boldsymbol{l} = \mathrm{D}_t \boldsymbol{F} \cdot \boldsymbol{f} \quad \longrightarrow \quad \mathrm{L}_t \boldsymbol{g} = 2\, [\, \boldsymbol{g} \cdot \boldsymbol{l} \,]^{\mathrm{sym}} \,, \quad \boldsymbol{l}_{\mathrm{p}} = \boldsymbol{F}_{\mathrm{e}} \cdot \mathrm{D}_t \boldsymbol{F}_{\mathrm{p}} \cdot \boldsymbol{f} \tag{3.60}$$

being obvious and the Kirchhoff–type stresses allow similar representation as the second Piola–Kirchhoff–type tensors in eq.(3.53), namely

$$\begin{aligned} &\tfrac{1}{2}\, \boldsymbol{F} \star \boldsymbol{S}^0 = \tfrac{1}{2}\, \boldsymbol{\tau}^0 = \boldsymbol{t}^0_{(m)} : \mathbf{p}_{(m)} \,, && \tfrac{1}{2}\, \boldsymbol{F}_{\mathrm{e}} \star \widehat{\boldsymbol{S}}^{\mathrm{e}} = \tfrac{1}{2}\, \boldsymbol{\tau}^{\mathrm{e}} = \boldsymbol{t}^{\mathrm{e}}_{(m)} : \mathbf{p}^{\mathrm{e}}_{(m)} && \text{with} \\ &\boldsymbol{F} \star \boldsymbol{T}^0_{(m)} = \boldsymbol{t}^0_{(m)} = \frac{\partial \psi^0_0}{\partial [\, \boldsymbol{c} \cdot \boldsymbol{k}_{(m)} \cdot \boldsymbol{g} \,]} \,, && \boldsymbol{F}_{\mathrm{e}} \star \widehat{\boldsymbol{T}}^{\mathrm{e}}_{(m)} = \boldsymbol{t}^{\mathrm{e}}_{(m)} = \frac{\partial \psi^{\mathrm{e}}_0}{\partial [\, \boldsymbol{c}_{\mathrm{e}} \cdot \boldsymbol{k}_{\mathrm{e}\,(m)} \cdot \boldsymbol{g} \,]} && \text{and} \\ &\boldsymbol{F} \star \mathbf{P}_{(m)} = \mathbf{p}_{(m)} = \frac{\partial [\, \boldsymbol{c} \cdot \boldsymbol{k}_{(m)} \cdot \boldsymbol{g} \,]}{\boldsymbol{g}} \,, && \boldsymbol{F}_{\mathrm{e}} \star \widehat{\mathbf{P}}^{\mathrm{e}}_{(m)} = \mathbf{p}^{\mathrm{e}}_{(m)} = \frac{\partial [\, \boldsymbol{c}_{\mathrm{e}} \cdot \boldsymbol{k}_{\mathrm{e}\,(m)} \cdot \boldsymbol{g} \,]}{\boldsymbol{g}} \,, \end{aligned} \tag{3.61}$$

compare eq.(3.47,3.48) and remark 3.4.1. The abbreviation $\mathrm{L}_t\{\bullet\}$, as applied in eqs.(3.59,3.60), denotes the Lie derivative of the quantity $\{\bullet\}$, i.e. $\mathrm{L}_t \boldsymbol{g} = \boldsymbol{f}^{\mathrm{d}} \cdot \mathrm{D}_t \boldsymbol{C} \cdot \boldsymbol{f} = [\, \boldsymbol{g} \cdot \boldsymbol{l}^{\mathrm{d}} \,] + [\, \boldsymbol{g} \cdot \boldsymbol{l}^{\mathrm{d}} \,]^{\mathrm{t}}$ with $\mathrm{D}_t \boldsymbol{g} = \boldsymbol{0}$.

Remark 3.4.1 *For convenience of the reader the general format of the projection tensors as introduced in eqs.(3.53,3.61) is highlighted in the following. To give an example, the particular operator* $\mathbf{P}_{(m)} = \partial_{\boldsymbol{C}} \boldsymbol{E}_{(m)}$ *reads*

$$\begin{aligned} \mathbf{P}_{(m)} = {} & \lambda_k^{m-2} \quad \boldsymbol{N}^k \otimes \boldsymbol{N}^k \otimes \boldsymbol{N}_k \otimes \boldsymbol{N}_k \\ & + \frac{1}{m}\, \frac{\lambda_k^m - \lambda_l^m}{\lambda_k^2 - \lambda_l^2} \,[\, \boldsymbol{N}^k \otimes \boldsymbol{N}^l \otimes \boldsymbol{N}_k \otimes \boldsymbol{N}_l + \boldsymbol{N}^k \otimes \boldsymbol{N}^l \otimes \boldsymbol{N}_l \otimes \boldsymbol{N}_k \,] \end{aligned} \tag{3.62}$$

for $l \neq k$ *and* $m > 0$*, wherein use of* $E_{(m)\,k} - E_{(m)\,l} = \frac{1}{m}\, [\, \lambda_k^m - \lambda_l^m \,]$ *has been made. For a general review the reader is referred to, for example, Ogden (1997) or Miehe and Lambrecht (2001) where the case of equal principal stretches is additionally addressed; in this regard, see also the contribution by Man (1994) and the discussion in Lu (2004).*

3.4.1 Relations between different stress tensors in one configuration

Based on the relations between different generalised strain measures as highlighted in section 3.2.1, it is now straightforward to derive transformations between correlated stresses in one configuration. To be specific, eq.(3.35) results in

$$\boldsymbol{T}_{(m)} = \left.\frac{\partial \psi_0^0}{\partial \boldsymbol{K}_{(m)}}\right|_{\boldsymbol{F}_{\mathrm{p}}} : \frac{\partial \boldsymbol{K}_{(m)}}{\partial \boldsymbol{E}_{(m)}} = \left[\, \boldsymbol{B}^{\frac{m}{2}} \cdot \boldsymbol{Y}_{(m)} \cdot \boldsymbol{G}^{-1} \,\right]^{\mathrm{sym}} \quad \text{with} \quad \boldsymbol{Y}_{(m)} = \left.\frac{\partial \psi_0^0}{\partial \boldsymbol{K}_{(m)}}\right|_{\boldsymbol{F}_{\mathrm{p}}} \tag{3.63}$$

so that $\boldsymbol{Y}_{(m)} = [\, \boldsymbol{C}^{\frac{m}{2}} \cdot \boldsymbol{T}_{(m)} \cdot \boldsymbol{G} \,]^{\mathrm{sym}}$, while similar elaborations based on eq.(3.36) render

$$\widehat{\boldsymbol{T}}^{\mathrm{e}}_{(m)} = \frac{\partial \psi_0^{\mathrm{e}}}{\partial \widehat{\boldsymbol{K}}_{\mathrm{e}\,(m)}} : \frac{\partial \widehat{\boldsymbol{K}}_{\mathrm{e}\,(m)}}{\partial \widehat{\boldsymbol{E}}_{\mathrm{e}\,(m)}} = \left[\, \widehat{\boldsymbol{B}}_{\mathrm{e}}^{\frac{m}{2}} \cdot \widehat{\boldsymbol{Y}}^{\mathrm{e}}_{(m)} \cdot \boldsymbol{G}_{\mathrm{p}}^{-1} \,\right]^{\mathrm{sym}} \quad \text{with} \quad \widehat{\boldsymbol{Y}}^{\mathrm{e}}_{(m)} = \frac{\partial \psi_0^{\mathrm{e}}}{\partial \widehat{\boldsymbol{K}}_{\mathrm{e}\,(m)}} \tag{3.64}$$

or $\widehat{\boldsymbol{Y}}_{(m)} = [\, \widehat{\boldsymbol{C}}_{\mathrm{e}}^{\frac{m}{2}} \cdot \widehat{\boldsymbol{T}}^{\mathrm{e}}_{(m)} \cdot \boldsymbol{G}_{\mathrm{p}} \,]^{\mathrm{sym}}$, respectively. By analogy with theses derivations, we observe for the corresponding spatial stresses

$$\boldsymbol{t}_{(m)} = \left.\frac{\partial \psi_0^0}{\partial \boldsymbol{e}_{(m)}}\right|_{\boldsymbol{F}_{\mathrm{p}}} : \frac{\partial \boldsymbol{e}_{(m)}}{\partial [\, \boldsymbol{c} \cdot \boldsymbol{k}_{(m)} \cdot \boldsymbol{g} \,]} = \left[\, \boldsymbol{b} \cdot \boldsymbol{c}^{\frac{m}{2}} \cdot \boldsymbol{z}_{(m)} \,\right]^{\mathrm{sym}} \quad \text{with} \quad \boldsymbol{z}_{(m)} = \left.\frac{\partial \psi_0^0}{\partial \boldsymbol{e}_{(m)}}\right|_{\boldsymbol{F}_{\mathrm{p}}} \tag{3.65}$$

so that $\boldsymbol{z}_{(m)} = [\, \boldsymbol{b}^{\frac{m}{2}} \cdot \boldsymbol{c} \cdot \boldsymbol{t}_{(m)} \,]^{\mathrm{sym}}$, as well as

$$\boldsymbol{t}^{\mathrm{e}}_{(m)} = \frac{\partial \psi_0^{\mathrm{e}}}{\partial \boldsymbol{e}_{\mathrm{e}\,(m)}} : \frac{\partial \boldsymbol{e}_{\mathrm{e}\,(m)}}{\partial [\, \boldsymbol{c}_{\mathrm{e}} \cdot \boldsymbol{k}_{\mathrm{e}\,(m)} \cdot \boldsymbol{g} \,]} = \left[\, \boldsymbol{b}_{\mathrm{e}} \cdot \boldsymbol{c}_{\mathrm{e}}^{\frac{m}{2}} \cdot \boldsymbol{z}^{\mathrm{e}}_{(m)} \,\right]^{\mathrm{sym}} \quad \text{with} \quad \boldsymbol{z}^{\mathrm{e}}_{(m)} = \frac{\partial \psi_0^{\mathrm{e}}}{\partial \boldsymbol{e}_{\mathrm{e}\,(m)}} \tag{3.66}$$

or $\boldsymbol{z}^{\mathrm{e}}_{(m)} = [\, \boldsymbol{b}_{\mathrm{e}}^{\frac{m}{2}} \cdot \boldsymbol{c}_{\mathrm{e}} \cdot \boldsymbol{t}^{\mathrm{e}}_{(m)} \,]^{\mathrm{sym}}$, respectively, whereby eq.(3.37) has been taken into account.

Remark 3.4.2 *By analogy with eq.(3.34), one can also relate different stress tensors in terms of different generalised strain measures with respect to one configuration. The lines of derivation in this regard are commonly based on the comparison of energetically conjugated quantities as, for example,* $\boldsymbol{T}^0_{(m)} : \mathrm{D}_t \boldsymbol{E}_{(m)} = \boldsymbol{T}^0_{(n)} : \mathrm{D}_t \boldsymbol{E}_{(n)}$ *and* $\widehat{\boldsymbol{T}}^{\mathrm{e}}_{(m)} : \mathrm{D}_t \widehat{\boldsymbol{E}}_{\mathrm{e}\,(m)} = \widehat{\boldsymbol{T}}^{\mathrm{e}}_{(n)} : \mathrm{D}_t \widehat{\boldsymbol{E}}_{\mathrm{e}\,(n)}$ *for* $m, n \geq 0$*, respectively. We do not place emphasis on these transformations in this work but refer the reader to the contributions by Guo and Man (1992), Guansuo et al. (2000), Farahani and Naghdabadi (2000, 2003), Rosati and Valoroso (2002), and Nicholson (2003) for detailed reviews.*

3.4.2 Relations between different stress tensors in different configurations

The transformation between the stress tensors $\{\, \boldsymbol{S}^0, \boldsymbol{\tau}^0 \,\}$, $\{\, \widehat{\boldsymbol{S}}^{\mathrm{e}}, \boldsymbol{\tau}^{\mathrm{e}} \,\}$, $\{\, \boldsymbol{T}^0, \boldsymbol{t}^0 \,\}$, and $\{\, \widehat{\boldsymbol{T}}^{\mathrm{e}}, \boldsymbol{t}^{\mathrm{e}} \,\}$ are determined by direct pushforward and pullback operations which have already been highlighted in section 3.4. Based on the relations between different generalised strain measures as reviewed in section 3.2.2, it is now straightforward to derive further transformations between correlated stresses in different configurations. To be specific, eq.(3.42) results in

$$\boldsymbol{z}_{(m)} = \boldsymbol{Y}_{(m)} : \frac{\partial \boldsymbol{K}_{(m)}}{\partial \boldsymbol{e}_{(m)}} = \left[\, \boldsymbol{F} \cdot \boldsymbol{G}^{-1} \cdot \boldsymbol{Y}_{(m)} \cdot \boldsymbol{f} \cdot \boldsymbol{g}^{-1} \,\right]^{\mathrm{sym}} \tag{3.67}$$

so that $\boldsymbol{Y}_{(m)} = [\, \boldsymbol{G} \cdot \boldsymbol{f} \cdot \boldsymbol{z}_{(m)} \cdot \boldsymbol{g} \cdot \boldsymbol{F} \,]^{\mathrm{sym}}$, while similar elaborations based on eq.(3.43) render

$$\boldsymbol{z}^{\mathrm{e}}_{(m)} = \widehat{\boldsymbol{Y}}^{\mathrm{e}}_{(m)} : \frac{\partial \widehat{\boldsymbol{K}}_{\mathrm{e}\,(m)}}{\partial \boldsymbol{e}_{\mathrm{e}\,(m)}} = \left[\, \boldsymbol{F}_{\mathrm{e}} \cdot \boldsymbol{G}_{\mathrm{p}}^{-1} \cdot \widehat{\boldsymbol{Y}}^{\mathrm{e}}_{(m)} \cdot \boldsymbol{f}_{\mathrm{e}} \cdot \boldsymbol{g}^{-1} \,\right]^{\mathrm{sym}} \tag{3.68}$$

or $\widehat{\boldsymbol{Y}}^{\mathrm{e}}_{(m)} = [\,\boldsymbol{G}_{\mathrm{p}} \cdot \boldsymbol{f}_{\mathrm{e}} \cdot \boldsymbol{z}^{\mathrm{e}}_{(m)} \cdot \boldsymbol{g} \cdot \boldsymbol{F}_{\mathrm{e}}\,]^{\mathrm{sym}}$, respectively.

With these observations and those elaborations highlighted in section 3.4.1 at hand, we can also relate the remaining stress tensors. For completeness, we finally mention the rather lengthy expressions

$$\begin{aligned} \boldsymbol{z}_{(m)} &= \big[\,\boldsymbol{F}\cdot\boldsymbol{G}^{-1}\cdot\big[\,\boldsymbol{C}^{\frac{m}{2}}\cdot\boldsymbol{T}_{(m)}\cdot\boldsymbol{G}\,\big]^{\mathrm{sym}}\cdot\boldsymbol{f}\cdot\boldsymbol{g}^{-1}\,\big]^{\mathrm{sym}}\,, \\ \boldsymbol{z}^{\mathrm{e}}_{(m)} &= \Big[\,\boldsymbol{F}_{\mathrm{e}}\cdot\boldsymbol{G}_{\mathrm{p}}^{-1}\cdot\big[\,\widehat{\boldsymbol{C}}_{\mathrm{e}}^{\frac{m}{2}}\cdot\widehat{\boldsymbol{T}}^{\mathrm{e}}_{(m)}\cdot\boldsymbol{G}_{\mathrm{p}}\,\big]^{\mathrm{sym}}\cdot\boldsymbol{f}_{\mathrm{e}}\cdot\boldsymbol{g}^{-1}\,\Big]^{\mathrm{sym}} \end{aligned} \tag{3.69}$$

and

$$\begin{aligned} \boldsymbol{T}_{(m)} &= \big[\,\boldsymbol{B}^{\frac{m}{2}}\cdot\big[\,\boldsymbol{G}\cdot\boldsymbol{f}\cdot\boldsymbol{z}_{(m)}\cdot\boldsymbol{g}\cdot\boldsymbol{F}\,\big]^{\mathrm{sym}}\cdot\boldsymbol{G}^{-1}\,\big]^{\mathrm{sym}}\,, \\ \widehat{\boldsymbol{T}}^{\mathrm{e}}_{(m)} &= \Big[\,\widehat{\boldsymbol{B}}_{\mathrm{e}}^{\frac{m}{2}}\cdot\big[\,\boldsymbol{G}_{\mathrm{p}}\cdot\boldsymbol{f}_{\mathrm{e}}\cdot\boldsymbol{z}^{\mathrm{e}}_{(m)}\cdot\boldsymbol{g}\cdot\boldsymbol{F}_{\mathrm{e}}\,\big]^{\mathrm{sym}}\cdot\boldsymbol{G}_{\mathrm{p}}^{-1}\,\Big]^{\mathrm{sym}}\,. \end{aligned} \tag{3.70}$$

3.4.3 Associated inelasticity

According to the (reduced) dissipation inequality (3.56), namely

$$\mathsf{D}_0 = \Big[\,\widehat{\boldsymbol{C}}_{\mathrm{e}}\cdot\widehat{\boldsymbol{S}}^{\mathrm{e}}\,\Big] : \widehat{\boldsymbol{L}}_{\mathrm{p}} \geq 0 \quad \text{with} \quad \widehat{\boldsymbol{L}}_{\mathrm{p}} = \mathrm{D}_t\,\boldsymbol{F}_{\mathrm{p}}\cdot\boldsymbol{f}_{\mathrm{p}}\,, \tag{3.71}$$

associated evolution equations are straightforwardly set up via

$$\widehat{\boldsymbol{L}}_{\mathrm{p}} = \mathrm{D}_t\lambda\,\frac{\partial\Phi\big(\widehat{\boldsymbol{C}}_{\mathrm{e}}\cdot\widehat{\boldsymbol{S}}^{\mathrm{e}},\boldsymbol{H}_{\mathrm{p}};\boldsymbol{X}\big)}{\partial\big[\,\widehat{\boldsymbol{C}}_{\mathrm{e}}\cdot\widehat{\boldsymbol{S}}^{\mathrm{e}}\,\big]} = \mathrm{D}_t\lambda\,\widehat{\boldsymbol{B}}_{\mathrm{e}}\cdot\frac{\partial\Phi\big(\widehat{\boldsymbol{C}}_{\mathrm{e}}\cdot\widehat{\boldsymbol{S}}^{\mathrm{e}},\boldsymbol{H}_{\mathrm{p}};\boldsymbol{X}\big)}{\partial\widehat{\boldsymbol{S}}^{\mathrm{e}}}\,, \tag{3.72}$$

wherein $\mathrm{D}_t\lambda \geq 0$ denotes a multiplier which is either derived from further constitutive assumptions, as for instance for viscous response, or determined by restricting the incorporated potential or rather yield function $\Phi \leq 0$ so that $\Phi\,\mathrm{D}_t\lambda = 0$. The tensorial variable $\boldsymbol{H}_{\mathrm{p}}$ denotes an additional argument that conveniently enables the formulation of, for instance, anisotropic flow rules. On the one hand, the introduction of the scalar–valued potential Φ, from which we derive associated flow rules, restricts the type of evolution equation as compared to the general anisotropic case or rather a comprehensive tensor function with respect to the arguments incorporated into Φ. On the other hand, the associated format is considered to be sufficiently general for the problem at hand. Alternatively to the representation in eq.(3.72), transformation of the derived relation to the material or spatial configuration, respectively, leads to

$$\boldsymbol{L}_{\mathrm{p}} = \mathrm{D}_t\lambda\,\frac{\partial\Phi\big(\boldsymbol{C}\cdot\boldsymbol{f}_{\mathrm{p}}\cdot\widehat{\boldsymbol{S}}^{\mathrm{e}}\cdot\boldsymbol{f}_{\mathrm{p}}^{\mathrm{d}},\boldsymbol{H}_0;\boldsymbol{X}\big)}{\partial\big[\,\boldsymbol{C}\cdot\boldsymbol{f}_{\mathrm{p}}\cdot\widehat{\boldsymbol{S}}^{\mathrm{e}}\cdot\boldsymbol{f}_{\mathrm{p}}^{\mathrm{d}}\,\big]} = \mathrm{D}_t\lambda\,\boldsymbol{B}\cdot\frac{\partial\Phi\big(\boldsymbol{C}\cdot\boldsymbol{F}_{\mathrm{p}}^{-1}\cdot\widehat{\boldsymbol{S}}^{\mathrm{e}}\cdot\boldsymbol{F}_{\mathrm{p}}^{-\mathrm{d}},\boldsymbol{H}_0;\boldsymbol{X}\big)}{\partial\big[\,\boldsymbol{f}_{\mathrm{p}}\cdot\widehat{\boldsymbol{S}}^{\mathrm{e}}\cdot\boldsymbol{f}_{\mathrm{p}}^{\mathrm{d}}\,\big]} \tag{3.73}$$

and

$$\boldsymbol{l}_{\mathrm{p}} = \mathrm{D}_t\lambda\,\frac{\partial\Phi\big(\boldsymbol{g}\cdot\boldsymbol{\tau}^{\mathrm{e}},\boldsymbol{H}_t;\boldsymbol{X}\big)}{\partial\big[\,\boldsymbol{g}\cdot\boldsymbol{\tau}^{\mathrm{e}}\,\big]} = \mathrm{D}_t\lambda\,\boldsymbol{g}^{-1}\cdot\frac{\partial\Phi\big(\boldsymbol{g}\cdot\boldsymbol{\tau}^{\mathrm{e}},\boldsymbol{H}_t;\boldsymbol{X}\big)}{\partial\boldsymbol{\tau}^{\mathrm{e}}_{\mathrm{e}}}\,, \tag{3.74}$$

wherein $\boldsymbol{H}_0 = \boldsymbol{f}_{\mathrm{p}} \star \boldsymbol{H}_{\mathrm{p}}$ and $\boldsymbol{H}_t = \boldsymbol{F}_{\mathrm{e}} \star \boldsymbol{H}_{\mathrm{p}}$. An alternative evolution equation in terms of spatial arguments is provided by $-\frac{1}{2}\,\mathrm{L}_t\boldsymbol{b}_{\mathrm{e}} = [\,\boldsymbol{l}_{\mathrm{p}}\cdot\boldsymbol{b}_{\mathrm{e}}\,]^{\mathrm{sym}} = -\frac{1}{2}\,\mathrm{D}_t\lambda\;\partial_{\boldsymbol{\xi}^{\mathrm{e}}}\Phi$, wherein $\boldsymbol{\xi}^{\mathrm{e}} = -\,\partial_{\boldsymbol{b}_{\mathrm{e}}}\psi^{\mathrm{e}}_0$; see Menzel and Steinmann (2003c) for a detailed discussion. Assuming an isotropic setting, i.e. $\boldsymbol{a}$ and $\boldsymbol{H}_t$ vanish, we obtain the well–established representation $-\frac{1}{2}\,\mathrm{L}_t\boldsymbol{b}_{\mathrm{e}} = \mathrm{D}_t\lambda\;\boldsymbol{g}^{-1}\cdot\partial_{\boldsymbol{\tau}^{\mathrm{e}}}\Phi\cdot\boldsymbol{b}_{\mathrm{e}}$ which allows similar representation with respect to the intermediate and material configuration via straightforward pullback transformations.

Apart from the fact that the Helmholtz free energy density is defined in terms of material, intermediate, and spatial generalised strain measures in addition to appropriate metric tensors and structural tensors, the evolution equations (3.73,3.74) represent well–established formats of associated flow rules for anisotropic finite inelasticity.

Remark 3.4.3 *The stress tensors of Mandel type which are incorporated into the potential Φ turn out to be un–symmetric for the general elastically anisotropic case. The eigenvalues of these tensors, however, remain real since the Mandel type stresses are determined by the product of two symmetric second–order tensors with one of them being positive definite, namely $\boldsymbol{C}$, $\widehat{\boldsymbol{C}}_{\mathrm{e}}$ and $\boldsymbol{g}$ for the problem at hand; compare e.g. Ericksen (1960). Due to the mixed–variant nature of these stress tensors, trace operations are defined with respect to appropriate identity tensors, so that for instance the deviatoric part of these stresses allows representation as*

$$\begin{aligned}
\big[\,\boldsymbol{C}\ \cdot\ \boldsymbol{f}_{\mathrm{p}}\cdot\widehat{\boldsymbol{S}}^{\mathrm{e}}\cdot\boldsymbol{F}_{\mathrm{p}}^{\mathrm{d}}\,\big]^{\mathrm{dev}} &= \boldsymbol{C}\ \cdot\ \boldsymbol{f}_{\mathrm{p}}\cdot\widehat{\boldsymbol{S}}^{\mathrm{e}}\cdot\boldsymbol{F}_{\mathrm{p}}^{\mathrm{d}} - \tfrac{1}{3}\big[\,\boldsymbol{C}\ :\big[\,\boldsymbol{f}_{\mathrm{p}}\cdot\widehat{\boldsymbol{S}}^{\mathrm{e}}\cdot\boldsymbol{F}_{\mathrm{p}}^{\mathrm{d}}\,\big]\,\big]\,\boldsymbol{I}_0^{\mathrm{d}}\,,\\
\big[\,\widehat{\boldsymbol{C}}_{\mathrm{e}}\cdot\ \widehat{\boldsymbol{S}}^{\mathrm{e}}\ \big]^{\mathrm{dev}} &= \widehat{\boldsymbol{C}}_{\mathrm{e}}\cdot\ \widehat{\boldsymbol{S}}^{\mathrm{e}} - \tfrac{1}{3}\big[\,\widehat{\boldsymbol{C}}_{\mathrm{e}}:\ \widehat{\boldsymbol{S}}^{\mathrm{e}}\ \big]\,\boldsymbol{I}_{\mathrm{p}}^{\mathrm{d}}\,,\\
\big[\,\boldsymbol{g}\ \cdot\ \boldsymbol{\tau}^{\mathrm{e}}\ \big]^{\mathrm{dev}} &= \boldsymbol{g}\ \cdot\ \boldsymbol{\tau}^{\mathrm{e}} - \tfrac{1}{3}\big[\,\boldsymbol{g}\ :\ \boldsymbol{\tau}^{\mathrm{e}}\ \big]\,\boldsymbol{I}_t^{\mathrm{d}}\,.
\end{aligned}\tag{3.75}$$

3.5 Green–Naghdi–type inelasticity

In contrast to the previous section, where finite inelasticity has been discussed in a rather general context, we next place emphasis on a particular approach which dates back to the pioneering work by Green and Naghdi (1965), see also the review article by Naghdi (1990). The fundamental kinematic assumption thereby consists in accepting ψ_0^{e} to take (with a slight misuse of notation) the representation

$$\begin{aligned}
\psi_0^{\mathrm{e}}(\boldsymbol{F},\boldsymbol{E}_{\mathrm{p}},\boldsymbol{A}_0;\boldsymbol{X}) &= \psi_0^{\mathrm{e}}(\ \ \boldsymbol{E}_{(m)}\ \ - \boldsymbol{E}_{\mathrm{p}},\boldsymbol{G}^{-1},\boldsymbol{A};\boldsymbol{X})\\
&= \psi_0^{\mathrm{e}}(\ \ \widehat{\boldsymbol{E}}_{(m)}\ \ - \widehat{\boldsymbol{E}}_{\mathrm{p}},\widehat{\boldsymbol{b}}_{\mathrm{p}},\boldsymbol{A}_{\mathrm{p}};\boldsymbol{X})\\
&= \psi_0^{\mathrm{e}}(\ \boldsymbol{c}\cdot\boldsymbol{k}_{(m)}\cdot\boldsymbol{g}\ - \boldsymbol{e}_{\mathrm{p}},\boldsymbol{b},\boldsymbol{A}_t;\boldsymbol{X})
\end{aligned}\tag{3.76}$$

so that

$$\begin{aligned}
I_j &= \boldsymbol{I}_0\ :\ \big[\,[\,\boldsymbol{E}_{(m)}-\boldsymbol{E}_{\mathrm{p}}\,]\cdot\boldsymbol{G}^{-1}\,\big]^j = \boldsymbol{I}_{\mathrm{p}}\ :\ \Big[\,\Big[\,\widehat{\boldsymbol{E}}_{(m)}-\widehat{\boldsymbol{E}}_{\mathrm{p}}\,\Big]\cdot\widehat{\boldsymbol{b}}_{\mathrm{p}}\,\Big]^j\\
&= \boldsymbol{I}_t\ :\ \big[\,[\,\boldsymbol{c}\cdot\boldsymbol{k}_{(m)}\cdot\boldsymbol{g}-\boldsymbol{e}_{\mathrm{p}}\,]\cdot\boldsymbol{b}\,\big]^j = \boldsymbol{I}_t\ :\ [\,\boldsymbol{g}\cdot\boldsymbol{k}_{(m)}-\boldsymbol{e}_{\mathrm{p}}\cdot\boldsymbol{b}\,]^j\,,\\
I_{\alpha+3} &= \boldsymbol{I}_0\ :\ \Big[\,[\,\boldsymbol{E}_{(m)}-\boldsymbol{E}_{\mathrm{p}}\,]\cdot\big[\,\boldsymbol{G}^{-1}\cdot[\,\boldsymbol{E}_{(m)}-\boldsymbol{E}_{\mathrm{p}}\,]\,\big]^{\alpha-1}\cdot\boldsymbol{A}_0\,\Big]\\
&= \boldsymbol{I}_{\mathrm{p}}\ :\ \Big[\,\Big[\,\widehat{\boldsymbol{E}}_{(m)}-\widehat{\boldsymbol{E}}_{\mathrm{p}}\,\Big]\cdot\Big[\,\widehat{\boldsymbol{b}}_{\mathrm{p}}\cdot\Big[\,\widehat{\boldsymbol{E}}_{(m)}-\widehat{\boldsymbol{E}}_{\mathrm{p}}\,\Big]\,\Big]^{\alpha-1}\cdot\boldsymbol{A}_{\mathrm{p}}\,\Big]\\
&= \boldsymbol{I}_t\ :\ \big[\,[\,\boldsymbol{c}\cdot\boldsymbol{k}_{(m)}\cdot\boldsymbol{g}-\boldsymbol{e}_{\mathrm{p}}\,]\cdot[\,\boldsymbol{b}\cdot[\,\boldsymbol{c}\cdot\boldsymbol{k}_{(m)}\cdot\boldsymbol{g}-\boldsymbol{e}_{\mathrm{p}}\,]\,]^{\alpha-1}\cdot\boldsymbol{A}_t\,\big]\,,
\end{aligned}\tag{3.77}$$

with $j=1,2,3$ and $\alpha=1,2$ in contrast to eqs.(3.46–3.48); see also remark 3.2.1. The incorporated symmetric strain measures $\boldsymbol{E}_{(m)}$, $\widehat{\boldsymbol{E}}_{(m)}$ and $\boldsymbol{c}\cdot\boldsymbol{k}_{(m)}\cdot\boldsymbol{g}$ are thereby referred to the total deformation while $\boldsymbol{E}_{\mathrm{p}}$, $\widehat{\boldsymbol{E}}_{\mathrm{p}}=\boldsymbol{F}_{\mathrm{p}}\star\boldsymbol{E}_{\mathrm{p}}$ and $\boldsymbol{e}_{\mathrm{p}}=\boldsymbol{F}\star\boldsymbol{E}_{\mathrm{p}}$ take the interpretation as symmetric internal variables similar to the generally un–symmetric irreversible distortion $\boldsymbol{F}_{\mathrm{p}}$. Conceptually speaking, this approach recaptures the formal structure of a small strain inelastic setting except that generalised strain measures – based on the total deformation – are incorporated and appropriate metric tensors are taken into account. Apparently, the representations in eq.(3.76)

in terms of material and spatial arguments are preferable compared to the intermediate format since neither $\boldsymbol{F}_{\mathrm{p}}$ nor $\boldsymbol{F}_{\mathrm{e}}$ are directly accessible within this framework. This aspect is also reflected by the considered metric tensors which differ from those applied in eq.(3.46). In this context, and also for the case of brevity, we will mainly place emphasis on formulations based on either material or, respectively, spatial arguments in the following.

3.5.1 Associated inelasticity

Similarly to eq.(3.71), the isothermal dissipation inequality, as based on the ansatz highlighted in eq.(3.76), now results in

$$\mathsf{D}_0 = -\left.\frac{\partial \psi_0^{\mathrm{e}}}{\partial \boldsymbol{E}_{\mathrm{p}}}\right|_{\boldsymbol{F}} : \mathrm{D}_t \boldsymbol{E}_{\mathrm{p}} = -\left.\frac{\partial \psi_0^{\mathrm{e}}}{\partial \widehat{\boldsymbol{E}}_{\mathrm{p}}}\right|_{\boldsymbol{F}} : \mathrm{L}_t^{\mathrm{p}} \widehat{\boldsymbol{E}}_{\mathrm{p}} = -\left.\frac{\partial \psi_0^{\mathrm{e}}}{\partial \boldsymbol{e}_{\mathrm{p}}}\right|_{\boldsymbol{F}} : \mathrm{L}_t \boldsymbol{e}_{\mathrm{p}} \geq 0 \tag{3.78}$$

with

$$-\left.\frac{\partial \psi_0^{\mathrm{e}}}{\partial \boldsymbol{E}_{\mathrm{p}}}\right|_{\boldsymbol{F}} = -\frac{\partial \psi_0^{\mathrm{e}}}{\partial [\, \boldsymbol{E}_{(m)} - \boldsymbol{E}_{\mathrm{p}} \,]} : \left.\frac{\partial [\, \boldsymbol{E}_{(m)} - \boldsymbol{E}_{\mathrm{p}} \,]}{\partial \boldsymbol{E}_{\mathrm{p}}}\right|_{\boldsymbol{F}} = \frac{\partial \psi_0^{\mathrm{e}}}{\partial [\, \boldsymbol{E}_{(m)} - \boldsymbol{E}_{\mathrm{p}} \,]} = \boldsymbol{T}^{\mathrm{e}}_{(m)} \tag{3.79}$$

as well as

$$\begin{aligned} -\left.\frac{\partial \psi_0^{\mathrm{e}}}{\partial \boldsymbol{e}_{\mathrm{p}}}\right|_{\boldsymbol{F}} &= -\frac{\partial \psi_0^{\mathrm{e}}}{\partial [\, \boldsymbol{c} \cdot \boldsymbol{k}_{(m)} \cdot \boldsymbol{g} - \boldsymbol{e}_{\mathrm{p}} \,]} : \left.\frac{\partial [\, \boldsymbol{c} \cdot \boldsymbol{k}_{(m)} \cdot \boldsymbol{g} - \boldsymbol{e}_{\mathrm{p}} \,]}{\partial \boldsymbol{e}_{\mathrm{p}}}\right|_{\boldsymbol{F}} \\ &= \frac{\partial \psi_0^{\mathrm{e}}}{\partial [\, \boldsymbol{c} \cdot \boldsymbol{k}_{(m)} \cdot \boldsymbol{g} - \boldsymbol{e}_{\mathrm{p}} \,]} = \boldsymbol{t}^{\mathrm{e}}_{(m)} \,, \end{aligned} \tag{3.80}$$

respectively, wherein the notation introduced in section 3.4 for stresses derived from generalised strain measures has been adopted. By analogy with eq.(3.73), we consequently define associated flow rules via

$$\mathrm{D}_t \boldsymbol{E}_{\mathrm{p}} = \mathrm{D}_t \lambda \, \frac{\partial \Phi\big(\boldsymbol{T}^{\mathrm{e}}_{(m)}, \boldsymbol{C}, \boldsymbol{H}_0; \boldsymbol{X}\big)}{\partial \boldsymbol{T}^{\mathrm{e}}_{(m)}} = \mathrm{D}_t \lambda \left[\boldsymbol{C}^{\frac{m}{2}} \cdot \frac{\partial \Phi\big(\boldsymbol{T}^{\mathrm{e}}_{(m)}, \boldsymbol{C}, \boldsymbol{H}_0; \boldsymbol{X}\big)}{\partial \boldsymbol{Y}^{\mathrm{e}}_{(m)}} \cdot \boldsymbol{G} \right]^{\mathrm{sym}}, \tag{3.81}$$

wherein $\boldsymbol{Y}^{\mathrm{e}}_{(m)} = \partial_{\boldsymbol{K}_{(m)}} \psi_0^{\mathrm{e}} \big|_{\boldsymbol{E}_{\mathrm{p}}}$ and use of the symmetry of $\partial_{\boldsymbol{Y}^{\mathrm{e}}_{(m)}} \Phi$ has been made; compare section 3.4.1. Similarly to eq.(3.74), the spatial representation of the sought evolution equation results in

$$\mathrm{L}_t \boldsymbol{e}_{\mathrm{p}} = \mathrm{D}_t \lambda \, \frac{\partial \Phi\big(\boldsymbol{t}^{\mathrm{e}}_{(m)}, \boldsymbol{g}, \boldsymbol{H}_t; \boldsymbol{X}\big)}{\partial \boldsymbol{t}^{\mathrm{e}}_{(m)}} = \mathrm{D}_t \lambda \left[\boldsymbol{c} \cdot \boldsymbol{b}^{\frac{m}{2}} \cdot \frac{\partial \Phi\big(\boldsymbol{t}^{\mathrm{e}}_{(m)}, \boldsymbol{g}, \boldsymbol{H}_t; \boldsymbol{X}\big)}{\partial \boldsymbol{z}^{\mathrm{e}}_{(m)}} \right]^{\mathrm{sym}}, \tag{3.82}$$

wherein $\boldsymbol{z}^{\mathrm{e}}_{(m)} = \partial_{\boldsymbol{e}_{(m)}} \psi_0^{\mathrm{e}} \big|_{\boldsymbol{e}_{\mathrm{p}}}$ and use of the symmetry of $\partial_{\boldsymbol{z}^{\mathrm{e}}_{(m)}} \Phi$ has been made; compare section 3.4.1. Based on the elaborations highlighted in section 3.4.2, we finally identify the relations

$$\begin{aligned} \mathrm{D}_t \boldsymbol{E}_{\mathrm{p}} &= \mathrm{D}_t \lambda \left[\boldsymbol{C}^{\frac{m}{2}} \cdot \left[\boldsymbol{f} \cdot \boldsymbol{g}^{-1} \cdot \frac{\partial \Phi\big(\boldsymbol{t}^{\mathrm{e}}_{(m)}, \boldsymbol{g}, \boldsymbol{H}_t; \boldsymbol{X}\big)}{\partial \boldsymbol{z}^{\mathrm{e}}_{(m)}} \cdot \boldsymbol{F} \right]^{\mathrm{sym}} \right]^{\mathrm{sym}} \\ &= \mathrm{D}_t \lambda \left[\boldsymbol{C}^{\frac{m}{2}} \cdot \left[\boldsymbol{f} \cdot \boldsymbol{g}^{-1} \cdot \left[\boldsymbol{c}^{\frac{m}{2}} \cdot \boldsymbol{b} \cdot \frac{\partial \Phi\big(\boldsymbol{t}^{\mathrm{e}}_{(m)}, \boldsymbol{g}, \boldsymbol{H}_t; \boldsymbol{X}\big)}{\partial \boldsymbol{t}^{\mathrm{e}}_{(m)}} \right]^{\mathrm{sym}} \cdot \boldsymbol{F} \right]^{\mathrm{sym}} \right]^{\mathrm{sym}} \\ &= \mathrm{D}_t \lambda \, \boldsymbol{F}^{\mathrm{d}} \cdot \frac{\partial \Phi\big(\boldsymbol{t}^{\mathrm{e}}_{(m)}, \boldsymbol{g}, \boldsymbol{H}_t; \boldsymbol{X}\big)}{\partial \boldsymbol{t}^{\mathrm{e}}_{(m)}} \cdot \boldsymbol{F} = \boldsymbol{F}^{\mathrm{d}} \cdot \mathrm{L}_t \boldsymbol{e}_i \cdot \boldsymbol{F} \end{aligned} \tag{3.83}$$

and

$$
\begin{aligned}
\mathrm{L}_t \boldsymbol{e}_{\mathrm{p}} \;&=\; \mathrm{D}_t\lambda \left[\boldsymbol{c}\cdot\boldsymbol{b}^{\frac{m}{2}} \cdot \left[\boldsymbol{g}\cdot\boldsymbol{F}\cdot \frac{\partial \Phi\big(\boldsymbol{T}^{\mathrm{e}}_{(m)},\boldsymbol{C},\boldsymbol{H}_0;\boldsymbol{X}\big)}{\partial \boldsymbol{Y}^{\mathrm{e}}_{(m)}} \cdot \boldsymbol{G}\cdot\boldsymbol{f} \right]^{\mathrm{sym}} \right]^{\mathrm{sym}} \\
&=\; \mathrm{D}_t\lambda \left[\boldsymbol{c}\cdot\boldsymbol{b}^{\frac{m}{2}} \cdot \left[\boldsymbol{g}\cdot\boldsymbol{F}\cdot \left[\boldsymbol{B}^{\frac{m}{2}} \cdot \frac{\partial \Phi\big(\boldsymbol{T}^{\mathrm{e}}_{(m)},\boldsymbol{C},\boldsymbol{H}_0;\boldsymbol{X}\big)}{\partial \boldsymbol{T}^{\mathrm{e}}_{(m)}} \cdot \boldsymbol{G}^{-1} \right]^{\mathrm{sym}} \cdot \boldsymbol{G}\cdot\boldsymbol{f} \right]^{\mathrm{sym}} \right]^{\mathrm{sym}} \\
&=\; \mathrm{D}_t\lambda\, \boldsymbol{f}^{\mathrm{d}} \cdot \frac{\partial \Phi\big(\boldsymbol{T}^{\mathrm{e}}_{(m)},\boldsymbol{C},\boldsymbol{H}_0;\boldsymbol{X}\big)}{\partial \boldsymbol{T}^{\mathrm{e}}_{(m)}} \cdot \boldsymbol{F}^{-1} \;=\; \boldsymbol{F}^{-\mathrm{d}} \cdot \mathrm{D}_t \boldsymbol{E}_i \cdot \boldsymbol{f}\,.
\end{aligned}
\tag{3.84}
$$

As previously mentioned in this section, the proposed Green–Naghdi–type framework takes the interpretation as an inelastic setting with respect to the reference configuration with the formal structure of a small strain setting being recaptured. This idea is also reflected by the flow rules in eq.(3.80) since the covariant metric $\boldsymbol{C}$ ($\boldsymbol{g}$) is additionally incorporated besides the symmetric generalised stress tensor $\boldsymbol{T}^{\mathrm{e}}_{(m)}$ ($\boldsymbol{t}^{\mathrm{e}}_{(m)}$). Analogous expressions have apparently not been introduced into the previously highlighted evolutions equations (3.72–3.74) since, for example, trace operations of the Mandel type stress tensors incorporated into these relations are performed with identity tensors which are redundant, compare remarks 3.4.3 and 3.5.1.

Remark 3.5.1 *Alternatively, the potential Φ could also be introduced with respect to different metric tensors, for instance $\Phi\big(\boldsymbol{T}^{\mathrm{e}}_{(m)},\boldsymbol{G},\boldsymbol{H}_0;\boldsymbol{X}\big) = \Phi\big(\boldsymbol{t}^{\mathrm{e}}_{(m)},\boldsymbol{c},\boldsymbol{h};\boldsymbol{X}\big)$. This ansatz, however, would not reflect the idea that corresponding trace operations in terms of spatial arguments are related to the spatial co–variant metric as, for example, in eqs.(3.74,3.75). Contrary, the particular choice highlighted in eq.(3.81) renders for instance the deviatoric stresses to take the representations*

$$
\begin{aligned}
\big[\,\boldsymbol{T}^{\mathrm{e}}_{(m)}\,\big]^{\mathrm{dev}} &= \boldsymbol{T}^{\mathrm{e}}_{(m)} \;-\; \tfrac{1}{3}\,\big[\,\boldsymbol{C}:\boldsymbol{T}^{\mathrm{e}}_{(m)}\,\big]\;\boldsymbol{B} \quad \textit{and} \\
\big[\,\boldsymbol{t}^{\mathrm{e}}_{(m)}\,\big]^{\mathrm{dev}} &= \boldsymbol{t}^{\mathrm{e}}_{(m)} \;-\; \tfrac{1}{3}\;\big[\,\boldsymbol{g}:\boldsymbol{t}^{\mathrm{e}}_{(m)}\,\big]\;\boldsymbol{g}^{-1}\,.
\end{aligned}
\tag{3.85}
$$

4 Kinematic hardening coupled with anisotropic damage for multiplicative elastoplasticity

In the context of computational material modelling, it is a desirable feature to develop finite strain formulations and algorithms that provide sufficient freedom to capture phenomenological effects like elastoplasticity, proportional and kinematic hardening, continuum damage, viscosity and finally anisotropy. Several recent monographs reflect the significance of this wide branch in computational mechanics; naming only a few, we refer to the works by Rappaz et al. (2003), Lubarda (2002), Haupt (2000), Besseling and v.d. Giessen (1994), Maugin (1992), Lubliner (1990), Lemaitre and Chaboche (1998) and in view of the underlying numerical treatment an outstanding contribution is given by the late Simo (1998). In this chapter we develop a sound constitutive framework that incorporates all of the previously mentioned phenomenological effects but, nevertheless, neglects any further influences resulting for instance from a thermal field. Several established concepts are thereby emphasised and joined together:

Hyperelastic formats for appropriate stress tensors are applied and the previously discussed assumption of a stress–free intermediated configuration, i.e. multiplicative elastoplasticity, is adopted. This framework enables us to incorporate commonly used formulations for the elastic behaviour and the effect of proportional hardening. For an alternative modelling ansatz see, for example, Svendsen (1998) or Bertram (1999, 2003).

Concerning the introduction of kinematic or rather anisotropic hardening, one could either directly set up evolution equations for a so–called back–stress tensor or introduce a corresponding internal variable that determines the back–stress via a hyperelastic format; compare Ekh and Runesson (2001), Diegele et al. (2000) or Svendsen (1998) and Svendsen et al. (1998) among others. In this chapter, we adopt the latter approach by analogy with the work by Wallin et al. (2003) (here without any restriction to elastic isotropy), i.e. an additional fictitious configuration is formally introduced whose underlying linear tangent map serves as an internal variable. It is then straightforward to proceed along the lines of multiplicative elastoplasticity such that an evolution equation for the corresponding kinematic hardening velocity gradient is a natural outcome.

Before coupling the plasticity framework with continuum damage mechanics, we must develop a physically sound formulation of degradation that provides sufficient freedom to capture the anisotropic nature of damage. Thus, the state of damage must at least be described by a second–order tensor, see Leckie and Onat (1981). In the following, the underlying mechanism to incorporate the effects of damage is provided by the hypothesis of strain energy equivalence between the intermediate configuration of multiplicative elastoplasticity and an additional fictitious or rather effective configuration; compare Betten (1981), Sidoroff (1981), Murakami (1988), Kattan and Voyiadjis (1990), Oller et al. (1995), Brünig (2003), Menzel and Steinmann (2001b), and references cited therein. The approach allows interpretation as covariance of the Helmholtz free energy with respect to superposed isomorphisms, which are identified here as the damage deformation gradient; see Marsden and Hughes (1994), Lu and Papadopoulos (2000) or Menzel and Steinmann (2003c, 2003d). As an interesting aspect, the present damage–metric–based formulation may formally be related to the classical understanding of damage as an area reduction since the damage tangent map determines the metric with respect to the intermediate configuration. Apparently, it turns out that this approach includes – besides the trivial case of isotropy for spherical damage mappings – specific elastic

symmetry classes, namely subclasses of transversal isotropy and orthotropy which are of cardinal interest for engineering applications; compare Menzel and Steinmann (2001a). Similar to the plastic part of the deformation gradient and the kinematic hardening mapping, the setup of a Lemaitre–type evolution equation for the damage velocity gradient is straightforward.

With these modelling approaches in hand, the coupling of the plasticity framework to continuum damage is performed by adopting the concept of effective stresses or rather strain equivalence; for a survey see, for example, Lämmer and Tsakmakis (2000), Steinmann et al. (1994) or Lemaitre and Chaboche (1998). In this chapter, effective stresses are incorporated via modified Mandel–type tensors. Conceptually speaking, the appropriate metric is varied such that anisotropic degradation enters the corresponding stress fields with respect to the intermediate configuration. Apart from proportional and kinematic hardening effects, as usually observed in metal plasticity, this approach enables us to describe typical path– or rather history dependent degradation of the material. Initially damaged configurations are conveniently introduced via initial damage metrics that differs from the, say, identity and thereby result in an initially anisotropic elastic response. By applying a spectral decomposition to the initial damage metric, it is obvious that eigenvalues smaller than one then denote degradation and eigenvalues greater than one characterise stiffening compared to a standard isotropic elastic setting where the metric boils down to the identity within an Euclidian setting. The product of these eigenvalues (if smaller than one) allows interpretation as being directly related to the initial content of isotropic damage or rather spherical voids. A distinction between different material behaviour in tension and compression, as for instance the microcrack–opening–closure effect which is addressed in Ekh and Runesson (2000) and Ekh et al. (2003), is not explicitly considered in the elastic response for conceptual clarity but allows to be shifted to a specific damage evolution law. In this context, the developed framework is not restricted to anisotropic failure of initially isotropic metals but additionally provides a convenient platform for the modelling of the material behaviour and failure of, for example, fibre reinforced composites and plastics. Furthermore, even constitutive models on the meso or micro level are captured in the presented formulation; compare Ekh et al. (2004) where special emphasis is placed on the modelling of single– and polycrystal–(visco)plasticity. Applications of the presented framework within small strain kinematics are given in Menzel et al. (2002) and Ekh et al. (2003) while the finite strain formulation is developed in Menzel and Steinmann (2003b).

Concerning the specific model that finally serves for several numerical examples concluding this chapter, we adopt constitutive equations as simple as possible, i.e. a St.–Venant–Kirchhoff–type ansatz and a v. Mises–type yield function; for an outline on anisotropic yield functions we refer the reader to the contributions by Steinmann et al. (1996), Miehe (1998), Hill (2000), Bruhns et al. (2003), and references cited in therein. While the underlying plastic evolution equation as well as the flow of proportional hardening contributions are of associated type and any plastic spin will be neglected, the kinematic hardening contribution is enhanced by an additional non–associated saturation–type term. The non–associated damage model itself is anisotropic and allows to account for different material behaviour in tension and compression with respect to the space of the driving damage force. In particular, we apply a Rankine–type model similar to Carol et al. (2001) and further elaborated in Menzel et al. (2003, 2005b). This ansatz closes the physically sound framework. Apparently, any appropriate isotropic or anisotropic damage model, which is based on an internal variable of for instance zeroth– or second–order and allowing representation via strain energy equivalence, can conveniently be incorporated into the developed framework since the introduced effective space is assumed to remain isotropic. Finally, the commonly applied exponential integration scheme is applied to the evolution equation of the plastic –, the kinematic hardening –, and the damage velocity gradient. Nevertheless, solely the evolution of the damage contribution with respect to the effective configuration allows representation within the standard spectral

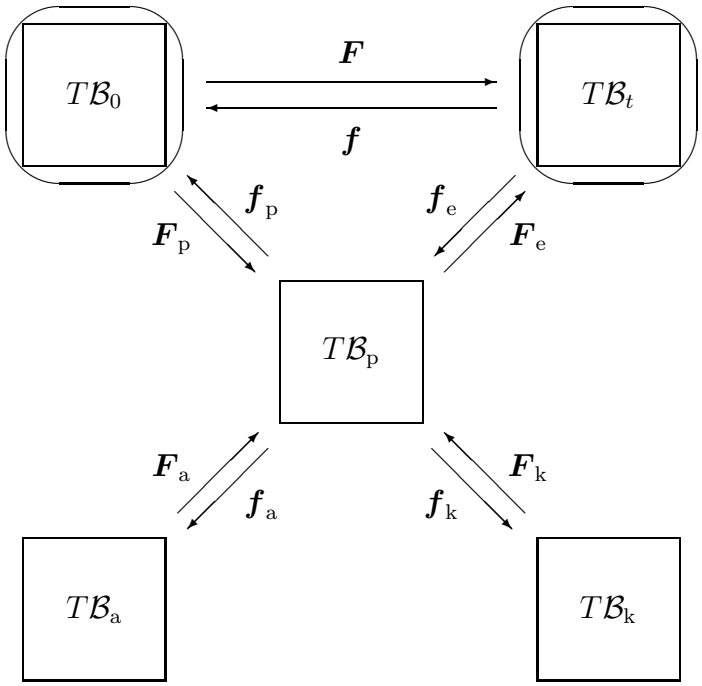

Figure 4.1: Graphical representation of tangent spaces and related linear tangent maps.

decomposition theorem for symmetric second–order tensors. Moreover, it turns out that the underlying Jacobians, which are used to solve the systems of nonlinear equations as based on Newton–type algorithms, can conveniently be approximated by a first–order difference scheme. Apart from that, different integration schemes and iteration techniques, as elaborated in Ekh and Menzel (2006), are reviewed for the so–called local problem.

The chapter is organised as follows: To set the stage, the underlying kinematics due to the introduction of fictitious configurations are reviewed in section 4.1. In order to obtain hyperelastic stress formats, we consequently apply the Coleman–Noll entropy principle within the framework of non–standard dissipative materials, see section 4.2. Additional emphasis is thereby placed on appropriate evolution equations and essential numerical aspects. A detailed outline of the application of the fictitious configuration concept is highlighted in section 4.4 so that later on, in section 4.5, a prototype model can be introduced. Finally, several numerical examples underline the applicability of the proposed framework, see section 4.6.

4.1 Essential kinematics

Based on the elaborations in chapter 2 and 3, the subsequent section summarises some essentials of the applied kinematical framework, whereby special emphasis is placed on the introduction of additional fictitious configurations and the underlying tangent maps. In this regard, we introduce – besides the material, spatial and intermediate configuration – two additional fictitious configurations, both being attached to the intermediate configuration; see figure 4.1 for a graphical illustration. On the one hand, a fictitious or rather effective configuration is assumed to be isotropic (as reflected by, for instance, the later on introduced Helmholtz free energy density), the corresponding tangent and dual space being denoted by $T\mathcal{B}_\mathrm{a}$ and $T^*\mathcal{B}_\mathrm{a}$, respectively. The underlying metric tensor, the second–order identity as well as the fictitious linear tangent map read as

$$\boldsymbol{G}_\mathrm{a} : T\mathcal{B}_\mathrm{a} \to T^*\mathcal{B}_\mathrm{a}\,, \quad \boldsymbol{I}_\mathrm{a} : T\mathcal{B}_\mathrm{a} \to T\mathcal{B}_\mathrm{a}\,, \quad \boldsymbol{F}_\mathrm{a} : T\mathcal{B}_\mathrm{a} \to T\mathcal{B}_\mathrm{p}\,, \quad \boldsymbol{f}_\mathrm{a} : T\mathcal{B}_\mathrm{p} \to T\mathcal{B}_\mathrm{a} \tag{4.1}$$

with $\boldsymbol{I}_{\mathrm{a}} = \boldsymbol{f}_{\mathrm{a}} \cdot \boldsymbol{F}_{\mathrm{a}}$ and $J_{\mathrm{a}} = \det(\boldsymbol{F}_{\mathrm{a}}) > 0$ so that $j_{\mathrm{a}} = \det(\boldsymbol{f}_{\mathrm{a}}) > 0$. These linear tangent maps allow interpretation as an affine pre–deformation and determine the elastic anisotropy of the considered body B as well as the degradation of the material. By analogy with chapter 3, one could introduce several kinematic tensors with respect to $\boldsymbol{F}_{\mathrm{a}}$. In the sequel, however, we are mainly interested in the pushforward of $\boldsymbol{G}_{\mathrm{a}}^{-1}$ and the pullback of the elastic Green–Lagrange strain tensor $\widehat{\boldsymbol{E}}_{\mathrm{e}} = \frac{1}{2}\,[\,\widehat{\boldsymbol{C}}_{\mathrm{e}} - \boldsymbol{G}_{\mathrm{p}}\,]$, i.e.

$$\boldsymbol{A}_{\mathrm{p}} \doteq \boldsymbol{F}_{\mathrm{a}} \star \boldsymbol{G}_{\mathrm{a}}^{-1} = \boldsymbol{F}_{\mathrm{a}} \cdot \boldsymbol{G}_{\mathrm{a}}^{-1} \cdot \boldsymbol{F}_{\mathrm{a}}^{\mathrm{d}}\,, \quad \bar{\boldsymbol{E}}_{\mathrm{e}} \doteq \boldsymbol{f}_{\mathrm{a}} \star \widehat{\boldsymbol{E}}_{\mathrm{e}} = \boldsymbol{F}_{\mathrm{a}}^{\mathrm{d}} \cdot \widehat{\boldsymbol{E}}_{\mathrm{e}} \cdot \boldsymbol{F}_{\mathrm{a}}\,. \tag{4.2}$$

On the other hand, the natural and dual tangent space of the second fictitious configuration is introduced as $T\mathcal{B}_{\mathrm{k}}$ and $T^*\mathcal{B}_{\mathrm{k}}$, respectively, so that the correlated metric tensor, the second order identity and the linear tangent maps consequently result in

$$\boldsymbol{G}_{\mathrm{k}} : T\mathcal{B}_{\mathrm{k}} \to T^*\mathcal{B}_{\mathrm{k}}\,, \quad \boldsymbol{I}_{\mathrm{k}} : T\mathcal{B}_{\mathrm{k}} \to T\mathcal{B}_{\mathrm{k}}\,, \quad \boldsymbol{F}_{\mathrm{k}} : T\mathcal{B}_{\mathrm{k}} \to T\mathcal{B}_{\mathrm{p}}\,, \quad \boldsymbol{f}_{\mathrm{k}} : T\mathcal{B}_{\mathrm{p}} \to T\mathcal{B}_{\mathrm{k}} \tag{4.3}$$

with $\boldsymbol{I}_{\mathrm{k}} = \boldsymbol{f}_{\mathrm{k}} \cdot \boldsymbol{F}_{\mathrm{k}}$ and $J_{\mathrm{k}} = \det(\boldsymbol{F}_{\mathrm{k}}) > 0$ so that $j_{\mathrm{k}} = \det(\boldsymbol{f}_{\mathrm{k}}) > 0$. Apparently, the underlying linear mappings serve as internal variables which allow to conveniently develop a sound kinematic hardening framework. Placing emphasis on corresponding deformation tensors, we are mainly interested in pushforward operations of $\boldsymbol{G}_{\mathrm{k}}$, namely

$$\widehat{\boldsymbol{K}} \doteq \boldsymbol{F}_{\mathrm{k}} \star \boldsymbol{G}_{\mathrm{k}} = \boldsymbol{f}_{\mathrm{k}}^{\mathrm{d}} \cdot \boldsymbol{G}_{\mathrm{k}} \cdot \boldsymbol{f}_{\mathrm{k}} \tag{4.4}$$

which enables us to set up a Green–Lagrange–type strain measure

$$\widehat{\boldsymbol{E}}_{\mathrm{k}} \doteq \tfrac{1}{2}\,[\,\widehat{\boldsymbol{K}} - \boldsymbol{G}_{\mathrm{p}}\,]\,, \quad \bar{\boldsymbol{E}}_{\mathrm{k}} = \boldsymbol{f}_{\mathrm{a}} \star \widehat{\boldsymbol{E}}_{\mathrm{k}} = \boldsymbol{F}_{\mathrm{a}}^{\mathrm{d}} \cdot \widehat{\boldsymbol{E}}_{\mathrm{k}} \cdot \boldsymbol{F}_{\mathrm{a}}\,. \tag{4.5}$$

Now, after discussing the transformation relations between different configurations, we place emphasis on the correlated velocity gradients or rather distortion velocities. In this context, we recall the physical velocity gradient and its pullback to the reference configuration

$$\boldsymbol{l} = \mathrm{D}_t\boldsymbol{F} \cdot \boldsymbol{f} = -\,\boldsymbol{F} \cdot \mathrm{D}_t\boldsymbol{f}\,, \quad \boldsymbol{L} = \boldsymbol{\varphi}^*\,\boldsymbol{l} = \boldsymbol{f} \star \boldsymbol{l} = \boldsymbol{f} \cdot \mathrm{D}_t\boldsymbol{F} = -\,\mathrm{D}_t\boldsymbol{f} \cdot \boldsymbol{F}\,, \tag{4.6}$$

whereby, as previously introduced, the notation $\mathrm{D}_t\{\bullet\}$ abbreviates the material time derivative. A pullback transformation with respect to the intermediate configuration results in

$$\widehat{\boldsymbol{L}} = \boldsymbol{f}_{\mathrm{e}} \star \boldsymbol{l} = \boldsymbol{f}_{\mathrm{e}} \cdot \mathrm{D}_t\boldsymbol{F} \cdot \boldsymbol{f}_{\mathrm{p}} = -\,\boldsymbol{F}_{\mathrm{p}} \cdot \mathrm{D}_t\,\boldsymbol{f} \cdot \boldsymbol{F}_{\mathrm{e}} \tag{4.7}$$

and referring to the adopted multiplicative decomposition we obtain the following additive decomposition

$$\widehat{\boldsymbol{L}} = \widehat{\boldsymbol{L}}_{\mathrm{e}} + \widehat{\boldsymbol{L}}_{\mathrm{p}} = \boldsymbol{f}_{\mathrm{e}} \cdot \mathrm{D}_t\boldsymbol{F}_{\mathrm{e}} + \mathrm{D}_t\boldsymbol{F}_{\mathrm{p}} \cdot \boldsymbol{f}_{\mathrm{p}} = -\,\mathrm{D}_t\boldsymbol{f}_{\mathrm{e}} \cdot \boldsymbol{F}_{\mathrm{e}} - \boldsymbol{F}_{\mathrm{p}} \cdot \mathrm{D}_t\boldsymbol{f}_{\mathrm{p}}\,, \tag{4.8}$$

compare chapter 3. A similar outline in, for example, $\mathcal{B}_0$ or $\mathcal{B}_t$ follows straightforwardly and is hence omitted here. By analogy with these well–established formats, the velocity 'gradients' with respect to the, say, damage and hardening mapping $\boldsymbol{F}_{\mathrm{a}}$ and $\boldsymbol{F}_{\mathrm{k}}$ are consequently introduced (similar to $\widehat{\boldsymbol{L}}_{\mathrm{p}}$) as

$$\widehat{\boldsymbol{L}}_{\mathrm{a}} \doteq \mathrm{D}_t\boldsymbol{F}_{\mathrm{a}} \cdot \boldsymbol{f}_{\mathrm{a}} = -\,\boldsymbol{F}_{\mathrm{a}} \cdot \mathrm{D}_t\boldsymbol{f}_{\mathrm{a}}\,, \quad \widehat{\boldsymbol{L}}_{\mathrm{k}} \doteq \mathrm{D}_t\boldsymbol{F}_{\mathrm{k}} \cdot \boldsymbol{f}_{\mathrm{k}} = -\,\boldsymbol{F}_{\mathrm{k}} \cdot \mathrm{D}_t\boldsymbol{f}_{\mathrm{k}}\,. \tag{4.9}$$

4.2 Coleman–Noll entropy principle

In this section we apply the Coleman–Noll entropy principle to the problem at hand. For a detailed review on the general underlying theory we refer the reader to the monographs by

Antman (1995), Maugin (1999) and Nemat–Nasser (2004) or the contribution by Miehe and Stein (1992), among others, and the elaborations summarised in section 3.4.

Let the Helmholtz free energy density take the following format

$$\psi_0(\boldsymbol{F}_{\mathrm{e}}, \boldsymbol{F}_{\mathrm{k}}, \boldsymbol{F}_{\mathrm{a}}, \kappa; \boldsymbol{X}) \doteq \psi_0^{\mathrm{e}}(\widehat{\boldsymbol{E}}_{\mathrm{e}}, \boldsymbol{A}_{\mathrm{p}}; \boldsymbol{X}) + \psi_0^{\mathrm{k}}(\widehat{\boldsymbol{E}}_{\mathrm{k}}, \boldsymbol{A}_{\mathrm{p}}; \boldsymbol{X}) + \psi_0^{\kappa}(\kappa; \boldsymbol{X})\,, \tag{4.10}$$

whereby a representation with respect to the intermediated setting has been chosen and, as outlined in the previous section, $\widehat{\boldsymbol{E}}_{\mathrm{e}}$, $\widehat{\boldsymbol{E}}_{\mathrm{k}}$, $\boldsymbol{A}_{\mathrm{p}}$ represent the elastic Green–Lagrange strain measure, the Green–Lagrange–type strain measure as based on the internal kinematic hardening variable as well as the damage metric, respectively, and κ defines an additional scalar–valued (internal) variable that accounts for proportional hardening. The local form of the isothermal Clausius–Duhem inequality consequently reads

$$\begin{aligned} \mathsf{D}_0 = \widehat{\boldsymbol{M}}_{\mathrm{e}}^{\mathrm{d}} : \widehat{\boldsymbol{L}} \;-\; \partial_{\widehat{\boldsymbol{E}}_{\mathrm{e}}}\psi_0\,\big|_{\widehat{\boldsymbol{E}}_{\mathrm{k}},\boldsymbol{A}_{\mathrm{p}},\kappa} : \mathrm{D}_t\widehat{\boldsymbol{E}}_{\mathrm{e}} \;-\; \partial_{\widehat{\boldsymbol{E}}_{\mathrm{k}}}\psi_0\,\big|_{\widehat{\boldsymbol{E}}_{\mathrm{e}},\boldsymbol{A}_{\mathrm{p}},\kappa} : \mathrm{D}_t\widehat{\boldsymbol{E}}_{\mathrm{k}} \\ -\; \partial_{\boldsymbol{A}_{\mathrm{p}}}\psi_0\,\big|_{\widehat{\boldsymbol{E}}_{\mathrm{e}},\widehat{\boldsymbol{E}}_{\mathrm{k}},\kappa} : \mathrm{D}_t\boldsymbol{A}_{\mathrm{p}} \;-\; \partial_{\kappa}\psi_0\,\big|_{\widehat{\boldsymbol{E}}_{\mathrm{e}},\widehat{\boldsymbol{E}}_{\mathrm{k}},\boldsymbol{A}_{\mathrm{p}}}\,\mathrm{D}_t\kappa \quad \geq 0 \end{aligned} \tag{4.11}$$

with $\widehat{\boldsymbol{M}}_{\mathrm{e}}^{\mathrm{d}}$ characterising the (elastic) Mandel stress which enters the computation of the stress power $\widehat{\boldsymbol{M}}_{\mathrm{e}}^{\mathrm{d}} : \widehat{\boldsymbol{L}}$. Based on the previously highlighted kinematical relations as outlined in eqs.(4.2, 4.4) and (4.8, 4.9), we observe the following correlations between material time derivatives of interest – namely those quantities which are incorporated into the dissipation inequality (4.11) – and the underlying distortion velocities

$$\mathrm{D}_t\widehat{\boldsymbol{E}}_{\mathrm{e}} = [\,\widehat{\boldsymbol{C}}_{\mathrm{e}} \cdot \widehat{\boldsymbol{L}}_{\mathrm{e}}\,]^{\mathrm{sym}}\,,\;\; \mathrm{D}_t\widehat{\boldsymbol{E}}_{\mathrm{k}} = -\,[\,\widehat{\boldsymbol{K}} \cdot \widehat{\boldsymbol{L}}_{\mathrm{k}}\,]^{\mathrm{sym}}\,,\;\; \mathrm{D}_t\boldsymbol{A}_{\mathrm{p}} = 2\,[\,\widehat{\boldsymbol{L}}_{\mathrm{a}} \cdot \boldsymbol{A}_{\mathrm{p}}\,]^{\mathrm{sym}}\,. \tag{4.12}$$

With these considerations at hand, the dissipation inequality (4.11) is rewritten as

$$\mathsf{D}_0 = \widehat{\boldsymbol{M}}_{\mathrm{e}}^{\mathrm{d}} : \widehat{\boldsymbol{L}}_{\mathrm{p}} + \widehat{\boldsymbol{M}}_{\mathrm{k}}^{\mathrm{d}} : \widehat{\boldsymbol{L}}_{\mathrm{k}} - \widehat{\boldsymbol{M}}_{\mathrm{a}}^{\mathrm{d}} : \widehat{\boldsymbol{L}}_{\mathrm{a}} - Y\,\mathrm{D}_t\kappa \geq 0\,, \tag{4.13}$$

whereby use of the symmetry of the derivatives of the Helmholtz free energy density ψ_0 with respect to $\widehat{\boldsymbol{E}}_{\mathrm{e}}$, $\widehat{\boldsymbol{E}}_{\mathrm{k}}$, $\boldsymbol{A}_{\mathrm{p}}$ has been made and, adopting the standard argumentation of rational thermodynamics, thestress tensors defined read

$$\begin{aligned} \widehat{\boldsymbol{M}}_{\mathrm{e}}^{\mathrm{d}} &\doteq \widehat{\boldsymbol{C}}_{\mathrm{e}} \cdot \partial_{\widehat{\boldsymbol{E}}_{\mathrm{e}}}\psi_0^{\mathrm{e}}\,\Big|_{\boldsymbol{A}_{\mathrm{p}}}\,, & \widehat{\boldsymbol{M}}_{\mathrm{k}}^{\mathrm{d}} &\doteq \widehat{\boldsymbol{K}} \cdot \partial_{\widehat{\boldsymbol{E}}_{\mathrm{k}}}\psi_0^{\mathrm{k}}\,\Big|_{\boldsymbol{A}_{\mathrm{p}}}\,, \\ \widehat{\boldsymbol{M}}_{\mathrm{a}}^{\mathrm{d}} &\doteq 2\,\partial_{\boldsymbol{A}_{\mathrm{p}}}[\,\psi_0^{\mathrm{e}} + \psi_0^{\mathrm{k}}\,]\,\big|_{\widehat{\boldsymbol{E}}_{\mathrm{e}},\widehat{\boldsymbol{E}}_{\mathrm{k}}} \cdot \boldsymbol{A}_{\mathrm{p}}\,, & Y &\doteq \partial_{\kappa}\psi_0^{\kappa}\,. \end{aligned} \tag{4.14}$$

Remark 4.2.1 *Even though the introduction of fictitious configurations whose underlying linear tangent maps define internal variables accounting for degradation and kinematic hardening might at first glance seem somehow artificial, we observe that the model includes well–established formulations of finite inelasticity if specific kinematic assumptions are incorporated. Choosing, for example, $\boldsymbol{F}_{\mathrm{a}}$ to be throughout represented by the identity, i.e. no degradation takes place and the model reflects the behaviour of an elastically isotropic material, and replacing the introduced strain measure by the appropriate metric tensor results in the standard format $\psi_0^{\mathrm{e}}(\widehat{\boldsymbol{C}}_{\mathrm{e}}, \widehat{\boldsymbol{G}}^{-1}; \boldsymbol{X}) = \psi_0^{\mathrm{e}}(\boldsymbol{C}, \boldsymbol{B}_{\mathrm{p}}; \boldsymbol{X}) = \psi_0^{\mathrm{e}}(\boldsymbol{g}, \boldsymbol{b}_{\mathrm{e}}; \boldsymbol{X})$. Alternatively, the representation $\psi_0^{\mathrm{e}}(\widehat{\boldsymbol{C}}_{\mathrm{e}} \cdot \boldsymbol{G}_{\mathrm{p}}^{-1}; \boldsymbol{X}) = \psi_0^{\mathrm{e}}(\boldsymbol{C} \cdot \boldsymbol{B}_{\mathrm{p}}; \boldsymbol{X}) = \psi_0^{\mathrm{e}}(\boldsymbol{g} \cdot \boldsymbol{b}_{\mathrm{e}}; \boldsymbol{X})$ can be applied; compare, for instance, Miehe (1995) ($\widehat{\psi}_{macro}$), Svendsen (1998) (ψ_E), or Govindjee and Reese (1997) (ψ^k). However, for the second contribution with tensorial arguments, ψ_0^{k}, we additionally assume $\boldsymbol{F}_{\mathrm{k}} \equiv \boldsymbol{F}_{\mathrm{p}}$ and introduce the metric $\widehat{\boldsymbol{b}}_{\mathrm{k}} \doteq \boldsymbol{F}_{\mathrm{k}} \star \boldsymbol{G}_{\mathrm{p}}^{-1}$ which enables us to obtain $\psi_0^{\mathrm{k}}(\boldsymbol{G}_{\mathrm{p}}, \widehat{\boldsymbol{b}}_{\mathrm{k}}; \boldsymbol{X}) = \psi_0^{\mathrm{k}}(\boldsymbol{C}_{\mathrm{p}}, \boldsymbol{G}^{-1}; \boldsymbol{X}) = \psi_0^{\mathrm{k}}(\boldsymbol{c}_{\mathrm{e}}, \boldsymbol{b}; \boldsymbol{X})$ with $\widehat{\boldsymbol{b}}_{\mathrm{k}} = \boldsymbol{F}_{\mathrm{k}} \star \boldsymbol{G}_{\mathrm{k}}^{-1} \equiv \boldsymbol{F}_{\mathrm{p}} \star \boldsymbol{G}^{-1}$ and $\boldsymbol{C}_{\mathrm{p}} = \boldsymbol{f}_{\mathrm{p}} \star \boldsymbol{G}_{\mathrm{p}}$ being obvious. The alternative representation reads $\psi_0^{\mathrm{k}}(\boldsymbol{G}_{\mathrm{p}} \cdot \widehat{\boldsymbol{b}}_{\mathrm{k}}; \boldsymbol{X}) = \psi_0^{\mathrm{k}}(\boldsymbol{C}_{\mathrm{p}} \cdot \boldsymbol{G}^{-1}; \boldsymbol{X}) = \psi_0^{\mathrm{k}}(\boldsymbol{c}_{\mathrm{e}} \cdot \boldsymbol{b}; \boldsymbol{X})$, see Svendsen (1998) ($\psi_P$).*

4.2.1 Non–standard dissipative materials

Next, following well–established lines of derivation for the modelling of inelastic response, we introduce an admissible elastic domain with respect to the intermediate configuration

$$\mathcal{A} = \left\{ \left(\widehat{\boldsymbol{M}}^{\mathrm{d}}_{\mathrm{r}}, Y\right) \,\middle|\, {}^{\mathrm{yie}}\Phi\left(\widehat{\boldsymbol{M}}^{\mathrm{d}}_{\mathrm{r}}, Y; \boldsymbol{X}\right) \leq 0 \right\} \quad \text{with} \quad \widehat{\boldsymbol{M}}^{\mathrm{d}}_{\mathrm{r}} \doteq \widehat{\boldsymbol{M}}^{\mathrm{d}}_{\mathrm{e}} - \widehat{\boldsymbol{M}}^{\mathrm{d}}_{\mathrm{k}} \tag{4.15}$$

determined by a (convex) yield function ${}^{\mathrm{yie}}\Phi(\widehat{\boldsymbol{M}}^{\mathrm{d}}_{\mathrm{r}}, Y; \boldsymbol{X}) \doteq {}^{\mathrm{pla}}\Phi(\widehat{\boldsymbol{M}}^{\mathrm{d}}_{\mathrm{r}}; \boldsymbol{X}) + {}^{\mathrm{har}}\Phi(Y; \boldsymbol{X})$, compare sections 3.4.3 and 3.5.1. Apparently, the relative stress $\widehat{\boldsymbol{M}}^{\mathrm{d}}_{\mathrm{r}}$ is introduced such that this Mandel–type tensor takes the commonly applied format for the formulation of kinematic hardening. Moreover, we assume the existence of a dissipation potential of Lemaitre–type, namely

$${}^{\mathrm{pot}}\Phi\left(\widehat{\boldsymbol{M}}^{\mathrm{d}}_{\mathrm{r}}, \widehat{\boldsymbol{M}}^{\mathrm{d}}_{\mathrm{a}}, Y; \boldsymbol{X}\right) \doteq {}^{\mathrm{yie}}\Phi\left(\widehat{\boldsymbol{M}}^{\mathrm{d}}_{\mathrm{r}}, Y; \boldsymbol{X}\right) + {}^{\mathrm{dam}}\Phi\left(\widehat{\boldsymbol{M}}^{\mathrm{d}}_{\mathrm{a}}; \boldsymbol{X}\right). \tag{4.16}$$

Based on these assumptions, appropriate evolution equations allow the following representations

$$\begin{aligned}
\widehat{\boldsymbol{L}}_{\mathrm{p}} &\doteq \mathrm{D}_t\lambda\, \partial_{\widehat{\boldsymbol{M}}^{\mathrm{d}}_{\mathrm{e}}} {}^{\mathrm{pot}}\Phi = \mathrm{D}_t\lambda\, \partial_{\widehat{\boldsymbol{M}}^{\mathrm{d}}_{\mathrm{e}}} {}^{\mathrm{pla}}\Phi \doteq \mathrm{D}_t\lambda\, \widehat{\boldsymbol{\nu}}_{\mathrm{p}}\,, \\
\widehat{\boldsymbol{L}}_{\mathrm{k}} &\doteq \mathrm{D}_t\lambda\, \partial_{\widehat{\boldsymbol{M}}^{\mathrm{d}}_{\mathrm{k}}} {}^{\mathrm{pot}}\Phi = \mathrm{D}_t\lambda\, \partial_{\widehat{\boldsymbol{M}}^{\mathrm{d}}_{\mathrm{k}}} {}^{\mathrm{pla}}\Phi \doteq \mathrm{D}_t\lambda\, \widehat{\boldsymbol{\nu}}_{\mathrm{k}}\,, \\
-\widehat{\boldsymbol{L}}_{\mathrm{a}} &\doteq \mathrm{D}_t\lambda\, \partial_{\widehat{\boldsymbol{M}}^{\mathrm{d}}_{\mathrm{a}}} {}^{\mathrm{pot}}\Phi = \mathrm{D}_t\lambda\, \partial_{\widehat{\boldsymbol{M}}^{\mathrm{d}}_{\mathrm{a}}} {}^{\mathrm{dam}}\Phi \doteq \mathrm{D}_t\lambda\, \widehat{\boldsymbol{\nu}}_{\mathrm{a}}\,, \\
-\mathrm{D}_t\kappa &\doteq \mathrm{D}_t\lambda\, \partial_{Y} {}^{\mathrm{pot}}\Phi \quad = \mathrm{D}_t\lambda\, \partial_{Y} {}^{\mathrm{har}}\Phi \quad \doteq \mathrm{D}_t\lambda\, \nu_{\kappa}\,,
\end{aligned} \tag{4.17}$$

whereby the Lagrange multiplier $\mathrm{D}_t\lambda$ is either restricted by the conditions $\mathrm{D}_t\lambda > 0$, $\mathrm{D}_t\lambda\, {}^{\mathrm{yie}}\Phi = 0$, $\mathrm{D}_t\lambda\, \mathrm{D}_t{}^{\mathrm{yie}}\Phi = 0$ or, for a viscoplastic setting, determined via $t^*\, \mathrm{D}_t\lambda \doteq \eta({}^{\mathrm{yie}}\Phi)$ with $t^* > 0$; furthermore $\eta \in C^1 \mid \eta({}^{\mathrm{yie}}\Phi \leq 0) = 0$ being a monotonically increasing functional. Obviously, we deal with associated evolution equations for the plasticity and hardening contributions but the damage part, nevertheless, remains non–associated.

Remark 4.2.2 *Different types of kinematic hardening are commonly applied in elastoplasticity, for instance so–called Prager –, Ziegler – or Armstrong–Frederick equations which are, in contrast to the present formulation, frequently combined with the assumption of elastic isotropy. Even though the proposed finite strain framework reflects a similar setup as linear kinematic hardening within a small strain setting, its extension to for example nonlinear Armstrong–Frederick–type hardening is potentially included; compare Haupt (2000), Diegele et al. (2000), or Svendsen (1998) and Svendsen et al. (1998) for detailed discussions. In this context, we obtain the classical non–associated format for the evolution of the Mandel–type back–stress tensor as* $\mathrm{L}^{\mathrm{p}}_t \widehat{\boldsymbol{M}}^{\mathrm{d}}_{\mathrm{k}} \doteq c\, \widehat{\boldsymbol{L}}^{\mathrm{d}}_{\mathrm{p}} - b\, \mathrm{D}_t\lambda\, \widehat{\boldsymbol{M}}^{\mathrm{d}}_{\mathrm{k}}$ *with* $\mathrm{L}^{\mathrm{p}}_t[\bullet] = \boldsymbol{F}_{\mathrm{p}} \star \mathrm{D}_t(\boldsymbol{f}_{\mathrm{p}} \star [\bullet])$ *denoting the Lie derivative with respect to the intermediate configuration. Moreover, non–associated saturation–type hardening is conveniently introduced via an extension of the corresponding evolution equation for* $\boldsymbol{F}_{\mathrm{k}}$*, namely* $\widehat{\boldsymbol{L}}_{\mathrm{k}} \doteq \mathrm{D}_t\lambda\, [\, \widehat{\boldsymbol{\nu}}_{\mathrm{k}} + a\, K^{-1}_{\infty}\, \widehat{\boldsymbol{M}}_{\mathrm{k}}\,]$ *with* $K_{\infty} > 0$*, see Ekh and Runesson (2001) for a comprehensive outline. In the progression of this chapter, we apply this approach to the framework at hand – further details being given when needed, see section 4.5.3.*

Remark 4.2.3 *In this chapter, we place no emphasis on the introduction of any additional constitutive spin equation. Applications of plastic spin for a similar kinematic hardening formulation which, however, has been restricted to elastic isotropy and does not address any degradation of the material, is developed in Wallin et al. (2003). For a general survey we refer the reader to Dafalias (1998) and the contributions by Cleja–Ţigoiu (2000), Tsakmakis (2004), Häusler et al. (2004), Haupt and Kersten (2003), and Paulun and Ręcherski (1992).*

4.2.2 Prototype constitutive integrator

Concerning numerical integration of the obtained evolution equations, the time domain of interest is subdivided into several intervals; $\mathcal{T} = \bigcup_{n=0}^{N} [\, t^n \,,\, t^{n+1} \,]$ with $\Delta t \doteq t^{n+1} - t^n > 0$ being obvious. From eqs.(4.8,4.17) and adopting the approach as advocated by Weber and Anand (1990), we obtain the relation

$$\boldsymbol{F}_{\mathrm{p}}^{n+1} \doteq \exp(\Delta\lambda\, \widehat{\boldsymbol{\nu}}_{\mathrm{p}}^{n+1}) \cdot \boldsymbol{F}_{\mathrm{p}}^{n} \quad \text{so that} \quad \boldsymbol{F}_{\mathrm{e}}^{n+1} = \boldsymbol{F}_{\mathrm{tri}} \cdot \exp(-\,\Delta\lambda\, \widehat{\boldsymbol{\nu}}_{\mathrm{p}}^{n+1}) \tag{4.18}$$

with $\boldsymbol{F}_{\mathrm{tri}} = \boldsymbol{F}^{n+1} \cdot \boldsymbol{f}_{\mathrm{p}}^{n}$. It turns out that $\widehat{\boldsymbol{\nu}}_{\mathrm{p}}$ is generally non–symmetric since we do not consider any specific restrictions to isotropy. In complete analogy, an exponential integration scheme can be applied to the kinematic hardening and the damage contribution

$$\boldsymbol{F}_{\mathrm{k}}^{n+1} \doteq \exp(\Delta\lambda\, \widehat{\boldsymbol{\nu}}_{\mathrm{k}}^{n+1}) \cdot \boldsymbol{F}_{\mathrm{k}}^{n} \,, \qquad \boldsymbol{F}_{\mathrm{a}}^{n+1} \doteq \exp(-\,\Delta\lambda\, \widehat{\boldsymbol{\nu}}_{\mathrm{a}}^{n+1}) \cdot \boldsymbol{F}_{\mathrm{a}}^{n} \,, \tag{4.19}$$

recall eq.(4.9), while an Euler backward approach may serve as integration rule for the hardening variable; i.e. $\kappa^{n+1} \doteq \kappa^n - \Delta\lambda\, \nu_{\kappa}^{n+1}$. Once more, it is the anisotropic material behaviour that causes generally non–symmetric flow directions $\widehat{\boldsymbol{\nu}}_{\mathrm{k}}$ and $\widehat{\boldsymbol{\nu}}_{\mathrm{a}}$. These implicit integration rules result in a nonlinear system of equations represented by the following residua

$$\begin{aligned}
\boldsymbol{R}_{\mathrm{e}} &= \boldsymbol{F}_{\mathrm{e}}^{n+1} - \boldsymbol{F}_{\mathrm{e}}^{\mathrm{tri}} \cdot \exp(-\,\Delta\lambda\, \widehat{\boldsymbol{\nu}}_{\mathrm{p}}^{n+1}) \,, \\
\boldsymbol{R}_{\mathrm{k}} &= \boldsymbol{F}_{\mathrm{k}}^{n+1} - \exp(\Delta\lambda\, \widehat{\boldsymbol{\nu}}_{\mathrm{k}}^{n+1}) \cdot \boldsymbol{F}_{\mathrm{k}}^{n} \,, \\
\boldsymbol{R}_{\mathrm{a}} &= \boldsymbol{F}_{\mathrm{a}}^{n+1} - \exp(-\,\Delta\lambda\, \widehat{\boldsymbol{\nu}}_{\mathrm{d}}^{n+1}) \cdot \boldsymbol{F}_{\mathrm{a}}^{n} \,, \\
R_{\kappa} &= \kappa^{n+1} - \kappa^n + \Delta\lambda\, \nu_{\kappa}^{n+1} \,,
\end{aligned} \tag{4.20}$$

which determine the Jacobian of a typical Newton–type iteration scheme, namely

$$\begin{bmatrix}
\partial_{\boldsymbol{F}_{\mathrm{e}}^{n+1}} \boldsymbol{R}_{\mathrm{e}} & \partial_{\boldsymbol{F}_{\mathrm{k}}^{n+1}} \boldsymbol{R}_{\mathrm{e}} & \partial_{\boldsymbol{F}_{\mathrm{a}}^{n+1}} \boldsymbol{R}_{\mathrm{e}} & \\
\partial_{\boldsymbol{F}_{\mathrm{e}}^{n+1}} \boldsymbol{R}_{\mathrm{k}} & \partial_{\boldsymbol{F}_{\mathrm{k}}^{n+1}} \boldsymbol{R}_{\mathrm{k}} & \partial_{\boldsymbol{F}_{\mathrm{a}}^{n+1}} \boldsymbol{R}_{\mathrm{k}} & \\
\partial_{\boldsymbol{F}_{\mathrm{e}}^{n+1}} \boldsymbol{R}_{\mathrm{a}} & \partial_{\boldsymbol{F}_{\mathrm{k}}^{n+1}} \boldsymbol{R}_{\mathrm{a}} & \partial_{\boldsymbol{F}_{\mathrm{a}}^{n+1}} \boldsymbol{R}_{\mathrm{a}} & \\
 & & & \partial_{\kappa^{n+1}} R_{\kappa}
\end{bmatrix} \circ \begin{bmatrix} \Delta\boldsymbol{F}_{\mathrm{e}} \\ \Delta\boldsymbol{F}_{\mathrm{k}} \\ \Delta\boldsymbol{F}_{\mathrm{a}} \\ \Delta\kappa \end{bmatrix} = \begin{bmatrix} -\,\boldsymbol{R}_{\mathrm{e}} \\ -\,\boldsymbol{R}_{\mathrm{k}} \\ -\,\boldsymbol{R}_{\mathrm{a}} \\ -\,R_{\kappa} \end{bmatrix} \tag{4.21}$$

whereby the notation $\circ$ abbreviates the appropriate contraction operation. It turns out that these 'local' Jacobians, as well as the 'global' Jacobian or rather the algorithmic tangent operator within a finite element setting, can conveniently be approximated via a first–order difference perturbation scheme. For a detailed outline of the underlying algorithm we refer the reader to Miehe (1996c) or Menzel and Steinmann (2003b); see also section 4.3.1.1 in this regard. The computation of the Lagrange multiplier follows either from the solution of the nonlinear equation ${}^{\mathrm{yie}}\Phi^{n+1}(\Delta\lambda, \dots) \doteq 0$ or by seeking the solution of the nonlinear relation $t^* \,\Delta\lambda - \Delta t\, \eta^{n+1}(\Delta\lambda, \dots) \doteq 0$, with $\Delta\lambda \equiv \Delta t\, \mathrm{D}_t\lambda$ being obvious (recall that $t^* \to 0$ leads to $\eta^{n+1} \to 0$ and ${}^{\mathrm{yie}}\Phi^{n+1} \to 0$ recovering the rate–independent case).

The integration scheme highlighted above will serve as a prototype integration technique in this chapter. In general, however, various algorithms can be applied to the integration of the underlying system of ordinary differential equations. Different approaches with a particular focus on efficiency are elaborated in the subsequent section 4.3. The subsequent finite element examples in section 4.6, however, are based on eqs.(4.18–4.21) together with a staggered iteration scheme wherein any (vanilla–type flavour) scalar–valued iteration can be applied to the calculation of the Lagrange multiplier. A brief summary is given in algorithm 4.1.

Algorithm 4.1 *Staggered solution technique: Newton–type algorithm to solve the set of nonlinear equations for $\boldsymbol{F}_{\mathrm{e}}^{n+1}$, $\boldsymbol{F}_{\mathrm{k}}^{n+1}$, $\boldsymbol{F}_{\mathrm{a}}^{n+1}$ and κ^{n+1} embedded into a scalar–valued iteration to compute the Lagrange multiplier $\Delta\lambda$.*

finite element method — **for** given $\boldsymbol{F}^{n+1}$, $\boldsymbol{F}_{\mathrm{p}}^{n}$, $\boldsymbol{F}_{\mathrm{k}}^{n}$, $\boldsymbol{F}_{\mathrm{a}}^{n}$, κ^{n} **do**

if ${}^{\mathrm{yie}}\Phi^{n+1} > 0$ **then**

scalar–valued iteration — **dowhile** $|\Delta\Delta\lambda| > \mathrm{tol}$

$\ldots$

$\Delta\lambda \hookleftarrow \Delta\lambda + \Delta\Delta\lambda$

Newton iteration — **dowhile** $\|\boldsymbol{R}_{\mathrm{e}}\| + \|\boldsymbol{R}_{\mathrm{k}}\| + \|\boldsymbol{R}_{\mathrm{a}}\| + |R_{\kappa}| > \mathrm{tol}$

$\ldots$

$\boldsymbol{F}_{\mathrm{e}}^{n+1} \hookleftarrow \boldsymbol{F}_{\mathrm{e}}^{n+1} + \Delta\boldsymbol{F}_{\mathrm{e}}$

$\boldsymbol{F}_{\mathrm{k}}^{n+1} \hookleftarrow \boldsymbol{F}_{\mathrm{k}}^{n+1} + \Delta\boldsymbol{F}_{\mathrm{k}}$

$\boldsymbol{F}_{\mathrm{a}}^{n+1} \hookleftarrow \boldsymbol{F}_{\mathrm{a}}^{n+1} + \Delta\boldsymbol{F}_{\mathrm{a}}$

$\kappa^{n+1} \hookleftarrow \kappa^{n+1} + \Delta\kappa$

enddo

enddo

endif

Remark 4.2.4 *Please note that the exponential of a generally non–symmetric second–order tensor is performed via a series expansion since no spectral decomposition is conveniently available. Higher–order powers thereby allow representation via the Cayley–Hamilton theorem which improves the numerical efficiency of the computation, compare Miehe (1996a). The specific case with the flow direction being the product of two symmetric second–order tensors (at least one of them positive definite), which results in a generalised eigenvalue problem, is discussed below; see section 4.5.2.*

4.3 Efficient integration / iteration schemes

In this section, we discuss two alternative but representative types of implicit integration schemes: a two–step backward differential rule (BDF2) and, as a special case of BDF2, the single–step Euler backward rule (EB). The reader is referred to, for example, Papadopoulos and Taylor (1994), Kirchner and Simeon (1999), and Ekh (2001) for reviews on the BDF2 algorithm. Higher–order multi–step integration schemes in the present context are also discussed in Menzel and Steinmann (2001b). Concerning notation, explicit denomination of variables referring to the actual state t^{n+1} is often omitted for notational simplicity.

The fundamental idea for the setup of multi–step algorithms consists in approximating the material time derivative via

$$\mathrm{D}_t\{\bullet\} \approx \frac{\{\bullet\}^{n+1} - \{\widetilde{\bullet}\}}{\widetilde{\Delta t}} \tag{4.22}$$

with the notation $\{\widetilde{\circ}\}$ representing an appropriate assembly with respect to the previous time

steps of interest. To be specific, we obtain for the BDF2 algorithm, which is of up to second–order accuracy, the relations

$$\begin{aligned} \widetilde{\bullet} \;&=\; \beta_1 \{\bullet\}^{n-1} + [\,1-\beta_1\,]\,\{\bullet\}^n\,, \qquad \widetilde{\Delta t} \,=\, \beta_2\,\Delta t\,, \\ \beta_1 \;&=\; -\,\frac{[\Delta t]^2}{\Delta t^n\,[\,\Delta t^n + 2\,\Delta t\,]}\,, \qquad \beta_2 \;=\, \frac{\beta_1\,\Delta t^n + \Delta t}{\Delta t}\,. \end{aligned} \tag{4.23}$$

By applying BDF2 to the system of non–linear equations as highlighted in eq.(4.17), namely

$$\mathrm{D}_t \boldsymbol{F}_{\mathrm{p,k}} = \mathrm{D}_t\lambda\,\widehat{\boldsymbol{\nu}}_{\mathrm{p,k}}\cdot\boldsymbol{F}_{\mathrm{p,k}}\,, \qquad \mathrm{D}_t\boldsymbol{F}_{\mathrm{a}} = -\,\mathrm{D}_t\lambda\,\widehat{\boldsymbol{\nu}}_{\mathrm{a}}\cdot\boldsymbol{F}_{\mathrm{a}} \doteq -\,\mathrm{D}_t\lambda\,\boldsymbol{F}_{\mathrm{a}}\cdot\bar{\boldsymbol{\nu}}_{\mathrm{a}}\,, \tag{4.24}$$

whereby proportional hardening contribution have been omitted for the sake of brevity, we obtain

$$\begin{aligned} \boldsymbol{R}_{\mathrm{p}}(\boldsymbol{f}_{\mathrm{p}},\boldsymbol{f}_{\mathrm{k}},\boldsymbol{f}_{\mathrm{a}},\widetilde{\Delta\lambda};\boldsymbol{C}) &= \boldsymbol{I}_{\mathrm{p}} - \widetilde{\boldsymbol{F}}_{\mathrm{p}}\cdot\boldsymbol{f}_{\mathrm{p}} - \widetilde{\Delta\lambda}\,\widehat{\boldsymbol{\nu}}_{\mathrm{p}}(\boldsymbol{f}_{\mathrm{p}},\boldsymbol{f}_{\mathrm{k}},\boldsymbol{f}_{\mathrm{a}};\boldsymbol{C})\,, \\ \boldsymbol{R}_{\mathrm{k}}(\boldsymbol{f}_{\mathrm{p}},\boldsymbol{f}_{\mathrm{k}},\boldsymbol{f}_{\mathrm{a}},\widetilde{\Delta\lambda};\boldsymbol{C}) &= \boldsymbol{I}_{\mathrm{p}} - \widetilde{\boldsymbol{F}}_{\mathrm{k}}\cdot\boldsymbol{f}_{\mathrm{k}} - \widetilde{\Delta\lambda}\,\widehat{\boldsymbol{\nu}}_{\mathrm{k}}(\boldsymbol{f}_{\mathrm{p}},\boldsymbol{f}_{\mathrm{k}},\boldsymbol{f}_{\mathrm{a}};\boldsymbol{C})\,, \\ \boldsymbol{R}_{\mathrm{a}}(\boldsymbol{f}_{\mathrm{p}},\boldsymbol{f}_{\mathrm{k}},\boldsymbol{f}_{\mathrm{a}},\widetilde{\Delta\lambda};\boldsymbol{C}) &= \boldsymbol{I}_{\mathrm{a}} - \boldsymbol{f}_{\mathrm{a}}\cdot\widetilde{\boldsymbol{F}}_{\mathrm{a}} + \widetilde{\Delta\lambda}\,\bar{\boldsymbol{\nu}}_{\mathrm{a}}(\boldsymbol{f}_{\mathrm{p}},\boldsymbol{f}_{\mathrm{k}},\boldsymbol{f}_{\mathrm{a}};\boldsymbol{C})\,, \end{aligned} \tag{4.25}$$

together with the Kuhn–Tucker conditions

$$\widetilde{\Delta\lambda} \geq 0\,, \qquad \Phi^{\mathrm{yie}} \leq 0\,, \qquad \widetilde{\Delta\lambda}\,\Phi^{\mathrm{yie}} = 0 \tag{4.26}$$

with $\widetilde{\Delta\lambda} \equiv \widetilde{\Delta t}\,\mathrm{D}_t\lambda$. As previously mentioned, viscous response can be included if the plastic multiplier is directly determined from $\widetilde{\Delta\lambda} = \widetilde{\Delta t}\,\eta(\Phi^{\mathrm{yie}})/t^*$.

However, setting $\beta_1 \doteq 0\ \forall\ \Delta t$ results in $\beta_2 = 1$ so that $\widetilde{\Delta t} = \Delta t$ and $\widetilde{\Delta\lambda} = \Delta\lambda = \Delta t\,\mathrm{D}_t\lambda$. Apparently, one obtains a single step algorithm which equals the classical implicit EB integration scheme. This enables us to easily switch between BDF2 and EB by solely minor changes in the computer code. Please note that the EB algorithm requires less additional data storage as compared to the BDF2 scheme (as well as to any other higher–order multi–step scheme).

Remark 4.3.1 *It is noted that the system of non–linear equations in eq.(4.25) can be reduced to a smaller system of non–linear equations by rephrasing them in terms of the symmetric tensors $\widehat{\boldsymbol{C}}_{\mathrm{e}}$ and $\widehat{\boldsymbol{K}}$ instead of the in general non–symmetric quantities $\boldsymbol{f}_{\mathrm{p}}$ and $\boldsymbol{f}_{\mathrm{k}}$. By doing so, however, the degree of non–linearity of the system of equations increases.*

4.3.1 Solution strategies

For inelastic loading processes, i.e. $\Delta\lambda > 0$, the system of non–linear equations (4.25,4.26) can be summarised as

$$\mathbf{R}(\mathbf{X},\widetilde{\Delta\lambda};\boldsymbol{C}) = \mathbf{0} \quad \text{and} \quad \mathrm{R}_\lambda(\mathbf{X};\boldsymbol{C}) = 0 \quad \text{or} \quad \mathbf{R}_{\mathrm{tot}}(\mathbf{X}_{\mathrm{tot}};\boldsymbol{C}) = \mathbf{0}\,, \tag{4.27}$$

wherein the abbreviations

$$\begin{aligned} \mathbf{R} \;&=\; [\,\boldsymbol{R}_{\mathrm{p}},\boldsymbol{R}_{\mathrm{k}},\boldsymbol{R}_{\mathrm{a}}\,]^{\mathrm{t}}\,, \qquad \mathbf{R}_{\mathrm{tot}} \;=\; [\,\boldsymbol{R}_{\mathrm{p}},\boldsymbol{R}_{\mathrm{k}},\boldsymbol{R}_{\mathrm{a}},R_\lambda\,]^{\mathrm{t}}\,, \\ \mathbf{X} \;&=\; [\,\boldsymbol{f}_{\mathrm{p}},\boldsymbol{f}_{\mathrm{k}},\boldsymbol{f}_{\mathrm{a}}\,]^{\mathrm{t}}\,, \qquad \mathbf{X}_{\mathrm{tot}} \;=\; [\,\boldsymbol{f}_{\mathrm{p}},\boldsymbol{f}_{\mathrm{k}},\boldsymbol{f}_{\mathrm{a}},\widetilde{\Delta\lambda}\,]^{\mathrm{t}} \end{aligned} \tag{4.28}$$

have been introduced. Furthermore, the unbalance R_λ corresponds to $\mathrm{R}_\lambda = \Phi^{\mathrm{yie}}$ for a rate–independent model and $\mathrm{R}_\lambda = t^*\,\widetilde{\Delta\lambda} - \widetilde{\Delta t}\,\eta$ for a rate–dependent model, respectively.

4.3.1.1 Newton type techniques

Different techniques can be applied in order to compute the solution $\mathbf{X}_{\mathrm{tot}}$ of $\mathbf{R}_{\mathrm{tot}} = \mathbf{0}$; see, for instance, the monograph by Engeln–Müllges and Uhlig (1996) where several appropriate algorithms are described. Apparently, Newton's method constitutes a standard approach, which has also been adopted in section 4.2.2, where $\mathbf{X}_{\mathrm{tot}}$ is iteratively updated (index (k)). The subsequent Newton algorithm 4.2 also includes a 'simple' line search (parameter α) and as such generalises algorithm 4.1.

Algorithm 4.2 *Monolithic solution technique: Newton algorithm including a 'simple' line search to solve the set of nonlinear equations for* $\boldsymbol{F}_{\mathrm{p}}^{n+1}$, $\boldsymbol{F}_{\mathrm{k}}^{n+1}$, $\boldsymbol{F}_{\mathrm{a}}^{n+1}$ *and* $\Delta\lambda$.

finite element method — **for** given $\boldsymbol{F}^{n+1}$, $\boldsymbol{F}_{\mathrm{p}}^{n}$, $\boldsymbol{F}_{\mathrm{k}}^{n}$, $\boldsymbol{F}_{\mathrm{a}}^{n}$ **do**

if $\Phi^{\mathrm{yie}} > 0$ **then**

Newton iteration — **dowhile** $\|\mathbf{R}_{\mathrm{tot}}^{(k)}\| > \mathrm{tol}$

$\mathbf{X}_{\mathrm{tot}}^{(k+1)} = \mathbf{X}_{\mathrm{tot}}^{(k)} - \left[\mathbf{J}_{\mathrm{tot}}^{(k)}\right]^{-1} \circ \mathbf{R}_{\mathrm{tot}}^{(k)}$

$\alpha = 1$

'simple' line search — **dowhile** $\|\mathbf{R}_{\mathrm{tot}}(\mathbf{X}_{\mathrm{tot}}^{(k+1)})\| > \|\mathbf{R}_{\mathrm{tot}}^{(k)}\|$

$\alpha \hookleftarrow 0.7\,\alpha$

$\mathbf{X}_{\mathrm{tot}}^{(k+1)} = \mathbf{X}_{\mathrm{tot}}^{(k)} - \alpha \left[\mathbf{J}_{\mathrm{tot}}^{(k)}\right]^{-1} \circ \mathbf{R}_{\mathrm{tot}}^{(k)}$

enddo

$k \hookleftarrow k + 1$

enddo

endif

The iteration matrix is commonly identified with the Jacobian $\mathbf{J}_{\mathrm{tot}}^{(k)} = \partial\mathbf{R}_{\mathrm{tot}}^{(k)}/\partial\mathbf{X}_{\mathrm{tot}}^{(k)}$ which turns out to be non–symmetric for the problem at hand. Furthermore, the notation $\circ$ characterises the appropriate contraction. In the sequel, we discuss three possible alternatives of how the iteration matrix $\mathbf{J}_{\mathrm{tot}}$ can be chosen:

Method 1 The iteration matrix is chosen as the analytically derived Jacobian

$$\mathbf{J}_{\mathrm{tot}}^{(k)} = \frac{\partial \mathbf{R}_{\mathrm{tot}}^{(k)}}{\partial \mathbf{X}_{\mathrm{tot}}^{(k)}} \,. \tag{4.29}$$

Essential expression for the derivation of this Jacobian within the later on chosen prototype model are summarised in appendix D.

Method 2 The iteration matrix is chosen as the approximate Jacobian via a first–order difference scheme for every entry $\mathrm{R}_{\mathrm{tot}\,i}^{(k)}$ in $\mathbf{R}_{\mathrm{tot}}^{(k)} \equiv \left[\,\mathrm{R}_{\mathrm{tot}\,1}^{(k)}, \ldots, \mathrm{R}_{\mathrm{tot}\,i}^{(k)}, \ldots, \mathrm{R}_{\mathrm{tot}\,28}^{(k)}\,\right]$ and $\mathrm{X}_{\mathrm{tot}\,j}^{(k)}$ in $\mathbf{X}_{\mathrm{tot}}^{(k)} \equiv \left[\,\mathrm{X}_{\mathrm{tot}\,1}^{(k)}, \ldots, \mathrm{X}_{\mathrm{tot}\,j}^{(k)}, \ldots, \mathrm{X}_{\mathrm{tot}\,28}^{(k)}\,\right]$ within each iteration step k:

$$\mathrm{J}_{\mathrm{tot}\,ij}^{(k)} \approx \frac{\mathrm{R}_{\mathrm{tot}\,i}^{(k)}\left(\left[\,\mathrm{X}_{\mathrm{tot}\,1}^{(k)}, \ldots, \mathrm{X}_{\mathrm{tot}\,j}^{(k)} + \varepsilon, \ldots, \mathrm{X}_{\mathrm{tot}\,28}^{(k)}\,\right]\right) - \mathrm{R}_{\mathrm{tot}\,i}^{(k)}\left(\mathbf{X}_{\mathrm{tot}}^{(k)}\right)}{\varepsilon} \,. \tag{4.30}$$

The optimal choice of the perturbation parameter $\varepsilon \ll 1$ depends on the machine precision. For a general outline on this and on other approximation schemes of higher–order, we refer the reader to the monograph by Dennis and Schnabel (1996); see also the contributions by Miehe (1996b), Menzel and Steinmann (2003b), Pérez–Foguet et al. (2000a, 2000b), or Fellin and Ostermann (2002) where a small strain setting is addressed.

Method 3 The iteration matrix is computed by means of method 1 or method 2 for $k = 1$ and from then on, $k > 1$, according to the Broyden update:

$$\Big[\mathbf{J}_{\text{tot}}^{(k)}\Big]^{-1} \approx \Big[\mathbf{J}_{\text{tot}}^{(k-1)}\Big]^{-1} + \frac{\Big[\boldsymbol{\Xi}_{\text{tot}} - \Big[\mathbf{J}_{\text{tot}}^{(k-1)}\Big]^{-1} \circ \boldsymbol{\Gamma}_{\text{tot}}\Big] \circ \boldsymbol{\Xi}^{\text{t}}}{\boldsymbol{\Xi}_{\text{tot}}^{\text{t}} \circ \Big[\mathbf{J}_{\text{tot}}^{(k-1)}\Big]^{-1} \circ \boldsymbol{\Gamma}_{\text{tot}}} \Big[\mathbf{J}_{\text{tot}}^{(k-1)}\Big]^{-1} \tag{4.31}$$

with $\boldsymbol{\Xi}_{\text{tot}} = \mathbf{X}_{\text{tot}}^{(k)} - \mathbf{X}_{\text{tot}}^{(k-1)}$ and $\boldsymbol{\Gamma}_{\text{tot}} = \mathbf{R}_{\text{tot}}^{(k)} - \mathbf{R}_{\text{tot}}^{(k-1)}$. The Broyden update gives a non–symmetric iteration matrix, as the Jacobian is for the problem at hand, while a corresponding BFGS method is designed for problems with symmetric Jacobians; compare for instance Engelman et al. (1981).

Apparently, methods 1–3 nicely fit into the monolithic algorithm 4.2 described above; that is, we solve for all unknowns at the same time. Alternatively, a staggered Newton iteration scheme could be chosen, see Johansson et al. (1999), or as we shall discuss in the sequel a staggered iteration technique combining fixed–point and quasi–Newton iterations.

4.3.1.2 Staggered iteration technique

The subsequently highlighted algorithm 4.3 will in the following be referred to as

Method 4 and is an example of a staggered iteration technique, where we combine a fixed–point procedure (index (l)) together with a quasi–Newton scheme (regula falsi, index (k)) for the plastic multiplier. Apparently, the essential idea of this particular algorithm 4.3 consists in performing simple updates instead of elaborated iterations.

This approach, which seems to be new in the present context, turns out to be a computationally very efficient algorithm. An alternative update procedure is developed in Johansson et al. (1999) where, however, all the components of the Jacobian must be computed. Owing to this, that algorithm is not considered here.

Remark 4.3.2 *When applying the presented constitutive framework within an implicit finite element context, one commonly also adopts a Newton scheme for the global system of non–linear equations; compare section 4.2.2. The underlying 'global' Jacobian or rather the algorithmic tangent operator is thereby defined via, for instance,*

$$\mathsf{E}_{\text{alg}} = 2\,\frac{\mathrm{d}\boldsymbol{S}_{\text{e}}}{\mathrm{d}\boldsymbol{C}} \quad \textit{with} \quad \boldsymbol{S}_{\text{e}} = \boldsymbol{f}_{\text{p}} \cdot \widehat{\boldsymbol{S}}_{\text{e}}\big(\boldsymbol{A}_{\text{p}}(\boldsymbol{F}_{\text{a}}), \widehat{\boldsymbol{C}}_{\text{e}}(\boldsymbol{f}_{\text{p}}, \boldsymbol{C})\big) \cdot \boldsymbol{f}_{\text{p}}^{\text{d}} \tag{4.32}$$

and $\widehat{\boldsymbol{S}}_{\text{e}} = \widehat{\boldsymbol{B}}_{\text{e}} \cdot \widehat{\boldsymbol{M}}_{\text{e}}^{\text{d}}$. *Based on these relations, straightforward computations yield*

$$\frac{\mathrm{d}\boldsymbol{S}_{\text{e}}}{\mathrm{d}\boldsymbol{C}} = \frac{\partial \boldsymbol{S}_{\text{e}}}{\partial \widehat{\boldsymbol{S}}_{\text{e}}} : \left[\frac{\partial \widehat{\boldsymbol{S}}_{\text{e}}}{\partial \boldsymbol{F}_{\text{a}}} : \frac{\mathrm{d}\boldsymbol{F}_{\text{a}}}{\mathrm{d}\boldsymbol{C}} + \frac{\partial \widehat{\boldsymbol{S}}_{\text{e}}}{\partial \widehat{\boldsymbol{C}}_{\text{e}}} : \left[\frac{\partial \widehat{\boldsymbol{C}}_{\text{e}}}{\partial \boldsymbol{f}_{\text{p}}} : \frac{\mathrm{d}\boldsymbol{f}_{\text{p}}}{\mathrm{d}\boldsymbol{C}} + \frac{\partial \widehat{\boldsymbol{C}}_{\text{e}}}{\partial \boldsymbol{C}}\right]\right] + \frac{\partial \boldsymbol{S}_{\text{e}}}{\partial \boldsymbol{f}_{\text{p}}} : \frac{\mathrm{d}\boldsymbol{f}_{\text{p}}}{\mathrm{d}\boldsymbol{C}} \,. \tag{4.33}$$

The total derivatives $\mathrm{d}\boldsymbol{F}_{\text{a}}/\mathrm{d}\boldsymbol{C}$, $\mathrm{d}\boldsymbol{f}_{\text{p}}/\mathrm{d}\boldsymbol{C}$ *can be obtained from* $\mathbf{R}_{\text{tot}}(\mathbf{X}_{\text{tot}}; \boldsymbol{C}) = \mathbf{0}\ \forall\, \boldsymbol{C}$ *with*

$$\frac{\mathrm{d}\mathbf{R}_{\text{tot}}}{\mathrm{d}\boldsymbol{C}} = \frac{\partial \mathbf{R}_{\text{tot}}}{\partial \mathbf{X}_{\text{tot}}} \odot \frac{\mathrm{d}\mathbf{X}_{\text{tot}}}{\mathrm{d}\boldsymbol{C}} + \frac{\partial \mathbf{R}_{\text{tot}}}{\partial \boldsymbol{C}} = \mathbf{0} \quad \textit{and} \quad \frac{\mathrm{d}\mathbf{X}_{\text{tot}}}{\mathrm{d}\boldsymbol{C}} = -\Big[\mathbf{J}_{\text{tot}}\Big]^{-1} \odot \frac{\partial \mathbf{R}_{\text{tot}}}{\partial \boldsymbol{C}} \,. \tag{4.34}$$

From this we observe that the properties of the local iteration algorithm might also influence the efficiency of the global finite element algorithm. Consequently, for methods that use the exact or an approximation of the Jacobian $\mathbf{J}_{\mathrm{tot}}$ *during the local iterations, we can conveniently compute at least a good estimate of* $\mathsf{E}_{\mathrm{alg}}$*. This is not the case for the staggered iteration technique. A possibility for this case is to apply numerical differentiation in the first iteration followed by Broyden updates to obtain approximations of* $\mathsf{E}_{\mathrm{alg}}$*. Concerning comparisons of efficiency, however, we solely focus on the local constitutive problem itself in this chapter.*

Algorithm 4.3 *Staggered solution technique: fixed–point procedure to solve the set of nonlinear equations for* $\boldsymbol{F}_{\mathrm{p}}^{n+1}$, $\boldsymbol{F}_{\mathrm{k}}^{n+1}$, $\boldsymbol{F}_{\mathrm{a}}^{n+1}$ *combined with a regula falsi scheme* $\Delta\lambda$*.*

finite element method — **for** given $\boldsymbol{F}^{n+1}$, $\boldsymbol{F}_{\mathrm{p}}^{n}$, $\boldsymbol{F}_{\mathrm{k}}^{n}$, $\boldsymbol{F}_{\mathrm{a}}^{n}$ **do**

if $\Phi^{\mathrm{yie}} > 0$ **then**

set $\widetilde{\Delta\lambda} = \Delta\lambda^{n}$ and $\widehat{\boldsymbol{\nu}}_{\mathrm{p,k,a}} = \widehat{\boldsymbol{\nu}}_{\mathrm{p,k,a}}^{n}$

regula falsi iteration — **dowhile** $|R_{\lambda}^{(k)}| > \mathrm{tol}$

fixed–point iteration — **dowhile** $\|\Delta\widehat{\boldsymbol{\nu}}_{\mathrm{p}}\| + \|\Delta\widehat{\boldsymbol{\nu}}_{\mathrm{k}}\| + \|\Delta\widehat{\boldsymbol{\nu}}_{\mathrm{a}}\| > \mathrm{tol}$

$$\boldsymbol{f}_{\mathrm{p}}^{(l+1)} = \widetilde{\boldsymbol{f}}_{\mathrm{p}} \cdot \left[\, \boldsymbol{I}_{\mathrm{p}} - \widetilde{\Delta\lambda}\, \widehat{\boldsymbol{\nu}}_{\mathrm{p}}^{(l)} \,\right]$$

$$\boldsymbol{f}_{\mathrm{k}}^{(l+1)} = \widetilde{\boldsymbol{f}}_{\mathrm{k}} \cdot \left[\, \boldsymbol{I}_{\mathrm{p}} - \widetilde{\Delta\lambda}\, \widehat{\boldsymbol{\nu}}_{\mathrm{k}}^{(l)} \,\right]$$

$$\boldsymbol{f}_{\mathrm{a}}^{(l+1)} = \left[\, \boldsymbol{I}_{\mathrm{a}} + \widetilde{\Delta\lambda}\, \widehat{\boldsymbol{\nu}}_{\mathrm{a}}^{(l)} \,\right] \cdot \widetilde{\boldsymbol{f}}_{\mathrm{a}}$$

$$\Delta\widehat{\boldsymbol{\nu}}_{\mathrm{p,k,a}} = \widehat{\boldsymbol{\nu}}_{\mathrm{p,k,a}}\big(\boldsymbol{f}_{\mathrm{p,k,a}}^{(l+1)}\big) - \widehat{\boldsymbol{\nu}}_{\mathrm{p,k,a}}^{(l)}$$

$$l \hookleftarrow l + 1$$

enddo

$$\widetilde{\Delta\lambda}^{(k+1)} = \widetilde{\Delta\lambda}^{(k)} - \frac{\widetilde{\Delta\lambda}^{(k)} - \widetilde{\Delta\lambda}^{(k-1)}}{R_{\lambda}^{(k)} - R_{\lambda}^{(k-1)}}\, R_{\lambda}^{(k)}$$

$$k \hookleftarrow k + 1$$

enddo

endif

4.4 Fictitious configuration concept

In the sequel, we give a detailed outline of how the introduced fictitious configurations or rather the corresponding linear tangent maps shape the proposed formulation. The damage mapping $\boldsymbol{F}_{\mathrm{a}}$ thereby defines an energy metric with respect to the stress–free intermediate configuration of multiplicative elastoplasticity, namely $\boldsymbol{A}_{\mathrm{p}} = \boldsymbol{F}_{\mathrm{a}} \star \boldsymbol{G}_{\mathrm{a}}^{-1} : T^{*}\mathcal{B}_{\mathrm{p}} \rightarrow T\mathcal{B}_{\mathrm{p}}$. Conceptually speaking, we deal with an Euclidian geometry which is based on a non–constant and possibly non–spherical metric that accounts for both anisotropy and degradation.

4.4.1 Helmholtz free energy density

The introduction of the Helmholtz free energy density was essentially based on an additive decomposition $\psi_0 \doteq \psi_0^{\mathrm{e}} + \psi_0^{\mathrm{k}} + \psi_0^{\kappa}$. By analogy with section 3.3, application of the general

covariance principle, or rather adopting the concept of strain energy equivalence, enables us to give the following representation

$$\begin{aligned}\psi_0 &= \psi_0^{\mathrm{e}}(\bar{\boldsymbol{E}}_{\mathrm{e}}, \boldsymbol{G}_{\mathrm{a}}^{-1}; \boldsymbol{X}) + \psi_0^{\mathrm{k}}(\bar{\boldsymbol{E}}_{\mathrm{k}}, \boldsymbol{G}_{\mathrm{a}}^{-1}; \boldsymbol{X}) + \psi_0^{\kappa}(\kappa; \boldsymbol{X}) \\ &= \psi_0^{\mathrm{e}}(\widehat{\boldsymbol{E}}_{\mathrm{e}}, \boldsymbol{A}_{\mathrm{p}}; \boldsymbol{X}) + \psi_0^{\mathrm{k}}(\widehat{\boldsymbol{E}}_{\mathrm{k}}, \boldsymbol{A}_{\mathrm{p}}; \boldsymbol{X}) + \psi_0^{\kappa}(\kappa; \boldsymbol{X})\,.\end{aligned} \tag{4.35}$$

We restrict ourselves to an outline with respect to the intermediate and the, say, effective configuration, since transformations to other configurations are straightforward. As the key idea of the proposed framework, the fictitious configuration is assumed to represent an initially isotropic setting such that we consequently obtain a set of only three invariants for each of the contributions ψ_0^{e} and ψ_0^{k}, i.e.

$$\begin{aligned}I_{\mathrm{e}\,i} &= \boldsymbol{I}_{\mathrm{a}} : [\,\bar{\boldsymbol{E}}_{\mathrm{e}} \cdot \boldsymbol{G}_{\mathrm{a}}^{-1}\,]^i = \boldsymbol{I}_{\mathrm{p}} : [\,\widehat{\boldsymbol{E}}_{\mathrm{e}} \cdot \boldsymbol{A}_{\mathrm{p}}\,]^i\,, \\ I_{\mathrm{k}\,i} &= \boldsymbol{I}_{\mathrm{a}} : [\,\bar{\boldsymbol{E}}_{\mathrm{k}} \cdot \boldsymbol{G}_{\mathrm{a}}^{-1}\,]^i = \boldsymbol{I}_{\mathrm{p}} : [\,\widehat{\boldsymbol{E}}_{\mathrm{k}} \cdot \boldsymbol{A}_{\mathrm{p}}\,]^i\end{aligned} \tag{4.36}$$

with $i = 1, 2, 3$. Based on this, we observe from eq.(4.14) that the Mandel–type stress tensors possess the relations

$$\begin{aligned}\widehat{\boldsymbol{M}}_{\mathrm{e}}^{\mathrm{d}} &= \sum_{i=1}^{3} i \quad \partial_{I_{\mathrm{e}\,i}} \psi_0^{\mathrm{e}}\, \widehat{\boldsymbol{C}}_{\mathrm{e}} \cdot \boldsymbol{A}_{\mathrm{p}} \cdot [\,\widehat{\boldsymbol{E}}_{\mathrm{e}} \cdot \boldsymbol{A}_{\mathrm{p}}\,]^{i-1}\,, \\ \widehat{\boldsymbol{M}}_{\mathrm{k}}^{\mathrm{d}} &= \sum_{i=1}^{3} i \quad \partial_{I_{\mathrm{k}\,i}} \psi_0^{\mathrm{k}}\, \widehat{\boldsymbol{K}} \cdot \boldsymbol{A}_{\mathrm{p}} \cdot [\,\widehat{\boldsymbol{E}}_{\mathrm{k}} \cdot \boldsymbol{A}_{\mathrm{p}}\,]^{i-1}\,, \\ \widehat{\boldsymbol{M}}_{\mathrm{a}}^{\mathrm{d}} &= 2 \sum_{i=1}^{3} i \,\big[\, \partial_{I_{\mathrm{e}\,i}} \psi_0^{\mathrm{e}} [\,\widehat{\boldsymbol{E}}_{\mathrm{e}} \cdot \boldsymbol{A}_{\mathrm{p}}\,]^i + \partial_{I_{\mathrm{k}\,i}} \psi_0^{\mathrm{k}} [\,\widehat{\boldsymbol{E}}_{\mathrm{k}} \cdot \boldsymbol{A}_{\mathrm{p}}\,]^i \,\big] \\ &= 2\, \widehat{\boldsymbol{E}}_{\mathrm{e}} \cdot \widehat{\boldsymbol{B}}_{\mathrm{e}} \cdot \widehat{\boldsymbol{M}}_{\mathrm{e}}^{\mathrm{d}} + 2\, \widehat{\boldsymbol{E}}_{\mathrm{k}} \cdot \widehat{\boldsymbol{K}}^{-1} \cdot \widehat{\boldsymbol{M}}_{\mathrm{k}}^{\mathrm{d}}\end{aligned} \tag{4.37}$$

and satisfy the following symmetry properties

$$\widehat{\boldsymbol{M}}_{\mathrm{e}}^{\mathrm{d}} \cdot \widehat{\boldsymbol{C}}_{\mathrm{e}} = \widehat{\boldsymbol{C}}_{\mathrm{e}} \cdot \widehat{\boldsymbol{M}}_{\mathrm{e}}\,, \qquad \widehat{\boldsymbol{M}}_{\mathrm{k}}^{\mathrm{d}} \cdot \widehat{\boldsymbol{K}} = \widehat{\boldsymbol{K}} \cdot \widehat{\boldsymbol{M}}_{\mathrm{k}}\,, \qquad \boldsymbol{A}_{\mathrm{p}} \cdot \widehat{\boldsymbol{M}}_{\mathrm{a}}^{\mathrm{d}} = \widehat{\boldsymbol{M}}_{\mathrm{a}} \cdot \boldsymbol{A}_{\mathrm{p}}\,. \tag{4.38}$$

It turns out that the underlying kinematic assumptions, i.e. the affine pre–deformation characterised by $\boldsymbol{F}_{\mathrm{a}}$, result either in an isotropic setting or subclasses of transversal or orthotropic symmetry. It is obvious, that the contribution $\psi_0^{\kappa}(\kappa; \boldsymbol{X})$ is not affected by the fictitious configuration concept, since only scalar–valued arguments are incorporated.

Remark 4.4.1 *Even for isotropic or rather proportional hardening, which is represented in the proposed formulation by the scalar–valued internal variable κ, one could alternatively introduce a tensorial quantity of second–order, see Menzel et al. (2002).*

Remark 4.4.2 *The elastic second Piola–Kirchhoff–type stresses are defined via $\widehat{\boldsymbol{S}}_{\mathrm{e}} \doteq \partial_{\widehat{\boldsymbol{E}}_{\mathrm{e}}} \psi_0^{\mathrm{e}} = \widehat{\boldsymbol{B}}_{\mathrm{e}} \cdot \widehat{\boldsymbol{M}}_{\mathrm{e}}^{\mathrm{d}}$ and $\bar{\boldsymbol{S}}_{\mathrm{e}} = \boldsymbol{f}_{\mathrm{a}} \star \widehat{\boldsymbol{S}}_{\mathrm{e}} = \boldsymbol{f}_{\mathrm{a}} \cdot \widehat{\boldsymbol{S}}_{\mathrm{e}} \cdot \boldsymbol{f}_{\mathrm{a}}^{\mathrm{d}}$, respectively. In view of the kinematic hardening contribution, we similarly introduce the stress tensors $\widehat{\boldsymbol{S}}_{\mathrm{k}} \doteq \partial_{\widehat{\boldsymbol{E}}_{\mathrm{k}}} \psi_0^{\mathrm{k}} = \widehat{\boldsymbol{K}}^{-1} \cdot \widehat{\boldsymbol{M}}_{\mathrm{k}}^{\mathrm{d}}$ and $\bar{\boldsymbol{S}}_{\mathrm{k}} = \boldsymbol{f}_{\mathrm{a}} \star \widehat{\boldsymbol{S}}_{\mathrm{k}} = \boldsymbol{f}_{\mathrm{a}} \cdot \widehat{\boldsymbol{S}}_{\mathrm{k}} \cdot \boldsymbol{f}_{\mathrm{a}}^{\mathrm{d}}$. The Cauchy stress however, which enters the spatial balance of linear momentum format, is obtained from eq.(4.37) via pushforward operation, i.e. $\boldsymbol{\sigma}_{\mathrm{e}} = j\, \boldsymbol{F}_{\mathrm{e}} \star \widehat{\boldsymbol{S}}_{\mathrm{e}} = j \sum_{i=1}^{3} i\, \partial_{I_{\mathrm{e}\,i}} \psi_0^{\mathrm{e}}\, \boldsymbol{A}_t \cdot [\,\boldsymbol{e}_{\mathrm{e}} \cdot \boldsymbol{A}_t\,]^{i-1}$ introducing the spatial energy metric $\boldsymbol{A}_t = \boldsymbol{F}_{\mathrm{e}} \star \boldsymbol{A}_{\mathrm{p}} = \boldsymbol{F}_{\mathrm{e}} \cdot \boldsymbol{A}_{\mathrm{p}} \cdot \boldsymbol{F}_{\mathrm{e}}^{\mathrm{d}}$ and the Almansi–type elastic strain measure $\boldsymbol{e}_{\mathrm{e}} = \boldsymbol{F}_{\mathrm{e}} \star \widehat{\boldsymbol{E}}_{\mathrm{e}} = \frac{1}{2}[\,\boldsymbol{g} - \boldsymbol{c}_{\mathrm{e}}\,]$. The corresponding definition of the deviatoric Cauchy stress reads $\boldsymbol{\sigma}_{\mathrm{e}}^{\mathrm{dev}} \doteq \boldsymbol{\sigma}_{\mathrm{e}} - \frac{1}{3}[\,\boldsymbol{g} : \boldsymbol{\sigma}_{\mathrm{e}}\,]\,\boldsymbol{g}^{-1}$ (note that the spatial format of the incorporated invariants results in $I_{\mathrm{e}\,i} = \boldsymbol{I}_t : [\,\boldsymbol{e}_{\mathrm{e}} \cdot \boldsymbol{A}_t\,]^i$ with $i = 1, 2, 3$).*

4.4.2 Damage potential

The same covariance concept is now adopted for the damage potential, i.e. we assume ${}^{\mathrm{dam}}\Phi(\bar{\boldsymbol{M}}^{\mathrm{d}}_{\mathrm{a}};\boldsymbol{X}) \doteq {}^{\mathrm{dam}}\Phi(\widehat{\boldsymbol{M}}^{\mathrm{d}}_{\mathrm{a}};\boldsymbol{X})$ with

$$\begin{aligned}\bar{\boldsymbol{M}}^{\mathrm{d}}_{\mathrm{a}} &= \boldsymbol{f}_{\mathrm{a}} \star \widehat{\boldsymbol{M}}^{\mathrm{d}}_{\mathrm{a}} = \boldsymbol{F}^{\mathrm{d}}_{\mathrm{a}} \cdot \widehat{\boldsymbol{M}}^{\mathrm{d}}_{\mathrm{a}} \cdot \boldsymbol{f}^{\mathrm{d}}_{\mathrm{a}} = 2\,\partial_{\boldsymbol{G}^{-1}_{\mathrm{a}}}[\,\psi^{\mathrm{e}}_0 + \psi^{\mathrm{k}}_0\,] \cdot \boldsymbol{G}^{-1}_{\mathrm{a}} \\ &= 2\sum_{i=1}^{3} i\,\big[\,\partial_{I_{\mathrm{e}\,i}}\psi^{\mathrm{e}}_0[\,\bar{\boldsymbol{E}}_{\mathrm{e}} \cdot \boldsymbol{G}^{-1}_{\mathrm{a}}\,]^i + \partial_{I_{\mathrm{k}\,i}}\psi^{\mathrm{k}}_0[\,\bar{\boldsymbol{E}}_{\mathrm{k}} \cdot \boldsymbol{G}^{-1}_{\mathrm{a}}\,]^i\,\big]\,,\end{aligned} \tag{4.39}$$

compare eq.(4.14). By analogy with the fictitious configuration representing an initially isotropic setting, let the damage potential be determined via the following three invariants

$$I_{\mathrm{a}\,i} = \boldsymbol{I}_{\mathrm{a}} : [\,2\,\partial_{\boldsymbol{G}^{-1}_{\mathrm{a}}}\psi \cdot \boldsymbol{G}^{-1}_{\mathrm{a}}\,]^i = \boldsymbol{I}_{\mathrm{a}} : [\,\bar{\boldsymbol{M}}^{\mathrm{d}}_{\mathrm{a}}\,]^i = \boldsymbol{I}_{\mathrm{p}} : [\,\widehat{\boldsymbol{M}}^{\mathrm{d}}_{\mathrm{a}}\,]^i = \boldsymbol{I}_{\mathrm{p}} : [\,2\,\partial_{\boldsymbol{A}_{\mathrm{p}}}\psi \cdot \boldsymbol{A}_{\mathrm{p}}\,]^i \tag{4.40}$$

with $i = 1,2,3$. Conceptually speaking, the definition of these invariants is based on a symmetric stress field ($2\,\partial_{\boldsymbol{G}^{-1}_{\mathrm{a}}}[\,\psi^{\mathrm{e}}_0 + \psi^{\mathrm{k}}_0\,]$ and $2\,\partial_{\boldsymbol{A}_{\mathrm{p}}}[\,\psi^{\mathrm{e}}_0 + \psi^{\mathrm{k}}_0\,]$) with respect to the appropriate metric ($\boldsymbol{G}^{-1}_{\mathrm{a}}$ and $\boldsymbol{A}_{\mathrm{p}}$). We consequently obtain for the related flow direction

$$\widehat{\boldsymbol{\nu}}_{\mathrm{a}} = \sum_{i=1}^{3} i\,\partial_{I_{\mathrm{a}\,i}}{}^{\mathrm{dam}}\Phi\,[\,\widehat{\boldsymbol{M}}_{\mathrm{a}}\,]^{i-1} = \sum_{i=1}^{3} i\,\partial_{I_{\mathrm{a}\,i}}{}^{\mathrm{dam}}\Phi\,\big[\,2\,\boldsymbol{A}_{\mathrm{p}} \cdot \partial_{\boldsymbol{A}_{\mathrm{p}}}[\,\psi^{\mathrm{e}}_0 + \psi^{\mathrm{k}}_0\,]\,\big]^{i-1} \tag{4.41}$$

which results in connection with eqs.(4.12, 4.17) in the following remarkable result

$$\begin{aligned}\mathrm{D}_t\boldsymbol{A}_{\mathrm{p}} &= \quad 2\,[\,\widehat{\boldsymbol{L}}_{\mathrm{a}} \cdot \boldsymbol{A}_{\mathrm{p}}\,]^{\mathrm{sym}} = \quad 2\,\widehat{\boldsymbol{L}}_{\mathrm{a}} \cdot \boldsymbol{A}_{\mathrm{p}} \\ &= -\,2\,\mathrm{D}_t\lambda\,\widehat{\boldsymbol{\nu}}_{\mathrm{a}} \cdot \boldsymbol{A}_{\mathrm{p}} = -\,2\,\mathrm{D}_t\lambda \sum_{i=1}^{3} i\,\partial_{I_{\mathrm{a}\,i}}{}^{\mathrm{dam}}\Phi\;\boldsymbol{A}_{\mathrm{p}} \cdot [\,\widehat{\boldsymbol{M}}^{\mathrm{d}}_{\mathrm{a}}\,]^{i-1}\,.\end{aligned} \tag{4.42}$$

Practically speaking, the covariance principle in the present context yields $\widehat{\boldsymbol{L}}_{\mathrm{a}}$ to be generally symmetric with respect to $\boldsymbol{A}_{\mathrm{p}}$. Next, applying pullback operations to the damage contributions in the dissipation inequality (4.11,4.13) with respect to the fictitious configuration leads to

$$\begin{aligned}&\partial_{\boldsymbol{A}_{\mathrm{p}}}\psi_0 : \mathrm{D}_t\boldsymbol{A}_{\mathrm{p}} = \partial_{\boldsymbol{G}^{-1}_{\mathrm{a}}}\psi_0 : \mathrm{l}^{\mathrm{a}}_t\,\boldsymbol{G}^{-1}_{\mathrm{a}} = \bar{\boldsymbol{M}}^{\mathrm{d}}_{\mathrm{a}} : \bar{\boldsymbol{L}}_{\mathrm{a}} = \widehat{\boldsymbol{M}}^{\mathrm{d}}_{\mathrm{a}} : \widehat{\boldsymbol{L}}_{\mathrm{a}} \quad \text{with} \\ &\mathrm{l}^{\mathrm{a}}_t\,\boldsymbol{G}^{-1}_{\mathrm{a}} = \boldsymbol{f}_{\mathrm{a}} \star \mathrm{D}_t\boldsymbol{A}_{\mathrm{p}} = 2\,[\,\bar{\boldsymbol{L}}_{\mathrm{a}} \cdot \boldsymbol{G}^{-1}_{\mathrm{a}}\,]^{\mathrm{sym}} \quad \text{and} \quad \boldsymbol{G}^{-1}_{\mathrm{a}} = \boldsymbol{f}_{\mathrm{a}} \star \boldsymbol{A}_{\mathrm{p}}\;,\end{aligned} \tag{4.43}$$

whereby the notation $\mathrm{l}^{\mathrm{a}}_t\{\bullet\}$ takes the interpretation as a Lie–derivative with respect to $\boldsymbol{f}_{\mathrm{a}}$, i.e. $\mathrm{l}^{\mathrm{a}}_t\{\bullet\} = \boldsymbol{f}_{\mathrm{a}} \star \mathrm{D}_t(\boldsymbol{F}_{\mathrm{a}} \star \{\bullet\})$. Furthermore, a pullback of the velocity gradient $\bar{\boldsymbol{L}}_{\mathrm{a}}$ yields

$$\bar{\boldsymbol{L}}_{\mathrm{a}} = \boldsymbol{f}_{\mathrm{a}} \star \widehat{\boldsymbol{L}}_{\mathrm{a}} = \boldsymbol{f}_{\mathrm{a}} \cdot \mathrm{D}_t\boldsymbol{F}_{\mathrm{a}} = -\,\mathrm{D}_t\boldsymbol{f}_{\mathrm{a}} \cdot \boldsymbol{F}_{\mathrm{a}}\,, \tag{4.44}$$

compare eq.(4.9). By analogy with eqs.(4.19,4.42), an exponential integration scheme with respect to $\bar{\boldsymbol{L}}_{\mathrm{a}}$ ends up in the equivalent expression

$$\begin{aligned}&\boldsymbol{F}^{n+1}_{\mathrm{a}} \doteq \boldsymbol{F}^{n}_{\mathrm{a}} \cdot \exp(-\,\Delta\lambda\,\bar{\boldsymbol{\nu}}^{n+1}_{\mathrm{a}}) \quad \text{with} \\ &\bar{\boldsymbol{\nu}}_{\mathrm{a}} \quad = \boldsymbol{f}_{\mathrm{a}} \star \widehat{\boldsymbol{\nu}}_{\mathrm{a}} = \mathrm{D}_t\lambda\,\partial_{\bar{\boldsymbol{M}}^{\mathrm{d}}_{\mathrm{a}}}{}^{\mathrm{dam}}\Phi = \mathrm{D}_t\lambda \sum_{i=1}^{3} i\,\partial_{I_{\mathrm{a}\,i}}{}^{\mathrm{dam}}\Phi\,[\,\bar{\boldsymbol{M}}_{\mathrm{a}}\,]^{i-1}\,.\end{aligned} \tag{4.45}$$

Moreover, we can apply the spectral decomposition theorem to the Mandel–type stress tensors (in the sense that the eigenvalues are real) since these mixed–variant fields are composed by the product of two symmetric second–order tensors with one of them always remaining positive definite; see, for example, Ericksen (1960), Eringen (1971b), or Lodge (1974) for a discussion.

Remark 4.4.3 *The damage stress tensor (as represented in eq.(4.39) with respect to the fictitious configuration) turns out to be symmetric, i.e.* $\bar{\boldsymbol{M}}^{\mathrm{t}}_{\mathrm{a}} = \boldsymbol{G}^{-1}_{\mathrm{a}} \cdot \bar{\boldsymbol{M}}^{\mathrm{d}}_{\mathrm{a}} \cdot \boldsymbol{G}_{\mathrm{a}} = \bar{\boldsymbol{M}}_{\mathrm{a}}$.

4.4.3 Yield function

While the introduction of the Helmholtz free energy density and the damage potential is conceptually based on the postulate of strain energy equivalence, as discussed by Sidoroff (1981), attention is now paid to the postulate of strain equivalence as commonly applied to the coupling of plasticity and continuum damage; see, for instance, Steinmann et at. (1994) or Lämmer and Tsakmakis (2000), where several coupling–types of isotropic continuum damage and plasticity are highlighted. In this context, we introduce with a small abuse of notation an effective elastic Mandel stress tensor

$$ {}^{\text{eff}}\widehat{\boldsymbol{M}}{}^{\text{d}}_{\text{e}} \equiv [\, \boldsymbol{f}^{\text{d}}_{\text{a}} \cdot \widehat{\boldsymbol{C}}_{\text{e}} \cdot \boldsymbol{f}_{\text{a}} \,] \cdot \partial_{\widehat{\boldsymbol{E}}_{\text{e}}} \psi^{\text{e}}_{0} \quad \text{with} \quad {}^{\text{eff}}\widehat{\boldsymbol{M}}{}^{\text{d}}_{\text{e}} \cdot \widehat{\boldsymbol{C}}_{\text{e}} \neq \widehat{\boldsymbol{C}}_{\text{e}} \cdot {}^{\text{eff}}\widehat{\boldsymbol{M}}_{\text{e}} \,. \tag{4.46} $$

The underlying kinematics are essentially based on the assumption ${}^{\text{eff}}\bar{\boldsymbol{M}}{}^{\text{d}}_{\text{e}} = \boldsymbol{f}_{\text{a}} \star {}^{\text{eff}}\widehat{\boldsymbol{M}}{}^{\text{d}}_{\text{e}} \equiv \widehat{\boldsymbol{C}}_{\text{e}} \cdot \bar{\boldsymbol{S}}_{\text{e}}$, i.e. the effective elastic Mandel tensor is defined by the composition of appropriate stresses and a modified metric tensor that accounts for the anisotropic degradation of the material, compare remark 4.4.2. A detailed discussion on the application of the equivalent strain concept in the present context is given in Menzel and Steinmann (2003b). With this effective quantity in hand, the yield function is assumed to be determined via an effective relative Mandel stress tensor

$$ {}^{\text{yie}}\Phi \doteq {}^{\text{yie}}\Phi\big({}^{\text{eff}}\widehat{\boldsymbol{M}}{}^{\text{d}}_{\text{r}}, Y; \boldsymbol{X} \big) \quad \text{with} \quad {}^{\text{eff}}\widehat{\boldsymbol{M}}{}^{\text{d}}_{\text{r}} = {}^{\text{eff}}\widehat{\boldsymbol{M}}{}^{\text{d}}_{\text{e}} - \widehat{\boldsymbol{M}}{}^{\text{d}}_{\text{k}} \,. \tag{4.47} $$

Apparently, we do not investigate the influence of different effective stress measures, as for example the incorporation of an effective back–stress tensor, since this is not within the scope of the present chapter; in this regard we refer the reader to the work by Lämmer and Tsakmakis (2000). Straightforward application of the evolution equations as highlighted in eq.(4.17), however, results in the following relations for the corresponding flow directions

$$ \begin{aligned} \widehat{\boldsymbol{\nu}}_{\text{p}} &= \frac{\partial\, {}^{\text{pla}}\Phi}{\partial\, {}^{\text{eff}}\widehat{\boldsymbol{M}}{}^{\text{d}}_{\text{r}}} : \frac{\partial\, {}^{\text{eff}}\widehat{\boldsymbol{M}}{}^{\text{d}}_{\text{r}}}{\partial \widehat{\boldsymbol{M}}{}^{\text{d}}_{\text{e}}} \equiv \quad \frac{\partial\, {}^{\text{pla}}\Phi}{\partial\, {}^{\text{eff}}\widehat{\boldsymbol{M}}{}^{\text{d}}_{\text{r}}} : \Big[\, [\, \boldsymbol{f}^{\text{d}}_{\text{a}} \cdot \widehat{\boldsymbol{C}}_{\text{e}} \cdot \boldsymbol{f}_{\text{a}} \cdot \widehat{\boldsymbol{B}}_{\text{e}} \,] \,\overline{\otimes}\, \boldsymbol{I}_{\text{p}} \Big] \,, \\ \widehat{\boldsymbol{\nu}}_{\text{k}} &= \frac{\partial\, {}^{\text{pla}}\Phi}{\partial\, {}^{\text{eff}}\widehat{\boldsymbol{M}}{}^{\text{d}}_{\text{r}}} : \frac{\partial\, {}^{\text{eff}}\widehat{\boldsymbol{M}}{}^{\text{d}}_{\text{r}}}{\partial \widehat{\boldsymbol{M}}{}^{\text{d}}_{\text{k}}} \equiv - \frac{\partial\, {}^{\text{pla}}\Phi}{\partial\, {}^{\text{eff}}\widehat{\boldsymbol{M}}{}^{\text{d}}_{\text{r}}} : [\, \boldsymbol{I}^{\text{d}}_{\text{p}} \,\overline{\otimes}\, \boldsymbol{I}_{\text{p}} \,] \,. \end{aligned} \tag{4.48} $$

For conceptual clarity, the hardening contribution ${}^{\text{har}}\Phi(Y; \boldsymbol{X})$ remains unchanged in this work, i.e. no further modifications with respect to the damage mapping are applied.

4.5 Prototype model

The following prototype model is introduced so that well–established constitutive equations are adopted as far as possible, for instance a St.–Venant–Kirchhoff ansatz or v. Mises–type yield functions. Both, the incorporation and examination of different prototype models as for example Neo–Hooke– or Hill–type models constitute future research. In that case, the identification of material parameters is of cardinal importance and a non–trivial task while the parameters for the prototype model chosen in this work are rather settled. With these assumptions in hand, we are able to discuss several (academic) numerical examples that present the general material behaviour of the developed framework in a clear and reasonable fashion.

4.5.1 Helmholtz free energy density

Based on the previously highlighted additive split of the Helmholtz free energy density, we adopt a simple ansatz of St.–Venant–Kirchhoff–type for the elastic and kinematic hardening

contribution, i.e.

$$\psi_0^{\mathrm{e}} \doteq \tfrac{1}{2}\, L\, I_{\mathrm{e}1}^2 + G\, I_{\mathrm{e}2} \quad \text{and} \quad \psi_0^{\mathrm{k}} \doteq H_3\, [\, I_{\mathrm{k}2} - \tfrac{1}{3}\, I_{\mathrm{k}1}^2\,] \tag{4.49}$$

with $G > 0$, $L > -\frac{2}{3}\, G$ and $H_3 > 0$. The chosen hardening contribution takes a standard format such that linear and saturation–type effects are modelled

$$\psi_0^{\kappa} \doteq [\, Y_\infty - Y_0\,]\, [\, \kappa + H_1^{-1}\, \exp(-\, H_1\, \kappa) - H_1^{-1}\,] + \tfrac{1}{2}\, H_2\, \kappa^2\,, \tag{4.50}$$

wherein $H_{1,2} \geq 0$ and $Y_\infty \geq Y_0 \geq 0$.

4.5.2 Damage potential

Since the fictitious configuration is assumed to represent an isotropic configuration, the damage potential ${}^{\mathrm{dam}}\Phi$ can either by defined in terms of the highlighted basic invariants $I_{\mathrm{a}\,1,2,3}$, the corresponding principal invariants or the correlated eigenvalues of $\widehat{\boldsymbol{M}}_{\mathrm{a}}^{\mathrm{d}}$ or $\bar{\boldsymbol{M}}_{\mathrm{a}}^{\mathrm{d}}$, respectively – all of them being real (in the sequel we restrict ourselves to these two configurations even though an outline with respect to $\mathcal{B}_0$ or $\mathcal{B}_t$ follows straightforwardly). Placing next emphasis on the corresponding generalised eigenvalue problem, the Mandel–type damage stress tensor can be decomposed as (recall section 4.4.2)

$$\begin{aligned}
\widehat{\boldsymbol{M}}_{\mathrm{a}}^{\mathrm{d}} &= \sum_{i=1}^{3} \lambda_{\mathrm{a}\,i}\, \widehat{\boldsymbol{n}}_{\mathrm{a}}^{i} \otimes \widehat{\boldsymbol{n}}_{\mathrm{a}\,i} \quad \text{with} \quad \|\widehat{\boldsymbol{n}}_{\mathrm{a}\,i}\|_{\boldsymbol{A}_{\mathrm{p}}} = 1\,, \qquad \boldsymbol{A}_{\mathrm{p}} = \sum_{i=1}^{3} \widehat{\boldsymbol{n}}_{\mathrm{a}}^{i} \otimes \widehat{\boldsymbol{n}}_{\mathrm{a}}^{i}\,, \\
\bar{\boldsymbol{M}}_{\mathrm{a}}^{\mathrm{d}} &= \sum_{i=1}^{3} \lambda_{\mathrm{a}\,i}\, \bar{\boldsymbol{n}}_{\mathrm{a}}^{i} \otimes \bar{\boldsymbol{n}}_{\mathrm{a}\,i} \quad \text{with} \quad \|\bar{\boldsymbol{n}}_{\mathrm{a}\,i}\|_{\boldsymbol{G}_{\mathrm{a}}} = 1\,, \qquad \boldsymbol{G}_{\mathrm{a}} = \sum_{i=1}^{3} \bar{\boldsymbol{n}}_{\mathrm{a}}^{i} \otimes \bar{\boldsymbol{n}}_{\mathrm{a}}^{i}\,,
\end{aligned} \tag{4.51}$$

with $\boldsymbol{A}_{\mathrm{p}} = \boldsymbol{F}_{\mathrm{a}} \star \boldsymbol{G}_{\mathrm{a}} = \boldsymbol{f}_{\mathrm{a}}^{\mathrm{d}} \cdot \boldsymbol{G}_{\mathrm{a}} \cdot \boldsymbol{f}_{\mathrm{a}}$ and $\widehat{\boldsymbol{n}}_{\mathrm{a}}^{i} = \boldsymbol{A}_{\mathrm{p}} \cdot \widehat{\boldsymbol{n}}_{\mathrm{a}\,i}$, $\bar{\boldsymbol{n}}_{\mathrm{a}}^{i} = \boldsymbol{G}_{\mathrm{a}} \cdot \bar{\boldsymbol{n}}_{\mathrm{a}\,i}$ as well as $\widehat{\boldsymbol{n}}_{\mathrm{a}}^{i} = \boldsymbol{f}_{\mathrm{a}}^{\mathrm{d}} \cdot \bar{\boldsymbol{n}}_{\mathrm{a}}^{i}$, $\widehat{\boldsymbol{n}}_{\mathrm{a}\,i} = \boldsymbol{F}_{\mathrm{a}} \cdot \bar{\boldsymbol{n}}_{\mathrm{a}\,i}$ (and usually $\lambda_{\mathrm{a}\,1} \geq \lambda_{\mathrm{a}\,2} \geq \lambda_{\mathrm{a}\,3}$).

Based on these elaborations, the setup of a Rankine–type model is straightforward: here we follow the outline given by Carol et al. (2001), further developed in Menzel et al. (2003), and introduce the damage potential

$${}^{\mathrm{dam}}\Phi(\widehat{\boldsymbol{M}}_{\mathrm{a}}^{\mathrm{d}}; \boldsymbol{X}) = {}^{\mathrm{dam}}\Phi(\bar{\boldsymbol{M}}_{\mathrm{a}}^{\mathrm{d}}; \boldsymbol{X}) \doteq \Big[\, \sum_{i=1}^{3} \langle \lambda_{\mathrm{a}\,i} \rangle^{D+1} \Big]^{\frac{1}{D+1}} \geq 0 \quad \text{with} \quad D \geq 0\,, \tag{4.52}$$

wherein the definition of the Macaulay bracket reads $\langle \{\bullet\} \rangle = \frac{1}{2}\, [\, \{\bullet\} + |\{\bullet\}|\,]$, $\{\bullet\} \in \mathbb{R}$. For $D \to 0$ the presented model reduces to (quasi) isotropic damage while $D > 0$ yields an anisotropic damage formulation. Independent of the specific choice of D, different material behaviour in, say, 'tension and compression' is generally included in this model (with respect to the space of the driving damage force). This concept is commonly applied in strain space, see for example Ekh et al. (2003) for an outline in the present context. With this damage potential in hand, the computation of the corresponding flow–direction results in

$$\begin{aligned}
\widehat{\boldsymbol{\nu}}_{\mathrm{a}} &= \sum_{i=1}^{3} {}^{\mathrm{dam}}\Phi^{-D}\, \langle \lambda_{\mathrm{a}\,i} \rangle^{D}\, \mathcal{H}(\lambda_{\mathrm{a}\,i})\, \widehat{\boldsymbol{n}}_{\mathrm{a}\,i} \otimes \widehat{\boldsymbol{n}}_{\mathrm{a}}^{i}\,, \\
\bar{\boldsymbol{\nu}}_{\mathrm{a}} &= \sum_{i=1}^{3} {}^{\mathrm{dam}}\Phi^{-D}\, \langle \lambda_{\mathrm{a}\,i} \rangle^{D}\, \mathcal{H}(\lambda_{\mathrm{a}\,i})\, \bar{\boldsymbol{n}}_{\mathrm{a}\,i} \otimes \bar{\boldsymbol{n}}_{\mathrm{a}}^{i}\,,
\end{aligned} \tag{4.53}$$

see eqs.(4.17,4.41,4.45). Please recall the fundamental relation $I_{\mathrm{e}\,1} = \lambda_{\mathrm{a}\,1} + \lambda_{\mathrm{a}\,2} + \lambda_{\mathrm{a}\,3}$ and that $\partial_{\{\bullet\}} \langle \{\bullet\} \rangle$ equals the Heaviside function ($\mathcal{H}(\{\bullet\}) = 1$ if $\{\bullet\} \geq 0$, $\mathcal{H}(\{\bullet\}) = 0$ if $\{\bullet\} < 0$

with $\{\bullet\} \in \mathbb{R}$) as well as the property $0 \leq {}^{\mathrm{dam}}\Phi^{-D}\,\langle\lambda_{\mathrm{a}\,i}\rangle^{D}\;\mathcal{H}(\lambda_{\mathrm{a}\,i}) \leq 1$. Moreover, we immediately observe that the chosen damage model is thermodynamically consistent since the obtained contribution to the dissipation inequality always remains non–negative

$$\begin{aligned} -\,\widehat{\boldsymbol{M}}^{\mathrm{d}}_{\mathrm{a}} : \widehat{\boldsymbol{L}}_{\mathrm{a}} &= \sum_{i=1}^{3} \mathrm{D}_t\lambda\;\lambda_{\mathrm{a}\,i}\;{}^{\mathrm{dam}}\Phi^{-D}\,\langle\lambda_{\mathrm{a}\,i}\rangle^{D}\;\mathcal{H}(\lambda_{\mathrm{a}\,i})\;[\,\widehat{\boldsymbol{n}}^{i}_{\mathrm{a}}\otimes\widehat{\boldsymbol{n}}_{\mathrm{a}\,i},]:[\,\widehat{\boldsymbol{n}}_{\mathrm{a}\,i}\otimes\widehat{\boldsymbol{n}}^{i}_{\mathrm{a}}\,]\geq 0\,, \\ -\,\bar{\boldsymbol{M}}^{\mathrm{d}}_{\mathrm{a}} : \bar{\boldsymbol{L}}_{\mathrm{a}} &= \sum_{i=1}^{3} \mathrm{D}_t\lambda\;\lambda_{\mathrm{a}\,i}\;{}^{\mathrm{dam}}\Phi^{-D}\,\langle\lambda_{\mathrm{a}\,i}\rangle^{D}\;\mathcal{H}(\lambda_{\mathrm{a}\,i})\;[\,\bar{\boldsymbol{n}}^{i}_{\mathrm{a}}\otimes\bar{\boldsymbol{n}}_{\mathrm{a}\,i}\,]:[\,\bar{\boldsymbol{n}}_{\mathrm{a}\,i}\otimes\bar{\boldsymbol{n}}^{i}_{\mathrm{a}}\,]\geq 0\,, \end{aligned} \tag{4.54}$$

compare eqs.(4.13, 4.17, 4.43).

Remark 4.5.1 *Please note that the 'pseudo–logarithmic' damage rate as advocated in the work by Carol et al. (2001), where the adopted Rankine–type model is outlined for the coupling of linear elasticity and continuum damage mechanics, corresponds to the Lie–derivative* $\mathrm{l}^{\mathrm{a}}_{t}\{\bullet\}$ *introduced in eq.(4.43). Moreover, when neglecting the kinematic hardening contribution* ψ^{k}_{0} *the damage stress tensor allows representation as* $\widehat{\boldsymbol{M}}^{\mathrm{d}}_{\mathrm{a}} = 2\,\partial_{\boldsymbol{A}_{\mathrm{p}}}\psi^{\mathrm{e}}_{0}\cdot\boldsymbol{A}_{\mathrm{p}} = 2\,\widehat{\boldsymbol{E}}_{\mathrm{e}}\cdot\partial_{\widehat{\boldsymbol{E}}_{\mathrm{e}}}\psi^{\mathrm{e}}_{0} = 2\,\widehat{\boldsymbol{E}}_{\mathrm{e}}\cdot\widehat{\boldsymbol{S}}_{\mathrm{e}}$ *or* $\bar{\boldsymbol{M}}^{\mathrm{d}}_{\mathrm{a}} = 2\,\bar{\boldsymbol{E}}_{\mathrm{e}}\cdot\bar{\boldsymbol{S}}_{\mathrm{e}}$*, respectively. By comparing this result with eq.(71) in Carol et al. (2001, Part I) we observe the relation* $\widehat{\boldsymbol{M}}_{\mathrm{a}} \equiv -\,4\,\boldsymbol{\mathcal{Y}}$.

4.5.3 Yield function

For the contribution ${}^{\mathrm{pla}}\Phi$ of the yield function ${}^{\mathrm{yie}}\Phi$, a well–established v. Mises–type model in connection with the concept of effective stresses is adopted; we choose in particular

$$\begin{aligned} {}^{\mathrm{pla}}\Phi &\doteq \sqrt{\tfrac{3}{2}}\,\left[\,\boldsymbol{I}_{\mathrm{p}} : \left[\,\left[\,{}^{\mathrm{eff}}\widehat{\boldsymbol{M}}^{\mathrm{d}}_{\mathrm{r}}\,\right]^{\mathrm{dev}}\right]^{2}\right]^{\frac{1}{2}} \doteq \sqrt{\tfrac{3}{2}}\,\left[\;{}^{\mathrm{eff}}I^{\mathrm{dev}}_{\mathrm{p}\,2}\,\right]^{\frac{1}{2}} \\ \text{with}\qquad & \left[\,{}^{\mathrm{eff}}\widehat{\boldsymbol{M}}^{\mathrm{d}}_{\mathrm{r}}\,\right]^{\mathrm{dev}} = {}^{\mathrm{eff}}\widehat{\boldsymbol{M}}^{\mathrm{d}}_{\mathrm{r}} - \tfrac{1}{3}\left[\,\boldsymbol{I}_{\mathrm{p}} : {}^{\mathrm{eff}}\widehat{\boldsymbol{M}}^{\mathrm{d}}_{\mathrm{r}}\,\right]\boldsymbol{I}^{\mathrm{d}}_{\mathrm{p}} \end{aligned} \tag{4.55}$$

which results in the following flow directions

$$\begin{aligned} \widehat{\boldsymbol{\nu}}_{\mathrm{p}} &= \frac{\partial\,{}^{\mathrm{pla}}\Phi}{\partial\widehat{\boldsymbol{M}}^{\mathrm{d}}_{\mathrm{e}}} \equiv \quad \sqrt{\tfrac{3}{2}}\,\left[\;{}^{\mathrm{eff}}I^{\mathrm{dev}}_{\mathrm{p}\,2}\,\right]^{-\frac{1}{2}}\,\widehat{\boldsymbol{B}}_{\mathrm{e}}\cdot\boldsymbol{f}^{\mathrm{d}}_{\mathrm{a}}\cdot\widehat{\boldsymbol{C}}_{\mathrm{e}}\cdot\boldsymbol{f}_{\mathrm{a}}\cdot\,\left[\,{}^{\mathrm{eff}}\widehat{\boldsymbol{M}}_{\mathrm{r}}\right]^{\mathrm{dev}}, \\ \widehat{\boldsymbol{\nu}}_{\mathrm{k}} &= \frac{\partial\,{}^{\mathrm{pla}}\Phi}{\partial\widehat{\boldsymbol{M}}^{\mathrm{d}}_{\mathrm{k}}} \equiv -\,\sqrt{\tfrac{3}{2}}\,\left[\;{}^{\mathrm{eff}}I^{\mathrm{dev}}_{\mathrm{p}\,2}\,\right]^{-\frac{1}{2}} \qquad\qquad \left[\,{}^{\mathrm{eff}}\widehat{\boldsymbol{M}}_{\mathrm{r}}\right]^{\mathrm{dev}}, \end{aligned} \tag{4.56}$$

recall eq.(4.48). The adopted (linear) format for the hardening potential is the simplest possible, namely

$${}^{\mathrm{har}}\Phi \doteq -\,[\,Y_0 + Y\,] \quad \text{such that} \quad \nu_{\kappa} = -\,1\,. \tag{4.57}$$

The proof that the chosen v. Mises–type model is thermodynamically consistent is straightforward and therefore omitted. For a viscoplastic setting, the commonly applied Norton–type format or rather power law

$$\eta({}^{\mathrm{yie}}\Phi) \doteq \left[\frac{\langle\,{}^{\mathrm{yie}}\Phi\rangle}{Y_0}\right]^{N} \quad \text{with} \quad N \geq 1 \tag{4.58}$$

is adopted. In order to account for nonlinear kinematic hardening, however, we expand eq.$(4.56)_2$ and assume

$$\widehat{\boldsymbol{\nu}}^{\mathrm{nonlin}}_{\mathrm{k}} = \widehat{\boldsymbol{\nu}}_{\mathrm{k}} + a\,K^{-1}_{\infty}\,\widehat{\boldsymbol{M}}_{\mathrm{k}} \quad \text{with} \quad a \doteq \tfrac{3}{2}\,, \tag{4.59}$$

whereby K_{∞} acts as a saturation value, recall remark 4.2.2 and see Ekh and Runesson (2001) for a comprehensive outline.

4.5.4 Weighting of the evolution equations

In order to switch between different models, for instance viscoplasticity coupled to anisotropic continuum damage without hardening effects or viscoplasticity with mixed hardening but without taking degradation into account, we introduce three weighting factors that scale the underlying evolution equations, namely

$$\widehat{\boldsymbol{\nu}}_{\mathrm{k}} \hookleftarrow [\,1 - r_{\mathrm{k}}\,]\,\widehat{\boldsymbol{\nu}}_{\mathrm{k}}\,, \qquad \widehat{\boldsymbol{\nu}}_{\mathrm{a}} \hookleftarrow [\,1 - r_{\mathrm{a}}\,]\,\widehat{\boldsymbol{\nu}}_{\mathrm{a}}\,, \qquad \nu_{\kappa} \hookleftarrow [\,1 - r_{\kappa}\,]\,\nu_{\kappa} \tag{4.60}$$

with $r_{\mathrm{k}}, r_{\mathrm{a}}, r_{\kappa} \in [\,0\,,\,1\,]$ being obvious.

4.6 Numerical examples

For conceptual simplicity and in order to place emphasis on characteristic properties of the proposed prototype model, we first restrict ourselves to a rate–independent setting in simple shear, whereby the effects of degradation and kinematic hardening are discussed separately. Even though loading and un–/reloading conditions are highlighted within these examples, we further elaborate on cyclic loading in simple shear and thereby additionally account for the rate–dependent case. Besides discussing fundamental constitutive properties as such, we next address numerical issues by focusing of different integration/iteration techniques based on the proposed methods 1–4, whereby representative simple shear loading is considered. Finally, a finite element setting is discussed, namely the classical example of a rod under torsion including all of the previously highlighted effects, i.e. viscoplasticity, anisotropic degradation, kinematic hardening and proportional hardening.

If not mentioned otherwise, the following material parameters serve for the subsequent numerical applications: $L \doteq 1.2 \times 10^5$, $G \doteq 8.1 \times 10^4$ (which approximately corresponds to $E = 2.1 \times 10^5$, $\nu = 0.3$), $Y_0 \doteq 5 \times 10^2$, $Y_\infty \doteq 1 \times 10^3$, $K_\infty = 2.5 \times 10^2$, $H_1 \doteq 20$, $H_2 \doteq 1$, $H_3 \doteq 2.5 \times 10^2$ and $D = 10$. Moreover, two different initial (elastic) settings are considered, namely an initially isotropic and an initially anisotropic material. The underlying damage mapping for the first type of material is consequently represented by the identity

$$\boldsymbol{F}_{\mathrm{a}}|_{t_0} \doteq \delta_{ij}\,\boldsymbol{e}_i \otimes \boldsymbol{e}_j\,, \qquad i,j = 1,2,3 \tag{4.61}$$

with δ_{ij} denoting the Kronecker delta and $\{\boldsymbol{e}_i\}$ being a space–attached Cartesian frame. The second material type, i.e. the initially anisotropic setting, is defined via

$$\begin{aligned} \boldsymbol{F}_{\mathrm{a}}|_{t_0} \doteq\ & 1.0315\,\boldsymbol{e}_1 \otimes \boldsymbol{e}_1 + 0.9846\,\boldsymbol{e}_2 \otimes \boldsymbol{e}_2 + 0.9846\,\boldsymbol{e}_3 \otimes \boldsymbol{e}_3 \\ & + 0.0938\,\boldsymbol{e}_1 \otimes \boldsymbol{e}_2 + 0.0469\,\boldsymbol{e}_1 \otimes \boldsymbol{e}_3 \end{aligned} \tag{4.62}$$

which results via the spectral decomposition theorem, $\boldsymbol{A}_{\mathrm{p}}|_{t_0} = \sum_{i=1}^{3} \alpha_{0\,i}\,\widehat{\boldsymbol{V}}_{0\,i} \otimes \widehat{\boldsymbol{V}}_{0\,i}$ with $\|\widehat{\boldsymbol{V}}_{0\,i}\|_{\boldsymbol{G}_{\mathrm{p}}} = 1$, in

$$\begin{aligned} \alpha_{0\,1} &= 0.9063\,, & \widehat{\boldsymbol{V}}_{0\,1} &= -\,0.5220\ \boldsymbol{e}_1 + 0.7629\ \boldsymbol{e}_2 + 0.3815\ \boldsymbol{e}_3\,, \\ \alpha_{0\,2} &= 0.9695\,, & \widehat{\boldsymbol{V}}_{0\,2} &= -\,0.4472\ \boldsymbol{e}_2 + 0.8944\ \boldsymbol{e}_3\,, \\ \alpha_{0\,3} &= 1.1381\,, & \widehat{\boldsymbol{V}}_{0\,3} &= \ \ 0.8530\ \boldsymbol{e}_1 + 0.4669\ \boldsymbol{e}_2 + 0.2334\ \boldsymbol{e}_3\,, \end{aligned} \tag{4.63}$$

with $\prod_{i=1}^{3} \alpha_{0\,i} = 1$. Please note that the restriction to initially unimodular mappings $\boldsymbol{F}_{\mathrm{a}}|_{t_0}$ is by no means necessary; the comparison of the initially isotropic and anisotropic setting, however, would somehow be misleading if $\det(\boldsymbol{F}_{\mathrm{a}}|_{t_0})$ took different values for both cases.

In order to visualise that two second–order tensors do not commutate, we introduce a scalar–valued quantity, called anisotropy measure, which takes in terms of, for example, strains and stresses the following format

$$\delta(\widehat{\boldsymbol{E}}_{\mathrm{e}} \cdot \widehat{\boldsymbol{S}}_{\mathrm{e}}) = \frac{\| [\, \widehat{\boldsymbol{E}}_{\mathrm{e}} \cdot \widehat{\boldsymbol{S}}_{\mathrm{e}} \,] - [\, \widehat{\boldsymbol{E}}_{\mathrm{e}} \cdot \widehat{\boldsymbol{S}}_{\mathrm{e}} \,]^{\mathrm{t}} \|}{\| \widehat{\boldsymbol{E}}_{\mathrm{e}} \cdot \widehat{\boldsymbol{S}}_{\mathrm{e}} \|} \,. \tag{4.64}$$

4.6.1 Simple shear

The considered homogeneous deformation in simple shear is related to the deformation gradient $\boldsymbol{F} \doteq \delta_{ij}\, \boldsymbol{e}_i \otimes \boldsymbol{e}_j + \gamma\, \boldsymbol{e}_1 \otimes \boldsymbol{e}_2$. The subsequently applied loading and un–/reloading path is determined by first increasing the shear number from zero to $\frac{1}{2}$, $\gamma \in [\, 0 \rightarrow \frac{1}{2} \,]$, and second decreasing the shear number back to zero, $\gamma \in [\, 0 \rightarrow \frac{1}{2}\,,\, \frac{1}{2} \rightarrow 0 \,]$. For the cyclic loading history (solely one cycle) the same deformation path is additionally attached, but with revers shear direction.

4.6.1.1 Elastoplasticity coupled with continuum damage without hardening

The modelling of elastoplasticity with degradation but without hardening is performed via $r_\kappa = r_{\mathrm{k}} = 1$, $r_{\mathrm{a}} = 0$. Figure 4.2 highlights the monotonic decrease of the eigenvalues of the damage metric for the initially isotropic setting. The considered shear deformation results in a high degree of damage evolution. Single components of the Cauchy stresses and the relative (or rather elastic) Mandel stresses are pictured in figures 4.3 and 4.4. Furthermore, the deviatoric norms of the Cauchy stresses and the effective relative Mandel stresses underline on the one hand the degradation of the material and on the other the hand the fact that no proportional hardening is taken into account, see figure 4.5. The rather small elastic range is clearly displayed in figures 4.3–4.5.

Next, initially anisotropic material response is discussed. Figures 4.6–4.9 visualise the damage metric and stress tensors of interest by analogy with the previous setting. The damage eigenvalues degrade similar to the isotropic case but follow distinctive evolutions, see figure 4.6. Both the Cauchy stresses and the relative Mandel stresses possess completely different properties compared to the previous setting, see figures 4.7 and 4.8, whereby the cyclic response apparently stems from the incorporated anisotropy. The deviatoric stress–norms, however, show once more the perfectly plastic behaviour, compare figure 4.9. For the initially anisotropic setting we place additional emphasis on two anisotropy measures, see figure 4.10. It is clearly seen that the overall response is anisotropic and, furthermore, that the principal directions of the damage metric evolve during the considered deformation process.

4.6.1.2 Elastoplasticity with kinematic hardening but without degradation

Elastoplasticity with solely kinematic hardening but without degradation is represented via $r_\kappa = r_{\mathrm{a}} = 1$, $r_{\mathrm{k}} = 0$. The initially isotropic setting clearly shows a typical behaviour as expected for kinematic hardening, see the visualisation of the Cauchy stresses, the relative Mandel stresses and the deviatoric norms of these stress fields in figures 4.11–4.13. We observe in particular the saturation–type effect and that the admissible domain is dragged along as well as that proportional hardening is not incorporated.

Figures 4.14–4.17 highlight the behaviour of the initially anisotropic material. The material response turns out be completely different compared to the Cauchy stresses and the relative

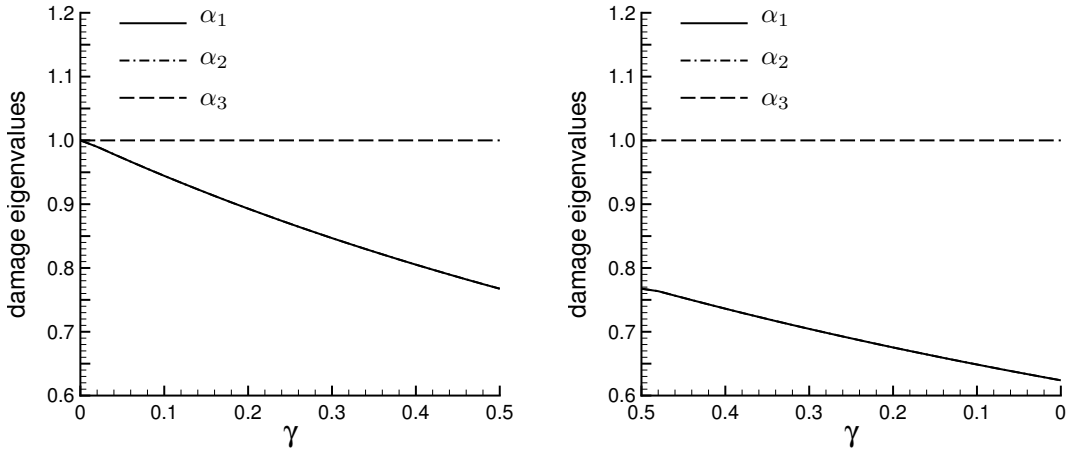

Figure 4.2: Simple shear, initially isotropic material (elastoplasticity): eigenvalues $\alpha_{1,2,3}$ of the damage metric $\boldsymbol{A}_{\mathrm{p}}$ for $\gamma \in [\,0 \to 0.5\,,\, 0.5 \to 0\,]$ and $r_\kappa = r_{\mathrm{k}} = 1$, $r_{\mathrm{a}} = 0$ (no hardening but anisotropic damage).

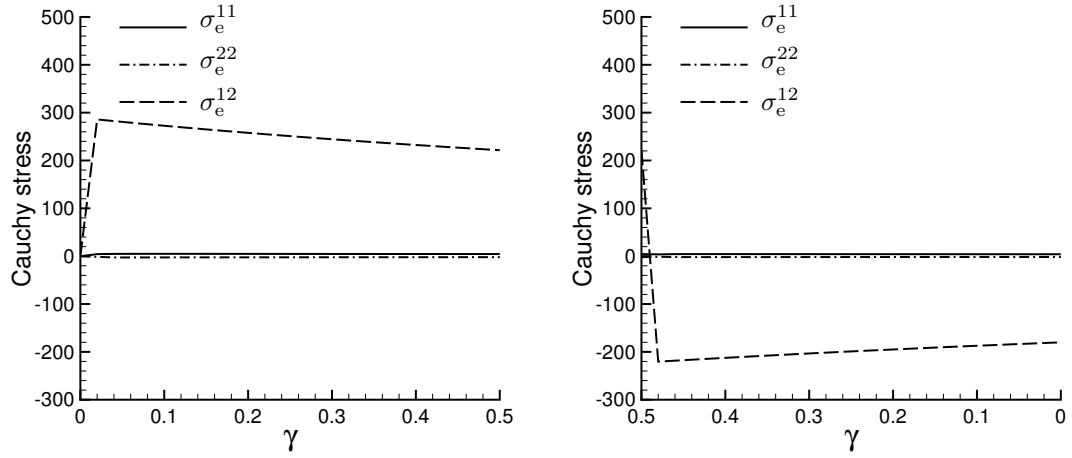

Figure 4.3: Simple shear, initially isotropic material (elastoplasticity): Cauchy stresses $\boldsymbol{\sigma}_{\mathrm{e}}$ for $\gamma \in [\,0 \to 0.5\,,\, 0.5 \to 0\,]$ and $r_\kappa = r_{\mathrm{k}} = 1$, $r_{\mathrm{a}} = 0$ (no hardening but anisotropic damage).

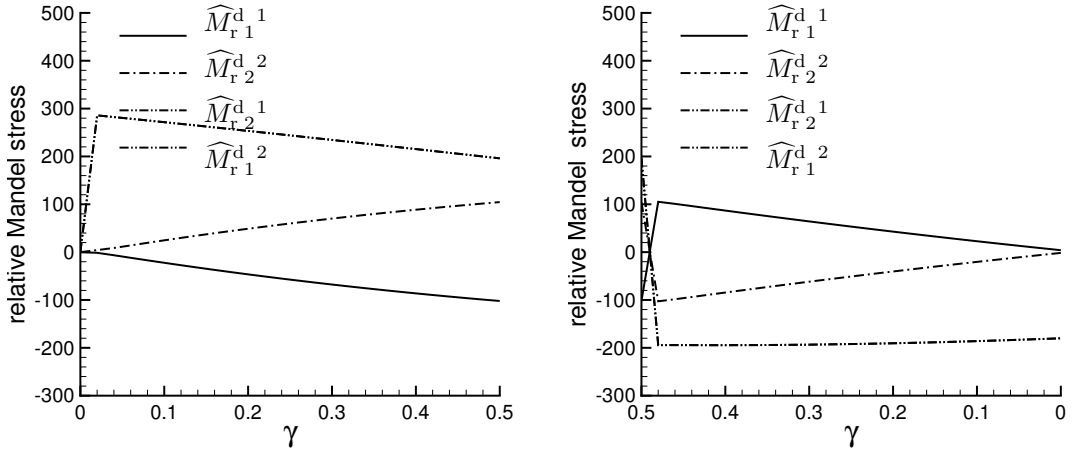

Figure 4.4: Simple shear, initially isotropic material (elastoplasticity): relative Mandel stresses $\widehat{\boldsymbol{M}}_{\mathrm{r}}^{\mathrm{d}}$ for $\gamma \in [\,0 \to 0.5\,,\, 0.5 \to 0\,]$ and $r_\kappa = r_{\mathrm{k}} = 1$, $r_{\mathrm{a}} = 0$ (no hardening but anisotropic damage).

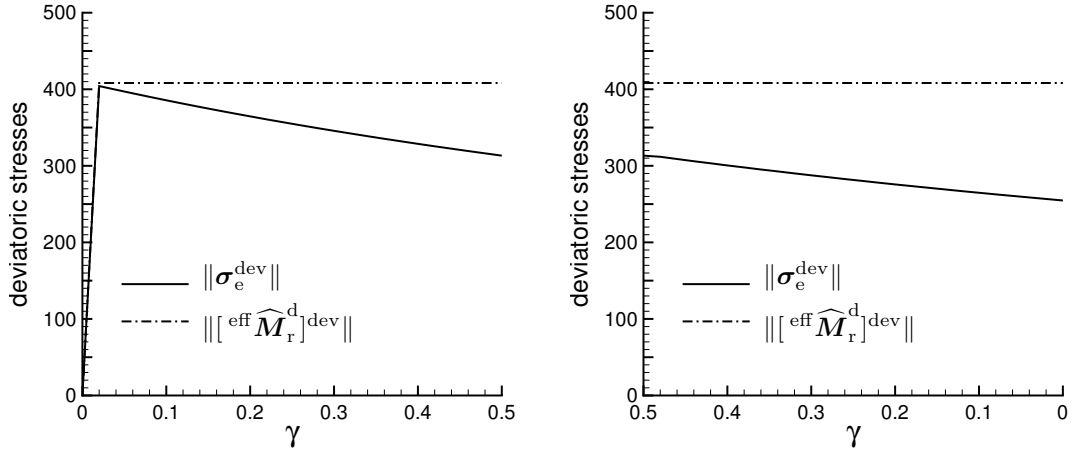

Figure 4.5: Simple shear, initially isotropic material (elastoplasticity): norm of the deviatoric stress tensors $\boldsymbol{\sigma}_{\mathrm{e}}^{\mathrm{dev}}$ and $[\,{}^{\mathrm{eff}}\widehat{\boldsymbol{M}}_{\mathrm{r}}^{\mathrm{d}}]^{\mathrm{dev}}$ for $\gamma \in [\,0 \to 0.5\,,\, 0.5 \to 0\,]$ and $r_\kappa = r_{\mathrm{k}} = 1$, $r_{\mathrm{a}} = 0$ (no hardening but anisotropic damage).

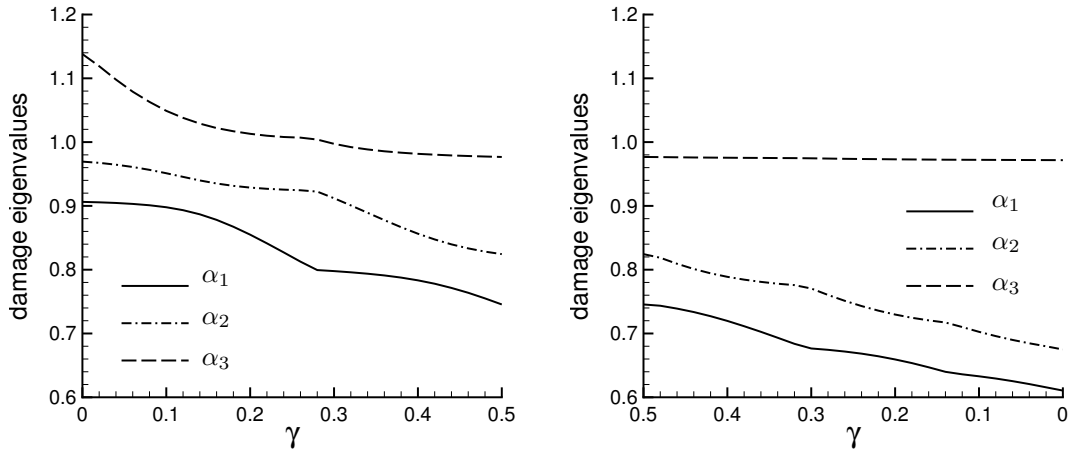

Figure 4.6: Simple shear, initially anisotropic material (elastoplasticity): eigenvalues $\alpha_{1,2,3}$ of the damage metric $\boldsymbol{A}_{\mathrm{p}}$ for $\gamma \in [\,0 \to 0.5\,,\, 0.5 \to 0\,]$ and $r_\kappa = r_{\mathrm{k}} = 1$, $r_{\mathrm{a}} = 0$ (no hardening but anisotropic damage).

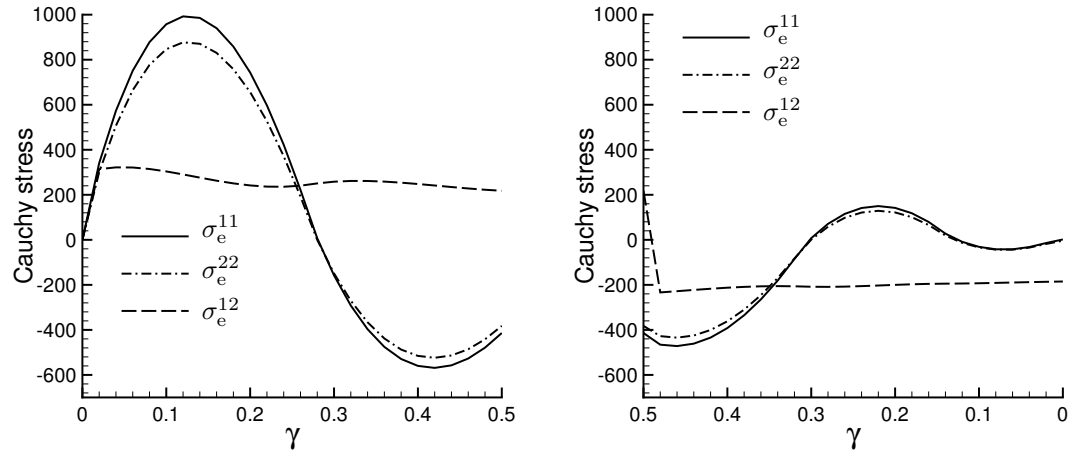

Figure 4.7: Simple shear, initially anisotropic material (elastoplasticity): Cauchy stresses $\boldsymbol{\sigma}_{\mathrm{e}}$ for $\gamma \in [\,0 \to 0.5\,,\, 0.5 \to 0\,]$ and $r_\kappa = r_{\mathrm{k}} = 1$, $r_{\mathrm{a}} = 0$ (no hardening but anisotropic damage).

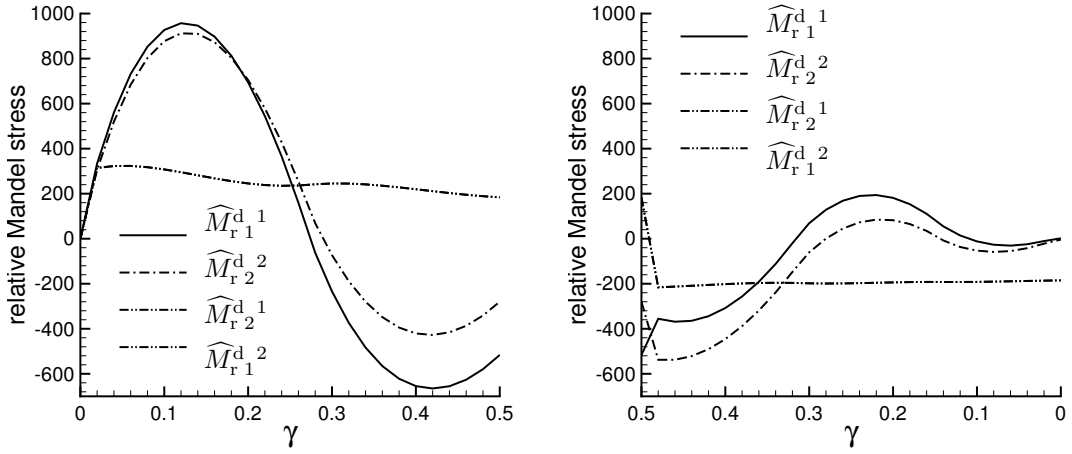

Figure 4.8: Simple shear, initially anisotropic material (elastoplasticity): relative Mandel stresses $\widehat{\boldsymbol{M}}^{\mathrm{d}}_{\mathrm{r}}$ for $\gamma \in [\,0 \to 0.5\,,\; 0.5 \to 0\,]$ and $r_\kappa = r_{\mathrm{k}} = 1$, $r_{\mathrm{a}} = 0$ (no hardening but anisotropic damage).

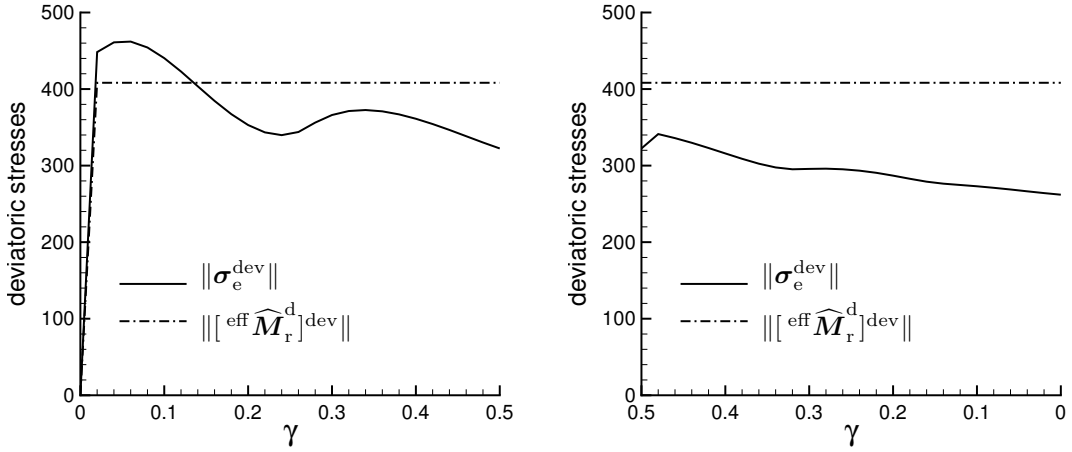

Figure 4.9: Simple shear, initially anisotropic material (elastoplasticity): norm of the deviatoric stress tensors $\boldsymbol{\sigma}^{\mathrm{dev}}_{\mathrm{e}}$ and $[\,{}^{\mathrm{eff}}\widehat{\boldsymbol{M}}^{\mathrm{d}}_{\mathrm{r}}]^{\mathrm{dev}}$ for $\gamma \in [\,0 \to 0.5\,,\; 0.5 \to 0\,]$ and $r_\kappa = r_{\mathrm{k}} = 1$, $r_{\mathrm{a}} = 0$ (no hardening but anisotropic damage).

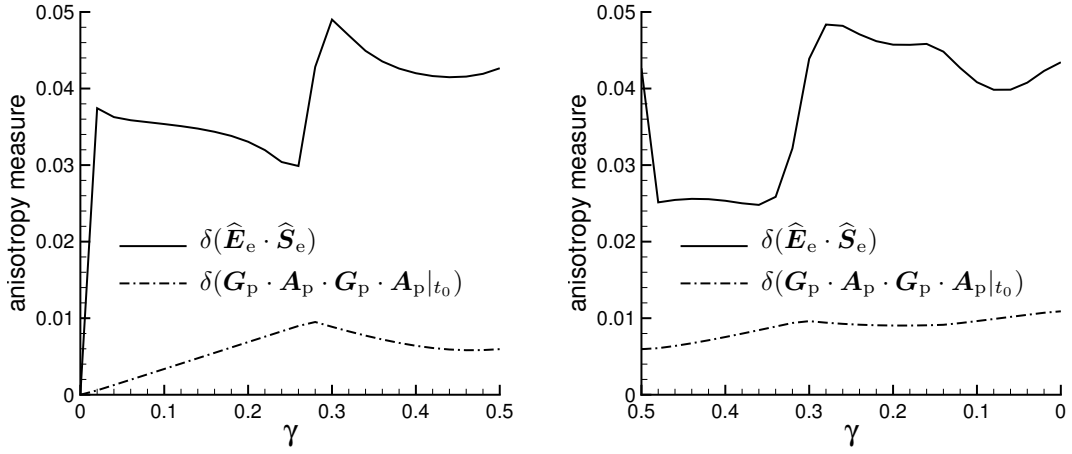

Figure 4.10: Simple shear, initially anisotropic material (elastoplasticity): anisotropy measures $\delta(\widehat{\boldsymbol{E}}_{\mathrm{e}} \cdot \widehat{\boldsymbol{S}}_{\mathrm{e}})$, $\delta(\boldsymbol{G}_{\mathrm{p}} \cdot \boldsymbol{A}_{\mathrm{p}} \cdot \boldsymbol{G}_{\mathrm{p}} \cdot \boldsymbol{A}_{\mathrm{p}}|_{t_0})$ for $\gamma \in [\,0 \to 0.5\,,\; 0.5 \to 0\,]$ and $r_\kappa = r_{\mathrm{k}} = 1$, $r_{\mathrm{a}} = 0$ (no hardening but anisotropic damage).

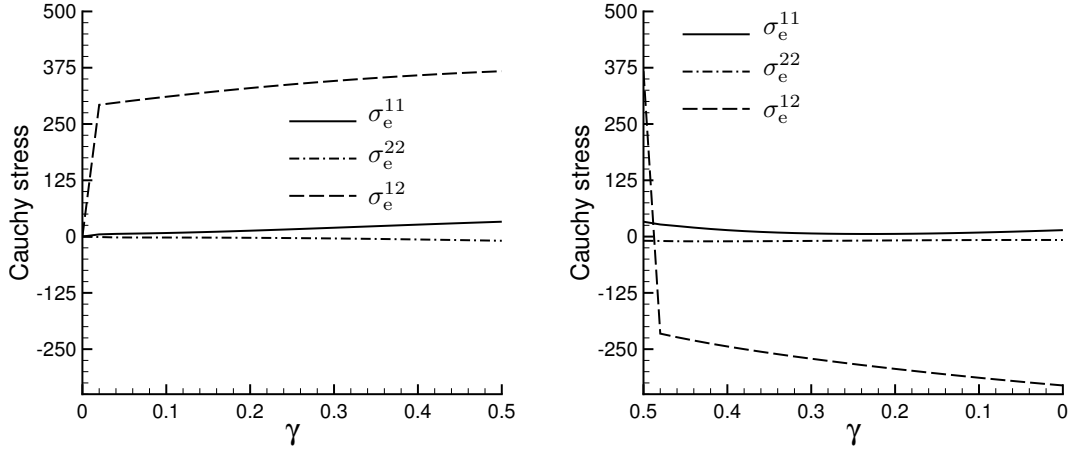

Figure 4.11: Simple shear, initially isotropic material (elastoplasticity): Cauchy stresses $\boldsymbol{\sigma}_{\mathrm{e}}$ for $\gamma \in [\,0 \rightarrow 0.5\,,\; 0.5 \rightarrow 0\,]$ and $r_{\kappa} = r_{\mathrm{a}} = 1$, $r_{\mathrm{k}} = 0$ (no proportional hardening and damage but kinematic hardening).

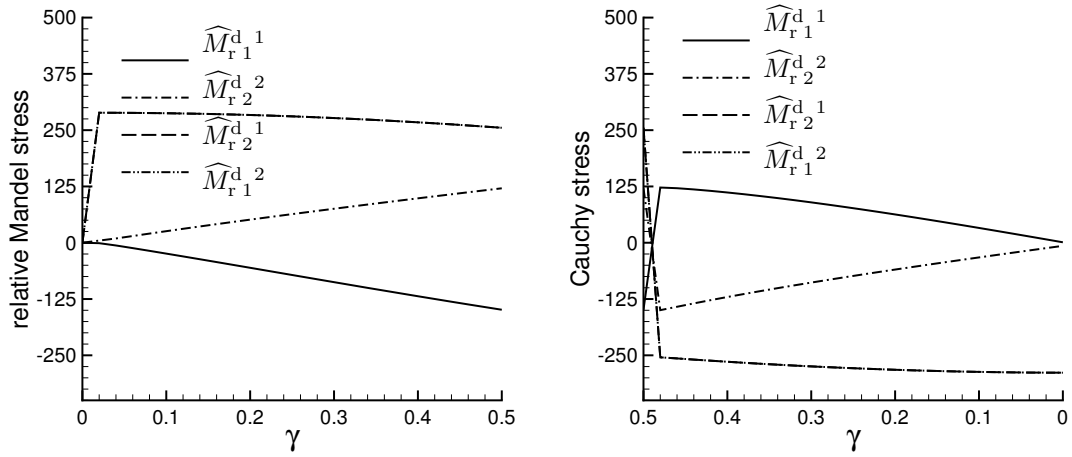

Figure 4.12: Simple shear, initially isotropic material (elastoplasticity): relative Mandel stresses $\widehat{\boldsymbol{M}}_{\mathrm{r}}^{\mathrm{d}}$ for $\gamma \in [\,0 \rightarrow 0.5\,,\; 0.5 \rightarrow 0\,]$ and $r_{\kappa} = r_{\mathrm{a}} = 1$, $r_{\mathrm{k}} = 0$ (no proportional hardening and damage but kinematic hardening).

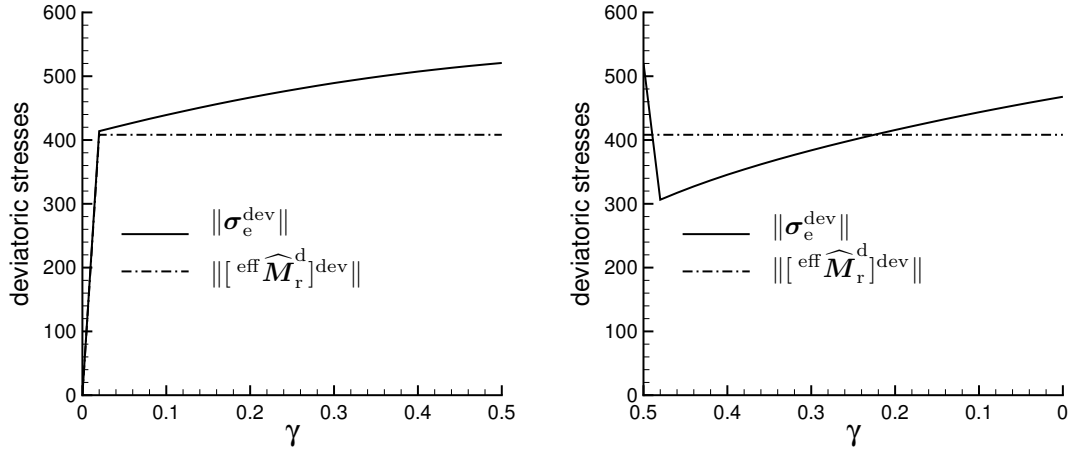

Figure 4.13: Simple shear, initially isotropic material (elastoplasticity): norm of the deviatoric stress tensors $\boldsymbol{\sigma}_{\mathrm{e}}^{\mathrm{dev}}$ and $[\,{}^{\mathrm{eff}}\widehat{\boldsymbol{M}}_{\mathrm{r}}^{\mathrm{d}}]^{\mathrm{dev}}$ for $\gamma \in [\,0 \rightarrow 0.5\,,\; 0.5 \rightarrow 0\,]$ and $r_{\kappa} = r_{\mathrm{a}} = 1$, $r_{\mathrm{k}} = 0$ (no proportional hardening and damage but kinematic hardening).

Mandel stresses for the isotropic setting in figures 4.11–4.13. The fact that proportional hardening is not activated is clearly visualised in figure 4.16. Due to the overall anisotropy of the material and the non–constant principal strain directions in simple shear, we compute several non–vanishing anisotropy measures. These scalar–valued functions, representing the non–commutativity of the considered tensorial quantities, are displayed in figure 4.17.

4.6.1.3 Cyclic loading

Next, a representative cyclic loading path is considered, whereby for the sake of clarity solely one cycle is taken into account. The subsequent graphs highlight the shear component of the (elastic) Cauchy stress tensor, σ_{e}^{12}, with respect to the space–attached Cartesian frame. For the initially isotropic setting, figure 4.18 visualises the response for kinematic hardening without and with degradation. We observe for the first case that the nonlinear saturation–type effect of kinematic hardening is captured by the applied prototype model. Both effects, the typical influence of the back–stresses as well as the decrease of the Cauchy stresses due to damage evolution are clearly monitored. Moreover, the computations displayed in figure 4.19 additionally account for viscoplastic behaviour. The time interval of the loading path is thereby set to $\mathcal{T} = 100$, which defines the time increments Δt; the relaxation time parameter has been chosen as $t^* = 100$ and in view of the power–type law we assumed $N = 2$.

Finally, figures 4.20 and 4.21 highlight similar results for the initially anisotropic material. Due to the incorporated anisotropy, it is thereby obvious that the shear stress components σ_{e}^{23} and σ_{e}^{13} do not vanish. By analogy with the previous setting we, nevertheless, restrict ourselves to visualising the response of σ_{e}^{12}.

4.6.1.4 Accuracy and efficiency studies

For the subsequent accuracy and efficiency analysis with respect to different integration / iteration techniques as discussed in section 4.3, we restrict ourselves to initial isotropy as well as to linear kinematic hardening and, moreover, neglect proportional hardening effects so that $r_{\mathrm{k}} = r_{\mathrm{a}} = 0$ but $r_{\kappa} = 1$. Monotonic loading for $\gamma \in [\,0 \rightarrow 2\,]$ is taken into account and $H_3 = 10^3$ together with $D = 2$ for anisotropic damage evolution, besides $D = 0$ for isotropic degradation, are applied. The overall response is assumed to remain rate–independent.

In order to illustrate how the four different methods1–4, as introduced in sections 4.3.1.1 and 4.3.1.2, perform regarding accuracy and efficiency, the logarithm of the error in σ_{e}^{12} at $\gamma = 2$ versus the normalised CPU time is shown in figures 4.22 and 4.23. For the results in figure 4.22 the EB integration technique was applied, while the results in figure 4.23 are based on the BDF2 integration technique.

By comparing the results for the different methods we observe that method 4 (staggered) is numerically the most efficient approach when using many time steps (N). Also the Broyden method is superior to the Newton methods when efficiency is compared. We can also note that the Newton method with numerical differentiation is computationally the most expensive scheme but the difference to the Newton method with analytical Jacobian is less than expected. This fact can be explained by the high cost to compute the analytical Jacobian for this complex material model.

Furthermore, both Newton methods converge for larger time steps as compared to the other methods. Especially, the staggered method needs rather small time steps in order to converge. Owing to this, we can see in figure 4.22 that the CPU time for the staggered method is increasing when decreasing the number of time steps; by decreasing the number of time steps further,

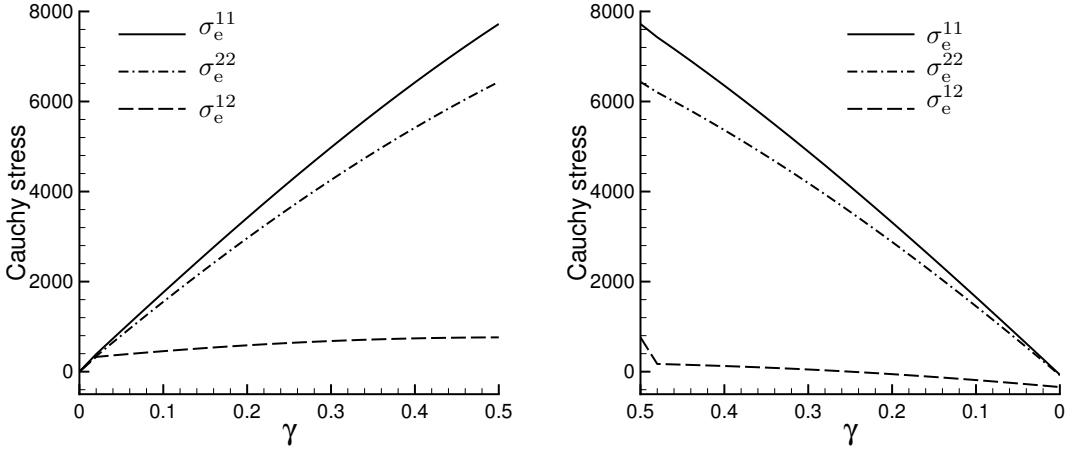

Figure 4.14: Simple shear, initially anisotropic material (elastoplasticity): Cauchy stresses $\boldsymbol{\sigma}_{\mathrm{e}}$ for $\gamma \in [\,0 \to 0.5\,,\; 0.5 \to 0\,]$ and $r_\kappa = r_{\mathrm{a}} = 1$, $r_{\mathrm{k}} = 0$ (no proportional hardening and damage but kinematic hardening).

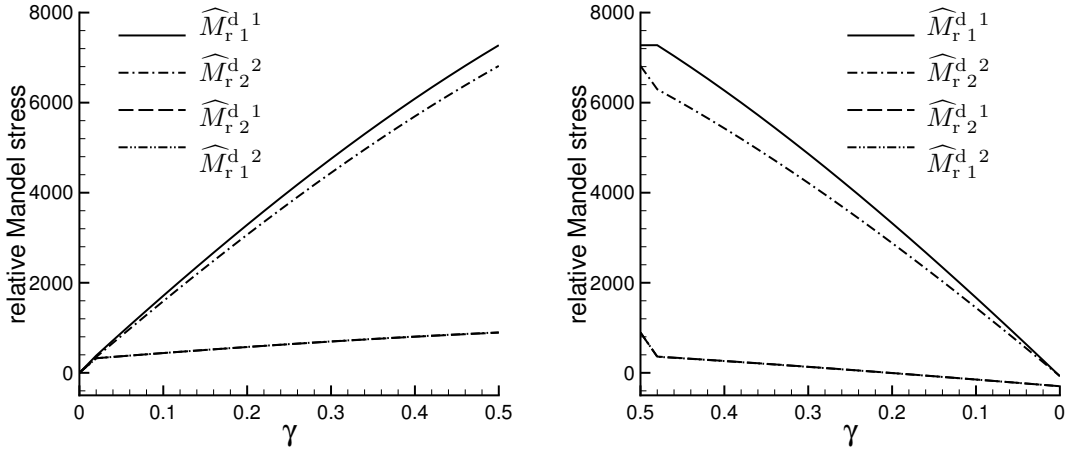

Figure 4.15: Simple shear, initially anisotropic material (elastoplasticity): relative Mandel stresses $\widehat{\boldsymbol{M}}_{\mathrm{r}}^{\mathrm{d}}$ for $\gamma \in [\,0 \to 0.5\,,\; 0.5 \to 0\,]$ and $r_\kappa = r_{\mathrm{a}} = 1$, $r_{\mathrm{k}} = 0$ (no proportional hardening and damage but kinematic hardening).

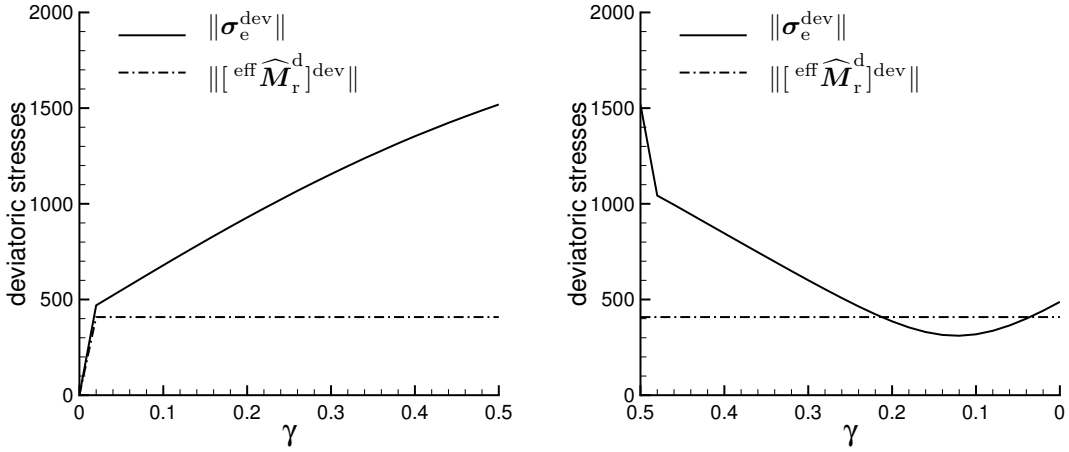

Figure 4.16: Simple shear, initially anisotropic material (elastoplasticity): norm of the deviatoric stress tensors $\boldsymbol{\sigma}_{\mathrm{e}}^{\mathrm{dev}}$ and $[\,{}^{\mathrm{eff}}\widehat{\boldsymbol{M}}_{\mathrm{r}}^{\mathrm{d}}]^{\mathrm{dev}}$ for $\gamma \in [\,0 \to 0.5\,,\; 0.5 \to 0\,]$ and $r_\kappa = r_{\mathrm{a}} = 1$, $r_{\mathrm{k}} = 0$ (no proportional hardening and damage but kinematic hardening).

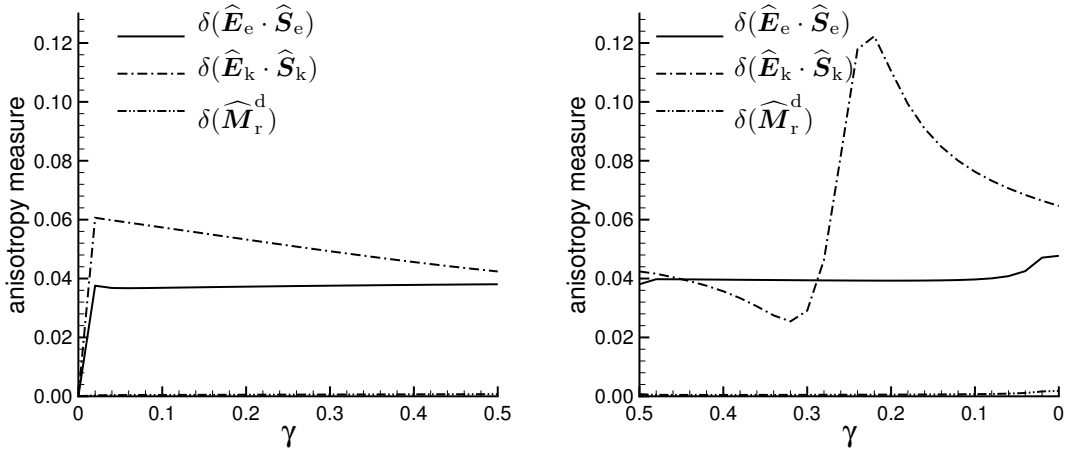

Figure 4.17: Simple shear, initially anisotropic material (elastoplasticity): anisotropy measures $\delta(\widehat{\boldsymbol{E}}_{\mathrm{e}} \cdot \widehat{\boldsymbol{S}}_{\mathrm{e}})$, $\delta(\widehat{\boldsymbol{E}}_{\mathrm{k}} \cdot \widehat{\boldsymbol{S}}_{\mathrm{k}})$, $\delta(\widehat{\boldsymbol{M}}_{\mathrm{r}}^{\mathrm{d}})$ for $\gamma \in [\,0 \to 0.5\,,\, 0.5 \to 0\,]$ and $r_\kappa = r_{\mathrm{a}} = 1$, $r_{\mathrm{k}} = 0$ (no proportional hardening and damage but kinematic hardening).

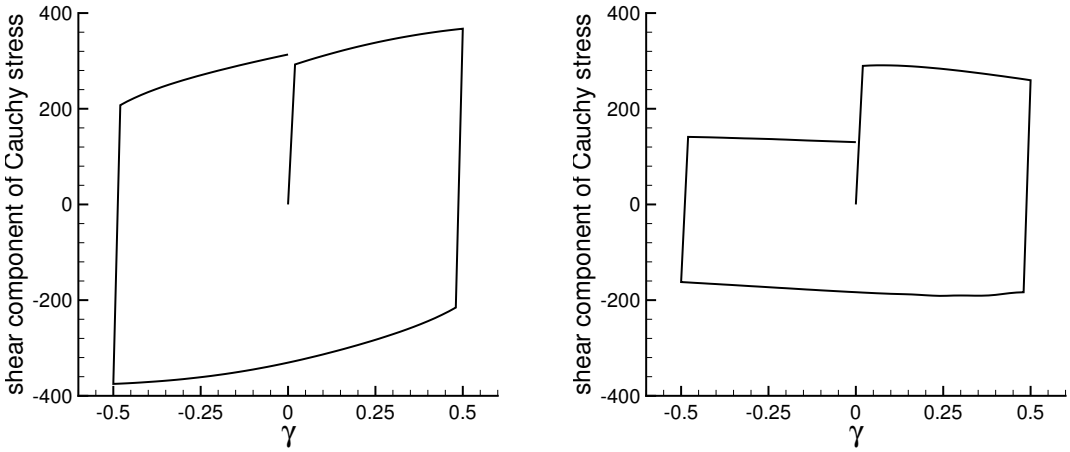

Figure 4.18: Simple shear, initially isotropic material (elastoplasticity): shear component of the Cauchy stress σ_{e}^{12} for $\gamma \in [\,0 \to 0.5\,,\, 0.5 \to -0.5\,,\, -0.5 \to 0\,]$ and $r_\kappa = r_{\mathrm{a}} = 1$, $r_{\mathrm{k}} = 0$ (no proportional hardening and damage but kinematic hardening; left) and $r_\kappa = 1$, $r_{\mathrm{k}} = r_{\mathrm{a}} = 0$ (no proportional hardening but kinematic hardening and anisotropic damage; right).

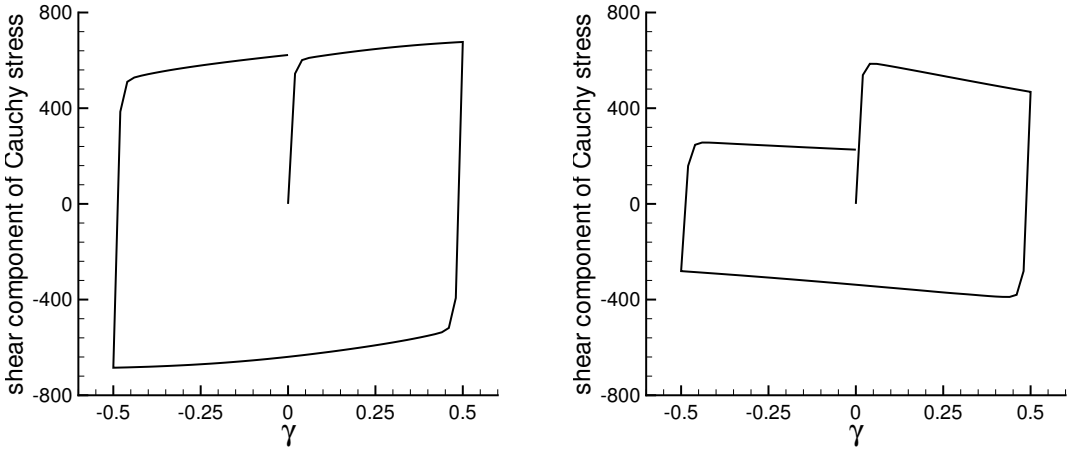

Figure 4.19: Simple shear, initially isotropic material (elasto–viscoplasticity): shear component of the Cauchy stress σ_{e}^{12} for $\gamma \in [\,0 \to 0.5\,,\, 0.5 \to -0.5\,,\, -0.5 \to 0\,]$ and $r_\kappa = r_{\mathrm{a}} = 1$, $r_{\mathrm{k}} = 0$ (no proportional hardening and damage but kinematic hardening; left) and $r_\kappa = 1$, $r_{\mathrm{k}} = r_{\mathrm{a}} = 0$ (no proportional hardening but kinematic hardening and anisotropic damage; right).

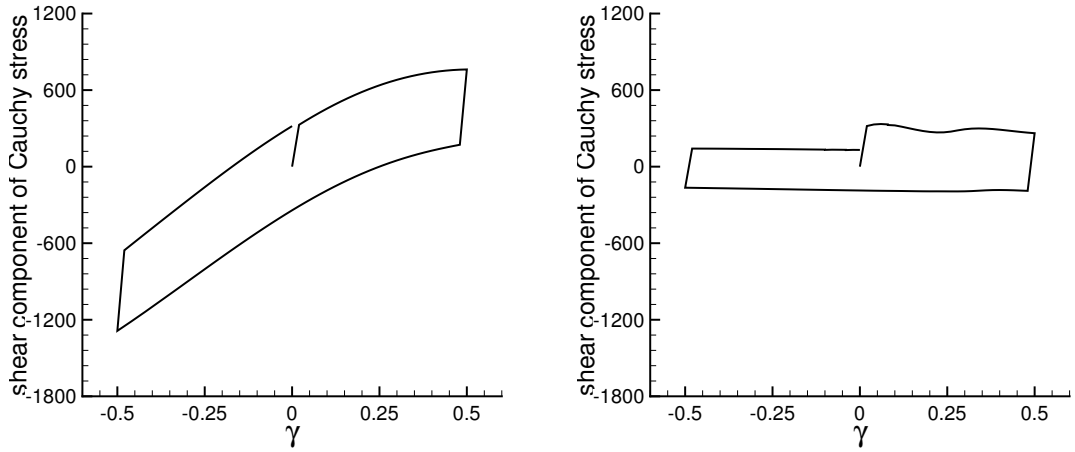

Figure 4.20: Simple shear, initially anisotropic material (elastoplasticity): shear component of the Cauchy stress σ_{e}^{12} for $\gamma \in [\,0 \rightarrow 0.5\,,\, 0.5 \rightarrow -0.5\,,\, -0.5 \rightarrow 0\,]$ and $r_\kappa = r_{\mathrm{a}} = 1$, $r_{\mathrm{k}} = 0$ (no proportional hardening and damage but kinematic hardening; left) and $r_\kappa = 1$, $r_{\mathrm{a}} = r_{\mathrm{k}} = 0$ (no proportional hardening but kinematic hardening and anisotropic damage; right).

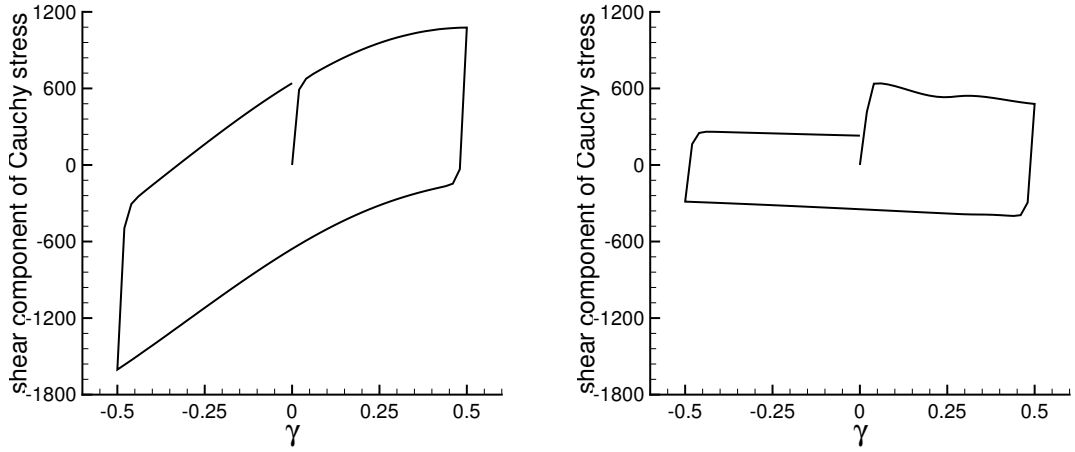

Figure 4.21: Simple shear, initially anisotropic material (elasto–viscoplasticity): shear component of the Cauchy stress σ_{e}^{12} for $\gamma \in [\,0 \rightarrow 0.5\,,\, 0.5 \rightarrow -0.5\,,\, -0.5 \rightarrow 0\,]$ and $r_\kappa = r_{\mathrm{a}} = 1$, $r_{\mathrm{a}} = 0$ (no proportional hardening and damage but kinematic hardening; left) and $r_\kappa = 1$, $r_{\mathrm{a}} = r_{\mathrm{k}} = 0$ (no proportional hardening but kinematic hardening and anisotropic damage; right).

the method will no longer converge. Nevertheless, in general we can conclude that for a given CPU time the staggered technique definitely gives the highest accuracy.

Finally, in these examples we also note, as expected, that the BDF2 algorithm gives higher accuracy than the EB algorithm. The extra cost for the BDF2 algorithm is that we must store internal variables from two time steps and not only from one time step as for EB integration. This, however, does not influence the CPU time in this simple example.

4.6.2 Torsion of a rod

Completing the numerical examples in this chapter, we lastly focus on a finite element application. The considered boundary value problem is a typical torsion problem of a rod as commonly elaborated in experimental and numerical investigations on the plastic behaviour of metallic materials. To be specific, the cross–section at the bottom of the rod is completely clamped while the cross–section at the top of the rod is rotated which allows to be measured

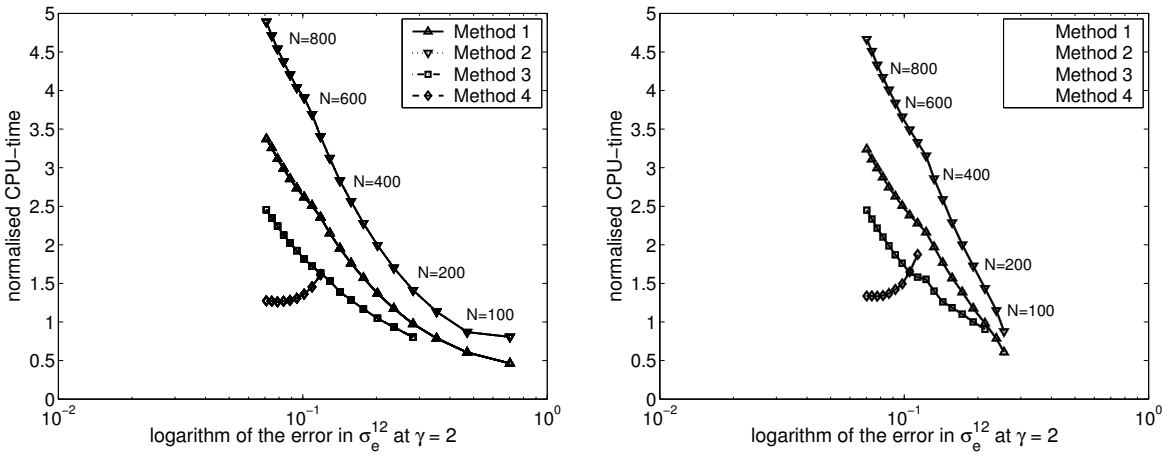

Figure 4.22: Accuracy versus numerical efficiency of different iteration schemes for EB integration: isotropic damage ($D = 0$), left; anisotropic damage ($D = 2$), right.

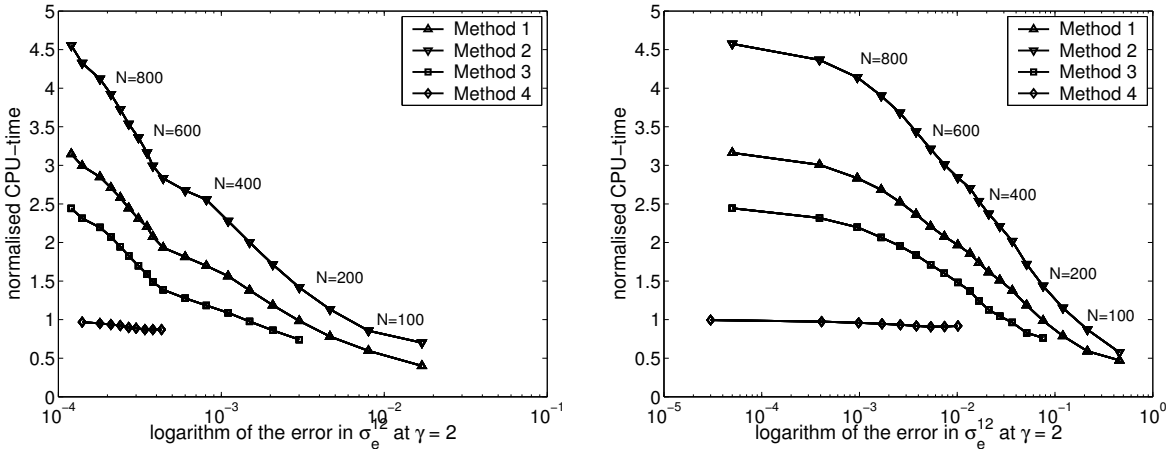

Figure 4.23: Accuracy versus numerical efficiency of different iteration schemes for BDF2 integration: isotropic damage ($D = 0$), left; anisotropic damage ($D = 2$), right.

in terms of an angle φ. Longitudinal displacements of the top cross–section are prevented so that a longitudinal force in addition to the torsional moment is observed. Figure 4.24 gives a graphical representation of the considered specimen. The geometry of the square rod is chosen as $1 \times 1 \times 5$ and the discretisation is performed by $5 \times 5 \times 10$ enhanced eight–node bricks (Q1E9) as advocated by Simo and Armero (1992). No emphasis is placed on the finite element implementation itself in this work but the reader is referred to the monographs by Oden (1972), Belytschko et al. (2000) or Dhondt (2004), and references cited therein.

In the sequel, we account for viscoplasticity, initial anisotropy, anisotropic degradation, kinematic and proportional hardening; $r_\kappa = 0.75$, $r_\mathrm{k} = 0.25$, $r_\mathrm{a} = 0$. The rotation or rather torsion angle φ is first increased from zero to $\frac{\pi}{2}$ and then reduced to zero so that loading and un–/reloading is modelled; $\varphi \in [\,0 \rightarrow \frac{\pi}{2}\,,\, \frac{\pi}{2} \rightarrow 0\,]$. Rate–dependency is characterised via the parameters $N = 1$, $t^* = 1000$ and the loading path from zero to $\varphi = \frac{\pi}{2}$ is related to the time interval $\mathcal{T} = 9$ (the un–/reloading path is related to the same time interval, i.e. $\varphi \in [\,0 \rightarrow \frac{\pi}{2}\,,\, \frac{\pi}{2} \rightarrow 0\,]$ corresponds to $\mathcal{T} = 18$). Figure 4.25 displays load/displacement curves for the loading and un–/reloading path. We observe that the torsional moment monitors the overall softening behaviour for loading and even for un–/reloading. Due to the chosen boundary conditions, the longitudinal force shows similar characteristics; at least at the end of the considered un–/reloading path softening is observed. For comparison reasons, we additionally highlight similar load/displacement curves for the (linear) kinematic hardening

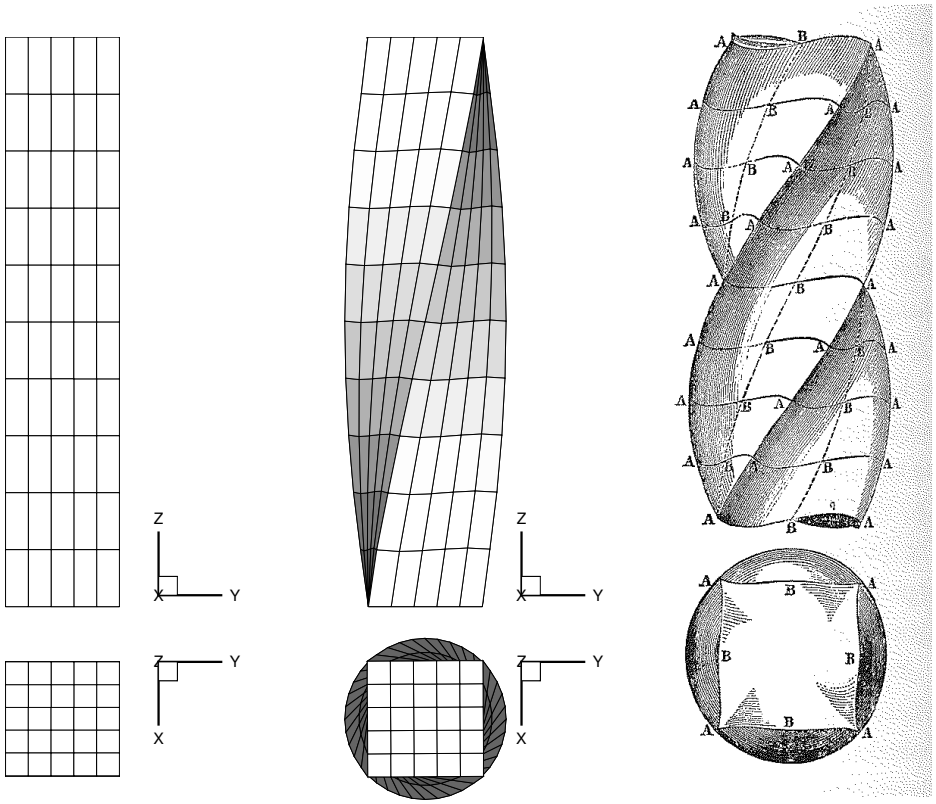

Figure 4.24: Torsion of a rod, initially anisotropic material: discretisation (left), deformed mesh for $\varphi \in [\, 0 \rightarrow \frac{\pi}{2} \,]$ (middle) and drawing by St.–Venant (right), taken from Fung and Tong (2001).

model in figure 4.26. These computations, which neglect the extension given in eq.(4.59), show higher peak values for the maximum torsional moment as well as for the maximum longitudinal force. This shift–effect underlines the influence of the non–linear saturation–type kinematic hardening model (the subsequent figures are based on the non–linear saturation–type model). Since initial anisotropy is considered, the response of the specimen is throughout un–symmetric. This property is clearly reflected by the deviatoric norm of the (elastic) Cauchy stresses and the effective relative Mandel stresses; see figures 4.27 and 4.28, where the loading and un–/reloading response is highlighted. The smallest damage eigenvalue, which in fact characterises the degree of damage, is visualised in figure 4.29. Note that the state of degradation is quite advanced and still increases for the un–/reloading path. Since the principal directions of the damage metric do not remain constant during the deformation process, we obtain a non–vanishing anisotropy measure with respect to the actual and initial damage metric as plotted in figure 4.30. Finally, the visualisation of the corresponding anisotropy measures for the elastic and kinematic hardening contributions are highlighted in figures 4.31 and 4.32. These plots underpin that the related Mandel–type stress tensors are throughout un–symmetric since the underlying related strain and stress tensors do not commutate.

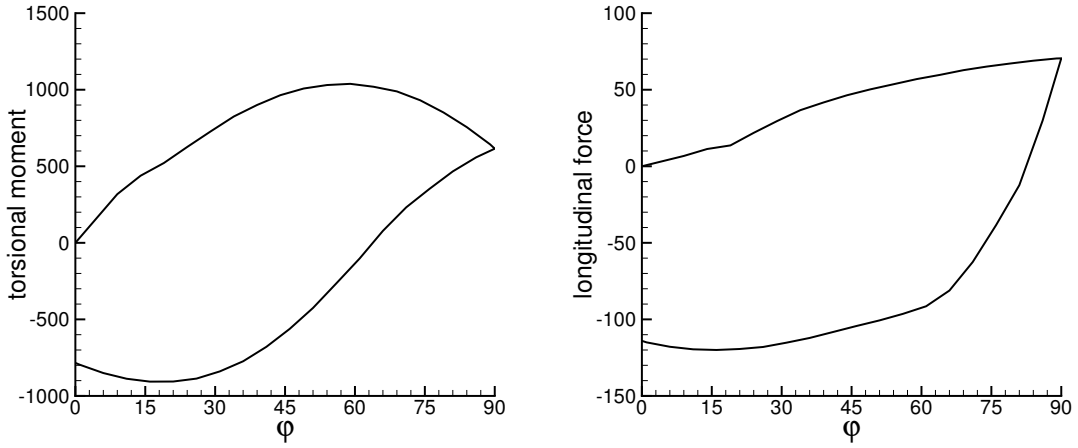

Figure 4.25: Torsion of a rod, initially anisotropic material (elasto–viscoplasticity): torsional moment (left), longitudinal force (right) for $\varphi \in [\,0 \rightarrow \frac{\pi}{2}\,,\, \frac{\pi}{2} \rightarrow 0\,]$ and $r_\kappa = 0.75$, $r_\mathrm{k} = 0.25$, $r_\mathrm{a} = 0$ (proportional and non–linear saturation–type kinematic hardening and anisotropic damage).

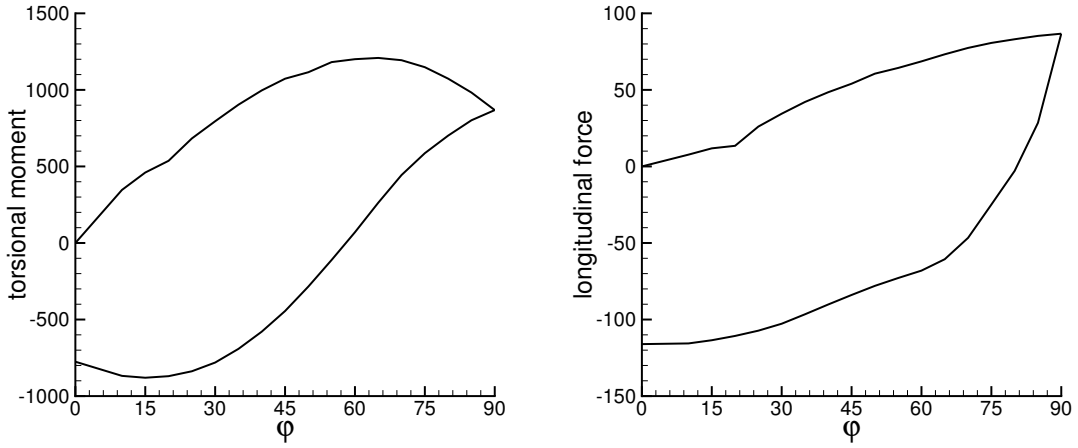

Figure 4.26: Torsion of a rod, initially anisotropic material (elasto–viscoplasticity): torsional moment (left), longitudinal force (right) for $\varphi \in [\,0 \rightarrow \frac{\pi}{2}\,,\, \frac{\pi}{2} \rightarrow 0\,]$ and $r_\kappa = 0.75$, $r_\mathrm{k} = 0.25$, $r_\mathrm{a} = 0$ (proportional and linear kinematic hardening and anisotropic damage).

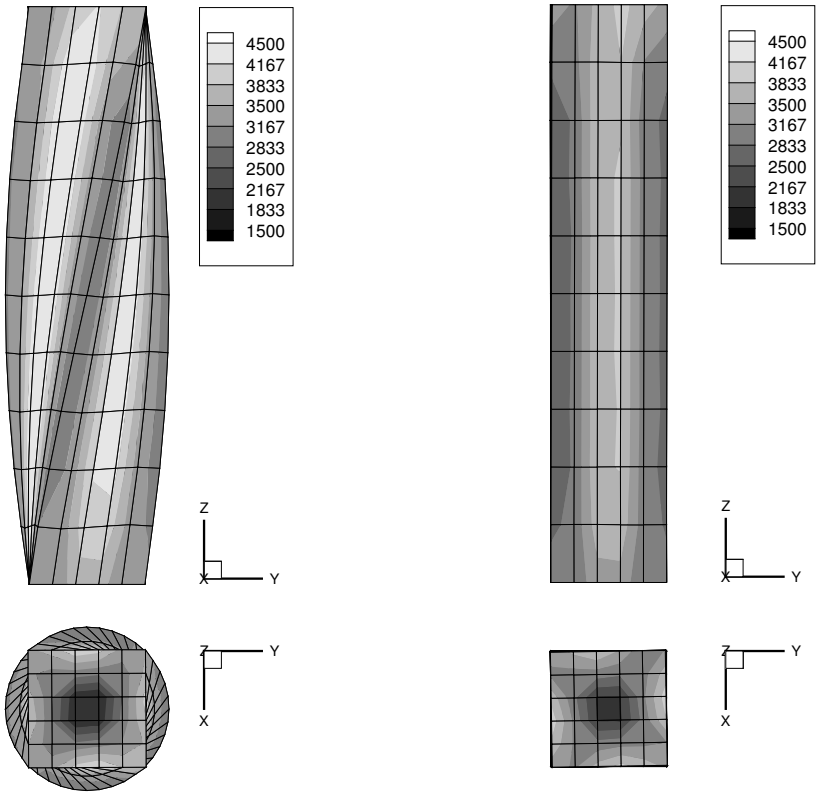

Figure 4.27: Torsion of a rod, initially anisotropic material (elasto–viscoplasticity): norm of $\boldsymbol{\sigma}_{\mathrm{e}}^{\mathrm{dev}}$ for $\varphi \in [\, 0 \rightarrow \frac{\pi}{2} \,]$ (left), $\varphi \in [\, 0 \rightarrow \frac{\pi}{2}\,,\, \frac{\pi}{2} \rightarrow 0 \,]$ (right) and $r_\kappa = 0.75$, $r_{\mathrm{k}} = 0.25$, $r_{\mathrm{a}} = 0$ (proportional and kinematic hardening and anisotropic damage).

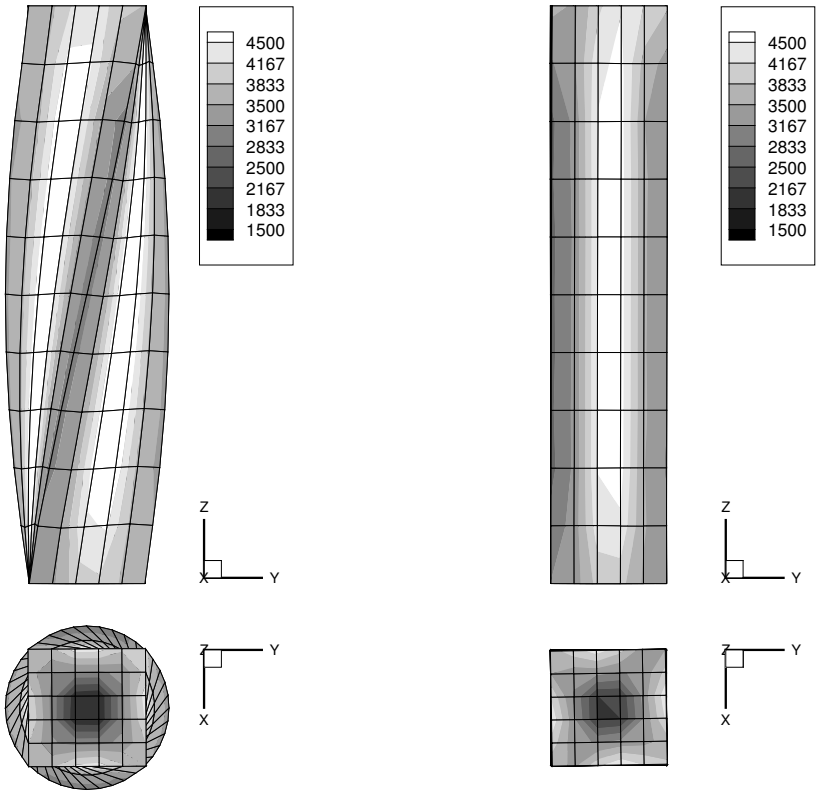

Figure 4.28: Torsion of a rod, initially anisotropic material (elasto–viscoplasticity): norm of $[{}^{\mathrm{eff}}\widehat{\boldsymbol{M}}_{\mathrm{r}}^{\mathrm{d}}]^{\mathrm{dev}}$ for $\varphi \in [\, 0 \rightarrow \frac{\pi}{2} \,]$ (left), $\varphi \in [\, 0 \rightarrow \frac{\pi}{2}\,,\, \frac{\pi}{2} \rightarrow 0 \,]$ (right) and $r_\kappa = 0.75$, $r_{\mathrm{k}} = 0.25$, $r_{\mathrm{a}} = 0$ (proportional and kinematic hardening and anisotropic damage).

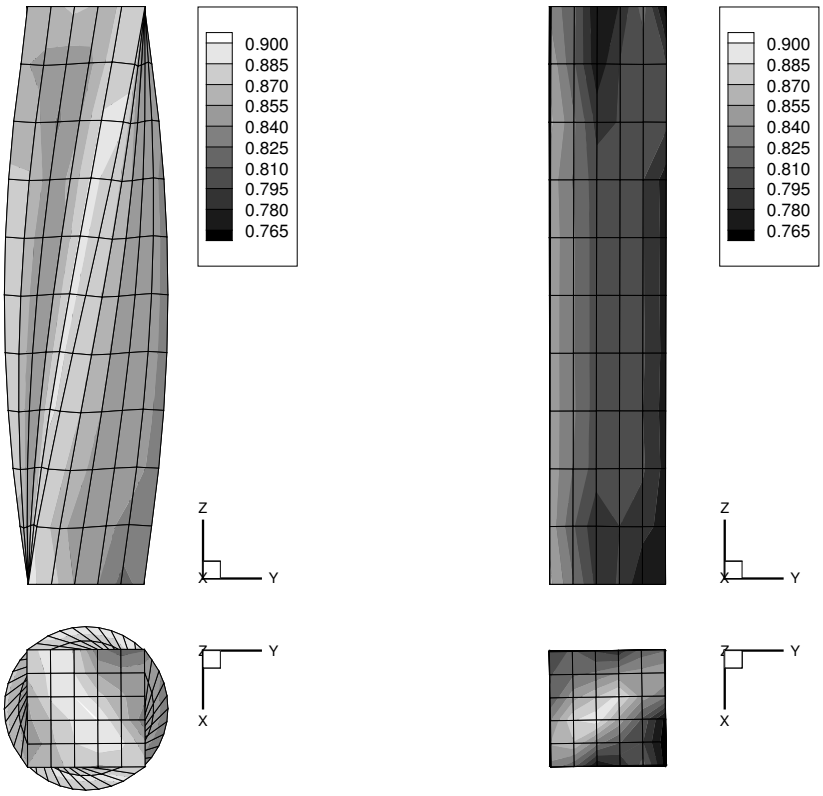

Figure 4.29: Torsion of a rod, initially anisotropic material (elasto–viscoplasticity): smallest damage eigenvalue α_1 for $\varphi \in [\,0 \rightarrow \frac{\pi}{2}\,]$ (left), $\varphi \in [\,0 \rightarrow \frac{\pi}{2}\,,\ \frac{\pi}{2} \rightarrow 0\,]$ (right) and $r_\kappa = 0.75$, $r_\mathrm{k} = 0.25$, $r_\mathrm{a} = 0$ (proportional and kinematic hardening and anisotropic damage).

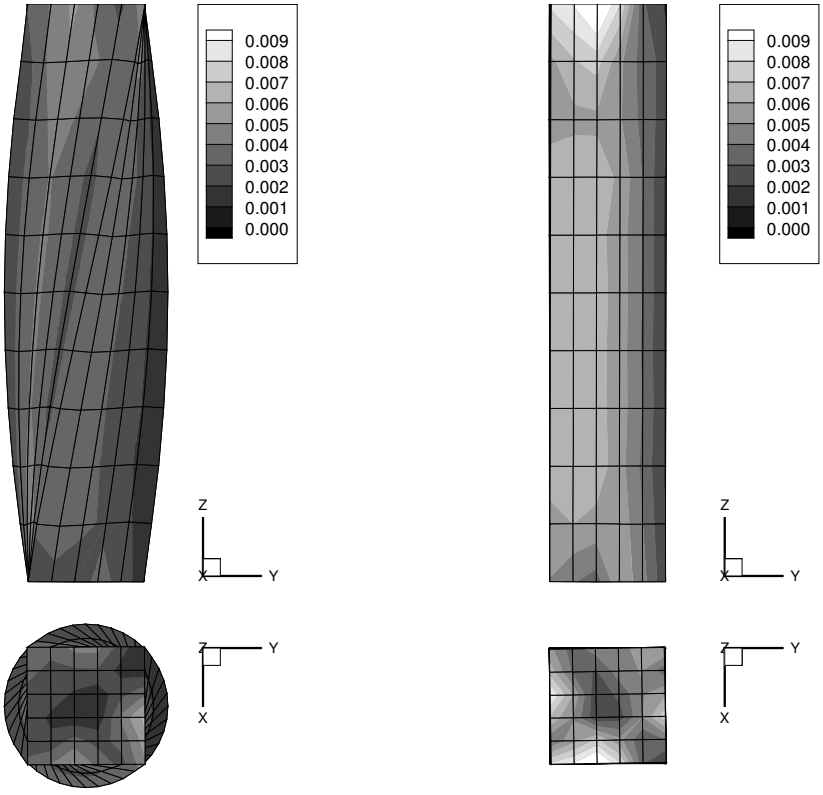

Figure 4.30: Torsion of a rod, initially anisotropic material (elasto–viscoplasticity): anisotropy measure $\delta(\boldsymbol{G}_\mathrm{p}\cdot\boldsymbol{A}_\mathrm{p}\cdot\boldsymbol{G}_\mathrm{p}\cdot\boldsymbol{A}_\mathrm{p}|_{t_0})$ for $\varphi \in [\,0 \rightarrow \frac{\pi}{2}\,]$ (left), $\varphi \in [\,0 \rightarrow \frac{\pi}{2}\,,\ \frac{\pi}{2} \rightarrow 0\,]$ (right) and $r_\kappa = 0.75$, $r_\mathrm{k} = 0.25$, $r_\mathrm{a} = 0$ (proportional and kinematic hardening and anisotropic damage).

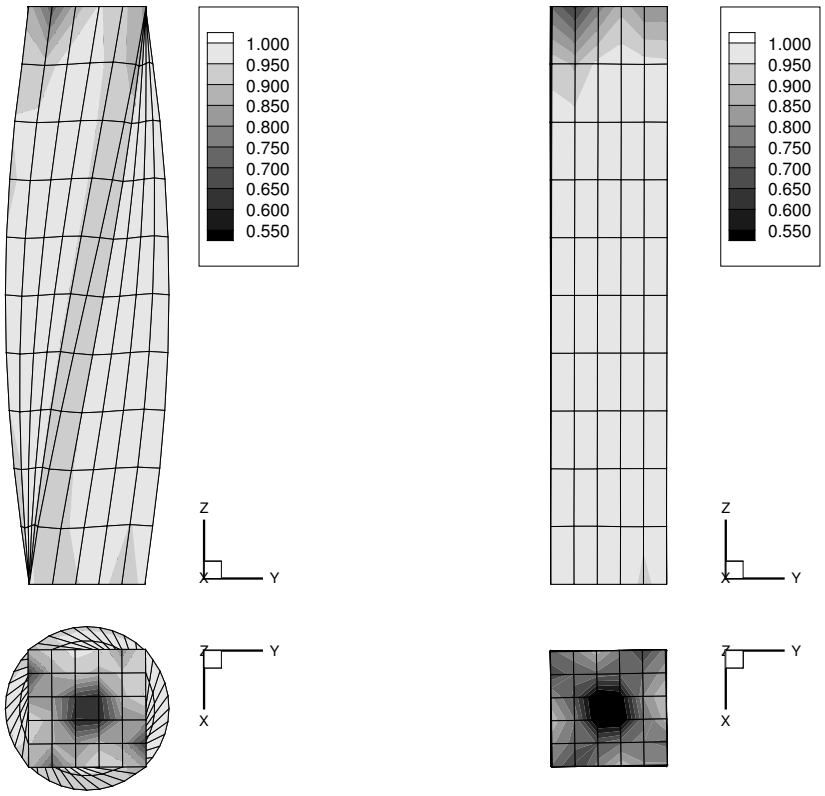

Figure 4.31: Torsion of a rod, initially anisotropic material (elasto–viscoplasticity): anisotropy measure $\delta(\widehat{\boldsymbol{E}}_{\mathrm{e}} \cdot \widehat{\boldsymbol{S}}_{\mathrm{e}})$ for $\varphi \in [\,0 \to \frac{\pi}{2}\,]$ (left), $\varphi \in [\,0 \to \frac{\pi}{2}\,,\, \frac{\pi}{2} \to 0\,]$ (right) and $r_\kappa = 0.75$, $r_{\mathrm{k}} = 0.25$, $r_{\mathrm{a}} = 0$ (proportional and kinematic hardening and anisotropic damage).

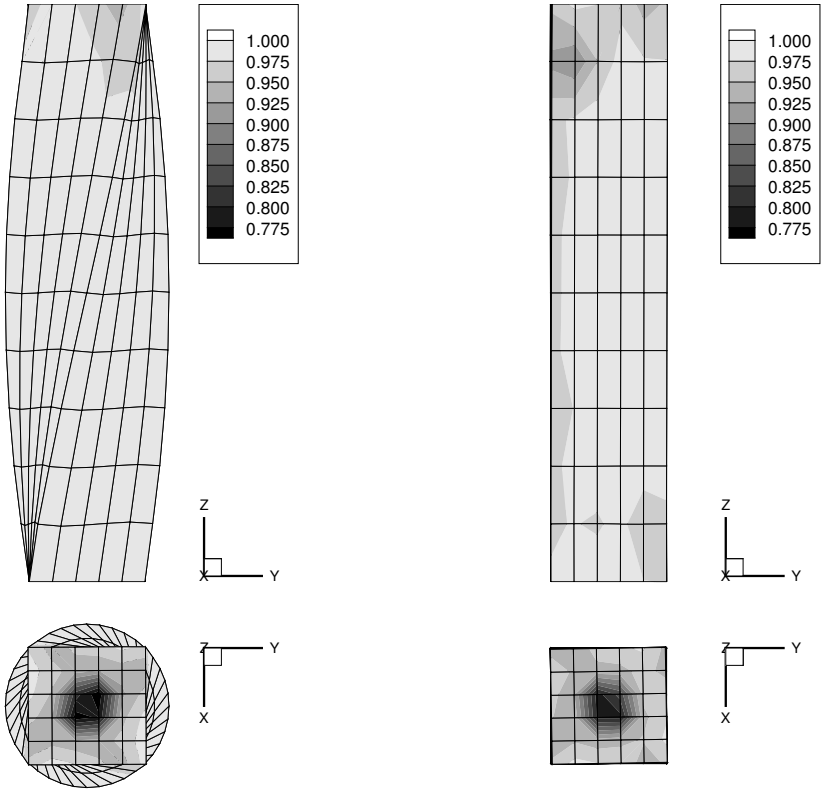

Figure 4.32: Torsion of a rod, initially anisotropic material (elasto–viscoplasticity): anisotropy measure $\delta(\widehat{\boldsymbol{E}}_{\mathrm{k}} \cdot \widehat{\boldsymbol{S}}_{\mathrm{k}})$ for $\varphi \in [\,0 \to \frac{\pi}{2}\,]$ (left), $\varphi \in [\,0 \to \frac{\pi}{2}\,,\, \frac{\pi}{2} \to 0\,]$ (right) and $r_\kappa = 0.75$, $r_{\mathrm{k}} = 0.25$, $r_{\mathrm{a}} = 0$ (proportional and kinematic hardening and anisotropic damage).

5 Deformation–induced substructure evolution for multiplicative elastoplasticity

In this chapter we extend the previously elaborated formulation (chapter 4) for kinematic hardening coupled with anisotropic damage to a, what we call, substructure evolution framework. In particular the former damage metric is thereby modified and deformation–induced anisotropy is again incorporated. The considered elastic symmetry group of interest is transversal isotropy. As a key feature of the developed approach, deformation–dependent reorientation of the underlying fibre direction is coupled with volumetric degradation of the bulk material such that the dissipation inequality is generally fulfilled.

Having materials in mind as, for instance, pearlitic steel, initial random orientation of individual grains is interpreted as initial macroscopic isotropy. These grains, however, tend to align after large shear deformation; compare, for example, Yokoyama et al. (2002) or Ivanisenko et al. (2003). In this regard, we propose a physically motivated framework for substructure or, in other words, texture evolution from a phenomenological or rather macroscopic point of view. By analogy with chapter 4, the developed model as such resembles formulations reported in the literature, see for instance Haupt (2000) or Tsakmakis (2004), while the macroscopic reorientation approach is inspired by Imatani and Maugin (2002), Maugin and Imatani (2003), Menzel (2005a), and Vincent et al. (2003); compare chapter 6. Furthermore, anisotropy is introduced via the previously highlighted fictitious configurations concept; compare Menzel and Steinmann (2003b), Menzel et al. (2005b), references cited in these works, and chapter 4. For additional relevant literature related to the modelling of substructure and large deformations, we refer to Dafalias (1984, 1985, 1998), Arvas (1992), Miehe (1998), Svendsen (1998), Böhlke and Bertram (2001), Menzel and Steinmann (2003c), Bucher et al. (2003), Johansson et al. (2005a, 2005b) and the contributions in Kocks et al. (2000).

The chapter is organised as follows: Section 5.1 gives an outline of the utilised modelling strategy, namely a short introduction on the introduced substructure metric. Application of the Coleman–Noll entropy principle to the problem at hand is briefly discussed in section 5.2. The main body of this chapter is section 5.3, where a prototype model is developed. The setup of appropriate yield functions, hardening potentials, reorientation and texture stiffness evolution together with elaborations of thermodynamic consistency are thereby addressed. Numerical integration techniques are reviewed in section 5.4 and used for the numerical examples in section 5.5 that highlight specific features of the proposed model.

5.1 Substructure metric

In the computational mechanics community the nowadays most frequently adopted method for the modelling of anisotropy is the introduction of structural tensors into the chosen Helmholtz free energy density and, for example, correlated inelastic potentials; see, for instance, Menzel and Steinmann (2003b, 2003d), and references cited therein. This method as such can be used to describe almost any possible symmetry group of a material provided that the appropriate order and number of tensors are used. Representation theorems can then be adopted to formulate the most general form of the Helmholtz free energy density expressed in terms of mixed invariants of deformation or stress tensors and the additionally introduced structural

tensors; see Spencer (1971) or the contributions in Boehler (1987) for a general survey. A more restricted method for the formulation of anisotropy, which is a subclass of the method with structural tensors, is to introduce the concept of fictitious configurations associated with tangent maps and so–called energy metrics; compare chapter 4. With the purpose to model special forms of evolving texture, we will set up evolution equations for the intermediate energy metric $\boldsymbol{A}_{\mathrm{p}} = \boldsymbol{F}_{\mathrm{a}} \cdot \boldsymbol{A}_{\mathrm{a}} \cdot \boldsymbol{f}_{\mathrm{a}}^{\mathrm{d}}$, whereby $\boldsymbol{A}_{\mathrm{a}} \doteq \boldsymbol{G}_{\mathrm{a}}^{-1}$ is assumed throughout. Apparently, this ansatz allows the incorporation of restricted forms of (elastic) anisotropy; compare Menzel and Steinmann (2001a).

Summarising, macroscopic texture, in terms of orientation and stiffness of the – for instance pearlite – substructure, is modelled in the following by means of the second–order symmetric anisotropy or substructure metric $\boldsymbol{A}_{\mathrm{p}}$. Application of the spectral decomposition theorem together with the assumption of transversally isotropic response leads to

$$\boldsymbol{A}_{\mathrm{p}} = \alpha\, \boldsymbol{G}_{\mathrm{p}}^{-1} + \beta\, \boldsymbol{a}_{\mathrm{p}} \otimes \boldsymbol{a}_{\mathrm{p}} \quad \text{with} \quad \|\boldsymbol{a}_{\mathrm{p}}\|_{\boldsymbol{G}_{\mathrm{p}}} = 1 \tag{5.1}$$

functions that determine the stiffness related to evolving anisotropy; compare remark 5.1.2. On the macroscopic scale, the preferred direction $\boldsymbol{a}_{\mathrm{p}}$ represents a vectorial quantity which is considered as the macroscopic conceptual counterpart to, for example, the orientation of the lattice structure in single crystals. The special format of $\boldsymbol{A}_{\mathrm{p}}$ in eq.(5.1) includes the modelling of isotropy ($\beta = 0 \;\forall\; t$) with evolution of the bulk stiffness (in terms of α). It also allows for the incorporation of initial anisotropy with a preferred direction ($\beta \neq 0$ at t_0) such that $\boldsymbol{A}_{\mathrm{p}} \neq \alpha\, \boldsymbol{G}_{\mathrm{p}}^{-1}$ at t_0 followed by evolution of both, stiffness (in terms of changing α and β) and reorientation (in terms of changing $\boldsymbol{a}_{\mathrm{p}}$), respectively. Moreover, the tensor $\boldsymbol{A}_{\mathrm{p}}$ defines the (elastic) material symmetry of the body B of interest; compare chapter 3 and 4. Reorientation of $\boldsymbol{a}_{\mathrm{p}}$ is defined by a rotation $\boldsymbol{R}_{\mathrm{a}} \in \mathbb{O}_{+}^{3}$ of the initial fibre direction $\boldsymbol{a}_0|_{t_0} \in T\mathcal{B}_0$ with $\|\boldsymbol{a}_0\| = 1 \;\forall\, t$, namely

$$\boldsymbol{a}_{\mathrm{p}} = \boldsymbol{R}_{\mathrm{a}} \cdot \boldsymbol{a}_0 \quad \text{so that} \quad \boldsymbol{a}_{\mathrm{p}} \neq \boldsymbol{F}_{\mathrm{p}} \cdot \boldsymbol{a}_0\,. \tag{5.2}$$

From the chain rule, the fact that $\boldsymbol{a}_0$ is assumed to remain constant and the orthogonality of $\boldsymbol{R}_{\mathrm{a}}$, it follows that $\mathrm{D}_t \boldsymbol{a}_{\mathrm{p}} = \boldsymbol{\Omega}_{\mathrm{a}} \cdot \boldsymbol{a}_{\mathrm{p}}$, whereby $\boldsymbol{\Omega}_{\mathrm{a}} = \mathrm{D}_t \boldsymbol{R}_{\mathrm{a}} \cdot \boldsymbol{R}_{\mathrm{a}}^{\mathrm{t}}$ constitutes the underlying (constitutive) spin tensor; compare chapter 6. The skew–symmetry of $\boldsymbol{\Omega}_{\mathrm{a}}$ together with the symmetry of $\boldsymbol{a}_{\mathrm{p}} \otimes \boldsymbol{a}_{\mathrm{p}}$ results in the following useful relation

$$\tfrac{1}{2}\, \mathrm{D}_t \|\boldsymbol{a}_{\mathrm{p}}\|^2 = \boldsymbol{a}_{\mathrm{p}} \cdot \boldsymbol{G}_{\mathrm{p}} \cdot \mathrm{D}_{\mathrm{t}} \boldsymbol{a}_p = \boldsymbol{a}_{\mathrm{p}} \cdot \boldsymbol{G}_{\mathrm{p}} \cdot \boldsymbol{\Omega}_{\mathrm{a}} \cdot \boldsymbol{a}_{\mathrm{p}} = 0 \tag{5.3}$$

which merely confirms that the rotation $\boldsymbol{R}_{\mathrm{a}}$ preserves the unit length of $\boldsymbol{a}_{\mathrm{p}}$.

Remark 5.1.1 *An alternative representation of eq.(5.1) reads* $\boldsymbol{A}_{\mathrm{p}} = \sum_{i=1}^{3} \beta_i \;\boldsymbol{a}_{\mathrm{p}\,i} \otimes \boldsymbol{a}_{\mathrm{p}\,i}$ *wherein the stiffness parameters* β_i *and the orientation of* $\boldsymbol{a}_{\mathrm{p}\,i}$ *are governed by evolution rules.*

Remark 5.1.2 *The particular format of* $\boldsymbol{A}_{\mathrm{p}}$ *in eq.(5.1) implies that the tangent mapping* $\boldsymbol{F}_{\mathrm{a}} = \widehat{\boldsymbol{v}}_{\mathrm{a}} \cdot \boldsymbol{R}_{\mathrm{a}}$ *in the definition of* $\boldsymbol{A}_{\mathrm{p}} = \boldsymbol{F}_{\mathrm{a}} \star \boldsymbol{G}_{\mathrm{a}}^{-1}$ *can be decomposed into a symmetric left stretch tensor* $\widehat{\boldsymbol{v}}_{\mathrm{a}}$ *and a rotation tensor* $\boldsymbol{R}_{\mathrm{a}} \in \mathbb{O}_{+}^{3}$ *so that*

$$\widehat{\boldsymbol{v}}_{\mathrm{a}} = \boldsymbol{F}_{\mathrm{a}} \cdot \boldsymbol{R}_{\mathrm{a}}^{\mathrm{t}} = \sqrt{\alpha}\; \boldsymbol{I}_{\mathrm{p}} - \left[\, \sqrt{\alpha} - \sqrt{\alpha + \beta}\, \right] \boldsymbol{a}_{\mathrm{p}} \otimes \left[\, \boldsymbol{a}_{\mathrm{p}} \cdot \boldsymbol{G}_{\mathrm{p}} \,\right]. \tag{5.4}$$

Combining eq.(5.4) with the Sherman–Morrison–Woodbury theorem results in $J_{\mathrm{a}} = \alpha \sqrt{\alpha + \beta}$ *and the requirement* $\alpha, \beta \in \{\, \alpha, \beta \,|\, \alpha > 0\,,\;\; \alpha + \beta > 0 \,\}$ *which ensures that* $J_{\mathrm{a}} > 0$ *and consequently* $\det(\boldsymbol{A}_{\mathrm{p}}) > 0$. *The rotation* $\boldsymbol{R}_{\mathrm{a}}$ *obviously does not influence the constitutive relations for the model presented below.*

5.2 Coleman–Noll entropy principle

The applied kinematical framework is one–to–one with the elaborations in chapter 4 and consequently based on the strain measures introduced in section 4.1, i.e. $\widehat{\boldsymbol{E}}_{\mathrm{e}} = \frac{1}{2}[\,\widehat{\boldsymbol{C}}_{\mathrm{e}} - \boldsymbol{G}_{\mathrm{p}}\,]$ and $\widehat{\boldsymbol{E}}_{\mathrm{k}} = \frac{1}{2}[\,\widehat{\boldsymbol{K}} - \boldsymbol{G}_{\mathrm{p}}\,]$; compare section 3.1. By analogy with eqs.(4.8,4.9), material time derivatives of the deformation and strain tensors are adopted in this chapter, namely

$$\mathrm{D}_t\widehat{\boldsymbol{E}}_{\mathrm{e}} = \tfrac{1}{2}\,\mathrm{D}_t\widehat{\boldsymbol{C}}_{\mathrm{e}} = \big[\,\widehat{\boldsymbol{C}}_{\mathrm{e}}\cdot\widehat{\boldsymbol{L}}_{\mathrm{e}}\,\big]^{\mathrm{sym}}\,, \qquad \mathrm{D}_t\widehat{\boldsymbol{E}}_{\mathrm{k}} = \tfrac{1}{2}\,\mathrm{D}_t\widehat{\boldsymbol{K}} = -\big[\,\widehat{\boldsymbol{K}}\cdot\widehat{\boldsymbol{L}}_{\mathrm{k}}\,\big]^{\mathrm{sym}} \tag{5.5}$$

and $\mathrm{D}_t\boldsymbol{A}_{\mathrm{p}} = 2\,[\,\widehat{\boldsymbol{L}}_{\mathrm{a}}\cdot\boldsymbol{A}_{\mathrm{p}}\,]$. As previously defined, for instance in remark 4.2.2 or in eq.(4.43), we will also make use of the following Lie derivatives

$$\begin{aligned}\mathrm{L}^{\mathrm{p}}_t\widehat{\boldsymbol{C}}_{\mathrm{e}} &= \boldsymbol{F}_{\mathrm{p}}\star\mathrm{D}_t\boldsymbol{C} \;=\; \mathrm{D}_t\widehat{\boldsymbol{C}}_{\mathrm{e}} \,+\, 2\,\big[\,\widehat{\boldsymbol{C}}_{\mathrm{e}}\cdot\widehat{\boldsymbol{L}}_{\mathrm{p}}\,\big]^{\mathrm{sym}}\\ \mathrm{L}^{\mathrm{p}}_t\widehat{\boldsymbol{E}}_{\mathrm{e}} &= \boldsymbol{F}_{\mathrm{p}}\star\mathrm{D}_t\boldsymbol{E}_{\mathrm{e}} \;=\; \mathrm{D}_t\widehat{\boldsymbol{E}}_{\mathrm{e}} \,+\, 2\,\big[\,\widehat{\boldsymbol{E}}_{\mathrm{e}}\cdot\widehat{\boldsymbol{L}}_{\mathrm{p}}\,\big]^{\mathrm{sym}}\end{aligned} \tag{5.6}$$

in the sequel. Based on the Helmholtz free energy density introduced in eq.(4.10), the isothermal Clausius–Duhem inequality – proportional hardening contributions being neglected – results in

$$\begin{aligned}\mathsf{D}_0 \;=\;& \tfrac{1}{2}\,\boldsymbol{S} : \mathrm{D}_t\boldsymbol{C}\\ &- \partial_{\widehat{\boldsymbol{E}}_{\mathrm{e}}}\psi_0\big|_{\widehat{\boldsymbol{E}}_{\mathrm{k}},\boldsymbol{A}_{\mathrm{p}}} : \mathrm{D}_t\widehat{\boldsymbol{E}}_{\mathrm{e}} - \partial_{\widehat{\boldsymbol{E}}_{\mathrm{k}}}\psi_0\big|_{\widehat{\boldsymbol{E}}_{\mathrm{e}},\boldsymbol{A}_{\mathrm{p}}} : \mathrm{D}_t\widehat{\boldsymbol{E}}_{\mathrm{k}} - \partial_{\boldsymbol{A}_{\mathrm{p}}}\psi_0\big|_{\widehat{\boldsymbol{E}}_{\mathrm{e}},\widehat{\boldsymbol{E}}_{\mathrm{k}}} : \mathrm{D}_t\boldsymbol{A}_{\mathrm{p}} \geq 0\end{aligned} \tag{5.7}$$

which, together with the elaborations above, can alternatively be rewritten as

$$\begin{aligned}\mathsf{D}_0 \;=\;& \big[\,\widehat{\boldsymbol{S}}_{\mathrm{e}} - \partial_{\widehat{\boldsymbol{E}}_{\mathrm{e}}}\psi_0\big|_{\widehat{\boldsymbol{E}}_{\mathrm{k}},\boldsymbol{A}_{\mathrm{p}}}\,\big] : \big[\,\mathrm{L}^{\mathrm{p}}_t\widehat{\boldsymbol{E}}_{\mathrm{e}} + \boldsymbol{G}_{\mathrm{p}}\cdot\widehat{\boldsymbol{L}}_{\mathrm{p}}\,\big]^{\mathrm{sym}}\\ &+\; \widehat{\boldsymbol{S}}_{\mathrm{e}} : \big[\,\widehat{\boldsymbol{C}}_{\mathrm{e}}\cdot\widehat{\boldsymbol{L}}_{\mathrm{p}}\,\big]^{\mathrm{sym}} + \widehat{\boldsymbol{S}}_{\mathrm{k}} : \big[\,\widehat{\boldsymbol{K}}\cdot\widehat{\boldsymbol{L}}_{\mathrm{k}}\,\big]^{\mathrm{sym}} + \widehat{\boldsymbol{S}}_{\mathrm{k}} : \big[\,\widehat{\boldsymbol{L}}_{\mathrm{a}}\cdot\boldsymbol{A}_{\mathrm{p}}\,\big]^{\mathrm{sym}} \geq 0\,,\end{aligned} \tag{5.8}$$

compare section 3.4, wherein use of the hyperelastic stress formats

$$\widehat{\boldsymbol{S}}_{\mathrm{e}} = \partial_{\widehat{\boldsymbol{E}}_{\mathrm{e}}}\psi_0\big|_{\widehat{\boldsymbol{E}}_{\mathrm{k}},\boldsymbol{A}_{\mathrm{p}}}\,, \qquad \widehat{\boldsymbol{S}}_{\mathrm{k}} = \partial_{\widehat{\boldsymbol{E}}_{\mathrm{k}}}\psi_0\big|_{\widehat{\boldsymbol{E}}_{\mathrm{e}},\boldsymbol{A}_{\mathrm{p}}}\,, \qquad \widehat{\boldsymbol{S}}_{\mathrm{a}} = -\,2\,\partial_{\boldsymbol{A}_{\mathrm{p}}}\psi_0\big|_{\widehat{\boldsymbol{E}}_{\mathrm{e}},\widehat{\boldsymbol{E}}_{\mathrm{k}}}\,, \tag{5.9}$$

has been made. Note that due to the special format of $\boldsymbol{A}_{\mathrm{p}}$, as established in eq.(5.1), the (reduced) dissipation inequality (5.8) also allows representations as

$$\begin{aligned}\mathsf{D}_0 \;=\;& \widehat{\boldsymbol{M}}^{\mathrm{d}}_{\mathrm{e}} : \widehat{\boldsymbol{L}}_{\mathrm{p}} + \widehat{\boldsymbol{M}}^{\mathrm{d}}_{\mathrm{k}} : \widehat{\boldsymbol{L}}_{\mathrm{k}}\\ &+\; \tfrac{1}{2}\,\widehat{\boldsymbol{S}}_{\mathrm{a}} : \big[\,\boldsymbol{G}_{\mathrm{p}}\,\mathrm{D}_t\alpha + \boldsymbol{a}_{\mathrm{p}}\otimes\boldsymbol{a}_{\mathrm{p}}\,\mathrm{D}_t\beta\,\big] + \beta\,\widehat{\boldsymbol{S}}_{\mathrm{a}} : \big[\,\boldsymbol{a}_{\mathrm{p}}\otimes\mathrm{D}_t\boldsymbol{a}_{\mathrm{p}}\,\big] \geq 0\,,\end{aligned} \tag{5.10}$$

see eq.(4.14) for the definition of the Mandel–type stresses. The particular format of eq.(5.10) turns out to be favourable for the model developed in this chapter since, in contrast to the formulation highlighted in the previous chapter 4, the force which drives the reorientation of $\boldsymbol{a}_{\mathrm{p}}$ can directly be addressed. Moreover, the evolution of α and β is combined such that the dissipation inequality is conveniently satisfied.

Remark 5.2.1 *An alternative formulation is defined upon introducing reorientation in the free energy via rotations, say $\boldsymbol{Q}_{\mathrm{p,k}} \in \mathbb{O}^3_+$; compare, for example, Tsakmakis (2004) or Haupt and Kersten (2003). The Helmholtz free energy density is then assumed to be a scalar–valued isotropic tensor function in terms of $\{\,\widehat{\boldsymbol{E}}_{\mathrm{e}}, \boldsymbol{Q}_{\mathrm{p}}, \widehat{\boldsymbol{E}}_{\mathrm{k}}, \boldsymbol{Q}_{\mathrm{k}}, \alpha, \beta\,\}$. By analogy with eq.(5.10), we end up with*

$$\begin{aligned}\mathsf{D}_0 \;=\;& \widehat{\boldsymbol{M}}^{\mathrm{d}}_{\mathrm{e}} : \big[\,\widehat{\boldsymbol{L}}_{\mathrm{p}} - \boldsymbol{W}_{\mathrm{p}}\,\big] \;+\; \widehat{\boldsymbol{M}}^{\mathrm{d}}_{\mathrm{k}} : \big[\,\widehat{\boldsymbol{L}}_{\mathrm{k}} - \boldsymbol{W}_{\mathrm{k}}\,\big]\\ &-\; \partial_{\alpha}\psi_0\big|_{\widehat{\boldsymbol{E}}_{\mathrm{e}},\ldots,\beta}\,\mathrm{D}_t\alpha \quad - \;\partial_{\beta}\psi_0\big|_{\widehat{\boldsymbol{E}}_{\mathrm{e}},\ldots,\alpha}\,\mathrm{D}_t\beta \quad \geq 0\,,\end{aligned} \tag{5.11}$$

wherein the constitutive spins $\boldsymbol{W}_{\mathrm{p,k}} = \mathrm{D}_t\boldsymbol{Q}_{\mathrm{p,k}}\cdot\boldsymbol{Q}^{\mathrm{t}}_{\mathrm{p,k}} \in \mathbb{W}^3$ have been introduced. Hence, evolution equations for $\widehat{\boldsymbol{L}}_{\mathrm{p}}$, $\widehat{\boldsymbol{L}}_{\mathrm{k}}$, $\mathrm{D}_t\alpha$, $\mathrm{D}_t\beta$, and $\boldsymbol{W}_{\mathrm{p}}$, $\boldsymbol{W}_{\mathrm{k}}$ need to be formulated such that the dissipation inequality is fulfilled.

5.3 Prototype model

Based on the elaborations above and by analogy with the pervious chapter, we next propose a prototype model which in particular includes a stress–driven fibre reorientation. Later on, this prototype model serves to perform representative numerical examples which are embedded into a finite element context.

5.3.1 Helmholtz free energy density

The applied Helmholtz free energy density coincides with the format chosen in section 4.5.1. For completeness, however, we additionally mention the particular representation of the corresponding hyperelastic stresses, namely

$$\begin{aligned}
\widehat{\boldsymbol{S}}_{\mathrm{e}} &= \quad 2\,G \quad \boldsymbol{A}_{\mathrm{p}} \cdot \widehat{\boldsymbol{E}}_{\mathrm{e}} \cdot \boldsymbol{A}_{\mathrm{p}} + \quad L \quad I_{\mathrm{e}\,1} \quad \boldsymbol{A}_{\mathrm{p}}, \\
\widehat{\boldsymbol{S}}_{\mathrm{k}} &= \quad 2\,H_3 \quad \boldsymbol{A}_{\mathrm{p}} \cdot \widehat{\boldsymbol{E}}_{\mathrm{k}} \cdot \boldsymbol{A}_{\mathrm{p}} - \tfrac{2}{3} \; H_3 \; I_{\mathrm{k}\,1} \quad \boldsymbol{A}_{\mathrm{p}}, \\
\widehat{\boldsymbol{S}}_{\mathrm{a}} &= -\,4\,G \quad \widehat{\boldsymbol{E}}_{\mathrm{e}} \cdot \boldsymbol{A}_{\mathrm{p}} \cdot \widehat{\boldsymbol{E}}_{\mathrm{e}} - 2 \; L \quad I_{\mathrm{e}\,1} \quad \widehat{\boldsymbol{E}}_{\mathrm{e}} \\
&\quad -\,4\,H_3 \; \widehat{\boldsymbol{E}}_{\mathrm{k}} \cdot \boldsymbol{A}_{\mathrm{p}} \cdot \widehat{\boldsymbol{E}}_{\mathrm{k}} + \tfrac{4}{3} \; H_3 \; I_{\mathrm{k}\,1} \quad \widehat{\boldsymbol{E}}_{\mathrm{k}}\,.
\end{aligned} \tag{5.12}$$

Moreover, it is also interesting to note, that the purely elastic tangent operator recaptures the standard isotropic St.–Venant–Kirchhoff stiffness tensor

$$\widehat{\mathsf{E}}_{\mathrm{e}} := \partial_{\widehat{\boldsymbol{E}}_{\mathrm{e}}} \widehat{\boldsymbol{S}}_{\mathrm{e}} = G \left[\boldsymbol{A}_{\mathrm{p}} \,\overline{\otimes}\, \boldsymbol{A}_{\mathrm{p}} + \boldsymbol{A}_{\mathrm{p}} \,\underline{\otimes}\, \boldsymbol{A}_{\mathrm{p}} \right] + L \left[\boldsymbol{A}_{\mathrm{p}} \otimes \boldsymbol{A}_{\mathrm{p}} \right] \tag{5.13}$$

despite the fact that $\boldsymbol{A}_{\mathrm{p}}$ replaces $\boldsymbol{G}_{\mathrm{p}}^{-1}$.

5.3.2 Yield function and kinematic hardening potential

By analogy with eq.(4.15), we next introduce an admissible elastic domain with respect to the intermediate configuration

$$\mathcal{A} = \left\{ \widehat{\boldsymbol{M}}_{\mathrm{r}}^{\mathrm{d}} \;\middle|\; {}^{\mathrm{yie}}\Phi\big(\widehat{\boldsymbol{M}}_{\mathrm{r}}^{\mathrm{d}}, \boldsymbol{A}_{\mathrm{p}}^{\mathrm{yie}}, \beta; \boldsymbol{X}\big) \leq 0 \right\} \quad \text{with} \quad \widehat{\boldsymbol{M}}_{\mathrm{r}}^{\mathrm{d}} \doteq \widehat{\boldsymbol{M}}_{\mathrm{e}}^{\mathrm{d}} - \widehat{\boldsymbol{M}}_{\mathrm{k}}^{\mathrm{d}}\,, \tag{5.14}$$

wherein the incorporated metric $\boldsymbol{A}_{\mathrm{p}}^{\mathrm{yie}}$ is assumed to take a similar format as $\boldsymbol{A}_{\mathrm{p}}$, i.e

$$\boldsymbol{A}_{\mathrm{p}}^{\mathrm{yie}} \doteq \boldsymbol{G}_{\mathrm{p}}^{-1} - \eta_{\mathrm{yie}} \left[1 - \exp(-|\beta|) \right] \boldsymbol{a}_{\mathrm{p}} \otimes \boldsymbol{a}_{\mathrm{p}} \quad \text{with} \quad \eta_{\mathrm{yie}} \in [\,0\,,\,1\,] \tag{5.15}$$

denoting a material parameter that governs the orientational influences of the yield function; compare also eq.(5.1). Apparently, $\boldsymbol{A}_{\mathrm{p}}^{\mathrm{yie}}$ defines the symmetry group of the yield function via

$$\mathbb{G}_{\mathrm{yie}} = \left\{ \boldsymbol{Q} \in \mathbb{O}^3 \;\middle|\; \boldsymbol{Q} \star \boldsymbol{A}_{\mathrm{p}}^{\mathrm{yie}} = \boldsymbol{A}_{\mathrm{p}}^{\mathrm{yie}} \right\} \tag{5.16}$$

and also allows interpretation as the pushforward (in terms of an additional tangent mapping) of a metric tensor settled in a configuration which represents, for instance, isotropic inelastic response if kinematic hardening effects would be neglected. Here, however, $\boldsymbol{A}_{\mathrm{p}}^{\mathrm{yie}}$ is the result of substituting α and β in eq.(5.1) with 1 and $-\,\eta_{\mathrm{yie}}\,[\,1 - \exp(-|\beta|)\,]$, respectively. It is then assured that the apparent yield stress increases with β in the direction of $\boldsymbol{a}_{\mathrm{p}}$. Note that $\det(\boldsymbol{A}_{\mathrm{p}}^{\mathrm{yie}}) = [\,1 - \eta_{\mathrm{yie}}\,] + \eta_{\mathrm{yie}} \exp(-|\beta|) \geq 0$ for $\eta_{\mathrm{yie}} \in [\,0\,,\,1\,]$ and that $\boldsymbol{A}_{\mathrm{p}}^{\mathrm{yie}}$ has the limiting values $\boldsymbol{G}_{\mathrm{p}}^{-1}$ for $\beta \to 0$ and $\boldsymbol{G}_{\mathrm{p}}^{-1} - \eta_{\mathrm{yie}}\,\boldsymbol{a}_{\mathrm{p}} \otimes \boldsymbol{a}_{\mathrm{p}}$ for $\beta \to \infty$, respectively. Thus, the metric $\boldsymbol{A}_{\mathrm{p}}^{\mathrm{yie}}$ is reduced in the direction of $\boldsymbol{a}_{\mathrm{p}}$.

Next, we assume that the yield function depends only on the symmetric part of the stress arguments and agree to a deviatoric v. Mises–type format, i.e.

$$ {}^{\mathrm{yie}}\Phi \doteq {}^{\mathrm{yie}}\Phi\big(\big[\, \widehat{\boldsymbol{M}}{}^{\mathrm{d}}_{\mathrm{r}} \cdot \boldsymbol{G}_{\mathrm{p}} \,\big]^{\mathrm{sym}}, \boldsymbol{A}^{\mathrm{yie}}_{\mathrm{p}}, \beta; \boldsymbol{X} \big) \doteq \tfrac{3}{2\,Y_{\mathrm{p}}}\, I^{\mathrm{dev}}_{\mathrm{r}\,2} - Y_{\mathrm{p}} \leq 0\,, \tag{5.17} $$

wherein

$$ I^{\mathrm{dev}}_{\mathrm{r}\,2} = \big[\, \widehat{\boldsymbol{M}}{}^{\mathrm{d}}_{\mathrm{r}} \cdot \boldsymbol{G}_{\mathrm{p}} \,\big]^{\mathrm{sym}} : \widehat{\mathsf{H}}^{\mathrm{dev}}_{\mathrm{yie}} : \big[\, \widehat{\boldsymbol{M}}{}^{\mathrm{d}}_{\mathrm{r}} \cdot \boldsymbol{G}_{\mathrm{p}} \,\big]^{\mathrm{sym}} \geq 0 \quad \text{and} \quad Y_{\mathrm{p}} = Y_{\mathrm{p}\,0}\,\sqrt{1+\beta^2} \tag{5.18} $$

together with

$$ \begin{aligned} \widehat{\mathsf{H}}^{\mathrm{dev}}_{\mathrm{yie}} \;\doteq\; & \boldsymbol{A}^{\mathrm{yie}}_{\mathrm{p}} \,\overline{\otimes}\, \boldsymbol{A}^{\mathrm{yie}}_{\mathrm{p}} + \tfrac{1}{9}\, I_{\mathrm{yie}\,2}\, \boldsymbol{G}^{-1}_{\mathrm{p}} \otimes \boldsymbol{G}^{-1}_{\mathrm{p}} \\ & - \tfrac{1}{3}\, \big[\boldsymbol{G}^{-1}_{\mathrm{p}} \otimes [\, \boldsymbol{A}^{\mathrm{yie}}_{\mathrm{p}} \cdot \boldsymbol{G}_{\mathrm{p}} \cdot \boldsymbol{A}^{\mathrm{yie}}_{\mathrm{p}} \,] + [\, \boldsymbol{A}^{\mathrm{yie}}_{\mathrm{p}} \cdot \boldsymbol{G}_{\mathrm{p}} \cdot \boldsymbol{A}^{\mathrm{yie}}_{\mathrm{p}} \,] \otimes \boldsymbol{G}^{-1}_{\mathrm{p}} \,\big] \end{aligned} \tag{5.19} $$

for $I_{\mathrm{yie}\,2} = \boldsymbol{I}_{\mathrm{p}} : [\, \boldsymbol{G}_{\mathrm{p}} \cdot \boldsymbol{A}^{\mathrm{yie}}_{\mathrm{p}} \,]^2$. The incorporation of β into the threshold $Y_{\mathrm{p}} \geq Y_{\mathrm{p}\,0} > 0$ allows interpretation as proportional harding evolution. A similar ansatz is applied to the kinematic hardening potential, to be specific

$$ {}^{\mathrm{har}}\Phi \doteq {}^{\mathrm{har}}\Phi\big(\big[\, \widehat{\boldsymbol{M}}{}^{\mathrm{d}}_{\mathrm{k}} \cdot \boldsymbol{G}_{\mathrm{p}} \,\big]^{\mathrm{sym}}, \boldsymbol{A}^{\mathrm{yie}}_{\mathrm{p}}, \beta; \boldsymbol{X} \big) \doteq \tfrac{3}{2\,Y_{\mathrm{k}}}\, I^{\mathrm{dev}}_{\mathrm{k}\,2} \quad \text{with} \quad Y_{\mathrm{k}} = Y_{\mathrm{k}\,0}\,\sqrt{1+\beta^2} \tag{5.20} $$

and $I^{\mathrm{dev}}_{\mathrm{k}\,2} = [\, \widehat{\boldsymbol{M}}{}^{\mathrm{d}}_{\mathrm{k}} \cdot \boldsymbol{G}_{\mathrm{p}} \,]^{\mathrm{sym}} : \widehat{\mathsf{H}}^{\mathrm{dev}}_{\mathrm{yie}} : [\, \widehat{\boldsymbol{M}}{}^{\mathrm{d}}_{\mathrm{k}} \cdot \boldsymbol{G}_{\mathrm{p}} \,]^{\mathrm{sym}} \geq 0$.

In view of setting up (non–associated) inelastic flow rules, we furthermore introduce the plastic or rather inelastic potential ${}^{\mathrm{pot}}\Phi = {}^{\mathrm{yie}}\Phi + {}^{\mathrm{har}}\Phi$. The dissipation inequality in eq.(5.10) motivates evolution equations for $\widehat{\boldsymbol{L}}_{\mathrm{p}}$ and $\widehat{\boldsymbol{L}}_{\mathrm{k}}$, respectively (besides $\mathrm{D}_t\alpha$, $\mathrm{D}_t\beta$ and $\mathrm{D}_t\boldsymbol{a}_{\mathrm{p}}$). The evolution of plastic flow is here proposed to be proportional to the gradient of the plastic potential in stress space as defined in eqs.(5.17–5.20) which obviously results in a purely symmetric gradient $\partial\, {}^{\mathrm{pot}}\Phi / \partial\, \widehat{\boldsymbol{M}}{}^{\mathrm{d}}_{\mathrm{e}}$. The general setting of constitutive equations for the plastic flow, however, includes also the plastic spin in addition to the (symmetric) rate of plastic deformation. Therefore, it is convenient to decompose $\widehat{\boldsymbol{L}}_{\mathrm{p}} = \boldsymbol{D}_{\mathrm{p}} + \boldsymbol{\Omega}_{\mathrm{p}}$ in its symmetric part $\boldsymbol{D}_{\mathrm{p}} = \widehat{\boldsymbol{L}}{}^{\mathrm{sym}}_{\mathrm{p}}$ and its skew–symmetric part $\boldsymbol{\Omega}_{\mathrm{p}} = \widehat{\boldsymbol{L}}{}^{\mathrm{skw}}_{\mathrm{p}}$. The evolution for the rate of plastic deformation is proposed as

$$ \begin{aligned} \boldsymbol{D}_{\mathrm{p}} \;&\doteq\; \mathrm{D}_t\lambda\; \partial_{\widehat{\boldsymbol{M}}{}^{\mathrm{d}}_{\mathrm{e}}}\, {}^{\mathrm{pot}}\Phi = \mathrm{D}_t\lambda\; \partial_{\widehat{\boldsymbol{M}}{}^{\mathrm{d}}_{\mathrm{e}}}\, {}^{\mathrm{yie}}\Phi \\ &=\; \mathrm{D}_t\lambda\; \tfrac{3}{Y_{\mathrm{p}}}\; \Big[\, \big[\, \widehat{\boldsymbol{M}}{}^{\mathrm{d}}_{\mathrm{r}} \cdot \boldsymbol{G}_{\mathrm{p}} \,\big]^{\mathrm{sym}} : \widehat{\mathsf{H}}^{\mathrm{dev}}_{\mathrm{yie}} \,\Big]^{\mathrm{sym}} \cdot \boldsymbol{G}_{\mathrm{p}}\,. \end{aligned} \tag{5.21} $$

Inspired by Dafalias (1998), we now introduce the skew–symmetric plastic spin $\boldsymbol{\Omega}^{\mathrm{iso}}_{\mathrm{p}} \doteq \boldsymbol{\Omega}_{\mathrm{p}}$; compare remark 5.2.1 with $\boldsymbol{\Omega}^{\mathrm{iso}}_{\mathrm{p}} \doteq \boldsymbol{\Omega}_{\mathrm{p}} - \boldsymbol{W}_{\mathrm{p}}$ which is isoclinic with respect to the constitutive spin $\boldsymbol{W}_{\mathrm{p}}$. Furthermore, as shown by Dafalias (1985) and Arvas (1992), the plastic spin for the considered symmetry group can be formulated as

$$ \boldsymbol{\Omega}^{\mathrm{iso}}_{\mathrm{p}} = \mathrm{D}_t\lambda\; |f_0(\boldsymbol{D}_{\mathrm{p}})|\; \widehat{\boldsymbol{M}}{}^{\mathrm{skw}}_{\mathrm{e}} \quad \text{with} \quad f_0(\boldsymbol{D}_{\mathrm{p}}) \doteq \eta_{\mathrm{p}}\, \boldsymbol{I}^{\mathrm{d}}_{\mathrm{p}} : \boldsymbol{D}_{\mathrm{p}} \tag{5.22} $$

where $\eta_{\mathrm{p}} \geq 0$ denotes a material parameter. From eq.(5.22) we conclude that the assumed format for f_0 is first–order homogeneous in the argument $\boldsymbol{D}_{\mathrm{p}}$ so that $f_0(\varepsilon\, \boldsymbol{D}_{\mathrm{p}}) = \varepsilon\, f_0(\boldsymbol{D}_{\mathrm{p}})$. An alternative formulation of the the scalar–valued function f_0 is obtained upon, for instance, replacing $\boldsymbol{I}^{\mathrm{d}}_{\mathrm{p}}$ in eq.(5.22) with a linear combination of $\boldsymbol{I}^{\mathrm{d}}_{\mathrm{p}}$, $\boldsymbol{G}_{\mathrm{p}} \cdot \boldsymbol{A}_{\mathrm{p}}$, $\widehat{\boldsymbol{M}}_{\mathrm{e}}$, and $\widehat{\boldsymbol{M}}_{\mathrm{k}}$, respectively.

In analogy to the decomposition of $\widehat{\boldsymbol{L}}_{\mathrm{p}} = \boldsymbol{D}_{\mathrm{p}} + \boldsymbol{\Omega}_{\mathrm{p}}$ we now make use of the decomposition of $\widehat{\boldsymbol{L}}_{\mathrm{k}} = \boldsymbol{D}_{\mathrm{k}} + \boldsymbol{\Omega}_{\mathrm{k}}$ in its symmetric part $\boldsymbol{D}_{\mathrm{k}} = \widehat{\boldsymbol{L}}{}^{\mathrm{sym}}_{\mathrm{k}}$ and its skew–symmetric part $\boldsymbol{\Omega}_{\mathrm{k}} = \widehat{\boldsymbol{L}}{}^{\mathrm{skw}}_{\mathrm{k}}$.

Similar to eq.(5.21), the evolution for the rate of kinematic hardening is introduced next as

$$\begin{aligned}\boldsymbol{D}_{\mathrm{k}} &\doteq \mathrm{D}_t\lambda\, \partial_{\widehat{\boldsymbol{M}}_{\mathrm{k}}^{\mathrm{d}}}{}^{\mathrm{pot}}\Phi = \mathrm{D}_t\lambda\, \big[\, \partial_{\widehat{\boldsymbol{M}}_{\mathrm{k}}^{\mathrm{d}}}{}^{\mathrm{har}}\Phi + \partial_{\widehat{\boldsymbol{M}}_{\mathrm{k}}^{\mathrm{d}}}{}^{\mathrm{yie}}\Phi \,\big] \\ &= \mathrm{D}_t\lambda\, \Big[\, \Big[\, \tfrac{3}{Y_{\mathrm{k}}} \big[\, \widehat{\boldsymbol{M}}_{\mathrm{k}}^{\mathrm{d}} \cdot \boldsymbol{G}_{\mathrm{p}} \,\big]^{\mathrm{sym}} - \tfrac{3}{Y_{\mathrm{p}}} \big[\, \widehat{\boldsymbol{M}}_{\mathrm{r}}^{\mathrm{d}} \cdot \boldsymbol{G}_{\mathrm{p}} \,\big]^{\mathrm{sym}} \Big] : \widehat{\mathsf{H}}_{\mathrm{yie}}^{\mathrm{dev}} \,\Big]^{\mathrm{sym}} \cdot \boldsymbol{G}_{\mathrm{p}}\,.\end{aligned} \tag{5.23}$$

and, moreover, the hardening spin is proposed as

$$\boldsymbol{\Omega}_{\mathrm{k}}^{\mathrm{iso}} = \mathrm{D}_t\lambda\, \eta_{\mathrm{k}}\, |f_0(\boldsymbol{D}_{\mathrm{p}})|\, \widehat{\boldsymbol{M}}_{\mathrm{k}}^{\mathrm{skw}}\,, \tag{5.24}$$

wherein $\eta_{\mathrm{k}} \geq 0$ is a material parameter and $\boldsymbol{\Omega}_{\mathrm{k}}^{\mathrm{iso}} \doteq \boldsymbol{\Omega}_{\mathrm{k}}$ or $\boldsymbol{\Omega}_{\mathrm{k}}^{\mathrm{iso}} \doteq \boldsymbol{\Omega}_{\mathrm{k}} - \boldsymbol{W}_{\mathrm{k}}$ in view of the case discussed in remark 5.2.1. For the modelling of more realistic response types, for instance of carbon steel under large deformations, cyclic loading, and multi–axial ratcheting we refer the reader to Johansson et al. (2005a) and references cited therein.

Remark 5.3.1 *In the special case of classical associative evolution rules, convexity (together with homogeneity) of* ${}^{\mathrm{yie}}\Phi$ *is a sufficient requirement for the postulate of maximum dissipation to be fulfilled. For the limiting cases* $\beta \to 0$ *and* $\beta \to \infty$ *combined with* $\eta_{\mathrm{yie}} \doteq 1$ *it is straightforward to show that the ansatz proposed in eq.(5.17) renders* $\mathcal{A}$ *to represent a convex domain in the space spanned by deviatoric symmetric relative Mandel stresses* $[\, \widehat{\boldsymbol{M}}_{\mathrm{r}}^{\mathrm{d}} \cdot \boldsymbol{G}_{\mathrm{p}} \,]^{\mathrm{sym}}$. *To be specific, eq.(5.19) leads to*

$$\begin{aligned}&\big[\, \widehat{\boldsymbol{M}}_{\mathrm{r}}^{\mathrm{d}} \cdot \boldsymbol{G}_{\mathrm{p}} \,\big]^{\mathrm{sym}} : \widehat{\mathsf{H}}_{\mathrm{yie}}^{\mathrm{dev}} : \big[\, \widehat{\boldsymbol{M}}_{\mathrm{r}}^{\mathrm{d}} \cdot \boldsymbol{G}_{\mathrm{p}} \,\big]^{\mathrm{sym}} \\ &\qquad = \big[\, \boldsymbol{G}_{\mathrm{p}} \cdot \widehat{\boldsymbol{M}}_{\mathrm{r}}^{\mathrm{dev}} \,\big]^{\mathrm{sym}} : \big[\, \boldsymbol{A}_{\mathrm{p}}^{\mathrm{yie}} \,\overline{\otimes}\, \boldsymbol{A}_{\mathrm{p}}^{\mathrm{yie}} \,\big] : \big[\, \boldsymbol{G}_{\mathrm{p}} \cdot \widehat{\boldsymbol{M}}_{\mathrm{r}}^{\mathrm{dev}} \,\big]^{\mathrm{sym}},\end{aligned} \tag{5.25}$$

wherein $\boldsymbol{A}_{\mathrm{p}} = \boldsymbol{G}_{\mathrm{p}}^{-1}$ *for* $\beta \to 0$ *and* $\boldsymbol{A}_{\mathrm{p}} = \boldsymbol{G}_{\mathrm{p}}^{-1} - \boldsymbol{a}_{\mathrm{p}} \otimes \boldsymbol{a}_{\mathrm{p}}$ *for* $\beta \to \infty$, *respectively. Both limiting scenarios apparently yield idempotent tensors* $\boldsymbol{A}_{\mathrm{p}}^{\mathrm{yie}}$ *so that* $\boldsymbol{A}_{\mathrm{p}}^{\mathrm{yie}} \otimes \boldsymbol{A}_{\mathrm{p}}^{\mathrm{yie}}$ *is, accordingly, positive (semi) definite.*

5.3.3 Reorientation evolution

Inspired by Imatani and Maugin (2002) and Maugin and Imatani (2003) we formulate the evolution rule for texture reorientation as follows

$$\mathrm{D}_t\boldsymbol{a}_{\mathrm{p}} \doteq \mathrm{D}_t\lambda\, \boldsymbol{G}_{\mathrm{p}}^{-1} \cdot \big[\, \boldsymbol{\Xi}_{\mathrm{a}} - \|\boldsymbol{a}_{\mathrm{p}}\|^{-2}\, \lambda_{\Xi_{\mathrm{a}}}\, \boldsymbol{G}_{\mathrm{p}} \,\big] \cdot \boldsymbol{a}_{\mathrm{p}}\,, \tag{5.26}$$

wherein $\boldsymbol{\Xi}_{\mathrm{a}}$ denotes a (co–variant) second–order tensor specified later on, $\lambda_{\Xi_{\mathrm{a}}} = \boldsymbol{a}_{\mathrm{p}} \cdot \boldsymbol{\Xi}_{\mathrm{a}} \cdot \boldsymbol{a}_{\mathrm{p}}$ characterises the projection of $\boldsymbol{\Xi}_{\mathrm{a}}$ on $\boldsymbol{a}_{\mathrm{p}}$ and $\mathrm{D}_{\mathrm{t}}\lambda$ is the Lagrange multiplier previously used; see Menzel (2006b) for a corresponding outline in terms of spatial arguments. The ansatz in eq.(5.26) will cause the direction $\boldsymbol{a}_{\mathrm{p}}$ to eventually align with a principal direction of $\boldsymbol{\Xi}_{\mathrm{a}}$ – the additional weighting factor $\|\boldsymbol{a}_{\mathrm{p}}\|^{-2}$ here being redundant since $\boldsymbol{a}_{\mathrm{p}}$ is a unit vector. Note also that eq.(5.26) guarantees the orthogonality condition between $\mathrm{D}_t\boldsymbol{a}_{\mathrm{p}}$ and $\boldsymbol{a}_{\mathrm{p}}$ as discussed in eq.(5.3). Following Vincent et al. (2003), where the direction of distortion follows a principal loading axis with a certain delay, we suggest that $\boldsymbol{\Xi}_{\mathrm{a}}$ is proportional to the thermodynamic (driving) force $\widehat{\boldsymbol{S}}_{\mathrm{a}}$, namely

$$\boldsymbol{\Xi}_{\mathrm{a}} \doteq \frac{1}{t^*\,\beta}\, \widehat{\boldsymbol{S}}_{\mathrm{a}} \tag{5.27}$$

with t^* constituting a constant proportionality factor – similar to the relaxation time in, for example, viscoelasticity – that governs the rate of evolution of $\boldsymbol{a}_{\mathrm{p}}$ so that $t^* \to \infty$ results in $\mathrm{D}_{\mathrm{t}}\boldsymbol{a}_{\mathrm{p}} \to \boldsymbol{0}$. The influence of the stiffness parameter β in eq.(5.27) is introduced with

the purpose to easier fulfil the dissipation inequality. Note that the evolution of $\boldsymbol{a}_\mathrm{p}$ depends on $\boldsymbol{F}_\mathrm{p}$ via $\mathrm{D}_t\lambda$ but is not convected, i.e. $\mathrm{D}_t\boldsymbol{a}_\mathrm{p} \neq \mathrm{D}_t\boldsymbol{F}_\mathrm{p} \cdot \boldsymbol{a}_0|_{t_0}$. Besides eq.(5.27) there are various alternative suggestion for $\boldsymbol{\Xi}_\mathrm{a}$, for instance $\boldsymbol{\Xi}_\mathrm{a} \propto \boldsymbol{G}_\mathrm{p} \cdot \widehat{\boldsymbol{S}}_\mathrm{e} \cdot \boldsymbol{G}_\mathrm{p}$, $\boldsymbol{\Xi}_\mathrm{a} \propto \widehat{\boldsymbol{M}}_\mathrm{e}^\mathrm{d} \cdot \boldsymbol{G}_\mathrm{p}$ or $\boldsymbol{\Xi}_\mathrm{a} \propto \boldsymbol{G}_\mathrm{p} \cdot \widehat{\boldsymbol{L}}_\mathrm{a}^\mathrm{sym}$ among others. The special case $\boldsymbol{\Xi}_\mathrm{a} \propto \widehat{\boldsymbol{E}}_\mathrm{e}$ (together with isotropic plasticity) results in commutating (conjugated) stress and strain tensors; compare chapter 6. Moreover, $\boldsymbol{\Xi}_\mathrm{a} = \boldsymbol{G}_\mathrm{p}$ or $\boldsymbol{\Xi}_\mathrm{a} = \boldsymbol{0}$ leads to $\mathrm{D}_t\boldsymbol{a}_\mathrm{p} = \boldsymbol{0}$.

Remark 5.3.2 *Combining eq.(5.4) with the Sherman–Morrison–Woodbury formula, we obtain closed form expressions for $\widehat{\boldsymbol{v}}_\mathrm{a}^{-1}$ and $\widehat{\boldsymbol{L}}_\mathrm{a}$ as*

$$\begin{aligned} \widehat{\boldsymbol{v}}_\mathrm{a}^{-1} &= \boldsymbol{R}_\mathrm{a} \cdot \boldsymbol{f}_\mathrm{a} = \frac{1}{\sqrt{\alpha}}\,\boldsymbol{I}_\mathrm{p} + \frac{1}{\sqrt{\alpha}}\left[\frac{\sqrt{\alpha}-\sqrt{\alpha+\beta}}{\sqrt{\alpha+\beta}}\right]\boldsymbol{a}_\mathrm{p}\otimes\boldsymbol{a}_\mathrm{p}\cdot\boldsymbol{G}_\mathrm{p} \\ \widehat{\boldsymbol{L}}_\mathrm{a} &= \mathrm{D}_t\boldsymbol{F}_\mathrm{a}\cdot\boldsymbol{f}_\mathrm{a} = \mathrm{D}_t\widehat{\boldsymbol{v}}_\mathrm{a}\cdot\widehat{\boldsymbol{v}}_\mathrm{a}^{-1} + \widehat{\boldsymbol{v}}_\mathrm{a}\cdot\mathrm{D}_t\boldsymbol{R}_\mathrm{a}\cdot\boldsymbol{R}_\mathrm{a}^\mathrm{t}\cdot\widehat{\boldsymbol{v}}_\mathrm{a} \end{aligned} \tag{5.28}$$

so that

$$\begin{aligned} \mathrm{D}_t\widehat{\boldsymbol{v}}_\mathrm{a}\cdot\widehat{\boldsymbol{v}}_\mathrm{a}^{-1} &= \frac{1}{2}\left[\frac{\mathrm{D}_t\alpha}{\alpha}\right]\left[\,\boldsymbol{I}_\mathrm{p} - \boldsymbol{a}_\mathrm{p}\otimes\boldsymbol{a}_\mathrm{p}\cdot\boldsymbol{G}_\mathrm{p}\,\right] + \frac{1}{2}\left[\frac{\mathrm{D}_t\alpha+\mathrm{D}_t\beta}{\alpha+\beta}\right]\boldsymbol{a}_\mathrm{p}\otimes\boldsymbol{a}_\mathrm{p}\cdot\boldsymbol{G}_\mathrm{p} \\ &\quad + \boldsymbol{a}_\mathrm{p}\otimes\mathrm{D}_t\boldsymbol{a}_\mathrm{p}\cdot\boldsymbol{G}_\mathrm{p} + \mathrm{D}_t\boldsymbol{a}_\mathrm{p}\otimes\boldsymbol{a}_\mathrm{p}\cdot\boldsymbol{G}_\mathrm{p} \end{aligned} \tag{5.29}$$

turns out so be symmetric.

5.3.4 Texture stiffness evolution

Based of the discussion in section 5.1, we now formulate evolution for the stiffness in terms of $\boldsymbol{A}_\mathrm{p}$, that initially increases due to the reorientation of $\boldsymbol{a}_\mathrm{p}$. After severe substructure deformation has taken place, we expect the evolution of stiffness to saturate. The thermodynamic (driving) forces related to texture stiffness, which here allow interpretation as Schmid–type stresses, are defined as

$$\begin{aligned} S_\alpha &\doteq -\,2\,\partial_\alpha\psi_0\big|_{\widehat{\boldsymbol{E}}_\mathrm{e},\widehat{\boldsymbol{E}}_\mathrm{k},\beta,\boldsymbol{a}_\mathrm{p}} = \widehat{\boldsymbol{S}}_\mathrm{a} : \partial_\alpha\boldsymbol{A}_\mathrm{p}\big|_{\beta,\boldsymbol{a}_\mathrm{p}} = \widehat{\boldsymbol{S}}_\mathrm{a} :\ \boldsymbol{G}_\mathrm{p} \\ S_\beta &\doteq -\,2\,\partial_\beta\psi_0\big|_{\widehat{\boldsymbol{E}}_\mathrm{e},\widehat{\boldsymbol{E}}_\mathrm{k},\alpha,\boldsymbol{a}_\mathrm{p}} = \widehat{\boldsymbol{S}}_\mathrm{a} : \partial_\beta\boldsymbol{A}_\mathrm{p}\big|_{\alpha,\boldsymbol{a}_\mathrm{p}} = \widehat{\boldsymbol{S}}_\mathrm{a} : [\,\boldsymbol{a}_\mathrm{p}\otimes\boldsymbol{a}_\mathrm{p}\,] \end{aligned} \tag{5.30}$$

with $\widehat{\boldsymbol{S}}_\mathrm{a}$ being given in eq.(5.12). Note that the forces $S_{\alpha,\beta}$ are almost linearly proportional to α and β, respectively. With these elaborations in hand, evolution of texture stiffness is formulated in terms of the function

$${}^\mathrm{fib}\Phi \doteq {}^\mathrm{fib}\Phi(S_\beta) \doteq H_4\left[\,-|S_\beta| + \tfrac{1}{2\,Y_{\mathrm{a}\,0}}\,S_\beta^2\,\right], \tag{5.31}$$

wherein $H_4, Y_{\mathrm{a}\,0} > 0$ are material parameters that govern the evolution rate and saturation of the texture stiffness, and the evolution of α and β is proposed as

$$\mathrm{D}_t\alpha \doteq -\,\tfrac{S_\beta}{S_\alpha}\,\mathrm{D}_t\beta \quad\text{and}\quad \mathrm{D}_t\beta \doteq \mathrm{D}_t\lambda\,\partial_{S_\beta}{}^\mathrm{pot}\Phi\,. \tag{5.32}$$

The weighting factor S_β/S_α is thereby chosen with the purpose to eliminate the corresponding contribution to the dissipation inequality, compare section 5.3.5. Note that β increases if α decreases as long as $S_\beta/S_\alpha > 0$.

5.3.5 Dissipation inequality

Finally, we discuss the dissipation inequality as introduced in eq.(5.10) by first additively decomposing D_0 into four parts

$$\mathsf{D}_0 = \mathsf{D}_0^{\mathrm{sym}} + \mathsf{D}_0^{\mathrm{skw}} + \mathsf{D}_0^{\mathrm{ori}} + \mathsf{D}_0^{\mathrm{sti}} \tag{5.33}$$

and then showing that each part remains non–negative. The first two contributions $\mathsf{D}_0^{\mathrm{sym}}$ and $\mathsf{D}_0^{\mathrm{skw}}$ are related to the plastic flow and the evolution of kinematic hardening. They are shown to be non–negative in a standard fashion

$$\begin{aligned} \mathsf{D}_0^{\mathrm{sym}} &= \widehat{\boldsymbol{M}}_{\mathrm{e}}^{\mathrm{d}} : \boldsymbol{D}_{\mathrm{p}} \; + \; \widehat{\boldsymbol{M}}_{\mathrm{k}}^{\mathrm{d}} : \boldsymbol{D}_{\mathrm{k}} \; = \mathrm{D}_t\lambda \; 2 \left[\, {}^{\mathrm{pot}}\Phi + Y_{\mathrm{p}} \right] \qquad \geq 0 \,, \\ \mathsf{D}_0^{\mathrm{skw}} &= \widehat{\boldsymbol{M}}_{\mathrm{e}}^{\mathrm{d}} : \boldsymbol{\Omega}_{\mathrm{p}}^{\mathrm{iso}} + \widehat{\boldsymbol{M}}_{\mathrm{k}}^{\mathrm{d}} : \boldsymbol{\Omega}_{\mathrm{k}}^{\mathrm{iso}} = \mathrm{D}_t\lambda \; |f_0| \left[\, \| \widehat{\boldsymbol{M}}_{\mathrm{e}}^{\mathrm{skw}} \|^2 + \eta_{\mathrm{k}} \, \| \widehat{\boldsymbol{M}}_{\mathrm{k}}^{\mathrm{skw}} \|^2 \right] \geq 0 \,, \end{aligned} \tag{5.34}$$

compare Haupt (2000) or Johansson et al. (2005a) among others. The third part $\mathsf{D}_0^{\mathrm{ori}}$ in eq.(5.33) is related to reorientation evolution and can be rewritten as

$$\begin{aligned} \mathsf{D}_0^{\mathrm{ori}} &= \beta \, \widehat{\boldsymbol{S}}_{\mathrm{a}} : \left[\, \boldsymbol{a}_{\mathrm{p}} \otimes \mathrm{D}_t \boldsymbol{a}_{\mathrm{p}} \right] \\ &= \mathrm{D}_t\lambda \, \tfrac{1}{t^*} \left[\left[\, \boldsymbol{a}_{\mathrm{p}} \cdot \widehat{\boldsymbol{S}}_{\mathrm{a}} \right] \cdot \boldsymbol{G}_{\mathrm{p}}^{-1} \cdot \left[\, \widehat{\boldsymbol{S}}_{\mathrm{a}} \cdot \boldsymbol{a}_{\mathrm{p}} \right] - \left[\, \boldsymbol{a}_{\mathrm{p}} \cdot \widehat{\boldsymbol{S}}_{\mathrm{a}} \cdot \boldsymbol{a}_{\mathrm{p}} \right]^2 \right] \\ &= \mathrm{D}_t\lambda \, \tfrac{1}{t^*} \left[\, \| \widehat{\boldsymbol{S}}_{\mathrm{a}} \cdot \boldsymbol{a}_{\mathrm{p}} \|^2 - \left[\, \boldsymbol{a}_{\mathrm{p}} \cdot \widehat{\boldsymbol{S}}_{\mathrm{a}} \cdot \boldsymbol{a}_{\mathrm{p}} \right]^2 \right] \geq 0 \,. \end{aligned} \tag{5.35}$$

The last transformation in inequality (5.35) follows from the unit length of $\boldsymbol{a}_{\mathrm{p}}$ and the Cauchy–Schwarz inequality, i.e. $\| \widehat{\boldsymbol{S}}_{\mathrm{a}} \cdot \boldsymbol{a}_{\mathrm{p}} \|^2 = \| \widehat{\boldsymbol{S}}_{\mathrm{a}} \cdot \boldsymbol{a}_{\mathrm{p}} \|^2 \, \| \boldsymbol{a}_{\mathrm{p}} \|^2 \geq [\, \boldsymbol{a}_{\mathrm{p}} \cdot \widehat{\boldsymbol{S}}_{\mathrm{a}} \cdot \boldsymbol{a}_{\mathrm{p}}]^2$. The fourth part $\mathsf{D}_0^{\mathrm{sti}}$ in eq.(5.33) is associated with the evolution of texture stiffness. Combining eqs.(5.30–5.32) leads to

$$\begin{aligned} \mathsf{D}_0^{\mathrm{sti}} &= \tfrac{1}{2} \left[\; \boldsymbol{G}_{\mathrm{p}}^{-1} \; \mathrm{D}_t\alpha \; + \; \boldsymbol{a}_{\mathrm{p}} \otimes \boldsymbol{a}_{\mathrm{p}} \; \mathrm{D}_t\beta \right] : \widehat{\boldsymbol{S}}_{\mathrm{a}} \\ &= \tfrac{1}{2} \left[\quad S_\alpha \; \mathrm{D}_t\alpha \; + \qquad S_\beta \; \mathrm{D}_t\beta \right] \\ &= \tfrac{1}{2} \left[\, - S_\beta \; \mathrm{D}_t\beta \; + \qquad S_\beta \; \mathrm{D}_t\beta \right] = 0 \,. \end{aligned} \tag{5.36}$$

Hence, we conclude that the proposed prototype model satisfies the dissipation inequality.

5.4 Constitutive integrator

The evolution rules in eqs.(5.21–5.24,5.26,5.32) are integrated using an implicit Euler backward scheme; compare section 4.3. Thus, the incremental format of the local strain–driven problem is (with a slight abuse of notation) expressed as the following system of algebraic equations

$$\begin{aligned} \boldsymbol{R}_{\mathrm{p}} &= \boldsymbol{I}_{\mathrm{p}} \; - \; \boldsymbol{F}_{\mathrm{p}}^n \cdot \boldsymbol{f}_{\mathrm{p}} \; - \; \Delta\lambda \qquad \left[\quad |f_0| \widehat{\boldsymbol{M}}_{\mathrm{e}}^{\mathrm{skw}} - \partial_{\widehat{\boldsymbol{M}}_{\mathrm{e}}^{\mathrm{d}}} {}^{\mathrm{pot}}\Phi \right] \\ \boldsymbol{R}_{\mathrm{k}} &= \boldsymbol{I}_{\mathrm{p}} \; - \; \boldsymbol{F}_{\mathrm{k}}^n \cdot \boldsymbol{f}_{\mathrm{k}} \; - \; \Delta\lambda \qquad \left[\, \eta_{\mathrm{k}} \, |f_0| \widehat{\boldsymbol{M}}_{\mathrm{k}}^{\mathrm{skw}} - \partial_{\widehat{\boldsymbol{M}}_{\mathrm{k}}^{\mathrm{d}}} {}^{\mathrm{pot}}\Phi \right] \\ \boldsymbol{R}_{\mathrm{a}} &= \boldsymbol{a}_{\mathrm{p}} \; - \; \boldsymbol{a}_{\mathrm{p}}^n \qquad - \; \Delta\lambda \quad \tfrac{1}{t^* \, \beta} \left[\, \boldsymbol{G}_{\mathrm{p}}^{-1} \cdot \widehat{\boldsymbol{S}}_{\mathrm{a}} - S_\beta \, \| \boldsymbol{a}_{\mathrm{p}} \|^{-2} \, \boldsymbol{I}_{\mathrm{p}} \right] \cdot \boldsymbol{a}_{\mathrm{p}} \\ R_\alpha &= \alpha \; - \; \alpha^n \qquad + \qquad \tfrac{S_\beta}{S_\alpha} \left[\, \beta - \beta^n \right] \\ R_\beta &= \beta \; - \; \beta^n \qquad - \; \Delta\lambda \; H_4 \, S_\beta \left[\, - |S_\beta|^{-1} + Y_{\mathrm{a}\,0}^{-1} \right] \\ R_\lambda &= {}^{\mathrm{yie}}\Phi \end{aligned} \tag{5.37}$$

so that $\mathbf{R}_{\mathrm{tot}} = [\, \boldsymbol{R}_{\mathrm{p}}, \boldsymbol{R}_{\mathrm{k}}, \boldsymbol{R}_{\mathrm{a}}, R_{\alpha}, R_{\beta}, R_{\lambda} \,]^{\mathrm{t}}$ and $\mathbf{X}_{\mathrm{tot}} = [\, \boldsymbol{f}_{\mathrm{p}}, \boldsymbol{f}_{\mathrm{k}}, \boldsymbol{a}_{\mathrm{p}}, \alpha, \beta, \Delta\lambda \,]^{\mathrm{t}}$; compare section 4.3. Subsequent numerical examples are based on (the monolithic) algorithm 4.2 combined with method 2 from section 4.3.1.1. The adopted Euler backward scheme, however, in general violates the constraint that $\boldsymbol{a}_{\mathrm{p}}$ has unit length. A possible remedy is to perform a normalisation after the iteration update, i.e. $\boldsymbol{a}_{\mathrm{p}} \hookleftarrow \boldsymbol{a}_{\mathrm{p}}/\|\boldsymbol{a}_{\mathrm{p}}\|$.

5.5 Numerical examples

In the following we illustrate, by simple numerical examples, the capabilities of the proposed constitutive model for hardening, reorientation, and stiffness evolution of texture. The utilised material parameters are: $G = 80$, $L = 120$, $H_3 = 1$, $\eta_{\mathrm{yie}} = \{0, 1\}$, $Y_{\mathrm{p}\,0} = 0.5$, $Y_{\mathrm{k}\,0} = 1$, $\eta_{\mathrm{p}} = 0$, $\eta_{\mathrm{k}} = 0$, $t^* = \{100, \infty\}$, $H_4 = \{0.0, 0.3\}$, $Y_{\mathrm{a}\,0} = 300$, whereby it is noted that the parameters η_{yie}, t^*, H_4 and $Y_{\mathrm{a}\,0}$ govern the influence of texture.

5.5.1 Cyclic simple shear

The influence of the modelled texture is studied during ten cycles of prescribed simple shear strain, i.e. $\boldsymbol{F} \equiv \boldsymbol{I}_0 + \gamma\, \boldsymbol{e}_1 \otimes \boldsymbol{e}_2$, whereby $\{\boldsymbol{e}_{1,2,3}\}$ denotes a (space–attached) Cartesian frame and $\gamma \in [\, 0\,,\, 1\,]$. The initial orientation $\boldsymbol{a}_{\mathrm{p}}|_{t_0}$ is determined by a principal direction of $\boldsymbol{E}_{\mathrm{e}}|_{t_0}$, or rather $\widehat{\boldsymbol{E}}_{\mathrm{e}}|_{t_0}$. This corresponds to $\boldsymbol{a}_{\mathrm{p}}|_{t_0} \equiv [\, \boldsymbol{e}_1 + \boldsymbol{e}_2 \,]/\sqrt{2}$ or equivalently $\theta \equiv \pi/4$ with $\tan(\theta) \doteq [\, \widetilde{\boldsymbol{a}}_{\mathrm{t}} \cdot \boldsymbol{e}_2 \,]/[\, \widetilde{\boldsymbol{a}}_{\mathrm{t}} \cdot \boldsymbol{e}_1 \,]$ for $\widetilde{\boldsymbol{a}}_{\mathrm{t}} = \boldsymbol{F}_{\mathrm{e}} \cdot \boldsymbol{a}_{\mathrm{p}}/\|\boldsymbol{F}_{\mathrm{e}} \cdot \boldsymbol{a}_{\mathrm{p}}\|$. Moreover, the initial stiffness parameters are chosen as $\alpha|_{t_0} = 1$ and $\beta|_{t_0} = 0.05$ so that $\boldsymbol{A}_{\mathrm{p}}|_{t_0} = \boldsymbol{G}_{\mathrm{p}}^{-1} + 0.05\ \boldsymbol{a}_{\mathrm{p}}|_{t_0} \otimes \boldsymbol{a}_{\mathrm{p}}|_{t_0}$. Thus, the spherical part of the substructure metric $\boldsymbol{A}_{\mathrm{p}}$ dominates at t_0. For purpose of illustration, we additionally introduce the (Kirchhoff) shear stress $\tau \doteq \boldsymbol{e}_1 \cdot \boldsymbol{F}_{\mathrm{e}} \cdot \widehat{\boldsymbol{S}}_{\mathrm{e}} \cdot \boldsymbol{F}_{\mathrm{e}}^{\mathrm{d}} \cdot \boldsymbol{e}_2$.

First, for comparison we show the nearly isotropic response in figure 5.1. Evolution of reorientation θ as well as of the stiffness parameters α and β are inactive, i.e. $t^* \to \infty$ and $H_4 = 0$. The influence of the stiffness parameter $\beta = 0.05$ on the orientation in figure 5.1 is rather small. Similarly, the parameter η_{yie} has practically no influence, since β is small. Next, the evolution of reorientation is activated, whereas the evolution rate is determined by the parameter value $\eta_{\mathrm{yie}} = 100$. The stress–strain relation in figure 5.2 is still the same as for the isotropic case since the stiffness parameter β is small and $H_4 = 0$. However, the reorientation evolves as shown in figure 5.2. Even for this case, we conclude that the parameter η_{yie} has practically no influence since β is small. Figure 5.3 displays the case where the stiffness parameters α and β evolve with a rate determined by the parameter value $H_4 = 0.3$. Evolution of reorientation, however, is inactive, namely $t^* \to \infty$. The evolution of the yield surface is now influenced by the parameter $\eta_{\mathrm{yie}} = 1$. The stress–strain relation nearly coincides with the isotropic case for the first cycle while the stiffness is small. For larger cycle numbers, β increases and decreases according to the evolution rule. As a consequence, the stress response shows a ratcheting character. The behaviour displayed in figure 5.3 is almost identical with the case where $\boldsymbol{a}_{\mathrm{p}}$ convects with $\boldsymbol{F}_{\mathrm{p}}$, i.e. $\boldsymbol{a}_{\mathrm{p}} \approx \boldsymbol{F}_{\mathrm{p}} \cdot \boldsymbol{a}_0|_{t_0}/\|\boldsymbol{F}_{\mathrm{p}} \cdot \boldsymbol{a}_0|_{t_0}\|$. Nevertheless, this does not need to be the case for general loading situations. Finally, in figure 5.4 both the orientation of $\boldsymbol{a}_{\mathrm{p}}$ as well as the stiffness parameters α and β evolve with rates determined by $t^* = 100$, $H_4 = 0.3$ and $\eta_{\mathrm{yie}} = 1$. It is clear from figure 5.4 that the evolution of reorientation saturates after sufficiently many loading cycles. This saturation occurs mainly due to the fact that $\boldsymbol{a}_{\mathrm{p}}$ approaches an eigenvector of $\boldsymbol{\Xi}_{\mathrm{a}}$. The saturation of α and β, which is governed by the parameter $Y_{\mathrm{a}\,0}$, is less pronounced. The dominant portion of the response in figures 5.1–5.4 is obviously inelastic. In figure 5.5 we show the case where $\eta_{\mathrm{yie}} = 0$ so that the influence of texture on the anisotropic evolution of the yield surface is eliminated. By comparing figures

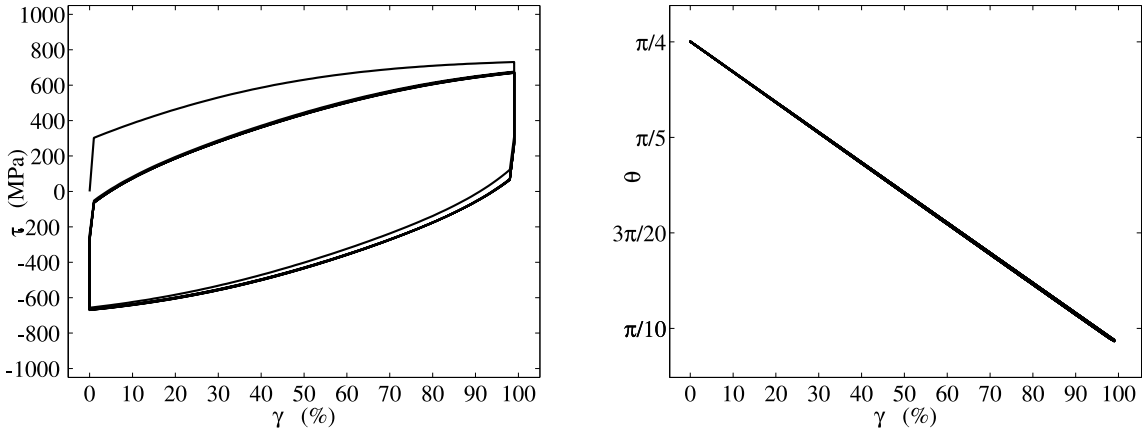

Figure 5.1: Cyclic simple shear – nearly isotropic with $H_4 = 0$ and $t^* \to \infty$: shear stress τ (left); texture orientation θ (right).

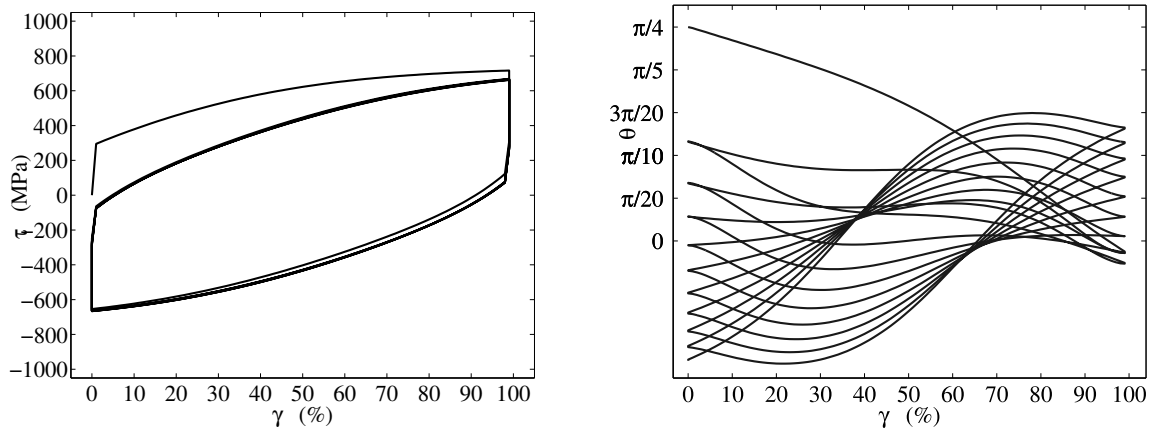

Figure 5.2: Cyclic simple shear – evolving texture with $H_4 = 0$ and $t^* = 100$: shear stress τ (left); texture orientation θ (right).

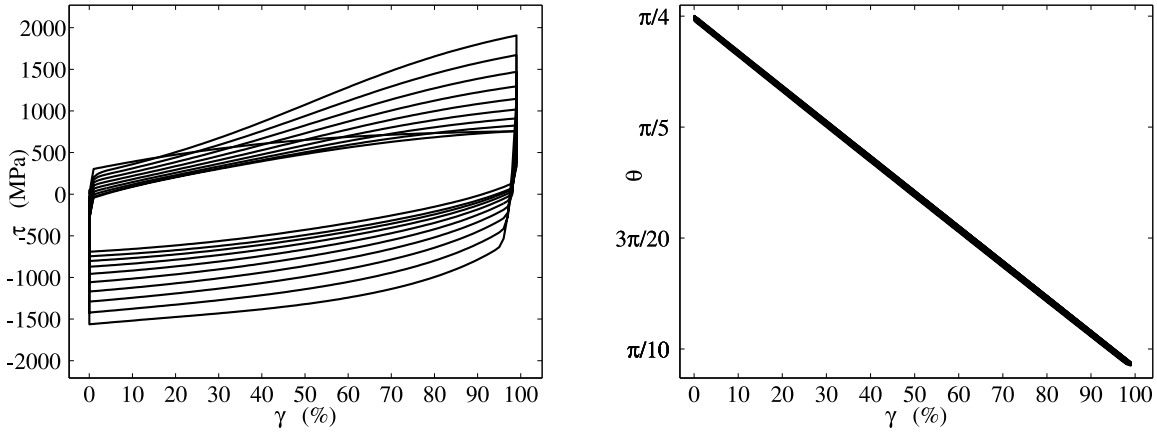

Figure 5.3: Cyclic simple shear – evolving texture with $H_4 = 0.3$, $Y_{\mathrm{a}\,0} = 300$, $t^* \to \infty$ and $\eta_{\mathrm{yie}} = 1$: shear stress τ (left); texture orientation θ (right).

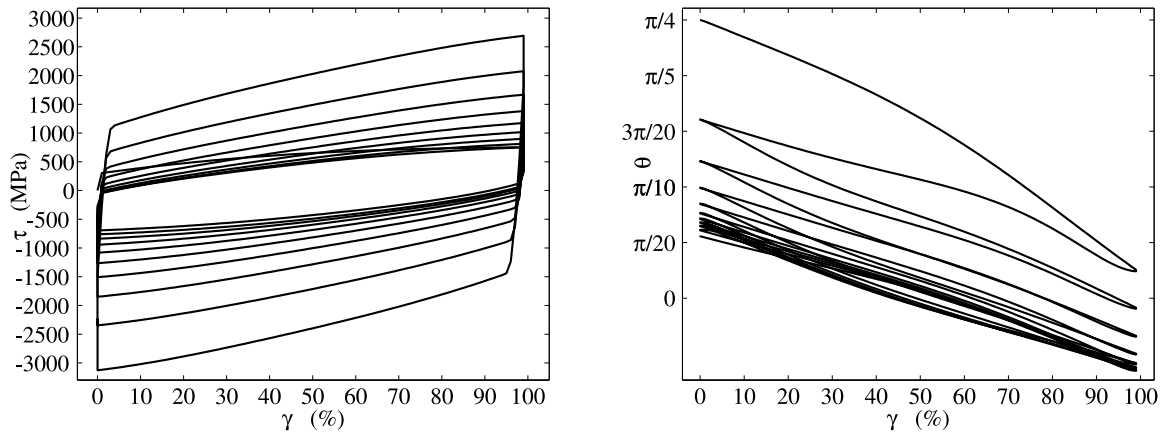

Figure 5.4: Cyclic simple shear – evolving texture with $H_4 = 0.3$, $Y_{\mathrm{a}\,0} = 300$, $t^* = 100$ and $\eta_{\mathrm{yie}} = 1$: shear stress τ (left); texture orientation θ (right).

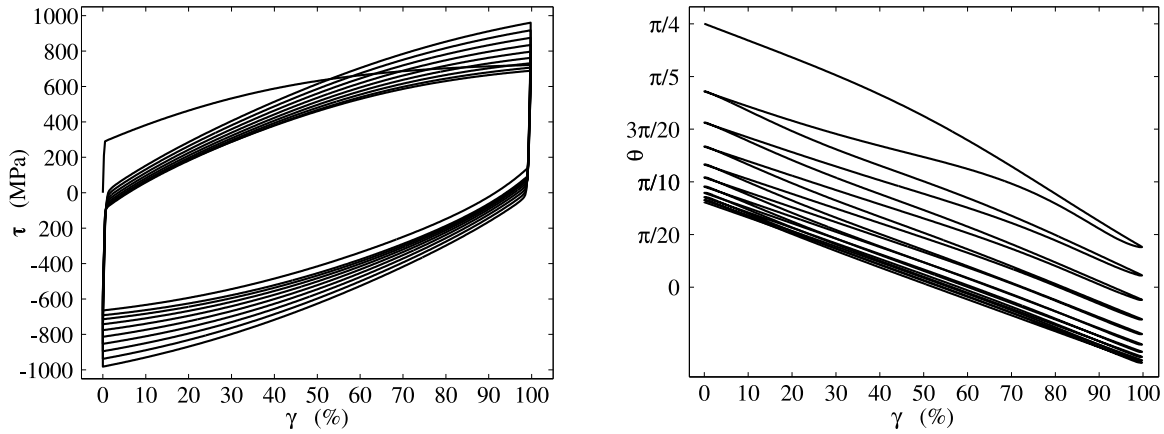

Figure 5.5: Cyclic simple shear – evolving texture with $H_4 = 0.3$, $Y_{\mathrm{a}\,0} = 300$, $t^* = 100$ and $\eta_{\mathrm{yie}} = 0$: shear stress τ (left); texture orientation θ (right).

5.4 and 5.5 it is concluded that the influence of η_{yie} on the overall stress–strain response is large.

5.5.2 Compression and cyclic shear of a square–shaped specimen

In the following, we illustrate the performance of the proposed model when used in a simple boundary value problem. The discretisation of a $l_0 \times l_0 \equiv 10 \times 10$ square–shaped specimen under plane strain conditions is realised with 8×8 four–node elements (Q1) as shown in figure 5.6. The lower side of the square is fixed while the opposite side has a prescribed displacement. The material parameters $H_4 = 0.3$, $t^* = 100$, and $\eta_{\mathrm{yie}} = 1$ are utilised in addition to the parameters mentioned above. The prescribed displacement is cyclic with the amplitude determined by the components l_x and l_y. For the ratio between the horizontal and vertical displacements of the prescribed side we choose $l_x/l_y = 4$. Moreover, figure 5.6 shows the deformed finite element mesh at the first load step. The lines in the centre of each element represent the initial orientation $\widetilde{\boldsymbol{a}}_t = \boldsymbol{F}_{\mathrm{e}} \cdot \boldsymbol{a}_{\mathrm{p}} / \| \boldsymbol{F}_{\mathrm{e}} \cdot \boldsymbol{a}_{\mathrm{p}} \|$ at $t \approx t_0$ evaluated as the integration point average in each element. This initial orientation is, by analogy with the previous section, determined by the predominant principal direction of $\widehat{\boldsymbol{E}}_{\mathrm{e}}$ at the first load step, whereas $\boldsymbol{a}_{\mathrm{p}}$ then evolves according to the proposed evolution rules. The initial stiffness is determined by $\alpha = 1$ and $\beta = 0.05$ so that $\boldsymbol{A}_{\mathrm{p}} = \boldsymbol{G}_{\mathrm{p}}^{-1} + 0.05\, \boldsymbol{a}_{\mathrm{p}} \otimes \boldsymbol{a}_{\mathrm{p}}$.

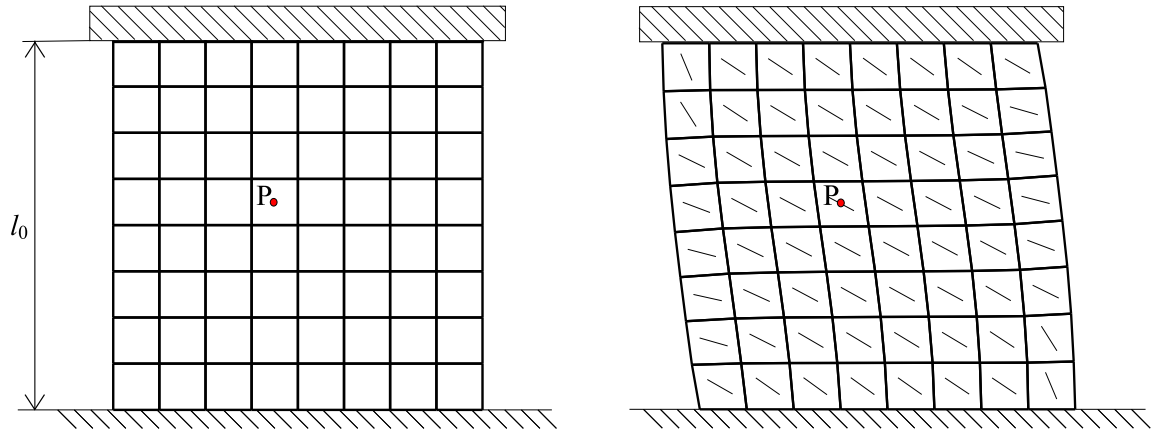

Figure 5.6: Compression and cyclic shear of a square–shaped specimen: finite element discretisation (left); substructure orientation $\widetilde{\boldsymbol{a}}_t$ at $t \approx t_0$ (right).

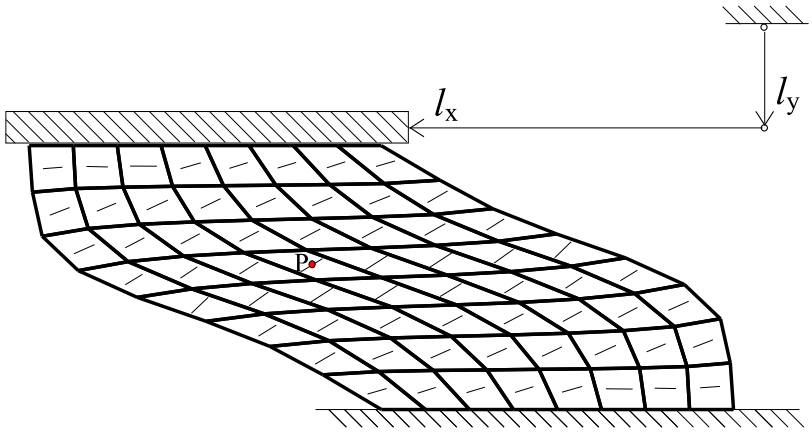

Figure 5.7: Compression and cyclic shear of a square–shaped specimen: boundary conditions and deformed mesh after 9.5 loading cycles.

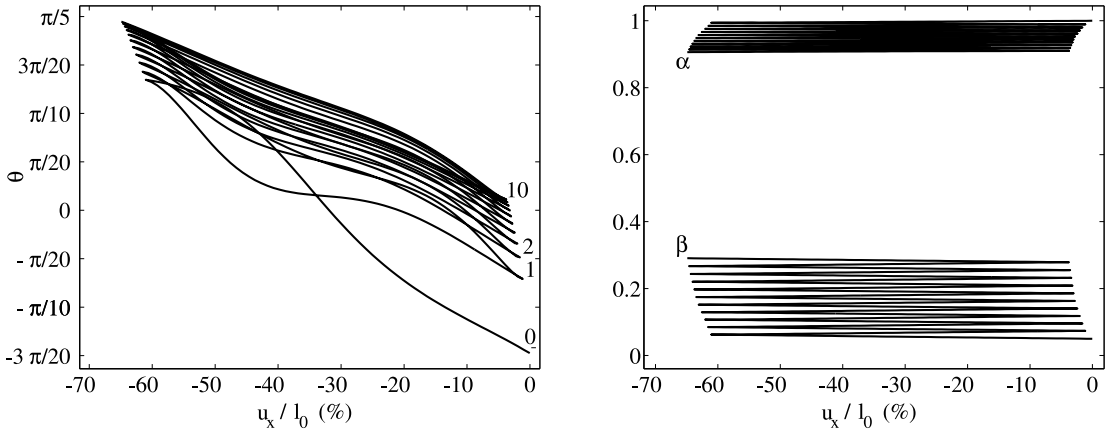

Figure 5.8: Compression and cyclic shear of a square–shaped specimen: texture orientation measure θ at P versus u_x/l_0 (left); stiffness parameters α and β at P versus u_x/l_0 (right).

Since the spherical part of the substructure metric dominates at $t \approx t_0$, initial orientations displayed in figure 5.6 have no practical influence on the response at $t \approx t_0$. However, figure 5.7 additionally shows the deformed finite element mesh. The lines in the centre of each element once more represent the mean value of the orientation $\widetilde{\boldsymbol{a}}_t$ over integration points values in each element. It is clearly observed from figure 5.7 that the orientation aligns with the lower and upper sides in the upper and lower parts of the mesh. Furthermore, the cyclic response in the point P (integration point average in the element) in figures 5.6 and 5.7 is shown in figure 5.8: on the one hand, the cyclic response of the orientation measure θ versus the normalised horizontal displacement or rather strain measure u_x/l_0 of P is visualised; on the other hand, the stiffness parameters α and β in P are plotted versus u_x/l_0. It is thereby clear that the evolution of the orientation tends to saturate after a few cycles, whereas the saturation of α and β is small. It is also noted that β increases faster than α decreases.

6 Fibre reorientation of biological tissues for multiplicative growth

The development of appropriate models for biological tissues that capture at least some of the essential biochemical and biophysical or rather biomechanical effects is a fundamental task and one of the challenging tasks in the wide research field of computational biomechanics. Both hard tissues, such as bones and teeth, and soft tissues, such as ligaments, tendons, muscles, skin and vessels, have attracted various studies over the last decades. Several outstanding monographs document the rapid development of this important scientific field of research; see for example Schneck (1990), Fung (1993), Humphrey (2002), Murray (2002), Cowin and Doty (2007), and the review articles by Taber (1995) and Cowin (1999b) or the contributions in Cowin (2001), Cowin and Humphrey (2000) as well as in Holzapfel and Ogden (2003) for a state–of–the–art overview. A typical classification of the biomechanical behaviour of tissues is thereby introduced by distinguishing between passive response, active response and remodelling or rather between non–adaptive and adaptive performance. One particular property of the first and second category consists in the assumption of conservation of mass while the latter category assembles effects like growth phenomena and the evolution on internal structures.

In view of soft biological tissues undergoing large deformations, the materials of interest commonly consist of cell assemblies and extracellular matrix – the properties of the latter being predominantly characterised by fibres as elastin and collagen; see for example the article by Cowin (2000) for a comprehensive overview and the survey on essential collagen properties with special emphasis on tendons by Silver et al. (2003). In general, biological tissues can be considered as composite materials which continuously change according to, for instance, growth (and atrophy) as well as remodelling effects. Various substructures are noted at different scales of observation and often render biological tissues to exhibit strongly directionally dependent properties. To give an example, the intracellular microrheology allows interpretation as an actin–rich network possessing different properties as expected for permanently cross–linked networks; compare Kole et al. (2005) and see also the survey in Boal (2002) as well as the contribution by Chandran and Barocas (2006). In order to account for such anisotropic characteristics – which are related to the observation and mechanical behaviour of for example actin, fibrils, different types of collagen and so forth – so–called fibre families are incorporated into the finite–deformation continuum approach proposed in this contribution so that anisotropic response is included on a phenomenological basis.

In addition to the modelling of interstitial growth, we are particularly interested in capturing remodelling and self–assembly represented by fibre reorientation or rather turnover in developing tissues. To give an example, collagen fibres, as those we are focusing on and which determine mechanical properties of for example tendons and extracellular matrix, are produced by fibroblast. Such fibroblasts secret collagen molecules that assemble into ordered polymers – so–called collagen fibrils. Cable–like bundles thereof finally form collagen fibres; the reader is referred to Alberts et al. (1994) for further details. Moreover, collagen fibres are aligned according to the orientation of these fibroblasts. Adaptation processes in general are on the one hand determined by genetic informations and, on the other hand, also driven by interactions with tissue environments; compare the discussion in Cowin (2004). Related experiments focus on different scales of observation by for example monitoring the mechanical response on the overall tissue level or investigating the behaviour of individual cells. Further

background information is provided in the contributions by Calve et al. (2004) and Borschel et al. (2005), among others, as well as in the survey article by Wang and Thampatty (2006) wherein numerous experimental results are reviewed.

Although it is accepted and experimentally verified that biological tissues adapt under the action of mechanical forces, the particular manner in which cells sense such loading conditions and convert them into biological responses remains largely unknown. Moreover, cells react not only to mechanical stimuli but also transform changes in, for instance, applied magnetic fields into biochemical processes; compare Torbet and Ronzière (1984) or Guido and Tranquillo (1993). Furthermore, the influence of different substances, as for example calcium and tyrosine, on fibre alignment has been studied by several research groups; see Malek and Izumo (1996) among others. Nowadays, it is well–established that various types of cells reorient with respect to the direction of representative mechanical forces acting on them – to name but a few, endothelial cells, fibroblasts, and smooth muscle cells all have been shown to exhibit such alignment processes. Cells may be considered to be strain–, respectively stress–sensing – see the discussion in Humphrey (2001) and Cowin (2004) as well as the different modelling approaches developed in Driessen (2006) – and, as an interesting side aspect, the rate and extent of cell reorientation has been observed to depend primarily on the magnitude of the stretches and not on the stretching rate; compare Wang et al. (2001). Depending on the specific type of tissue or rather cells together with the particular type of loading conditions, fibre and cell alignment was reported to take place according to the directions of maximum and minimum principal stretches; see for instance Eastwood et al. (1998) and Malek and Izumo (1996) or, respectively, Breen (2000) and Wang (2000) while a general overview is given in Wang and Thampatty (2006). The computational reorientation framework developed in this contribution is motivated by these observations.

The modelling of passive response even of soft tissues as arteries is nowadays highly developed, see Holzapfel (2001, 2005, 2002b) and references cited therein. Nevertheless, the characterisation of the (fibre–) morphology of biological tissues remains an elaborate but fundamental task in order to link computational models and in vivo materials; see for instance the review article by Zysset (2003) and references cited therein, where special emphasis is placed on hard tissues – namely bones. The overall behaviour of commonly considered biological materials is obviously anisotropic such that concepts from classical continuum mechanics, as highlighted in the contributions in Boehler (1987) and Spencer (1984), serve as a convenient backbone; see also Weiss et al. (1996) and Almeida and Spilker (1998) for the modelling of the anisotropic elastic behaviour of soft tissues and Cowin (1985), Zysset and Curnier (1995) and Menzel and Steinmann (2001a) for alternative frameworks. Passive response, however, is not at all restricted to non–dissipative processes; in other words, anisotropic viscoelastic and anisotropic elastoplastic behaviour occur – see, for example, the formulation by Holzapfel and Gasser (2001) or Kaliske (2000) and the contribution by Gasser and Holzapfel (2002).

In contrast to the viscous behaviour within passive response, one observes that remodelling effects take place on a different, drastically larger, time scale; see Currey (2003) with application to bones. Consequently, we adopt the viewpoint that any applied load or boundary condition represents an assembly of driving effects averaged over time. Therefore, viscoelastic constitutive laws are not incorporated into the formulation developed in this chapter, but remodelling is addressed, namely isotropic and anisotropic growth together with reorientation. Having for example a soft tissue in mind, consider an assembly or bundles of collagen fibrils that form fibres. From a macroscopic point of view, collections of fibres are essentially characterised via a representative diameter and a corresponding orientation or rather direction. Apparently, the direction naturally evolves such that the loading capacity of the in–vivo material is optimised – the transcription of this effect in terms of mathematical equations being a non–trivial task.

Moreover, it is accepted that the fibre diameter increases in response to mechanical stimuli like stress (which means that the diameter is correlated to the strength of the fibre), but that the fibre diameter is also age–dependent. In addition, initially randomly–distributed fibre directions (the modelling thereof within a numerical setting being straightforward) that later on adapt according to a particular type of loading path would provide further insight and understanding of the mechanical remodelling process of the in–vivo material. Since the temperature of a living tissues is almost constant, thermal coupling is usually neglected. However, electric effects and stimuli as well as age–dependency should also be addressed – especially for the modelling of muscle contraction, see e.g. Schneck (1992) or Wren (2003) among others. These properties, as well as observations like regeneration after injury or surface growth, as discussed by e.g. Skalak et al. (1997), are, nevertheless, not in the focus of this chapter wherein we restrict ourselves to purely mechanical stimuli.

From the continuum mechanics point of view, it is an old but ongoing discussion concerning the adoption of the theory of mixtures, porous media, or open systems for the modelling of growth (or resorption) phenomena; see e.g. the early and pioneering contributions by Truesdell and Toupin (1960), Bowen (1976), Cowin and Hegedus (1976) and the survey article by Cowin (1999a) or the monographs by de Groot (1961), Kestin (1966) and Katchalsky and Curran (1965), where detailed background information on the underlying theories are provided. In the following, we firstly adopt the latter approach, as further developed in Epstein and Maugin (2000), Kuhl and Steinmann (2003a), Klisch and Hoger (2003), Huang (2004), and by Guillou and Ogden in (2006, pp. 47–62). Numerical simulations of biological materials, in particular bones, were initiated more than two decades ago, as reviewed by Huiskes and Chao (1983). Stable computational models for the (Wolff–type) adaption of hard tissues, however, were devised in the late 1980s and early 1990s by Huiskes et al. (1987), Weinans et al. (1992) and Harrigan and Hamilton (1992, 1993, 1994). Based on these isotropic remodelling formulations, several numerical approaches were further elaborated, see for example Jacobs et al. (1995), Nackenhorst (1996) or Kuhl and Steinmann (2003b) where, in contrast to the previously cited references, the incorporation and computational treatment of an additional mass flux term is developed. For a discussion on various aspects of the underlying numerical techniques and a comparison of two different discretisation approaches for the density field, we refer the reader to Kuhl et al. (2003). Remodelling and growth of transversely isotropic continua has been investigated in Menzel (2005a).

Since the response and adaption of biomaterials is usually anisotropic, models for anisotropic growth or anisotropic remodelling were (are) consequently developed. At first glance, several proposed formulations seem similar to well–established frameworks in computational finite inelasticity, but, if at least growth and resorption is appropriately incorporated, should additionally be embedded into the theory of open systems. In this regard, the concept of a growth mapping, as typically represented in terms of a corresponding linear tangent map or rather growth tensor, is advocated in the pioneering work by Rodriguez et al. (1994), and further discussed and elaborated in for example Taber (1995), Taber and Eggers (1996), Cowin (1996), Hoger (1997), Taber and Perucchio (2000), Chen and Hoger (2000), Klisch et al. (2001), DiCarlo and Quiligotti (2002), and Quiligotti (2002); see also the investigations on evolving natural configurations in the context of biomechanics by Ambrosi and Mollica (2002), Humphrey and Rajagopal (2002), and Rao et al. (2003). With the general thermodynamic and kinematic framework at hand, the remaining task consists in setting up appropriate evolution equations for the growth distortion and a reasonable fibre reorientation model. However, since the development of these anisotropic growth theories is currently still under discussion, it is not astonishing that these formulations are somehow ahead of the setup of appropriate computational frameworks. To be specific, most of the pioneering contributions that address robust algorithms to simulate anisotropic remodelling within a finite element setting were mainly re-

stricted to small strains and hard tissues, compare Jacobs et al. (1997), Weng (1998) or Krstin et al. (2000). First numerical elaborations as based on finite deformation finite element techniques and a multiplicative decomposition of the deformation gradient in the present context are discussed in Himpel et al. (2005) wherein isotropic response is addressed. In the following, we adopt the approach recently proposed by Lubarda and Hoger (2002), namely that material fibre families constitute principal directions of the growth distortion itself; see also the elaborations by Hoger et al. (2004) and Lubarda (2004) as well as Menzel (2006a, 2006b, 2007) for first numerical applications of transversely isotropic continua in this regard. Contrary to previous works, we assume two different types of anisotropic growth evolution: on the one hand an energy–driven format will be discussed while, on the other hand, the growth evolution is driven by a configurational stress conjugated to the growth distortion itself. The general format and interpretation of this stress tensor and related transformations thereof is directly associated with Eshelbian stress tensors in classical finite plasticity formulations as developed in chapter 2; see also Svendsen (2001), Maugin (1994, 2003), Epstein (2002) and the contribution by Garikipati et al. in Steinmann and Maugin (2005, pp. 77–84) in this regard. As such, this particular choice of a driving stress tensor or, in other words, driving force seems to be natural when accepting the adopted kinematical framework. Nevertheless, one should note that the interpretation and incorporation of growth factors suitable for continuum growth theories is non–trivial and that adaptation stimuli of purely mechanical nature, as those proposed in this contribution, are a priori oversimplifying. In this regard, it is of cardinal importance to design experiments which are guided by appropriate theoretical approaches so that essential modelling parameters can be confined or even identified; see Humphrey (2002) for an overview on experimental techniques. Such parameters are, however, often not directly accessible from measured data in contrast to changes in tissue mass, shape and geometry of the particular specimen of interest, mechanical properties as local stiffness parameters and so forth. Accordingly, several experiments should be performed at different growth stages and – in future – combined with a so–called inverse finite–element–based parameter identification; for a general outline the reader is referred to Mahnken (2000), Kleuter et al. (2007), and references cited therein. Investigating these usually ill–posed problems is expected to significantly further the derivation and validation of biomechanical growth and remodelling laws. Based on such elaborations, it is presumed that theoretical models can be simplified and that physically meaningful material parameters related to growth and remodelling may become accessible.

While particular energy expression or the considered configurational stress, respectively, essentially drive growth evolution, we develop a purely kinematics–based remodelling or rather reorientation formulation. In general, two different reorientation effects can be incorporated: on the one hand, kinematic and constitutive relations could be modified; see for instance the contributions by Ericksen with application to phase transformation collected in Beatty and Hayes (2005). On the other hand, representative (state) variables might be directly reoriented by means of constitutive or balance equations; see for example Virga (1994) for an overview with application to liquid crystals or Arockiarajan and Menzel (2007) in view of ferroelectric phase transitions. The remodelling framework proposed in the following will affect both, the incorporated deformation tensors as well as representative state variables. Concerning finite transversely isotropic inelasticity, different approaches have been proposed in the literature as for instance an alignment with respect to principal stress directions; compare Imatani and Maugin (2002) or the outline in chapter 5 where special emphasis has been placed on a thermodynamically consistent elastoplasticity framework. In the sequel, we develop two different kinematics–based reorientation models with application to either transversely isotropic or orthotropic tissues. Both frameworks inherently preserve the underlying symmetry group. The overall approach is motivated by the contributions by Vianello (1996a, 1996b) and Sgarra and Vianello (1997) to which we will refer to as Vianello's 'coaxiality' theory; in this regard,

see also the contributions by Pedersen (1989) and Cowin (1994, 1995). As a key result, it has been shown that the strain energy reaches a critical point if conjugated stress and stretch tensors commutate. Moreover, it has also been proven that at least three different orthogonal (symmetry) transformations exist, which can be superposed onto the material constitutive relation and thereby enable the construction of commutating stress and strain tensors for a generally anisotropic material. Since energy optimisation is commonly considered as a basic modelling axiom, these ideas are carried over to the problem at hand. To be specific, the introduced fibre family or fibre families, respectively, are (locally) aligned with respect to principal stretch directions (note that an alignment of the anisotropy variables according to principal stress directions renders, in general, non–commutating stress and strain tensors). For the transversely isotropic case, the related angular velocity vector is constitutively determined such that a so–called drilling rotation is a priori excluded; see for instance Betsch et al. (1998) where numerical concepts for this particular case are discussed. Concerning orthotropic response, we constitutively derive the related angular velocity vector from a (pseudo) rotation vector which is extracted with the help of a singularity–free quaternion–based algorithm; for detailed background information concerning quaternion theory we refer the reader to the review article by Argyris (1982), the monographs by Altman (1986) or the general survey in Angeles (1988). The ansatz for the underlying rotation tensor is thereby, in general, not unique, which might also reflected the fact that universal constitutive relations are not obvious for orthotropic materials; see for instance Pucci and Saccomandi (1997) and Saccomandi and Beatty (2002) for an overview on universal relations for fibre reinforced materials or the general survey by Saccomandi (2001). Consequently, for the orthotropic model further constitutive assumptions are incorporated into the proposed symmetry group preserving reorientation approach. Both approaches automatically guarantee saturation–type reorientation behaviour whereby the time–dependent formulation itself is straightforwardly based on concepts well–established for instance for the algorithmic treatment of viscoelasticity.

To give a classical example of an orthotropic soft biological tissue, walls of elastic as well as of muscular arteries are composed of three different layers – the intima, media, and adventitia. While the intima of a young and healthy artery does not carry much of the stresses acting on the artery, both the media as well as the adventitia significantly contribute to the overall mechanical properties of the artery; the reader is referred to the monograph by Humphrey (2002) for a detailed survey on vascular wall mechanics. Moreover, both the media and the adventitia possess fibrous helix–type structures which are accepted to be sufficient accurately mirrored by cylindrically orthotropic symmetry. For an overview on experimental methods to identify such fibre orientation distributions see Marquez (2006) or the overview by Sachse (2004). In addition, inelastic effects as softening, so–called pseudoelastic response, viscoelastic behaviour and so forth are observed and in particular attributed to the media layer; related continuum formulations are highlighted in Holzapfel et al. (2002a) and Gasser and Holzapfel (2002). Typical arteries of interest, as for instance the aorta, show no substantial (additional) adaptation if a full–grown state of the blood vessel is examined. Contrary to such pre–conditioned and healthy scenarios, injury of vessel walls stemming for example from balloon dilatation causes cells to adapt, reorient, migrate and so forth.

The chapter is organised as follows: after briefly reviewing fundamental balance equations in section 6.1, key features of constitutive framework are introduced in section 6.2.1. We thereby address in particular the underlying kinematical framework, the considered mass source as well as the introduction of hyperelastic stress formats in the present context. The later on proposed fibre reorientation models are motivated in section 6.3 wherein first general coaxiality relations between conjugated stress and stretch tensors are elaborated which are next applied or rather extended to the model at hand. Apart from that, the main body of this chapter consists of sections 6.4 and 6.5: on the one hand, an energy–driven growth formulation

is developed whereby the intermediate and material configurations are assumed to coincide. The reorientation model in section 6.4 incorporates one fibre family so that the symmetry groups corresponds to transversal isotropy. On the other hand, the intermediate configuration is taken into account in section 6.5 and, moreover, two orthogonal fibre families are introduced which results in orthotropic response. Various numerical examples show the applicability of the developed formulations.

6.1 Balance equations

For convenience of the reader and in order to introduce the applied notation, we first summarise essential balance equations for the problem at hand. In this context, let ρ_0 characterise the material density at a particular $\boldsymbol{X}$ of the body B. Balancing this scalar–valued field introduces the mass flux $\boldsymbol{R}$ and the mass source term R_0, namely

$$\mathrm{D}_t \rho_0 = \nabla_{\boldsymbol{X}} \cdot \boldsymbol{R} + R_0 \,. \tag{6.1}$$

For conceptual simplicity, we neglect the flux term in the sequel, $\boldsymbol{R} \doteq \boldsymbol{0}$, such that $\mathrm{D}_t \rho_0 \doteq R_0$, which however does not restrict the proposed constitutive framework itself. Nevertheless, it is of cardinal importance for the progression of this work on open systems that the source term does not vanish as for the standard mass–conserving approach, which has been denoted as passive response above. It is thereby obvious that with the mass being a non–conserved quantity, non–standard representations compared to the commonly considered balance laws are obtained. Based on the assumed mass–balance format, we observe for instance, that an analogous balance relation of linear momentum (e.g. $\rho_0 \, \mathrm{D}_t \boldsymbol{\varphi}$) now reads

$$\mathrm{D}_t (\rho_0 \, \mathrm{D}_t \boldsymbol{\varphi}) = \nabla_{\boldsymbol{X}} \cdot \boldsymbol{\Pi}^{\mathrm{t}} + \boldsymbol{b}_0 + R_0 \, \mathrm{D}_t \boldsymbol{\varphi} \tag{6.2}$$

with $\boldsymbol{b}_0 + R_0 \, \mathrm{D}_t \boldsymbol{\varphi}$ denoting the modified momentum source (the momentum flux here appears in standard format since an additional mass flux has been neglected). Similarly, we obtain the relation

$$\mathrm{D}_t (\rho_0 \, \epsilon) = \boldsymbol{\Pi}^{\mathrm{t}} : \mathrm{D}_t \boldsymbol{F} - \nabla_{\boldsymbol{X}} \cdot \boldsymbol{Q} + Q_0 + R_0 \, \epsilon \tag{6.3}$$

for the balance of internal energy $(\rho_0 \, \epsilon)$, wherein $-\boldsymbol{Q}$ represents the flux of non–mechanical energy and $Q_0 + R_0 \, \epsilon$ characterises the non–mechanical source term. Furthermore, the balance of entropy $(\rho_0 \, \eta)$ is determined by

$$\mathrm{D}_t (\rho_0 \, \eta) = -\nabla_{\boldsymbol{X}} \cdot \boldsymbol{H} + H_0 + R_0 \, \eta + \gamma_0 \tag{6.4}$$

with $-\boldsymbol{H}$ and $H_0 + R_0 \, \eta$ denoting the entropy flux and source, whereas $\gamma_0 \geq 0$ abbreviates the entropy production. Next, by introducing the absolute temperature $\theta > 0$ such that the volume specific Helmholtz free energy takes the format $\psi \doteq \epsilon - \theta \, \eta$, we obtain, after some straightforward transformations, the well–established Clausius–Duhem inequality as

$$\begin{aligned} \theta \, \gamma_0 \; &= \; \mathsf{D}_0 = J_{\mathrm{g}} \, \mathsf{D}_{\mathrm{g}} = J \, \mathsf{D}_t \\ &= \; \boldsymbol{\Pi}^{\mathrm{t}} : \mathrm{D}_t \boldsymbol{F} - \rho_0 \, \mathrm{D}_t \psi - \rho_0 \, \eta \, \mathrm{D}_t \theta - \theta \, \Gamma_0 - \theta^{-1} \, \boldsymbol{Q} \cdot [\, \nabla_{\boldsymbol{X}} \, \theta \,] \; \geq \; 0 \,. \end{aligned} \tag{6.5}$$

Thereby, the relations $\boldsymbol{H} \doteq \theta^{-1} \, \boldsymbol{Q}$ as well as $H_0 \doteq \theta^{-1} \, Q_0 + \Gamma_0$, respectively, have been assumed and $\psi \, \mathrm{D}_t \rho_0 = R_0 \, \epsilon - \theta \, R_0 \, \eta$ stems from the incorporated version of the balance of mass. In fact, the additional contribution Γ_0, which can be additively decomposed into growth and remodelling contributions for the subsequently developed formulations, accounts for the entropy supply caused by the ambient material of the considered particle or rather local chart.

6.2 Constitutive framework

Before addressing the formulation of growth and remodelling, we first briefly review essentials of the applied constitutive framework itself. Thereby, a multiplicative decomposition of the deformation gradient is adopted and, later on, hyperleastic stress formats are defined; compare section 2.3. As this study progresses, two different reorientation formulations are developed: (i) the subsequently elaborated intermediate configuration is chosen to coincide with the material configuration and energy–driven growth evolution is introduced; (ii) deformation tensors take the intermediate configuration into account and stress–driven growth evolution is proposed.

6.2.1 Essential kinematics

Similar to the multiplicative decomposition of the deformation gradient $\boldsymbol{F}$ applied in the previous chapters 2–5, we assume

$$\nabla_{\boldsymbol{X}}\boldsymbol{\varphi} = \boldsymbol{F} = \boldsymbol{F}_{\mathrm{e}} \cdot \boldsymbol{F}_{\mathrm{g}} : T\mathcal{B}_0 \to T\mathcal{B}_t\,, \qquad J, J_{\mathrm{e}}, J_{\mathrm{g}} > 0 \tag{6.6}$$

with $J = \det(\boldsymbol{F})$ and $j = J^{-1}$, $\boldsymbol{f} = \boldsymbol{F}^{-1}$, etc. The linear tangent maps $\boldsymbol{F}_{\mathrm{g}} : T\mathcal{B}_0 \to T\mathcal{B}_{\mathrm{g}}$ and $\boldsymbol{F}_{\mathrm{e}} : T\mathcal{B}_{\mathrm{g}} \to T\mathcal{B}_t$ characterise a linear growth map and the reversible distortion, respectively, both being generally incompatible. Based on this kinematic assumption, typical deformation tensors can be introduced by analogy with section 3.1, namely

$$\begin{aligned} \boldsymbol{C} &= \boldsymbol{F}^{\mathrm{d}} \cdot \boldsymbol{g} \cdot \boldsymbol{F}\,, & \boldsymbol{B}_{\mathrm{g}} &= \boldsymbol{f}_{\mathrm{g}} \cdot \boldsymbol{G}_{\mathrm{g}}^{-1} \cdot \boldsymbol{f}_{\mathrm{g}}^{\mathrm{d}}, \\ \boldsymbol{C}_{\mathrm{e}} &= \boldsymbol{F}_{\mathrm{e}}^{\mathrm{d}} \cdot \boldsymbol{g} \cdot \boldsymbol{F}_{\mathrm{e}}\,, & \boldsymbol{b}_{\mathrm{g}} &= \boldsymbol{F}_{\mathrm{g}} \cdot \boldsymbol{G}^{-1} \cdot \boldsymbol{F}_{\mathrm{g}}^{\mathrm{d}}\,, \\ \boldsymbol{c} &= \boldsymbol{f}^{\mathrm{d}} \cdot \boldsymbol{G} \cdot \boldsymbol{f}\,, & \boldsymbol{b}_{\mathrm{e}} &= \boldsymbol{F}_{\mathrm{e}} \cdot \boldsymbol{G}_{\mathrm{g}}^{-1} \cdot \boldsymbol{F}_{\mathrm{e}}^{\mathrm{d}}\,, \end{aligned} \tag{6.7}$$

wherein $\boldsymbol{G}_{\mathrm{g}}$ denotes the co–variant metric tensors with respect to the growth or rather intermediate configuration; compare figure 6.1. As such, the adopted kinematic growth framework is directly embedded into well–established modelling concepts for multiplicative elastoplasticity; to give an example, for instance $\widehat{\boldsymbol{L}}_{\mathrm{g}} = \mathrm{D}_t\boldsymbol{F}_{\mathrm{g}} \cdot \boldsymbol{f}_{\mathrm{g}}$ represents a growth distortion velocity with respect to the intermediate configuration.

6.2.2 Mass source

As a key feature of the proposed framework, the total mass $m = \int_{\mathcal{B}_0} \mathrm{d}m = \int_{\mathcal{B}_0} \rho_0\,\mathrm{d}V_0$ of the body B of interest is not conserved. In this regard, we consider the (material) mass source R_0 introduced in eq.(6.1) so that

$$\mathrm{d}m = \mathrm{d}m^* + \int_{t_0}^{t} R_0\,\mathrm{d}t\,\mathrm{d}V_0 = \rho_0\,\mathrm{d}V_0 = \rho_{\mathrm{g}}\,\mathrm{d}V_{\mathrm{g}} = \rho_t\,\mathrm{d}V_t \tag{6.8}$$

wherein $\mathrm{d}m^* = \rho_0^*\,\mathrm{d}V_0$ refers to a fixed initial material mass density $\rho_0^* = \rho_0|_{t_0}$ (any additional mass flux being neglected). It is obvious from eq.(6.8) that infinitesimal volume elements and densities consequently transform via

$$\mathrm{d}V_0 = j_{\mathrm{g}}\,\mathrm{d}V_{\mathrm{g}} = j\,\mathrm{d}V_t \quad \text{and} \quad \rho_0 = J_{\mathrm{g}}\,\rho_{\mathrm{g}} = J\,\rho_t\,, \tag{6.9}$$

respectively. Note that the particular case when the intermediate density ρ_{g} is assumed to remain constant, i.e. $\mathrm{D}_t\rho_{\mathrm{g}} = \mathrm{D}_t(j_{\mathrm{g}}\,\rho_0) = 0$, results in

$$\mathrm{D}_t\rho_0 = -\,\rho_0\,J_{\mathrm{g}}\,\mathrm{D}_t j_{\mathrm{g}} = \rho_0\,\mathrm{D}_t\boldsymbol{F}_{\mathrm{g}} : \boldsymbol{f}_{\mathrm{g}}^{\mathrm{d}} = \rho_0\,\mathrm{tr}\big(\widehat{\boldsymbol{L}}_{\mathrm{g}}\big) = R_0 \tag{6.10}$$

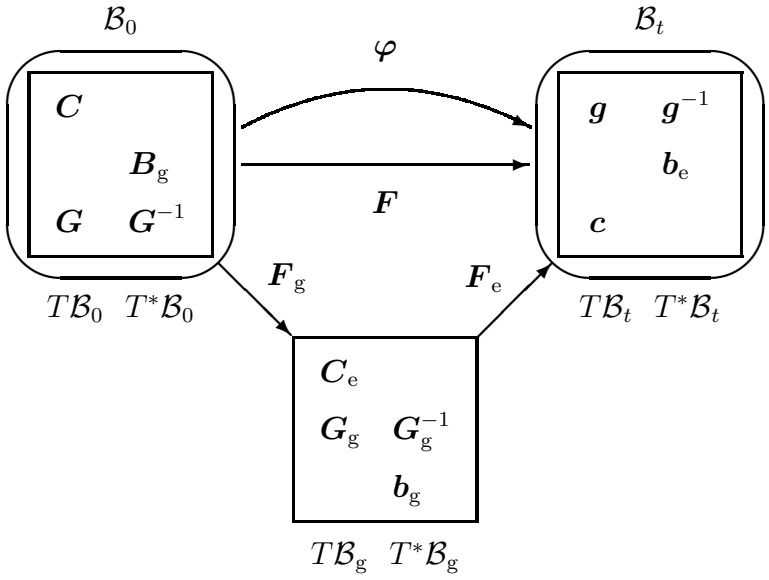

Figure 6.1: Essential kinematics and related deformation tensors.

so that $\mathrm{tr}\big(\widehat{\boldsymbol{L}}_{\mathrm{g}}\big) \neq 0$ which is in contrast to classical formulations in continuum plasticity theory. For convenience of the reader, figure 6.2 gives a graphical representation of the transformations between infinitesimal volume elements and densities.

6.2.3 Helmholtz free energy density and hyperelastic stress formats

By analogy with eqs.(2.54,2.55,3.45,3.46,4.10) we now introduce the mass specific (ψ) and volume specific (e.g. ψ_0) Helmholtz free energy as an isotropic tensor function

$$\begin{aligned} &\psi = \rho_0^{-1}\,\psi_0 = \rho_{\mathrm{g}}^{-1}\,\psi_{\mathrm{g}} = \rho_t^{-1}\,\psi_t \qquad\qquad \text{with} \\ &\psi_0\big(\boldsymbol{g}, \boldsymbol{F}, \boldsymbol{F}_{\mathrm{g}}, \boldsymbol{G}_{\mathrm{g}}^{-1}, \boldsymbol{A}_0^{\alpha}; \boldsymbol{X}\big) = J_{\mathrm{g}}\,\psi_{\mathrm{g}} = J\,\psi_t \ , \end{aligned} \tag{6.11}$$

whereby any influence of the temperature field θ has been neglected. The additional symmetric second–order tensors $\boldsymbol{A}_0^{\alpha}$, with $\boldsymbol{A}_0^{\alpha=1,2,\cdots} : T^*\mathcal{B}_0 \to T\mathcal{B}_0$, take the modelling of anisotropic (for instance orthotropic) elastic response into account. Incorporation of the reversible distortion as well as standard invariance relations together with the fundamental covariance principle render the Helmholtz free energy density to take (with a slight misuse of notation) the format

$$\begin{aligned} \psi_0 \;&=\; \psi_0\big(\boldsymbol{g}, \boldsymbol{F}_{\mathrm{e}}, \boldsymbol{G}_{\mathrm{g}}^{-1}, \boldsymbol{A}_{\mathrm{g}}^{\alpha}; \boldsymbol{X}\big) \;=\; \psi_0\big(\boldsymbol{C}_{\mathrm{e}}, \boldsymbol{G}_{\mathrm{g}}^{-1}, \boldsymbol{A}_{\mathrm{g}}^{\alpha}; \boldsymbol{X}\big) \\ &=\; \psi_0\big(\boldsymbol{C}, \boldsymbol{B}_{\mathrm{g}}, \boldsymbol{A}_0^{\alpha}; \boldsymbol{X}\big) \qquad\quad =\; \psi_0\big(\boldsymbol{g}, \boldsymbol{b}_{\mathrm{e}}, \boldsymbol{A}_t^{\alpha}; \boldsymbol{X}\big) \end{aligned} \tag{6.12}$$

with the pushforward transformations $\boldsymbol{A}_{\mathrm{g}}^{\alpha} = \boldsymbol{F}_{\mathrm{g}} \cdot \boldsymbol{A}_0^{\alpha} \cdot \boldsymbol{F}_{\mathrm{g}}^{\mathrm{d}}$ and $\boldsymbol{A}_t^{\alpha} = \boldsymbol{F} \cdot \boldsymbol{A}_0^{\alpha} \cdot \boldsymbol{F}^{\mathrm{d}}$ being obvious. Following well–established arguments of rational mechanics as previously adopted in chapters 2–5, hyperelastic formats result in

$$\begin{aligned} \boldsymbol{\Pi}^{\mathrm{d}} &= \quad \rho_0\,\partial_{\boldsymbol{F}}\ \psi\big|_{\rho_0, \boldsymbol{F}_{\mathrm{g}}, \boldsymbol{A}_0^{\alpha}}\,, \\ \boldsymbol{\Pi}_{\mathrm{g}}^{\mathrm{d}} &= \quad \rho_0\,\partial_{\boldsymbol{F}_{\mathrm{g}}}\,\psi\big|_{\rho_0, \boldsymbol{F}, \boldsymbol{A}_0^{\alpha}}\,, \\ \boldsymbol{Z}_0^{\alpha} &= -\ \rho_0\,\partial_{\boldsymbol{A}_0^{\alpha}}\psi\big|_{\rho_0, \boldsymbol{C}, \boldsymbol{B}_{\mathrm{g}}} = [\,\boldsymbol{Z}_0^{\alpha}\,]^{\mathrm{t}}\,. \end{aligned} \tag{6.13}$$

Based on eqs.(6.11,6.12), one straightforwardly obtains

$$\boldsymbol{\Pi}^{\mathrm{d}} = \rho_0\,\partial_{\boldsymbol{F}}[\,\rho_0^{-1}\,\psi_0\,]\big|_{\rho_0, \boldsymbol{F}_{\mathrm{g}}, \boldsymbol{A}_0^{\alpha}} = \boldsymbol{g} \cdot \boldsymbol{F}_{\mathrm{e}} \cdot \boldsymbol{S}_{\mathrm{e}} \cdot \boldsymbol{f}_{\mathrm{g}}^{\mathrm{d}} \quad \text{with} \quad \boldsymbol{S}_{\mathrm{e}} = 2\,\partial_{\boldsymbol{C}_{\mathrm{e}}}\psi_0\big|_{\rho_0, \boldsymbol{A}_{\mathrm{g}}^{\alpha}} = \boldsymbol{S}_{\mathrm{e}}^{\mathrm{t}} \tag{6.14}$$

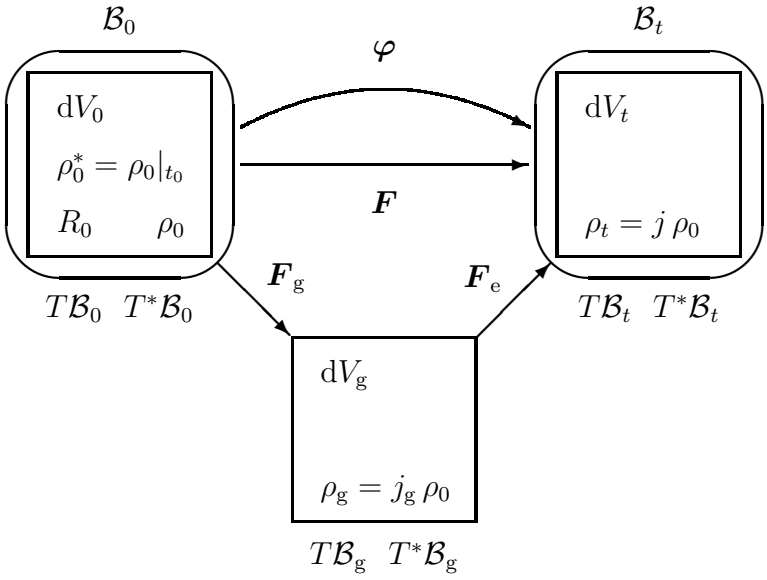

Figure 6.2: Mass source, density and volume transformations.

for the total Piola stress tensor. The derivation of the Piola–type or rather configurational stress tensor conjugated to the linear growth map proceeds along similar lines, namely

$$\boldsymbol{\Pi}^\mathrm{d}_\mathrm{g} = \rho_0\,\partial_{\boldsymbol{F}_\mathrm{g}}[\,\rho_0^{-1}\,J_\mathrm{g}\,\psi_\mathrm{g}\,]\big|_{\rho_0,\boldsymbol{F},\boldsymbol{A}^\alpha_0} = \Big[\,\psi_0\,\boldsymbol{I}^\mathrm{d}_\mathrm{g} - \boldsymbol{C}_\mathrm{e}\cdot\boldsymbol{S}_\mathrm{e} + 2\,\boldsymbol{Z}^\alpha_\mathrm{g}\cdot\boldsymbol{A}^\alpha_\mathrm{g}\,\Big]\cdot\boldsymbol{f}^\mathrm{d}_\mathrm{g} \tag{6.15}$$

with $\boldsymbol{I}_\mathrm{g} = \boldsymbol{F}_\mathrm{g}\cdot\boldsymbol{f}_\mathrm{g}$ denoting the intermediate second–order identity and $\boldsymbol{Z}^\alpha_\mathrm{g} = -\,\partial_{\boldsymbol{A}^\alpha_\mathrm{g}}\psi_0\big|_{\rho_0,\boldsymbol{C}_\mathrm{e}} = \boldsymbol{f}^\mathrm{d}_\mathrm{g}\cdot\boldsymbol{Z}^\alpha_0\cdot\boldsymbol{f}_\mathrm{g}$. Please note that $\boldsymbol{\Pi}^\mathrm{d}_\mathrm{g}$ corresponds to the intermediate motion plastic Piola stress $\widetilde{\boldsymbol{\Pi}}^\mathrm{t}$ introduced in eqs.(2.51,2.64).

Remark 6.2.1 *The total Piola stress tensor $\boldsymbol{\Pi}^\mathrm{d}$ allows alternative representations as*

$$\boldsymbol{\Pi}^\mathrm{d} = \boldsymbol{g}\cdot\boldsymbol{F}\cdot\boldsymbol{S} = -\,2\,\big[\,\boldsymbol{Y}_t\cdot\boldsymbol{b}_\mathrm{e} + \boldsymbol{Z}^\alpha_t\cdot\boldsymbol{A}^\alpha_t\,\big]\cdot\boldsymbol{f}^\mathrm{d} \tag{6.16}$$

with $\boldsymbol{S} = 2\,\partial_{\boldsymbol{C}}\psi_0|_{\rho_0,\boldsymbol{B}_\mathrm{g},\boldsymbol{A}^\alpha_0} = \boldsymbol{f}_\mathrm{g}\cdot\boldsymbol{S}_\mathrm{e}\cdot\boldsymbol{f}^\mathrm{d}_\mathrm{g}$ as well as $\boldsymbol{Y}_t = -\,\partial_{\boldsymbol{b}_\mathrm{e}}\psi_0|_{\rho_0,\boldsymbol{A}^\alpha_t} = \boldsymbol{Y}^\mathrm{t}_t$ and $\boldsymbol{Z}^\alpha_t = -\,\partial_{\boldsymbol{A}^\alpha_t}\psi_0|_{\rho_0,\boldsymbol{b}_e} = \boldsymbol{f}^\mathrm{d}\cdot\boldsymbol{Z}^\alpha_0\cdot\boldsymbol{f}$, respectively; see Menzel and Steinmann (2003c) for further details. Moreover, the growth–induced (configurational) Piola stress $\boldsymbol{\Pi}^\mathrm{d}_\mathrm{g}$ can be rewritten as

$$\boldsymbol{\Pi}^\mathrm{d}_\mathrm{g} = \Big[\,\psi_0\,\boldsymbol{I}^\mathrm{d}_\mathrm{g} + 2\,\boldsymbol{Y}_\mathrm{g}\cdot\boldsymbol{G}^{-1}_\mathrm{g}\,\Big]\cdot\boldsymbol{f}^\mathrm{d}_\mathrm{g} \tag{6.17}$$

wherein $\boldsymbol{Y}_\mathrm{g} = -\,\partial_{\boldsymbol{G}^{-1}_\mathrm{g}}\psi_0|_{\rho_0,\boldsymbol{C}_e,\boldsymbol{A}^\alpha_\mathrm{g}} = \boldsymbol{F}^\mathrm{d}_\mathrm{e}\cdot\boldsymbol{Y}_t\cdot\boldsymbol{F}_\mathrm{e}$. Besides similar transformations as highlighted in eq.(6.16), it is also interesting to note that the related intermediate Cauchy stress $\boldsymbol{\sigma}^\mathrm{t}_\mathrm{g} = \boldsymbol{\Pi}^\mathrm{d}_\mathrm{g}\cdot\mathrm{cof}(\boldsymbol{f}_\mathrm{g})$, which is often introduced as an Eshelby–type stress tensor, turns out to be generally – even for anisotropic elastic response – symmetric

$$\boldsymbol{\sigma}^\mathrm{t}_\mathrm{g} = \psi_\mathrm{g}\,\boldsymbol{I}^\mathrm{d}_\mathrm{g} + 2\,J^{-1}_\mathrm{g}\,\boldsymbol{Y}_\mathrm{g}\cdot\boldsymbol{G}^{-1}_\mathrm{g} = \boldsymbol{\sigma}_\mathrm{g}\,, \tag{6.18}$$

compare $\widetilde{\boldsymbol{\sigma}}^\mathrm{t}$ in eqs.(2.51,2.65) and the contributions by Svendsen (2001), Lu and Papadopoulos (2000) or Menzel and Steinmann (2003c).

6.3 Vianello's 'coaxiality' theory

In the progression of this work, we will assume that $\boldsymbol{A}^\alpha_{0,\mathrm{g},t}$ are (sign–independent) rank one tensors, namely $\boldsymbol{A}^\alpha_0 \doteq \boldsymbol{a}^\alpha_0\otimes\boldsymbol{a}^\alpha_0$. As such, the modelling of so–called reorientation effects is

incorporated via reorientation of, for instance, $\boldsymbol{a}_0^\alpha$. The evolution of these vectors can either be stress– or strain–driven. The latter approach will be elaborated in the sequel and allows interpretation as a purely kinematics–based reorientation framework. In this regard, let $\boldsymbol{R}_\mathrm{a}$ transform some given fibre or rather direction vector $\boldsymbol{a}_0^n$, namely $\boldsymbol{a}_0 \doteq \boldsymbol{a}_0^{n+1} = \boldsymbol{R}_\mathrm{a} \cdot \boldsymbol{a}_0^n$. Accordingly, we observe the relation

$$\mathrm{D}_t \boldsymbol{a}_0 = \mathrm{D}_t \boldsymbol{R}_\mathrm{a} \cdot \boldsymbol{a}_0^n = \boldsymbol{\Omega}_\mathrm{a} \cdot \boldsymbol{a}_0 = \boldsymbol{G}^{-1} \cdot [\, \boldsymbol{\omega}_\mathrm{a} \times \boldsymbol{a}_0 \,] \quad \text{with} \quad \mathrm{D}_t \boldsymbol{a}_0 \cdot \boldsymbol{G} \cdot \boldsymbol{a}_0 = 0 \tag{6.19}$$

but, in general, $\boldsymbol{\omega}_\mathrm{a} \cdot \boldsymbol{G} \cdot \boldsymbol{a}_0 \neq 0$; compare section 5.1. Consequently, the remaining task consists in choosing a constitutive ansatz either for $\boldsymbol{R}_\mathrm{a}$ or $\mathrm{D}_t \boldsymbol{R}_\mathrm{a}$, respectively – to give an example

$$\mathrm{D}_t \boldsymbol{a}_0 = \big[\, \boldsymbol{S} \cdot \boldsymbol{C} - [\, \boldsymbol{a}_0 \cdot \boldsymbol{G} \cdot \boldsymbol{S} \cdot \boldsymbol{C} \cdot \boldsymbol{a}_0 \,] \boldsymbol{I}_0 \big] \cdot \boldsymbol{a}_0 \tag{6.20}$$

compare eq.(5.26) – or to directly define $\boldsymbol{\Omega}_\mathrm{a}$ or $\boldsymbol{\omega}_\mathrm{a}$. Before elaborating the reorientation model itself, essential ideas of Vianello's 'coaxiality' theory of stress and stretch tensors are briefly reviewed (section 6.3.1) and then extended or rather modified for the problem at hand (section 6.3.2) which motivates the subsequently proposed reorientation framework for transversely isotropic continua in section 6.4 whereas reorientation for orthotropic tissues is developed in section 6.5.

6.3.1 Anisotropic tensor functions

For conceptual simplicity we here restrict ourselves to purely elastic response and assume the Helmholtz free energy density, as represented by a possibly anisotropic tensor function, to take the format $\psi(\boldsymbol{C})$ so that the underlying symmetry group $\mathbb{G}$ is defined via

$$\mathbb{G} = \big\{\, \boldsymbol{Q} \in \mathbb{O}^3 \,\big|\, \psi(\boldsymbol{C}^*) = \psi(\boldsymbol{C}) \,\big\} \,, \tag{6.21}$$

wherein $\boldsymbol{C}^* = \boldsymbol{Q} \cdot \boldsymbol{C} \cdot \boldsymbol{Q}^\mathrm{t}$. It has been proven that at least three different proper orthogonal transformations $\boldsymbol{Q} \in \mathbb{O}^3_+$ exist such that conjugated stress and stretch tensors commutate, i.e. $\mathrm{skw}(\boldsymbol{S}^* \cdot \boldsymbol{C}^*) = \frac{1}{2}\,[\, \boldsymbol{S}^* \cdot \boldsymbol{C}^* \,] - \frac{1}{2}\,[\, \boldsymbol{S}^* \cdot \boldsymbol{C}^* \,]^\mathrm{t} = \boldsymbol{0}$ with $\boldsymbol{S}^* = \boldsymbol{S}(\boldsymbol{C}^*) = \boldsymbol{Q} \cdot \boldsymbol{S}(\boldsymbol{C}) \cdot \boldsymbol{Q}^\mathrm{t}$. In other words, the principal stretches are fixed while the principal stretch directions are transformed in terms of $\boldsymbol{Q}$, namely

$$\boldsymbol{C}^* = \lambda_i^C \, \boldsymbol{n}_{C^*}^i \otimes \boldsymbol{n}_{C^*}^i \quad \text{with} \quad \boldsymbol{n}_{C^*}^i = \boldsymbol{Q} \cdot \boldsymbol{n}_C^i \,. \tag{6.22}$$

A trivial solution for the coaxiality of conjugated stretch and stress tensors is provided by the relation $\boldsymbol{n}_{C^*}^i \cdot \boldsymbol{n}_j^{S^*} = \delta_i^{\,j}$ – with the incorporated principal values λ_i^C and λ_S^j not necessarily following the same order of sequence, compare section 6.5.3 – wherein

$$\boldsymbol{S}^* = \lambda_S^i \, \boldsymbol{n}_i^{S^*} \otimes \boldsymbol{n}_i^{S^*} \quad \text{with} \quad \boldsymbol{n}_i^{S^*} = \boldsymbol{Q} \cdot \boldsymbol{n}_i^S \,. \tag{6.23}$$

Moreover, it turns out that states at which stress and stretches commutate render the (isothermal) Helmholtz free energy density to take an extremal value. In this regard, let

$$\Psi = \psi(\boldsymbol{C}^*)|_{\boldsymbol{C}} = \Psi(\boldsymbol{Q}) \tag{6.24}$$

and also note that the directional derivative, say, of $\boldsymbol{Q}$ results in $\frac{\mathrm{d}}{\mathrm{d}\varepsilon} \boldsymbol{Q}_\varepsilon|_{\varepsilon=0} = \boldsymbol{W}_\mathrm{I} \cdot \boldsymbol{Q}$ with $\boldsymbol{Q}_\varepsilon = \exp(\varepsilon\, \boldsymbol{W}_\mathrm{I})$ and $\boldsymbol{W}_\mathrm{I} \in \mathbb{W}^3$, i.e. $\boldsymbol{W}_\mathrm{I} = -\, \boldsymbol{W}_\mathrm{I}^\mathrm{t}$. Critical points of Ψ apparently correspond to

$$\partial_{\boldsymbol{Q}} \Psi : [\, \boldsymbol{W}_\mathrm{I} \cdot \boldsymbol{Q} \,] = \mathrm{skw}(\boldsymbol{S}^* \cdot \boldsymbol{C}^*) : \boldsymbol{W}_\mathrm{I} = 0 \quad \forall\, \boldsymbol{W}_\mathrm{I} \tag{6.25}$$

so that $\mathrm{skw}(\boldsymbol{S}^* \cdot \boldsymbol{C}^*) = \boldsymbol{0}$ which underlines the physical interpretation mentioned above. Furthermore, one could additionally investigate stability conditions at a critical point $\boldsymbol{Q}_\mathrm{crt}$ of

Ψ by computing the corresponding Hessian $\mathsf{H}_C = \partial_{\boldsymbol{Q}_{\mathrm{crt}}}[\,\partial_{\boldsymbol{Q}_{\mathrm{crt}}}\Psi \cdot \boldsymbol{Q}_{\mathrm{crt}}^{\mathrm{t}}\,] \cdot \boldsymbol{Q}_{\mathrm{crt}}^{\mathrm{t}}$ and performing a correlated eigenvalue analysis. Following similar lines as for the derivation of the critical points themselves, one finally ends up with

$$\begin{aligned} \mathsf{H}_C &= \boldsymbol{W}_{\mathrm{I}} : \mathbf{H}_C : \boldsymbol{W}_{\mathrm{II}} = \boldsymbol{W}_{\mathrm{II}} : \mathbf{H}_C : \boldsymbol{W}_{\mathrm{I}} \\ &= \left[\, \boldsymbol{C}^* \cdot \mathbf{E}_C^* : \mathrm{skw}(\boldsymbol{C}^* \cdot \boldsymbol{W}_{\mathrm{II}}) - 2\,\boldsymbol{S}^* \cdot \mathrm{skw}(\boldsymbol{C}^* \cdot \boldsymbol{W}_{\mathrm{II}}) \,\right] : \boldsymbol{W}_{\mathrm{I}}\,, \end{aligned} \tag{6.26}$$

wherein $\mathbf{E}_C^* = 2\,\partial_{\boldsymbol{C}^*}\boldsymbol{S}^*$ and $\boldsymbol{W}_{\mathrm{II}} \in \mathbb{W}^3$. Moreover, use of $\boldsymbol{D} : \boldsymbol{W} = -\,\boldsymbol{D}^{\mathrm{t}} : \boldsymbol{W}\ \forall\, \boldsymbol{W} \in \mathbb{W}^3$ has been made which holds for all second–order tensors $\boldsymbol{D}$. Due to symmetry properties of $\mathbf{E}_C^*$, eq.(6.26) might be further condensed.

6.3.2 Isotropic tensor functions

The Helmholtz free energy density has been introduced as an isotropic tensor function in eq.(6.11) so that the underlying elastic symmetry group takes (for instance) the representation

$$\mathbb{G} = \left\{\, \boldsymbol{Q} \in \mathbb{O}^3 \;\middle|\; \boldsymbol{A}_0^{\alpha} = \boldsymbol{A}_0^{\alpha\,*} = \boldsymbol{Q} \cdot \boldsymbol{A}_0^{\alpha} \cdot \boldsymbol{Q}^{\mathrm{t}} \,\right\}\,. \tag{6.27}$$

By analogy with section 6.3.1, we are in particular interested in orthogonal transformations $\boldsymbol{Q} \in \mathbb{O}_+^3$ which render ψ to take an extremum at fixed deformation. Similar to the previous section and eq.(6.27) we introduce

$$\Psi = \psi(\rho_0, \boldsymbol{C}, \boldsymbol{B}_{\mathrm{g}}, \boldsymbol{A}_0^{\alpha\,*})\big|_{\rho_0, \boldsymbol{C}, \boldsymbol{B}_{\mathrm{g}}} = \Psi(\boldsymbol{Q}) \tag{6.28}$$

and $\boldsymbol{T}_0^{\alpha\,*} = \boldsymbol{T}_0^{\alpha}(\rho_0, \boldsymbol{C}, \boldsymbol{B}_{\mathrm{g}}, \boldsymbol{A}_0^{\alpha\,*})$ with $\boldsymbol{T}_0^{\alpha} = -\,2\,\boldsymbol{Z}_0^{\alpha}$, respectively. In general, the orthogonal transformation $\boldsymbol{Q}$ should also act on $\boldsymbol{B}_{\mathrm{g}}$. For the problem at hand, however, it is sufficient to consider solely $\boldsymbol{A}_0^{\alpha\,*}$ and to neglect $\boldsymbol{B}_{\mathrm{g}}^*$, since the subsequently derived alignment of $\boldsymbol{A}_0^{\alpha}$ with respect to $\boldsymbol{C}$ also renders $\boldsymbol{B}_{\mathrm{g}}$ and $\boldsymbol{C}$ to commutate.

Based on these relations, critical points of Ψ are consequently identified via

$$\partial_{\boldsymbol{Q}}\Psi : [\,\boldsymbol{W}_{\mathrm{I}} \cdot \boldsymbol{Q}\,] = \mathrm{skw}(\boldsymbol{T}_0^{\alpha\,*} \cdot \boldsymbol{A}_0^{\alpha\,*}) : \boldsymbol{W}_{\mathrm{I}} = 0 \quad \forall\, \boldsymbol{W}_{\mathrm{I}} \tag{6.29}$$

so that $\mathrm{skw}(\boldsymbol{T}_0^{\alpha\,*} \cdot \boldsymbol{A}_0^{\alpha\,*}) = \boldsymbol{0}$. In the following, we assume a somehow trivial solution of eq.(6.29), namely that each individual (transversely isotropic) structural tensor contribution vanishes identically

$$\mathrm{skw}(\boldsymbol{T}_0^{1\,*} \cdot \boldsymbol{A}_0^{1\,*}) = \mathrm{skw}(\boldsymbol{T}_0^{2\,*} \cdot \boldsymbol{A}_0^{2\,*}) = \boldsymbol{0}\,. \tag{6.30}$$

Taking general representation theorems of isotropic tensor functions into account and incorporating the hyperelastic formats introduced in section 6.3.2, it is straightforward to show that eq.(6.30) corresponds to

$$\mathrm{skw}(\boldsymbol{C} \cdot \boldsymbol{A}_0^{1,2\,*}) = \mathrm{skw}(\boldsymbol{G} \cdot \boldsymbol{A}_0^{1\,*} \cdot \boldsymbol{C} \cdot \boldsymbol{A}_0^{2\,*}) = \boldsymbol{0} \tag{6.31}$$

which, following the same lines of derivation, results in a similar relation as eq.(6.25), namely

$$\mathrm{skw}(\boldsymbol{S}^* \cdot \boldsymbol{C}) = \boldsymbol{0}\,. \tag{6.32}$$

Conceptually speaking, conjugated stress and stretch tensors commutate if the incorporated structural tensors are aligned according to the principal stretch directions. Contrary, coaxiality of stress and structural tensors would, in general, not result in an extremal value of the Helmholtz free energy. Nevertheless, coaxiality of stretch and structural tensors constitutes a somehow trivial (but non–unique) solution for the problem at hand since, in general, additional critical points exist; compare the assumption made in eq.(6.30). By analogy with eq.(6.26),

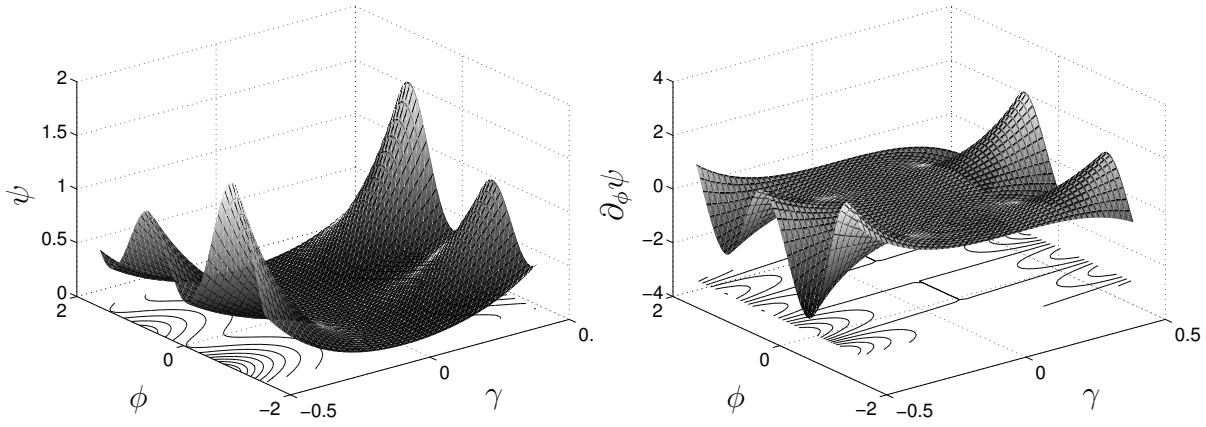

Figure 6.3: Graphical illustration of $\psi(\phi,\gamma)$ and $\partial_\phi\psi(\phi,\gamma)$ for orthotropic finite elasticity under simple shear loading.

one could, moreover, elaborate on stability conditions of the derived critical points via the Hessian relation

$$\begin{aligned}\mathsf{H}_{A_0^1} &= \boldsymbol{W}_{\mathrm{I}} : \mathbf{H}_{A_0^1} : \boldsymbol{W}_{\mathrm{II}} = \boldsymbol{W}_{\mathrm{II}} : \mathbf{H}_{A_0^1} : \boldsymbol{W}_{\mathrm{I}} \\ &= \big[\, \boldsymbol{A}_0^{1*} \cdot \mathbf{E}^{1*}_{A_0^1} : \mathrm{skw}(\boldsymbol{A}_0^{1*} \cdot \boldsymbol{W}_{\mathrm{II}}) + \boldsymbol{A}_0^{1*} \cdot \mathbf{E}^{1*}_{A_0^2} : \mathrm{skw}(\boldsymbol{A}_0^{2*} \cdot \boldsymbol{W}_{\mathrm{II}}) \\ &- \quad 2\,\boldsymbol{T}_0^{1*} \cdot \mathrm{skw}(\boldsymbol{A}_0^{1*} \cdot \boldsymbol{W}_{\mathrm{II}}) \,\big] : \boldsymbol{W}_{\mathrm{I}}\,,\end{aligned} \tag{6.33}$$

wherein $\mathbf{E}^{1*}_{A_0^{1,2}} = 2\,\partial_{\boldsymbol{A}_0^{1,2*}} \boldsymbol{T}_0^{1*}$. Eq.(6.33) might be further condensed due to symmetry properties of $\mathbf{E}^*_{A_0^\alpha}$ and the related representation of $\mathsf{H}_{A_0^2}$ follows by analogy.

Example 6.3.1 *In order to give a simple illustrative example of critical points of the Helmholtz free energy density, we restrict ourselves to orthotropic finite elasticity in the following ($\boldsymbol{B}_{\mathrm{g}} = \boldsymbol{G}^{-1}$, $\rho_0 = \rho_{\mathrm{g}} = \mathrm{const}$) and discuss a homogeneous deformation in simple shear, namely $\boldsymbol{F} = \boldsymbol{I}_0 + \gamma\, \boldsymbol{e}_1 \otimes \boldsymbol{e}_2$. Fibres defining the referential structural tensors are assumed to lie in the $\boldsymbol{e}_1 - \boldsymbol{e}_2$ plane so that one single angle is sufficient to determine the two sets of perpendicular direction vectors, i.e. $\boldsymbol{Q}(\phi\, \boldsymbol{e}_3)$. To be specific, we choose $\boldsymbol{a}_0^1 = \cos(\phi)\, \boldsymbol{e}_1 + \sin(\phi)\, \boldsymbol{e}_2$ and $\boldsymbol{a}_0^2 = -\sin(\phi)\, \boldsymbol{e}_1 + \cos(\phi)\, \boldsymbol{e}_2$ (the material response in the direction of $\boldsymbol{a}_0^1$ being stiffer than for $\boldsymbol{a}_0^2$) as well as $\phi \in [\,-\frac{\pi}{2}\,,\,\frac{\pi}{2}\,]$ and $\gamma \in [\,-\frac{1}{2}\,,\,\frac{1}{2}\,]$. Further details, as for instance the adopted Helmholtz free energy density, are given in section 6.5.4.*

Figure 6.3 highlights the pronounced dependence of the Helmholtz free energy (ψ) on the incorporated fibre directions (ϕ) at fixed state of deformation (γ). The overall non–convex nature is clearly reflected by the fact that different orientation angles render identical energy levels for a given shear number so that several energy extrema come into the picture.

Remark 6.3.1 *The analysis highlighted above has been based on an alignment of the structural tensors $\boldsymbol{A}_0^\alpha$ with respect to the principal directions of $\boldsymbol{C}$. Alternatively, one could also enforce coaxiality of $\boldsymbol{A}_{\mathrm{g}}^\alpha$ and $\boldsymbol{C}_{\mathrm{e}}$ or, formally, even of $\boldsymbol{A}_0^\alpha$ and $\boldsymbol{C}_{\mathrm{e}}$, respectively, since, in view of the growth model proposed in section 6.5, $\boldsymbol{C}$ and $\boldsymbol{C}_{\mathrm{e}}$ commutate for both scenarios. A corresponding outline in terms of spatial arguments is addressed in Menzel (2006b).*

Remark 6.3.2 *Note that restricting the orthogonal transformation $\boldsymbol{Q} \in \mathbb{O}^3$, as introduced in eqs.(6.21,6.27), to $\boldsymbol{Q} \in \mathbb{O}^3_+$ so that $\det(\boldsymbol{Q}) = 1$ does not result in any un–physical constraints, since $\boldsymbol{Q}$ acts on tensors of even order (reflections can be identified with rotations together with a change in sign).*

6.4 Energy–driven growth coupled with reorientation of one fibre family

In this section we propose an energy driven growth evolution coupled with reorientation for one fibre family. As such, we deal with transversely isotropic continua so that the index $\alpha \equiv 1$ will be neglected, i.e. $\boldsymbol{A}_0 = \boldsymbol{A}_0^1$ and $\boldsymbol{a}_0 = \boldsymbol{a}_0^1$. Moreover, we assume the intermediate and material configuration to coincide by setting $\boldsymbol{F}_{\mathrm{g}} \doteq \boldsymbol{I}_0$. Practically speaking, the developed growth formulation is embedded into a finite elasticity framework for open systems wherein growth and remodelling is incorporated via evolution of the material density (ρ_0), the fibre strength $(\|\boldsymbol{a}_0\|)$ – which, until now, has not been addressed in this chapter – and the fibre orientation $(\boldsymbol{\omega}_a)$. Consequently, the Helmholtz free energy reduces (with a slight misuse of notation) to

$$\begin{aligned} &\psi = \psi(\theta, \rho_0, \boldsymbol{F}, \boldsymbol{a}_0; \boldsymbol{X}) \doteq \psi(\theta, \rho_0, \boldsymbol{C}, \boldsymbol{A}_0; \boldsymbol{X}) \\ &\text{with} \quad \boldsymbol{A}_0 = \boldsymbol{a}_0 \otimes \boldsymbol{a}_0 \doteq \lambda^{A_0}\, \boldsymbol{n}^{A_0} \otimes \boldsymbol{n}^{A_0} \quad \text{for} \\ &\|\boldsymbol{n}^{A_0}\| = 1\,, \quad \lambda^{A_0} = \boldsymbol{a}_0 \cdot \boldsymbol{G} \cdot \boldsymbol{a}_0\,, \quad \lambda^{A_0}|_{t_0} \doteq 1\ . \end{aligned} \tag{6.34}$$

To address at least two representations of stress tensors of interest, the most general format of the (material) second Piola–Kirchhoff stress $\boldsymbol{S}$, recall eq.(6.16), results in

$$\begin{aligned} \boldsymbol{S} = 2\,\rho_0 \Big[\sum_{i=1}^{3} S_i\, [\, \boldsymbol{G}^{-1} \cdot \boldsymbol{C}\,]^{i-1} \cdot \boldsymbol{G}^{-1} + S_7\, \boldsymbol{A}_0 + 2\, S_8\, [\, \boldsymbol{A}_0 \cdot \boldsymbol{C}\,]^{\mathrm{sym}} \cdot \boldsymbol{G}^{-1} \\ + \ S_9\, \boldsymbol{A}_0 \cdot \boldsymbol{G} \cdot \boldsymbol{A}_0 + 2\, S_{10}\, \boldsymbol{A}_0 \cdot \boldsymbol{C} \cdot \boldsymbol{A}_0 \Big] \end{aligned} \tag{6.35}$$

whereby the scalars $S_{1,2,3,7,\ldots,10}$ are functions of θ, ρ_0 and the underlying (polynomial) invariants. Moreover, the spatial Cauchy stress tensor $\boldsymbol{\sigma}^{\mathrm{t}} = j\, \boldsymbol{F} \cdot \boldsymbol{S} \cdot \boldsymbol{F}$ reads in general

$$\begin{aligned} \boldsymbol{\sigma}^{\mathrm{t}} = 2\,\rho_t \Big[\sum_{i=1}^{3} S_i\, [\, \boldsymbol{b} \cdot \boldsymbol{g}\,]^{i-1} \cdot \boldsymbol{b} + S_7\, \boldsymbol{A}_t + 2\, S_8\, [\, \boldsymbol{A}_t \cdot \boldsymbol{b}\,]^{\mathrm{sym}} \\ + \ S_9\, \boldsymbol{A}_t \cdot \boldsymbol{c} \cdot \boldsymbol{A}_t + 2\, S_{10}\, \boldsymbol{A}_t \cdot \boldsymbol{g} \cdot \boldsymbol{A}_t \Big]\,. \end{aligned} \tag{6.36}$$

With these relations in hand, the Clausius–Duhem inequality (6.5) can be further elaborated. Here we are in particular interested in the contribution stemming from the structural tensor which allows representation as

$$\begin{aligned} &-\rho_0\, \partial_{\boldsymbol{A}_0}\psi : \mathrm{D}_t \boldsymbol{A}_0 \equiv -\rho_0\, \partial_{\lambda^{A_0}}\psi\, \mathrm{D}_t\lambda^{A_0} - \rho_0\, \partial_{\boldsymbol{n}^{A_0}}\psi \cdot \mathrm{D}_t \boldsymbol{n}^{A_0} \quad \text{with} \\ &\partial_{\lambda^{A_0}}\psi = \partial_{\boldsymbol{A}_0}\psi : [\, \boldsymbol{n}^{A_0} \otimes \boldsymbol{n}^{A_0}\,] \quad \text{and} \quad \partial_{\boldsymbol{n}^{A_0}}\psi = 2\,\lambda^{A_0}\, \partial_{\boldsymbol{A}_0}\psi \cdot \boldsymbol{n}^{A_0}\ . \end{aligned} \tag{6.37}$$

Together with the hyperelastic stress tensors introduced in section 6.2.3, we conclude

$$\begin{aligned} \mathsf{D}_0 \ &= \ \theta \big[\ - \ {}^{\rho_0}\Gamma_0 - \theta^{-1}\, \rho_0\, \partial_{\rho_0}\psi\, R_0 \,\big] \\ &+ \ \theta \big[\ - \ {}^{\lambda^{A_0}}\Gamma_0 - \theta^{-1}\, \rho_0\, \partial_{\boldsymbol{A}_0}\psi : [\, \boldsymbol{n}^{A_0} \otimes \boldsymbol{n}^{A_0}\,]\, \mathrm{D}_t\lambda^{A_0} \,\big] \\ &+ \ \theta \big[\ - \ {}^{n^{A_0}}\Gamma_0 - 2\,\theta^{-1}\, \rho_0\, \lambda^{A_0}\, \boldsymbol{n}^{A_0} \cdot \partial_{\boldsymbol{A}_0}\psi \cdot \mathrm{D}_t \boldsymbol{n}^{A_0} \,\big] \\ &+ \ \theta \big[\ - \theta^{-2}\, \boldsymbol{Q} \cdot [\, \nabla_{\boldsymbol{X}}\theta\,] \,\big] \\ &\doteq \ \theta \big[\, {}^{\rho_0}\gamma_0 + {}^{\lambda^{A_0}}\gamma_0 + {}^{n^{A_0}}\gamma_0 + {}^{\theta}\gamma_0 \,\big] \ \geq \ 0\,. \end{aligned} \tag{6.38}$$

For the course of this section, we adopt the commonly applied (reduced) ansatz that each individual contribution is non–negative, so that ${}^{\rho_0}\gamma_0, {}^{\lambda^{A_0}}\gamma_0, {}^{n^{A_0}}\gamma_0, {}^{\theta}\gamma_0 \geq 0$ whereby $\theta^2\, {}^{\theta}\gamma_0 \geq 0$

is established as Fourier's inequality. Conceptually speaking, the entropy supply terms ${}^{\rho_0}\Gamma_0$, ${}^{\lambda^{A_0}}\Gamma_0$ and ${}^{n^{A_0}}\Gamma_0$ compensate for stiffening and remodelling effects of the biomaterial due to isotropic growth ($\mathrm{D}_t\rho_0 \neq 0$), growth of the fibre diameter ($\mathrm{D}_t\lambda^{A_0} \neq 0$) and fibre reorientation ($\mathrm{D}_t\boldsymbol{n}^{A_0} \neq \boldsymbol{0}$), respectively.

For the subsequent prototype model as well as for the subsequent numerical examples, we restrict ourselves to an isothermal setting, $\theta \doteq \mathrm{const}$, so that $\nabla_{\boldsymbol{X}}\theta = \boldsymbol{0}$ and consequently ${}^{\theta}\gamma_0 = 0$ which motivates to cancel out the temperature field from the list of arguments that enter the Helmholtz free energy. In the following, the frequently applied additive split of the Helmholtz free energy into a purely isotropic contribution and an additional anisotropic part is adopted. Moreover, the material density is assumed to weight the Helmholtz free energy via

$$\psi(\rho_0, \boldsymbol{C}(\boldsymbol{F}), \boldsymbol{A}_0(\lambda^{A_0}, \boldsymbol{n}^{A_0}); \boldsymbol{X}) \doteq \left[\tfrac{\rho_0}{\rho_0^*}\right]^n \left[\, \psi^{\mathrm{iso}}(\rho_0, \boldsymbol{C}; \boldsymbol{X}) + \psi^{\mathrm{ani}}(\rho_0, \boldsymbol{C}, \boldsymbol{A}_0; \boldsymbol{X}) \,\right] \tag{6.39}$$

with $1 \leq n \leq 3.5$, which is a well–established ansatz, whereby $\rho_0^* = \rho_0|_{t_0} > 0$ denotes some fixed initial value for the density field. We choose in particular

$$\begin{aligned} \rho_0\, \psi^{\mathrm{nh}} &\doteq \tfrac{\mu}{2}\,[\, I_1 - 3\,]\,, \\ \rho_0\, \psi^{\mathrm{iso}} &\doteq \rho_0\, \psi^{\mathrm{nh}} - \mu\, \ln(J) + \tfrac{\lambda}{2}\, \ln^2(J)\,, \\ \rho_0\, \psi^{\mathrm{ani}} &\doteq \tfrac{\alpha}{2\,\beta}\left[\, \exp(\beta\,[\, I_7 - I_4\,]^2) - 1\,\right], \end{aligned} \tag{6.40}$$

wherein

$$I_1 = \boldsymbol{G}^{-1} : \boldsymbol{C} = \boldsymbol{b} : \boldsymbol{g}\,, \quad I_4 = \boldsymbol{A}_0 : \boldsymbol{G} = \boldsymbol{A}_t : \boldsymbol{c}\,, \quad I_7 = \boldsymbol{A}_0 : \boldsymbol{C} = \boldsymbol{A}_t : \boldsymbol{g} \tag{6.41}$$

and $\lambda, \mu, \alpha, \beta > 0$. Setting up appropriate evolution equations for the referential density ρ_0 and the structural tensor in terms of λ^{A_0} and $\boldsymbol{n}^{A_0}$, respectively, remains to be completed.

6.4.1 Material density evolution

Concerning the evolution of the density field, it has been shown by Harrigan and Hamilton (1992, 1993, 1994) that the evolution equation

$$\mathrm{D}_t\rho_0 = R_0 \doteq [\, 1 - q_{\rho_0}\,] \left[\left[\tfrac{\rho_0}{\rho_0^*}\right]^{-m} \rho_0\, \psi - {}^{\rho_0}\psi_0^* \right] \tag{6.42}$$

for the referential density guarantees (for an isotropic and small strain setting) existence and uniqueness of a global minimum of the stored energy if $m > n$, see also remark 6.4.4, whereby ${}^{\rho_0}\psi_0^* > 0$ denotes a fixed initial value for the Helmholtz free energy or rather density stimulus and $q_{\rho_0} \in [\, 0\,,\, 1\,]$ is a constant scaling factor. When choosing the ansatz ${}^{\rho_0}\Gamma_0 \doteq \theta^{-1}\,[\, 1 - n\,]\,\psi\, R_0$ for the extra entropy supply, we observe that the density contribution to the dissipation inequality as highlighted in eq.(6.38) disappears, namely ${}^{\rho_0}\gamma_0 = -\,{}^{\rho_0}\Gamma_0 - \theta^{-1}\,\rho_0\,\partial_{\rho_0}\psi\, R_0 = -\,{}^{\rho_0}\Gamma_0 + \theta^{-1}\,[\, 1 - n\,]\,\psi\, R_0 = 0$. Practically speaking, any ${}^{\rho_0}\Gamma_0 \dot{\leq} -\,\theta^{-1}\,\rho_0\,\partial_{\rho_0}\psi\, R_0$ satisfies this particular fraction of the dissipation inequality, in other words ${}^{\rho_0}\gamma_0 \geq 0$.

6.4.2 Fibre strength evolution

In analogy to the density contribution, we now introduce a constitutive equation for the length, the diameter or, in other words, the strength of the fibre $\boldsymbol{a}_0$ which is directly related to the norm of the structural tensor $\boldsymbol{A}_0$, namely λ^{A_0}. It is thereby obvious that an increase of λ^{A_0} stiffens

the material while decreasing λ^{A_0} characterises degradation. In order to set up an energy–driven evolution equation, we define the projected right Cauchy–Green tensor

$$\begin{aligned} \boldsymbol{C}^{A_0} &\doteq \boldsymbol{G} + [\, \boldsymbol{n}^{A_0} \cdot \boldsymbol{C} \cdot \boldsymbol{n}^{A_0} - 1 \,]\; \boldsymbol{G} \cdot \boldsymbol{n}^{A_0} \otimes \boldsymbol{n}^{A_0} \cdot \boldsymbol{G} \\ &= \boldsymbol{G} + \big[\, [\lambda^{A_0}]^{-1}\, I_7 - 1 \,\big] \qquad \boldsymbol{G} \cdot \boldsymbol{n}^{A_0} \otimes \boldsymbol{n}^{A_0} \cdot \boldsymbol{G} \end{aligned} \tag{6.43}$$

which accounts solely for the stretch (to the power of two) along the direction of the fibre and determines a modified Neo–Hooke contribution ${}^{A_0}\psi^{\mathrm{nh}}(\rho_0, \boldsymbol{C}^{A_0}; \boldsymbol{X})$ in the sequel. Based on this projected deformation tensor, we choose

$$\mathrm{D}_t\lambda^{A_0} \doteq [\, 1 - q_{\lambda^{A_0}} \,] \left[[\, \tfrac{\alpha}{2\,\beta}\, \exp(\beta\, [\, I_7 - I_4 \,]^2) + \tfrac{\mu}{2}\, I_7 \,]^{-l} \left[\tfrac{\rho_0}{\rho_0^*}\right]^n \rho_0\, [\, {}^{A}\psi^{\mathrm{nh}} + \psi^{\mathrm{ani}} \,] - {}^{\lambda^{A_0}}\psi_0^* \right] \tag{6.44}$$

with $l > 1$, see remark 6.4.4, wherein $q_{\lambda^{A_0}} \in [\, 0\,,\, 1 \,]$ is a constant scaling factor. Adopting the previously applied approach once more, one obtains from ${}^{\lambda^{A_0}}\Gamma_0 \doteq -\,2\,\beta\,\theta^{-1}\,\rho_0\, I_4^{-1}\, [\, I_7 - I_4 \,]^2\, [\, \rho_0/\rho_0^* \,]^n\, [\, \psi^{\mathrm{ani}} + 1 \,]\, \mathrm{D}_t\lambda^{A_0}$ a vanishing contribution of λ^{A_0} to the dissipation inequality in eq.(6.38), in other words ${}^{\lambda^{A_0}}\gamma_0 = -\,{}^{\lambda^{A_0}}\Gamma_0 - \theta^{-1}\,\rho_0\, \partial_{\boldsymbol{A}_0}\psi : [\, \boldsymbol{n}^{A_0} \otimes \boldsymbol{n}^{A_0} \,]\, \mathrm{D}_t\lambda^{A_0} = 0$; see also eq.(6.49) below for the derivation of this particular ansatz. Nevertheless, any ${}^{\lambda^{A_0}}\Gamma_0 \overset{!}{\leq} -\,\theta^{-1}\,\rho_0\, \partial_{\boldsymbol{A}_0}\psi : [\, \boldsymbol{n}^{A_0} \otimes \boldsymbol{n}^{A_0} \,]\, \mathrm{D}_t\lambda^{A_0}$ apparently guarantees ${}^{\lambda^{A_0}}\gamma_0 \geq 0$.

6.4.3 Fibre direction evolution

Next, emphasis is placed on the evolution of the fibre direction as characterised by the unit vector $\boldsymbol{n}^{A_0}$. Due to the nature of elements of unit spheres, the evolution reduces to a rotation and the correlated velocity allows representation as

$$\mathrm{D}_t\boldsymbol{n}^{A_0} = \boldsymbol{G}^{-1} \cdot [\, \boldsymbol{\omega}_{\mathrm{a}} \times \boldsymbol{n}^{A_0} \,] = \boldsymbol{G}^{-1} \cdot [\, -\,\boldsymbol{e}_0 \cdot \boldsymbol{\omega}_{\mathrm{a}} \,] \cdot \boldsymbol{n}^{A_0}\,, \tag{6.45}$$

wherein $\boldsymbol{\omega}_{\mathrm{a}}$ and $\boldsymbol{e}_0$ denote the underlying angular velocity and permutation tensor, respectively; recall eqs.(5.2,5.3,6.19) and see appendix A. It is obvious from the elaborations highlighted in section 6.3 that conjugated stress and deformation tensors commutate if the anisotropy axis $\boldsymbol{a}_0$ shares its direction with one of the principal stretch directions. This motivates the alignment of the fibre vector $\boldsymbol{n}^{A_0}$ with, for instance, the eigenvector $\boldsymbol{n}_C^1$ of the right Cauchy–Green tensor, whereby $\lambda_1^C \geq \lambda_2^C \geq \lambda_3^C$. In this regard, we propose the ansatz

$$\begin{aligned} \boldsymbol{\omega}_{\mathrm{a}} &\doteq [\, 1 - q_{\boldsymbol{n}^{A_0}} \,]\, \tfrac{\pi}{2\,t^*}\, \boldsymbol{G}^{-1} \cdot \big[\, \boldsymbol{n}^{A_0} \times [\, \boldsymbol{G}^{-1} \cdot \boldsymbol{n}_C^1 \,] \,\big] \\ &\text{together with} \quad \boldsymbol{n}_C^1 \hookleftarrow -\,\boldsymbol{n}_C^1 \quad \text{if} \quad \boldsymbol{n}^{A_0} \cdot \boldsymbol{n}_C^1 < 0 \end{aligned} \tag{6.46}$$

wherein $t^* > 0$ acts in a similar way to a relaxation time parameter in viscoelasticity and the interval of the constant scaling factor $q_{\boldsymbol{n}^{A_0}} \in [\, 0\,,\, 1 \,]$ being obvious (recall that the considered eigenvectors are independent of sign); see also remark 6.4.3 in this context. For equal eigenvalues, i.e. $\lambda_1^C = \lambda_2^C > \lambda_3^C$ or $\lambda_1^C = \lambda_2^C = \lambda_3^C$ (but not $\lambda_1^C > \lambda_2^C = \lambda_3^C$), any evolution of the fibre direction is neglected by simply setting $\mathrm{D}_t\boldsymbol{n}^{A_0} \doteq \boldsymbol{0}$. Consequently, the fibre $\boldsymbol{a}_0$ aligns according to the predominant stretch direction so that the modelled adaptation process increases the loading capacity of the material. From the modelling point of view, the ansatz in eq.(6.46) a priori excludes, say, drilling rotations, namely $\boldsymbol{n}^{A_0} \cdot \boldsymbol{G} \cdot \boldsymbol{\omega}_{\mathrm{a}} = 0$, which eliminates any rotation with respect to the fibre direction itself. In general, however, the computation of the vector product of eq.(6.45) with $\boldsymbol{n}^{A_0}$ (from the left) together with application of the '$\varepsilon\,\delta$–rule' yields

$$\boldsymbol{\omega}_{\mathrm{a}} = \boldsymbol{G}^{-1} \cdot [\, \boldsymbol{n}^{A_0} \times \mathrm{D}_t\boldsymbol{n}^{A_0} \,] + [\, \boldsymbol{n}^{A_0} \cdot \boldsymbol{G} \cdot \boldsymbol{\omega}_{\mathrm{a}} \,]\, \boldsymbol{n}^{A_0}\,. \tag{6.47}$$

Furthermore, the required orthogonality of $\mathrm{D}_t\boldsymbol{n}^{A_0}$ and $\boldsymbol{n}^{A_0}$ becomes obvious by applying the '$\varepsilon\,\delta$ – rule' with respect to eqs.(6.45,6.46), which results in

$$\mathrm{D}_t\boldsymbol{n}^{A_0} \propto \left[\, \boldsymbol{G}^{-1}\cdot\boldsymbol{n}^1_C - [\,\boldsymbol{n}^1_C\cdot\boldsymbol{n}^{A_0}\,]\,\boldsymbol{n}^{A_0}\,\right] \quad \text{so that} \quad \mathrm{D}_t\boldsymbol{n}^{A_0}\cdot\boldsymbol{G}\cdot\boldsymbol{n}^{A_0} = 0\,. \tag{6.48}$$

Alternatively, one could align $\boldsymbol{n}^{A_0}$ with the principal stress direction $\boldsymbol{n}^S_1$ instead of $\boldsymbol{n}^1_C$. As previously mentioned, conjugated stress and strain fields then in general no longer commutate (even for $t\to\infty$).

Concerning the dissipation inequality, we first compute the derivative

$$\partial_{\boldsymbol{A}_0}\psi = 2\,\beta\,[\,I_7 - I_4\,]\,\left[\tfrac{\rho_0}{\rho_0^*}\right]^n\,[\,\psi^{\mathrm{ani}}+1\,]\,[\,\boldsymbol{C}-\boldsymbol{G}\,] \tag{6.49}$$

and then observe from $\boldsymbol{n}^{A_0}\cdot\boldsymbol{G}\cdot\mathrm{D}_t\boldsymbol{n}^{A_0} = 0$ that the assumption ${}^{n^{A_0}}\Gamma_0 \doteq -\,4\,\lambda^{A_0}\,\beta\,\theta^{-1}\,\rho_0\,[\,\rho_0/\rho_0^*\,]^n\,[\,I_7-I_4\,]\,[\,\psi^{\mathrm{ani}}+1\,]\,\boldsymbol{n}^{A_0}\cdot\boldsymbol{C}\cdot\mathrm{D}_t\boldsymbol{n}^{A_0}$ results in ${}^{n^{A_0}}\gamma_0 = -\,{}^{n^{A_0}}\Gamma_0 - 2\,\theta^{-1}\,\rho_0\,\lambda^{A_0}\,\boldsymbol{n}^{A_0}\cdot\partial_{\boldsymbol{A}_0}\psi\cdot\mathrm{D}_t\boldsymbol{n}^{A_0} = 0$. However, any choice with ${}^{n^{A_0}}\Gamma_0 \dot{\leq} -\,2\,\theta^{-1}\,\rho_0\,\lambda^{A_0}\,\boldsymbol{n}^{A_0}\cdot\partial_{\boldsymbol{A}_0}\psi\cdot\mathrm{D}_t\boldsymbol{n}^{A_0}$ satisfies the reorientation part in the dissipation inequality as highlighted in eq.(6.38).

Remark 6.4.1 *The anisotropic part of the chosen Helmholtz free energy as highlighted in eq.(6.40) is essentially based on the computation of the difference between the invariants I_7 (trace of the product of the right Cauchy–Green tensor and the structural tensor) and I_4 (trace of the structural tensor). The incorporation of I_4 instead of some constant value, typically one, stems from the fact that the structural tensor itself is not constant for the proposed framework. The assumed format, namely $I_7 - I_4$, allows interpretation as a strain measure in fibre direction since $I_7 \to I_4$ for $\boldsymbol{F}\to\boldsymbol{I}_0$, and apparently guarantees a stress–free setting upon local unloading. However, if I_4 is replaced by, for instance, some constant $i_4 \doteq I_4|_{t_0}$ one might end up with a convenient model that allows the formulation of residual stresses stemming from the remodelling of the fibres (softening and strengthening).*

Remark 6.4.2 *The anisotropic contribution of the chosen format for the Helmholtz free energy in eq.(6.40) cannot (as yet) be proven to fulfil the condition of polyconvexity; see Ball (1977), Ciarlet (1988) and Šilhavý (1997) or Dacorogna (1989) and Giusti (2003) for general surveys. The specific case with $\boldsymbol{a}_0 = \mathrm{const}$ and $\lambda^{A_0} = 1$ is discussed by Schröder and Neff (2003); see also the discussion on convexity and material stability in the contributions by Ogden in Holzapfel and Ogden (2003, pp. 65–108) and Ogden (2001a) as well as Merodio and Ogden (2003). To the knowledge of the author, however, there is no analysis to date available (and moreover not in the focus of this work) that provides polyconvex functions within the present context, in other words $\lambda^{A_0} \neq \mathrm{const}$ and $\boldsymbol{n}^{A_0} \neq \mathrm{const}$. In view of the application of relaxation techniques to the problem at hand we refer the reader to, e.g., Conti et al. (2002) or Dolzmann (2003) and references cited therein. Stability properties of the reorientation framework proposed in this section with application to a transversely isotropic chain network model are studied in Kuhl et al. (2006).*

Remark 6.4.3 *An alternative but rather reduced ansatz for the anisotropic constitutive equation is based on the idea that conjugated stress and stretch tensors commutate during the entire deformation process so that, for the problem at hand, the fibre direction is a priori attached to one of the related principal stretch directions. An even further limited formulation is to adopt the format of the universal isotropic relation*

$$\boldsymbol{S} \doteq 2\,\rho_0\sum_{i=1}^{3} s_i\,[\,\boldsymbol{G}^{-1}\cdot\boldsymbol{C}\,]^{i-1}\cdot\boldsymbol{G}^{-1}\,, \qquad \boldsymbol{\sigma} \doteq 2\,\rho_t\sum_{i=1}^{3} s_i\,[\,\boldsymbol{b}\cdot\boldsymbol{g}\,]^{i-1}\cdot\boldsymbol{b}\,, \tag{6.50}$$

wherein, however, the scalars s_i remain functions of the set of invariants of the original anisotropic problem; see for instance Beatty (1987) or Imatani and Maugin (2002) with application to isotropic elasticity and anisotropic growth, respectively. Nevertheless, the assumed type of evolution equation (6.46) obviously does, even for $t \to \infty$, not result in eq.(6.50).

Remark 6.4.4 *The Wolff–type law as highlighted in eq.(6.42) guarantees a saturation–type evolution of the density field for $m > n$. Practically speaking, the rate of the material density (here the mass source term) must vanish at a biological equilibrium state. Since $\rho_0\,\psi$ embodies the material density to the power of n, see eq.(6.39), it is obvious that the saturation effect sought can only be obtained by scaling $\rho_0\,\psi$ with ρ_0 to the power of a factor which is smaller than $-n$, in other words $m > n$; recall that ${}^{\rho_0}\psi_0^* = \text{const}$. Even though the particular representation of the evolution of λ^{A_0} looks rather lengthy at first glance, it is the same concept as for the density which is adopted in eq.(6.44) and thereby, the range of the exponent l is consequently also restricted.*

Moreover, the assumed evolution type for ρ_0 and λ^{A_0} is very convenient on the one hand but also elementary on the other hand since a simple difference relation serves as the basic connection between the considered driving forces and (constant) stimuli. The incorporation of so–called dead zones however, is frequently applied in the literature and naturally extends the proposed framework. In addition, different remodelling response for an increasing / decreasing density field or tension / compression loading of the fibres, respectively, can be modelled – a particular case being the ansatz that fibres under compression are simply not taken into account by setting $\mathrm{D}_t\lambda^{A_0} \doteq 0$, $\mathrm{D}_t\boldsymbol{n}^{A_0} \doteq \boldsymbol{0}$ or even $\lambda^{A_0} \doteq 0$ if $\lambda_1^C < 1$ or $\lambda_S^1 < 0$, respectively; see e.g. Reese et al. (2001) or De Hart et al. (2004) for a similar approach. Since the incorporation of these additional enhancements and constraints is somehow straightforward, we do not focus on these aspects in the following.

Remark 6.4.5 *As previously mentioned in the introduction, modelling approaches in computational inelasticity are usually based on internal variables, which are driven by their dual forces. In this context, the driving force of the structural tensor is determined by eq.(6.49) for the problem at hand, see for instance chapter 5 or Menzel and Steinmann (2003c) for a comprehensive discussion in the context of anisotropic multiplicative elastoplasticity. Here, however, we chose an alternative approach, which enabled us to separately address the evolution of anisotropic growth in terms of fibre strengthening and reorientation.*

6.4.4 Constitutive integrator

Implicit integration schemes are applied in the sequel; to be specific, an Euler backward rule serves for the integration of the density ρ_0 as well as for λ^{A_0} while the setup of an exponential scheme enables us to obtain the classical Euler–Rodrigues formula for the rotation of the direction $\boldsymbol{n}^{A_0}$. Accordingly, integration of the material density is performed via

$$\begin{aligned} \rho_0 &\doteq \rho_0|_{t_n} + [\,1 - q_{\rho_0}\,]\,\Delta t \left[\, \left[\tfrac{\rho_0}{\rho_0^*}\right]^{-m} \rho_0\,\psi \;-\; {}^{\rho_0}\psi_0^* \right] \\ &= \rho_0|_{t_n} + [\,1 - q_{\rho_0}\,]\,\Delta t \left[\, \rho_0\psi_0 \;-\; {}^{\rho_0}\psi_0^* \right] \end{aligned} \tag{6.51}$$

or rather

$$\begin{aligned} \xi &\doteq \xi|_{t_n} + [\,1 - q_{\rho_0}\,]\,\Delta t \;\left[\; \xi^{1-m} \qquad \psi \qquad - \tfrac{1}{\rho_0^*}\,{}^{\rho_0}\psi_0^* \,\right] \\ &= \xi|_{t_n} + [\,1 - q_{\rho_0}\,]\,\Delta t \;\left[\; \xi^{1+n-m}\,[\;\psi^{\mathrm{iso}} + \psi^{\mathrm{ani}}\,] - \tfrac{1}{\rho_0^*}\,{}^{\rho_0}\psi_0^* \,\right] \end{aligned} \tag{6.52}$$

with $\xi \doteq \rho_0/\rho_0^*$ denoting the material relative density. For λ^{A_0}, we consequently obtain

$$\begin{aligned}\lambda^{A_0} \doteq\ & \lambda^{A_0}|_{t_n} + [\,1 - q_{\lambda^{A_0}}\,]\,\Delta t \Big[\ [\,\tfrac{\alpha}{2\beta}\,\exp(\beta\,[\,I_7 - I_4\,]^2) + \tfrac{\mu}{2}\,I_7\,]^{-l}\,\xi^n\,\rho_0\,[\,{}^A\psi^{\rm nh} + \psi^{\rm ani}\,] \\ & \qquad\qquad - {}^{\lambda^{A_0}}\psi_0^*\Big] \\ =\ & \lambda^{A_0}|_{t_n} + [\,1 - q_{\lambda^{A_0}}\,]\,\Delta t \Big[\qquad\qquad {}^{\lambda^{A_0}}\psi_0 - {}^{\lambda^{A_0}}\psi_0^*\Big]\end{aligned} \tag{6.53}$$

while the applied exponential integration scheme for $\boldsymbol{n}^{A_0}$ leads to

$$\boldsymbol{n}^{A_0} = \exp(-\,\Delta t\ \boldsymbol{G}^{-1}\cdot\boldsymbol{e}_0\cdot\boldsymbol{\omega}_{\rm a})\cdot\boldsymbol{n}^{A_0}|_{t_n} = \boldsymbol{R}_{\rm a}(\Delta t\,\boldsymbol{\omega}_{\rm a})\cdot\boldsymbol{n}^{A_0}|_{t_n}\,. \tag{6.54}$$

The proper orthogonal tensor $\boldsymbol{R}_{\rm a}$ possesses a closed form representation, taking, for example, the format

$$\begin{aligned}\boldsymbol{R}_{\rm a}(\Delta t\,\omega_{\rm a}\,\boldsymbol{n}^{\omega_{\rm a}}) =\ & \cos(\Delta t\,\omega_{\rm a})\ \boldsymbol{I}_0 + [\,1 - \cos(\Delta t\,\omega_{\rm a})\,]\ \boldsymbol{n}^{\omega_{\rm a}}\otimes\boldsymbol{n}^{\omega_{\rm a}}\cdot\boldsymbol{G} \\ & - \sin(\Delta t\,\omega_{\rm a})\ \boldsymbol{G}^{-1}\cdot\boldsymbol{e}_0\cdot\boldsymbol{n}^{\omega_{\rm a}}\end{aligned} \tag{6.55}$$

with $\boldsymbol{\omega}_{\rm a} = \omega_{\rm a}\,\boldsymbol{n}^{\omega_{\rm a}}$ and $\|\boldsymbol{n}^{\omega_{\rm a}}\| = 1$ being obvious. Alternatively, the rotated vector can be directly written as

$$\begin{aligned}\boldsymbol{n}^{A_0} =\ & \cos(\Delta t\,\omega_{\rm a})\ \boldsymbol{n}^{A_0}|_{t_n} + [\,1 - \cos(\Delta t\,\omega_{\rm a})\,]\ [\,\boldsymbol{n}^{\omega_{\rm a}}\cdot\boldsymbol{G}\cdot\boldsymbol{n}^{A_0}|_{t_n}\,]\,\boldsymbol{n}^{\omega_{\rm a}} \\ & + \sin(\Delta t\,\omega_{\rm a})\ \boldsymbol{G}^{-1}\cdot[\,\boldsymbol{n}^{\omega_{\rm a}}\times\boldsymbol{n}^{A_0}|_{t_n}\,]\,.\end{aligned} \tag{6.56}$$

Summarising, we obtain a system of non–linear equations, which is solved by means of the Newton–type algorithm and reviewed in section 4.3; to be specific, algorithm 4.2 is combined with method 2. The residual system to be solved, as based on eqs.(6.52,6.53,6.56), reads

$$\begin{aligned}R_\xi \quad =\ & \xi \quad - \xi|_{t_n} \quad - [\,1 - q_{\rho_0}\,]\ \ \Delta t\,\big[\,\xi^{1+n-m}\,[\,\psi^{\rm iso} + \psi^{\rm ani}\,] - \tfrac{1}{\rho_0^*}\,\rho_0\psi_0^*\,\big]\,, \\ R_{\lambda^{A_0}} =\ & \lambda^{A_0} - \lambda^{A_0}|_{t_n} - [\,1 - q_{\lambda^{A_0}}\,]\ \Delta t\,\Big[\,[\,\tfrac{\alpha}{2\beta}\,\exp(\beta\,[\,I_7 - I_4\,]^2) + \tfrac{\mu}{2}\,I_7\,]^{-l} \\ & \qquad\qquad \xi^n\,\rho_0\,[\,{}^A\psi^{\rm nh} + \psi^{\rm ani}\,] - {}^{\lambda^{A_0}}\psi_0^*\Big]\,, \\ \boldsymbol{R}_{\boldsymbol{n}^{A_0}} =\ & \boldsymbol{n}^{A_0} - \cos(\Delta t\,\omega_{\rm a})\ \boldsymbol{n}^{A_0}|_{t_n} - [\,1 - \cos(\Delta t\,\omega_{\rm a})\,]\ [\,\boldsymbol{n}^{\omega_{\rm a}}\cdot\boldsymbol{G}\cdot\boldsymbol{n}^{A_0}|_{t_n}\,]\boldsymbol{n}^{\omega_{\rm a}} \\ & - \sin(\Delta t\,\omega_{\rm a})\ \boldsymbol{G}^{-1}\cdot[\,\boldsymbol{n}^{\omega_{\rm a}}\times\boldsymbol{n}^{A_0}|_{t_n}\,]\,.\end{aligned} \tag{6.57}$$

While the corresponding linearisation for the two scalar–valued equations in eq.(6.57) is straightforward, one must guarantee that $\boldsymbol{n}^{A_0}$ remains a unit vector. Practically speaking, one can either introduce additional penalty of Lagrange multiplier contributions, which account for the normalisation constraint or perform the linearisation with respect to the appropriate manifold (in terms of generalised coordinates often denoted as rotation parameters). In order to keep the formulation as concise and efficient as possible, we choose a parametrisation of the unit vector $\boldsymbol{n}^{A_0}$ in terms of spherical coordinates, say $\vartheta_{1,2}$ or $\theta_{1,2}$, that refer to a space–attached Cartesian frame $\{\boldsymbol{e}_{1,2,3}\}$, for example

$$\begin{aligned}&\text{parametrisation 1:}\quad \boldsymbol{n}^{A_0} = \sin(\vartheta_1)\sin(\vartheta_2)\ \boldsymbol{e}_1 + \qquad \cos(\vartheta_2)\ \boldsymbol{e}_2 + \cos(\vartheta_1)\sin(\vartheta_2)\ \boldsymbol{e}_3\,, \\ &\text{parametrisation 2:}\quad \boldsymbol{n}^{A_0} = \cos(\theta_1)\sin(\theta_2)\ \boldsymbol{e}_1 + \sin(\theta_1)\sin(\theta_2)\ \boldsymbol{e}_2 + \qquad \cos(\theta_2)\ \boldsymbol{e}_3\,.\end{aligned} \tag{6.58}$$

The first parametrisation is chosen throughout as long as $\mathrm{tol} < \vartheta_2 < [\,\pi - \mathrm{tol}\,]$ with $0 < \mathrm{tol} \ll 1$; the second parametrisation is applied otherwise (a third parametrisation is possible but not needed). For a general survey on the numerical treatment of finite rotations we refer the reader

to Betsch et al. (1998) and references cited therein. With these relations in hand, the setup of the (local monolithic) system of linear equations, which is solved for any iteration step, reads

$$\begin{bmatrix} \partial_\xi R_\xi & \partial_{\lambda^{A_0}} R_\xi & \partial_{\vartheta_1} R_\xi & \partial_{\vartheta_2} R_\xi \\ \partial_\xi R_{\lambda^{A_0}} & \partial_{\lambda^{A_0}} R_{\lambda^{A_0}} & \partial_{\vartheta_1} R_{\lambda^{A_0}} & \partial_{\vartheta_2} R_{\lambda^{A_0}} \\ \partial_\xi R_{\vartheta_1} & \partial_{\lambda^{A_0}} R_{\vartheta_1} & \partial_{\vartheta_1} R_{\vartheta_1} & \partial_{\vartheta_2} R_{\vartheta_1} \\ \partial_\xi R_{\vartheta_2} & \partial_{\lambda^{A_0}} R_{\vartheta_2} & \partial_{\vartheta_1} R_{\vartheta_2} & \partial_{\vartheta_2} R_{\vartheta_2} \end{bmatrix} \circ \begin{bmatrix} \Delta\xi \\ \Delta\lambda^{A_0} \\ \Delta\vartheta_1 \\ \Delta\vartheta_2 \end{bmatrix} = \begin{bmatrix} -R_\xi \\ -R_{\lambda^{A_0}} \\ -R_{\vartheta_1} \\ -R_{\vartheta_2} \end{bmatrix} \tag{6.59}$$

with

$$\begin{aligned} R_{\vartheta_2} &= \vartheta_2 - \bar{\vartheta}_2(\vartheta_{1,2}, \dots)\,, & R_{\vartheta_1} &= \vartheta_1 - \bar{\vartheta}_1(\vartheta_{1,2}, \dots)\,, \\ \vartheta_2 &\doteq \arccos(n_2^{A_0})\,, & \vartheta_1 &\doteq \arccos(n_3^{A_0})/\sin(\vartheta_2)\,, \\ \bar{\vartheta}_2 &\doteq \arccos(\bar{n}_2^{A_0})\,, & \bar{\vartheta}_1 &\doteq \arccos(\bar{n}_3^{A_0})/\sin(\bar{\vartheta}_2)\,, \\ \boldsymbol{n}^{A_0} &= \textstyle\sum_{i=1}^{3} n_i^{A_0}\, \boldsymbol{e}_i\,, & \bar{\boldsymbol{n}}^{A_0} &= \boldsymbol{n}^{A_0} - \boldsymbol{R}_{\boldsymbol{n}^{A_0}} = \textstyle\sum_{i=1}^{3} \bar{n}_i^{A_0}\, \boldsymbol{e}_i\,, \end{aligned} \tag{6.60}$$

wherein the residuals $R_{\vartheta_{1,2}}$ take different formats for parametrisation 2 in terms of $\theta_{1,2}$.

6.4.5 Numerical examples

For the subsequent numerical examples, a homogeneous deformation in uniaxial tension as well as three–dimensional finite element settings are considered, whereby enhanced eight node bricks (Q1E9) as advocated by Simo and Armero (1992) are adopted. The choice of appropriate material parameters, however, is a non–trivial task and constitutes future research. In this (first) study we choose similar data as applied in the contribution by Holzapfel et al. in Cowin and Humphrey (2000, pp. 1–48) for the Helmholtz free energy density, namely $\lambda = 147$, $\mu = 3$ (which corresponds to $E = 8.94$, $\nu = 0.49$), $\alpha = 2$, $\beta = 1$ and $\rho_0^* = \rho_0|_{t_0} = 1$. The previously mentioned stability criterion is satisfied by, for instance, the exponents $n = 2$, $m = 4$ and in view of the fibre evolution we assume $l = 2.5$. The initial stimuli are chosen as ${}^{\rho_0}\psi_0^* = 2$ and ${}^{\lambda^{A_0}}\psi_0^* = 0.1$. Concerning the evolution or rather rotation of the fibre direction, $t^* = 100$ is assumed such that the relation $\Delta t \ll t^*$ holds for a typical time step size of $\Delta t = 1$. In order to visualise that two second–order tensors do not commutate, we once more apply the so–called anisotropy measure, compare eq.(4.64), which in the present context takes the format

$$\delta(\boldsymbol{C}\cdot\boldsymbol{S}) = \frac{\| [\,\boldsymbol{C}\cdot\boldsymbol{S}\,] - [\,\boldsymbol{C}\cdot\boldsymbol{S}\,]^{\mathrm{t}} \|}{\| \boldsymbol{C}\cdot\boldsymbol{S} \|}\,. \tag{6.61}$$

6.4.5.1 Uniaxial tension

To set the stage, we first discuss a homogeneous deformation in uniaxial tension, in other words $\boldsymbol{F} \doteq \boldsymbol{I}_0 + [\,\lambda_1^U - 1\,]\,\boldsymbol{e}_1 \otimes \boldsymbol{e}_1$. The scalar λ_1^U obviously denotes the longitudinal stretch and the chosen loading path is determined by $\lambda_1^U = 1.15$ for $t \in (\,0\,,\,25\,]$ and $\lambda_1^U = 1.30$ for $t \in (\,25\,,\,50\,]$. The initial fibre (direction) takes the representation $\boldsymbol{a}_0|_{t_0} = 0.866\,\boldsymbol{e}_1 + 0.5\,\boldsymbol{e}_2$ such that the initial angle between $\boldsymbol{a}_0|_{t_0}$ and the Cartesian axis $\boldsymbol{e}_1$, say $\phi_{\boldsymbol{a}_0} = \angle(\boldsymbol{a}_0, \boldsymbol{e}_1)$, corresponds to $\phi_{\boldsymbol{a}_0}|_{t_0} = \frac{\pi}{6}$. In analogy to $\phi_{\boldsymbol{a}_0}$, we also calculate the angles $\phi_{\boldsymbol{C}} = \angle(\boldsymbol{n}_C^1, \boldsymbol{e}_1)$ and $\phi_{\boldsymbol{S}} = \angle(\boldsymbol{n}_1^S, \boldsymbol{e}_1)$ in the following. Moreover, $\sigma^{11} = \boldsymbol{e}_1 \cdot \boldsymbol{\sigma} \cdot \boldsymbol{e}_1$ denotes the component of the spatial Cauchy stress in longitudinal direction.

Now, let all three arguments, ρ_0 or ξ, λ^{A_0}, and $\boldsymbol{n}^{A_0}$, develop during the deformation process, with $q_{\boldsymbol{n}^{A_0}} = q_{\rho_0} = q_{\lambda^{A_0}} = 0$. Figure 6.4 shows the results for $\boldsymbol{n}^{A_0}$ following $\boldsymbol{n}_C^1$. We observe

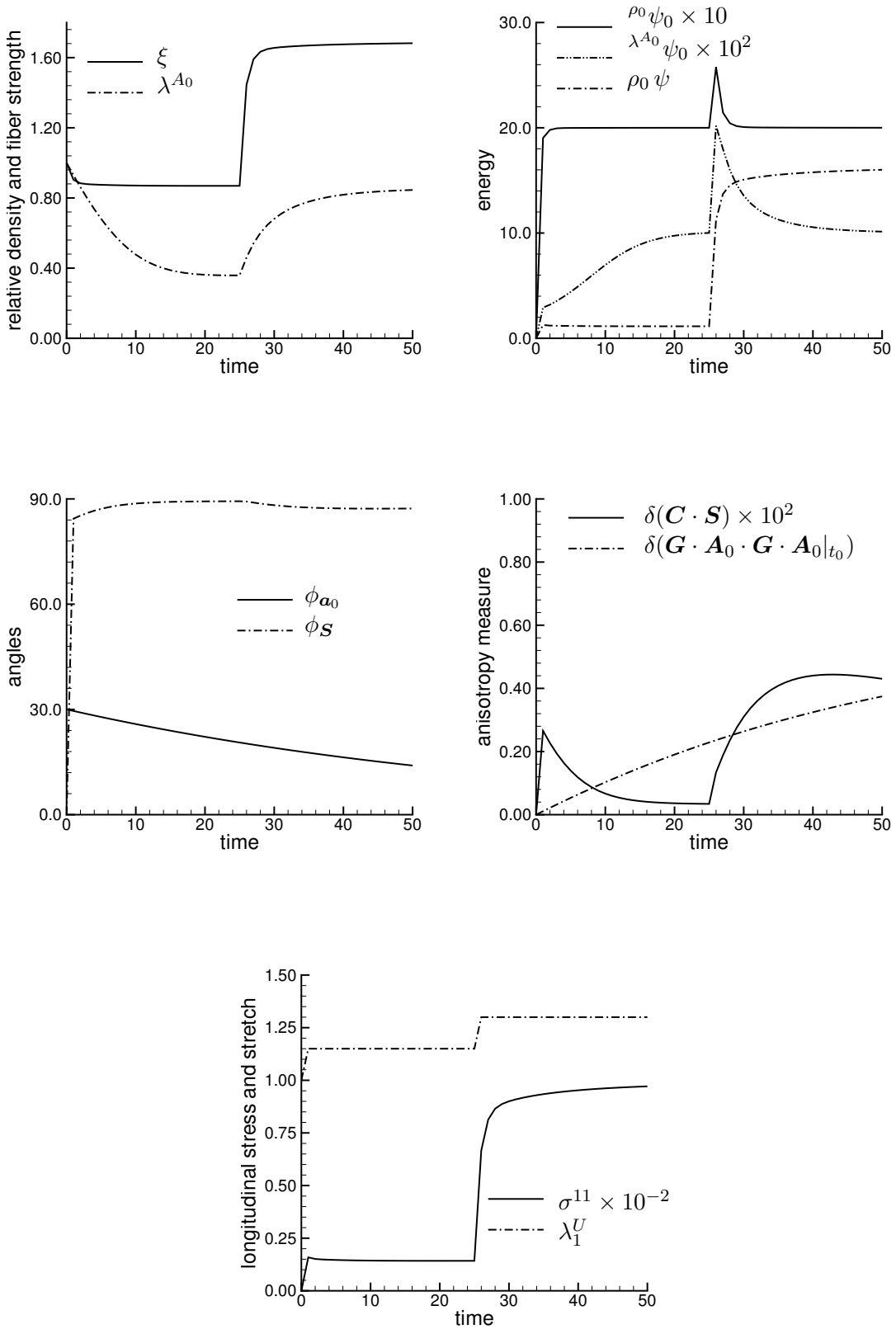

Figure 6.4: Uniaxial tension: evolution of the density, the fibre strength and – direction, aligned with $\boldsymbol{n}_C^1$ for $q_{\boldsymbol{n}^{A_0}} = q_{\rho_0} = q_{\lambda^{A_0}} = 0$.

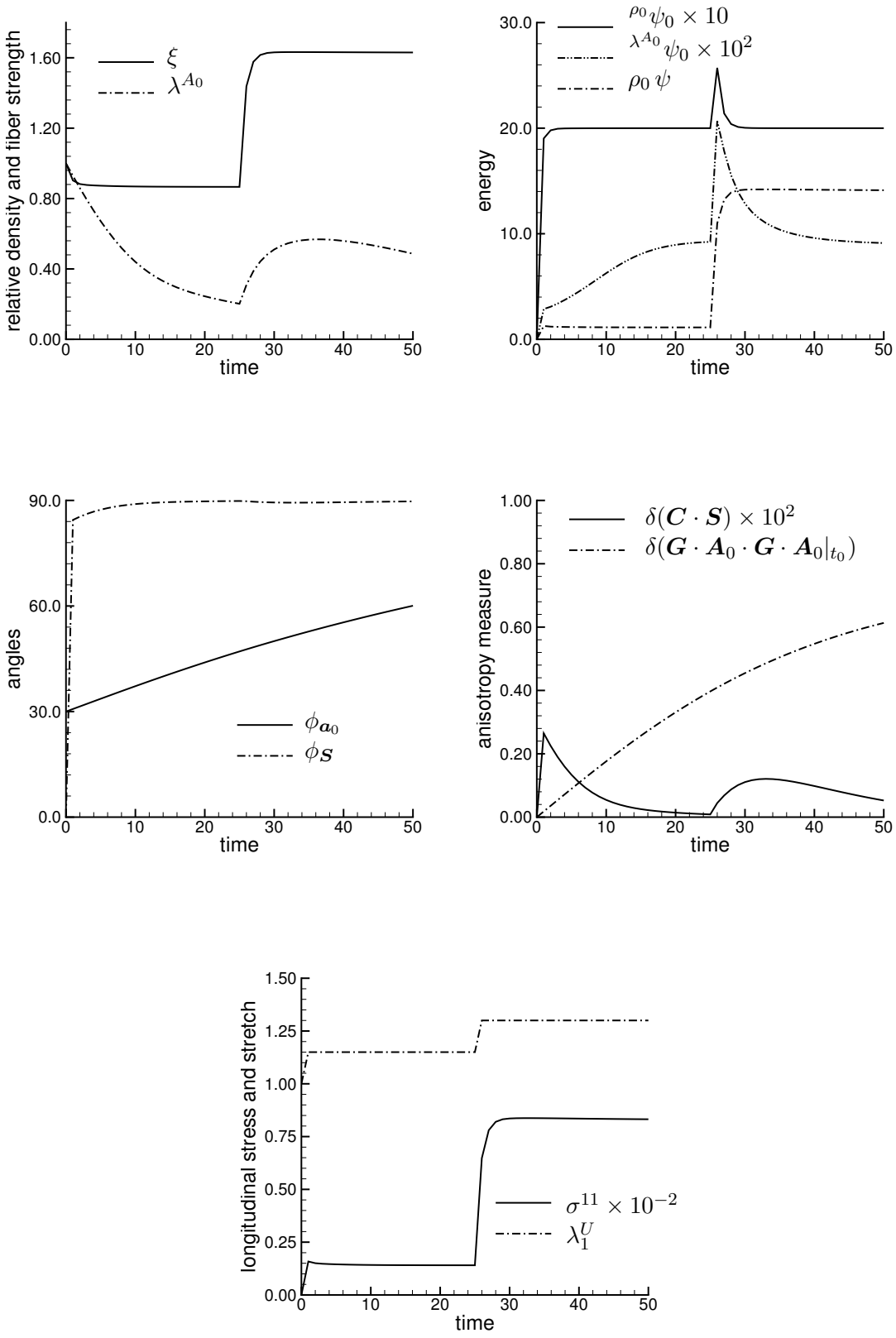

Figure 6.5: Uniaxial tension: evolution of the density, the fibre strength and – direction, aligned with $\boldsymbol{n}_1^S$ for $q_{\boldsymbol{n}^{A_0}} = q_{\rho_0} = q_{\lambda^{A_0}} = 0$.

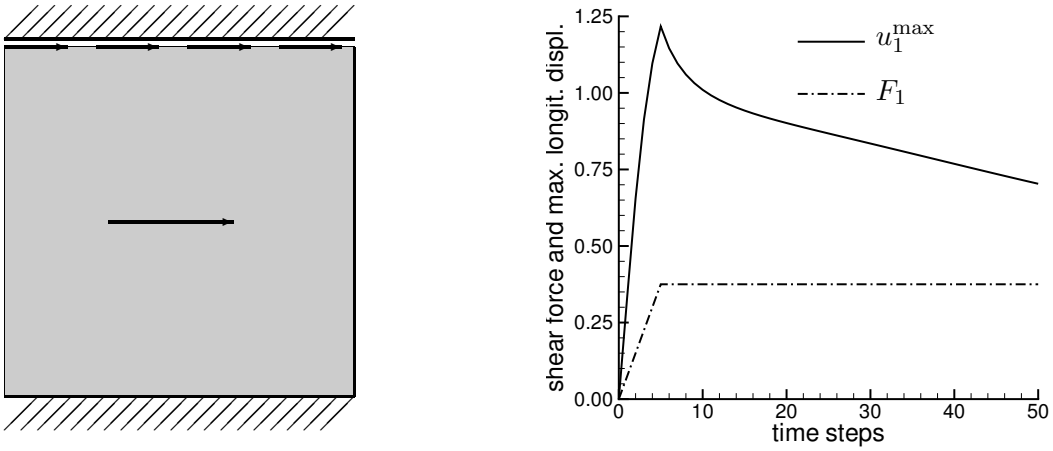

Figure 6.6: Specimen under shear: geometry and boundary conditions (left); maximal horizontal displacement $u_1^{\max}$ and loading history F_1 (right).

in particular that ρ_0 or ξ and λ^{A_0} first decrease and then increase. The adjustment of the driving terms ${}^{\rho_0}\psi_0$ and ${}^{\lambda^{A_0}}\psi_0$ in figure 6.4 (recall eqs.(6.51,6.53)) with the stimuli ${}^{\rho_0}\psi_0^*$ and ${}^{\lambda^{A_0}}\psi_0^*$ corresponds to the cessation of the evolution of ξ and λ^{A_0} which allows interpretation as approaching biological equilibrium. Moreover, the Helmholtz free energy results in a plateau–type graph. It is obvious for the considered model–type that the anisotropy measure $\delta(\boldsymbol{C}\cdot\boldsymbol{S})$ is directly related to the processing of λ^{A_0}. Similarly, the stress component σ^{11} displays the block–type loading path. Monotonically decreasing and increasing properties characterise the evolution of $\phi_{\boldsymbol{a}_0}$ and $\delta(\boldsymbol{G}\cdot\boldsymbol{A}_0\cdot\boldsymbol{G}\cdot\boldsymbol{A}_0|_{t_0})$, respectively.

Next, let $\boldsymbol{n}^{A_0}$ evolve with $\boldsymbol{n}_1^S$ for $q_{\boldsymbol{n}^{A_0}} = q_{\rho_0} = q_{\lambda^{A_0}} = 0$. Figure 6.5 presents the obtained results in analogy to figure 6.4. Placing emphasis on only two properties of this computation, we point out that both, the Helmholtz free energy ($\rho_0\,\psi$) as well as the longitudinal stress (σ^{11}) possess smaller values as for the previous setting, compare figure 6.4, which reflects the fact that fibre reorientation according to the predominant stretch direction increases the loading capacity of the material (note that the deformation is prescribed for the homogeneous deformation considered here).

6.4.5.2 Specimen under shear

In the following, we discuss a three–dimensional finite element setting whereby the body of interest is loaded under shear. The dimensions of the considered specimen are $1\times1\times0.1$ and the discretisation is performed with $10\times10\times2$ eight node bricks (Q1E9). Compared to the elaborations in section 6.4.5.1, some material parameters are slightly modified, namely: $\lambda = 32$, $\mu = 3.3$ (so that $E = 8.94$ and $\nu = 0.4$), $m = 3$, $l = 1.1$, $t^* = 5 \gg \Delta t = 0.05$, ${}^{\rho_0}\psi_0^* = 1$ and the fibre direction reorients with the predominant principal stretch direction (together with $q_{\rho_0} = q_{\lambda^{A_0}} = q_{\boldsymbol{n}^{A_0}} = 0$). Moreover, the initial fibre direction has been aligned with the moving direction of the upper edge, in other words $\boldsymbol{a}_0|_{t_0} \doteq \boldsymbol{e}_1$, compare figure 6.6 where the boundary and loading conditions are shown (note in particular that the bottom edge is clamped). The overall deformation process is therefore highly inhomogeneous right from the start. Practically speaking, the top edge is constrained such that all relevant finite element nodes are subjected to the same displacement field. The resultant force in the horizontal direction of these nodes (F_1) is incrementally increased within five time steps and then held constant for another 45 time steps. As a result, we observe that the maximal horizontal displacements ($u_1^{\max}$), which is located constantly at the top edge, increases during the first five time steps and then decreases.

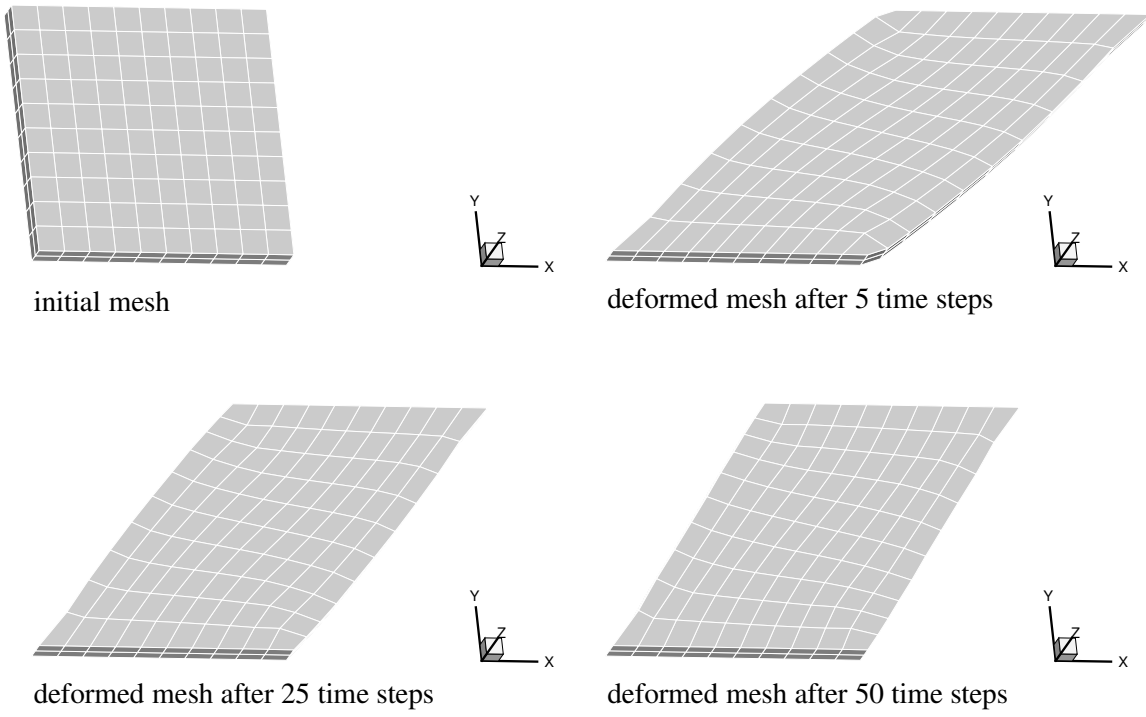

Figure 6.7: Specimen under shear: initial mesh and deformed meshes after 5 –, 25 – and 50 time steps.

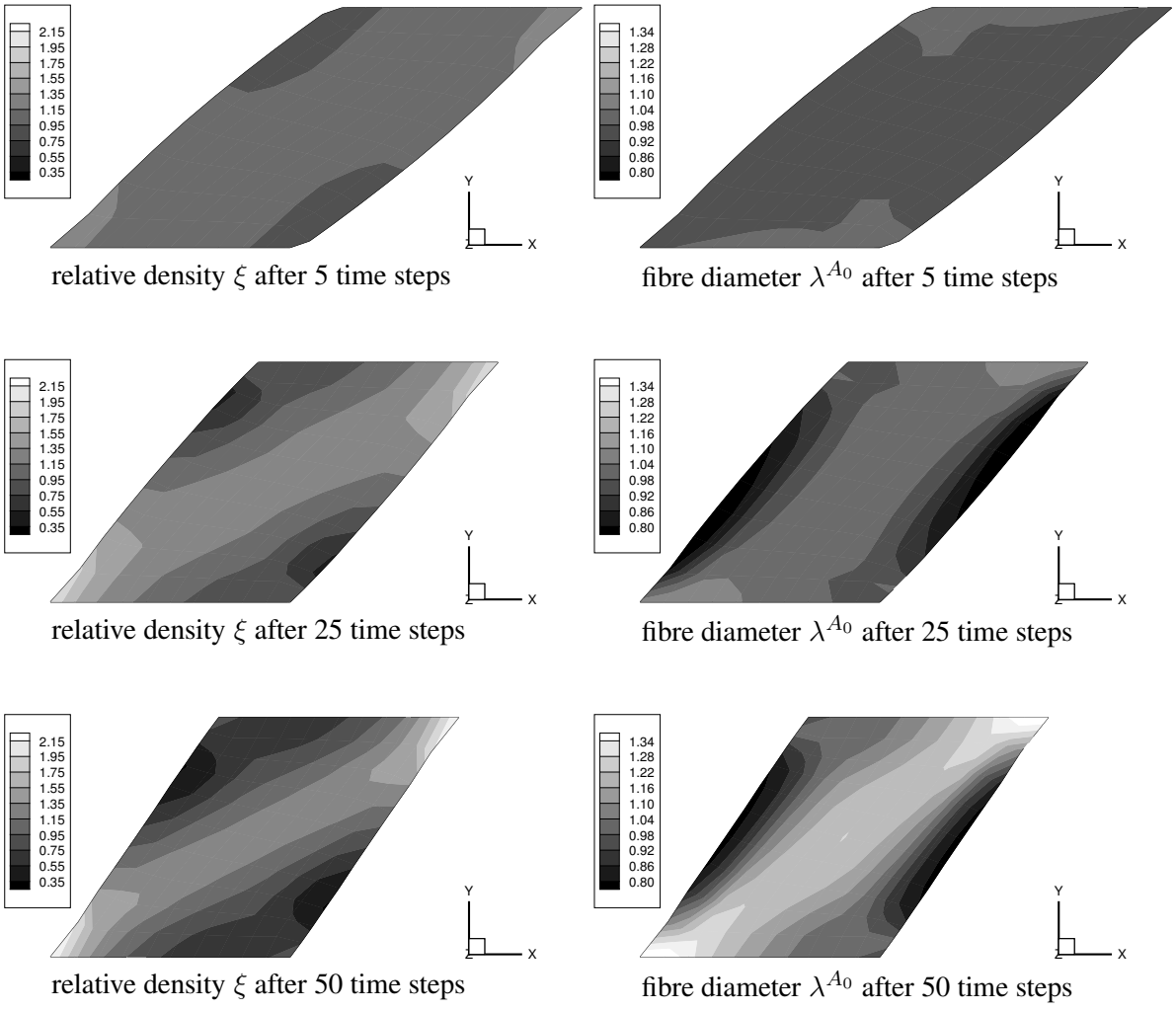

Figure 6.8: Specimen under shear: relative density ξ (left) and fibre diameter λ^{A_0} (right) after 5 –, 25 – and 50 time steps.

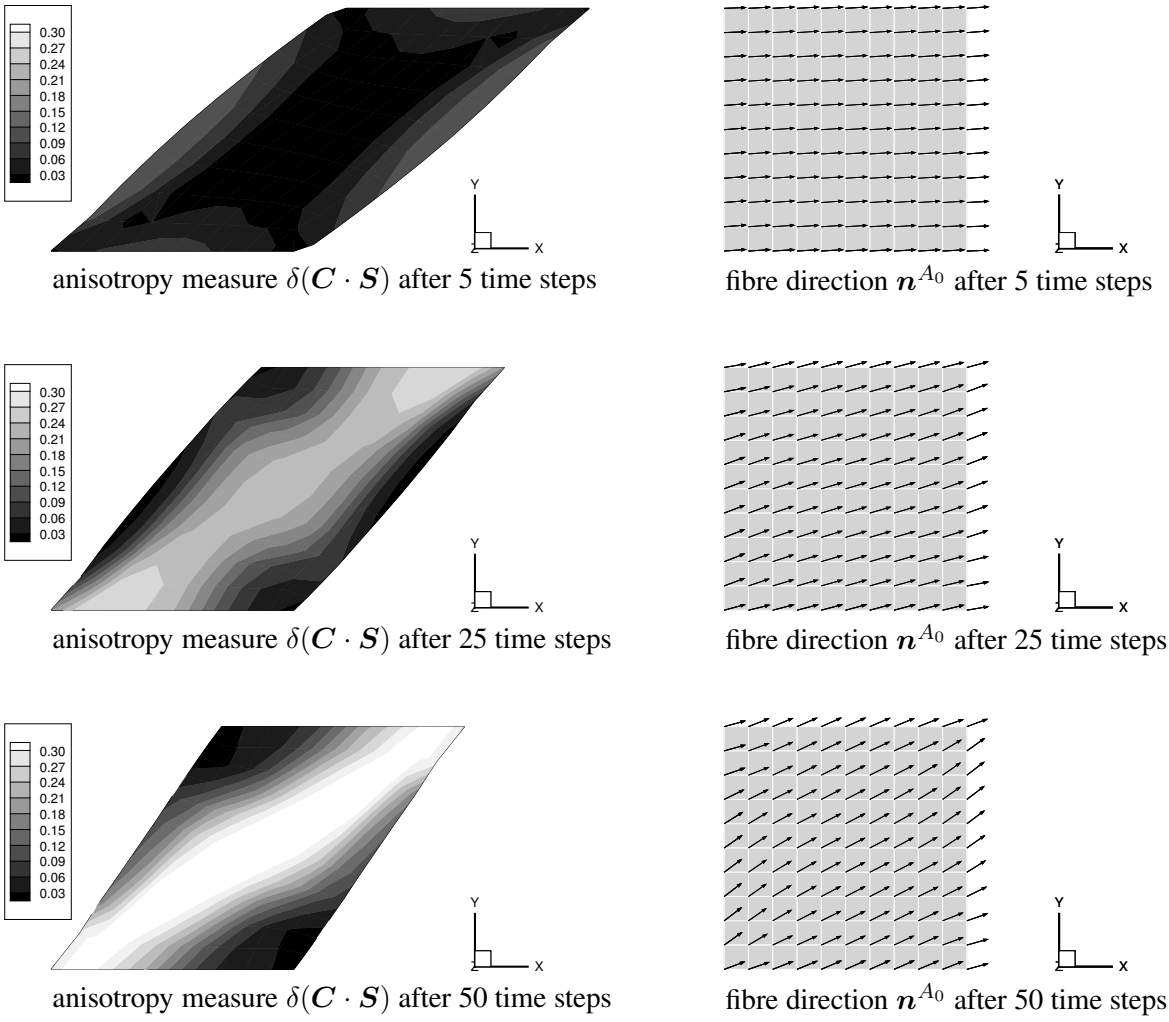

anisotropy measure $\delta(\boldsymbol{C}\cdot\boldsymbol{S})$ after 5 time steps | fibre direction $\boldsymbol{n}^{A_0}$ after 5 time steps

anisotropy measure $\delta(\boldsymbol{C}\cdot\boldsymbol{S})$ after 25 time steps | fibre direction $\boldsymbol{n}^{A_0}$ after 25 time steps

anisotropy measure $\delta(\boldsymbol{C}\cdot\boldsymbol{S})$ after 50 time steps | fibre direction $\boldsymbol{n}^{A_0}$ after 50 time steps

Figure 6.9: Specimen under shear: anisotropy measure $\delta(\boldsymbol{C}\cdot\boldsymbol{S})$ (left) and fibre direction $\boldsymbol{n}^{A_0}$ (right) after 5 –, 25 – and 50 time steps.

This effect stems from the stiffening of the remodelling process, compare figure 6.6 and 6.7 where the deformed mesh is presented for different time steps. The distributions of the density, the fibre strength, the anisotropy measure and the reorientation of the fibre are presented for different time steps, see figure 6.8 and 6.9. These results clearly show that the specimen tends to stiffen (ρ_0 as well as λ^{A_0}) along the diagonal in the $\boldsymbol{e}_1$–$\boldsymbol{e}_2$ plane. The anisotropy measure $\delta(\boldsymbol{C}\cdot\boldsymbol{S})$ apparently also approaches its peak values in this domain and, moreover, the visualisation of the fibre direction underlines the alignment with respect to the predominant principal stretch direction.

6.4.5.3 Specimen with surface cut

Finally, we discuss a specimen with a surface cut, which is again subject to tension–type loading. The denomination of this example as a 'cut' might be somehow misleading since many additional responses are involved when biological tissues are disrupted. For conceptual simplicity however, we refer to this setting as a cut with the overall behaviour reflecting some effects of wound healing.

The dimensions of the specimen are chosen as $2 \times 1 \times 0.5$, and the discretisation is performed with $16 \times 8 \times 4$ eight node bricks (Q1E9); see figure 6.10 and 6.11. To be spe-

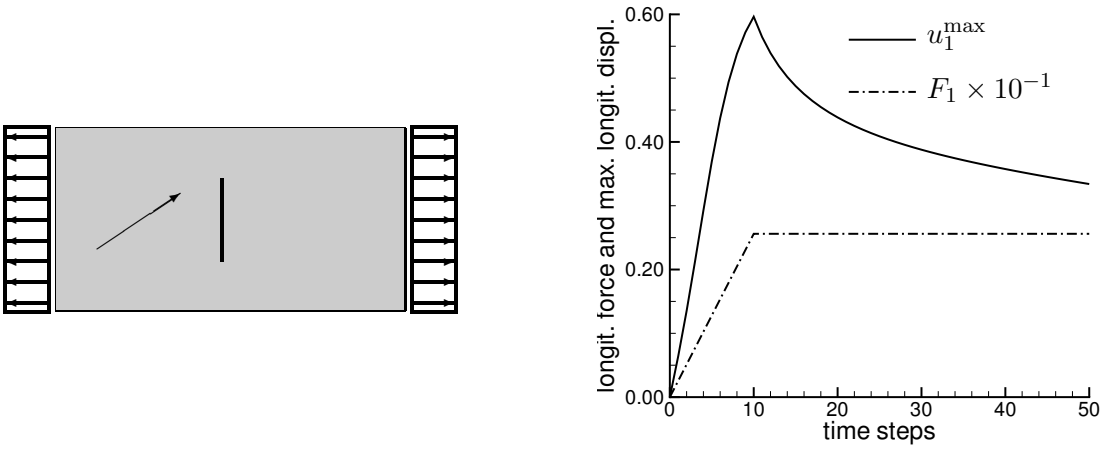

Figure 6.10: Specimen with surface cut, $\phi_{\text{cut}} = 0$: geometry and boundary conditions (left); maximal longitudinal displacement $u_1^{\max}$ and loading history F_1 (right).

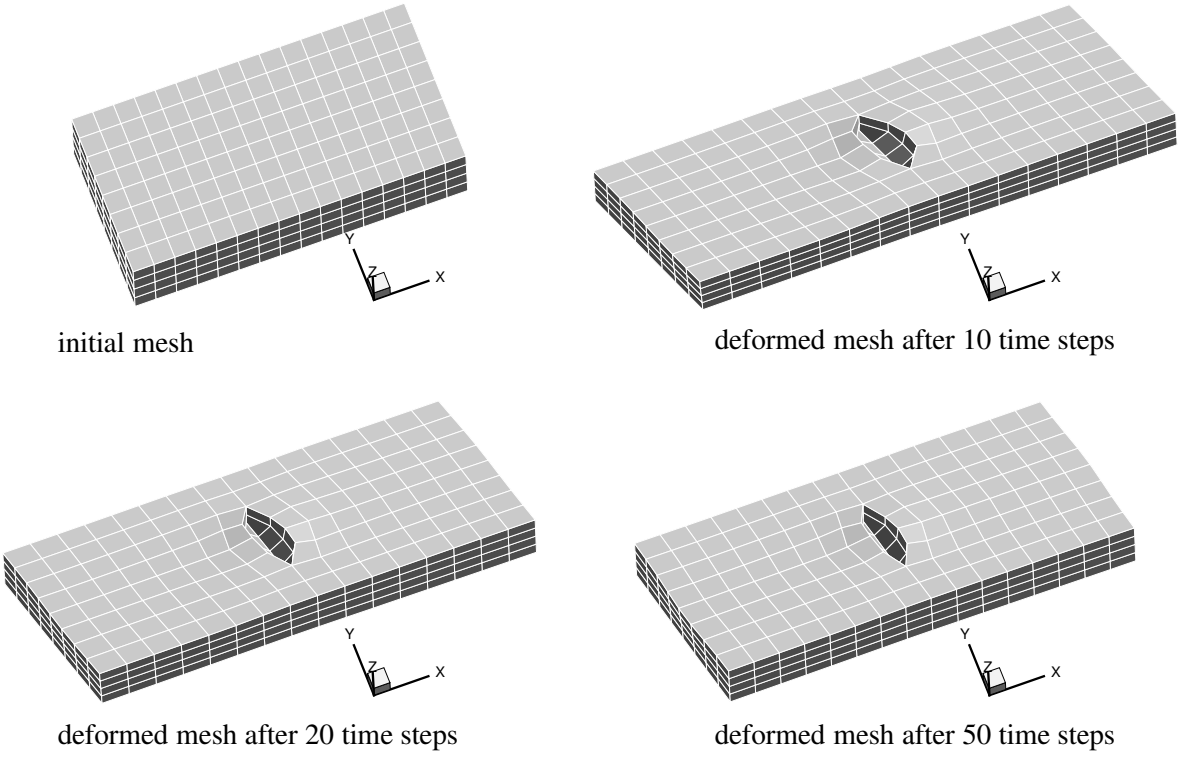

initial mesh

deformed mesh after 10 time steps

deformed mesh after 20 time steps

deformed mesh after 50 time steps

Figure 6.11: Specimen with surface cut, $\phi_{\text{cut}} = 0$: initial mesh and deformed meshes after 10 –, 20 – and 50 time steps.

cific, the force–driven loading conditions correspond to initially uniform longitudinal stresses at the endings. For notational simplicity, let this axial loading direction be aligned with the Cartesian axis $\boldsymbol{e}_1$ (such that the initial configuration of the body lies in the domain $\{-1 \leq X_1 \leq 1\,,\, -\frac{1}{2} \leq X_2 \leq \frac{1}{2}\,,\, 0 \leq X_3 \leq \frac{1}{2}\}$). The initial (closed) surface cut is perpendicular to the loading direction, namely collinear with $\boldsymbol{e}_2$ ($\phi_{\text{cut}}|_{t_0} = \angle(\text{cut}, \boldsymbol{e}_2)|_{t_0} = 0$), and its dimensions are correlated with half of the width and thickness of the specimen. Even though the underlying material is anisotropic, it is sufficient to constrain the degrees of freedom of solely a few nodes. In particular, the displacements of only three nodes, namely the mid–nodes under the bottom of the cut, are controlled; in other words $u^{\text{pr}}_{1,2,3}|_{\boldsymbol{X}=\frac{1}{4}\boldsymbol{e}_3} = 0$ and $u^{\text{pr}}_{1,2}|_{\boldsymbol{X}=\frac{1}{8}\boldsymbol{e}_3, \boldsymbol{0}} = 0$. Moreover, the incorporated material parameters are identical to the set for-

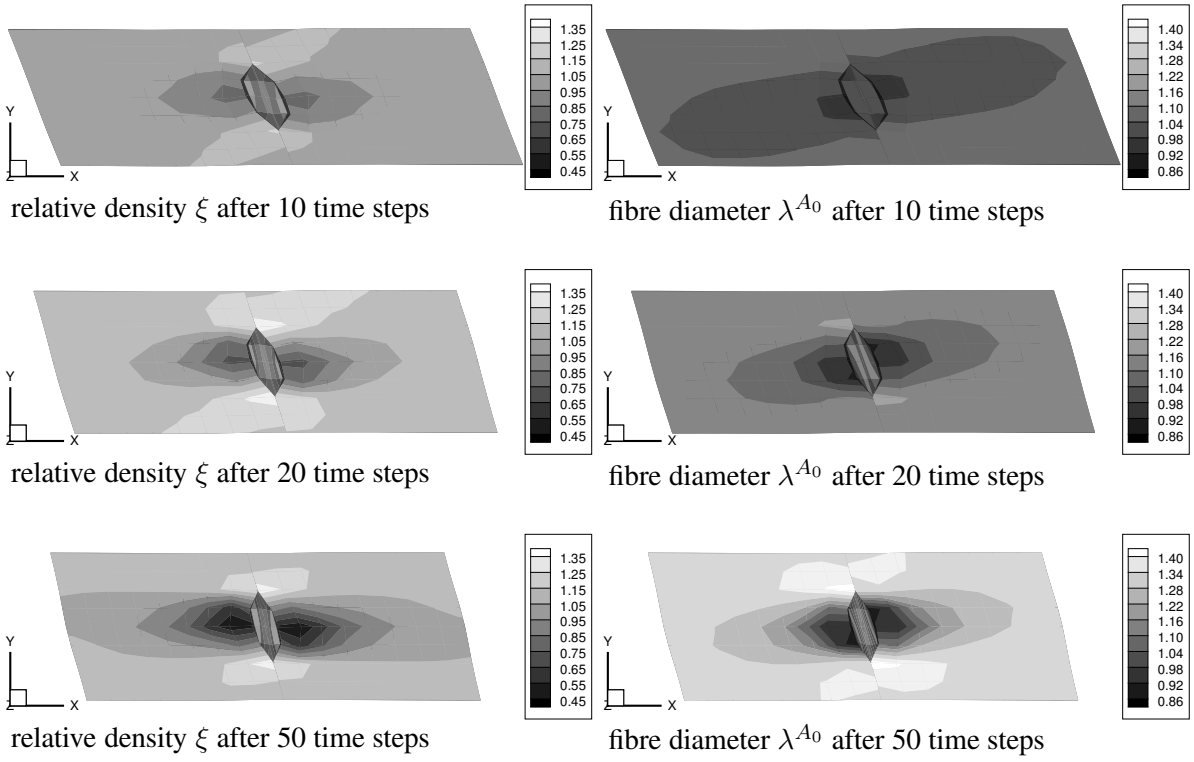

Figure 6.12: Specimen with surface cut, $\phi_{\text{cut}} = 0$: relative density ξ (left) and fibre diameter λ^{A_0} (right) after 10 –, 20 – and 50 time steps.

merly applied in section 6.4.5.2 with ${}^{\rho_0}\psi_0^* = 0.5$ and ${}^{\lambda^{A_0}}\psi_0^* = 0.05$ being the only exceptions. The initial fibre direction is chosen as $\boldsymbol{a}_0|_{t_0} = 0.866\,\boldsymbol{e}_1 + 0.5\,\boldsymbol{e}_2$ and, in analogy to the previous settings, all remodelling contributions are active ($q_{\rho_0} = q_{\lambda^{A_0}} = q_{\boldsymbol{n}^{A_0}} = 0$).

Besides the chosen boundary conditions, figure 6.10 additionally highlights the entire load versus displacement curve in terms of the longitudinal force (F_1) and the maximal longitudinal displacement, which refers constantly to the top left ($-u_1^{\max}$) and bottom right nodes ($u_1^{\max}$). It is clearly apparent that the chosen loading path corresponds to a linear increase of the resultant longitudinal force within a period of ten time steps while this force is held constant for the subsequent 40 time steps. Similar to the numerical examples discussed above, we observe that the maximal longitudinal displacement first increases with increasing load, but, due to the remodelling of the material, decreases in the progression. This stiffening effect is shown in figure 6.11, where deformed meshes for different time steps are highlighted. By analogy with section 6.4.5.2, figure 6.12 and 6.13 visualise the distributions of the density, the fibre diameter, the anisotropy measure as well as the fibre direction for different time steps. As expected, one observes on the one hand that the material stiffens at the tips of the cut, where ρ_0 and λ^{A_0} take their peak values. On the other hand, it is apparent that the material softens in the areas on the left–hand and right–hand sides of the edges of the cut. From a medical point of view, this cut orientation is therefore often disadvantageous since the cut is not collinear with the dominant principal stress (or stretch) direction; in other words it is not collinear with respect to the corresponding (Langer's) cleavage lines. Finally, the graphical representation of the anisotropy measure and the fibre direction itself in figure 6.13 underpins that the stress tensor, or the fibre respectively, aligns with the related stretch tensor (in time).

The influence of a deviation of the orientation of the cut is displayed in figure 6.14. Even though the overall response, namely the longitudinal force versus maximal longitudinal displacement curve, turns out to be almost independent of the chosen orientation of the cut (here $\phi_{\text{cut}}|_{t_0} \in \{-\frac{\pi}{6},\, 0,\, \frac{\pi}{6}\}$), we obtain different density and fibre contributions.

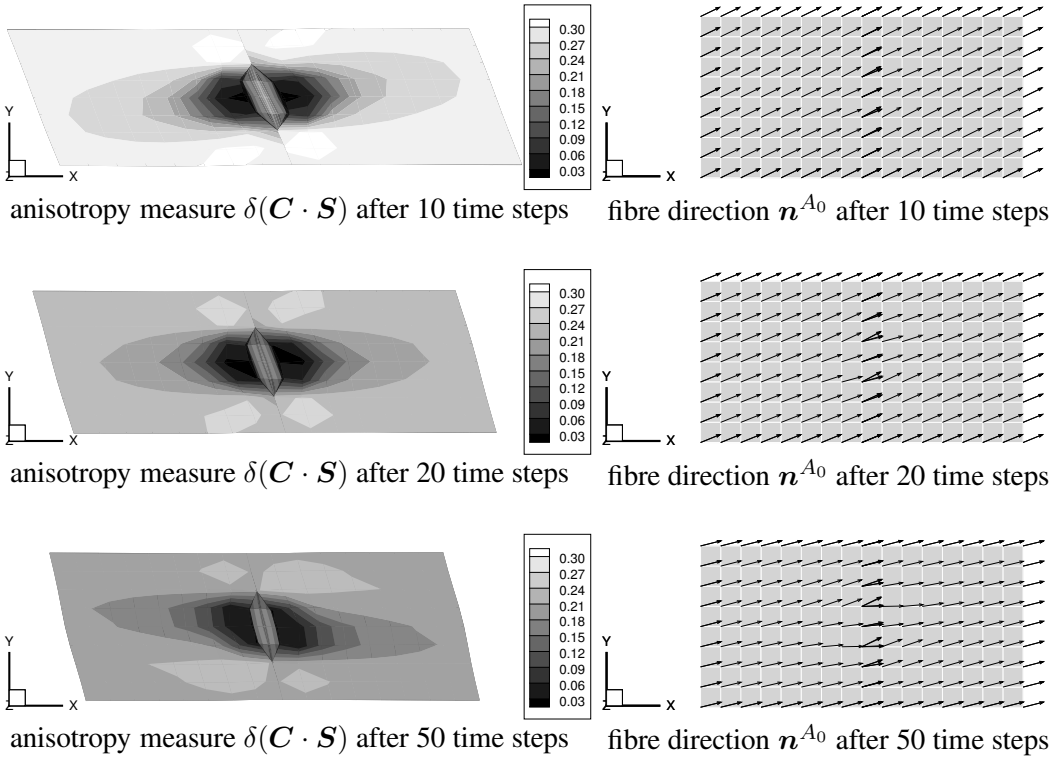

Figure 6.13: Specimen with surface cut, $\phi_{\text{cut}} = 0$: anisotropy measure $\delta(\boldsymbol{C}\cdot\boldsymbol{S})$ (left) and fibre direction $\boldsymbol{n}^{A_0}$ (right) after 10 –, 20 – and 50 time steps.

6.5 Stress–driven growth coupled with reorientation of two fibre families

The stress–driven growth model developed in this section is based on the multiplicative decomposition highlighted in section 6.2. Besides the incorporation of structural tensors into the Helmholtz free energy, also the evolution of the growth distortion $\boldsymbol{F}_{\mathrm{g}}$ will directly be related to these tensors $\boldsymbol{A}_0^\alpha$. To be specific, two rank one structural tensors $\boldsymbol{A}_0^\alpha = \boldsymbol{a}_0^\alpha \otimes \boldsymbol{a}_0^\alpha$, with $\alpha = 1, 2$ and $\|\boldsymbol{a}_0^\alpha\| = 1$, are introduced, whereby $\boldsymbol{a}_0^\alpha$ allow interpretation as two referential fibre families which, in the following, are supposed to be orthogonal.

Assume $\boldsymbol{F}_{\mathrm{g}}$ to map $\boldsymbol{a}_0^\alpha$ collinearly to themselves – in other words, the fibre families $\boldsymbol{a}_0^\alpha$ are principal directions of $\boldsymbol{F}_{\mathrm{g}}$, which consequently results in

$$\boldsymbol{F}_{\mathrm{g}} = \vartheta\, \boldsymbol{I}_0 + [\,\zeta_\alpha - \vartheta\,]\, \boldsymbol{A}_0^\alpha \cdot \boldsymbol{G} = [\,\vartheta\, \boldsymbol{A}_0^3 + \zeta_\alpha\, \boldsymbol{A}_0^\alpha\,] \cdot \boldsymbol{G}\,, \tag{6.62}$$

wherein $\boldsymbol{I}_0 = \sum_i \boldsymbol{A}_0^i \cdot \boldsymbol{G}$ denotes the material second–order identity and a third fibre direction $\boldsymbol{G} \cdot \boldsymbol{a}_0^3 = \boldsymbol{a}_0^1 \times \boldsymbol{a}_0^2$ has been introduced so that $\boldsymbol{a}_0^i \cdot \boldsymbol{G} \cdot \boldsymbol{a}_0^j = G_{ij}$ for $i, j = 1, 2, 3$ and $\boldsymbol{A}_0^3 = \boldsymbol{a}_0^3 \otimes \boldsymbol{a}_0^3$. With these elaborations in hand, it is straightforward to verify the assumed ansatz, namely

$$\boldsymbol{F}_{\mathrm{g}} \cdot \boldsymbol{a}_0^\alpha = \boldsymbol{a}_{\mathrm{g}}^\alpha = \zeta_\alpha\, \boldsymbol{a}_0^\alpha\,, \quad \boldsymbol{F}_{\mathrm{g}} \cdot \boldsymbol{a}_0^3 = \boldsymbol{a}_{\mathrm{g}}^3 = \vartheta\, \boldsymbol{a}_0^3 \tag{6.63}$$

with $\boldsymbol{F}_{\mathrm{g}} = \boldsymbol{a}_{\mathrm{g}}^i \otimes \boldsymbol{a}_0^i \cdot \boldsymbol{G}$ and $J_{\mathrm{g}} = \vartheta\, \zeta_1\, \zeta_2$ being obvious. We furthermore define spatial fibre directions as $\boldsymbol{a}_t^i = \boldsymbol{F} \cdot \boldsymbol{a}_0^i$ so that the spatial and intermediate structural tensors read $\boldsymbol{A}_t^i = \boldsymbol{a}_t^i \otimes \boldsymbol{a}_t^i$ and

$$\boldsymbol{A}_{\mathrm{g}}^\alpha = \boldsymbol{a}_{\mathrm{g}}^\alpha \otimes \boldsymbol{a}_{\mathrm{g}}^\alpha = \zeta_\alpha^2\, \boldsymbol{a}_0^\alpha \otimes \boldsymbol{a}_0^\alpha \quad \text{together with} \quad \boldsymbol{A}_{\mathrm{g}}^3 = \boldsymbol{a}_{\mathrm{g}}^3 \otimes \boldsymbol{a}_{\mathrm{g}}^3 = \vartheta^2\, \boldsymbol{a}_0^3 \otimes \boldsymbol{a}_0^3\,, \tag{6.64}$$

respectively. The incorporation of $\boldsymbol{A}_{\mathrm{g}}^\alpha$ into the isotropic tensor function $\psi_0\big(\boldsymbol{C}_{\mathrm{e}}, \boldsymbol{G}_{\mathrm{g}}^{-1}, \boldsymbol{A}_{\mathrm{g}}^{1,2}\big)$ apparently enables the modelling of orthotropic elastic response. Moreover, it is clearly observed from eq.(6.64) that the structural tensors $\boldsymbol{A}_{\mathrm{g}}^\alpha$ do in general not remain constant even for

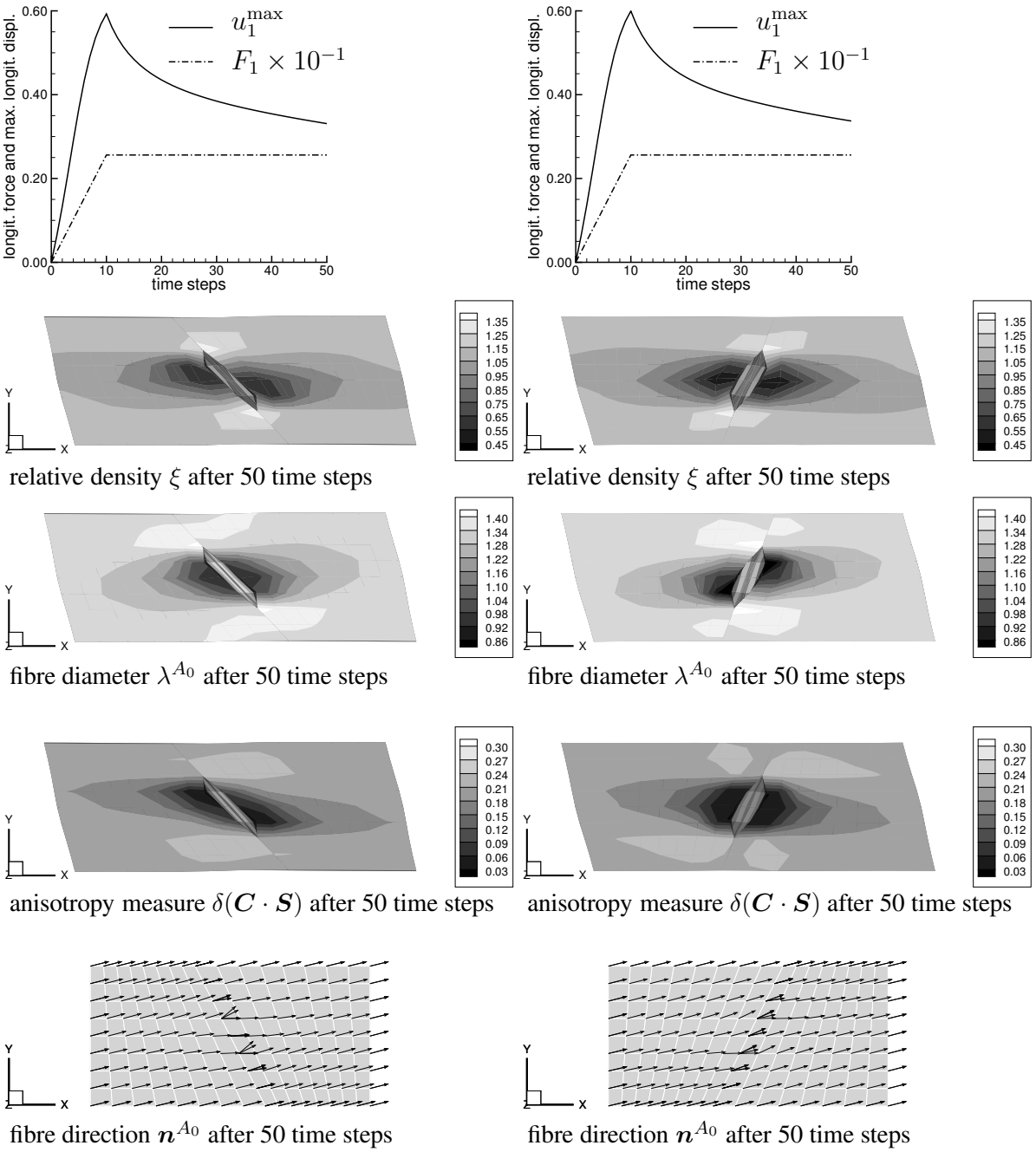

Figure 6.14: Specimen with surface cut, $\phi_{\text{cut}} = \frac{\pi}{6}$ (left) and $\phi_{\text{cut}} = -\frac{\pi}{6}$(right): load versus displacement curve (F_1 vs. $u_1^{\max}$), anisotropy measure $\delta(\boldsymbol{C} \cdot \boldsymbol{S})$, fibre diameter λ^{A_0} and fibre direction $\boldsymbol{n}^{A_0}$ after 50 time steps.

fixed fibre directions $\boldsymbol{a}_0^\alpha$. From the physical point of view, the non–constant contributions ζ_α allow interpretation as fibre weighting factors, fibre diameters or rather fibre strengths. This interpretation is also reflected by the incorporated deformation measure $\boldsymbol{C}_{\text{e}}$ since the elastic stretches at fixed total deformation – as captured within $\boldsymbol{F}_{\text{e}} = \boldsymbol{F} \cdot \boldsymbol{F}_{\text{g}}^{-1}|_{\boldsymbol{F}}$ – decrease for increasing values of ζ_α (and ϑ) which is clearly observed from eq.(6.62), namely

$$\boldsymbol{F}_{\text{g}}^{-1} = \vartheta^{-1}\, \boldsymbol{I}_0 + [\, \zeta_\alpha^{-1} - \vartheta^{-1}\,]\, \boldsymbol{A}_0^\alpha \cdot \boldsymbol{G} = [\, \vartheta^{-1}\, \boldsymbol{A}_0^3 + \zeta_\alpha^{-1}\, \boldsymbol{A}_0^\alpha\,] \cdot \boldsymbol{G}\,. \tag{6.65}$$

Remark 6.5.1 *On the one hand, the adopted assumption that $\boldsymbol{a}_0^\alpha$ constitute principal directions of $\boldsymbol{F}_{\text{g}}$ rather restricts the proposed formulation but, on the other hand, conveniently enables to represent the growth distortion in a symmetric format as highlighted in eq.(6.62).*

A, say, growth spin is addressed in section 6.5.3 later on by means of a direct fibre reorientation formulation. For a general inelastic and anisotropic constitutive framework based on evolving structural tensors the reader is referred to Menzel and Steinmann (2003c). In that work, structural tensors determining the elastic properties and those affecting the evolution of further internal variables do in general not coincide.

6.5.1 Material density evolution

In the following we assume $\rho_{\mathrm{g}} \doteq \mathrm{const}$. Accordingly, the material mass source is directly related to the trace of the growth distortion velocity as previously highlighted in eq.(6.10). As such, integration of the mass source over time results in

$$\rho_0 = \rho_0^* + \int_{t_0}^{t} R_0 \, \mathrm{d}t = J_{\mathrm{g}} \, \rho_{\mathrm{g}} = \vartheta \, \zeta_1, \zeta_2 \, \rho_{\mathrm{g}} \, . \tag{6.66}$$

In other words, the (determinant of the) growth distortion determines the material density for given ρ_{g}.

6.5.2 Fibre strength evolution

The reorientation of the fibre directions $\boldsymbol{a}_0^\alpha$ is addressed in section 6.5.3 so that the remaining task at this stage consists in setting up appropriate evolution equations for ϑ and ζ_α. The driving forces of these scalars are motived by the Clausius–Duhem inequality – the related contribution to eq.(6.5) reading

$$\rho_0 \, \mathrm{D}_t \psi \big|_{\rho_0, \boldsymbol{F}, \boldsymbol{A}_0^\alpha} = \boldsymbol{\Pi}_{\mathrm{g}}^{\mathrm{t}} : \left[\frac{\partial \boldsymbol{F}_{\mathrm{g}}}{\partial \vartheta} \, \mathrm{D}_t \vartheta + \frac{\partial \boldsymbol{F}_{\mathrm{g}}}{\partial \zeta_\alpha} \, \mathrm{D}_t \zeta_\alpha \right] . \tag{6.67}$$

Based on eq.(6.62), it is straightforward to identify

$$\partial_\vartheta \boldsymbol{F}_{\mathrm{g}} = \boldsymbol{A}_0^3 \cdot \boldsymbol{G} \quad \text{and} \quad \partial_{\zeta_\alpha} \boldsymbol{F}_{\mathrm{g}} = \boldsymbol{A}_0^\alpha \cdot \boldsymbol{G} \, . \tag{6.68}$$

With these elaborations in hand, we abbreviate notation and introduce projected stresses or rather driving forces

$$H_i = - \, \boldsymbol{\Pi}_{\mathrm{g}}^{\mathrm{t}} : [\, \boldsymbol{A}_0^i \cdot \boldsymbol{G} \,] \tag{6.69}$$

so that the contribution of interest to the Clausius–Duhem inequality results in

$$- \, \boldsymbol{\Pi}_{\mathrm{g}}^{\mathrm{t}} : \mathrm{D}_t \boldsymbol{F}_{\mathrm{g}} \big|_{\boldsymbol{A}_0^\alpha} = H_3 \, \mathrm{D}_t \vartheta + H_\alpha \, \mathrm{D}_t \zeta_\alpha \, . \tag{6.70}$$

As a fundamental modelling part, evolution equations for ζ_i – with $\zeta_3 = \vartheta$ for notational simplicity – are assumed to be determined by monotonically increasing functions in terms of their (dual) driving forces. The simplest choice consist of linear relations $\mathrm{D}_t \zeta_i = k_{\zeta_i} \, H_i$ – the additional scalars k_{ζ_i} being further weighting factors. In this work, however, we propose the ansatz

$$\mathrm{D}_t \zeta_i = k_{\zeta_i} \, \mathrm{sign}(H_i) \, \ln(|H_i| + 1) \, , \tag{6.71}$$

whereby saturation–type weighting factors are adopted

$$k_{\zeta_i} = \begin{cases} k_{\zeta_i}^+ \left[\dfrac{\zeta_i^+ - \zeta_i}{\zeta_i^+ - 1} \right]^{m_{\zeta_i}^+} & \text{for } H_i > 0 \\ k_{\zeta_i}^- \left[\dfrac{\zeta_i - \zeta_i^-}{1 - \zeta_i^-} \right]^{m_{\zeta_i}^-} & \text{for } H_i < 0 \end{cases} \tag{6.72}$$

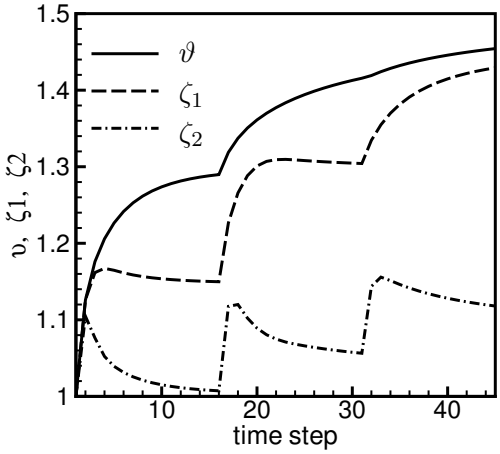

Figure 6.15: Typical evolution of the growth parameters ϑ and ζ_α under pure tension at different loading levels.

so that ${\zeta_i}^+$ and ${\zeta_i}^-$ denote upper and lower limit values for ζ_i, respectively, and different response in, say, tension ($H_i > 0$) and compression ($H_i < 0$) can be modelled.

For the subsequent numerical examples, an implicit Euler backward scheme is applied to integrate eq.(6.71), namely

$$\zeta_{i\,n+1} = \zeta_{i\,n} + \Delta t\, \mathrm{D}_t \zeta_{i\,n+1} \quad \text{with} \quad \zeta_i\big|_{t_0} = 1\,. \tag{6.73}$$

Moreover, algorithm 4.2 is applied and combined with method 2; compare section 4.3.1.1.

Example 6.5.1 *For illustration purpose and by analogy with section 6.4.5.1, we briefly highlight the qualitative behaviour of the proposed growth model under pure tension with respect to a constant loading direction $\boldsymbol{e}_3$, namely $\boldsymbol{F} = \boldsymbol{I}_0 + [\,\lambda_3^U - 1\,]\,\boldsymbol{e}_3 \otimes \boldsymbol{e}_3$. Initial growth conditions are determined by $\boldsymbol{F}_{\mathrm{g}}|_{t_0} = \boldsymbol{I}_0$, so that $\zeta_i|_{t_0} = 1$, and the (constant) directions of the fibre families are chosen as $\boldsymbol{a}_0^1 = [\,\boldsymbol{e}_1 + \boldsymbol{e}_3\,]/\sqrt{2}$ and $\boldsymbol{a}_0^2 = \boldsymbol{e}_2$ whereby $\{\boldsymbol{e}_i\}$ denotes a Cartesian frame. Further details as for instance the adopted Helmholtz free energy density are given in section 6.5.4.*

Figure 6.15 shows the typical time–dependent biological equilibrium evolution for different loading levels – the growth parameters ϑ and ζ_α approach load–dependent saturation plateaus. The particular loading levels, in other words the total stretch in loading direction, have thereby been fixed over certain time intervals:

$$\lambda_3^U = \begin{cases} 1.5 & \text{for} \quad 0 < \text{time step} \leq 15 \\ 2.0 & \text{for} \quad 15 < \text{time step} \leq 30 \\ 2.5 & \text{for} \quad 30 < \text{time step} \leq 45 \end{cases} \tag{6.74}$$

Remark 6.5.2 *Isotropic as well as transversely isotropic growth are inherently included in the proposed orthotropic growth model. For isotropic growth ($\boldsymbol{F}_{\mathrm{g}} = \vartheta\,\boldsymbol{I}_0$ with $\mathrm{D}_t\vartheta \neq 0$ and $\mathrm{D}_t\zeta_\alpha = 0$ being obvious) the driving force boils down to $H_3^{\mathrm{iso}} = \sum_i H_i$ while the projected stresses for transversely isotropic growth (for example $\boldsymbol{F}_{\mathrm{g}} = \vartheta\,\boldsymbol{I}_0 + [\,\zeta_1 - \vartheta\,]\,\boldsymbol{A}_0^1 \cdot \boldsymbol{G}$ with $\mathrm{D}_t\vartheta, \mathrm{D}_t\zeta_1 \neq 0$ and $\mathrm{D}_t\zeta_2 = 0$ being obvious) read $H_3^{\mathrm{tra}} = H_2 + H_3$ and $H_1^{\mathrm{tra}} = H_1$, respectively. Depending on the type of tissue investigated and related experimental observations, one might also choose the Helmholtz free energy density to reflect the same symmetry as the particular format of the adopted growth law.*

6.5.3 Fibre direction evolution

Motivated by the coaxiality relations between stretches and structural tensors, recall section 6.3, a symmetry group preserving remodelling approach is developed in the following. The two fibre families $\boldsymbol{a}_0^1$ and $\boldsymbol{a}_0^2$, which allow to incorporate orthotropic response, thereby throughout remain perpendicular. Apparently, the Helmholtz free energy density is directly affected by, on the one hand, the reorientation of structural tensors since these quantities serve as arguments of ψ. On the other hand, also appropriate deformation measures incorporated into ψ substantially depend on the direction of $\boldsymbol{a}_0^\alpha$. We restrict ourselves to an outline with respect to arguments settled in the material configuration – transformation to the growth or spatial configuration as well as an alignment of the structural tensors with respect to, for example, $\boldsymbol{C}_\mathrm{e}$ or $\boldsymbol{b}_\mathrm{e}$, respectively, being straightforward; compare Menzel (2006b).

The proposed reorientation framework is based on one single rotation $\boldsymbol{R}_\mathrm{a}$ for both fibre families $\boldsymbol{a}_0^{1,2}$. The related angular velocity vector $\boldsymbol{\omega}_\mathrm{a}$ is assumed to be proportional with respect to the pseudo rotation vector $\boldsymbol{\theta}_\mathrm{a}$ which is extracted from the constitutively determined rotation tensor. As such, the ansatz for $\boldsymbol{R}_\mathrm{a}$ is of cardinal importance and should ensure that $\boldsymbol{R}_\mathrm{a} \to \boldsymbol{I}_0$ for $\mathrm{skw}(\boldsymbol{T}_0^{\alpha\,*} \cdot \boldsymbol{A}_0^{\alpha\,*}) \to \boldsymbol{0}$. A natural choice for $\boldsymbol{R}_\mathrm{a}$ might consist in $\boldsymbol{R}_\mathrm{a} = \exp(\boldsymbol{\Theta})$ with (the stress– and kinematics–based quantity) $\boldsymbol{\Theta} \propto \mathrm{skw}(\boldsymbol{S} \cdot \boldsymbol{C})$ while we propose

$$\boldsymbol{R}_\mathrm{a} = \boldsymbol{G}^{-1} \cdot \boldsymbol{n}_C^i \otimes \boldsymbol{a}_0^i \cdot \boldsymbol{G} \tag{6.75}$$

which, in general, offers more modelling flexibility compared to the former ansatz. Commonly, the principal stretch directions are arranged according to the values of the principal stretches themselves, $\lambda_1^C \geq \lambda_2^C \geq \lambda_3^C$ say, so that $\{\boldsymbol{n}_C^1, \boldsymbol{n}_C^2, \boldsymbol{n}_C^3\} \in \mathbb{O}_+^3$. Similarly, the fibre families also define an orthonormal base system, $\{\boldsymbol{a}_0^1, \boldsymbol{a}_0^2, \boldsymbol{a}_0^3\} \in \mathbb{O}_+^3$, whereby the material parameters related to $\boldsymbol{a}_0^1$ can, for instance, be assumed to be 'stiffer' or identical compared to those which are attributed to $\boldsymbol{a}_0^2$. Furthermore, one could rearrange the sequence of $\boldsymbol{n}_C^i$ so that $\boldsymbol{a}_0^1$ is not necessarily aligned with the predominant stretch direction. In this regard, three different orientation preserving transformations are introduced, i.e.

$$\begin{aligned}
\boldsymbol{R}_{\mathrm{a}\,123} &= \boldsymbol{G}^{-1} \cdot \big[\, \boldsymbol{n}_C^1 \otimes \boldsymbol{a}_0^1 + \boldsymbol{n}_C^2 \otimes \boldsymbol{a}_0^2 + \boldsymbol{n}_C^3 \otimes \boldsymbol{a}_0^3 \,\big] \cdot \boldsymbol{G}\,, \\
\boldsymbol{R}_{\mathrm{a}\,231} &= \boldsymbol{G}^{-1} \cdot \big[\, \boldsymbol{n}_C^2 \otimes \boldsymbol{a}_0^1 + \boldsymbol{n}_C^3 \otimes \boldsymbol{a}_0^2 + \boldsymbol{n}_C^1 \otimes \boldsymbol{a}_0^3 \,\big] \cdot \boldsymbol{G}\,, \\
\boldsymbol{R}_{\mathrm{a}\,312} &= \boldsymbol{G}^{-1} \cdot \big[\, \boldsymbol{n}_C^3 \otimes \boldsymbol{a}_0^1 + \boldsymbol{n}_C^1 \otimes \boldsymbol{a}_0^2 + \boldsymbol{n}_C^2 \otimes \boldsymbol{a}_0^3 \,\big] \cdot \boldsymbol{G}\,.
\end{aligned} \tag{6.76}$$

For notational simplicity, however, we denote this orthogonal tensor by $\boldsymbol{R}_\mathrm{a}$ in the following and specify its particular representation according to eq.(6.76) when needed.

The remaining task consists in the determination of the pseudo rotation vector $\boldsymbol{\theta}_\mathrm{a} = \theta_\mathrm{a}\, \boldsymbol{n}^{\theta_\mathrm{a}}$ related to $\boldsymbol{R}_\mathrm{a}$ with

$$\begin{aligned}
\theta_\mathrm{a} &= \arccos([\,\mathrm{tr}(\boldsymbol{R}_\mathrm{a}) - 1\,]/2) \quad \text{and} \\
\boldsymbol{n}^{\theta_\mathrm{a}} &= \tfrac{1}{2}\, \sin^{-1}(\theta) \big[\, [\, R_{\mathrm{a}\,32} - R_{\mathrm{a}\,23}\,]\, \boldsymbol{e}_1 + [\, R_{\mathrm{a}\,13} - R_{\mathrm{a}\,31}\,]\, \boldsymbol{e}_2 + [\, R_{\mathrm{a}\,21} - R_{\mathrm{a}\,12}\,]\, \boldsymbol{e}_3 \,\big]
\end{aligned} \tag{6.77}$$

for $\theta_\mathrm{a} \neq \pi$, whereby $R_{\mathrm{a}\,ij} = \boldsymbol{e}_i \cdot \boldsymbol{R}_\mathrm{a} \cdot \boldsymbol{e}_j$ and $\|\boldsymbol{n}^{\theta_\mathrm{a}}\| = 1$, which is later on weighted by a scalar quantity in order to constitutively define the sought angular velocity vector $\boldsymbol{\omega}_\mathrm{a} \doteq \omega_\mathrm{a}\, \boldsymbol{n}^{\theta_\mathrm{a}}$. A singularity–free algorithm for the computation of $\boldsymbol{\theta}_\mathrm{a}$ for given $\boldsymbol{R}_\mathrm{a}$, as based on the extraction of the quaternion

$$\mathbf{q}_\mathrm{a} = [\, q_{\mathrm{a}\,0}\,,\, \boldsymbol{q}_\mathrm{a}\,] = [\, \cos(\theta_\mathrm{a}/2)\,,\, \sin(\theta_\mathrm{a}/2)\, \boldsymbol{n}^{\theta_\mathrm{a}}\,] \equiv [\, q_{\mathrm{a}\,0}\,,\, q_{\mathrm{a}\,1}\,,\, q_{\mathrm{a}\,2}\,,\, q_{\mathrm{a}\,3}\,]\,, \tag{6.78}$$

is summarised in algorithm 6.1. The adopted algorithm performs very robust since off–diagonal terms of the coefficients of $\boldsymbol{R}_\mathrm{a}$ are taken into account, which prevents inaccuracies

stemming for instance from

$$\begin{aligned} \mathrm{tr}(\boldsymbol{R}_{\mathrm{a}}(\theta_{\mathrm{a}}\,\boldsymbol{n}^{\theta_{\mathrm{a}}}) &= 1 + 2\,\cos(\theta_{\mathrm{a}}) \\ &\approx 1 + 2\,\cos(\theta_{\mathrm{a}} + \varepsilon) = \mathrm{tr}(\boldsymbol{R}_{\mathrm{a}}([\,\theta_{\mathrm{a}} + \varepsilon\,]\,\boldsymbol{n}^{\theta_{\mathrm{a}}}) \quad \text{for} \quad \theta_{\mathrm{a}} = 0, \pi, 2\,\pi, \ldots \end{aligned} \tag{6.79}$$

with $|\varepsilon| \ll 1$. Reorientation of both fibre families is assumed to occur whenever $\lambda_1^C > \lambda_2^C > \lambda_3^C$ and $\|\mathrm{skw}(\boldsymbol{S}\cdot\boldsymbol{C})\| > 0$ (otherwise the fibre direction remains unchanged, in other words $\boldsymbol{\omega}_{\mathrm{a}} = \boldsymbol{0}$) according to

$$\boldsymbol{\omega}_{\mathrm{a}} = \frac{\theta_{\mathrm{a}}}{\pi\,t^*}\,\boldsymbol{n}^{\theta_{\mathrm{a}}}\,, \tag{6.80}$$

wherein t^* acts similar to a relaxation time parameter in viscoelastic constitutive models. With this ansatz in hand, the algorithmic update is performed by means of an exponential integration scheme (recall $\Delta t = t_{n+1} - t_n > 0$)

$$\boldsymbol{a}_0^{\alpha} = \exp(-\,\Delta t\,\boldsymbol{G}^{-1}\cdot\boldsymbol{e}_0\cdot\boldsymbol{\omega}_{\mathrm{a}})\cdot\boldsymbol{a}_0^{\alpha}\big|_{t_n}\,. \tag{6.81}$$

Alternative representations of eq.(6.81) might be based on, for instance, the Euler–Rodrigues formula – the particular format has been reviewed in section 6.4.4 and is therefore omitted here.

Algorithm 6.1 *Singularity–free extraction of the pseudo rotation vector based on the quaternionian algorithm reported in Spurrier (1978) and constitutive determination of the angular velocity vector* $(i, j, k$ *is a cyclic permutation of* $1, 2, 3)$.

(i) quaternion $\mathbf{q}_{\mathrm{a}} = [\,q_{\mathrm{a}\,0}, \boldsymbol{q}_{\mathrm{a}}\,]$

if $R_{\mathrm{a}\,ii} > R_{\mathrm{a}\,11}, R_{\mathrm{a}\,22}, R_{\mathrm{a}\,33}$ **then**

$$\begin{aligned} q_{\mathrm{a}\,0} &= \tfrac{1}{2}\sqrt{1 + R_{\mathrm{a}\,ii}} \\ q_{\mathrm{a}\,i} &= \tfrac{1}{4\,q_{\mathrm{a}\,0}}\,[\,R_{\mathrm{a}\,kj} - R_{\mathrm{a}\,jk}\,] \end{aligned}$$

else $R_{\mathrm{a}\,ii} > R_{\mathrm{a}\,jj} \geq R_{\mathrm{a}\,kk}$

$$\begin{aligned} q_{\mathrm{a}\,i} &= \sqrt{\tfrac{1}{2}\,R_{\mathrm{a}\,(ii)} + \tfrac{1}{4}\,[\,1 - R_{\mathrm{a}\,ii}\,]} \\ q_{\mathrm{a}\,0} &= \tfrac{1}{4\,q_{\mathrm{a}\,i}}\,[\,R_{\mathrm{a}\,kj} - R_{\mathrm{a}\,jk}\,] \\ q_{\mathrm{a}\,l} &= \tfrac{1}{4\,q_{\mathrm{a}\,i}}\,[\,R_{\mathrm{a}\,li} + R_{\mathrm{a}\,il}\,] \qquad l = j, k \end{aligned}$$

(ii) pseudo rotation vector $\boldsymbol{\theta}_{\mathrm{a}} = \theta_{\mathrm{a}}\,\boldsymbol{n}^{\theta_{\mathrm{a}}}$

$$\begin{aligned} \theta_{\mathrm{a}} &= 2\,\arccos\,(q_{\mathrm{a}\,0}) \\ \boldsymbol{n}^{\theta_{\mathrm{a}}} &= \boldsymbol{q}_{\mathrm{a}}/\sin(\theta_{\mathrm{a}}/2) \end{aligned}$$

(iii) angular velocity vector $\boldsymbol{\omega}_{\mathrm{a}} = \omega_{\mathrm{a}}\,\boldsymbol{n}^{\theta_{\mathrm{a}}}$

if $\lambda_1^C > \lambda_2^C > \lambda_3^C$ **and** $\|\mathrm{skw}(\boldsymbol{S}\cdot\boldsymbol{C})\| > 0$ **then**

$$\omega_{\mathrm{a}} = \theta_{\mathrm{a}}/[\,\pi\,t^*\,]$$

else

$$\omega_{\mathrm{a}} = 0$$

Remark 6.5.3 *The existence of several states at which conjugated stress and stretch tensors commutate or even share identical principal directions, as discussed in section 6.3.2 (and 6.3.1), is also reflected by the fact that one and the same symmetry group allows representation in terms of different sets of (two) fibre families. In this regard, mechanically non–equivalent but orthogonal fibre directions $\boldsymbol{a}_0^\alpha$ can (initially) also be referred to two mechanically equivalent but non–orthogonal fibre families, $\bar{\boldsymbol{a}}_0^\alpha$, say. To be specific, $\boldsymbol{a}_0^\alpha$ take the representation $\boldsymbol{a}_0^1 = [\,\bar{\boldsymbol{a}}_0^1 + \bar{\boldsymbol{a}}_0^2\,]/[\,2\,\cos(\phi)\,]$ as well as $\boldsymbol{a}_0^2 = [\,\bar{\boldsymbol{a}}_0^1 - \bar{\boldsymbol{a}}_0^2\,]/[\,2\,\sin(\phi)\,]$ with $\phi = \bar{\boldsymbol{a}}_0^1 \cdot \bar{\boldsymbol{a}}_0^2/2$; compare the contribution by Spencer in Spencer (1984, pp. 1–32). While orientation distributions related to $\bar{\boldsymbol{a}}_0^\alpha$ might be directly accessible from experimental investigations, the (alternative) incorporation of $\boldsymbol{a}_0^\alpha$ into the various constitutive relations turns out to be useful in this work.*

6.5.4 Numerical examples

By analogy with eq.(6.40), the following numerical examples are based on a Helmholtz free energy density split into an isotropic Neo–Hooke part and an additional anisotropic extension

$$\begin{aligned}\rho_0^*\,\psi \;=\; & \tfrac{\mu}{2}\,[\,I_1 - 3\,] - \mu\,\ln(J_{\rm e}) + \tfrac{\lambda}{2}\,\ln^2(J_{\rm e}) \\ & + \tfrac{\alpha_1}{2\,\beta_1}\,\big[\,\exp\left(\beta_1\,[\,I_7 - I_4\,]^2\right) - 1\,\big] + \tfrac{\alpha_2}{2\,\beta_2}\,\big[\,\exp\left(\beta_2\,[\,I_{14} - I_{11}\,]^2\right) - 1\,\big]\,,\end{aligned} \tag{6.82}$$

wherein

$$\begin{aligned} I_1 \quad &= \boldsymbol{C} \;:\; \boldsymbol{B}_{\rm g} \;=\; \boldsymbol{C}_{\rm e} : \boldsymbol{G}_{\rm g}^{-1} = \boldsymbol{g} \;:\; \boldsymbol{b}_{\rm e}\,, \\ I_{4,11} &= \boldsymbol{C}_{\rm g} : \boldsymbol{A}_0^{1,2} = \boldsymbol{G}_{\rm g} : \boldsymbol{A}_{\rm g}^{1,2} = \boldsymbol{c}_{\rm e} : \boldsymbol{A}_t^{1,2}\,, \\ I_{7,14} &= \boldsymbol{C} \;:\; \boldsymbol{A}_0^{1,2} = \boldsymbol{C}_{\rm e} : \boldsymbol{A}_{\rm g}^{1,2} = \boldsymbol{g} \;:\; \boldsymbol{A}_t^{1,2}\,, \end{aligned} \tag{6.83}$$

recall that $\boldsymbol{A}_{\rm g}^{1,2} \neq \text{const}$. The isotropic material parameters are chosen as $\lambda = 12.77$ and $\mu = 3.19$ ($E = 8.94$ and $\nu = 0.4$). Standard eight–node bricks (Q1) are applied for the subsequent finite element computations. In order to visualise the non–coaxiality of conjugated stress and stretch tensors, we, once more, apply the the scalar–valued anisotropy measure introduced in eqs.(4.64,6.61).

6.5.4.1 Torsion of a rod

To set the stage and to illustrate the reorientation model itself, any growth influence is neglected ($\boldsymbol{F}_{\rm g} = \boldsymbol{I}_0$) within the following example. The discretisation of the block–type specimen (of dimension $1 \times 1 \times 5$) is performed by $5 \times 5 \times 10$ elements. Further material parameters are chosen as $\alpha_1 = 3.5$, $\alpha_2 = 2.5$, $\beta_{1,2} = 2$, $\rho_0^* = 1$, $\Delta t = 0.05$, $t^* = 1$ and the reorientation is based on $\boldsymbol{R}_{\rm a\,123}$, compare eq.(6.76)$_1$. Moreover, initial fibre directions are randomly generated for each individual integration point. To be specific, Eulerian angles $\varphi_1, \varphi_3 \in [0, 2\,\pi)$ and $\cos(\varphi_2) \in [-1, 1)$ are randomly determined to compute

$$\begin{aligned} \boldsymbol{a}_0^1 \;=\; & [\,{\rm c}_1{\rm c}_3 - {\rm s}_1{\rm c}_2\,{\rm s}_3\,]\,\boldsymbol{e}_1 - [\,{\rm c}_1{\rm s}_3 + {\rm s}_1{\rm c}_2\,{\rm c}_3\,]\,\boldsymbol{e}_2 + [\,{\rm s}_1{\rm s}_2\,]\,\boldsymbol{e}_3 \\ \boldsymbol{a}_0^2 \;=\; & [\,{\rm s}_1{\rm c}_3 + {\rm c}_1{\rm c}_2\,{\rm s}_3\,]\,\boldsymbol{e}_1 - [\,{\rm s}_1{\rm s}_3 - {\rm c}_1{\rm c}_2\,{\rm c}_3\,]\,\boldsymbol{e}_2 - [\,{\rm c}_1{\rm s}_2\,]\,\boldsymbol{e}_3 \end{aligned} \tag{6.84}$$

with ${\rm c}_1 = \cos(\varphi_1)$, ${\rm s}_1 = \sin(\varphi_1)$, etc. (and $\boldsymbol{a}_0^{1,2} \leftrightarrows -\boldsymbol{a}_0^{1,2}$ if $\boldsymbol{a}_0^{1,2} \cdot \boldsymbol{e}_3 < 0$); for a graphical representation of $\boldsymbol{a}_0^{1,2}|_{t_0}$ see figure 6.16. The bottom of the specimen is totally clamped while solely longitudinal displacements at the top surface are set equal to zero – the remaining top–displacements being chosen such that the rod is loaded under torsion; compare figure 6.16 and section 4.6.2. A torsion angle of π is achieved after six time steps (t_6). From then on, the incorporated displacement constraints are fixed for 144 time steps (t_{150}). The time–dependent reorientation of the fibre directions is clearly seen in figure 6.16 by means of a

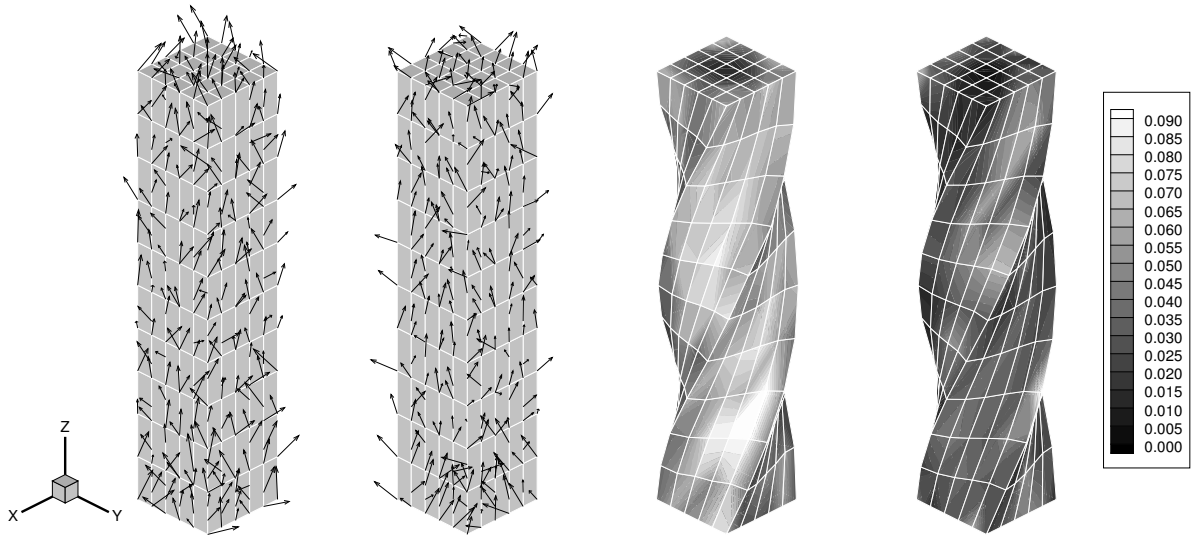

Figure 6.16: Torsion of a rod: $\boldsymbol{a}_0^1|_{t_0}$, $\boldsymbol{a}_0^2|_{t_0}$ with respect to undeformed mesh and $\delta(\boldsymbol{C}\cdot\boldsymbol{S})|_{t_6}$, $\delta(\boldsymbol{C}\cdot\boldsymbol{S})|_{t_{150}}$ with respect to deformed mesh.

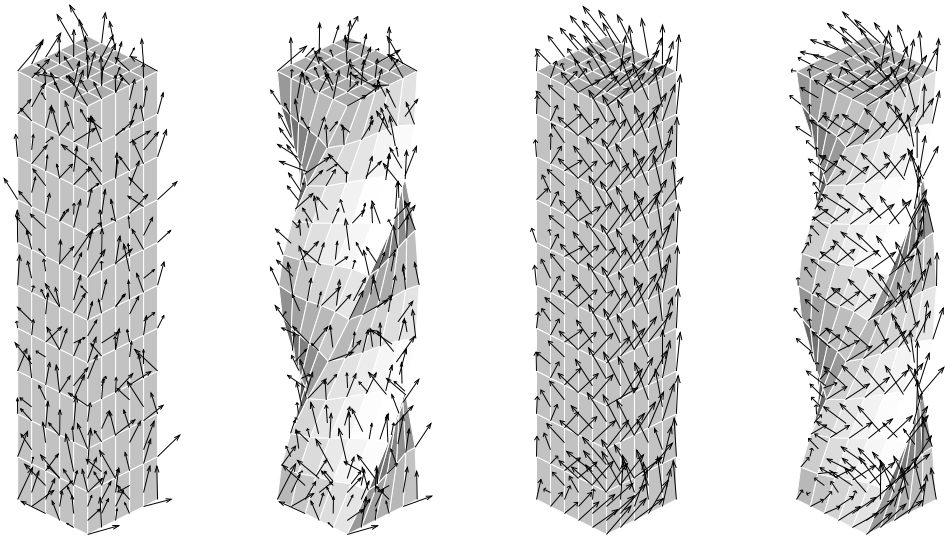

Figure 6.17: Torsion of a rod: $\boldsymbol{a}_0^1|_{t_6}$, $\widetilde{\boldsymbol{a}}_t^1|_{t_6}$ and $\boldsymbol{a}_0^1|_{t_{150}}$, $\widetilde{\boldsymbol{a}}_t^1|_{t_{150}}$ with respect to undeformed and deformed mesh.

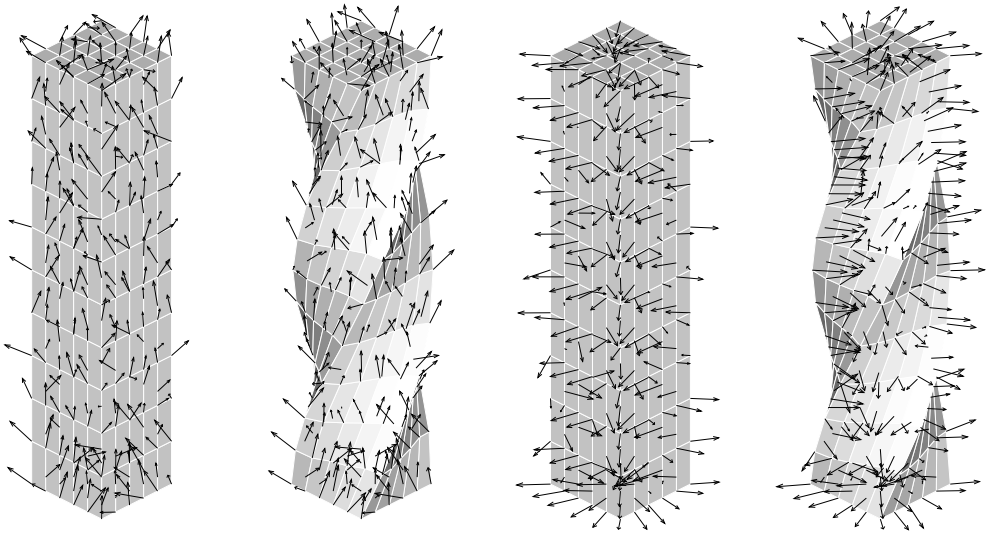

Figure 6.18: Torsion of a rod: $\boldsymbol{a}_0^2|_{t_6}$, $\widetilde{\boldsymbol{a}}_t^2|_{t_6}$ and $\boldsymbol{a}_0^2|_{t_{150}}$, $\widetilde{\boldsymbol{a}}_t^2|_{t_{150}}$ with respect to undeformed and deformed mesh.

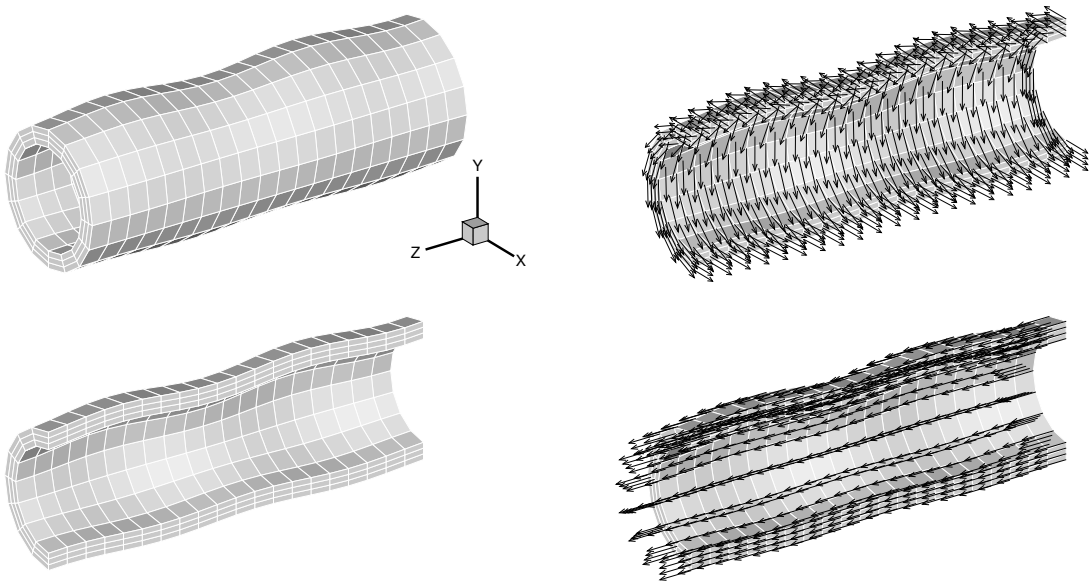

Figure 6.19: Artery–type tube: perturbed geometry and initial orientation of the circumferential ($\boldsymbol{a}_0^1|_{t_0}$) and longitudinal fibre family ($\boldsymbol{a}_0^2|_{t_0}$).

time–dependently decreasing coaxiality measure $0.000 \leq \delta(\boldsymbol{S} \cdot \boldsymbol{C}) \leq 0.163$ – here displayed with respect to the time steps t_6 and t_{150}. The particular reorientation of both fibre families according to the principal stretch directions is shown in figures 6.17 and 6.18, whereby material ($\boldsymbol{a}_0^{1,2}$) and spatial fibre orientations ($\widetilde{\boldsymbol{a}}_t^{1,2} = \boldsymbol{a}_t^{1,2}/\|\boldsymbol{a}_t^{1,2}\|$) are visualised for t_6 and t_{150}, respectively.

6.5.4.2 Artery–type tube

Within the next example, growth evolution as well as fibre reorientation is activated. We discuss a tube or rather artery–type segment of length $l = 6$ and assume the inner and outer radii to take the values $r_i = 3/4$ and $r_o = 1$, respectively. The finite element discretisation is thereby performed with 20 elements in longitudinal direction, 16 elements in circumferential direction and three elements in radial direction; compare figure 6.19. In order to incorporate a 'more realistic' geometry, we apply a small (periodic) perturbation so that the entire specimen possesses no axial symmetry, namely

$$\boldsymbol{X}_{\text{per}} = \text{per}\,[\,\sin(\phi)\,\cos(\varphi+\phi)\,]\,\boldsymbol{e}_r \quad \text{with} \quad \phi = 2\,\pi\,X_z/l \tag{6.85}$$

for $\text{per} = -\,2.5\times10^{-2}$ and $X_z = \boldsymbol{X}\cdot\boldsymbol{e}_z$, whereby φ denotes the angle related to the cylindrical base system $\{\boldsymbol{e}_r, \boldsymbol{e}_\varphi, \boldsymbol{e}_z\}$; to be specific: $\boldsymbol{e}_r = \cos(\varphi)\,\boldsymbol{e}_1 + \sin(\varphi)\,\boldsymbol{e}_2$, $\boldsymbol{e}_\varphi = -\sin(\varphi)\,\boldsymbol{e}_1 + \cos(\varphi)\,\boldsymbol{e}_2$ and $\boldsymbol{e}_z = \boldsymbol{e}_3$, respectively.

In vivo fibre directions ($\bar{\boldsymbol{a}}_0^\alpha|_{t_0}$), identified with identical mechanical properties, are observed under an angle of, for example, $30°$ ($150°$) with respect to $\boldsymbol{e}_\varphi$. Within the subsequent analysis, we account for this particular symmetry by aligning $\boldsymbol{a}_0^1|_{t_0}$ according to the circumferential direction of the perturbed geometry and consequently choose $\boldsymbol{a}_0^2|_{t_0} = \boldsymbol{e}_z$; compare remark 6.5.3 and see figure 6.19 for a graphical illustration. The applied set of material parameters can be related to the response of the arterial media layer: $\lambda = 12.77$, $\mu = 3.19$ ($E = 8.94$ and $\nu = 0.4$), $\alpha_1 = 2.165$, $\alpha_2 = 1.25$, $\beta_1 = 0.866$ and $\beta_2 = 0.5$ – the remaining constants reading $\rho_0^* = 1$, $\Delta t = 0.01$, $t^* = 1$, $k_{\zeta_i}^{+,-} = 2$, $\zeta_i^+ = 1.5$, $\zeta_i^- = 0.5$, $m_{\zeta_i}^{+,-} = 1.25$ and $\boldsymbol{R}_{\text{a}\,123}$ being chosen for the reorientation, compare eqs.(6.72) and $(6.76)_1$.

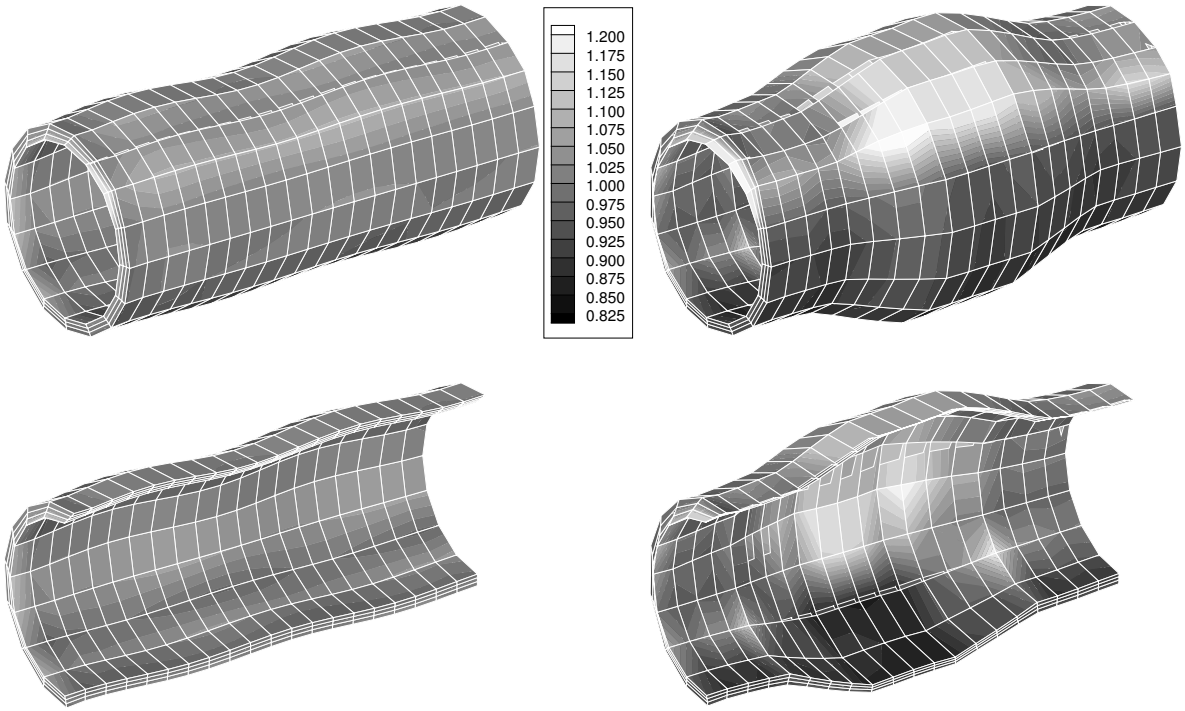

Figure 6.20: Artery–type tube: referential density $\rho_0|_{t_{50}}$, $\rho_0|_{t_{100}}$ before and after stenting–like loading.

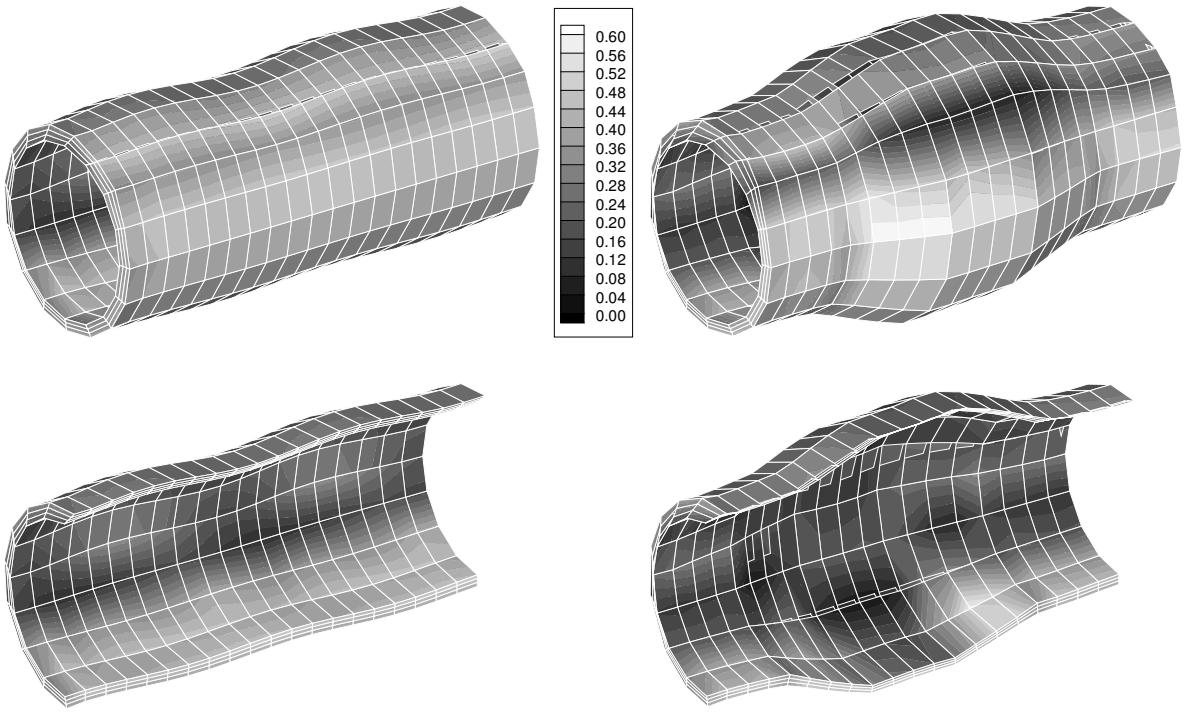

Figure 6.21: Artery–type tube: anisotropy measure $\delta(\boldsymbol{C}\cdot\boldsymbol{S})|_{t_{50}}$, $\delta(\boldsymbol{C}\cdot\boldsymbol{S})|_{t_{100}}$ before and after stenting–like loading.

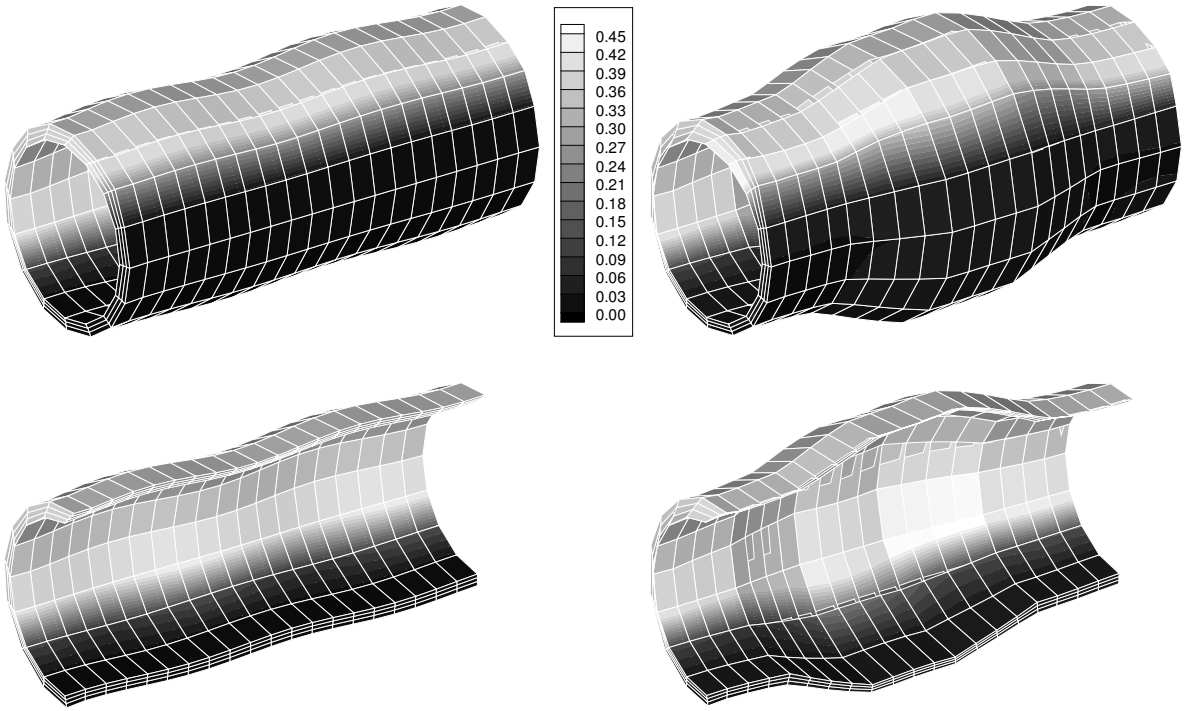

Figure 6.22: Artery–type tube: reorient. measure $\delta(\boldsymbol{G}\cdot\boldsymbol{A}_0^1|_{t_0}\cdot\boldsymbol{G}\cdot\boldsymbol{A}_0^1|_{t_{50}})$, $\delta(\boldsymbol{G}\cdot\boldsymbol{A}_0^1|_{t_0}\cdot\boldsymbol{G}\cdot\boldsymbol{A}_0^1|_{t_{100}})$ before and after stenting–like loading.

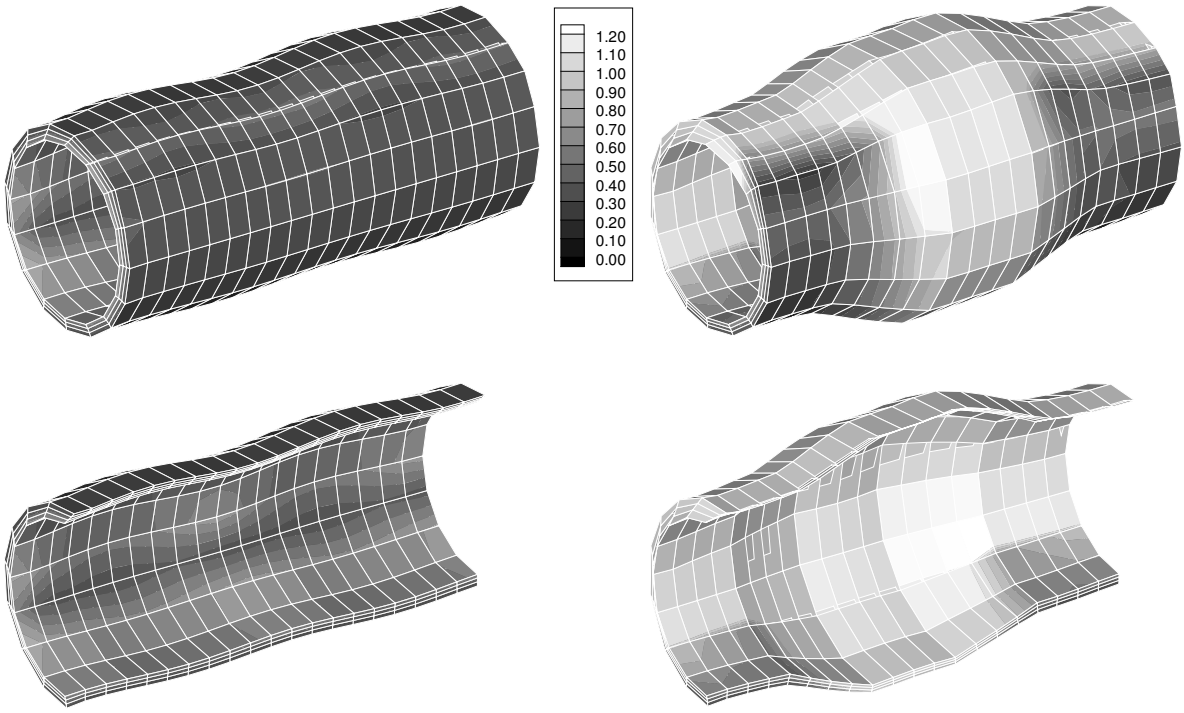

Figure 6.23: Artery–type tube: deviatoric norm of Cauchy stress $\|[\boldsymbol{\sigma}^{\mathrm{t}}]^{\mathrm{dev}}|_{t_{50}}\|$, $\|[\boldsymbol{\sigma}^{\mathrm{t}}]^{\mathrm{dev}}|_{t_{100}}\|$ before and after stenting–like loading.

Realistic loading conditions of arterial structures should account for different arterial layers (especially growth of the intima), initial stress contributions, plaques, internal pressure, etc. among other relevant effects. As a first attempt towards applying the proposed growth and reorientation model to the simulation of arteries, we choose purely displacement–driven loading for those finite element nodes located at r_i. Besides a longitudinal stretch of $\lambda_z^U = 1.1$ (longitudinal displacements at $X_z = 0$ and $X_z = 6$ are constrained), radial displacements $u_r|_{(X_r=r_i)} = 0.5$ are applied – both within one time step. These Dirichlet boundary conditions are then fixed for 49 times steps until a stenting–like loading is introduced (t_{50}). For this second loading step, another radial displacement $u_r|_{(X_r=r_i)} = 0.5$ is applied to the middle segment of the specimen and linearly decreased towards the endings within one time step – the boundary condition once more being fixed for the subsequent 49 time steps so that growth and fibre reorientation evolve (t_{100}). As such, the analysis accounts for growth–induced residual stresses before the second stenting–like deformation is applied. The entire simulation itself, however, is not claimed to realistically monitor the behaviour of arteries but rather to show the applicability of the developed modelling framework to typical biological structures – detailed numerical elaborations constituting future research.

Figure 6.20 highlights the (non–conserved) referential density $\rho_0 = J_{\mathrm{g}}\,\rho_{\mathrm{g}} = \vartheta\,\zeta_1\,\zeta_2\,\rho_0^*$ after the initial (t_{50}) and stenting–like loading (t_{100}), respectively, with $0.869 \leq \rho_0 \leq 1.615$. The slight inhomogeneity induced by the perturbed geometry as well as the rather substantial inhomogeneity after stenting are clearly shown. The contribution of the anisotropy measure $\delta(\boldsymbol{C}\cdot\boldsymbol{S})$, however, possesses a qualitatively different distribution, compare figure 6.21 with $0.001 \leq \delta(\boldsymbol{C}\cdot\boldsymbol{S}) \leq 0.717$. This effect mainly stems from the fact that the referential geometry has been perturbed, which induced an initial inhomogeneity concerning the initial fibre orientations and renders also the reorientation measure $\delta(\boldsymbol{G}\cdot\boldsymbol{A}_0^1|_{t_0}\cdot\boldsymbol{G}\cdot\boldsymbol{A}_0^1)$ to be inhomogeneously distributed in circumferential direction; compare figure 6.22 with $0.000 \leq \delta(\boldsymbol{G}\cdot\boldsymbol{A}_0^1|_{t_0}\cdot\boldsymbol{G}\cdot\boldsymbol{A}_0^1) \leq 0.707$. Finally, even not that common for biological applications, the deviatoric norm of the (spatial) Cauchy stress $\boldsymbol{\sigma}^{\mathrm{t}} = \boldsymbol{\Pi}^{\mathrm{d}}\cdot\mathrm{cof}(\boldsymbol{f})$ is visualised in figure 6.23 with $[\boldsymbol{\sigma}^{\mathrm{t}}]^{\mathrm{dev}} = \boldsymbol{\sigma}^{\mathrm{t}} - \frac{1}{3}\,\mathrm{tr}(\boldsymbol{\sigma}^{\mathrm{t}})\;\boldsymbol{I}_t^{\mathrm{t}}$ and $0.209 \leq \|[\boldsymbol{\sigma}^{\mathrm{t}}]^{\mathrm{dev}}\| \leq 64.950$.

7 Summary

The main goal of this work was to examine various aspects of 'inelastic continuum mechanics': first, fundamental aspects of a general finite deformation theory based on a multiplicative decomposition of the deformation gradient with special emphasis on the incompatibility of the so–called intermediate configuration have been discussed in detail. Moreover, various balance of linear momentum representations together with the corresponding volume forces were derived in a configurational mechanics context. The subsequent chapters have consequently been based on these elaborations so that the applied multiplicative decomposition generally serves as a fundamental modelling concept in this work; after generalised strain measures had been introduced, a kinematic hardening model coupled with anisotropic damage, a substructure evolution framework as well as two different growth and remodelling formulations for biological tissues were presented. The key contents of chapters 2–6 are summarised below.

Chapter 2 In this chapter we aimed at the derivation of particular configurational volume forces. The concept of a multiplicative decomposition of the deformation gradient has been adopted as a general framework for finite inelasticity. Due to the general incompatibility of the underlying intermediate configuration, several (geometrically necessary) dislocation density tensors were elaborated. These quantities naturally contributed to the sought configurational volume forces. The derivation of these fields was based on the comparison of balance of linear momentum representations for the spatial, intermediate, and material motion problem. The intermediate volume forces enabled us to recover the classical format of the Peach–Koehler force. This key result would, apparently, not have been observed when considering the balance of linear momentum relation with respect to the material configuration. On the one hand, the main drawback of an outline with respect to the material configuration in view of the derivation of Peach–Koehler forces relies on the fact that solely gradients of the plastic distortion, but not appropriate dislocation density tensors, contribute to the corresponding volume forces. On the other hand, we observed two different material balance of linear momentum representations. In addition to the material format which incorporated the classical Eshelby stress tensor, a representation based on the material Mandel stress $\widetilde{\boldsymbol{\Sigma}}^{\mathrm{t}} = \boldsymbol{F}^{\mathrm{t}} \cdot \boldsymbol{\Pi}^{\mathrm{t}}$ was derived. The related volume force included solely the gradient of the total deformation gradient so that, in view of a computational finite element setting, no gradients of internal variables as for example the plastic distortion are required. In view of numerical applications, this property is very attractive, since for instance the material force method can, more or less, be implemented as a 'black box' independent of the particular inelastic constitutive law; to be specific

$$
\begin{aligned}
0 \quad &= \int_{\mathcal{B}_0} \boldsymbol{W} \cdot \big[\, \nabla_{\boldsymbol{X}} \cdot \widetilde{\boldsymbol{\Sigma}}^{\mathrm{t}} + \widetilde{\boldsymbol{B}}_0 \, \big] \, \mathrm{d}V_0 \quad \forall \, \boldsymbol{W} \quad \text{with} \\
\widetilde{\boldsymbol{B}}_0 \quad &= - \, \boldsymbol{\Pi}^{\mathrm{t}} : \nabla_{\boldsymbol{X}} \boldsymbol{F} - \boldsymbol{F}^{\mathrm{t}} \cdot \boldsymbol{b}_0^{\mathrm{ext}} \qquad\qquad \text{so that} \\
\mathbf{F}^{h}_{\mathrm{sur}\, K} \quad &= \mathop{\mathsf{A}}_{e=1}^{n_{\mathrm{el}}} \int_{\mathcal{B}_0^e} \widetilde{\boldsymbol{\Sigma}}^{\mathrm{t}} \cdot \nabla_{\boldsymbol{X}} N^k - N^k \, \widetilde{\boldsymbol{B}}_0 \, \mathrm{d}V_0 \, ,
\end{aligned}
\tag{7.1}
$$

compare the discussions in section 2.6 and 1.3.4. Apart from recovering fundamental aspects of nowadays classical crystal plasticity formulations, we finally also addressed a continuum plasticity framework incorporating dislocation density tensors and intermediate volume forces

as driving forces. The development of a robust finite element formulation constitutes future research; it is, however, expected that representative examples based on this rather general ansatz reflect, for example, the Bauschinger and the Hall–Petch effect.

Chapter 3 The main goal of this chapter was the elaboration of pushforward and pullback transformations between different Seth–Hill type strain measures embedded into the kinematical framework established in chapter 2, namely the multiplicative decomposition of the deformation gradient into a reversible elastic distortion and an irreversible plastic distortion. A fundamental backbone of the highlighted derivations was provided by the application of the spectral decomposition theorem as well as absolute tensor representations. These considerations enabled us to develop equivalent sets of material, intermediate, and spatial generalised strain measures. Based on the fundamental covariance of the Helmholtz free energy, related stress tensors – settled in different configurations – have been introduced. With these elaborations in hand, two different associated inelasticity approaches were discussed, whereby neither the particular elasticity law nor the incorporated flow rule had been restricted to isotropic response. Summarising, the basic sets of constitutive equations of finite inelasticity based on material, intermediate, and spatial generalised strain measures were highlighted. From the modelling point of view, this variability or rather general framework broadens the spectrum of possible particular formulations for finite inelasticity which is of special interest, for instance, for (subsequent) numerical applications and serves as a convenient platform in view of the implementation of efficient algorithmic settings.

Chapter 4 Based on the fundamental elaborations in chapter 2 and 3, a rather general formulation of finite anisotropic inelasticity was developed in chapter 4. We considered in particular a viscoplastic setting that accounted for anisotropic degradation and kinematic as well as proportional hardening. As a key idea, an isotropic fictitious or rather effective configuration has been introduced which is related to the intermediate configuration of multiplicative elastoplasticity via a fictitious or rather damage tangent map. Practically speaking, the covariance principle serves as a basic concept to develop the proposed finite strain setting by assuming the Helmholtz free energy to remain invariant under the action of this mapping. In other words, we dealt with an Euclidian space with respect to a non–constant metric that allowed to model transversal and orthotropic material symmetry if this damage metric possessed non–spherical properties. By analogy with the damage or rather anisotropy mapping, another tangent has been introduced that served as an internal variable to define a Mandel–type back–stress tensor and therefore allowed to incorporate kinematic hardening.

Straightforward application of the framework of non–standard dissipative materials enabled the definition of appropriate evolution equations. While a generally non–symmetric effective relative Mandel stress tensor has been employed into the yield function, the Mandel–type damage tensor allowed a generally symmetric representation in the effective configuration. The proposed thermodynamically consistent prototype model was based on well–established potentials. However, the kinematic hardening contribution accounted for an additional saturation–type term and in view of the damage evolution, a Rankine–type ansatz, as based on a spectral decomposition of the Mandel–type damage stresses, has been adopted. The developed formulation therefore accounts for the modelling of different material behaviour in tension and compression with respect to the space spanned by the damage stress tensor. Based on this, exponential integration schemes have been applied to the underlying (inelastic) tangent maps. Moreover, different methods for the solution of this so–called local constitutive problem, that arises when integrating the constitutive model implicitly, have been studied. The four additionally investigated methods are of Newton or quasi–Newton type and of a staggered

type. It is also shown how to obtain the algorithmic consistent tangent stiffness useful in Newton iterations within a global finite element problem. Besides the exponential scheme, these iteration methods are based on two implicit time stepping techniques: Euler backward (EB) and a two step backward differential rule (BDF2).

Several numerical examples underlined the applicability of the developed framework. Different properties of the model were investigated for the rate–independent and rate–dependent case with respect to a homogeneous deformation in simple shear. Both, loading and un– / reloading as well as cyclic loading have been discussed in detail. Concerning the investigations on different integration and iteration techniques, it can be concluded that the proposed staggered method is superior concerning accuracy for a certain CPU time. But the staggered method demands the time steps to be sufficiently small in order to converge. By comparing the Newton method based on an analytically derived Jacobian with the Newton method with the computed Jacobian via numerical differentiation, the difference in CPU time is notably small. This is believed to be caused by the high computational effort to compute the analytical Jacobian for the chosen constitutive model. Also the Broyden method is computationally more efficient than the Newton methods. Similarly to the staggered method, the Broyden method demands smaller time steps than the Newton methods in order to converge. Obviously, the BDF2 method is superior to the EB method when comparing accuracy. The conclusions regarding the different iteration methods hold for both the EB and the BDF2 methods. Finally, a finite element setting was applied to a classical torsion problem which showed the capability of the proposed formulation to model overall softening behaviour, initial anisotropy, kinematic and proportional hardening, as well as anisotropic degradation.

Chapter 5 A model for the analysis of deformation induced anisotropy due to substructure evolution at large strains was proposed in chapter 5. The modelled evolution of stiffness and orientation was inspired by recent developments in bio–mechanics; compare chapter 6. In particular, we adopted a special ansatz for the anisotropy or rather substructure metric that influenced both the Helmholtz free energy as well as evolution rules. Although the texture reorientation depended on the plastic part of the deformation gradient, it was not convected. Modelling restrictions were established such that the dissipation inequality is fulfilled. The fictitious configurations approach investigated in chapter 4 for introducing anisotropy in the constitutive model resulted in a relatively simple format of the governing equations as compared to the structural tensor approach applied in chapter 6. This simplicity was favourable for the problem at hand when the model had been implemented in a finite element code. The studied numerical examples showed how the material parameters influence the stress–strain response. In particular, we focused on large shear deformations which is motivated by observations of the surface layer of railway track components. Texture in the elastic part of the Helmholtz free energy, however, has only small influence on the stress–strain response in the studied numerical examples. Hardening in the inelastic stress–strain response could be classified as isotropic (due to the stiffness evolution), kinematic (via conventional formulation), and a special form of distortional hardening (due to the stiffness evolution and the orientation of $\boldsymbol{a}_{\mathrm{p}}$). In the present context, the special form of distortional hardening concerned reorientation of the initially isotropic yield surface and also the change of proportions between the principal axes of the corresponding ellipsoidal yield surface. The model calibration was outside the scope of this study. However, by comparing the numerical examples with graphical images from so–called twin–disc experiments (although they represent completely different loading cases), it seems reasonable to anticipate that parts of the model can be calibrated (by an inverse analysis assuming strongly inhomogeneous stress and strain states). It is obviously possible to introduce additional material parameters in the model (for instance in eqs.(5.15,5.18,5.20)) with the purpose to increase the modelling flexibility. The modelling of deformation–induced

anisotropy due to substructure evolution does not require the fictitious configurations approach as such. A comparison between the fictitious configurations approach and the more general structural tensor approach is an interesting challenge. A meaningful comparison may require that the material parameters for the two approaches are identified. Such a parameter identification is considered non–trivial.

Chapter 6 This chapter aimed at the development of a theoretical and computational framework, which captures the remodelling of biological tissues. Typical examples of such adaptation processes are, for instance, growth phenomena and rearrangements of internal substructures. The orientation of these substructures was incorporated via fibre families, whereby we first investigated transversal isotropy and later on discussed orthotropic response. Evolution of these direction vectors was, in contrast to the stress–driven formulation in chapter 5, based on purely kinematical considerations. Motivated by, what we called Vianello's 'coaxiality' theory, a time–dependent alignment of the incorporated fibres with respect to principal stretch directions was proposed. In view of the growth models themselves, wherein an additional mass flux was throughout neglected for conceptual simplicity, two different frameworks have been developed:

Energy–driven growth For the energy–driven growth model presented in section 6.4 we assumed the intermediate and material configuration to coincide. Isotropic growth has thereby been addressed via a Wolff–type evolution law for the material density. We introduced the underlying microstructure of the tissue via incorporation of one fibre direction so that a transversely isotropic response was taken into account. The direction and the strength or diameter of the fibre were both not constrained to remain constant during the deformation of the considered body. In analogy to the density field, we also adopted an energy–driven Wolff–type law for the fibre strength which, accordingly, rendered similar saturation–type characteristics as the density evolution. It is then the combination of both contributions which is consequently classified as isotropic and anisotropic growth or simply as anisotropic growth. The advantage of the proposed formulation is the opportunity to separately address the anisotropic growth, or rather the strengthening and the reorientation of the fibre. Furthermore, issues of implementation were developed so that the theoretical framework is especially suited for numerical applications, like those based on the finite element method. As an interesting side aspect, the proposed formulation fits nicely into common finite element codes since the standard framework of internal variables has been adopted. Nevertheless, there are still several (known) factors left that apparently influence the remodelling process but are not addressed here, including electric stimuli, age–dependency, damage effects after peak loads or particular healing mechanisms, even though a number of remodelling effects are captured within the proposed framework. The applied format of the Wolff–type evolution laws seems to be quite powerful in the present context. Their particular representation however, could be extended in order to include so–called dead zones and different response characteristics for growth and resorption.

Stress–driven growth The stress–driven growth model developed in section 6.5 is consequently based on the multiplicative decomposition of the total deformation gradient into an elastic distortion and a so–called growth distortion, respectively. We aimed at the development of a continuum model which captures orthotropic response, growth in volume and density as well as reorientation of the two incorporated fibre families. Saturation–type evolution, which nicely enables time dependent convergence towards biological equilibrium, has been applied. The suggested driving force itself took the interpretation as an Eshelbian or configurational stress as established in mechanics in material space or rather configurational mechanics; compare chapter 2. Then a kinematics–based symmetry–group–preserving fibre reorientation model was developed. Conceptually speaking, referential fibre directions are

time–dependently aligned according to appropriate principal stretch directions. Finally, numerical examples based on a correlated finite element implementation have been discussed: first, a rod was loaded under torsion, whereby the effect of the fibre reorientation model was clearly displayed; second, an artery–type tube was loaded under stenting–like loading conditions starting from a growth–induced residually stressed state. Future investigations will in particular focus on biologically more realistic loading conditions, the consideration of different material properties attached to different arterial layers and the incorporation of plaques. Moreover, explicit elaborations on residual stresses, as for instance the computation of the so–called opening angle stemming from deformation–induced growth distortions, seem to be of special interest.

In summary, the key contribution of this work is the in–depth analysis of various fundamental aspects relevant for the modelling of inelastic continua undergoing finite deformations. The multiplicative decomposition of the total deformation gradient or, in other words, the introduction of a local rearrangement has thereby been adopted as a fundamental kinematical framework. Due to the general incompatibility of the introduced intermediate configuration, related differential operations had to be modified. In this regard, the standard Piola identity was extended, which enabled the transformation of, for instance, divergence operations to different configurations. The observed relation will also be useful in different (scientific) fields of application. Based on these elaborations, various balance relations and volume forces were investigated. As a new result, the Peach–Koehler force is now available for inelastic continua undergoing finite deformations – the purely elastic case being generally included as a special application. With these relations at hand, established inelastic modelling concepts, as for example the introduction of a projected Schmid stress in crystal–plasticity, were embedded into a configurational mechanics context. Moreover, the developed set of driving forces also serves as a platform for new formulations. In this regard, a continuum plasticity framework based on driving forces in terms of Peach–Koehler forces and dislocation density tensors has been proposed. In addition, an until now unrecognised material balance of linear momentum representation was found. This format is particularly attractive for numerical applications within, for instance, a finite element context. Apart from these fundamental aspects concerning the elastic and plastic distortion, dislocation density tensors, balance relations, and related flux and source terms, further invariance conditions constrain for example representative deformation measure to particular formats. Apparently, the introduction of strain measures is part of the constitutive modelling itself. While the definition of different strain families is rather established, their transformation to different configurations is considered as non–trivial for the generally anisotropic case. These relations were investigated in detail in this work, whereby special emphasis has been placed on the multiplicative decomposition of the deformation gradient. Accordingly, the extension of the celebrated Murnaghan–Truesdell formula, usually applied for isotropic response, is now also available for generalised strain measures combined with anisotropic material behaviour. As such, the developed kinematical framework motivates subsequent and future investigations in the context of computational inelasticity. Based on these fundamental elaborations, further constitutive models have been developed:

The coupling of kinematic hardening with damage is of cardinal importance for engineering applications. A key feature of the model developed in this work consists in the possibility to couple kinematic hardening with anisotropic continuum damage approaches. Consequently, the elastic response is not restricted to remain isotropic. Both, the damage as well as the kinematic hardening model have thereby been based on the introduction of internal variables which allow interpretation as linear tangent maps. Related fictitious configurations are thereby attached to the intermediate configuration. As such, the developed modelling concept turns

out to be rather general and can be used for different types of application. In this regard, a phenomenological substructure evolution model has been developed in a subsequent chapter. The underlying substructure is thereby incorporated via fibre direction vectors which align according to related stress measures. The development of such phenomenological texture evolution models is believed to continuously attract studies from different research fields in future. In this regard, the substructure evolution approach suggested in this study provides an essential modelling ansatz. A similar kinematics–based reorientation approach was applied to biological tissues in this work. The formulation of so–called remodelling effects is of cardinal importance for related biomechanical applications. As such, the newly developed framework substantially contributes to the computational modelling of growth in biomaterials. First numerical results based on the suggested approaches motivate or rather support evaluation and validation of these models based on appropriate experiments. Such investigations will further extend the understanding of inelasticity, substructure evolution, remodelling processes and so forth and might also enable the identification of material parameters. Interdisciplinary cooperations between scientists from different research fields like materials sciences and physics as well as biology and medicine are of significant relevance. Although related experiments are rather elaborate, complex, and difficult to implement, they appear to promise great benefits in future.

A Transformations of third–order permutation tensors

Within a finite deformation context, different representations of (isotropic) third–order permutation tensors can be introduced, namely purely contra– or co–variant and various mixed–variant formats. In this work, particular use of the material representations

$$\boldsymbol{E}_0 :\ T^*\mathcal{B}_0 \times T^*\mathcal{B}_0 \times T^*\mathcal{B}_0 \to \mathbb{R} \quad \text{and} \quad \boldsymbol{e}_0 :\ T\mathcal{B}_0 \times T\mathcal{B}_0 \times T\mathcal{B}_0 \to \mathbb{R}\,, \tag{A.1}$$

is made, with

$$\begin{aligned} E_0{}^{ijk} = e_{0\,ijk}^{-1} = \begin{cases} \det{}^{\frac{1}{2}}(\boldsymbol{G}^{-1}) & \text{if } \{i,j,k\} \text{ is an even permutation of } \{1,2,3\} \\ -\det{}^{\frac{1}{2}}(\boldsymbol{G}^{-1}) & \text{if } \{i,j,k\} \text{ is an odd permutation of } \{1,2,3\} \end{cases} \\ E_0{}^{ijk} = e_{0\,ijk} = \qquad 0 \qquad\qquad \text{otherwise}\,, \end{aligned} \tag{A.2}$$

wherein $\boldsymbol{G}$ denotes the co–variant metric in $\mathcal{B}_0$ so that

$$\begin{aligned} \boldsymbol{E}_0 &= \det(\boldsymbol{G}^{-1})\ [\,\boldsymbol{G}^{-1} \mathbin{\overline{\otimes}} \boldsymbol{G}^{-1}\,] : \boldsymbol{e}_0 \cdot \boldsymbol{G}^{-1}\,, \\ \boldsymbol{e}_0 &= \det(\boldsymbol{G}) \quad [\,\boldsymbol{G} \quad \mathbin{\overline{\otimes}} \boldsymbol{G} \quad\,] : \boldsymbol{E}_0 \cdot \boldsymbol{G}\,. \end{aligned} \tag{A.3}$$

It is now straightforward to prove the relations,

$$\begin{aligned} &\boldsymbol{E}_0 : \boldsymbol{E}_0 = \tfrac{2}{\det(\boldsymbol{G}^{-1})}\,\boldsymbol{G}^{-1}\,, \qquad \boldsymbol{e}_0 : \boldsymbol{e}_0 = \tfrac{2}{\det(\boldsymbol{G})}\,\boldsymbol{G}\,, \qquad \boldsymbol{E}_0 : \boldsymbol{e}_0 = 2\,\boldsymbol{I}_0\,, \\ &\boldsymbol{E}_0 \cdot \boldsymbol{E}_0 = \tfrac{2}{\det(\boldsymbol{G}^{-1})}\,\mathsf{G}^{-1\,\mathrm{skw}}\,, \qquad \boldsymbol{e}_0 \cdot \boldsymbol{e}_0 = \tfrac{2}{\det(\boldsymbol{G})}\,\mathsf{G}^{\mathrm{skw}}\,, \qquad \boldsymbol{E}_0 \cdot \boldsymbol{e}_0 = 2\,\mathsf{I}^{\mathrm{skw}}\,, \end{aligned} \tag{A.4}$$

with $\mathsf{G}^{-1\,\mathrm{skw}} = \frac{1}{2}\,[\,\boldsymbol{G}^{-1} \mathbin{\overline{\otimes}} \boldsymbol{G}^{-1} - \boldsymbol{G}^{-1} \mathbin{\underline{\otimes}} \boldsymbol{G}^{-1}\,]$, etc.

Based on these definitions, we next place emphasis on the demanded transformations of the permutation tensors in eq.(A.1) to the intermediate and spatial configuration. The coefficients of the permutation tensors are thereby weighted with the determinant of the corresponding linear tangent map, compare for instance Ogden (1997), so that the relations

$$\begin{aligned} &\boldsymbol{E}_{\mathrm{p}} = j_{\mathrm{p}}\ [\,\boldsymbol{F}_{\mathrm{p}} \mathbin{\overline{\otimes}} \boldsymbol{F}_{\mathrm{p}}\,] : \boldsymbol{E}_0 \cdot \boldsymbol{F}_{\mathrm{p}}^{\mathrm{t}}\,, \qquad \boldsymbol{e}_{\mathrm{p}} = J_{\mathrm{p}}\ [\,\boldsymbol{f}_{\mathrm{p}}^{\mathrm{t}} \mathbin{\overline{\otimes}} \boldsymbol{f}_{\mathrm{p}}^{\mathrm{t}}\,] : \boldsymbol{e}_0 \cdot \boldsymbol{f}_{\mathrm{p}}\,, \\ &\boldsymbol{E}_t = j\ \ [\,\boldsymbol{F} \ \ \mathbin{\overline{\otimes}} \boldsymbol{F}\ \ ] : \boldsymbol{E}_0 \cdot \boldsymbol{F}^{\mathrm{t}}\,, \qquad \boldsymbol{e}_t = J\ \ [\,\boldsymbol{f}^{\mathrm{t}} \mathbin{\overline{\otimes}} \boldsymbol{f}^{\mathrm{t}}\,] : \boldsymbol{e}_0 \cdot \boldsymbol{f} \end{aligned} \tag{A.5}$$

are obtained similarly to eq.(A.3). For completeness, we finally conclude

$$\boldsymbol{E}_t = j_{\mathrm{e}}\ [\,\boldsymbol{F}_{\mathrm{e}} \mathbin{\overline{\otimes}} \boldsymbol{F}_{\mathrm{e}}\,] : \boldsymbol{E}_{\mathrm{p}} \cdot \boldsymbol{F}_{\mathrm{e}}^{\mathrm{t}}\,, \qquad \boldsymbol{e}_t = J_{\mathrm{e}}\ [\,\boldsymbol{f}_{\mathrm{e}}^{\mathrm{t}} \mathbin{\overline{\otimes}} \boldsymbol{f}_{\mathrm{e}}^{\mathrm{t}}\,] : \boldsymbol{e}_{\mathrm{p}} \cdot \boldsymbol{f}_{\mathrm{e}} \tag{A.6}$$

with the reverse representations of eqs.(A.5,A.6) being obvious. Apparently, one could also relate $\boldsymbol{E}_{\mathrm{p}}$, $\boldsymbol{E}_t$ and $\boldsymbol{e}_{\mathrm{p}}$, $\boldsymbol{e}_t$ in analogy with eq.(A.3) which, however, is omitted for the sake of brevity.

B A note on the incorporation of dislocation density tensors into configurational volume forces

It is self–evident that gradients of tangent maps are directly related to, or rather define, dislocation density tensors. The double contraction of these quantities with appropriate stress tensors is frequently applied in this work and therefore discussed in detail for the simplest case in the sequel, namely in terms of the spatial motion gradient $\boldsymbol{F}$. Similar derivations with respect to the material motion gradient or the elastic and plastic distortions follow by analogy and are omitted for the sake of brevity.

In this context, a full length derivation of eq.(2.106) reads

$$\begin{aligned}
\nabla_{\boldsymbol{X}} \boldsymbol{F}^{\mathrm{t}} : \boldsymbol{\Pi}^{\mathrm{t}} &= \boldsymbol{\Pi}^{\mathrm{t}} : \nabla_{\boldsymbol{X}} \boldsymbol{F} + 2\, \boldsymbol{\Pi}^{\mathrm{t}} : [\, \nabla_{\boldsymbol{X}} \boldsymbol{F} : \mathbf{I}^{\mathrm{skw}} \,] \\
&= \boldsymbol{\Pi}^{\mathrm{t}} : \nabla_{\boldsymbol{X}} \boldsymbol{F} - \boldsymbol{\Pi}^{\mathrm{t}} : [\, \nabla^{\mathrm{t}}_{\boldsymbol{X}} \times \boldsymbol{F} \cdot \boldsymbol{e}_0 \,] \\
&= \boldsymbol{\Pi}^{\mathrm{t}} : \nabla_{\boldsymbol{X}} \boldsymbol{F} + \boldsymbol{\Pi}^{\mathrm{t}} : [\, \boldsymbol{A}^{\mathrm{t}} \cdot \boldsymbol{e}_0 \,] \\
&= \boldsymbol{\Pi}^{\mathrm{t}} : \nabla_{\boldsymbol{X}} \boldsymbol{F} - [\, \boldsymbol{\Pi} \cdot \boldsymbol{A}^{\mathrm{t}} \,] : \boldsymbol{e}_0 \\
&= \boldsymbol{\Pi}^{\mathrm{t}} : \nabla_{\boldsymbol{X}} \boldsymbol{F} - \boldsymbol{\Pi} \times \boldsymbol{A} \,,
\end{aligned} \tag{B.1}$$

whereby use of the notation introduced in section 1.5, eq.(2.4), and appendix A has been made. Note that the left–hand side of eq.(B.1) also allows representation in terms of a spatial gradient operator, namely $\nabla_{\boldsymbol{X}} \boldsymbol{F}^{\mathrm{t}} : \boldsymbol{\Pi}^{\mathrm{t}} = [\, \nabla_{\boldsymbol{x}} \boldsymbol{F}^{\mathrm{t}} \cdot \boldsymbol{F} \,] : \boldsymbol{\Pi}^{\mathrm{t}}$. These elaborations together with eqs.(2.4,2.43) finally enable us to reformulate the second term on the right–hand side of eq.(B.1) as

$$\begin{aligned}
\boldsymbol{\Pi} \times \boldsymbol{A} = [\, \boldsymbol{\Pi} \cdot \boldsymbol{A}^{\mathrm{t}} \,] : \boldsymbol{e}_0 &= [\, \mathrm{cof}(\boldsymbol{F}^{\mathrm{t}}) \cdot \boldsymbol{\sigma} \cdot \boldsymbol{d}^{\mathrm{t}} \cdot \mathrm{cof}(\boldsymbol{F}) \,] : \boldsymbol{e}_0 \\
&= J^2 \, [\, \boldsymbol{\sigma} \cdot \boldsymbol{d}^{\mathrm{t}} \,] : [\, \boldsymbol{f}^{\mathrm{t}} \,\overline{\otimes}\, \boldsymbol{f}^{\mathrm{t}} \,] : \boldsymbol{e}_0 \\
&= J \, [\, \boldsymbol{\sigma} \cdot \boldsymbol{d}^{\mathrm{t}} \,] : \boldsymbol{e}_t \cdot \boldsymbol{F} \\
&= J \, \boldsymbol{F}^{\mathrm{t}} \cdot [\, \boldsymbol{\sigma} \times \boldsymbol{d} \,] \,,
\end{aligned} \tag{B.2}$$

compare appendix A. Note that the stress tensor $\boldsymbol{\sigma}^{\mathrm{t}}$ and the dislocation density tensor $\boldsymbol{d}^{\mathrm{t}}$ on the right–hand side of eq.(B.2) are entirely settled in one configuration, here the spatial setting, while $\boldsymbol{\Pi}^{\mathrm{t}}$ and $\boldsymbol{A}^{\mathrm{t}}$ in eq.(B.1) are two–point tensors. Along the same lines of derivation, similar relations as for instance

$$\boldsymbol{f} \times \boldsymbol{A}^{\mathrm{t}} = [\, \boldsymbol{f} \cdot \boldsymbol{d}^{\mathrm{t}} \cdot \mathrm{cof}(\boldsymbol{F}) \,] : \boldsymbol{e}_0 = \boldsymbol{d}^{\mathrm{t}} : \boldsymbol{e}_{\mathrm{t}} \cdot \boldsymbol{F} = \boldsymbol{F}^{\mathrm{t}} \cdot [\, \boldsymbol{I}_t \times \boldsymbol{d} \,] \tag{B.3}$$

follow straightforwardly.

C Divergence operation with respect to incompatible configurations

In the following, we discuss the Piola identity in the context of an incompatible configuration. Special emphasis is placed on the application of the divergence operation to a second–order tensor as based on the differential operations introduced in eqs.(2.12,2.13). To set the stage, recall that Gauß' theorem results for sufficient smoothness in

$$\int_{\mathcal{A}_0} \boldsymbol{\Xi} \cdot \boldsymbol{N} \, \mathrm{d}A_0 = \int_{\mathcal{V}_0} \nabla_{\boldsymbol{X}} \cdot \boldsymbol{\Xi} \, \mathrm{d}V_0 = \int_{\mathcal{V}_t} \nabla_{\boldsymbol{x}} \cdot \boldsymbol{\xi} \, \mathrm{d}V_t = \int_{\mathcal{A}_t} \boldsymbol{\xi} \cdot \boldsymbol{n} \, \mathrm{d}A_t \,, \tag{C.1}$$

wherein $\boldsymbol{\Xi}$ denotes either a two–point or entirely referential second–order tensor. The tensor $\boldsymbol{\xi}$ is related to $\boldsymbol{\Xi}$ via the Piola transformation $\boldsymbol{\Xi} = \boldsymbol{\xi} \cdot \mathrm{cof}(\boldsymbol{F})$. Consequently, $\boldsymbol{N}$ and $\boldsymbol{n}$ characterise outward unit vectors in $\mathcal{B}_0$ and $\mathcal{B}_t$, respectively, so that $\boldsymbol{N} \, \mathrm{d}A_0 = \mathrm{cof}(\boldsymbol{f}) \cdot \boldsymbol{n} \, \mathrm{d}A_t$. The underlying relation for eq.(C.1) is given by the Piola identity

$$\nabla_{\boldsymbol{X}} \cdot \boldsymbol{\Xi} = \nabla_{\boldsymbol{X}} \cdot (\boldsymbol{\xi} \cdot \mathrm{cof}(\boldsymbol{F})) = [\nabla_{\boldsymbol{X}} \cdot \boldsymbol{\xi}] \cdot \mathrm{cof}(\boldsymbol{F}^{\mathrm{t}}) = J \, \nabla_{\boldsymbol{x}} \cdot \boldsymbol{\xi} \,, \tag{C.2}$$

i.e. the divergence of the corresponding cofactor vanishes identically

$$\begin{aligned} \nabla_{\boldsymbol{X}} \cdot \mathrm{cof}(\boldsymbol{F}) \; &= \quad \boldsymbol{f}^{\mathrm{t}} \cdot \nabla_{\boldsymbol{X}} J \qquad + \; J \, \nabla_{\boldsymbol{X}} \cdot \boldsymbol{f}^{\mathrm{t}} \\ &= \quad \partial_{\boldsymbol{f}} J : \nabla_{\boldsymbol{X}} \boldsymbol{f} \cdot \boldsymbol{f} \; + \; J \, \nabla_{\boldsymbol{x}} \boldsymbol{f}^{\mathrm{t}} : \boldsymbol{F}^{\mathrm{t}} \\ &= - \; J \, \boldsymbol{F}^{\mathrm{t}} : \nabla_{\boldsymbol{x}} \boldsymbol{f} \qquad + \; J \, \boldsymbol{F}^{\mathrm{t}} : \nabla_{\boldsymbol{x}} \boldsymbol{f} \; - \; J \, \boldsymbol{F} \times \boldsymbol{a} \\ &= \quad \boldsymbol{0} \quad \text{for} \quad \boldsymbol{a}^{\mathrm{t}} = \boldsymbol{0} \,; \end{aligned} \tag{C.3}$$

see, for example, the contribution by Ericksen (1960), or the monographs by Marsden and Hughes (1994), Ciarlet (1988), and Šilhavý (1997). The incorporation of the dislocation density tensor in eq.(C.3) is based on similar considerations as highlighted in eq.(B.1) and $\nabla_{\boldsymbol{x}} \cdot \mathrm{cof}(\boldsymbol{f}) = \boldsymbol{0}$ follows by analogy with the elaborations above. By deriving the Piola identity, however, compatibility of the overall motion has been assumed, namely $\boldsymbol{a}^{\mathrm{t}} = \boldsymbol{0}$; compare eq.(2.8). Apparently, dislocation density tensors with respect to the plastic or elastic distortion do not vanish in general, so that the relation between the intermediate divergence and the material or spatial divergence of a, for instance, second–order tensor possesses a different format compared to eq.(C.1). To be specific, we obtain on the one hand

$$\int_{\mathcal{A}_0} \boldsymbol{\Upsilon} \cdot \boldsymbol{N} \, \mathrm{d}A_0 = \int_{\mathcal{V}_0} \nabla_{\boldsymbol{X}} \cdot \boldsymbol{\Upsilon} \, \mathrm{d}V_0 = \int_{\mathcal{V}_{\mathrm{p}}} \widetilde{\nabla} \cdot \widetilde{\boldsymbol{\Upsilon}} - \widetilde{\boldsymbol{\Upsilon}} \cdot [\boldsymbol{F}_{\mathrm{p}} \times \widetilde{\boldsymbol{a}}] \, \mathrm{d}V_{\mathrm{p}} \,, \tag{C.4}$$

wherein $\boldsymbol{\Upsilon} = \widetilde{\boldsymbol{\Upsilon}} \cdot \mathrm{cof}(\boldsymbol{F}_{\mathrm{p}})$ denotes either a two–point or entirely referential second–order tensor and $\widetilde{\boldsymbol{a}}^{\mathrm{t}}$ has been introduced in eq.(2.31). On the other hand, one similarly observes

$$\int_{\mathcal{A}_t} \boldsymbol{\upsilon} \cdot \boldsymbol{n} \, \mathrm{d}A_t = \int_{\mathcal{V}_t} \nabla_{\boldsymbol{x}} \cdot \boldsymbol{\upsilon} \, \mathrm{d}V_t = \int_{\mathcal{V}_{\mathrm{p}}} \bar{\nabla} \cdot \bar{\boldsymbol{\upsilon}} - \bar{\boldsymbol{\upsilon}} \cdot [\boldsymbol{f}_{\mathrm{e}} \times \bar{\boldsymbol{A}}] \, \mathrm{d}V_{\mathrm{p}} \,, \tag{C.5}$$

wherein $\boldsymbol{\upsilon} = \bar{\boldsymbol{\upsilon}} \cdot \mathrm{cof}(\boldsymbol{f}_{\mathrm{e}})$ characterises either a two–point or entirely spatial second–order tensor and $\bar{\boldsymbol{A}}^{\mathrm{t}}$ has been introduced in eq.(2.29). In contrast to eq.(C.2), the corresponding local representations consequently result in the (two alternative sets of) relations

$$\begin{aligned} \nabla_{\boldsymbol{X}} \cdot \boldsymbol{\Upsilon} \; &= J_{\mathrm{p}} \, \widetilde{\nabla} \cdot \widetilde{\boldsymbol{\Upsilon}} \; - \; J_{\mathrm{p}} \, \widetilde{\boldsymbol{\Upsilon}} \cdot [\boldsymbol{F}_{\mathrm{p}} \times \widetilde{\boldsymbol{a}}] \\ \nabla_{\boldsymbol{x}} \cdot \boldsymbol{\upsilon} \; &= j_{\mathrm{e}} \; \bar{\nabla} \cdot \bar{\boldsymbol{\upsilon}} \; - \; j_{\mathrm{e}} \; \bar{\boldsymbol{\upsilon}} \cdot [\boldsymbol{f}_{\mathrm{e}} \times \bar{\boldsymbol{A}}] \end{aligned} \quad \text{or} \quad \begin{aligned} \nabla_{\boldsymbol{X}} \cdot \boldsymbol{\Upsilon} \; + \; \boldsymbol{\Upsilon} \cdot \boldsymbol{F}_{\mathrm{p}}^{\mathrm{t}} \cdot [\boldsymbol{F}_{\mathrm{p}} \times \widetilde{\boldsymbol{a}}] \; &= J_{\mathrm{p}} \, \widetilde{\nabla} \cdot \widetilde{\boldsymbol{\Upsilon}} \\ \nabla_{\boldsymbol{x}} \cdot \boldsymbol{\upsilon} \; + \; \boldsymbol{\upsilon} \cdot \boldsymbol{f}_{\mathrm{e}}^{\mathrm{t}} \cdot [\boldsymbol{f}_{\mathrm{e}} \times \bar{\boldsymbol{A}}] \; &= j_{\mathrm{e}} \; \bar{\nabla} \cdot \bar{\boldsymbol{\upsilon}} \end{aligned} \tag{C.6}$$

D Essential steps for the derivation of the local Jacobian in chapter 4

Differentiation of the flow directions derived in section 4.2 and 4.4 together with the prototype model introduced in section 4.5 (proportional hardening contributions being neglected) renders

$$\begin{aligned}
\mathrm{d}\,\widehat{\boldsymbol{\nu}}_{\mathrm{p}} &= \frac{\partial\,\widehat{\boldsymbol{\nu}}_{\mathrm{p}}}{\partial\,\widehat{\boldsymbol{B}}_{\mathrm{e}}} : \mathrm{d}\widehat{\boldsymbol{B}}_{\mathrm{e}} + \frac{\partial\,\widehat{\boldsymbol{\nu}}_{\mathrm{p}}}{\partial\,{}^{\mathrm{eff}}\widehat{\boldsymbol{C}}_{\mathrm{e}}} : \mathrm{d}\,{}^{\mathrm{eff}}\widehat{\boldsymbol{C}}_{\mathrm{e}} + \frac{\partial\,\widehat{\boldsymbol{\nu}}_{\mathrm{p}}}{\partial\,{}^{\mathrm{eff}}\widehat{\boldsymbol{M}}_{\mathrm{r}}^{\mathrm{dev}}} : \mathrm{d}\,{}^{\mathrm{eff}}\widehat{\boldsymbol{M}}_{\mathrm{r}}^{\mathrm{dev}}\,, \\
\mathrm{d}\,\widehat{\boldsymbol{\nu}}_{\mathrm{k}} &= -\,\frac{3}{2\,Y_0}\,\mathrm{d}\,{}^{\mathrm{eff}}\widehat{\boldsymbol{M}}_{\mathrm{r}}^{\mathrm{dev}}\,, \\
\mathrm{d}\,\bar{\boldsymbol{\nu}}_{\mathrm{a}} &= \frac{\partial\,\bar{\boldsymbol{\nu}}_{\mathrm{a}}}{\partial\,\bar{\lambda}_{\mathrm{a}\,i}}\,\mathrm{d}\,\bar{\lambda}_{\mathrm{a}\,i} + \frac{\partial^2\,\bar{\boldsymbol{\nu}}_{\mathrm{a}}}{\partial\,\bar{\boldsymbol{n}}_{\mathrm{a}}^{i}\otimes\bar{\boldsymbol{n}}_{\mathrm{a}\,i}} : \mathrm{d}\,(\bar{\boldsymbol{n}}_{\mathrm{a}}^{i}\otimes\bar{\boldsymbol{n}}_{\mathrm{a}\,i})\,.
\end{aligned} \tag{D.1}$$

The partial derivatives included in eq.(D.1) allow representation as

$$\begin{aligned}
\frac{\partial\,\widehat{\boldsymbol{\nu}}_{\mathrm{p}}}{\partial\,\widehat{\boldsymbol{B}}_{\mathrm{e}}} &= \frac{3}{2\,Y_0}\,\boldsymbol{I}_{\mathrm{p}}\,\overline{\otimes}\,\big[\,[\,{}^{\mathrm{eff}}\widehat{\boldsymbol{M}}_{\mathrm{r}}^{\mathrm{dev}}]^{\mathrm{d}}\cdot{}^{\mathrm{eff}}\widehat{\boldsymbol{C}}_{\mathrm{e}}\,\big]\,, \\
\frac{\partial\,\widehat{\boldsymbol{\nu}}_{\mathrm{p}}}{\partial\,{}^{\mathrm{eff}}\widehat{\boldsymbol{C}}_{\mathrm{e}}} &= \frac{3}{2\,Y_0}\,\widehat{\boldsymbol{B}}_{\mathrm{e}}\,\overline{\otimes}\,[\,{}^{\mathrm{eff}}\widehat{\boldsymbol{M}}_{\mathrm{r}}^{\mathrm{dev}}\,]^{\mathrm{d}}\,, \\
\frac{\partial\,\widehat{\boldsymbol{\nu}}_{\mathrm{p}}}{\partial\,{}^{\mathrm{eff}}\widehat{\boldsymbol{M}}_{\mathrm{r}}^{\mathrm{dev}}} &= \frac{3}{2\,Y_0}\,\big[\,\widehat{\boldsymbol{B}}_{\mathrm{e}}\cdot{}^{\mathrm{eff}}\widehat{\boldsymbol{C}}_{\mathrm{e}}\,\big]\,\overline{\otimes}\,\boldsymbol{I}_{\mathrm{p}}\,, \\
\frac{\partial^2\,\bar{\boldsymbol{\nu}}_{\mathrm{a}}}{\partial\,\bar{\boldsymbol{n}}_{\mathrm{a}}^{i}\otimes\bar{\boldsymbol{n}}_{\mathrm{a}\,i}} &= {}^{\mathrm{dam}}\Phi^{-D}\,\mathcal{H}(\bar{\lambda}_{\mathrm{a}\,i})\,\langle\bar{\lambda}_{\mathrm{a}\,i}\rangle^{D}\,\boldsymbol{I}_{\mathrm{a}}\,\overline{\otimes}\,\boldsymbol{I}_{\mathrm{a}}\,, \\
\frac{\partial\,\bar{\boldsymbol{\nu}}_{\mathrm{a}}}{\partial\,\bar{\lambda}_{\mathrm{a}\,i}} &= {}^{\mathrm{dam}}\Phi^{-D}\,\mathcal{H}(\bar{\lambda}_{\mathrm{a}\,i})\,D\,\big[\,\langle\bar{\lambda}_{\mathrm{a}\,i}\rangle^{D-1}\,\bar{\boldsymbol{n}}_{\mathrm{a}}^{i}\otimes\bar{\boldsymbol{n}}_{\mathrm{a}\,i} - {}^{\mathrm{dam}}\Phi^{-1}\langle\bar{\lambda}_{\mathrm{a}\,i}\rangle^{D}\,\bar{\boldsymbol{\nu}}_{\mathrm{a}}\,\big]\,,
\end{aligned} \tag{D.2}$$

whereby use of ${}^{\mathrm{eff}}\widehat{\boldsymbol{M}}_{\mathrm{e}}^{\mathrm{d}} = {}^{\mathrm{eff}}\widehat{\boldsymbol{C}}_{\mathrm{e}}\cdot\widehat{\boldsymbol{S}}_{\mathrm{e}}$ has been made. Moreover, eq.(D.1) also demands the computation of

$$\begin{aligned}
\mathrm{d}\widehat{\boldsymbol{B}}_{\mathrm{e}} &= -\,\big[\,\widehat{\boldsymbol{B}}_{\mathrm{e}}\,\overline{\otimes}\,\widehat{\boldsymbol{B}}_{\mathrm{e}}\,\big] : \mathrm{d}\widehat{\boldsymbol{C}}_{\mathrm{e}}\,, \\
\mathrm{d}\widehat{\boldsymbol{C}}_{\mathrm{e}} &= \big[\,\boldsymbol{I}_{\mathrm{p}}\,\underline{\otimes}\,[\,\boldsymbol{f}_{\mathrm{p}}^{\mathrm{d}}\cdot\boldsymbol{C}\,] + [\,\boldsymbol{f}_{p}^{\mathrm{d}}\cdot\boldsymbol{C}\,]\,\overline{\otimes}\,\boldsymbol{I}_{\mathrm{p}}\,\big] : \mathrm{d}\boldsymbol{f}_{\mathrm{p}}\,, \\
\mathrm{d}\,{}^{\mathrm{eff}}\widehat{\boldsymbol{C}}_{\mathrm{e}} &= \frac{\partial\,{}^{\mathrm{eff}}\widehat{\boldsymbol{C}}_{\mathrm{e}}}{\partial\,\boldsymbol{f}_{\mathrm{a}}} : \mathrm{d}\boldsymbol{f}_{\mathrm{a}} + \frac{\partial\,{}^{\mathrm{eff}}\widehat{\boldsymbol{C}}_{\mathrm{e}}}{\partial\widehat{\boldsymbol{C}}_{\mathrm{e}}} : \mathrm{d}\,\widehat{\boldsymbol{C}}_{\mathrm{e}}\,, \\
\mathrm{d}\,{}^{\mathrm{eff}}\widehat{\boldsymbol{M}}_{\mathrm{r}}^{\mathrm{dev}} &= \big[\,\boldsymbol{I}_{\mathrm{p}}\,\overline{\otimes}\,\boldsymbol{I}_{\mathrm{p}} - \tfrac{1}{3}\,\boldsymbol{I}_{\mathrm{p}}\otimes\boldsymbol{I}_{\mathrm{p}}\,\big] : \mathrm{d}\,{}^{\mathrm{eff}}\widehat{\boldsymbol{M}}_{\mathrm{r}}\,, \\
\mathrm{d}\,{}^{\mathrm{eff}}\widehat{\boldsymbol{M}}_{\mathrm{r}} &= \mathrm{d}\,{}^{\mathrm{eff}}\widehat{\boldsymbol{M}}_{\mathrm{e}} - \mathrm{d}\,\widehat{\boldsymbol{M}}_{\mathrm{k}}
\end{aligned} \tag{D.3}$$

together with

$$\begin{aligned}
\mathrm{d}\,{}^{\mathrm{eff}}\widehat{\boldsymbol{M}}_{\mathrm{e}} &= \big[\,\boldsymbol{I}_{\mathrm{p}}\,\overline{\otimes}\,{}^{\mathrm{eff}}\widehat{\boldsymbol{C}}_{\mathrm{e}}\,\big] : \mathrm{d}\widehat{\boldsymbol{S}}_{\mathrm{e}} + \big[\,\widehat{\boldsymbol{S}}_{\mathrm{e}}\,\overline{\otimes}\,\boldsymbol{I}_{\mathrm{p}}\,\big] : \mathrm{d}\,{}^{\mathrm{eff}}\widehat{\boldsymbol{C}}_{\mathrm{e}}\,,\\
\mathrm{d}\widehat{\boldsymbol{S}}_{\mathrm{e}} &= \frac{\partial\widehat{\boldsymbol{S}}_{\mathrm{e}}}{\partial\widehat{\boldsymbol{E}}_{\mathrm{e}}} : \mathrm{d}\widehat{\boldsymbol{E}}_{\mathrm{e}} + \frac{\partial\widehat{\boldsymbol{S}}}{\partial\boldsymbol{A}_{\mathrm{p}}} : \mathrm{d}\boldsymbol{A}_{\mathrm{p}}\,,\\
\mathrm{d}\widehat{\boldsymbol{E}}_{\mathrm{e}} &= \tfrac{1}{2}\,\mathrm{d}\widehat{\boldsymbol{C}}_{\mathrm{e}}\,,\\
\mathrm{d}\boldsymbol{A}_{\mathrm{p}} &= \big[\,-\boldsymbol{F}_{\mathrm{a}}\,\overline{\otimes}\,\boldsymbol{A}_{\mathrm{p}} - \boldsymbol{A}_{\mathrm{p}}\,\underline{\otimes}\,\boldsymbol{F}_{\mathrm{a}}\,\big] : \mathrm{d}\boldsymbol{f}_{\mathrm{a}}
\end{aligned} \tag{D.4}$$

as well as

$$\begin{aligned}
\mathrm{d}\widehat{\boldsymbol{M}}_{\mathrm{k}} &= \big[\,\boldsymbol{I}_{\mathrm{p}}\,\overline{\otimes}\,\widehat{\boldsymbol{K}}\,\big] : \mathrm{d}\widehat{\boldsymbol{S}}_{\mathrm{k}} + \big[\,\widehat{\boldsymbol{S}}_{\mathrm{k}}\,\overline{\otimes}\,\boldsymbol{I}_{\mathrm{p}}\,\big] : \mathrm{d}\widehat{\boldsymbol{K}}\,,\\
\mathrm{d}\widehat{\boldsymbol{S}}_{\mathrm{k}} &= \frac{\partial\widehat{\boldsymbol{S}}_{\mathrm{k}}}{\partial\widehat{\boldsymbol{E}}_{\mathrm{k}}} : \mathrm{d}\widehat{\boldsymbol{E}}_{\mathrm{k}} + \frac{\partial\widehat{\boldsymbol{S}}_{\mathrm{k}}}{\partial\boldsymbol{A}_{\mathrm{p}}} : \mathrm{d}\boldsymbol{A}_{\mathrm{p}}\,,\\
\mathrm{d}\widehat{\boldsymbol{E}}_{\mathrm{k}} &= \tfrac{1}{2}\,\mathrm{d}\widehat{\boldsymbol{K}}\,,\\
\mathrm{d}\widehat{\boldsymbol{K}} &= \big[\,\boldsymbol{f}_{\mathrm{k}}^{\mathrm{d}}\,\overline{\otimes}\,\boldsymbol{I}_{\mathrm{p}} + \boldsymbol{I}_{\mathrm{p}}\,\underline{\otimes}\,\boldsymbol{f}_{\mathrm{k}}^{\mathrm{d}}\,\big] : \mathrm{d}\boldsymbol{f}_{\mathrm{k}}
\end{aligned} \tag{D.5}$$

with $\widehat{\boldsymbol{M}}_{\mathrm{k}}^{\mathrm{d}} = \widehat{\boldsymbol{K}}\cdot\widehat{\boldsymbol{S}}_{\mathrm{k}}$. Eqs.(D.3–D.5), however, involve the elaboration of further partial derivatives, namely

$$\frac{\partial\,{}^{\mathrm{eff}}\widehat{\boldsymbol{C}}_{\mathrm{e}}}{\partial\boldsymbol{f}_{\mathrm{a}}} = \big[\,\boldsymbol{f}_{\mathrm{a}}^{\mathrm{d}}\cdot\widehat{\boldsymbol{C}}_{\mathrm{e}}\,\big]\,\overline{\otimes}\,\boldsymbol{I}_{\mathrm{p}} + \boldsymbol{I}_{\mathrm{p}}\,\underline{\otimes}\,\big[\,\boldsymbol{f}_{\mathrm{a}}^{\mathrm{d}}\cdot\widehat{\boldsymbol{C}}_{\mathrm{e}}\,\big]\,, \qquad \frac{\partial\,{}^{\mathrm{eff}}\widehat{\boldsymbol{C}}_{\mathrm{e}}}{\partial\widehat{\boldsymbol{C}}_{\mathrm{e}}} = \boldsymbol{f}_{\mathrm{a}}^{\mathrm{d}}\,\overline{\otimes}\,\boldsymbol{f}_{\mathrm{a}}^{\mathrm{d}}\,, \tag{D.6}$$

and

$$\begin{aligned}
\frac{\partial\widehat{\boldsymbol{S}}_{\mathrm{e}}}{\partial\widehat{\boldsymbol{E}}_{\mathrm{e}}} &= L\,\big[\,\boldsymbol{A}_{\mathrm{p}}\otimes\boldsymbol{A}_{\mathrm{p}}\,\big] + 2\,G\,\big[\boldsymbol{A}_{\mathrm{p}}\,\overline{\otimes}\,\boldsymbol{A}_{\mathrm{p}}\,\big]\,,\\
\frac{\partial\widehat{\boldsymbol{S}}_{\mathrm{e}}}{\partial\boldsymbol{A}_{\mathrm{p}}} &= L\,\Big[\,\boldsymbol{A}_{\mathrm{p}}\otimes\widehat{\boldsymbol{E}}_{\mathrm{e}} + \big[\,\boldsymbol{A}_{\mathrm{p}} : \widehat{\boldsymbol{E}}_{\mathrm{e}}\,\big]\,\boldsymbol{I}_{\mathrm{p}}\,\overline{\otimes}\,\boldsymbol{I}_{\mathrm{p}}\Big]\\
&\quad + 2\,G\,\Big[\,\boldsymbol{I}_{\mathrm{p}}\,\overline{\otimes}\,\big[\,\boldsymbol{A}_{\mathrm{p}}\cdot\widehat{\boldsymbol{E}}_{\mathrm{e}}\,\big] + \big[\,\boldsymbol{A}_{\mathrm{p}}\cdot\widehat{\boldsymbol{E}}_{\mathrm{e}}\,\big]\,\overline{\otimes}\,\boldsymbol{I}_{\mathrm{p}}\,\Big]\,,\\
\frac{\partial\widehat{\boldsymbol{S}}_{\mathrm{k}}}{\partial\widehat{\boldsymbol{E}}_{\mathrm{k}}} &= 2\,H\,\big[\,\boldsymbol{A}_{\mathrm{p}}\,\overline{\otimes}\,\boldsymbol{A}_{\mathrm{p}} - \tfrac{1}{3}\,\boldsymbol{A}_{\mathrm{p}}\otimes\boldsymbol{A}_{\mathrm{p}}\,\big]\,,\\
\frac{\partial\widehat{\boldsymbol{S}}_{\mathrm{k}}}{\partial\boldsymbol{A}_{\mathrm{p}}} &= 2\,H\,\Big[\,\boldsymbol{I}_{\mathrm{p}}\,\overline{\otimes}\,\big[\,\boldsymbol{A}_{\mathrm{p}}\cdot\widehat{\boldsymbol{E}}_{\mathrm{k}}\,\big] + \big[\,\boldsymbol{A}_{\mathrm{p}}\cdot\widehat{\boldsymbol{E}}_{\mathrm{k}}\,\big]\,\overline{\otimes}\,\boldsymbol{I}_{\mathrm{p}}\\
&\quad - \tfrac{1}{3}\;\boldsymbol{A}_{\mathrm{p}}\otimes\widehat{\boldsymbol{E}}_{\mathrm{k}} - \tfrac{1}{3}\,\big[\,\boldsymbol{A}_{\mathrm{p}} : \widehat{\boldsymbol{E}}_{\mathrm{k}}\,\big]\,\boldsymbol{I}_{\mathrm{p}}\,\overline{\otimes}\,\boldsymbol{I}_{\mathrm{p}}\Big]\,.
\end{aligned} \tag{D.7}$$

Furthermore, differentiation of the eigenvalues and the eigenbases of $\bar{\boldsymbol{M}}_{\mathrm{a}}^{\mathrm{d}}$ in eq.(D.5)$_3$ yields

$$\mathrm{d}\,\bar{\lambda}_{\mathrm{a}i} = [\,\bar{\boldsymbol{n}}_{\mathrm{a}}^{i}\otimes\bar{\boldsymbol{n}}_{\mathrm{a}i}\,] : \mathrm{d}\,\bar{\boldsymbol{M}}_{\mathrm{a}}^{\mathrm{d}}\,, \qquad \mathrm{d}\,(\bar{\boldsymbol{n}}_{\mathrm{a}}^{i}\otimes\bar{\boldsymbol{n}}_{\mathrm{a}i}) = \frac{\partial\,\bar{\boldsymbol{n}}_{\mathrm{a}}^{i}\otimes\bar{\boldsymbol{n}}_{\mathrm{a}i}}{\partial\bar{\boldsymbol{M}}_{\mathrm{a}}^{\mathrm{d}}} : \mathrm{d}\,\bar{\boldsymbol{M}}_{\mathrm{a}}^{\mathrm{d}}\,, \tag{D.8}$$

wherein

$$\mathrm{d}\,\bar{\boldsymbol{M}}_{\mathrm{a}}^{\mathrm{d}} = \big[\,\boldsymbol{F}_{\mathrm{a}}^{\mathrm{d}}\,\overline{\otimes}\,\boldsymbol{f}_{\mathrm{a}}\,\big] : \mathrm{d}\,\widehat{\boldsymbol{M}}_{\mathrm{a}}^{\mathrm{d}} + \Big[\,\big[\,\boldsymbol{F}_{\mathrm{a}}^{\mathrm{d}}\cdot\widehat{\boldsymbol{M}}_{\mathrm{a}}^{\mathrm{d}}\,\big]\,\underline{\otimes}\,\boldsymbol{I}_{\mathrm{p}} - \boldsymbol{F}_{\mathrm{a}}^{\mathrm{d}}\,\underline{\otimes}\,\big[\,\boldsymbol{f}_{\mathrm{a}}\cdot\widehat{\boldsymbol{M}}_{\mathrm{a}}\cdot\boldsymbol{F}_{\mathrm{a}}\,\big]\,\Big] : \mathrm{d}\boldsymbol{f}_{\mathrm{a}} \tag{D.9}$$

together with

$$\mathrm{d}\,\widehat{\boldsymbol{M}}_{\mathrm{a}}^{\mathrm{d}} = \mathrm{d}\,\widehat{\boldsymbol{M}}_{\mathrm{e}}^{\mathrm{d}} + \mathrm{d}\,\widehat{\boldsymbol{M}}_{\mathrm{k}}^{\mathrm{d}} = \big[\,\widehat{\boldsymbol{S}}_{\mathrm{e}}\,\overline{\otimes}\,\boldsymbol{I}_{\mathrm{p}}\,\big] : \mathrm{d}\widehat{\boldsymbol{C}}_{\mathrm{e}} + \big[\,\widehat{\boldsymbol{C}}_{\mathrm{e}}\,\overline{\otimes}\,\boldsymbol{I}_{\mathrm{p}}\,\big] : \mathrm{d}\widehat{\boldsymbol{S}}_{\mathrm{e}} + \mathrm{d}\,\widehat{\boldsymbol{M}}_{\mathrm{k}}^{\mathrm{d}}\,. \tag{D.10}$$

For simplicity we apply numerical differentiation to calculate $\partial\,(\bar{\boldsymbol{n}}_{\mathrm{a}}^{i}\otimes\bar{\boldsymbol{n}}_{\mathrm{a}i})\,/\,\partial\,\bar{\boldsymbol{M}}_{\mathrm{a}}^{\mathrm{d}}$ – it would, however, be possible, but not necessarily numerical efficient, to use Serrin's formula; compare for instance Miehe (1993).

Author Index

Bibliography

A. Acharya. A model of crystal plasticity based on the theory of continuously distributed dislocations. *J. Mech. Phys. Solids*, 49:761–784, 2001.

A. Acharya. Driving forces and boundary conditions in continuum dislocation mechanics. *Proc. Roy. Soc. London A*, 459:1343–1363, 2003.

A. Acharya. Constitutive analysis of finite deformation field dislocation mechanics. *J. Mech. Phys. Solids*, 52:301–316, 2004.

A. Acharya and J.L. Bassani. Lattice incompatibility and the gradient theory of crystal plasticity. *J. Mech. Phys. Solids*, 48(8):1565–1595, 2000.

B. Alberts, D. Bray, J. Lewis, M. Raff, K. Roberts, and J.D. Watson. *Molecular Biology of the Cell*. Garland Publishing, 3rd edition, 1994.

E.S. Almeida and R.L. Spilker. Finite element formulations for hyperelastic transversely isotropic biphasic soft tissues. *Comput. Methods Appl. Mech. Engrg.*, 151:513–538, 1998.

S.L. Altmann. *Rotation, Quaternions and Double Groups*. Oxford University Press, 1986.

D. Ambrosi and F. Mollica. On the mechanics of a growing tumor. *Int. J. Engng. Sci.*, 40:1297–1316, 2002.

J. Angeles. *Rational Kinematics*, volume 34 of *Springer Tracts in Natural Philosopy*. Springer, 1988.

S.S. Antman. *Nonlinear Problems of Elasticity*, volume 107 of *Applied Mathematical Sciences*. Springer, 1st edition, 1995.

J.H. Argyris. An excursion into large rotations. *Comput. Methods Appl. Mech. Engrg.*, 32:85–155, 1982.

A. Arockiarajan and A. Menzel. On the modelling of rate–dependent domain switching in piezoelectric materials under superimposed stresses. *Comput. Model. Eng. Sci.*, 19(2):163–180, 2007. printed version: 20(1), 55–72.

N. Arvas. Finite elastoplasticity transformations of transversely isotropic materials. *Int. J. Solids Struct.*, 29:2137–2157, 1992.

R.J. Asaro and V.A. Lubarda. *Mechanics of Solid Materials*. Cambridge, 2006.

J.M. Ball. Convexity conditions and existence theorems in nonlinear elasticity. *Arch. Rational Mech. Anal.*, 63:337–403, 1977.

M.F. Beatty. A class of universial relations in isotropic elasticity theory. *J. Elasticity*, 17:113–121, 1987.

M.F. Beatty and M.A. Hayes, editors. *Mechanics and Mathematics of Crystals – Selected Papers of J L Ericksen*. World Scientific, 2005.

M. Beck, T. Dürr, A. Rieke, and M.B. Schmidt. In der Bewegung liegt die Kraft. In *Die 4. Dimension, Neues Land*. Sony, 1993.

T. Belytschko, W.K. Liu, and B. Moran. *Nonlinear Finite Elements for Continua and Structures*. Wiley, 2000.

A. Bertram. An alternative approach to finite plasticity based on material isomorphisms. *Int. J. Plasticity*, 15(3):353–374, 1999.

A. Bertram. Finite thermoplasticity based on isomorphisms. *Int. J. Plasticity*, 19:2027–2050, 2003.

A. Bertram. *Elasticity and Plasticity of Large Deformations*. Springer, 2005.

J.F. Besseling and E. van der Giessen. *Mathematical Modelling of Inelastic Deformation*, volume 5 of *Applied Mathematics and Mathematical Computations*. Chapman & Hall, 1994.

P. Betsch, A. Menzel, and E. Stein. On the parametrization of finite rotations in computational mechanics. A classification of concepts with application to smooth shells. *Comput. Methods Appl. Mech. Engrg.*, 155:273–305, 1998.

J. Betten. Representation of constitutive equations in creep mechanics of isotropic and anisotropic materials. In A.R.S. Ponter and D.R. Hayhurst, editors, *Creep in Structures*, pages 179–201. IUTAM Symposium Leicester/UK 1980, Springer, 1981.

B.A. Bilby, R. Bullough, and E. Smith. Continuous distributions of dislocations: a new application of the methods of non–Riemannian geometry. *Proc. Roy. Soc. A*, 231:263–273, 1955.

E.W. Billington. Constitutive equation for a class of isotropic, perfectly elastic solids using a new measure of finite strain and corresponding stress. *J. Elasticity*, 45:117–134, 2003.

M.A. Biot. *Mechanics of Incremental Deformations*. Wiley, 1965.

D. Boal. *Mechanics of the Cell*. Cambridge, 2002.

N. Böck and G.A. Holzapfel. A new two–point deformation tensor and its relation to the classical kinematical framework and the stress concept. *Int. J. Solids Struct.*, 41:7459–7469, 2004.

J.P. Boehler. A simple derivation of representations for non–polynomial constitutive equations in some cases of anisotropy. *Z. angew. Math. Mech.*, 59:157–167, 1979.

J.P. Boehler, editor. *Applications of Tensor Functions in Solid Mechanics*. Number 292 in CISM Courses and Lectures. Springer, 1987.

T. Böhlke and A. Bertram. The evolution of Hooke's law due to texture development in FCC polycrystals. *Int. J. Solids Struct.*, 38:9437–9459, 2001.

G.H. Borschel, Y.-C. Huang, S.C. Calve, E.M. Arruda, J.B. Lynch, D.E. Dow, W.M. Kuzon, R.G. Dennis, and D.L. Brown. Tissue engineering of recellularized small-diameter vascular grafts. *Tissue Engineering*, 11(5–6):778–786, 2005.

R.M. Bowen. Theory of Mixtures. In A.C. Eringen, editor, *Continuum Physics*, volume III – Mixtures and EM Field Theories, pages 1–127. Academic Press, 1976.

M. Braun. Configurational forces induced by finite–element discretization. *Proc. Estonian Acad. Sci. Phys. Math.*, 46(1–2):24–31, 1997.

E.C. Breen. Mechanical strain increases type I collagen expression in pulmonary fibroblasts in vitro. *J. Appl. Physiol.*, 88:203–209, 2000.

O.T. Bruhns, H. Xiao, and A. Meyers. Constitutive inequalities for an isotropic elastic strain–energy function based on Hencky's logarithmic strain tensor. *Proc. Roy. Soc. London A*, 457:2207–2226, 2001.

O.T. Bruhns, H. Xiao, and A. Meyers. Some basic issues in traditional Eulerian formulations of finite elastoplasticity. *Int. J. Plasticity*, 19:2007–2026, 2003.

M. Brünig. An anisotropic ductile damage model based on irreversible thermodynamics. *Int. J. Plasticity*, 19:1679–1714, 2003.

A. Bucher, U.-J. Görke, and R. Kreißig. A material model for finite elasto–plastic deformations considering a substructure. *Int. J. Plasticity*, 20:619–642, 2003.

V.V. Bulatov and W. Cai. *Computer Simulation of Dislocations*, volume 3 of *Oxford Series on Materials Modelling*. Oxford, 2006.

R. Burridge and J.B. Keller. Peeling, slipping and cracking – some one–dimensional free–boundary problems in mechanics. *SIAM Review*, 20(1):31–61, 1978.

S.C. Calve, R.G. Dennis, P.E. Kosnik, K. Baar, K. Grosh, and E.M. Arruda. Engineering of functional tendon. *Tissue Engineering*, 10(5–6):755–761, 2004.

G. Capriz. *Continua with Microstructure*, volume 35 of *Springer Tracts in Natural Philosophy*. Springer, 1989.

I. Carol, E. Rizzi, and K. Willam. On the formulation of anisotropic elastic degradation. Part I: Theory based on a pseudo–logarithmic damage tensor rate, Part II: Generalized pseudo–Rankine model for tensile damage. *Int. J. Solids Struct.*, 38:491–518, 519–546, 2001.

P. Cermelli and M.E. Gurtin. On the characterization of geometrically necessary dislocations in finite plasticity. *J. Mech. Phys. Solids*, 49(7):1539–1568, 2001.

P. Cermelli and M.E. Gurtin. Geometrically necessary dislocations in viscoplastic single crystals and bicrystals undergoing small deformations. *Int. J. Solids Struct.*, 39(26):6281–6309, 2002.

P. Chadwick. *Continuum Mechanics*. Dover, 1999.

P.L. Chandran and V.H. Barocas. Affine versus non–affine fibril kinematics in collagen networks: theoretical studies of network behavior. *ASME J. Biomech. Eng.*, 128:259–270, 2006.

Y.-C. Chen and A. Hoger. Constitutive functions of elastic materials in finite growth and deformation. *J. Elasticity*, 59:175–193, 2000.

P.G. Ciarlet. *Mathematical Elasticity – Volume 1: Three Dimensional Elasticity*, volume 20 of *Studies in Mathematics and its Applications*. North–Holland, 1988.

M. Ciarletta and D. Ieşan. *Non–classical elastic solids*, volume 293 of *Pitman Research Notes in Mathematics Series*. Longman, 1993.

S. Cleja-Ţigoiu. Nonlinear elasto–plastic deformations of transversely isotropic material and plastic spin. *Int. J. Engng. Sci.*, 38:737–763, 2000.

S. Cleja-Ţigoiu and G.A. Maugin. Eshelby's stress tensors in finite elastoplasticity. *Acta Mech.*, 139: 231–249, 2000.

A. Conti, A. DeSimone, and G. Dolzmann. Soft elastic response of stretched sheets of nematic elastomers: A numerical study. *J. Mech. Phys. Solids*, 50:1431–1451, 2002.

B. Cotterell, G. Williams, J. Hutchinson, and M. Thouless. Announcement of a round robin on the analysis of the peel test. *Int. J. Fracture*, 119:L55–L59, 2003.

S.C. Cowin. The relationship between the elasticity tensor and the fabric tensor. *Mech. Mater.*, 4: 137–147, 1985.

S.C. Cowin. Optimization of the strain energy density in linear anisotropic elasticity. *J. Elasticity*, 34: 45–68, 1994.

S.C. Cowin. On the minimization and maximization of the strain energy density in cortical bone tissue. *J. Biomechanics*, 28(4):445–447, 1995. Technical Note.

S.C. Cowin. Strain or deformation rate dependent finite growth in soft tissues. *J. Biomechanics*, 29(5): 647–649, 1996. Technical Note.

S.C. Cowin. Bone poroelasticity. *J. Biomechanics*, 32:217–238, 1999a.

S.C. Cowin. Structural change in living tissues. *Meccanica*, 34:379–398, 1999b.

S.C. Cowin. How is a tissue built? *ASME J. Biomech. Eng.*, 122:553–569, 2000.

S.C. Cowin, editor. *Bone Mechanics Handbook*. CRC Press, 2nd edition, 2001.

S.C. Cowin. Tissue growth and remodeling. *Annu. Rev. Biomed. Eng.*, 6:77–107, 2004.

S.C. Cowin and S.B. Doty. *Tissue Mechanics*. Springer, 2007.

S.C. Cowin and D.H. Hegedus. Bone remodeling I: Theory of adaptive elasticity. *J. Elasticity*, 6(3): 313–326, 1976.

S.C. Cowin and J.D. Humphrey, editors. *Cardiovascular Soft Tissue Mechanics*. Kluwer, 2000.

S.C. Cowin and M.M. Mehrabadi. Anisotropic symmetries of linear elasticity. *ASME Appl. Mech. Rev.*, 48(5):247–285, 1995.

J.D. Currey. The many adaptions of bone. *J. Biomechanics*, 36:1487–1495, 2003.

B. Dacorogna. *Direct Methods in the Calculus of Variations*, volume 78 of *Applied Mathematical Sciences*. Springer, 1989.

Y.F. Dafalias. The plastic spin concept and a simple illustration of its role in finite plasticity transformations. *Mech. Mater.*, 3:223–233, 1984.

Y.F. Dafalias. The plastic spin. *ASME J. Appl. Mech.*, 52:865–871, 1985.

Y.F. Dafalias. Plastic spin: Necessity or redundancy? *Int. J. Plasticity*, 14(9):909–931, 1998.

G. Dassiso and I.V. Lindell. On the Helmholtz decomposition for polyadics. *Quart. Appl. Math.*, 59 (4):787–796, 2001.

C. Davini. Elastic invariants in crystal theory. In J.M. Ball, editor, *Material Instabilities in Continuum Mechanics and Related Mathematical Problems*, pages 85–105. Oxford, 1988.

G. de Saxcé. Divergence and curl of a product of linear mapping fileds and applications to the large deformations. *Int. J. Engng. Sci.*, 39:555–561, 2001.

R. de Wit. A view of the relation between the continuum theory of lattice defects and non–Euclidian geometry in the linear approximation. *Int. J. Engng. Sci.*, 19:1475–1506, 1981.

G. del Piero and D.R. Owen, editors. *Multiscale Modeling in Continuum Mechanics and Structured Deformations*. Number 447 in CISM Courses and Lectures. Springer, 2004.

J.E. Dennis, Jr. and R.B. Schnabel. *Numerical Methods for Unconstrained Optimization and Nonlinear Equations*. Number 16 in Classics in Applied Mathematics. SIAM, 1996.

G. Dhondt. *The Finite Element Method for Three–Dimensional Thermomechanical Applications*. Wiley, 2004.

A. DiCarlo and S. Quiligotti. Growth and balance. *Mech. Res. Comm.*, 29:449–456, 2002.

E. Diegele, W. Jansohn, and Ch. Tsakmakis. Finite deformation plasticity and viscoplasticity laws exhibiting nonlinear hardening rules: Part I: Constitutive theory and numerical integration, Part II: Representative examples. *Comput. Mech.*, 25:1–12, 13–27, 2000.

P. Dłużewski. Anisotropic hyperelasticity based upon general strain measures. *J. Elasticity*, 60:119–129, 2000.

P. Dłużewski, G. Maciejewski, G. Jurczak, S. Kret, and J.-Y. Laval. Nonlinear FE analysis of residual stresses induced by dislocations in heterostructures. *Comput. Mater. Sci.*, 29:379–395, 2004.

G. Dolzmann. *Variational Methods for Crystalline Microstructure – Analysis and Computation*, volume 1803 of *Lecture Notes in Mathematics*. Springer, 2003.

N. Driessen. *Modeling and remodelling of the collagen architecture in cardiovascular tissues*. PhD thesis, TU Eindhoven, Department of Biomedical Engineering, 2006.

M. Eastwood, V.C. Mudera, D.A. McGrouther, and R.A. Brown. Effect of precise mechanical loading on fibroblast populated collagen lattices: morphological changes. *Cell Motil. Cytoskeleton*, 40:13–21, 1998.

M. Ekh. Thermo–elastic–viscoplastic modeling of IN792. *J. Mech. Behavior Mat.*, 12(6):359–387, 2001.

M. Ekh, R. Lillbacka, and K. Runesson. A model framework for anisotropic damage coupled to crystal (visco)plasticity. *Int. J. Plasticity*, 20:2143–2159, 2004.

M. Ekh and A. Menzel. Efficient iteration schemes for anisotropic hyperelasto-plasticity. *Int. J. Numer. Methods Engng.*, 66:707–721, 2006.

M. Ekh, A. Menzel, K. Runesson, and P. Steinmann. Anisotropic damage with the MCR effect coupled to plasticity. *Int. J. Engng. Sci.*, 41:1535–1551, 2003.

M. Ekh and K. Runesson. Bifurcation results for plasticity coupled to damage with mcr–effect. *Int. J. Solids Struct.*, 37(14):1975–1996, 2000.

M. Ekh and K. Runesson. Modelling and numerical issues in hyperelasto–plasticity with anisotropy. *Int. J. Solids Struct.*, 38(52):9461–9478, 2001.

D. Elata and M.B. Rubin. Isotropy of strain energy functions which depend only on a finite number of directional strain measures. *ASME J. Appl. Mech.*, 61:284–289, 1994.

M. Elżanowski and S. Preston. A model of the self–driven evolution of a defective continuum. *Math. Mech. Solids*, 12:450–465, 2007.

M.S. Engelman, G. Strang, and K.-J. Bathe. The application of quasi–Newton methods in fluid mechanics. *Int. J. Numer. Methods Engng.*, 17:707–718, 1981.

G. Engeln-Müllges and F. Uhlig. *Numerical Algorithms with FORTRAN*. Springer, 1996.

M. Epstein. The Eshelby tensor and the theory of continuous distributions of dislocations. *Mech. Res. Comm.*, 29:501–506, 2002.

M. Epstein and I. Bucataru. Continuous distributions of dislocations in bodies with microstructure. *J. Elasticity*, 70:237–254, 2003.

M. Epstein and M. Elżanowski. A model of the evolution of a two–dimensional defective structure. *J. Elasticity*, 70:255–265, 2003.

M. Epstein and G.A. Maugin. The energy–momentum tensor and material uniformity in finite elasticity. *Acta Mech.*, 83:127–133, 1990.

M. Epstein and G.A. Maugin. On the geometrical material structure of anelasticity. *Acta Mech.*, 115: 119–131, 1996.

M. Epstein and G.A. Maugin. Thermomechanics of volumetric growth in uniform bodies. *Int. J. Plasticity*, 16:951–978, 2000.

J.L. Ericksen. Tensor fields. In S. Flügge, editor, *Encyclopedia of Physics*, volume III/1, pages 794–858. Springer, 1960.

J.L. Ericksen. Special topics in elastostatics. In C.-S. Yih, editor, *Advances in Applied Mechanics*, volume 17, pages 189–244. Academic Press, 1977.

J.L. Ericksen. Remarks concerning forces on line defects. *Z. angew. Math. Phys.*, 46:S247–S271, 1995.

J.L. Ericksen. *Introduction to the Thermodynamics of Solids*, volume 131 of *Applied Mathematical Science*. Springer, revised edition, 1998a.

J.L. Ericksen. On nonlinear elasticity theory for crystal defects. *Int. J. Plasticity*, 14:9–24, 1998b.

A.C. Eringen. *Nonlinear Theory of Continuous Media*. Series in Engineering Science. McGraw–Hill, 1962.

A.C. Eringen. Basic Principles – Deformation and Motion. In A.C. Eringen, editor, *Continuum Physics*, volume II – Continuum Mechanics of Single–Substance Bodies, pages 3–67. Academic Press, 1971a.

A.C. Eringen. Tensor Analysis. In A.C. Eringen, editor, *Continuum Physics*, volume I – Mathematics, pages 1–155. Academic Press, 1971b.

A.C. Eringen. *Nonlocal Continuum Field Theories*. Springer, 2002.

J.D. Eshelby. The force on an elastic singulatity. *Phil. Trans. Roy. Soc. London*, 244:87–112, 1951.

J.D. Eshelby. The continuum theory of lattice defect. In F. Seitz and D. Turnbull, editors, *Progess in Solid State Physics*, volume 3, pages 79–144. Academic Press, 1956.

L.P. Evers, W.A.M. Brekelmans, and M.G.D. Geers. Non–loacal plasticity model with intrinsic SSD and GND effects. *J. Mech. Phys. Solids*, 52:2379–2401, 2004a.

L.P. Evers, W.A.M. Brekelmans, and M.G.D. Geers. Scale dependent crystal plasticity framework with dislocation density and grain boundary effects. *Int. J. Solids Struct.*, 41:5209–5230, 2004b.

K. Farahani and R. Naghdabadi. Conjugate stresses of the Seth–Hill strain tensors. *Int. J. Solids Struct.*, 37:5247–5255, 2000.

K. Farahani and R. Naghdabadi. Basis free relations for the conjugate stresses of the strains based on the right stretch tensor. *Int. J. Solids Struct.*, 40:5887–5900, 2003.

W. Fellin and A. Ostermann. Consistent tangent operators for constitutive rate equations. *Int. J. Numer. Anal. Meth. Geomech.*, 26:1213–1233, 2002.

L.B. Freund. *Dynamic Fracture Mechanics*. Cambridge Monographs on Mechanics and Applied Mathematics. Cambridge, 1990.

Y.C. Fung. *Biomechanics: Mechanical Properties of Living Tissues*. Springer, 2nd edition, 1993.

Y.C. Fung and P. Tong. *Classical and Computational Solid Mechanics*, volume 1 of *Advanced Series in Engineering Science*. World Scientific, 2001.

T.C. Gasser and G.A. Holzapfel. A rate–independent elastoplastic constitutive model for biological fiber–reinforced composites at finite strains: continuum basis, algorithmic formulation and finite element implementation. *Comput. Mech.*, 29:340–360, 2002.

E. Giusti. *Direct Methods in the Calculus of Variations*. World Scientific, 2003.

J.D. Goddard and K. Ledniczky. On the spectral representation of stretch and rotation. *J. Elasticity*, 47:255–259, 1997.

S. Govindjee and A. Mihalic. Computational methods for inverse finite elastostatics. *Comput. Methods Appl. Mech. Engrg.*, 136:47–57, 1996.

S. Govindjee and A. Mihalic. Computational methods for inverse deformations in quasi–incompressible finite elasticity. *Int. J. Numer. Methods Engng.*, 43:821–838, 1998.

S. Govindjee and S. Reese. A presentation and comparison of two large strain deformation visoelasticity models. *ASME J. Eng. Mat. Tech.*, 119:251–255, 1997.

A.E. Green and J.E. Adkins. *Large Elastic Deformations*. Oxford University Press, 2nd edition, 1970.

A.E. Green and P.M. Naghdi. A general theory of an elastic–plastic continuum. *Arch. Rational Mech. Anal.*, 18:251–281, 1965.

A.E. Green, R.S. Rivlin, and R.T. Shield. General theory of small elastic deformations superposed on finite elastic deformations. *Proc. Roy. Soc. London A*, 211:128–154, 1952.

S.R. de Groot. *Thermodynamics of Irreversible Processes*. North Holland, 1961.

D. Gross, S. Kolling, R. Müller, and I. Schmidt. Configurational forces and their application in solid mechanics. *Euro. J. Mech. A/Solids*, 22:669–692, 2003.

D. Guansuo, R. Qingwen, and S. Zhujiang. Conjugate stresses to Seth's strain class. *Mech. Res. Comm.*, 27(5):539–542, 2000.

S. Guido and R.T. Tranquillo. A methodology for the systematic and quantitative study of cell contact guidance in oriented collagen gels – Correlation of fibroblast orientation and gel birefringence. *J. Cell Sci.*, 105:317–331, 1993.

Z.-H. Guo and C.S. Man. Conjugate stress and tensor equation $\sum_{r=1}^{m} \mathrm{U}^{m-r}\,\mathrm{X}\,\mathrm{U}^{r-1}=\mathrm{C}$. *Int. J. Solids Struct.*, 29(16):2063–2076, 1992.

M.E. Gurtin. The nature of configurational forces. *Arch. Rational Mech. Anal.*, 131:67–100, 1995.

M.E. Gurtin. *Configurational Forces as Basic Concept in Continuum Physics*, volume 137 of *Applied Mathematical Sciences*. Springer, 2000a.

M.E. Gurtin. On the plasticity of single crystals: free energy, microforces, plastic–strain gradients. *J. Mech. Phys. Solids*, 48:989–1036, 2000b.

M.E. Gurtin. A gradient theory of single–crystal viscoplasticity that accounts for geometrically necessary dislocations. *J. Mech. Phys. Solids*, 50(1):5–32, 2002.

M.E. Gurtin. A gradient theory of small–deformation isotropic plasticity that accounts for the Burgers vector and for dissipation due to plastic spin. *J. Mech. Phys. Solids*, 52(11):2545–2568, 2004.

M.E. Gurtin and A. Needleman. Boundary conditions in small–deformation, single–crystal plasticity that account for the Burgers vector. *J. Mech. Phys. Solids*, 53:1–31, 2005.

C.-S. Han, H. Gao, Y. Huang, and W.D. Nix. Mechanism–based strain gradient crystal plasticity – I. Theory, II. Analysis. *J. Mech. Phys. Solids*, 53:1188–1203, 1204–1222, 2005.

A. Hanyga. *Mathematical Theory of Non–Linear Elasticity*. Polish Scientific Publishers – Ellis Horwood, 1985.

T.P. Harrigan and J.J. Hamilton. An analytical and numerical study of the stability of bone remodelling theories: dependence on microstructural stimulus. *J. Biomechanics*, 25(5):477–488, 1992. Corrigendum 26(3):365–366, 1993.

T.P. Harrigan and J.J. Hamilton. Finite element simulation of adaptive bone remodelling: a stability criterion and a time stepping method. *Int. J. Numer. Methods Engng.*, 36:837–854, 1993.

T.P. Harrigan and J.J. Hamilton. Necessary and sufficient conditions for global stability and uniqueness in finite element simulations of adaptive bone remodelling. *Int. J. Solids Struct.*, 31:97–107, 1994.

J. De Hart, G.W.M. Peters, P.J.G. Schreurs, and F.P.T. Baaijens. Collagen fibers reduce stresses and stabilize motion of aortic valve leaflets during systole. *J. Biomechanics*, 37:303–311, 2004.

P. Haupt. *Continuum Mechanics and Theory of Materials*. Advanced Texts in Physics. Springer, 2000.

P. Haupt and Th. Kersten. On the modelling of anisotropic material behaviour in viscoplasticity. *Int. J. Plasticity*, 19:1885–1915, 2003.

P. Haupt, Y.-H. Pao, and K. Hutter. Theory of incremental motion in a body with initial elasto–plastic deformation. *J. Elasticity*, 28:193–221, 1992.

O. Häusler, D. Schick, and Ch. Tsakmakis. Description of plastic anisotropy effects at large deformations. Part II: The case of transverse isotropy. *Int. J. Plasticity*, 20:199–223, 2004.

K.S. Havner. *Finite Plastic Deformation of Crystalline Solids*. Cambridge Monographs on Mechanics and Applied Mathematics. Cambridge, 1992.

R. Hill. On constitutive inequalities for simple materials – I. *J. Mech. Phys. Solids*, 16:229–242, 1968.

R. Hill. Plastic anisotropy and the geometry of yield surfaces in stress space. *J. Mech. Phys. Solids*, 48: 1093–1106, 2000.

G. Himpel, E. Kuhl, A. Menzel, and P. Steinmann. Computational modelling of isotropic multiplicative growth. *Comput. Model. Eng. Sci.*, 8(2):119–134, 2005.

A. Hoger. The stress conjugate to logarithmic strain. *Int. J. Solids Struct.*, 23(12):1645–1656, 1987.

A. Hoger. The constitutive equation for finite deformations of a transversely isotropic hyperelastic material with residual stress. *J. Elasticity*, 33:107–118, 1993a.

A. Hoger. The dependence of the elasticity tensor on residual stress. *J. Elasticity*, 33:145–165, 1993b.

A. Hoger. The elasticity tensors of a residually stressed material. *J. Elasticity*, 31:219–237, 1993c.

A. Hoger. The elasticity tensor of a transversely isotropic hyperelastic material with residual stress. *J. Elasticity*, 42:115–132, 1996.

A. Hoger. Virtual configurations and constitutive equations for residually stressed bodies with material symmetry. *J. Elasticity*, 48:125–144, 1997.

A. Hoger, T.J. Van Dyke, and V.A. Lubarda. Symmetrization of the growth deformation and velocity gradients in residually stressed biomaterials. *Z. angew. Math. Phys.*, 55:848–860, 2004.

G.A. Holzapfel. Biomechanics of soft tissue. In J. Lemaitre, editor, *The Handbook of Materials Behavior Models*, volume 3, Multiphysics Behaviors, chapter 10, Composite Media, Biomaterials, pages 1049–1063. Academic Press, 2001.

G.A. Holzapfel and T.C. Gasser. A viscoelastic model for fibre–reinforced composites at finite strains: Continuum basis, computational aspects and applications. *Comput. Methods Appl. Mech. Engrg.*, 190:4379–4403, 2001.

G.A. Holzapfel, T.C. Gasser, and M. Stadler. A structural model for the viscoelastic behavior of arterial walls: Continuum formulation and finite element analysis. *Euro. J. Mech. A/Solids*, 21:441–463, 2002a.

G.A. Holzapfel and R.W. Ogden, editors. *Biomechanics of Soft Tissue in Cardiovascular Systems*. Number 441 in CISM Courses and Lectures. Springer, 2003.

G.A. Holzapfel and R.W. Ogden, editors. *Mechanics of Biological Tissue*. Springer, 2006.

G.A. Holzapfel, M. Stadler, and T.C. Gasser. Changes in the mechanical environment of stenotic arteries during interaction with stents: computational assessment of parametric stent designs. *ASME J. Biomech. Eng.*, 127:166–180, 2005.

G.A. Holzapfel, M. Stadler, and C.A.J. Schulze-Bauer. A layer–specific three–dimensional model for the simulation of balloon angioplasty using magnetic resonance imaging and mechanical testing. *Ann. Biomed. Eng.*, 30:753–767, 2002b.

Z. Huang. The equilibrium equations and constitutive equations of the growing deformable body in the framework of continuum theory. *Int. J. Non–Linear Mechanics*, 39:951–962, 2004.

R. Huiskes and E.Y.S. Chao. A survey of finite element analysis in orthopedic biomechanics: the first decade. *J. Biomechanics*, 16(6):385–409, 1983.

D. Hull and D.J. Bacon. *Introduction to Dislocations*. Elsevier, 4th edition, 2001.

J.D. Humphrey. Stress, strain, and mechanotransduction in cells. *ASME J. Biomech. Eng.*, 123:638–641, 2001.

J.D. Humphrey. *Cardiovascular Solid Mechanics. Cells, Tissues, and Organs*. Springer, 2002.

J.D. Humphrey and K.R. Rajagopal. A constrained mixture model for growth and remodeling of soft tissues. *Math. Models Meth. Appl. Sci.*, 12:407–430, 2002.

R. Husikes, H. Weinans, H.J. Grootenboer, M. Dalastra, B. Fudala, and T.J. Sloof. Adaptive bone–remodeling theory applied to prothetic–design analysis. *J. Biomechanics*, 20(11/12):1135–1150, 1987.

D. Ieşan. *Prestressed bodies*, volume 195 of *Pitman Research Notes in Mathematics Series*. Longman, 1989.

S. Imatani and G.A. Maugin. A constitutive model for material growth and its application to three–dimensional finite element analysis. *Mech. Res. Comm.*, 29:477–483, 2002.

V.L. Indenbom and A.N. Orlov. Physical foundations of dislocation theory. In E. Kröner, editor, *Mechanics of Generalized Continua*, pages 166–179. IUTAM, Springer, 1968.

Y. Ivanisenko, W. Lojkowski, R.Z. Valiev, and H.-J. Fecht. The mechanism of formation of nanostructure and dissolution of cementite in a pearlitic steel during high pressure. *Acta Mater.*, 51:5555–5570, 2003.

C.R. Jacobs, M.E. Levenston, G.S. Beaupré, J.C. Simo, and D.R. Carter. Numerical instabilities in bone remodelling simultaneous: The advantages of a node–based finite element approach. *J. Biomechanics*, 28(4):449–459, 1995.

C.R. Jacobs, J.C. Simo, G.S. Beaupré, and D.R. Carter. Adaptive bone remodelling incorporationg simultaneous density and anisotropy considerations. *J. Biomechanics*, 30(6):603–613, 1997.

G. Johansson, M. Ekh, and K. Runesson. Computational modeling of inelastic large ratcheting strains. *Int. J. Plasticity*, 20:955–980, 2005a.

G. Johansson, A. Menzel, and K. Runesson. Modeling of anisotropic inelasticity in pearlitic steel at large strains due to deformation induced substructure evolution. *Euro. J. Mech. A/Solids*, 24(6): 899–918, 2005b.

M. Johansson, R. Mahnken, and K. Runesson. Efficient integration technique for generalized viscoplasticity coupled to damage. *Int. J. Numer. Methods Engng.*, 44:1727–1747, 1999.

D.H. Kaelble. *Physical Chemistry of Adhesion*. Wiley, 1971.

M. Kaliske. A formulation of elasticity and viscoelasticity for fibre reinforced material at small and finite strains. *Comput. Methods Appl. Mech. Engrg.*, 185:225–243, 2000.

A. Katchalsky and P.F. Curran. *Nonequilibrium Thermodynamics in Biophysics*, volume 1 of *Harvard Books in Biophysics*. Havard University Press, 1965.

P.I. Kattan and G.Z. Voyiadjis. A coupled theory of damage mechanics and finite strain elasto–plasticity – I. Damage and elastic deformations. *Int. J. Engng. Sci.*, 28(5):421–435, 1990.

H. Kauderer. Über ein nichtlineares Elastizitätsgesetz. *Ingenieur–Archiv*, XVII:450–480, 1949.

H. Kauderer. *Nichtlineare Mechanik*. Springer, 1958.

J. Kestin. *A Course in Thermodynamics*. Blaisdell, 1966.

R. Kienzler and G. Hermann. *Mechanics in Material Space – with Application to Defect and Fracture Mechanics*. Springer, 2000.

A.J. Kinloch, C.C. Lau, and J.G. Williams. The peeling of flexible laminates. *Int. J. Fracture*, 66: 45–70, 1994.

E. Kirchner and B. Simeon. A higher–order integration method for viscoplasticity. *Comput. Methods Appl. Mech. Engrg.*, 175:1–18, 1999.

B. Kleuter, A. Menzel, and P. Steinmann. Generalized parameter identification for finite viscoelasticity. *Comput. Methods Appl. Mech. Engrg.*, 196:3315–3334, 2007.

S.M. Klisch, T.J. Van Dyke, and A. Hoger. A theory of volumetric growth for compressible elastic biological materials. *Math. Mech. Solids*, 6:551–575, 2001.

S.M. Klisch and A. Hoger. Volumetric growth of thermoelastic materials and mixtures. *Math. Mech. Solids*, 8:377–402, 2003.

U.F. Kocks, C.N. Tomé, and H.-R. Wenk, editors. *Texture and Anisotropy – Preferred Orientations in Polycrystals and their Effect on Material Properties*. Cambridge University Press, 2000.

T.P. Kole, Y. Tseng, I. Jiang, J.L. Katz, and D. Witz. Intracellular mechanics of migrating fibroblasts. *Mol. Biol. Cell*, 16:328–338, 2005.

K. Kondo. On the geometrical and physical foundations of the theory of yielding. In *Proc. 2. Japan Nat. Congress Appl. Mech.*, pages 41–47, 1952.

A.M. Kosevich. Crystal dislocations and the theory of elasticity. In F.R.N. Nabarro, editor, *Dislocations in Solids (The Elastic Theory)*, volume 1, pages 33–141. North–Holland Publishing Company, 1979.

E. Kröner. *Kontinuumstheorie der Versetzungen und Eigenspannungen*, volume 5 of *Erg. Angew. Math.* Springer, 1958.

E. Kröner. Allgemeine Kontinuumstheorie der Versetzungen und Eigenspannungen. *Arch. Rational Mech. Anal.*, 4:273–334, 1960.

E. Kröner. Continuum theory of defects. In *Physics of Defects*, pages 215–315. North–Holland, 1981.

E. Kröner and A. Seeger. Nichtlineare Elastizitätstheorie der Versetzungen und Eigenspannungen. *Arch. Rational Mech. Anal.*, 3:97–119, 1959.

N. Krstin, U. Nackenhorst, and R. Lammering. Zur konstitutiven Beschreibung des anisotropen beanspruchungsadaptiven Knochenumbaus. *Technische Mechanik*, 20(1):31–40, 2000.

E. Kuhl, A. Menzel, and K. Garikipati. On the convexity of transversely isotropic chain network models. *Phil. Mag.*, 86(21–22):3241–3258, 2006.

E. Kuhl, A. Menzel, and P. Steinmann. Computational modeling of growth – A critical review, a classification of concepts and two new consistent approaches. *Comput. Mech.*, 32:71–88, 2003.

E. Kuhl and P. Steinmann. Mass – and volume specific views on thermodynamics for open systems. *Proc. Roy. Soc. London A*, 459:2547–2568, 2003a.

E. Kuhl and P. Steinmann. Theory and numerics of geometrically nonlinear open system mechanics. *Int. J. Numer. Methods Engng.*, 58:1593–1615, 2003b.

H. Lämmer and Ch. Tsakmakis. Discussion of coupled elastoplasticity and damage constitutive equations for small and finite deformations. *Int. J. Plasticity*, 16:495–523, 2000.

K.C. Le and H. Stumpf. Strain measures, integrability condition and frame indifference in the theory of oriented media. *Int. J. Solids Struct.*, 35(9):783–798, 1998.

F.A. Leckie and E.T. Onat. Tensorial nature of damage measuring internal variables. In J. Hult and J. Lemaitre, editors, *Physical Non–Linearities in Structural Analysis*, pages 140–155. IUTAM Symposium Senlis/France 1980, Springer, 1981.

E. Lee. Elastic–plastic deformation at finite strains. *ASME J. Appl. Mech.*, 36:1–6, 1969.

J. Lemaitre and J.-L. Chaboche. *Mechanics of Solid Materials*. Cambridge, 2nd edition, 1998.

T. Liebe, A. Menzel, and P. Steinmann. Theory and numerics of a thermodynamically consistent framework for geometrically non–linear gradient plasticity. *Int. J. Engng. Sci.*, 41:1603–1629, 2003.

W.K. Liu, E.G. Karpov, and H.S. Park. *Nano Mechanics and Materials – Theory, Multiscale Methods and Applications*. Wiley, 2006.

A.S. Lodge. The compatibility conditions for large strains. *Quart. J. Mech. Appl. Math.*, IV(1):85–93, 1951.

A.S. Lodge. *Elastic Liquids – An Introductury Vector Treatment of Finite–Strain Polymer Rheology*. Academic Press, 1964.

A.S. Lodge. *Body Tensor Fields in Continuum Mechanics – With Application to Polymer Rheology*. Academic Press, 1974.

J. Lu. Exact expansion of arbitrary tensor functions $\mathbf{F}(\mathbf{A})$ and their derivatives. *Int. J. Solids Struct.*, 41:337–349, 2004.

J. Lu and P. Papadopoulos. A covariant constitutive description of anisotropic non–linear elasicity. *Z. angew. Math. Phys.*, 51:204–217, 2000.

V.A. Lubarda. Duality in constitutive formulation of finite–strain elastoplasticity based on $\mathrm{F}=\mathrm{F}_e\,\mathrm{F}_p$ and $\mathrm{F}=\mathrm{F}^p\,\mathrm{F}^e$ decompositions. *Int. J. Plasticity*, 15:1277–1290, 1999.

V.A. Lubarda. *Elastoplasticity Theory*. Mechanical Engineering series. CRC Press, 2002.

V.A. Lubarda. Constitutive theories based on the multiplicative decomposition of deformation gradient: Thermoelasticity, elastoplasticity, and biomechanics. *ASME Appl. Mech. Rev.*, 57(2):95–108, 2004.

V.A. Lubarda and A. Hoger. On the mechanics of solids with a growing mass. *Int. J. Solids Struct.*, 39: 4627–4664, 2002.

J. Lubliner. *Plasticity Theory*. MacMillan Publishing Company, 1990.

G. Maciejewski and P. Dłużewski. Nonlinear finite element calculations of residual stresses in dislocated crystals. *Comput. Mater. Sci.*, 30:44–49, 2004.

R. Mahnken. A comprehensive study of a multiplicative elastoplasticity model coupled to damage including parameter identification. *Comput. Struct.*, 74:179–200, 2000.

A.M. Malek and S. Izumo. Mechanism of endothelia cell shape and cytoskeletal remodeling in response to fluid shear stress. *J. Cell Sci.*, 109:713–726, 1996.

C.-S. Man. Remarks on the continuity of the scalar coefficients in the representation $\mathrm{H(A)}=\alpha\,\mathrm{I}+\beta\,\mathrm{A}+\gamma\,\mathrm{A}^2$ for isotropic tensor functions. *J. Elasticity*, 34:229–238, 1994.

J. Mandel. Thermodynamics and plasticity. In J.J. Delgado Domingos, M.N.R. Nina, and J.H. Whitelaw, editors, *Foundations of Continuum Thermodynamics*, pages 283–304. MacMillan, 1974.

X. Markenscoff and A. Gupta, editors. *Collected Works of J.D. Eshelby – The Mechanics of Defects and Inhomogeneities*, volume 133 of *Solid Mechanics and its Applications*. Springer, 2006.

J.P. Marquez. Fourier analysis and automated measurement of cell and fiber angular orientation distributions. *Int. J. Solids Struct.*, 43(21):6413–6423, 2006.

J.E. Marsden and T.J.R. Hughes. *Mathematical Foundations of Elasticity*. Dover, 1994.

L.C. Martins. The representation theorem for linear, isotropic material revisited. *J. Elasticity*, 54: 89–92, 1999.

G.A. Maugin. *The Thermomechanics of Plasticity and Fracture*. Cambridge Texts in Applied Mathematics. Cambridge University Press, 1992.

G.A. Maugin. *Material Inhomogeneities in Elasticity*, volume 3 of *Applied Mathematics and Mathematical Computation*. Chapman & Hall, 1993.

G.A. Maugin. Eshelby stress in elastoplasticity and ductile fracture. *Int. J. Plasticity*, 10(4):393–408, 1994.

G.A. Maugin. Material forces: Concepts and applications. *ASME Appl. Mech. Rev.*, 48(5):213–245, 1995.

G.A. Maugin. *The Thermodynamics of Nonlinear Irreversible Behaviors*, volume 27 of *World Scientific Series on Nonlinear Science: Series A*. World Scientific Publishing, 1999.

G.A. Maugin. Pseudo–plasticity and pseudo–inhomogeneity effects in materials mechanics. *J. Elasticity*, 71:81–103, 2003.

G.A. Maugin. Remarks on Eshelbian thermomechanics of materials. *Mech. Res. Comm.*, 29:537–542, 2006.

G.A. Maugin and M. Epstein. Geometrical material structure of elastoplasticity. *Int. J. Plasticity*, 14 (1–3):109–115, 1998.

G.A. Maugin and S. Imatani. Material growth in solid–like materials. In C. Miehe, editor, *Computational Mechanics of Solid Materials at Large Strains*, volume 108 of *Solid Mechanics and its Applications*, pages 221–234. IUTAM, Kluwer, 2003.

Á. Meggyes. Multiple decomposition in finite deformation theory. *Acta Mech.*, 146:169–182, 2001.

M.M. Mehrabadi and S.C. Cowin. Eigentensors of linear anisotropic elastic materials. *Quart. J. Mech. Appl. Math.*, 43(1):15–41, 1990.

A. Menzel. Modelling of anisotropic growth in biological tissues – A new approach and computational aspects. *Biomech. Model. Mechanobio.*, 3(3):147–171, 2005a.

A. Menzel. Relations between material, intermediate and spatial generalised strain measures for anisotropic multiplicative inelasticity. *Acta Mech.*, 182:231–252, 2005b.

A. Menzel. Adaptation of biological tissues – a fibre reorientation model for orthotropic multiplicative growth. In C.A. Mota Soares et al., editor, *III European Conference on Computational Mechanics*, 2006a.

A. Menzel. Anisotropic remodelling of biological tissues. In G.A. Holzapfel and R.W. Ogden, editors, *Mechanics of Biological Tissue*, pages 91–104. Springer, 2006b.

A. Menzel. A fibre reorientation model for orthotropic multiplicative growth – Configurational driving stresses, kinematics–based reorientation, and algorithmic aspects. *Biomech. Model. Mechanobio.*, 6 (5):303–320, 2007.

A. Menzel, I. Carol, and P. Steinmann. A framework for (visco)plasticity coupled to anisotropic damage. In *Proceedings of COMPLAS VII*, Barcelona, 2003.

A. Menzel, R. Denzer, and P. Steinmann. On the comparison of two approaches to compute material forces for inelastic materials. Application to single–slip crystal–plasticity. *Comput. Methods Appl. Mech. Engrg.*, 193(48–51):5411–5428, 2004.

A. Menzel, R. Denzer, and P. Steinmann. Material forces in computational single–slip crystal–plasticity. *Comput. Mater. Sci.*, 32(3–4):446–454, 2005a.

A. Menzel, M. Ekh, K. Runesson, and P. Steinmann. A framework for multiplicative elastoplasticity with kinematic hardening coupled to anisotropic damage. *Int. J. Plasticity*, 21:397–434, 2005b.

A. Menzel, M. Ekh, P. Steinmann, and K. Runesson. Anisotropic damage coupled to plasticity: Modelling based on the effective configuration concept. *Int. J. Numer. Methods Engng.*, 54(10):1409–1430, 2002.

A. Menzel and P. Steinmann. On the formulation of higher gradient single and polycrystal plasticity. *J. Phys. IV France*, 8:239–247, 1998.

A. Menzel and P. Steinmann. On the continuum formulation of higher gradient plasticity for single and polycrystals. *J. Mech. Phys. Solids*, 48(8):1777–1796, 2000. Erratum 49(5):1179–1180, 2001.

A. Menzel and P. Steinmann. On the comparison of two strategies to formulate orthotropic hyperelasticity. *J. Elasticity*, 62:171–201, 2001a.

A. Menzel and P. Steinmann. A theoretical and computational setting for anisotropic continuum damage mechanics at large strains. *Int. J. Solids Struct.*, 38(52):9505–9523, 2001b.

A. Menzel and P. Steinmann. Formulation and computation of geometrically nonlinear anisotropic inelasticity. In C. Miehe, editor, *Computational Mechanics of Solid Materials at Large Strains*, volume 108 of *Solid Mechanics and its Applications*, pages 181–190. IUTAM, Kluwer, 2003a.

A. Menzel and P. Steinmann. Geometrically nonlinear anisotropic inelasticity based on fictitious configurations: Application to the coupling of continuum damage and multiplicative elasto–plasticity. *Int. J. Numer. Methods Engng.*, 56:2233–2266, 2003b.

A. Menzel and P. Steinmann. On the spatial formulation of anisotropic multiplicative elasto–plasticity. *Comput. Methods Appl. Mech. Engrg.*, 192:3431–3470, 2003c.

A. Menzel and P. Steinmann. A view on anisotropic finite hyper–elasticity. *Euro. J. Mech. A/Solids*, 22:71–87, 2003d.

A. Menzel and P. Steinmann. A note on material forces in finite inelasticity. *Arch. Appl. Mech.*, 74: 800–807, 2005.

A. Menzel and P. Steinmann. On configurational forces in multiplicative elastoplasticity. *Int. J. Solids Struct.*, 44(13):4442–4471, 2007.

J. Merodio and R.W. Ogden. Instabilities and loss of ellipticity in fiber–reinforced compressible non–linearly elastic solids under plane deformation. *Int. J. Solids Struct.*, 40:4707–4727, 2003.

C. Miehe. Computation of isotropic tensor functions. *Commun. Numer. Methods Engng.*, 9:889–896, 1993.

C. Miehe. A theory of large–strain isotropic thermoplasticity based on metric transformation tensors. *Arch. Appl. Mech.*, 66:45–64, 1995.

C. Miehe. Exponential map algorithm for stress updates in anisotropic multiplicative elastoplasticity for single crystals. *Int. J. Numer. Methods Engng.*, 39:3367–3390, 1996a.

C. Miehe. Multisurface thermoplasticity for single crystals at large strains in terms of Eulerian vector updates. *Int. J. Solids Struct.*, 33(20–22):3103–3130, 1996b.

C. Miehe. Numerical computation of algorithmic (consistent) tangent moduli in large–strain computational inelasticity. *Comput. Methods Appl. Mech. Engrg.*, 134:223–240, 1996c.

C. Miehe. A constitutive frame of elastoplasticity at large strains based on the notion of a plastic metric. *Int. J. Solids Struct.*, 35(30):3859–3897, 1998.

C. Miehe, N. Apel, and M. Lambrecht. Anisotropic additive plasticity in the logarithmic strain space: modular kinematic formulation and implementation based on incremental minimization principles for standard materials. *Comput. Methods Appl. Mech. Engrg.*, 191:5383–5425, 2002.

C. Miehe and M. Lambrecht. Algorithms for computation of stresses and elasticity moduli in terms of Seth–Hill's family of generalized strain tensors. *Commun. Numer. Methods Engng.*, 17:337–353, 2001.

C. Miehe and J. Schröder. A comparative study of stress update algorithms for rate–independent and rate–dependent crystal plasticity. *Int. J. Numer. Methods Engng.*, 50:273–298, 2001.

C. Miehe and E. Stein. A canonical model of multiplicative elasto–plasticity: Formulation and aspects of the numerical implementation. *Euro. J. Mech. A/Solids*, 11:25–43, 1992. Special issue.

S. Murakami. Mechanical modeling of material damage. *ASME J. Appl. Mech.*, 55:280–286, 1988.

F.D. Murnaghan. Finite deformations of an elastic solid. *Am. J. Math.*, 59:235–260, 1937.

F.D. Murnaghan. *Finite Deformations of an Elastic Solid*. Applied Mathematics Series. Wiley, 1951.

J.D. Murray. *Mathematical Biology II: Spatial Models and Biomedical Applications*, volume 18 of *Interdisciplinary Applied Mathematics*. Springer, 3rd edition, 2002.

U. Nackenhorst. Numerical simulation of stress stimulated bone remodelling. *Technische Mechanik*, 17(1):31–40, 1996.

P.M. Naghdi. A critical review of the state of finite plasticity. *Z. angew. Math. Phys.*, 41:315–394, 1990.

S. Nemat-Nasser. *Plasticity – A Treatise on Finite Deformation of Heterogeneous Inelastic Materials*. Cambridge Monographs on Mechanics. Cambridge, 2004.

E. Nembach. *Particle Strengthening of Metals and Alloys*. Wiley, 1997.

T.D. Nguyen, S. Govindjee, P.A. Klein, and H. Gao. A material force method for inelastic fracture mechanics. *J. Mech. Phys. Solids*, 53:91–121, 2005.

D.W. Nicholson. On stresses conjugate to Eulerian strains. *Acta Mech.*, 165:87–98, 2003.

W. Noll. A mathematical theory of the mechanical behavior of continuous media. *Arch. Rational Mech. Anal.*, 2:197–226, 1958.

W. Noll. Materially uniform simple bodies with inhomogeneities. *Arch. Rational Mech. Anal.*, 27: 1–32, 1967.

W. Noll. A new mathematical theory of simple materials. *Arch. Rational Mech. Anal.*, 48:1–50, 1972.

J.T. Oden. *Finite Elements of Nonlinear Continua*. Advanced Engineering Series. McGraw–Hill, 1972.

R.W. Ogden. *Non–Linear Elastic Deformations*. Dover, 1997.

R.W. Ogden. Elements of the theory of finite elasticity. In Y.B. Fu and R.W. Ogden, editors, *Nonlinear Elasticity: Theory and Applications*, number 283 in London Mathematical Society Lecture Notes Series, pages 1–57. Cambridge, 2001a.

R.W. Ogden. Non–smooth changes in elastic material properties under finite deformation. In D.Y. Gao, R.W. Ogden, and G.E. Stavroulakis, editors, *Nonsmooth/Nonconvex Mechanics: Modeling, Analysis and Numerical Methods*, pages 277–299. Kluwer, 2001b.

S. Oller, S. Botello, J. Miquel, and E. Oñate. An anisotropic elastoplastic model based on an isotropic formulation. *Engng. Comput.*, 12:245–262, 1995.

P.J. Olver. *Application of Lie Groups to Differential Equations*, volume 107 of *Graduate Texts in Mathematics*. Springer, 2nd edition, 1993.

O.M. O'Reilly. A material momentum balance law for rods. *J. Elasticity*, 86:155–172, 2007.

P. Papadopoulos and J. Lu. A general framework for the numerical solution of problems in finite elasto–plasticity. *Comput. Methods Appl. Mech. Engrg.*, 159:1–18, 1998.

P. Papadopoulos and J. Lu. On the formulation and numerical solution of problems in anisotropic finite plasticity. *Comput. Methods Appl. Mech. Engrg.*, 190:4889–4910, 2001.

P. Papadopoulos and R.L. Taylor. On the application of multi–step integration methods to infinitesimal elastoplasticity. *Int. J. Numer. Methods Engng.*, 37:3169–3184, 1994.

J.E. Paulun and R.B. Ręcherski. On the relation for plastic spin. *Arch. Appl. Mech.*, 62:376–385, 1992.

M.O. Peach and J.S. Koehler. The forces exerted on dislocations and the stress field produced by them. *Phys. Rev.*, 80:436–439, 1950.

N. Pede, P. Podio-Guidugli, and G. Tomassetti. Balancing the force that drives the peeling of an adhesive tape. *Nuovo Cimento – Societa Italiana di Fisica Sezione B*, 121(5):531–543, 2006.

P. Pedersen. On optimal orientation of orthotropic materials. *Structural Optimization*, 1:101–106, 1989.

A. Pérez-Foguet, A. Rodriguez-Ferran, and A. Huerta. Numerical differentiation for local and global tangent operators in computational plasticity. *Comput. Methods Appl. Mech. Engrg.*, 189:277–296, 2000a.

A. Pérez-Foguet, A. Rodriguez-Ferran, and A. Huerta. Numerical differentiation for non–trivial consistent tangent matrices: An application to the MRS–Lade model. *Int. J. Numer. Methods Engng.*, 48:159–184, 2000b.

K.A. Pericak-Spector, J. Silvaloganathan, and S.J. Spector. The representation theorem for linear, isotropic tensor functions in even dimensions. *J. Elasticity*, 57:157–164, 1999.

R. Phillips. *Crystals, Defects and Microstructures – Modeling Across Scales*. Cambridge University Press, 2001.

P. Podio-Guidugli. A Primer in Elasticity. *J. Elasticity*, 58:1–104, 2000. Kluwer.

P. Podio-Guidugli. Configurational balances via variational arguments. *Interfaces and Free Boundaries*, 3:223–232, 2001.

P. Podio-Guidugli. Configurational forces: are they needed? *Mech. Res. Comm.*, 29:513–519, 2002.

E. Pucci and G. Saccomandi. On universal relations in continuum mechanics. *Continuum Mech. Thermodyn.*, 9:61–72, 1997.

S. Quiligotti. On bulk growth mechanics of solid–fluid mixtures: kinematics and invariance requirements. *Theor. Appl. Mech.*, 28–29:277–288, 2002.

I.J. Rao, J.D. Humphrey, and K.R. Rajagopal. Biological growth and remodelling: a uniaxial example with possible application to tendons and ligaments. *Comput. Model. Eng. Sci.*, 4(3–4):439–455, 2003.

M. Rappaz, M. Bellet, and M. Deville. *Numerical Modeling in Material Science and Engineering*, volume 32 of *Springer Series in Computational Mathematics*. Springer, 2003.

S. Reese, T. Raible, and P. Wriggers. Finite element modelling of orthotropic material behaviour in pneumatic membranes. *Int. J. Solids Struct.*, 38(52):9525–9544, 2001.

H. Richter. Zur Elastizitätstheorie endlicher Verformungen. *Math. Nachr.*, 8:65–73, 1952.

R.S. Rivlin and A.G. Thomas. Rupture of rubber. I. Characteristic energy for tearing. *J. Polymer Sci.*, 10(3):291–318, 1953.

E.K. Rodriguez, A. Hoger, and D. McCulloch. Stress–dependent finite growth in soft elastic tissues. *J. Biomechanics*, 27(4):455–467, 1994.

D. Rogula. Forces in material space. *Acta Mech.*, 29:705–713, 1977.

D. Rogula, editor. *Nonlocal Theory of Material Media*. Number 268 in CISM Courses and Lectures. Springer, 1982.

L. Rosati and N. Valoroso. Evaluation of conjugate stresses to Seth's strain tensors. *Technische Mechanik*, 22(1):26–35, 2002.

J. Rychlewski. Unconventional approach to linear elasticity. *Arch. Rat. Mech.*, 47(2):147–171, 1995.

G. Saccomandi. Universal results in finite elasticity. In Y.B. Fu and R.W. Ogden, editors, *Nonlinear Elasticity: Theory and Applications*, number 283 in London Mathematical Society Lecture Notes Series, pages 97–134. Cambridge, 2001.

G. Saccomandi and M.F. Beatty. Universal relations for fibre–reinforced elastic materials. *Math. Mech. Solids*, 7:95–110, 2002.

F.B. Sachse. *Computational Cardiology – Modeling of Anatomy, Electrophysiology, and Mechanics*, volume 2966 of *Lecture Notes in Computer Science*. Springer, 2004.

R.J. Sanford. *Principles of Fracture Mechanics*. Pearson, 2003.

C. Sansour. On the dual variable of the logarithmic strain tensor, the dual variable of the Cauchy stress tensor, and related issues. *Int. J. Solids Struct.*, 38:9221–9232, 2001.

K.N. Sawyers and R.S. Rivlin. The trousers test for rupture. *Engng. Fract. Mech.*, 6:557–562, 1974.

M. Schmidt-Baldassari. Numerical concepts for rate–independent single crystal plasticity. *Comput. Methods Appl. Mech. Engrg.*, 192:1261–1280, 2003.

D.J. Schneck. *Engineering Principles of Physiological Function*. New York University Biomedical Engineering Series. New York University Press, 1990.

D.J. Schneck. *Mechanics of Muscle*. New York University Biomedical Engineering Series. New York University Press, 2nd edition, 1992.

J.A. Schouten. *Tensor Analysis for Physicists*. Dover, 2nd edition, 1989.

J. Schröder, F. Gruttmann, and J. Löblein. A simple orthotropic finite elasto–plasticity model based on generalized stress–strain measures. *Comput. Mech.*, 30:48–64, 2002.

J. Schröder and P. Neff. Invariant formulation of hyperelastic transverse isotropy based on polyconvex free energy functions. *Int. J. Solids Struct.*, 40:401–445, 2003.

A. Seeger. Theorie der Gitterfehlstellen. In S. Flügge, editor, *Encyclopedia of Physics*, volume VII/1, pages 383–665. Springer, 1955.

B.R. Seth. Generalized strain measure with application to physical problems. In M. Reiner and D. Abir, editors, *Second–Order Effects in Elasticity, Plasticity and Fluid Dynamics*, pages 162–172, 1964.

C. Sgarra and M. Vianello. Rotations which make strain and stress coaxial. *J. Elasticity*, 47:217–224, 1997.

F. Sidoroff. Description of anisotropic damage application to elasticity. In J. Hult and J. Lemaitre, editors, *Physical Non–Linearities in Structural Analysis*, pages 237–244, 1981. IUTAM Symposium Senlis/France, 27.–30.05.1980, Springer.

M. Šilhavý. *The Mechanics and Thermomechanics of Continuous Media*. Texts and Monographs in Physics. Springer, 1997.

F.H. Silver, J.W. Freeman, and G.P. Seehra. Collagen self–assembly and the development of tendon mechanical properties. *J. Biomechanics*, 36:1529–1553, 2003.

J.C. Simo. Numerical analysis and simulation of plasticity. In P.G. Ciarlet and J.L. Lions, editors, *Numerical Methods for Solids (Part 3)*, volume VI of *Handbook of Numerical Analysis*, pages 183–499. North–Holland, 1998.

J.C. Simo and F. Armero. Geometrically non–linear enhanced strain mixed methods and the method of incompatible modes. *Int. J. Numer. Methods Engng.*, 33:1413–1449, 1992.

R. Skalar, D.A. Farrow, and A. Hoger. Kinematics of surface growth. *J. Math. Biol.*, 35:869–907, 1997.

R. Skalar, S. Zargaryan, R.K. Jain, P.A. Netti, and A. Hoger. Compatibility and the genesis of residual stress by volumetic growth. *J. Math. Biol.*, 34:889–914, 1996.

A.J.M. Spencer. Theory of Invariants. In A.C. Eringen, editor, *Continuum Physics*, volume I – Mathematics, pages 239–353. Academic Press, 1971.

A.J.M. Spencer, editor. *Continuum Theory of the Mechanics of Fibre–Reinforced Composites*. Number 282 in CISM Courses and Lectures. Springer, 1984.

R.A. Spurrier. Comment on "singularity–free extraction of a quaternion from a direction–cosine matrix". *J. Spacecraft*, 15(4):255, 1978.

P. Steinmann. Views on multiplicative elastoplasticity and the continuum theory of dislocations. *Int. J. Engng. Sci.*, 34(15):1717–1735, 1996.

P. Steinmann. Application of material forces to hyperelastostatic fracture mechanics. I. Continuum mechanical setting. *Int. J. Solids Struct.*, 37:7371–7391, 2000.

P. Steinmann. On spatial and material settings of hyperelastostatic crystal defects. *J. Mech. Phys. Solids*, 50(8):1743–1766, 2002a.

P. Steinmann. On spatial and material settings of thermo–hyperelastodynamics. *J. Elasticity*, 66:109–157, 2002b.

P. Steinmann and G.A. Maugin, editors. *Mechanics of Material Forces*, volume 11 of *Advances in Mechanics and Mathematics*, 2005. Springer.

P. Steinmann, C. Miehe, and E. Stein. Comparison of different finite deformation inelastic damage models within multiplicative elastoplasticity for ductile materials. *Comput. Mech.*, 13:458–474, 1994.

P. Steinmann, C. Miehe, and E. Stein. Fast transient dynamic plane stress analysis of orthotropic Hill-type solids at finite elastoplastic strains. *Int. J. Solids Struct.*, 33:1543–1562, 1996.

S. Sutcliffe. Spectral decomposition of the elasticity tensor. *ASME J. Appl. Mech.*, 59:762–773, 1992.

B. Svendsen. A thermodynamic formulation of finite–deformation elastoplasticity with hardening based on the concept of material isomorphism. *Int. J. Plasticity*, 14(6):473–488, 1998.

B. Svendsen. On the modeling of anisotropic elastic and inelastic material behaviour at large deformation. *Int. J. Solids Struct.*, 38(52):9579–9599, 2001.

B. Svendsen, S. Arndt, D. Klingbeil, and R. Sievert. Hyperelastic models for elastoplasticity with non–linear isotropic and kinematic hardening at large deformation. *Int. J. Solids Struct.*, 35(25): 3363–3389, 1998.

L.A. Taber. Biomechanics of growth, remodelling, and morphogenesis. *ASME Appl. Mech. Rev.*, 48 (8):487–545, 1995.

L.A. Taber and D.W. Eggeres. Theoretical study of stress–modulated growth in the aorta. *J. Theor. Biol.*, 180:343–357, 1996.

L.A. Taber and R. Perucchio. Modeling heart development. *J. Elasticity*, 61:165–197, 2000.

Lord Kelvin (W. Thomson). Elements of a mathematical theory of elasticity. *Phil. Trans. Roy. Soc. London*, 166:481–498, 1856.

J. Torbet and M.-C. Ronzière. Magnetic alignment of collagen during self–assembly. *Biochem. J.*, 219: 1057–1059, 1984.

C. Truesdell. *Continuum Mechanics I: The Mechanical Foundations of Elasticity and Fluid Dynamics*, volume 8 of *International Science Review Series*. Gordon and Beach, 1966.

C. Truesdell. *A First Course in Rational Continuum Mechanics*, volume I General Concepts of *Pure and Applied Mathematics*. Academic Press, 1977.

C. Truesdell and W. Noll. *The Non–Linear Field Theories of Mechanics*. Springer, 3rd edition, 2004. edited by S.S. Antman.

C. Truesdell and R.A. Toupin. The classical field theories. In S. Flügge, editor, *Encyclopedia of Physics*, volume III/1, pages 226–793. Springer, 1960.

Ch. Tsakmakis. Description of plastic anisotropy effects at large deformations. Part I: Restrictions imposed by the second law and the postulate of Il'iushin. *Int. J. Plasticity*, 20:167–198, 2004.

K.C. Valanis and V.P. Panoskaltsis. Material metric, connectivity and dislocations in continua. *Acta Mech.*, 175:77–103, 2005.

M. Vianello. Coaxiality of strain and stress in anisotropic linear elasticity. *J. Elasticity*, 42:283–289, 1996a.

M. Vianello. Optimization of the stored energy and coaxiality of strain and stress in finite elasticity. *J. Elasticity*, 44:193–202, 1996b.

L. Vincent, S. Calloch, and D. Marquis. A general plasticity model taking into account yield surface distortion for multiaxial ratcheting. *Int. J. Plasticity*, 20:1817–1850, 2003.

E.G. Virga. *Variational Theories for Liquid Crystals*, volume 8 of *Applied Mathematics and Mathematical Computation*. Chapman & Hall, 1994.

M. Wallin, M. Ristinmaa, and N.S. Ottosen. Kinematic hardening in large strain plasticity. *Euro. J. Mech. A/Solids*, 22:341–356, 2003.

C.C. Wang and F. Bloom. Material uniformity and inhomogeneity in anelastic bodies. *Arch. Rational Mech. Anal.*, 53:246–276, 1974.

C.C. Wang and C. Truesdell. *Introduction to Rational Elasticity*. Monographs and Textbooks on Mechanics of Solids and Fluids – Mechanics of Continua. Noordhoff International Publishing, 1973.

J.H.-C. Wang. Substrate deformation determines actin cytoskeleton reoganization: a mathematical modeling and experimental study. *J. Theor. Biol.*, 202:33–41, 2000.

J.H.-C. Wang, P. Goldschmidt-Clermont, J. Wille, and F.C.-P. Yin. Specifity of endothelial cell reorientation in response to cyclic mechanical stretching. *J. Biomechanics*, 34:1563–1572, 2001.

J.H.-C. Wang and B.P. Thampatty. An introductory review of cell mechanobiology. *Biomech. Model. Mechanobio.*, 5:1–16, 2006.

G. Weber and L. Anand. Finite deformation constitutive equations and a time integration procedure for isotropic, hyperelastic–viscoplastic solids. *Comput. Methods Appl. Mech. Engrg.*, 79:173–202, 1990.

H. Weinans, R. Huiskes, and H.J. Grootenboer. The behavior of adaptive bone–remodelling simulation models. *J. Biomechanics*, 25(12):1425–1441, 1992.

J.A. Weiss, B.N. Maker, and S. Govindjee. Finite element implementation of incompressible, transversely isotropic hyperelasticity. *Comput. Methods Appl. Mech. Engrg.*, 135:107–128, 1996.

S. Weng. Ein anisotropes Knochenumbaumodell und dessen Anwendung. *Technische Mechanik*, 18 (3):173–180, 1998.

T.A.L. Wren. A computational model for the adaption of muscle and tendon length to average muscle length and minimum tendon strain. *J. Biomechanics*, 36:1117–1124, 2003.

H. Xiao. On isotropic invariants of the elasticity tensor. *J. Elasticity*, 46:115–149, 1997.

H. Xiao and L.-S. Chen. Hencky's logarithmic strain and dual stress–strain and strain–stress relations in isotropic finite hyperelasticity. *Int. J. Solids Struct.*, 40:1455–1463, 2003.

A. Yavari, J.E. Marsden, and M. Ortiz. On spatial and material covariant balance laws in leasticity. *J. Appl. Phys.*, 47:042903/1–53, 2006.

H. Yokoyama, S. Miato, S. Yamamoto, and M. Fujikake. Effect of angle of attack on flanking behaviour in perlitic steel rails. *Wear*, 253:60–66, 2002.

M. Zelin. Microstructure evolution in pearlitic steels during wire drawing. *Acta Mater.*, 50(17):4431–4447, 2002.

J.M. Zhang and J. Rychlewsky. Structural tensors for anisotropic solids. *Arch. Rat. Mech.*, 42(3): 267–277, 1990.

Q.-S. Zheng and A.J.M. Spencer. Tensors which characterize anisotropies. *Int. J. Engng. Sci.*, 31(5): 679–693, 1993.

P.K. Zysset. A review of morphology–elasticity relationships in human trabecular bone: theories and experiments. *J. Biomechanics*, 36:1469–1485, 2003.

P.K. Zysset and A. Curnier. An alternative model for anisotropic elasticity based on fabric tensors. *Mech. Mater.*, 21:243–250, 1995. see also Technical Note by S.C. Cowin, *J. Biomechanics*, 31:759–762, 1998.

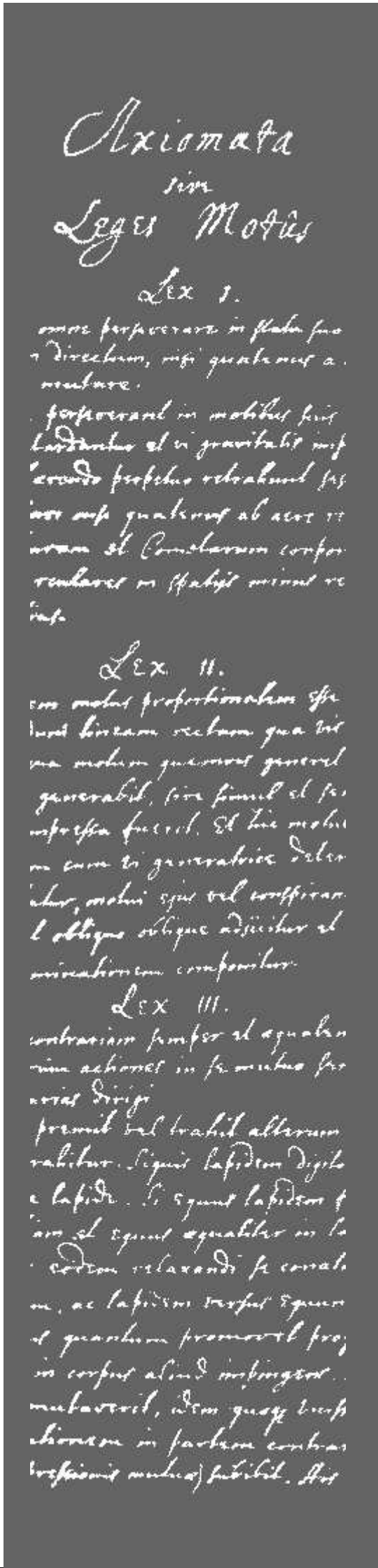

ISSN 1610–4641
ISBN 978–3–939432–55–5